ZBORNIK RADOVA
CONFERENCE PROCEEDINGS

MATRIB 2005

HOTEL POSEJDON, VELA LUKA
OTOK / ISLAND KORČULA, HRVATSKA
23-25. lipnja / June 2005.

ORGANIZATORI / ORGANIZED BY:

HRVATSKO DRUŠTVO ZA MATERIJALE I TRIBOLOGIJU
CROATIAN SOCIETY FOR MATERIALS AND TRIBOLOGY
DUBLIN INSTITUTE OF TECHNOLOGY
INSTITUTE OF MATERIALS AND MACHINE MECHANICS
(SLOVAK ACADEMY OF SCIENCES)

SPONZORI / SPONZORS:

INA INDUSTRIJA NAFTE – ZAGREB
STSI, Integrirani tehnički servisi d.d., član INA grupe

IZDAVAČ / PUBLISHER:
Hrvatsko društvo za materijale i tribologiju
Croatian Society for Materials and Tribology
c/o FSB, Ivana Lučića 5, 10000 Zagreb
tel.: +385 1 61 68 389; fax: +385 1 61 57 126
e-mail: hdmt@fsb.hr, http://www.fsb.hr/hdmt

UREDNIK / EDITOR: Krešimir Grilec

Svi radovi su tiskani u izvornom obliku.
All papers are printed in their original form

NAKLADA / ISSUE: 100

TISAK / PRINT: Logo-press d.o.o., Zagreb

ORGANIZATOR / ORGANIZED BY:

HRVATSKO DRUŠTVO ZA MATERIJALE I TRIBOLOGIJU
CROATIAN SOCIETY FOR MATERIALS AND TRIBOLOGY
c/o FSB, Ivana Lučića 5, 10000 Zagreb
tel.: +385 1 61 68 581; fax: +385 1 61 57 126
e-mail: hdmt@fsb.hr, http://www.fsb.hr/hdmt
DUBLIN INSTITUTE OF TECHNOLOGY
INSTITUTE OF MATERIALS AND MACHINE MECHANICS
(SLOVAK ACADEMY OF SCIENCES)

SPONZORI / SPONSORS:

INA – INDUSTRIJA NAFTE, Zagreb
STSI, Integrirani tehnički servisi d.d., član INA grupe

ORGANIZACIJSKI ODBOR / ORGANIZING COMMITTEE:

Krešimir Grilec (Zagreb) - predsjednik / president
Danijela Andreis (Vela Luka)
Darko Andreis (Vela Luka)
Denis Andreis (Vela Luka)
Suzana Jakovljević (Zagreb)
Dario Karlovčan (Zagreb)
Ivan Kramer (Zagreb)
Josip Lovričević (Vela Luka)
Željko Maričić (Vela Luka)
Gojko Marić (Zagreb)
Gorki Miletić (Vela Luka)
Želimir Oršanić (Zagreb)
Dinko Prižmić (Vela Luka)
Ana Žuvela (Vela Luka)
Danko Žuvela (Vela Luka)
Krešo Žuvela (Vela Luka)
Dražen Živković (Split)

PROGRAMSKI ODBOR / PROGRAMME COMMITTEE:

Vinko Ivušić (Zagreb) – predsjednik / president
Tomislav Filetin (Zagreb)
Mladen Franz (Zagreb)
Maurice Grech (Msida, Malta)
Jaroslav Jerz (Bratislava, Slovak Republic)
David Kennedy (Dublin, Ireland)
Slobodan Kralj (Zagreb)
Jan Meneve (Mol, Belgium)
Vedran Mudronja (Zagreb)
Ljiljana Pedišić (Zagreb)
Massimo Rogante (Civitanova Marche, Italy)
Zdravko Schauperl (Zagreb)
František Simančik (Bratislava, Slovak Republic)
Ivo Štepanek (Pilsen, Czech Republic)
Toma Udiljak (Zagreb)

SADRŽAJ

10. Savjetovanje o materijalima, tehnologijama, trenju i trošenju
10. Conference on Materials, Processes, Friction and Wear
MATRIB'05, Vela Luka, 23-25.06.2005.

RELATION BETWEEN THE RESISTANCE TO PERFORATION AND FLAT PRESSURE FORCE IN DEPENDENCE ON THE RELATIVE HUMIDITY OF THE CORRUGATED BOARD

ODNOS IZMEĐU PROBOJNE ČVRSTOĆE I RAVNE TLAČNE SILE U OVISNOSTI O RELATIVNOJ VLAZI VALOVITOG KARTONA

D. Babić, B. Lajić, D. Jurečić,
Grafički fakultet, Getaldićeva 2, 10000 Zagreb
Katedra za ambalažu i projektiranje grafičkih proizvoda

Abstract: The quality and the strength of the transport boxes produced from corrugated board depend on many factors. It is not only the quality of material, construction of the box or the way of production, but the relative humidity of the area in which the box is transported or stored. This investigation observes the mechanical properties of the material (ECT and CT) in dependence on the change of relative humidity (RH) in the environment.

Key words: circumferential resistance to perforation, resistance to perforation, relative humidity, strength of the transport boxes

Sažetak: Kvaliteta i čvrstoća transportnih kutija od valovitog kartona ovisi o mnogim faktorima. To nije samo kvaliteta materijala, konstrukcija kutije ili način formiranja kutije, nego svakako i vlažnost prostora u kojem se kutija ili skladišti ili transportira. Ovo istraživanje promatra mehanička svojstva materijala (ECT i CT) u ovisnosti o promjeni RV okoliša.

Ključne riječi: Obodna čvrstoća, probojna čvrstoća, relativna vlaga, čvrstoća transportne kutije

1. Introduction

In the segment of transport packaging the board covers about 40% of materials. More than 80% is corrugated board. According to that it is necessary to know this material very well. For the quality of the produced packaging from corrugated board, not only the physical and chemical properties are important but many mechanical properties that define that material are important as well. Finally, many investigations about that theme in our country as well as in the world have been performed. Our investigation is connected to the very often problem of storing the transport packaging in inadequate warehouses. Unfortunately, inadequate storage can be improved partially by better quality of the packaging, and consequently to that, more expensive packaging is produced, which leads to the income decrease; so such solutions are avoided. We are interested in the fact how much the materials strength is decreased by the increase of humidity as the main factor in the inadequate warehouses. If the humidity increase decreases the strength of the corrugated board according to some linear regulations or is there some other kind of the relation humidity/materials strength. Material strength was tested by ECT test (Fig. 1) and CT test (Fig. 2).

2. Method and material

We have tested one-wave double face corrugated board with the grammage 560g/m^2. Corrugated board was produced in the factory IPA Bilokalnik, in the town of Koprivnica. The flat layers were done from test-liner 170 g/m^2 produced in Belišće and wave-material was fluting 150 g/m^2 also from Belišće. The glue was Austrian starch glue from the producer Agram with the sign 8501. The glue consumption was 9 g/m², and as we have two layers the total consumption was 18 g/m². The production mark is 2K/3. Testing was done on the apparatus ECT (edge crash test) or crushing the corrugated board perpendicularly to waves (Fig 3), of the producer Loretzen & Wettre, type 048. The method was performed according to standard ISO 7263. Results are presented in table 1.

Figure 1. Apparatus for ECT test

Figure 2. Apparatus for measuring resistance to perforation CT

Values are chose according to standard humidity which is about 35%. Greater problem is presented by greater humidity than the humidity in the dry area; so only the increased humidity was investigated. CT (crash test) results were compared as well with the resistance to perforation results on the apparatus Karl Frank type 53809. This resistance was presented in table 2. According to the suggestion of the standard ISO 3036, determination of the resistance to perforation was done from the face of the material and from the back side of the material (Fig. 4) as well.

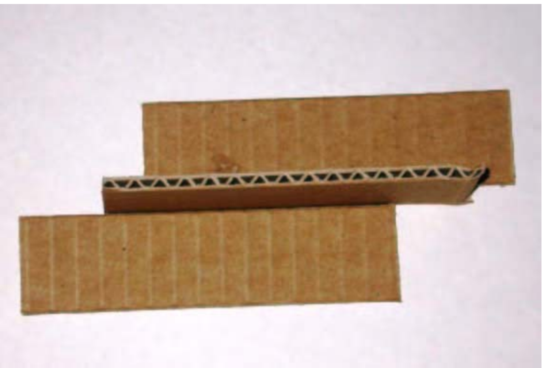

Figure 3. Sample outlook for ECT test
ISO 7263

Figure 4. Sample outlook for CT test
ISO 3036

By comparing both resistance values it will be possible to find the dependence of the resistance to perforation to material humidity. The obtained results are given in the table 2.

3. Results

Table 1. Testing results of the sample by ECT-testom

Ordinal number of testing	Testing results of the circumferential resistance to perforation expressed in (kN/m) in dependence on RH of the environment (%)			
	35	45	65	83
1	6.24	5.79	6.25	5.65
2	6.10	6.05	6.06	4.48
3	5.95	5.81	6.20	5.33
4	5.52	6.30	5.72	5.18
5	5.87	5.97	6.36	5.26
6	5.97	6.03	5.95	5.26
7	5.85	5.50	5.95	5.46
8	6.07	6.29	6.11	4.90
9	5.92	5.67	5.33	4.79
10	5.87	5.61	4.86	5.44
X	5.936	5.902	5.879	5.156
σ	0,190916	0.273569	0.463476	0,409151

Table 2. Investigation of the dynamic perforation of the corrugated board (in J)

Ordinal number of investigation	Perforation of the corrugated bord face				Perforation of the coruugated bord back side			
	Humidity (%)				Humidity (%)			
	35	45	65	83	35	45	65	83
1.	4.5	4.35	4.45	4.85	4.50	4.25	4.45	4.65
2.	4.35	4.50	4.50	4.55	4.35	4.30	4.25	4.60
3.	4.55	4.30	4.45	4.55	4.35	4.50	4.45	4.30
4.	4.45	4.50	4.55	4.25	4.35	4.15	4.05	4.50
5.	4.55	3.95	4.65	4.80	4.45	4.35	4.25	4.45
6.	4.55	4.55	3.95	4.55	4.35	4.30	4.55	4.45
7.	4.45	4.35	4.30	4.75	4.00	4.15	4.50	4.55
8.	4.45	4.30	4.55	4.55	4.60	4.25	4.55	4.45
9.	4.40	4.10	4.55	4.20	4.40	4.25	4.55	4.40
10.	4.40	4.35	4.75	4.25	4.15	4.25	4.45	4.25
X	4.465	4.325	4.470	4.530	4.350	4.275	4.405	4.460
σ	0.07097	0.184466	0.218835	0.233571	0.169967	0.100692	0.167415	0.124276

4. Result analysis

It is visible from the diagram 1 that there is a small percentage of the circumferential resistance decrease (about 0,1%) for RH between 35 and 65 %, and essentially greater decrease of the circumferential resistance for RH of 83% which is 23% (relationship of the average X R V (35, 45 and 65)% and RH 83%). It can be concluded that the circumferential resistance begins to change essentially at RH greater than 50%, which is good to know because a good constructed and formed box can stand up to strain during transport and storage even in relative unsuitable conditions. The following investigations will stronger define the limits of indulgence. Another conclusion can be drawn from the diagram 1. It is known that the resistance to perforation the corrugated board face in relation to the resistance to perforation of the corrugated board back side differs between 0,02 and 0,03% which was obtained in this investigation. The only unexpected value obtained from the table 2 graphically visible in diagram 1 is the smallest resistance to perforation at 45% of RH and the greatest one is at the greatest RH content. The increase of the resistance to perforation caused by the increase of humidity can be explained by the type of paper of the flat layer of the corrugated board the testliner 170 g/m^2 which is extremely resilient material. It is much more difficult to find the explanation for a bad result at RH of 45%. So this phenomena has to be investigated in the following works as well.

Diagram 1. Presentation of the table 1 and the table 2

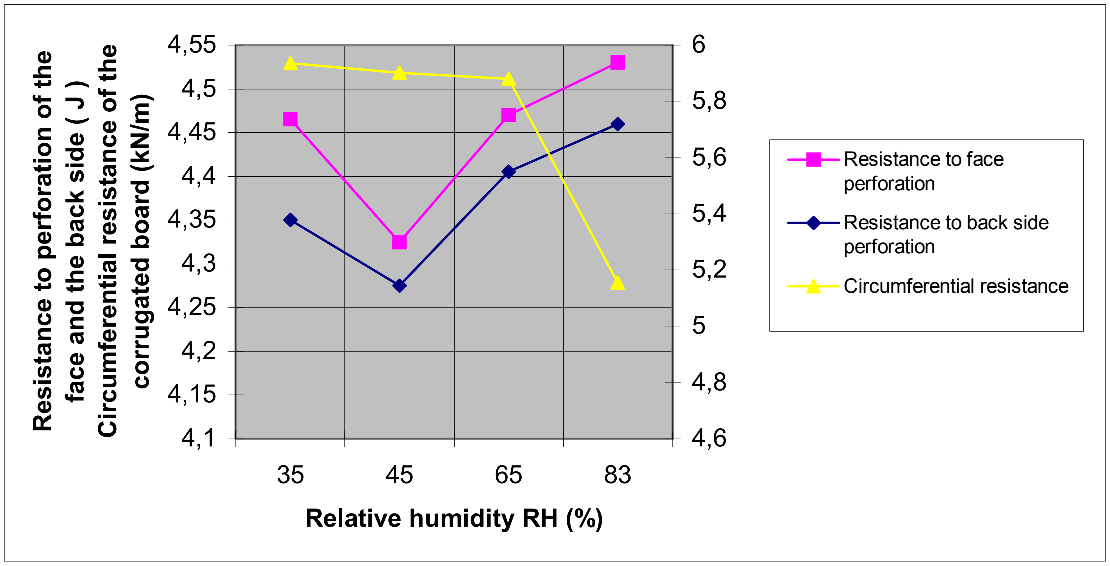

5. Conclusion

Transport boxes made from corrugated board, whose properties change by the change of the relative humidity RH according to the presented results during transport and storage, should not have essentially decreased resistance to perforation. In order to define this conclusion unambiguously, the finished boxes subjected to different relative humidity values have to be tested. The way of producing the boxes during the change of the RH of the environment, definitely influences the quality and the strength of the boxes. It is not the same if the box is made with the glue, adhesive stripe or wire-stitched. Only when the answers to that questions are obtained, one will be able to define the quality of boxes connected with the relative humidity of the environment, with a relative security.

6. Literatura

1. Brody, A. & Marsh, K. S. (1997). *The Wiley Encyclopaedia of Packaging Technology (2nd edition)*, John Wiley & Sons, Inc, ISBN 0-471-06397-5, New York
2. Bureau, W. H. (1989). *What the Printer Should Know about Paper*, Graphic Arts Technical Foundation, ISBN 0-88362-119-3, Pittsburgh
3. Hanlon, J. F.; Kelsey, R. J. & Forcinio, H. E. (1998). *Handbook of Package Engineering (3rd edition),* CRS Press, ISBN 1-56676-306-1, London
4. Mark, R. E. (1983). *Handbook of Physical and Mechanical Testing of Paper and Paperboard,* Marcel Dekker, INC., ISBN 0-8247-1871-2, New York
5. Day, S. G. (1984). *Strategic Market Planning,* The Pursuit of Compettive Advantages, ISBN 953-7040-01-1, West
6. Niskanen, K. (1998). *Paper Physics*, Book 16, Fapet Oy, ISBN 952-5216-16-0, Helsinki
7. Tenzer, H. J. (1989). *Leitfaden dr Papierverarbeitungstechnik*, VEB Fachbuchverlag, ISBN 3-343-00448-0, Leipzig

IZBOR OSNOVNOG I DODATNOG MATERIJALA ZA IZRADU TVRDOLEMLJENOG SPOJA NA ROTORIMA VISOKONAPONSKIH ASINHRONIH MOTORA

SELECTION OF PARENT AND FILLER MATERIAL FOR HARD-SOLDERED JOINTS ON ROTORS OF HIGH-VOLTAGE ASYNCHRONY ENGINES

Dr. sci. Kazafer Bečić, dipl.maš.inž.
Elektroremont d.d.,Banovići

Dr. sci. Sead Pašić, van. prof.
Univerzitet Džemal Bijedić,
Mašinski fakultet u Mostaru

Banovići, Mostar – Bosna i Hercegovina

Sažetak: Analiza potreba tehnologije tvrdog lemljenja u elektroindustriji ukazuje na veliku zastupljenost lemljenja kao termičkog postupka spajanja. Često je slučaj da se za razradu električnih i konstruktivnih funkcija proizvoda daju detaljna obrazloženja na naučnim principima, a da pri tom, zbog nepoznavanja teorije lemljenja, problemi lemljenja ostaju bez potrebnih razjašnjenja. Zato je, za rješavanje kompleksa problema iz ovog područja, važno poznavati različite faktore koji učestvuju u realizaciji zalemljenog spoja, jer to može imati presudan značaj za tok lemnog procesa, cijenu i valjnost spojnog mjesta.

Ključne riječi: tvrdo lemljenje, lem, topitelj.

Abstract: Analyses of hard-soldering technology application in electric industry shows that soldering, as form (procedure) of thermal (thermic) connection, is quite common. It is often the case that very detailed scientific based explanations of electric and constructive functions of products are being given, but because of the ignorance of soldering theory, the main problems of soldering remain unexplained. Therefore, for solving problems in this field, it is very important to understand different factors that are involved in making a soldered connection, for this could be of decisive (crucial) importance for soldering procedure, price and quality of connection. (connected spot).

Key words: hard-soldering, solder, flux

1. Uvod

Zalemljeni spoj nije homogeno tijelo, već je heterogeni sklop različitih materijala, s različitim fizičkim i hemijskim svojstvima. U najjednostavnijem slučaju sklop se sastoji iz osnovnog i dodatnog metala. Pri proučavanju čvrstoće takvog heterogenog spoja ne vrijede pojednostavljene pretpostavke teorije elastičnosti, koje vrijede za homogena metalna tijela, gdje se deformacije usljed vanjskih sila prenose jednoliko od površine ili mase na susjedna područja. Nije dovoljno poznavanje čvrstoće dodatnog i osnovnog metala da bi se mogla predvidjeti i čvrstoća zalemljenog spoja kao cjeline, već treba uzeti u obzir i mnogobrojne utjecajne faktore.

U zavisnosti o izabranom postupku lemljenja i obliku radnog komada, rastopljeni lem je u dodiru s površinom radnog komada u vremenu od nekoliko sekundi do nekoliko minuta. Usljed toga dodira dolazi do međusobne difuzije između lema i osnovnog materijala. Širina te zone zavisi od vrsti osnovnog materijala i primijenjenom lemu te o parametrima lemljenja. Vrsta i veličina difuzione zone i njezina istezljivost ima veliki utjecaj i na mehanička svojstva cjelokupnog zalemljenog spoja. Na *slici 1.* je shematski prikazan presjek kroz zalemljeni spoj.

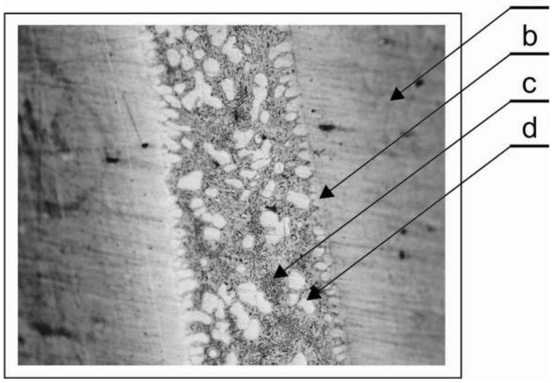

Slika 1. *– Mikrostruktura zalemljenog spoja: a) nepromijenjeni osnovni materijal; b) vijenac primarnih kristala na granici lem-osnovni materijal; c) eutektikum; d) primarni kristali u eutektikumu[2].*

2. Materijali za lemljenje

Materijali koji se upotrebljavaju za lemljenje su:

- lemovi (dodatni materijali),
- topitelji,
- zaštitni plinovi (zaštitna atmosfera).

2.1. *Lemovi (dodatni materijali)*

Legure za lemljenje teških metala dijele se prema svojoj kristalnoj građi [1] na sljedeće grupe:

- Grupa 1 obuhvata jednofazne lemove, to jest lemove sastavljene iz jedinstvenih kristala. To su čisti Cu – lem i Cu/Sn – lemovi,
- Grupa 2 obuhvata dvo-ili više-fazne lemove, sastavljene iz najmanje dvije različite kristalne vrste. To su Cu/Zn; Cu/Ni/Zn i Ag/Cu/Zn-legure,
- Grupa 3 obuhvata četverokomponentne legure sastavljene iz više kristalnih vrsta. To su Ag/Cd/Cu/Zn-legure,
- Grupa 4 obuhvata legure s fosforom koje se sastoje iz dvije ili više kristalnih vrsta. To su Cu/P; Ag/Cu/P-lemovi.

Tabela 1. *- Hemijski sastav, temperaturne i mehaničke osobine lemova za tvrdo lemljenje [1].*

Grupa i red. broj	Oznaka lema		Hemijski sastav lema u masenim % Solidus									Podruèje topljenja [K]		Radna temp. [K]	Svojstvo lema kod 293 K	
	DIN 8513	JUS	Ag	Cd	Cu	Zn	P	Si	Sn	Ni	Mn	Solidus	Likvidus		Èvrstoæa [MPa]	Spec.elek. otpor 10^{-3}[Ω m]
Grupa 1																
1	L-Cu				99,9 min		0,02 do 0,05					1356		1373	400	0,020
2	L-SnBz6				91 min		0 do 0,4		5 do 8			1283	1313	1313		
3	L-SnBz12				86 min		0 do 0,4		11 do 13			1098	1263	1263	300	0,100
Grupa 2		JUS C.D2.307														
4	**L-Ag44**	**S.Cu32ZnAg44**	**44**		**30**	**ost.**						948	1008	1003	460	0,087
5	L-Ag20		20		44	ost.		0 do 0,2				963	1083	1083	520	0,073
6	L-Ag12	S.Cu32ZnAg12	12		48	ost.						1073	1103	1103	540	0,074
7	L-Ag27	S.Cu32ZnAg27Mn	26 do 28		37 do 39	ost.				5 do 6	8,5 do 10,5	953	1103	1113	500	0,250
		JUS C.D2.306														
8	L-AgMs60	S.Cu60Zn			58 do 62	ost.		0,1 do 0,5	0,1 do 0,5			1163	1173	1173	420	0,069
9	L-AgNs				46 do 50	ost.		0,1 do 0,3		8 do 11		1163	1193	1183	550	0,200
Grupa 3		JUS C.D2.307														
10	L-Ag20Cd	S.Cu43ZnAg20Cd	20	15	40	ost.						878	968	1023	400	0,083
11	L-Ag30Cd	S.Cu36ZnAg30Cd	30	21	28	ost.						873	963	953	400	0,077
12	L-Ag40Cd		40	20	19	ost.						868	1176	883	470	0,071
Grupa 4																
13	L-Ag15P		15		ost.		5					923	1073	983	500	0,121
14	L-Ag5P		5		ost.		6					923	1083	983	500	0,230
15	L-CuP8				ost.		8					983	983-1043	983	450	0,280

2.2. *Topitelji (talila)*

Topitelji su nemetalni materijali. Oni se nanose na površine koje se žele lemiti nakon dobrog prethodnog čišćenja, da bi se odstranili postojeći oksidni slojevi i spriječilo stvaranje novih. Time se omogućava vlaženje površina koje se spajaju. Vrijeme djelotvornosti topitelja u obliku otopine je ograničeno.

Talilo ima dvije glavne funkcije:

- dezoksidira površinu i održava je u čistom stanju za vrijeme lemljenja,
- pomiče ravnotežu napetosti površine u smjeru širenja lema, smanjenjem ugla kvašenja.

Topitelji se uglavnom primjenjuju kod lemljenja na zraku, rjeđe u kisikom siromašnoj zaštitnoj atmosferi. Oni moraju zadovoljiti dva osnovna zahtjeva:

- nižu tačku topljenja za oko 50 K od lema za koji su namijenjeni,
- dobru zaštitu radnog komada stvaranjem nepropusnog filma u periodu zagrijavanja.

Kod dužeg zagrijavanja dostigne se granica topivosti oksida, i osnovni metal ostaje presvučen oksidom. Ovo objašnjava činjenicu da presporo zagrijavanje radnog komada onemogućava proces lemljenja.

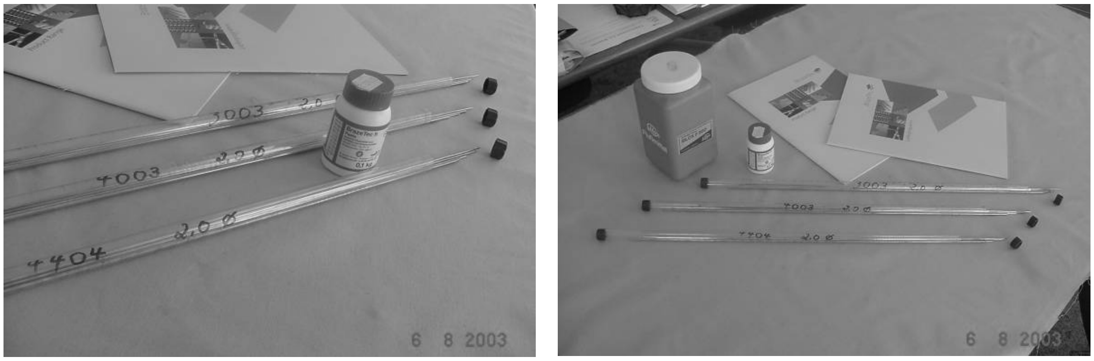

Slika 2. *– Dodatni materijali potrebni za tvrdo lemljenje.*

3. Izrada tvrdolemljenih spojeva na rotorima visokonaponskih asinhronih motora

Rotori visokonaposkih asinhronih motora su izuzetno opterećeni strojni dijelovi. Usljed velikih zagrijavanja rotora mogu se javiti naprezanja zbog kojih vrlo često dolazi do oštećenja namota rotora, posebno na dijelu štapa na mjestu spoja sa prstenom. Razlog ovome je umanjeno odvođenje topline u odnosu na dio smješten u lim paket rotora, što dovodi do velikih izduženja pojedinih štapova. Ovo ima za poslijedicu, kod konstrukcija rotora koje nisu adekvatno izrađene, defekt na spoju štapa sa kratkospojnim prstenom *(Slika 3).*

Reparatura oštećenih rotora asinhronih motora tehnički je vrlo zahtjevna operacija, kako u pogledu izrade pojedinih elemenata i pripreme spojeva, tako i pri izboru odgovarajućeg dodatnog materijala za tvrdo lemljenje (lema i topitelja) i adekvatne tehnologije lemljenja.

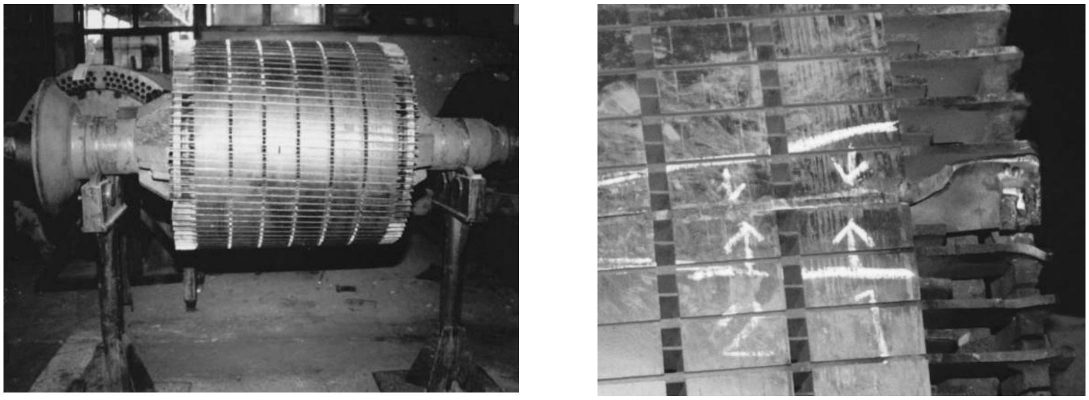

Slika 3 *–Defekt na mjestu zalemljenog spoja štapa i kratkospojnog prstena na rotoru visokonaoonskog asinhronog motora snage 1050 kW, TE Tuzla.*

Izbor optimalnog dodatnog materijala za tvrdo lemljenje štapa i kratkospojnog prstena na rotoru visokonaponskog asinhronog motora izvršen je na osnovu eksperimentalnih istraživanja koja su provedena u pogonima tvornice Elektroremont, Banovići, d.d. Izgled eksperimentalnih uzoraka koji su korišteni tokom istraživanja prikazani su na slici 4.

Slika 4. *- Reakcija talila s oksidima i kisikom iz zraka pri lemljenju eksperimentalnih uzoraka štapa i kratkospojnog prstena*

Analizirajući tabelarne vrijednosti čvrstoće lema, specifičnog električnog otpora, radne temperature, područja topljenja, hemijskog sastava i cijene, a na preporuku proizvođača lemova, za izradu uzoraka štapa i kratkospojnog prstena, koji je korišten za eksperimentalno ispitivanje, izabrani su lemovi iz grupe 2 i 3, sa oznakama L-Ag44, L-Ag40Cd i L-Ag30Cd. Podaci o odabranim dodatnim materijalima koji su korišteni za lemljenje namota rotora za kratkospojni prsten rotora visokonaponskih asinhronih motora dati su u *tabeli 2.*

Tabela 2. *- Područje topljenja, radna temperatura, mehaničke i električne osobine srebrenog lema L-Ag44, L-Ag40Cd i L-Ag30Cd.*

Grupa	Oznaka BrazeTec Hartlot		Hemijski sastav lema u masenim procentima [%]					Radna temp. [K]	Gustoća [kg/m^3]	mehaničke osobine lema	
	ISO9001	DIN 8513	Ag	Cu	Zn	Cd	ostalo			Čvrstoća [MPa]	Spec.elek otpor 10^{-3}[Ω m]
2	4404	L-Ag44	44	30	26	-	-	1003	9100	460	0.087
3	4003	L-Ag40Cd	40	19	21	20	-	883	9300	470	0.071
3	3003	L-Ag30Cd	30	28	21	21	-	953	9200	400	0.077

U procesu lemljenja namota rotora za kratkospojni prsten kod rotora visokonaponskih asinhronih motora, uz naprijed navedene lemove, koristio se topitelj za tvrdo lemljenje teških metala oznake Braze Tech Typ FH 10, po DIN EN 1045 ili SILOX F 500, proizvođača Zlatarna Celje, čiji je temperaturni opseg upotrebe od 773 K do 1073 K.

4. Zaključak

Pravilnim izborom postupka, kao i materijala za tvrdo lemljenje sa nižom tačkom topljenja i sa dobrim mehaničkim karakteristikama, postiže se ravnomjerna eutotektoidna struktura bez zaostalih grešaka u spojnom mjestu kao i bolje karakteristike spojnog mjesta, kako u pogledu mehaničkih, tako i električnih osobina lemljenih spojeva. Na ovaj način se značajno može povećati pouzdanost u radu visokonaponskih asinhronih motora i produžiti njihov vijek trajanja.

5. Literatura

1. Hrestak, M.; *Fizikalno-hemijske pojave u procesu tvrdog lemljenja i njihov utjecaj na* svojstva zalemljenog spoja I dio, Zavarivanje, HDTZ, Zagreb, 1977.

2. Bečić, K.; *Utjecaj reparature namota rotora na čvrstoću konstrukcije kod visokonaponskih asinhronih motora,* Doktorska disertacija, Mašinski fakultet u Tuzli, 2004.

3. Kralj, S.; *Ispitivanje čvrstoće zalemljenih spojeva,* Zavarivanje, HDTZ, Zagreb, 1980.

ZAMJENA ISTROŠENIH, ORIGINALNIH STROJNIH DIJELOVA NEORIGINALNIM

REPLACEMANT OF WORN-OUT ORIGINAL MACHINE PARTS WITH UNORIGINAL COMPONENTS

Srećko Brkić, PLIVA HRVATSKA D.O.O.- Prilaz baruna Filipovića 25, Zagreb

Sažetak

Predmet ovog rada je sklop na glavi omekšivača vode, preciznije rečeno njegov kritičan tribološki sustav. Prije izrade novog dijela nije bilo vremena za analizu tribosustava i traženja drugih varijanti rješenja, jer je zastoj postrojenja za proizvodnju pročišćene vode bio neprihvatljiv. Brzo se rješenje, obzirom na dosadašnje iskustvo pokazalo više nego zadovoljavajuće.

Ključne riječi: Trošenje, omekšivač, sapnica

Abstract

This paper describes the nozzle on the head of softener, or more precisely its critical tribologic system. Before a new nozzle was made there had been no time to analyse the tribologic systems or other options, since a longer standstill of the plant for production of purified water is not acceptable. Our previous experience revealed that this quick solution is more than satisfactory.

Key words: Wear, softener, nozzle

1. UVOD

Uvozni dijelovi na postrojenjima za farmaceutsku industriju su vrlo skupi, a i dugo se čeka njihova isporuka. Za svaku ozbiljnu proizvodnju to je neprihvatljivo tako da se u nuždi dijelovi strojeva ili postrojenja rade kao kopije originalnih dijelova. U ovom radu opisano je kako i zašto se morao mijenjati materijal originalnog dijela (sapnice) na omekšivaču pitke vode koji je sastavni dio linije-postrojenja za proizvodnju pročišćene vode.

2. IZBOR MATERIJALA SAPNICE

Renomirana tvrtka "Grunbeck" (Njemačka) je na svom novom tipu omekšivača (GENO-mat WF "S") ugradila sapnicu napravljenu od nehrđajućeg čelika kvalitete AISI 304. Sapnica je u radu sve do potpunog uništenja izdržala najviše 45 dana. Nakon toga ugrađena je nova originalna sapnica koja se potpuno istrošila nakon 40 dana (vidi sliku 1).

Slika 1

Uništena originalna sapnica 1 i zamjenska teflonska (PTFE) sapnica oznaka 2

Kratka analiza oštećenja sapnice ukazivala je da sapnica nije otporna na medij koji kroz nju prolazi. Medij je otopina NaCl uz dodatni slobodni klor. Originalna sapnica napravljena je iz materijala kvalitete AISI 304 (DIN WNr. 1.4301). Nehrđajući čelik kvalitete AISI 304 je austenitni čelik (18/10 Cr-Ni čelik). Otporan je na kiseline, vodu, vodenu paru i vlažni zrak. Klor i njegovi spojevi (kloridi) u interakciji sa organskim kiselinama uzrokuju jamičastu koroziju (pitting) na nehrđajućim čelicima. Kloridi nepovoljno utiču, jer izazivaju i stres koroziju na nehrđajućim čelicima.

Kemijski sastav nahrđajućeg čelika kvalitete AISI 304 je: C- 0,07%
Cr- 18,0%
Ni- 11,0%
(Ostatak se uglavnom odnosi na Fe)

Odabrao sam zamjenski materijal za izradu sapnice i to: POLI (TETRAFLUORETILEN)-PTFE. Ovaj plastomer poznat je pod nazivom "TEFLON". Taj je naziv u stvari komercijalni naziv nekih proizvođača tog materijala. Kemijska postojanost ovog materijala je na visokoj razini. Na TEFLON (PTFE) kemijski negativno utječu jedino rastaljeni ili otopljeni alkalni elementi. Na sve ostale elemente redom:

- voda,
- slabe kiseline,
- jake kiseline,
- oksidirajuće kiseline,
- fluorovodične kiseline,
- organske kiseline,
- slabe lužine,
- jake lužine
- anorganske soli,
- alkoholi,
- eteri,
- esteri,
- ketoni,
- aldehidi,
- amini,
- aromatski spojevi,
- benzini,
- masti/ulja

Teflon je otporan. Navedena visoka kemijska otpornost bila je razlog radi čega sam smatrao da bi sapnica trebala biti teflonska (PTFE). Nova sapnica iz potpuno različitog materijala napravljena je u radionici strojne obrade Pliva Hrvatska d.o.o.

3. ZAKLJUČAK

Trajnost originalnih sapnica pri radu omekšivača (24 sata na dan) je bila najviše 45 dana. Zamjenska teflonska sapnica je ugrađena 07.01.2005 godine. Dana 09.03.2005 došao je ovlašteni tehničar tvrtke Grunbeck (Njemačka) i pregledao teflonsku sapnicu. Na teflonskoj (PTFE) sapnici nije pronašao ni najmanjih tragove oštećenja koje bi mogli nastati erozijom i korozijom. Nakon detaljnog pregleda ovlašteni serviser ugradio je u omekšivač ponovno teflonsku sapnicu umjesto originalne napravljene iz nehrđajućeg čelika (kvalitete AISI 304). Bitno je napomenuti da se ugrađeni dio nalazi na postrojenju koje je u garantnom roku. Zamjenska teflonska (PTFE) sapnica ukazuje da je dobar izbor za rješenje ovoga problema. Zamjenom originalne sapnice neoriginalnom smanjili su se zastoji u radu farmaceutskih proizvodnji (Galenski, Injekcije i Oprema), budući da je riješen uzrok zastoja postrojenja za proizvodnju pročišćene vode radi zamjene sapnice i čestih pokretanja ručnih regeneracija ionskih masa u omekšivaču. Time su se svakako smanjili i troškovi u proizvodnjama.

4. LITERATURA

1. Filetin T., Kovačićek F., Indof J.: Svojstva i primjena materijala, Zagreb 2002
2. Ivušić V.: Tribologija- Zagreb: HDMT 1998
3. Evans T.J.: THE INSTITUTION OF CHEMICAL ENGINEERS-UK 1986

PREPARATION AND CHARACTERIZATION OF POLY(METHYL METHACRYLATE)- SILICA HYBRIDS

Ivan Brnardić,Gloria Gallego Ferrer*, Marica Ivanković & Hrvoje Ivanković
University of Zagreb, Faculty of Chemical Engineering and Technology, Marulićev trg 19,
HR-10001 Zagreb,Croatia
* Polytechnic University of Valencia, Dept.Appl.Thermodynam., Camino de Vera 14, E-46071 Valencia, Spain

Abstract:

The sol-gel process, with its associated mild conditions, offers a new approach to the synthesis of composite materials with domain sizes approaching the molecular level. For example, metal alkoxides can be mixed with monomers to be polymerized or polymers, which have functional groups that react with metal hydroxide, resulting in homogeneous organic-inorganic hybrid materials. In the hybrid materials, the existence of primary bonding forces (e.g. controllable number of covalent bonds) between the organic and inorganic components results in a reduced tendency of macroscopic phase separation as caused often by the thermodynamic incompatibility of the components.

In this work hybrid materials for biomedical applications were studied. Poly(methyl methacrylate)-silica hybrids were prepared by a simultaneous polymerization of organic monomer methyl methacrylate (MMA) and an organically modified silicon alkoxide, 3-glycidyloxypropyltrimethoxysilane (GLYMO), using a poly(oxypropylene)diamine as a crosslinking agent. Prepared hybrid materials were studied by differential scanning calorimetry (DSC), dynamic mechanical analysis (DMA) and thermogravometric analysis (TGA). Inorganic phase formed as a result of GLYMO´s hydrolysis and condensation in the sol-gel process influences the glass transition temperature of poly(methyl methacrylate) and improves the heat resistance of hybrid materials.

TVRDOĆA TOPLINSKI OBRAĐENE Cu-SLITINE S EFEKTOM PRISJETLJIVOSTI OBLIKA

Danko Ćorić, Mladen Franz
Fakultet strojarstva i brodogradnje
Ivana Lučića 5, Zagreb, Hrvatska

Sažetak:
Bakrena slitina s efektom prisjetljivosti oblika toplinski je obrađena u području temperatura 600°C do 800°C. Tvrdoća slitine izmjerena je metodom po Vickersu s nekoliko različitih opterećenja utiskivanja indentora: 0,098 N (HV 0,01), 4,9 N (HV 0,5), 9,8 N (HV 1) i 98,1 N (HV 10). Kada se tvrdoća ispituje metodom HV 0,01 slijedi stvarna tvrdoća strukturnih faza, a mjerenja s većim opterećenjima rezultiraju pojavom pseudo-tvrdoća uslijed mehanički inducirane martenzitne transformacije. Promjene kemijskog sastava koje nastupaju porastom temeperature betatizacije unutar dvofaznog područja $600°C \leq \vartheta_{\beta} \leq 670°C$ vode blagom snižavanju stvarne tvrdoće β-faze i značajnom porastu tvrdoće α-faze. Vrijednosti izmjerenih pseudo-tvrdoća determiniranih silom utiskivanja indentora ne ovise o provedenoj toplinskoj obradi.

Ključne riječi: Cu-slitina s efektom prisjetljivosti oblika, toplinska obrada, tvrdoća

1. UVOD

Kod konvencionalnih materijala (čelik, Al-slitina i sl.) mjerenje tvrdoće predstavlja jedan od najčešće primjenjivanih postupaka na području ispitivanja mehaničkih svojstava. Prema definiciji tvrdoća predstavlja otpornost materijala prema prodiranju nekog drugog znatno tvrđeg tijela. Utiskivanjem indentora, u obliku stošca, kugle ili piramide, ispitivani materijal deformira se prvo elastično pa potom plastično. Elastična deformacija nestaje odmah po rasterećenju, ali ostaje sačuvana plastična deformacija koja predstavlja mjeru otpornosti materijala trajnom deformiranju i ova se otpornost može izmjeriti. Što je veličina plastično deformiranog područja veća to je vrijednost tvrdoće materijala niža. Veličina plastične deformacijske komponente određena je strukturnim stanjem materijala koje se postiže obradom materijala određenog kemijskog sastava putem određenih tehnoloških postupaka (npr. toplinska obrada), ali isto tako ovisi i o obliku indentora i sili utiskivanja /1/. Kod mjerenja tvrdoće konvencionalnih materijala metodom po Vickersu izmjerene tvrdoće neće ovisiti o sili utiskivanja dijamantne piramide. Međutim, postoje materijali kao što su slitine s efektom prisjetljivosti oblika (skraćeno: SEPO) kod kojih izmjerena tvrdoća značajno varira s obzirom na primijenjeno opterećenje utiskivanja indentora /2/, /3/.

2. SASTAV SLITINE I EKSPERIMENTALNI POSTUPAK

Ispitivana bakrena slitina s prisjetljivošću oblika proizvedena je indukcijskim pretaljivanjem i lijevanjem u specijaliziranoj ljevaonici za lijevanje SEPO materijala Wieland-Werke A.G. u Njemačkoj. Proizvodnja legure zahtijeva visoku točnost legiranja, veću od 0,1 %, budući da su pretvorbene temperature koje imaju signifikantni utjecaj na eksploatacijske karakteristike slitine vrlo osjetljive na promjenu kemijskog sastava /4/.

Za eksperimentalno istraživanje odabrana je trokomponentna bakrena slitina s efektom prisjetljivosti oblika slijedećeg kemijskog sastava: Cu 69,51 % mase, Zn 27,32 % mase, Al 3,17 % mase. Sadržaj bakra i cinka određen je elektrogravimetrijskom metodom, a kontrola eventualno preostalih količina nakon selektivne depozicije metala provedena je u elektrolitu spektrofotometrijski. Za određivanje sadržaja aluminija korištena je atomsko-apsorpciona spektrofotometrija. Aluminij kao legirajući element značajno utječe na mehanička svojstva slitine i njeno transformacijsko ponašanje.

Lijevani SEPO uzorci toplinski su obrađeni u području temperatura gdje nastupaju visoko toplinski aktivirani procesi. Betatizacijsko zagrijavanje u trajanju 20 minuta provedeno je na temperaturama: 600°C, 620°C, 650°C, 660°C, 670°C, 680°C, 700°C, 725°C, 750°C, 775°C i 800°C. Uzorci su potom brzo hlađeni (gašeni) kako bi se izbjegle nepoželjne transformacije čvrstog stanja ("masivna", eutektoidna, bainitna reakcija, precipitacija) koje mijenjaju strukturu visoko temperatrurne β-faze (austenit) /5/. Gašenje brzinom većom od kritične (nadkritično gašenje) ostvareno je uranjanjem uzoraka u hladnu vodu. Brzina nadkritičnog gašenja određena je kemijskim sastavom slitine i veličinom austenitnog zrna.

Mjerenja tvrdoće provedena su na tvrdomjeru čiji je proizvođač Zwick, Njemačka, vrsta: 3212001. Ispitivanja su obavljena metodom po Vickersu s nekoliko različitih opterećenja utiskivanja indentora: 0,098 N (HV 0,01), 4,9 N (HV 0,5), 9,8 N (HV 1) i 98,1 N (HV 10). Za svako toplinski obrađeno stanje, ovisno o sili utiskivanja indentora, načinjeno je 15 mjerenja s ciljem smanjenja mjerne nesigurnosti iskazanog rezultata. Ovo je osobito važno kod mjerenja tvrdoće s malim opterećenjem kada je očekivano veće rasipanje rezultata. Tvrdoća je ispitana na sobnoj temperaturi iznad A_f (temperatura završetka austenitne transformacije).

3. REZULTATI EKSPERIMENATA

Mjerenjem tvrdoće pri temperaturi većoj od M_s (temperatura početka toplinski inducirane martenzitne transformacije), a nižoj od M_d (najviša temperatura pri kojoj nastupa mehanički inducirana martenzitna pretvorba) analizirani su efekti toplinske obradbe na dobivene tvrdoće.

Već provedena istraživanja pokazala su da je kod uzoraka betatiziranih u području temperatura $600°C \leq \vartheta_\beta \leq 670°C$ prisutna dvofazna $\alpha+\beta$-struktura, za razliku od uzoraka obrađenih na višim temperaturama ($680°C \leq \vartheta_\beta \leq 800°C$) koji imaju monofaznu austenitnu strukturu /6/.

U tablici 1 prikazani su rezultati mjerenja tvrdoće β-faze toplinski obrađenih uzoraka. Tvrdoća je izmjerena metodom po Vickersu s opterećenjem 0,098 N (HV 0,01).

Tablica 1: Vrijednosti tvrdoće β-faze toplinski obrađene CuZn27,32Al3,17 slitine

	ϑ_β, °C										
	600	620	650	660	670	680	700	725	750	775	800
HV 0,01	239	235	230	228	226	226	229	224	229	228	225

Slike 1 i 2 prikazuju tijek tvrdoće β-faze za temperature betatizacijskog zagrijavanja u dvofaznom $\alpha+\beta$-području odnosno monofaznom austenitnom području.

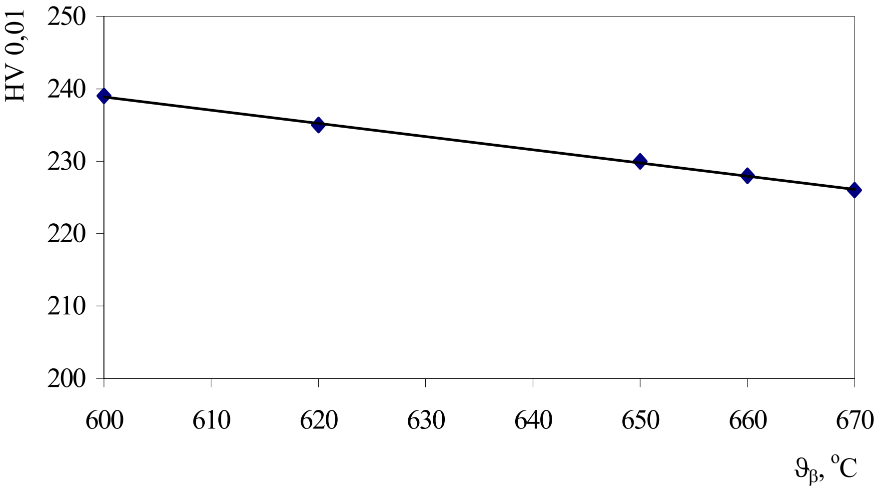

S

Slika 1: Ovisnost tvrdoće β-faze CuZn27,32Al3,17 slitine o temperaturi toplinske obrade unutar dvofaznog $\alpha+\beta$-područja

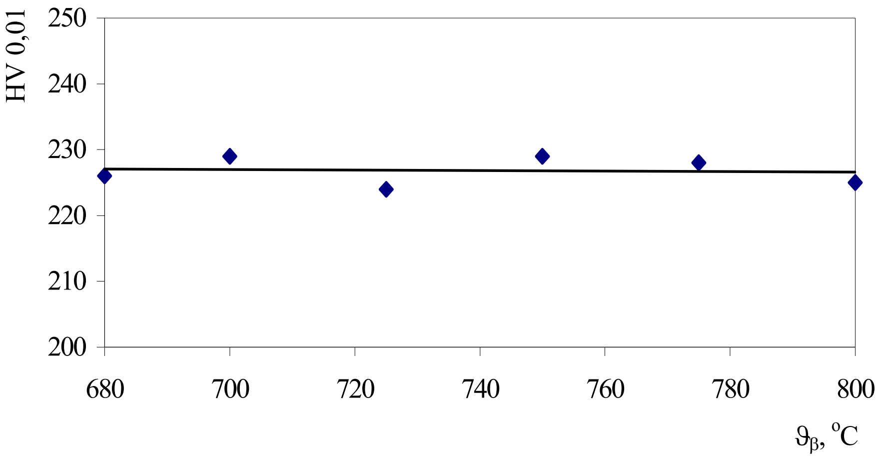

S

Slika 2: Ovisnost tvrdoće β-faze CuZn27,32Al3,17 slitine o temperaturi toplinske obrade unutar monofaznog β-područja

Iz slike 1 jasno je vidljivo blago linearno snižavanje tvrdoće β-faze s porastom temperature betatizacije prema 670°C. Tvrdoća austenita smanjuje se otprilike 2 HV na svakih 10°C promjene betatizacijske temperature. Nasuprot tome tvrdoća β-faze uzoraka toplinski obrađenih u području viših temperatura $680°C \leq \vartheta_\beta \leq 800°C$ približno je nepromijenjena i ne ovisi o temperaturi provedenog zagrijavanja.

U tablici 2 navedene su izmjerene tvrdoće α-faze CuZn27,32Al3,17 slitine gašene s temperatura $600°C \leq \vartheta_\beta \leq 670°C$, a na slici 3 prikazana je nastupajuća promjena tvrdoće.

Tablica 2: Vrijednosti tvrdoće α-faze toplinski obrađene CuZn27,32Al3,17 slitine

	ϑ_β, °C				
	600	620	650	660	670
HV 0,01	116	131	157	168	178

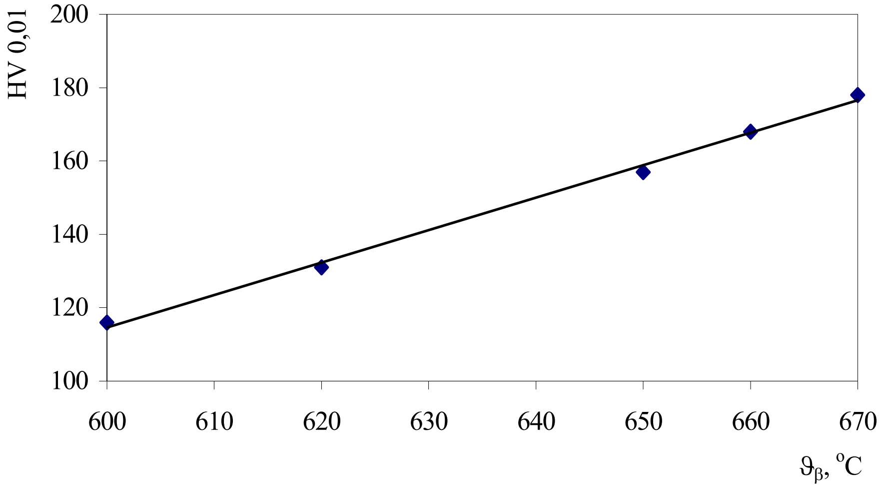

S

Slika 3: Ovisnost tvrdoće α-faze CuZn27,32Al3,17 slitine o temperaturi toplinske obrade unutar dvofaznog α+β-područja

Porastom temperature prema 670 °C dolazi do linearnog povećanja tvrdoće α-faze, pri čemu se za svaki stupanj promjene betatizacijske temeperature tvrdoća α-faze povećava ~1 HV. Usporede li se tvrdoće α- i β-faze proizlazi da je β-faza - intermetalni spoj znatno tvrđa, osobito za niže temperature betatizacijske obrade.

Tablica 3 sadrži vrijednosti tvrdoća izmjerenih većim opterećenjima 4,9 N (HV 0,5), 9,8 N (HV 1) i 98,1 N (HV 10).

Tablica 3: Tvrdoće toplinski obrađene CuZn27,32Al3,17 slitine izmjerene različitim opterećenjima

	ϑ_β, °C										
	600	620	650	660	670	680	700	725	750	775	800
HV 0,5	170	171	172	171	170	169	170	169	173	170	171
HV 1	160	162	163	161	161	161	161	160	163	160	162
HV 10	-	-	-	-	-	141,5	139,2	138,4	142,3	140,7	140,7

Kod metode HV 10, usljed pojave relativno velikog otiska, nije moguće mjerenje tvrdoće svih uzoraka već samo onih betatiziranih u području monofazne austenitne strukture (680 °C≤ϑ_β≤800 °C). Sve navedene tvrdoće izmjerene su na sobnoj temperaturi u području mehanički inducirane martenzitne pretvorbe. Slika 4 prikazuje položaj tvrdoća s obzirom na temperaturu betatizacije i korišteno opterećenje utiskivanja indentora.

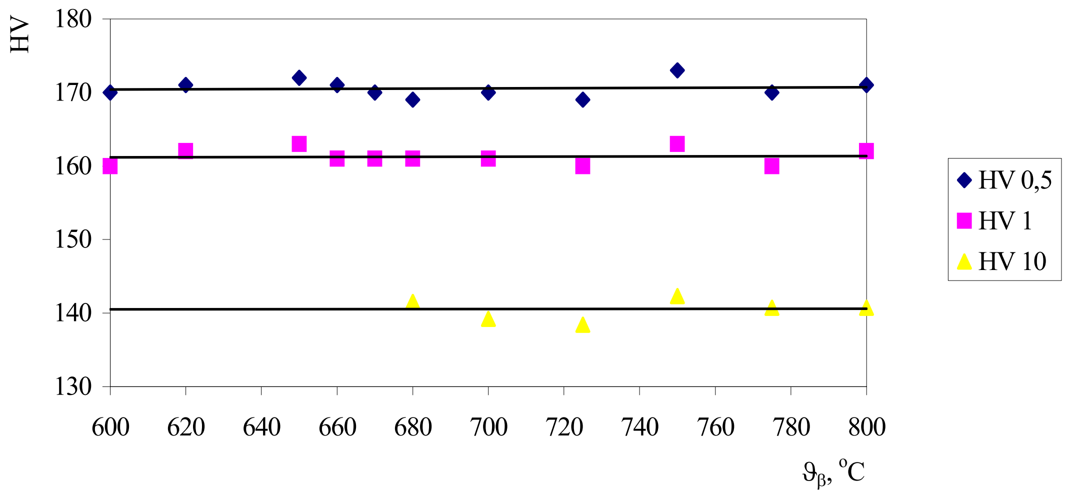

S

Slika 4: Ovisnost tvrdoća CuZn27,32Al3,17 slitine o temperaturi toplinske obrade i primijenjenom opterećenju

Vidljivo je da su tvrdoće toplinski obrađenih uzoraka neovisne o temperaturi betatizacijskog zagrijavanja. Međutim kako slika 4 pokazuje izmjerene tvrdoće značajno se mijenjaju s obzirom na metodu ispitivanja (HV 0,5, HV 1, HV 10). Premda su sva mjerenja obavljena utiskivanjem indentora u austenitnu strukturu slitine dobivene tvrdoće znatno su niže od tvrdoće austenita izmjerene malim opterećenjem (HV 0,01). Očito je dakle da izmjerene tvrdoće ne odgovaraju stvarnoj tvrdoći β-faze te se zapravo radi o pseudo-tvrdoćama. Pod djelovanjem većih opterećenja utiskivanja indentora na svim uzorcima mehanički se inducira transformacija tvrđe austenitne faze u mekšu martenzitnu fazu čime se snižava vrijednost izmjerene tvrdoće. Nepromjenjivost pseudo-tvrdoća unutar ispitivanog područja betatizacijskih temperatura ($600°C \leq \vartheta_\beta \leq 800$ °C) mogla se i očekivati, uzme li se u obzir da je tvrdoća mehanički induciranog martenzita ovisna o tvrdoći izvorne austenitne faze, a ispitivanja su pokazala da se tvrdoća austenita tek neznatno mijenja s promjenom temperature toplinske obrade.

4. RASPRAVA REZULTATA I ZAKLJUČAK

Budući da prisjetljivost oblika zahtijeva bezdifuzijsku reverzibilnu austenitno martenzitnu pretvorbu, toplinskom obradom lijevanih CuZnAl slitina postiže se visokotemperaturna austenitna struktura na kojoj počiva transformacijsko ponašanje SEPO materijala. Kako je austenitna struktura nastala homogenizacijskom obradom u području toplinski aktiviranih difuzijskih procesa po svojoj prirodi metastabilna, da bi se očuvala do sobne temperature nužno je kontrolirano hlađenje u vidu nadkritičnog gašenja. Homogena austenitna struktura slijedi gašenjem s temperatura viših od ϑ_β=670°C, a nižih od temperature taljenja (ϑ_m).

Tvrdoća austenita izmjerena na sobnoj temperaturi ($\vartheta > A_f$) metodom HV 0,01 pokazuje tendenciju blagog linearnog snižavanja s porastom temperature betatizacijske obrade unutar dvofaznog α+β-područja ($600°C \leq \vartheta_\beta \leq 670°C$). Istodobno nastupa veći porast tvrdoće α-faze pri čemu se tvrdoća povećava od 116 HV (ϑ_β=600°C) sve do 178 HV (ϑ_β=670°C). Promjena tvrdoća strukturnih faza uzrokovana je promjenom kemijskog sastava. Naime, istraživanja su pokazala da se porastom temperature izlučuje α-faza sve bogatija cinkom čime dolazi do osiromašenja austenitne matrice. S druge strane gašenjem iz monofaznog austenitnog područja ($680°C \leq \vartheta_\beta \leq 800°C$) kemijski sastav tek se neznatno mijenja pa su stvarne tvrdoće β-faze približno konstantne. Nadalje, potrebno je istaknuti da je tvrdoća austenita kod svih toplinski obrađenih uzoraka veća od tvrdoće α-faze. Ova razlika osobito dolazi do izražaja nakon toplinske obrade u području nižih temperatura.

Osim stvarne tvrdoće α- i β-faze kod slitina s efektom prisjetljivosti oblika moguće je izmjeriti i pseudo-tvrdoće. Odstupanje stvarne i izmjerene tvrdoće nastaje zbog niza anomalija koje slitina pokazuje kod mjerenja tvrdoće većim opterećenjima pri temperaturi manjoj od M_d. Pojava pseudo-tvrdoća u području temperatura $M_s<A_f<\vartheta<M_d$ dovodi se u vezu s naprezanjem ili deformacijom potaknutom martenzitnom pretvorbom. Deformacijom inducirana martenzitna transformacija javlja se nakon plastične deformacije austenita dok naprezanjem inducirani martenzit nastaje iz elastično deformiranog austenita. U ovom potonjem slučaju promjena strukture može se opisati izrazom $\beta \Rightarrow \alpha_M^+ \Rightarrow \alpha_{Md}^+$ kada iz austenita nastaju naprezanjem inducirani orijentirani martenzitni kristali α_M^+ koji pod djelovanjem mehaničkog opterećenja sadrže dislokacije i time nastaje α_{Md}^+ - defektna martenzitna struktura /7/, /8/. Zbog pojave mehanički induciranog martenzita izmjerene pseudo-tvrdoće značajno su niže od stvarne tvrdoće β-faze. Ranija istraživanja su pokazala da je ovaj mehanički inducirani martenzit manje pogodan za toplinsku povratnu austenitnu pretvorbu nego toplinski formiran martenzit. Martenzit nastao pod djelovanjem naprezanja toplinski je stabiliziran i transformira se u austenit tek nakon zagrijavanja znatno iznad nominalne A_f temperature. Pretpostavlja se da je uzrok takvom ponašanju deformacija α_M-kristala koja se nastavlja i nakon njihovog formiranja čime se uvode brojne dislokacije koje očvršćavaju strukturu, ali istodobno povećavaju stupanj neuređenosti.

Vrijednosti izmjerenih pseudo-tvrdoća determinirane su silom utiskivanja indentora. Veća opterećenja uzrokuju formiranje više martenzitnih iglica oko otiska, a kako su one mekanije od austenitne matrice dolazi do pada tvrdoće. Stoga su tvrdoće izmjerene metodom HV 0,5 i HV 1 pokazatelj mehaničke otpornosti dvofazne $\beta+\alpha_M$-strukture dok tvrdoća HV 10 karakterizira mehanički induciranu martenzitnu strukturu.

Pseudo-tvrdoće izmjerene određenom metodom približno su konstantne za cijelo ispitivano područje betatizacijskih temperatura ($600°C \leq \vartheta_\beta \leq 800°C$). Ovo se objašnjava činjenicom da je tvrdoća mehanički induciranog martenzita određena tvrdoćom izvorne β-faze, dakle tvrdoćom koja se vrlo malo mijenja s promjenom temperature betatizacijskog zagrijavanja.

Iz iznesenog je očito da tvrdoća toplinski obrađenih slitina s efektom prisjetljivosti oblika predstavlja vrlo kompleksno mehaničko svojstvo koje ne ovisi samo o materijalu i njegovom kemijskom sastavu te provedenoj toplinskoj obradi, što je slučaj kod konvencionalnih materijala, već u obzir treba uzeti i čimbenike kao što su temperatura ispitivanja i opterećenje utiskivanja indentora.

LITERATURA:

/1/ M. Franz: Mehanička svojstva materijala, Fakultet strojarstva i brodogradnje, Zagreb, 1998.

/2/ D. Ćorić, M. Franz: Mjerenje tvrdoće Cu-slitine s efektom prisjetljivosti oblika, Međunarodno savjetovanje MATRIB '99, str. 31 do 38, Trogir, svibanj 1999.

/3/ E. Hornbogen, E. Kobus: Characterization of Shape Memory Alloys by Hardness Indentations, Prakt. Metallogr. 30 (1993) 10, str. 507 do 519.

/4/ M. Franz: Slitine s efektom prisjetljivosti oblika, Hrvatska akademija znanosti i umjetnosti, Zagreb, 1995, s. 9

/5/ M. Franz, E. Hornbogen: Ausforming of a β-CuZn24Al9 Shape Memory Alloy, Zeitschrift fur Metallkunde 86, Carl Hanser Verlag, Munchen, 1995, p. 31 to 34

/6/ D. Ćorić, M. Franz: Influence of Betatisation Temperature on Thermal Transformation Behaviour of CuZn27Al 3 Alloy, Transactions of Famena, Vol. 28, No. 1, Zagreb (2004), p. 27 do 34

/7/ M. Franz, E. Hornbogen: Martensitic Transformation of a CuZnAl-Shape Memory Alloy Strengthened by Hot-Rolling, Materials Science and Engineering A252, Elsevier Science S.A., 1998, s. 157 do 165

/8/ J. Spielfeld, E. Hornbogen, M. Franz: Ausforming and Marforming of a Cu-Zn26,3-Al3,9 Shape Memory Alloy, ESOMAT'97, European Symposium on Martensitic Transformations, Enschede, Journal de Physique IV, 1997, s. C5 239-244

10. Savjetovanje o materijalima, tehnologijama, trenju i trošenju
10. Conference on Materials, Processes, Friction and Wear
MATRIB'05, Vela Luka, 23-25.06.2005.

ODREĐIVANJE KINETIČKIH PARAMETARA NEIZOTERMNE RAZGRADNJE PHB-a IKP METODOM

DETERMINATION OF THE KINETIC PARAMETERS FOR THE NON-ISOTHERMAL DEGRADATION OF PHB USING IKP METHOD

Matko Erceg, Tonka Kovačić & Ivka Klarić

Zavod za organsku kemijsku tehnologiju, Kemijsko-tehnološki fakultet
Teslina 10/V, 21 000 Split, Hrvatska
E-mail: merceg@ktf-split.hr

Abstract

The thermal degradation of biodegradable poly(3-hydroxybutyrate) (PHB) at processing temperatures is one of the main obstacles for its broad application. From the data obtained from non-isothermal thermogravimetric analysis, information about the kinetics of thermal degradation can be obtained. Therefore, the non-isothermal degradation of PHB was investigated in the temperature range 50···650ºC at four heating rates (2.5, 5, 10 and 20ºCmin^{-1}). The present work uses invariant kinetic parameters method (IKP method) to calculate the invariant kinetic parameters, i.e. activation energy (E_{inv}) and pre-exponential factor (A_{inv}). The IKP method is applied on the conversion range $0{,}10 \leq \alpha \geq 0{,}90$. The calculated value of E_{inv} is compared and practically equals the values obtained by isoconversional Flynn-Wall-Ozawa method. In order to explain the thermal degradation of the investigated material, it is necessary to know the kinetic triplet (E, A and conversion function, $f(\alpha)$). The IKP method allows evaluating numerically $f(\alpha)$. The values of invariant kinetic parameters were used for numerical evaluation of $f(\alpha)$. The plot $f(\alpha)$ *vs.* α exhibits a maximum what suggests that the non-isothermal degradation of PHB occurs through a mechanism like those represented by the Avrami-Erofeev equations (with m>1). However, the values of $f(\alpha)$ can not be fitted exactly by any of the ideal Avrami-Erofeev kinetic model. The exact analytical form of $f(\alpha)$ is difficult to be find.

Key words: invariant kinetic parameters method (IKP method), non-isothermal kinetics, PHB thermal degradation

Ključne riječi: metoda invarijantnih kinetičkih parametara (IKP metoda), neizotermna kinetika, toplinska razgradnja PHB-a

UVOD

Neizotermna termogravimetrijska analiza se često koristi za istraživanje kinetike i mehanizma toplinske razgradnje polimera. Ispravno određivanje kinetičkih parametara iz termogravimetrijskih podataka jedan je od najkompliciranijih kinetičkih problema.

Bilo koja kinetička analiza neizotermnih podataka osniva se na izrazu za brzinu reakcije:

$$\beta \frac{d\alpha}{dt} = A \cdot f(\alpha) \cdot \exp\left(-\frac{E}{RT}\right) \tag{1}$$

gdje je: α stupanj konverzije, β brzina zagrijavanja, t vrijeme, T temperatura, A predeksponencijalni faktor, $f(\alpha)$ kinetički model i R opća plinska konstanta. Stupanj konverzije izračunava se prema izrazu: $\alpha = (m_0 - m)/(m_0 - m_f)$, gdje su m_0, m i m_f početna, trenutna i konačna masa uzorka.

Primjena izraza (1) pretpostavlja da se poznavanjem vrijednosti kinetičkih parametara, E i A, te kinetičkog modela $f(\alpha)$ može opisati proces, bez obzira na njegovu kompleksnost. Polazeći od izraza (1) razvijene su različite metode njihovog određivanja. Jedan dio tih metoda zahtijeva pretpostavljanje $f(\alpha)$, što rezultira različitim vrijednostima kinetičkih parametara ovisno o pretpostavljenom $f(\alpha)$. Toplinska razgradnja uzoraka u čvrstom stanju heterogeni je proces popraćen oslobađanjem plinovitih produkata i često ga je teško opisati samo jednim mehanizmom razgradnje, odnosno jednim kinetičkim modelom. Stoga je ispravnije, u cilju točnog određivanja kinetičkih parametara, ne pretpostavljati unaprijed $f(\alpha)$.

Metoda invarijantnih kinetičkih parametara (IKP)[1,2], koja je primijenjena u ovom radu, omogućuje izračunavanje invarijantnih kinetičkih parametara (E_{inv} i A_{inv}) bez pretpostavljanja $f(\alpha)$. E_{inv} i A_{inv} ne ovise o eksperimentalnim uvjetima, te stoga predstavljaju stvarne vrijednosti kinetičkih parametara za pojedini proces. IKP metoda se osniva na činjenici da se ista eksperimentalna krivulja $\alpha=\alpha(T)$ može relativno dobro opisati s nekoliko različitih $f(\alpha)$, te da su kinetički parametri dobiveni primjenom različitih $f(\alpha)$ za istu eksperimentalnu krivulju povezani preko izraza za kompenzacijski efekt:

$$\ln A = \alpha^* + \beta^* E \tag{2}$$

gdje su α^* i β^* kompenzacijski parametri. Metoda zahtijeva snimanje TG krivulja pri više brzina zagrijavanja, β_v. U ovom radu primijenjeni su teorijski kinetički modeli prikazani u tablici 1.

Tablica 1. Kinetički modeli koji se najčešće koriste za reakcije u čvrstom stanju[3,4].

Mehanizam	Oznaka	f(α)	g(α)
Red reakcije	F_n	$(1-\alpha)^n$	$-\ln(1-\alpha)$, za n=1 (A1) $(1-(1-\alpha)^{(-n+1)})/(-n+1)$,za $n\neq1$
Nukleacija i rast (Avrami-Erofeev)	A_m $(0{,}5\leq m\geq4)$	$n(1-\alpha)[-\ln(1-\alpha)]^{(1-1/n)}$	$[-\ln(1-\alpha)]^{1/n}$
1D difuzija	D1	$1/2\alpha$	α^2
2D difuzija	D2	$1/[-\ln(1-\alpha)]$	$(1-\alpha)\ln(1-\alpha)+\alpha$
3D difuzija (Jander)	D3	$(3(1-\alpha)^{2/3})/(2[1-(1-\alpha)^{1/3}])$	$[1-(1-\alpha)^{1/3}]^2$
3D difuzija (Ginstring-Brounstein)	D4	$3/(2[(1-\alpha)^{-1/3}-1])$	$(1-2\alpha/3)-(1-\alpha)^{2/3}$
Power law	P_n	$n\alpha^{[1-1/n]}$	$\alpha^{1/n}$
Reakcija na granici faza	R_n $(1\leq n\geq3)$	$n(1-\alpha)^{1-1/n}$	$1-(1-\alpha)^{1/n}$

Za svaku brzinu zagrijavanja, β_v, primjenom Coats-Redfern metode[5], tj. izraza:

$$\ln\frac{g(\alpha)}{T^2}=\ln\left[\frac{AR}{\beta E}\left(1-\frac{2RT}{E}\right)\right]-\frac{E}{RT}\cong\ln\frac{AR}{\beta E}-\frac{E}{RT};\quad g(\alpha)=\int_0^{\alpha}\frac{d\alpha}{f(\alpha)} \tag{3}$$

izračunaju su kinetički parametri (E_v i A_v) za svaki $f(\alpha)$ iz tablice 1. Naime, iz nagiba pravca $\ln g(\alpha)/T^2$ vs. $1/T$ odredi se E_v, a iz odsječka na y-osi A_v.

Zatim se, uvođenjem tih kinetičkih parametara u izraz (2) i crtanjem krivulja $\ln A_v$ vs. E_v za svaku brzinu zagrijavanja odrede kompenzacijski parametri (α_v^* i β_v^*) iz nagiba pravca i odsječka na y-osi. Invarijantni kinetički parametri (E_{inv} i A_{inv}) izračunaju se iz tzv. superkorelacijskog izraza:

$$\alpha_v^* = \ln A_{inv} - \beta_v^* E_{inv} \tag{4}$$

Crtanjem ovisnosti α_v^* vs. β_v^* dobije se pravac čiji je nagib E_{inv}, a odsječak na y-osi $\ln A_{inv}$.

IKP metoda se može primijeniti i za brojčano određivanje $f(\alpha)$, uvođenjem vrijednosti E_{inv} i A_{inv} u izraz (1). Crtanjem ove ovisnosti $f(\alpha)$ vs. α, te njenom usporedbom s ovisnošću $f(\alpha)$ vs. α za teorijske kinetičke modele, može se donijeti zaključak o mehanizmu procesa, te eventualno odrediti točan izraz za $f(\alpha)$.

IKP metoda je primjenjiva samo za područje konverzija gdje se E ne mijenja s α. Ovisnost E o α određuje se iz termogravimetrijskih podataka primjenom izokonverzijske Flynn-Wall-Ozawa (FWO) metoda[6,7]. Vrijednosti E_{inv} dobivene IKP metodom uspoređene su s vrijednostima E dobivenim FWO metodom, a njihovo slaganje je uzeto kao kriterij ispravnosti određivanja kinetičkih parametara. U radu su kombiniranjem IKP i FWO metode određeni kinetički parametri, te brojčana vrijednost $f(\alpha)$.

EKSPERIMENTALNI DIO

Za ispitivanja je upotrijebljen polimer poli(3-hidroksibutirat) (PHB), (Biomer, Njemačka). Toplinska razgradnja PHB-a istraživana je termogravimetrijski (Perkin-Elmer TGS-2). Prije početka rada sustav je stabiliziran oko 1 sat. Istraživanja su provedena u neizotermnim uvjetima u području od 50···650ºC, pri različitim brzinama zagrijavanja (2,5; 5; 10; 20ºCmin^{-1}) u struji dušika (30 cm^{-3}min^{-1}). Masa uzoraka je bila 2,8 ± 0,2 mg.

REZULTATI I RASPRAVA

Termogravimetrijske krivulje (TG) neizotermne razgradnje PHB prikazane su na slici 1.

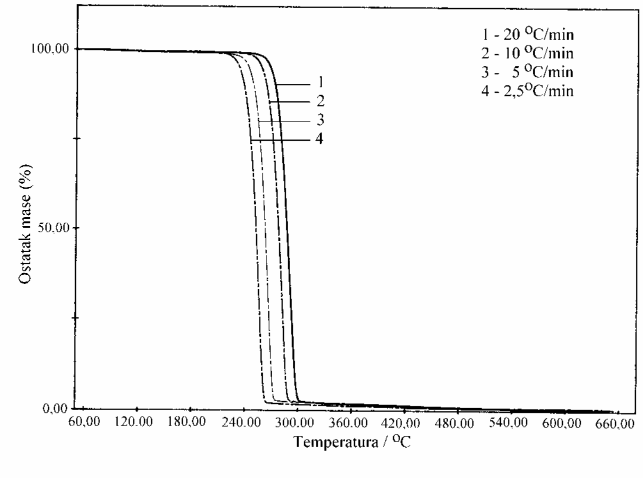

Slika 1. TG krivulje neizotermne razgradnje PHB-a.

Vrijednost E, dobivena FWO metodom[8], praktički je konstantna u području konverzija α=0,10-0,90 i iznosi E=135 ± 1,3 kJmol^{-1}, te je IKP metoda primijenjena na to područje konverzija.

U cilju određivanja invarijantnih kinetičkih parametara korišteno je 20 kinetičkih modela. Za svaki kinetički model i za svaku brzinu zagrijavanja izračunati su kinetički parametri Coats-Redfernovom metodom, čije su vrijednosti prikazane u tablici 2.

Tablica 2. Kinetički parametri izračunati primjenom Coats-Redfern metode.

	β=2,5 °Cmin^{-1}			β=5 °Cmin^{-1}			β=10 °Cmin^{-1}					
Kinetički model	E_v (kJmol^{-1})	ln A_v (A/s^{-1})	r^2	E_v (kJmol^{-1})	ln A_v (A/s^{-1})	r^2	E_v (kJmol^{-1})	ln A_v (A/s^{-1})	r^2	E_v (kJmol^{-1})	ln A_v (A/s^{-1})	r^2
A0.5	620,6	140,94	0,99869	651,9	145,81	0,99914	646,2	141,34	0,99918	647,0	139,80	0,99908
A1	305,9	68,57	0,99866	321,5	71,36	0,99912	318,5	69,44	0,99916	318,9	69,00	0,99905
A1.5	201,1	44,26	0,99862	211,4	46,36	0,99910	209,3	45,29	0,99914	209,5	45,21	0,99902
A2	148,6	32,02	0,99859	156,3	33,76	0,99907	154,7	33,12	0,99912	154,8	33,22	0,99899
A2.5	117,2	24,61	0,99855	123,3	26,45	0,99905	121,9	25,76	0,99909	122,0	25,98	0,99895
A3	96,2	19,64	0,99851	101,2	21,04	0,99903	100,1	20,82	0,99907	100,1	21,11	0,99891
A4	70,0	13,35	0,99843	73,7	14,57	0,99898	72,8	14,56	0,99902	72,8	14,95	0,99883
F0.5	257,8	57,17	0,99866	270,8	59,61	0,99829	268,3	58,07	0,99794	267,7	57,62	0,99145
F2/3	273,0	60,76	0,99972	286,8	63,31	0,99963	284,1	61,65	0,99942	283,8	61,20	0,99509
D1	493,1	110,26	0,99619	517,7	114,22	0,99552	513,0	110,75	0,99503	511,4	109,18	0,98633
D2	493,1	110,26	0,99619	517,7	114,22	0,99552	513,0	110,75	0,99503	511,4	109,18	0,98633
D3	554,6	123,24	0,99973	582,4	127,64	0,99965	577,3	123,69	0,99944	576,8	122,13	0,99526
D4	513,3	113,53	0,99799	539,0	117,63	0,99752	534,1	114,01	0,99713	533,0	112,44	0,99002
P1	217,5	47,58	0,98913	228,4	49,74	0,98795	226,2	48,52	0,98713	224,9	48,08	0,97418
P2	104,4	21,34	0,98816	109,8	22,77	0,98692	108,5	22,47	0,98599	107,8	22,58	0,97189
P3	66,7	12,39	0,98707	70,2	13,58	0,98575	69,3	13,59	0,98469	68,8	13,87	0,96930
P4	47,8	7,81	0,98583	50,4	8,88	0,98443	49,7	9,04	0,98321	49,3	9,41	0,96635
R1	217,5	47,58	0,98913	228,4	49,74	0,98795	226,2	48,52	0,98713	224,9	48,08	0,97418
R2	104,4	21,34	0,98816	109,8	22,77	0,98692	108,5	22,47	0,98599	107,8	22,58	0,97189
R3	66,7	12,39	0,98707	70,2	13,58	0,98575	69,3	13,59	0,98469	68,8	13,87	0,96930

Izračunate vrijednosti E odstupaju od vrijednosti izračunate FWO metodom, što znači da niti jedan testirani kinetički model ne odgovara stvarnom kinetičkom modelu procesa toplinske razgradnje PHB-a.

Kinetički parametri povezani su tzv. kompenzacijskim efektom (2), te su kompenzacijski parametri izračunati za svaku brzinu zagrijavanja prikazani u tablici 3.

Tablica 3. Vrijednosti kompenzacijskih parametara za podatke iz tablice 2.

β(°Cmin^{-1})	$-\alpha_v$* (A/s^{-1})	β_v* (molkJ^{-1})	r^2
2,5	2,3742	0,2289	0,99970
5	1,6409	0,2242	0,99972
10	1,0434	0,2184	0,99970
20	0,3908	0,2147	0,99969

Iz ovisnosti α_v^* vs. β_v^* dobivene su vrijednosti invarijantnih kinetičkih parametara: E_{inv}=134,2 kJmol^{-1} i $ln\ A_{inv}$= 28,38 (A_{inv}/s^{-1}). Vrijednosti E_{inv} praktički je jednaka vrijednosti E prema FWO metodi (E=135 ± 1,3 kJmol^{-1}), što znači da se IKP metodom dobije točna vrijednost energije aktivacije iako niti jedan kinetički model nije u potpunosti kinetički opisao eksperimentalne podatke.

Nadalje, temeljem vrijednosti E_{inv} i $ln\ A_{inv}$ i jednadžbe (1), izračunate su brojčane vrijednosti $f(\alpha)$. Ovisnost $f(\alpha)$ vs. α za različite brzine zagrijavanja prikazana je na slici 1.

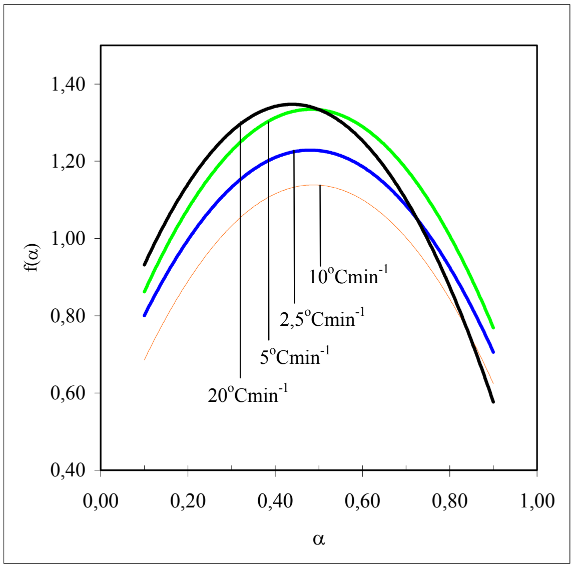

Slika 1. Ovisnost *f(α)* vs. *α* za neizotermnu razgradnju PHB-a.

Krivulje *f(α)* vs. *α* pokazuju isti oblik što ukazuje na isti reakcijski mehanizam. Usporedbom ovih krivulja s krivuljama *f(α)* vs. *α* za različite teorijske kinetičke modele može se zaključiti da se neizotermna razgradnja PHB-a odvija mehanizmom sličnom mehanizmu opisanom Avrami-Eroffevim kinetičkim modelom (m>1). Ipak, točan matematički oblik *f(α)* teško je odrediti.

ZAKLJUČAK

Kinetička analiza podataka neizotermne razgradnje PHB-a provedena je IKP i Flynn-Wall-Ozawa metodom. U području konverzija α=0,10-0,90 E ne ovisi o α. Vrijednosti E_{inv} izračunate IKP metodom dobro se slažu s vrijednostima izračunatim FWO metodom, što ukazuje na ispravnost ovakvog načina određivanja kinetičkih parametara. Vrijednosti invarijantnih kinetičkih parametara iskorištene su za brojčano određivanje *f(α).* Oblik krivulje *f(α)* vs. *α* ukazuje da se neizotermna razgradnja PHB-a odvija mehanizmom sličnom mehanizmu opisanom Avrami-Eroffevim kinetičkim modelom (m>1).

LITERATURA

1. A.I. Lesnikovich, S.V. Levchik, *Journal of Thermal Analysis*, 1983;27:83.
2. A.I. Lesnikovich, S.V. Levchik, *Journal of Thermal Analysis*, 1985;30;667.
3. P. Budrugeac, E. Segal, *International Journal of Chemical Kinetics*, 2001;33(10):564.
4. H. Tanaka, *Thermochimica Acta*, 1995;267:29.
5. A.W. Coats, J.P. Redfern, *Nature*, 1964;201:68.
6. J.H. Flynn, L.A. Wall, *Journal of Research of the National Bureau of Standards*, 1966;70A:487.
7. T. Ozawa, *Bulletin of the Chemical Society of Japan*, 1965;38:1881.
8. M. Erceg, T. Kovačić, I. Klarić, *International Conference MATRIB 2004, Conference Proceedings*, 62-66.

CONTACT FATIGUE DAMAGE OF GEARS

G. Fajdiga, M. Šraml and J. Flašker

University of Maribor
Faculty of Mechanical Engineering,
Smetanova ul. 17, 2000 Maribor
Slovenia

Abstract:

Two kinds of teeth damage can occur on gears under cyclic contact loading due to material fatigue - the pitting of gear teeth flanks and tooth breakage in the tooth root. In this study only the pitting phenomenon is addressed and the developed two-dimensional computational model for simulation of contact fatigue of gear teeth flanks is used for determination of pitting resistance, *i.e.* the service life of gear teeth flanks. The fatigue process leading to pitting is divided into crack initiation and crack propagation period that leads to the appearance of small pits on the contact surface.

The model for prediction of identification of critical material areas and the number of loading cycles, required for initial fatigue crack to appear, is based on Coffin-Manson relations between deformations and loading cycles, and comprise characteristic material fatigue parameters. The computational approach is based on continuum mechanics, where homogenous and elastic material model is assumed and results of cyclic loading conditions are obtained using the finite element method analysis.

The short crack theory together with the finite element method is then used for simulation of the fatigue crack growth. The governing factors are the initial crack length, crack angle, contact pressure which takes into account the EHD-lubrication conditions, tangential loading due to friction between contacting surfaces, moving contact conditions, residual stresses due to heat treatment of the material and the hydraulic pressure of trapped fluid acting on the crack surface. The virtual crack extension (VCE) method, implemented in the finite element method, is than used for simulating the fatigue crack propagation from the initial crack up to the formation of the surface pit. The relationship between the stress intensity factor K and crack length a, which is needed for determination of the required number of loading cycles N_p for a crack propagation from the initial to the critical length, is shown and with consideration of some particular material parameters, the service life of gear teeth flanks is estimated.

Keywords: contact fatigue, fracture mechanics, pitting, computational analysis

1 Introduction

The fatigue process of mechanical elements is a material characteristic and depends upon cyclic plasticity, local deformation, dislocation motion, formation of micro- and macro-cracks and their propagation. Contact fatigue is extremely important for all engineering applications involving localized contacts, such as gears, brakes, clutches, rolling bearings, wheels, rails, screw and riveted joints. Contact fatigue process can be divided into two main parts: (i) initiation of micro-cracks due to local accumulation of dislocations, high stresses in local points, plastic deformation around inhomogeneous inclusions or other imperfections on or under contact surface; (ii) crack propagation, which causes permanent damage to a mechanical element, i.e. exceeding of fracture toughness of the material.

The process of surface pitting can be visualized as the formation of small surface initial cracks, which grow under repeated contact loading. Eventually, the crack becomes large enough for unstable growth to occur, which causes the material surface layer to break away. The resulting void is surface pit [1, 4, 5] (Fig. 1).

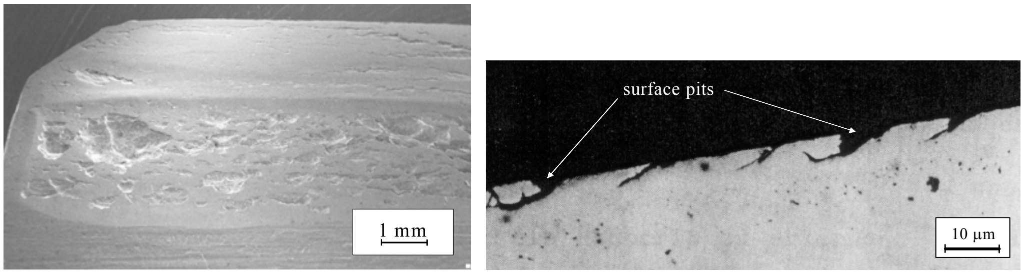

Figure 1: Typical surface pits on gear tooth flank [2].

The number of stress cycles N required for pitting of a gear teeth flank to occur can be determined from the number of stress cycles N_i required for the appearance of the initial crack in the material and the number of stress cycles N_p required for a crack to propagate from the initial to the critical crack length, when the final failure can be expected to occur [1, 4]

$$N = N_i + N_p \ . \tag{1}$$

2 Computational model of the pitting phenomena

Initial surface cracks leading to surface pitting of gears are, generally, observed to appear in the contact areas, where high normal contact pressure is combined with significant sliding velocities, which result in additional frictional loading of the surface material layer. There are several locations where pitting is apt to occur. However, the most critical contact loading conditions for initial crack formation and propagation are identified for the rolling contact with sliding, where the contact sliding, and with that the effect of friction, is opposite to the direction of the rolling contact motion. Thus, the worst contact loading conditions appear when the gears teeth are in contact at the inner point of single teeth pair engagement (point B on Fig. 2a), where the surface-breaking initial cracks are expected to develop first. This fact is valid for the pinion gear in case of revolutions reduction (reduction gear).

For computational determination of fatigue crack initiation and crack propagation at gear teeth flanks, an equivalent contact model (Hertzian theory) [7, 9, 14] is used (Fig. 2b). The equivalent cylinders have the same radii, as are the curvature radii of gear flanks at the observed point (the inner point of single teeth pair engagement – point *B*).

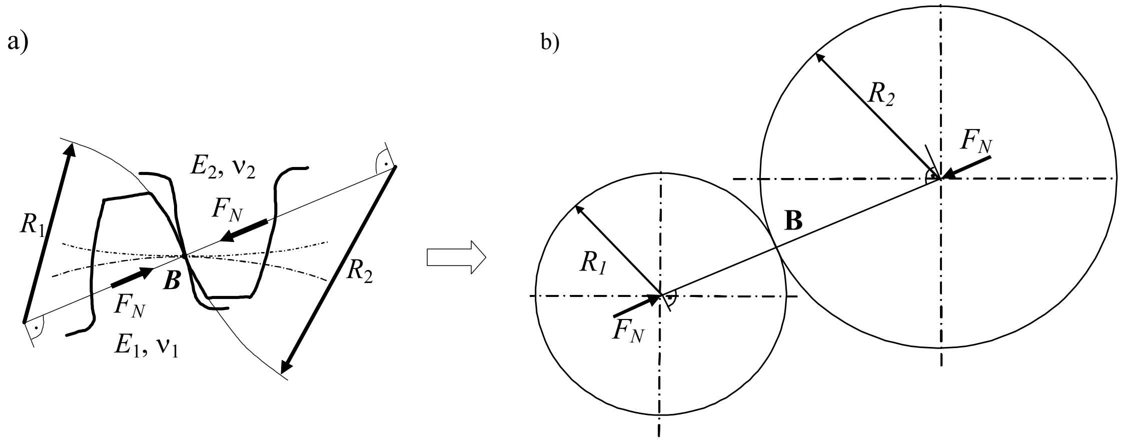

Figure 2: Model transformation of meshing gears (a) to the equivalent model of two cylinders for the meshing point *B* (b).

In analysing real mechanical components, some partial sliding occurs during time depended contact loading, which can originate from different effects (complex loading conditions, geometry, surface etc.) and it is often modelled by traction force due to the pure Coulomb friction law [9]. In the analysed case frictional contact loading $q(x)$ is a result of the traction force action (tangential loads) due to relative sliding of the contact bodies and is determined here by utilising Coulomb friction law [9]

$$q(x) = \mu \cdot p(x), \tag{2}$$

where μ is the local coefficient of friction between contacting bodies. For general case of elastic contact between two deformable bodies in a standstill situation, the analytical solutions are well known. However, using general Hertzian equations [9] it is difficult to provide the loading cycle history and/or simulation of a contact pressure distribution of moving contact in the analytical manner. Therefore, the finite element method (FEM) is used for simulating two-dimensional friction contact loading in this case and the same procedure is usually used when dealing with complex contact loading conditions (i.e. in case of gears analysis).

3 Fatigue crack initiation analysis

Standards for gears determination and design, such as American Gear Manufacturers Association (AGMA) standards or German DIN standards, indicate the possibility of dimensioning the so-called "time gearing". However, all standard models are rough and give not accurate enough results since they do not take into account the actual operational conditions. Therefore, our research group decided to develop models and procedures of calculations, that will give more reliable and, in particular, more accurate results [7, 14].

When the stress loading cycles are determined, the fatigue analysis for each observed material point can be performed. The methods for fatigue analysis are most frequently based on the relation between deformations, stresses and the number of loading cycles and are usually modified to fit the nature of the stress cycle, i.e. repeated or reversed stress cycle [15]. The number of stress cycles required for fatigue crack to appear, can be determined iteratively with the strain-life method ε-N, where the relationship between the specific deformation increment $\Delta\varepsilon$, and the number of loading cycles N_f, is fully characterized with the following equation [15]

$$\frac{\Delta\varepsilon}{2}=\frac{\sigma_a}{E}+\frac{\Delta\varepsilon_p}{2}=\frac{\sigma'_f}{E}\left(2N_f\right)^b+\varepsilon'_f\left(2N_f\right)^c, \tag{3}$$

where σ_f' is the fatigue strength coefficient, b the strength exponent, ε_f' the fatigue ductility coefficient and c the fatigue ductility exponent. Generally, the following modified approaches of strain-life method are most often used for fatigue calculations: Coffin-Manson's hypothesis (ε-N method), Morrow's analysis, Smith-Watson-Topper (SWT) method [15].

4 Fatigue crack propagation analysis

By considering initiation of micro crack in the contact area of gear teeth flank of meshing gears (Fig. 3), the short crack theory can be used for describing crack propagation from the initial to the critical crack length, when the pit occur on the gear teeth flank.

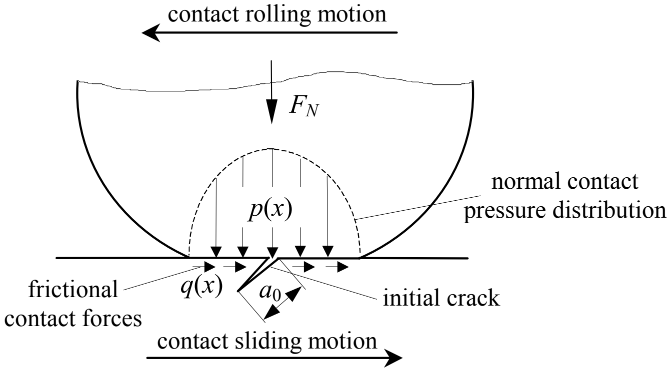

Figure 3: Orientation of the initial surface-breaking crack and contact loading.

The short crack growth is characterised by a successive blocking of persistent slip bands (PSB) with grain boundaries, which implies the discontinuous character of the crack growth process. Navarro and Rios [11] and Sun *et al.* [12] proposed the model where the crack growth rate $\mathrm{d}a/\mathrm{d}N$ is assumed to be proportional to the crack tip plastic displacement $\Delta\delta_{pl}$

$$\frac{\mathrm{d}a}{\mathrm{d}N}=C_o\left(\delta_{pl}\right)^{m_o}, \tag{4}$$

where C_o and m_o are material constants that are determined experimentally. In view of the numerical simulation, it is beneficial to express the crack tip plastic displacement δ_{pl} in terms of the stress intensity range ΔK. This relationship has been provided in the form [11]

$$\Delta\delta_{pl}=\frac{2\kappa}{G\sqrt{\pi}}\cdot\frac{\sqrt{1-n^2}}{n}\Delta K\sqrt{a}, \tag{5}$$

where G is the shear modulus, and $\kappa=1$ or $\kappa=1-\nu$ depending on whether screw or edge dislocations are being considered, with ν being Poisson's ratio. Parameter n describes the relative position of the crack tip to the grain boundary. The number of stress cycles required for a crack to propagate through each crystal grain is obtained with integration of Eq. (4)

$$N_j = \int_{a_{j-1}}^{a_j} \frac{da}{C_o\left(\delta_{pl}\right)^{m_o}} \; ; \; j = 1, 2, 3, ..., z \quad , \tag{6}$$

in which z is the number of grains transverse by the crack ($z=a/D$). The total number of stress cycles N required for a short crack to propagate from the initial crack length a_o to any crack length a can then be determined as

$$N = \sum_{j=1}^{z} N_j \; . \tag{7}$$

As the crack extends through ten or more grains, the influence of the material structure on the crack growth becomes negligible and linear elastic fracture mechanic (LEFM) theory can be applied thereafter [6].

Expressing the plastic displacement $\Delta\delta_{pl}$ in Eq. (5) in terms of the stress intensity range ΔK enables treatment of short and long cracks in a similar fashion. If the relationship between the stress intensity range and the crack length $\Delta K=f(a)$ can be derived in some way, the remaining service life of a mechanical element with the crack can be estimated with appropriate integration of rate Eq. (4). Considering small crack lengths observed during pitting in the contact area of mechanical elements, only the theory of short cracks is usually needed for describing crack propagation from the initial to the critical crack length.

For simple cases, the relationship between the stress intensity factor and the crack length $K=f(a)$ is available in the technical literature in analytical form [6]. However, for cases with complicated geometry and boundary conditions, it is necessary to use alternative methods for its determination. Here, the numerical procedure based on the virtual crack extension method (VCE) in the framework of the finite element analysis is used for this purpose [8].

5 Application of the computational model

The proposed computational model is applied to the analysis of the fatigue crack initiation and crack propagation on the tooth flank of a real gear pair, with material and geometric data set given in Table 1.

The determination of loading cycles at the contact region of meshing gears (at teeth flanks) appears to be difficult task. Indeed, the worst case of pitting phenomena, i.e. the area around the inner point of a single teeth pair engagement, is often simulated with maximum value of contact pressure via point force put at this point B. However, this is way out of the fact that the loading cycles are competent for evaluating fatigue process. For the treated gear pair the contact point B can be identified with equivalent radius, as well as other characteristics points (see Fig. 4). Following, the prediction of time depended loading cycles and evaluation of number of critical loading cycles of real meshing gears are presented [13].

Table 1: Data set for the gear pair.

Parameter	Pinion		Gear
Normal module		$m_n = 4{,}5$ mm	
Number of teeth	$z_1 = 16$		$z_2 = 24$
Pressure angle on pitch line		$\alpha_n = 20°$	
Helical angle		$\beta_0 = 0°$	
Coefficient of profile displacement	$x_1 = 0{,}182$		$x_2 = 0{,}171$
Centre distance		$a = 91{,}5$ mm	
Tooth width		$b_1 = b_2 = 14$ mm	
Pitch diameter	$d_1 = 72$ mm		$d_2 = 108$ mm
Material of gear pair		42CrMo4, case hardened	
Torque of a pinion: M_1=183,4 Nm; rotational velocity of pinion n_1=2175 min^{-1}			

5.1 Moving contact loading of meshing gears

Comprehensive model for contact fatigue life prediction of single mechanical elements should consider time history of applied contact loads, regarding both their magnitude and shape. For more realistic simulation of the fatigue crack initiation and crack propagation at teeth flanks it is necessary to consider the influence of moving contact in the vicinity of expected initial crack(s). The moving contact can be simulated with different loading configurations, as it is shown in Fig. 4.

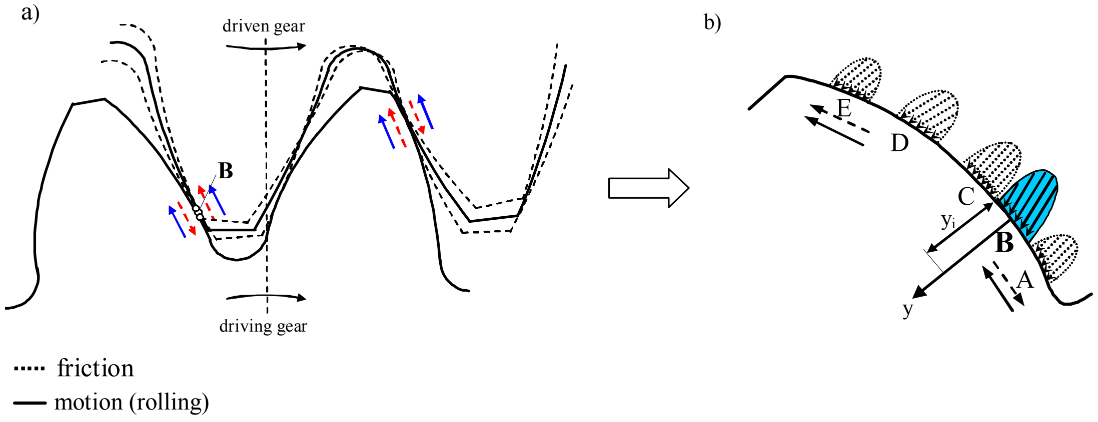

Figure 4: Moving contact loading configurations in respect to the initial crack position: meshing of gear pair (a), equivalent contact model of meshing gears (b).

Characteristic contact points (A, A-B, B, C, D and E – Fig. 4) of meshing gears have been considered, each with the specific normal $p(x)$ and tangential $q(x)$ contact loading distributions. The values of basic contact parameters have been considered using Hertzian theory and DIN 3990 standard procedure. On the basis of discussed facts and restrictions, the contact analysis, using FEM (Fig. 4b) was performed for evaluating loading cycles. Generally, obtained times are very short, since in presented case, the rotational velocity of the pinion is 2175 rpm [13]. In the case of Tresca stress comparative cycles, the time dependent normalised distribution of loading cycles, are presented in Fig. 5. Obtained loading cycle (considering point B), corresponds well with the fact that, in most cases, the compressive stress on spur gear teeth occurred at the lowest point on a pinion tooth at which full load is carried by a single pair of teeth. Theoretically, if one pair of teeth carries full load and the position of loading is at considered point *B*, there is the worst-load condition for Hertzian contact stress corresponding to the worst-load position [4] for strength. The values of normalised stress cycles are higher under contact surface, which is influenced particularly by the coefficient of friction and this fact is also in agreement with basic contact theory. Anyway, in critical area, the high contact pressure is combined with significant amount of gear sliding velocities, which results in the frictional loading of the surface layer. On the basis of the defined contact loading cycles of meshing gears, considering teeth flanks loading, the fatigue analyses can then be performed.

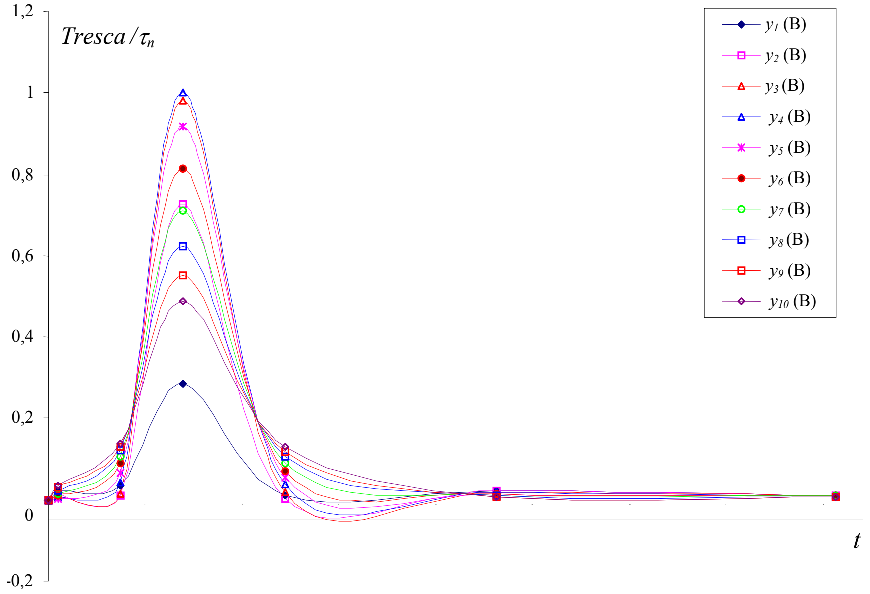

Figure 5: Normalised Tresca comparative stress cycles at meshing gears, on and under contact point *B* (see Figure 4b).

5.2 Fatigue crack initiation

The strain-life method (ε-N) and its modified forms, present in Chapter 3, was used to determine the number of stress cycles N_i required for the fatigue crack initiation (starting of pitting damage process), in the framework of the FEM program package MSC/FATIGUE [10]. Fatigue material parameters for the generalised contact model used in analysis are: modulus of elasticity $E = 2{,}06 \cdot 10^5$ MPa, Poisson ratio $\nu = 0{,}3$, fatigue strength coefficient $\sigma_f' =$ 1820 MPa, fatigue ductility coefficient $\varepsilon_f' = 0{,}65$, exponent of strength $b = -0{,}08$, fatigue ductility exponent $c = -0{,}76$, hardening exponent $n' = 0{,}14$, strength coefficient $K' = 2259$ MPa and surface finish factor $C_{surf} = 0{,}6 \div 0{,}9$. Additional factors, influencing fatigue life, are particularly: machine component size C_{size}, the type of loading C_{load} and effect of surface finish and treatment C_{surf}. Practically all fatigue failures start at the surface. So, it is evident, that fatigue properties are very sensitive to surface condition [4]. The usual way to account for these effects is through the calculation and application of specific modifying factors, influencing actual fatigue (endurance) limit S_e for a real component (spur gears)

$$S_{\mathrm{e}} = S_{\mathrm{e}}' \cdot \mathrm{C}_{\mathrm{surf}} \cdot \mathrm{C}_{\mathrm{size}} \cdot \mathrm{C}_{\mathrm{load}}, \qquad (8)$$

where S_e' is measured material endurance limit. The influence of surface finishing on fatigue strength was considered with the surface finishing factor C_{sur}, for different surface roughness R_a. Surface finishing is categorized by means of qualitative terms such as polished, machined and surface treatment is categorized by means of nitrided and shot peened, which provide the state of residual stresses in a compressive layer that have the effect of decreasing the likelihood of fatigue failure.

Table 2: Case studied: quality and material treatment description.

Case studied (Examples)	Case description
Ex 1	Averaged machined and "shot peened"
Ex 2	Averaged machined
Ex 3	Good machined and nitride
Ex 4	Polished
Ex 5	Averaged machined and nitride
Ex 6	Polished and "shot peened"
Ex 7	"Shot peened"
Ex 8	Poor machined

Results of number of loading cycles for crack initiation are presented in Fig. 6. Dealing with Tresca based loading cycles and ε-*N* method for determination of initiation damage, first damage appears at ($10^4 \div 3{\cdot}10^7$) loading cycles (at approximately 0,12 mm under observed inner point of single teeth pair engagement - point *B*).

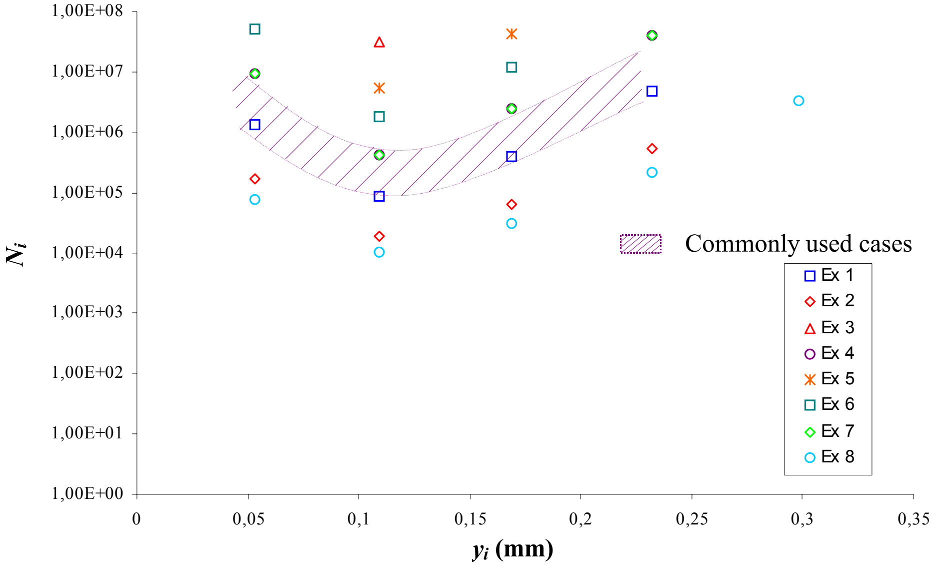

Figure 6: Results: number of loading cycles, when initial crack appear at the observed material points (y_i) – Tresca comparative stresses, ε-N analysis method.

Modified Coffin-Manson methods for determination of crack initiation are used, regarding different nature of loading cycles. The treated problems of mechanical treatment (Examples 1-8 in Table 2) result in different numbers of critical loading cycles for crack initiation. Hatched areas on presented diagram (Fig. 6) are valid for most frequently used gear pairs in practice. Thus, average values of critical number of loading cycles are in the range of ($1{,}2\ {\cdot}10^4 \div 7{,}1{\cdot}10^7$) loading cycles, defined in the proposed model.

5.3 Fatigue crack propagation

With regard to the results of crack initiation model the initial crack is presume to be located at the inner point of single teeth pair engagement (point *B*). The configuration of initial crack follows from metallographic investigation, see Chapter 5.3.2. After the crack is initiated at the surface of gear teeth flank the crack propagation model has been used for simulation of surface crack propagation on a gear teeth flank.
The gear pair is made of case hardened steel 42CrMo4 with Young's modulus E=$2.06\cdot10^5$ N/mm^2 and Poisson ratio ν=0.3. The maximum contact pressure acting at point *B* is p_0=1453 N/mm^2, with the equivalent radius of gear teeth flanks R_B^*=7,2562 mm. Using Hertzian theory [5], the half-length of the contact area is equal to b=0,1778 mm. The Hertzian normal loading distribution $p(x)$ along the entire contact width of the gear flanks has then been determined using Eq. (1). For all computations, the coefficient of friction μ_B = 0,1075 has been used. Therefore, the tangential loading $q(x)$ has been determined using Eq. (2).

5.3.1 Moving contact and the influence of fluid lubricant on crack propagation

For a more realistic simulation of fatigue crack growth, it is necessary to consider the influence of moving contact in the vicinity of initial crack (see Chapter 5.1). The moving contact can be simulated with different loading configurations as shown in Fig. 7. Five contact loading configurations have been considered, each with the same normal $p(x)$ and tangential $q(x)$ contact loading distributions, but acting at different positions in respect to the initial crack.

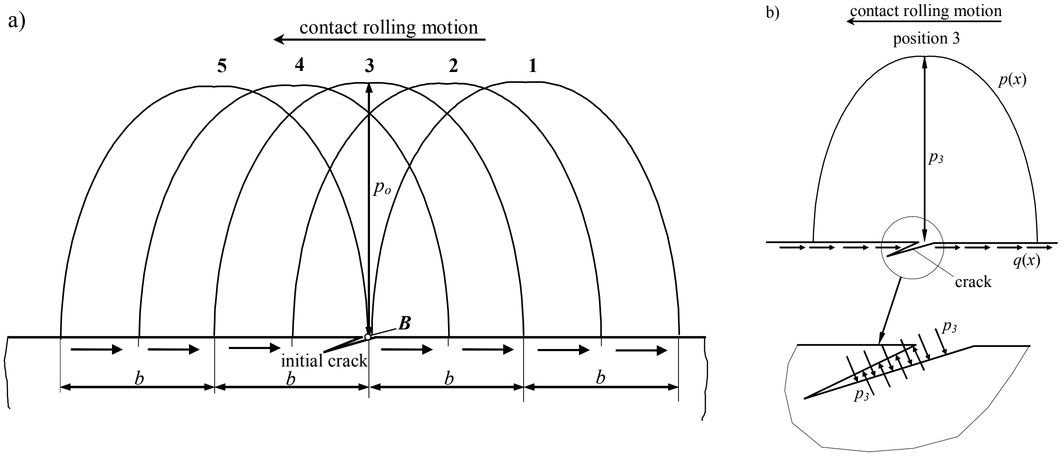

Figure 7: Moving contact loading configurations in respect to the initial crack position a) and modelling of the lubricant driven in the crack by the hydraulic pressure mechanism b).

5.3.2 The influence of fluid lubricant on crack propagation

The simulation of the surface initiated crack propagation should also consider the influence of the lubricant on crack propagation. Several mechanisms and models have been proposed in the past [3]. In the present computational procedure the hydraulic pressure mechanism has been adopted, where the lubricant pressure inside the crack is simply approximated with a uniform pressure distribution along the crack faces [3]. The level of lubricant pressure is equal to the current pressure determined at the crack mouth, i.e. the pressure depends on the contact pressure distribution position in respect to the crack mouth. Fig. 7b illustrates crack face pressure determination and distribution for two consecutive contact loading configurations. The finite element mesh shown in Fig. 8, and the boundary conditions as described above, have been used in subsequent analyses. For the configuration of the initial crack on the surface, located at point *B*, it was assumed that the initial length of the crack is equal to a_o=15 μm, with the initial inclination angle towards the contact surface equal to $\alpha_o = 22°$. It is recognised, that the predicted crack growth heavily depends on the size and orientation of the initial crack. However, the used configuration follows from metallographic investigations of initial cracks appearing on gears [5, 16]. A thorough investigation of the crack growth dependence on position and size of various initial defects is to be performed in future investigations with parametric simulations based on the proposed model.

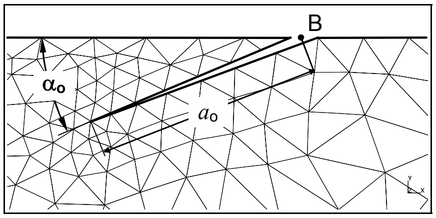

Figure 8: FE discretisation and configuration of the initial crack.

In this study, the FE analysis program BERSAFE [2], based on VCE method, has been used for computational estimation of the stress intensity factor *K* and subsequent incremental crack growth simulation. Five different loading configurations have been considered in each computation for the purpose of simulating the effect of the moving contact of the gear flanks (see Fig. 7). For each crack increment, the crack was actually extended in the direction of the recorded K_{max} from all calculated load cases. Figure 9 shows the relationship between stress intensity factor *K* and the crack length *a*, and also the shape and magnitude of the surface pit. It can be noticed that the computed stress intensity factor *K* is very small at the beginning, but later increases as the crack propagates towards the contact surface.

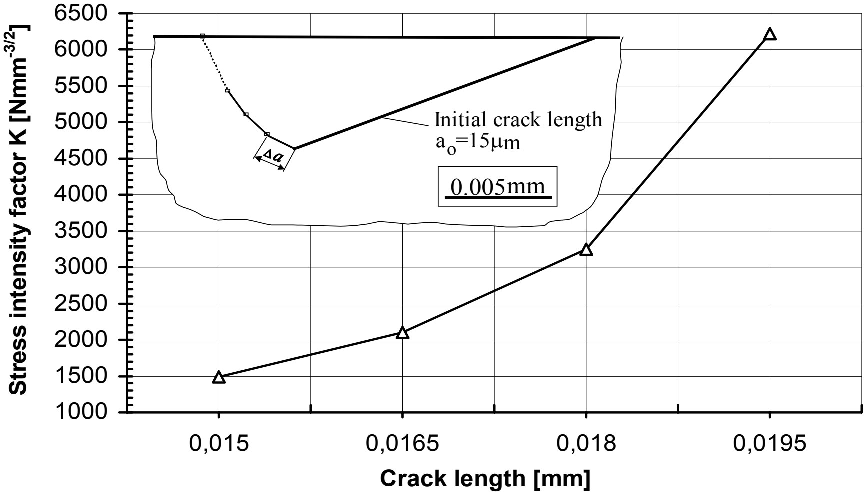

Figure 9: Stress intensity factor for initial surface micro crack propagation.

Numerical simulations have shown that at the moment when the crack reaches the vicinity of the contact surface, the stress intensity factor is extremely high. At that moment it can be expected that the material surface layer breaks away and the pit occurs on the surface. Because of the very small dimensions of surface pits, they can be termed "micro-pitting".

Micro pitting as shown in Fig. 9 is not the final and most critical surface failure. Further operation of the gear pair results in the formation of larger pits, and consequently progressive pitting. Following the above procedure, one can numerically determine the functional relationship $K=f(a)$, which is needed for determining the required number of loading cycles N_p for a crack propagating from the initial to the critical length (see Chapter 4 in this paper).

Figure 10 shows that the shape and magnitude of the numerically determined pits correspond well with available experimental data, as determined by experimental testing of a spur gear pair using the FZG - pitting test machine according to DIN 51354 standard. The tested gears have been subjected to the same operating conditions and loading parameters as used in the numerical computations.

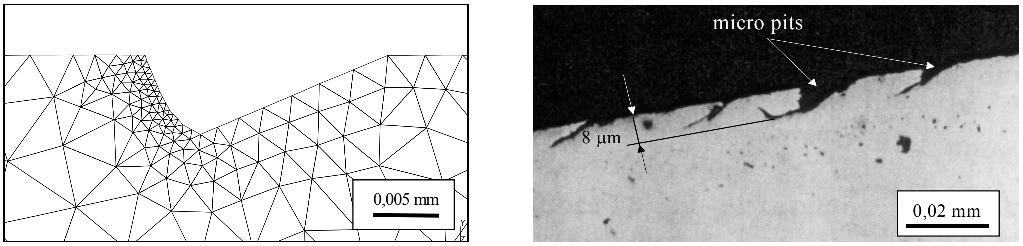

Figure 10: Numerically (left) and experimentally (right) determined pit shapes [2].

6 Concluding remarks

The paper presents a computational model for determining the service life of gears with regard to pitting on the gear teeth flanks. The process of surface pitting can be visualized as the formations of small surface initial cracks grow under repeated contact loading. Eventually, the crack becomes large enough for unstable growth to occur, which causes the material surface layer to break away. The resulting void is a surface pit. The fatigue process leading to pitting of gear teeth flank is divided into crack initiation (N_i) and crack propagation (N_p) periods, which enables the determination of total service life as $N = N_i+N_p$.

An equivalent contact model of a cylinder and flat surface is used for the simulation of the contact fatigue crack initiation and the crack propagation under conditions of rolling and sliding contact loading of meshing gears.

A general computational model for the determination of initiation fatigue loading cycles in meshing gears is based on material model which is assumed to be homogenous, without imperfections and/or inclusions and elastic shakedown of the material model is considered. The modified Coffin-Manson method, in the framework of finite element analysis (FEA), is used for iterative analyses of contact fatigue crack initiation. The number of loading cycles and places (on/under the contact surface) for contact fatigue are presented. Generally, regardless of select stress component, the number of loading cycles, required for initial fatigue damages, is in the range of $N_i = (10^4 \div 10^7)$ and where (on the contact surface or subsurface) the contact fatigue damage first occur mostly depends on the coefficient of friction, material parameters and contact geometry.

On the basis of results of fatigue crack initiation analysis the initial micro crack on gear teeth flank is assumed. A two-dimensional finite element approach is applied together with the short fatigue crack growth theories to predict the surface initiated crack propagation. The numerical model attempts to account for the different parameters influencing the crack propagation process (Hertzian contact pressure, friction between contacting surfaces, hydraulic pressure in the crack, meshing of gears, etc.) leading to pitting, starting from the initial surface fatigue crack to the critical crack length, when the occurrence of a surface pit is expected. The virtual crack extension (VCE) method in the framework of FEA is used for two-dimensional simulation of fatigue crack propagation from the initial crack up to the formation of the surface pit. Consequent computational determination of the functional relationship $K= f(a)$ from Fig. 9 enables the estimation of the crack propagation period in regard to the surface pitting, if combined with the previously developed model [6, 7], short fatigue crack growth theory and with consideration of some particular material parameters. Comparison of numerically predicted and experimentally recorded pit shapes show that they are in a very good agreement.

References

[1] Alban L. E, (1985): "Systematic Analysis of Gear Failures", *American Society for Materials*, Ohio.

[2] BERSAFE (1988): Users's Guides.

[3] Bower A.F., (1988): "The influence of crack face friction and trapped fluid on surface initiated rolling contact fatigue cracks", *ASME Journal of Tribology*, 110, pp. 704-711.

[4] Dudley D. W., (1996): "Fatigue and Life Prediction of Gears", *Fatigue Strength Prediction and Analysis*, 19: pp. 345-354.

[5] Elstorpff M.G., (1993): "Einflüsse auf die Grübchentragfähigkeit", Ph.D. thesis, TU Munich.

[6] Ewalds H.L. and Wanhill R.J.H., (1991): "Fracture Mechanics", Delftse U.M., *Co-publication of Edward Arnold*, Delft.

[7] Flašker J., Fajdiga G., Glodež S. and Hellen T. K., (2001): "Numerical simulation of surface pitting due to contact loading", *International Journal of Fatigue*, 23: pp. 599-605.

[8] Hellen T.K., (1975): "On the method of virtual crack extensions", *International Journal for Numerical Methods in Engineering*, 9, pp. 187-207.

[9] Johnson K. L., (1985): "Contact mechanics", Cambridge University press.

[10] Msc/Corporation (1999): MSC/FATIGUE Quick Start Guide, Version 8, The MacNeal-Schwendler Corporation, Los Angeles.

[11] Navarro A. and Rios E.R., (1988): "Short and long fatigue crack growth- a unified model", *Philosophical Magazine*, 57, pp. 15-36.

[12] Sun Z., Rios E.R. and Miller K.J., (1991): "Modelling small fatigue cracks interacting with grain boundaries", *Fatigue Fract. Engng. Mater.*, 14, pp. 277-291.

[13] Šraml, M., (2001): Modeling of contact fatigue of mechanical elements, Ph.D. Thesis, Abstract in English, Maribor.

[14] Šraml M., Flašker J. and Potrč I., (2003): "Numerical procedure for predicting the rolling contact fatigue crack initiation", *International Journal of Fatigue*, 25: pp. 585-595.

[15] Zahavi E., Torbilo V., (1996): "Fatigue Design-Life Expectancy of Machine Parts", *A Solomon Press book*, by CRC Press, Florida.

[16] Winter H., Knauer G., (1990): "Einfluss von Schmierstoff und Betriebstemperatur auf die Grübchentragfähigkeit einsatzgehärteter Zahnräder", *Antriebstechnik* 29, pp. 65-84.

10. Savjetovanje o materijalima, tehnologijama, trenju i trošenju
10. Conference on Materials, Processes, Friction and Wear
MATRIB'05, Vela Luka, 23-25.06.2005.

ANALIZA PROMJENA KARAKTERISTIKA PRIJENOSNOG ETALONA SILE Z4-20 kN TIJEKOM EKSPLOATACIJE

ANALYSIS OF PERFORMANCE CHANGE OF TRAVELLING FORCE STANDARD Z4-20 kN DURING EXPLOITATION

Željko Alar, Mladen Franz
Sveučilište u Zagrebu, Fakultet strojarstva i brodogradnje
Ivana Lučića 5, 10000 Zagreb,
E-mail: zeljko.alar@fsb.hr;

Sažetak

Pri umjeravanju mjerila sile prijenosni etaloni sile podvrgnuti su određenim uvjetima koji tijekom vremena dovode do promjena njihovih karakteristika. Postavlja se pitanje da li je moguće, na temelju praćenja promjena karakterstika prijenosnog etalona sile tijekom uporabe, predvidjeti vrijednost promjene pojedine karakteristike u slijedećem umjernom razdoblju etalona sile i kao takvu je uvrsitit u proračun mjerne nesigurnosti umjeravanja mjerila sile. U radu je provedeno praćenje karakteristika prijenosnog etalona sile Z4-20 kN tijekom tri umjerna perioda, gdje je u svakom intervalu s ovim etalonom provedeno umjeravanje oko pedestipet mjerila sile. Analiza je provedena na rezultatima umjeravanja ovog prijenosnog etalona sile 1998, 2000, 2002. i 2005. godine u PTB-u, Njemačka. Na temelju provedene analize dani su određeni zaključci.

Ključne riječi: sila, prijenosni etalon sile, umjeravanje, mjerna nesigurnost

Abstract

During calibration of force measuring equipment the travelling standards have been submitted to certain conditions, which changed their performances during the time. The question is, if tracing the travelling force standard performance changes can be the basis for prediction of certain performance changes in the following calibration period and as such incorporated to the calculation of measurement uncertainty during calibration of force measuring equipments. Tracing of Z4-20kN travelling force standard performances, during three calibration periods is described and in each period 55 force measuring equipments have been calibrated with this standard. The analysis is made with calibration results on this travelling force standard in 1998, 2000, 2002 and 2005 in PTB, Germany. This analysis is the basis for certain conclusions.

Key words: force, travelling standard, calibration, measurement uncertainty

1. Uvod

Mjerenje sile je osnova za određivanje mehaničkih svojstava nekog materijala ili proizvoda. Sila je matematički predstavljena kao vektor koji djeluje u određenoj točki, stoga mjerenje sile uključuje određivanje njene veličine i smjera djelovanja. Samo ispitivanje sile provodi se na uređajima za mjerenje sile a najčešće su to kidalice različitih tipova i oblika. Tijekom uporabe ti uređaji gube na preciznosti a posljedice koje nastanu uporabom takovih uređaja mogu biti dalekosežne. Zbog toga se provodi sistematska periodična kontrola ili provjera (umjeravanjem) uređaja za mjerenje sile kroz jedno umjerno razdoblje, čija je najveća dopuštena vremenska granica propisana normama.

Umjeravanje mjerila sile može se provesti jednom od ove dvije metode:

- direktna ili
- indirektna [1].

Direktna metoda obuhvaća izravnu usporedbu sa poznatom gravitacijskom silom utega standardne mase. Vrijednosti mase i gravitacije moraju biti točno poznate.
Indirektna metoda obuhvaća mjerenje učinka sile na neko tijelo. Primjeri primjene ove metode su:

- mjerenja akceleracije tijela sa poznatom masom koje je izloženo djelovanju sile,
- mjerenje rezultantnog učinka (deformacije) kada se silom djeluje na elastične elemente.

Metoda s elastičnim elementima ima veću primjenu. Razlozi većoj primjeni elastičnih elemenata su slijedeći:

- veliki raspon mjerenja,
- mogućnosti kontinuiranog praćenja,
- jednostavnija uporaba,
- te njihova otpornost.

Na slici 1 je prikazan jedan prijenosni etalon sile Laboratorija za ispitivanje mehaničkih svojstava (LIMS) Fakulteta strojarstva i brodogradnje Sveučilišta u Zagrebu, koji se primjenjuje za umjeravanje mjerila sile a metoda rada mu je mjerenje deformacije na elastičnom elementu (dinamometar) uslijed djelovanja opterećenja.

a) b) c)

Slika 1: Prijenosni etalon sile Z4-20 kN s prihvatnim napravama
a) MGC-plus mjerno pojačalo sa softverom CATMAN
b) dinamometar Z4-20 kN
c) prihvatne naprave za tlak i vlak

Ovaj prijenosni etalon se sastoji od dinamometra kao deformacijskog tijela i mjernog pojačala kao pretvarača signala.

Tijekom uporabe prijenosni etalon je izložen različitim utjecajima (okolišni uvjeti, djelovanje opterećenja, rukovanje više mjeritelja, transport i itd.) što se kroz duži vremenski period odražava na njegova svojstva. Postavlja se osnovno pitanje da li je moguće predvidjeti promjenu njegovih karakteristika u slijedećem umjernom razdoblju i da li bi se ta promjena mogla uvrstiti u mjernu nesigurnost rezultata mjerenja ovim etalonom.

U ovom radu provedeno je praćenje promjena karakteristika prijenosnog etalona sile Z4-20 kN u periodu od 1998. – 2005. godine. Analiza promjena karakteristika provedena je na temelju rezultata umjeravanja ovog prijenosnog etalona u tom periodu i evidencije uvjeta pri kojim je etalon bio upotrebljavan. Umjeravanja prijenosnog etalona sile provedena su u PTB-u (Physikalische Technische Bundesanstalt) koji posjeduje nacionalne etalone za silu u Njemačkoj čija je najveća mjerna sposobnost ***≤ 0,002 %***. Prijenosni etalon sile Z4-20 kN upotrebljava se za smjer opterećenja vlak i tlak, ali ovdje u radu su analizirani rezultati umjeravanja samo za tlak.

2. Umjeravanje prijenosnog etalona sile

Umjeravanje se provodi prema normi ISO 376 [2]. Ova norma je predviđena za umjeravanje uređaja za mjerenje sile čija svrha je daljnje umjeravanje jednoosnih ispitnih kidalica za statička ispitivanja. Sam umjerni postupak sastoji se iz uvođenja točno poznatih sila s utvrđenom mjernom nesigurnošću u deformacijsko tijelo (dinamometar), a na uređaju za očitanje sile, koji je sastavni dio cijelog mjernog sustava, se očitava deformacijska vrijednost *X,* mV/V koju je inicirala zadana poznata sila. Primjenom odgovarajućih izraza te statističkom obradom, provodi se usporedba dobivenih vrijednosti s poznatim uvedenim silama prilikom samog umjeravanja [3].

Postupak umjeravanja provodi se prema slici 2, gdje je vidljivo da se provodi šest mjernih nizova. Prva dva mjerna niza (R1, R2) su za slučaj kada se ne mijenja položaj dinamometra. Nakon toga se dinamometar zakreće za 120^o i izmjeri se mjerni niz R3. Za sva prva tri niza sile se uvode u rastućem tonu za određeni korak sile. Korak sile mora biti takav da unutar mjernog područja dinamometra bude najmanje osam točaka koje su ravnomjerno raspoređene unutar mjernog područja. Dostizanjem najveće sile u nizu R3 nastavlja se mjerenje sile ali pod uvjetima opadajuće sile istim korakom, čime se dobije mjerni niz R4′. Sve to isto ponavlja za mjerne nizove R5 i R6′, s time da je dinamometar sada zakrenut za 240^o.

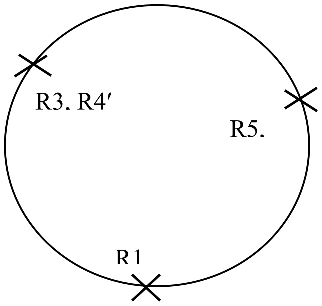

Slika 2: Raspored mjernih nizova pri umjeravanju prijenosnog etalona sile [2]

Kriteriji praćenje karakteristike prijenosnog etalona bili su ponovljivost, interpolacijsko odstupanje, nulto odstupanje, histerezna mjerenja i proširena mjerna nesigurnost.

U tablici 1 dani su izrazi i vrijednosti za pojedine parametre za pojedine klase prema normi ISO 376. Dovoljno je samo da jedan parametar ne zadovoljava granične vrijednosti za pojedinu klasu, prijenosnom etalonu bit će pridružena niža klasa.

Tablica 1: Izrazi i granične vrijednosti parametara za klasifikaciju prema EN ISO 376 [2]

Klasifikacijski parametar	**Izraz**	**Relativne pogreške za klasu, %**			
		00	**0,5**	**1**	**2**
Relativna pogreška ponovljivosti pri različitim ugradbenim položajima	$b = \frac{X_{\max} - X_{\min}}{X_r} \times 100\,\%$	0,05	0,10	0,20	0,40
Relativna pogreška ponovljivosti pri istim ugradbenim položajima	$b' = \frac{X_2 - X_1}{X_{wr}} \times 100\,\%$	0,025	0,05	0,10	0,20
Relativna pogreška histereznog mjerenja	$v = \frac{i' - i}{i} \times 100\,\%$	0,07	0,15	0,30	0,50
Relativno nulto odstupanje	$f_0 = \frac{i_f - i_0}{X_N} \times 100\,\%$	±0,012	±0,025	±0,050	±0,10
Relativno interpolacijsko odstupanje	$f_c = \frac{\overline{X}_r - X_a}{X_a} \times 100\,\%$	±0,025	±0,05	±0,10	±0,20

4. Analiza pojedinih parametara

Prijenosni etalon sile Z4-20 kN je prvi put umjeravan 24. 02. 1998. godine a slijedeća umjeravanja su provedena u granicama od 26 mjeseci. Unutar umjernog razdoblja ovim prijenosnim etalonom je provedeno prosječno oko 55 umjeravanja kidalica koja su provedena pri normalnim okolišnim uvjetima (temperatura u intervalu od 18 do 20 °C). Ova umjeravanja su provodili djelatnici LIMS-a (tri ovlaštena djelatnika).
Uvjeti umjeravanja prijenosnog etalona sile u PTB-u, Njemačka su bili približno jednaki pri svakom umjeravanju i prikazani su u tablici 2.

Tablica 2: Osnovni parametri pri umjeravanju dinamometra Z4-20 kN

Okolišni uvjeti	Temperatura	Tlak	Vlažnost
	22 ± 1 °C	**1035 hPa**	**45% rel.**

Davatelj sile		**Prijenosni etalon**		
Mjerno područje	**0 – 2,5 kN**	Mjerno pojačalo		**ML - 38**
Najbolja mjerna sposobnost	**≤ 0,002%**	Kabel	Dužina	**6 m**
			Priključak	**6 - žilni**
Pribor	**DKD-standard**	Dinamometar		**Z4-20 kN**
		Očitavač		**AB12**

U tablicama 3 i 4 su prikazani svi rezultati pojedinih parametara koji su praćeni za svako umjeravanje.

Tablica 3: Promjena vrijednosti nul-signala

Provedeno umjeravanje	Vrijednost nula - signala, mV/V
24. 02. 1998.	-0,00792
18. 08. 2000.	-0,01546
31. 10. 2002.	-0,01665
20. 01. 2005.	-0,01858

Nula signala je parametar koji se svakodnevno prati i njegova promjena govori nam o stanju prijenosnog etalona sile odnosno da li je bilo nekakvih značajnih utjecaja na etalon. No tijekom vremena vidljivo je da dolazi do promjene vrijednosti nula signala a time dolazi i do promjene ishodišta umjerne krivulje etalona.

Tablica 4: Promjena pogrešaka ponovljivosti, histereze, klase i proširene mjerne nesigurnosti u razdoblju od 1998. do 2005. godine

Parametar	Mjerni niz / God. umjeravanja	2	4	6	8	10	12	14	16	18	20
b, %	1998	0,000	0,000	0,002	0,001	0,001	0,001	0,001	0,001	0,000	0,000
	2000	0,000	0,003	0,002	0,003	0,002	0,003	0,002	0,001	0,001	0,001
	2002	0,000	0,003	0,002	0,003	0,002	0,002	0,001	0,001	0,001	0,001
	2005	0,005	0,005	0,003	0,004	0,003	0,003	0,003	0,003	0,002	0,003
b`, %	1998	0,010	0,005	0,005	0,005	0,004	0,003	0,003	0,004	0,004	0,004
	2000	0,000	0,003	0,002	0,001	0,001	0,001	0,001	0,001	0,001	0,002
	2002	0,005	0,003	0,002	0,001	0,002	0,001	0,001	0,001	0,002	0,002
	2005	0,010	0,000	0,002	0,003	0,002	0,002	0,001	0,002	0,001	0,002
v, %	1998	0,023	0,026	0,023	0,017	0,013	0,010	0,010	0,003	0,003	
	2000	0,068	0,053	0,042	0,036	0,028	0,020	0,015	0,008	0,008	
	2002	0,080	0,060	0,050	0,039	0,032	0,023	0,017	0,011	0,005	
	2005	0,083	0,063	0,053	0,042	0,033	0,025	0,018	0,011	0,006	
Klasa	1998	00	00	00	00	00	00	00	00	00	00
	2000	00	00	00	00	00	00	00	00	00	00
	2002	05	00	00	00	00	00	00	00	00	00
	2005	05	00	00	00	00	00	00	00	00	00
U, %	1998	0,035	0,028	0,024	0,022	0,017	0,014	0,010	0,010	0,009	0,009
	2000	0,040	0,032	0,026	0,023	0,019	0,015	0,012	0,011	0,010	0,010
	2002	0,047	0,035	0,029	0,023	0,019	0,016	0,013	0,011	0,010	0,010
	2005	0,050	0,036	0,031	0,025	0,019	0,016	0,014	0,012	0,011	0,010

Analizom promjene pojedinih paramatara kroz uporabno razdoblje prijenosnog etalona sile vidljiva je tendencija pogoršavanja odnosno približavanja graničnim vrijednostima za klasu 00 kojoj je odgovarao ovaj etalon pri prvom umjeravanju. Kroz promatranje vrijednosti relativne pogreške ponovljivosti pri istim i različitim ugradbenim položajima ne može se dati egzaktna ocjena da se stanje pogoršava no može se vidjeti raspodjela pogreške po pojedinim mjernim točkama (slika 3 a i b). Vidljivo je da na mjernim točkama do 40% nazivne sile postoji nestabilnost vrijednosti a da dalje dolazi do smirivanja vrijednosti pogrešaka. No analiza relativne greške histereznog mjerenja (slika 3 c) pokazuje nam kako prijenosni etalon gubi sposobnost tokom uporabe. Zbog ove pogreške je etalon 2002. i 2005. godine na prvoj mjernoj točki prešao u klasu 0,5. Na drugoj mjernoj točki može se očekivati pri slijedećem umjeravanju također do probijanja graničnih vrijednosti za klasu 00.

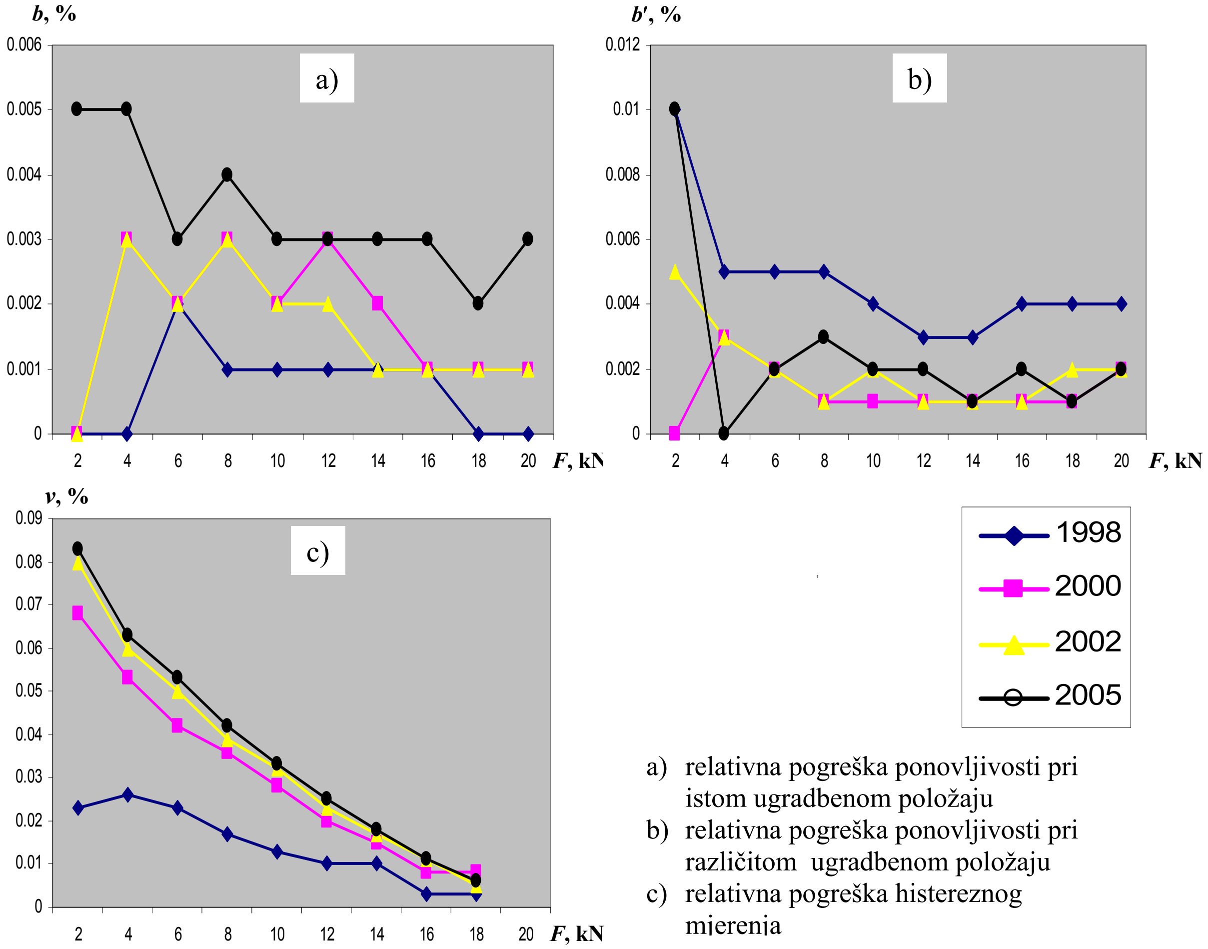

a) relativna pogreška ponovljivosti pri istom ugradbenom položaju
b) relativna pogreška ponovljivosti pri različitom ugradbenom položaju
c) relativna pogreška histereznog mjerenja

Slika 3: Raspodjela vrijednosti pojedinih pogrešaka po mjernom području prijenosnog etalona sile Z4-20 kN

Relativna pogreška interpolacijske krivulje je kod ovog prijenosnog etalona bila jako mala te je u radu dalje zanemarena jer je bio upotrijebljen polinom trećeg stupnja Y (izraz 1) kojim je jako dobro interpolirana krivulja umjeravanja. Promjena koeficijenata polinoma je dana u tablici 5.

$$Y = \mathrm{A}^{*}X + \mathrm{B}^{*}X^{2} + \mathrm{C}^{*}\, X^{3} \qquad (1)$$

Tablica 5: Koeficijenti polinoma

Polinom	Koeficijent God. umjeravanja	**A**	**B**	**C**
Y	1998	9,994500962 E-02	4,8057890026 E-05	-9,333878864 E-07
	2000	9,996454023 E-02	1,3809604441 E-06	-1,069236938 E-07
	2002	9,996695324 E-02	6,5254164706 E-07	-8,616775710 E-08
	2005	9,996426816 E-02	6,4077920258 E-07	-8,712253403 E-08

Procjena mjerne nesigurnosti je provedena u skladu s dokumentima [4] i [5]. U tablici 4 su dane vrijednosti proširene mjerne nesigurnosti (*U*) uz faktor pokrivanja *k*=2 i razinu povjerenja od 95% za svaku mjernu točku pri svakom umjeravanju. Na slici 4 dan je grafički prikaz promjene mjerne nesigurnosti s obzirom na uporabu. Vidljiva je tendencija porasta vrijednosti mjerne nesigurnosti pogotovo u početnom dijelu mjernog područja do 40 % nazivne sile. Za očekivati je da će i proširena mjerna nesigurnost na prvoj mjernoj točki probiti graničnu vrijednost za klasu 00 pri slijedećem umjeravanju prijenosnog etalona sile Z4-20 kN.

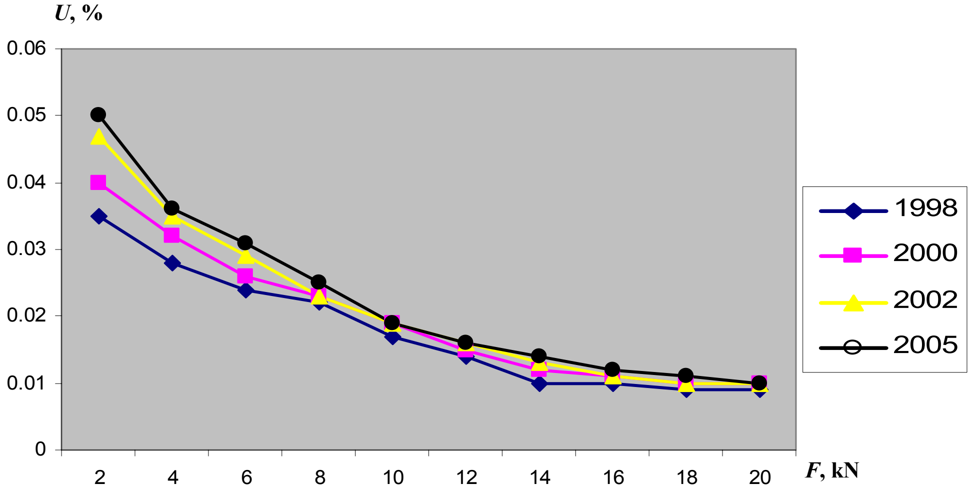

Slika 3: Raspodjela vrijednosti proširene mjerne nesigurnosti po mjernom području prijenosnog etalona sile Z4-20 kN

5. Zaključak

Temeljno pitanje ovog rada je bila da li je moguće na temelju praćenja pojedinih parametara za određeni prijenosni etalon sile predvidjeti promjenu njegovih karakteristika tijekom uporabe te iste uvrstiti u procjenu i proračun mjerne nesigurnosti umjeravanja mjerila sile u slijedećem razdoblju njegove primjene. Iz prethodno provedene analize za prijenosni etalon sile Z4-20 kN mogu se donijeti slijedeći zaključci:

- Najbolji pokazatelji promjena karakteristika prijenosnog etalona sile su relativna pogreška histereze te mjerna nesigurnost. Na temelju ovih vrijednosti moguće je za slijedeće umjerno razdoblje predvidjeti promjenu karakteristike etalona te to uvrstiti u procjenu i proračun ukupne mjerne nesigurnosti pri umjeravanju nekog mjerila sile ovim etalonom. No ovo vrijedi pod uvjetom da na prijenosni etalon nije bilo utjecaja tijekom uporabe koji su izvan uvjeta koje je propisao proizvođač i norma po kojoj se provodi umjeravanje..

- Uočena je nestabilnost parametara u mjernom području do 40% nazivne sile prijenosnog etalona sile. Ako se etalon sile primjenjuje u tom području i ako se vrijednosti pojedinog parametra približavaju graničnim vrijednostima za klasu koja je dobivena na prethodnom umjeravanju etalona, tada je potrebno dodatno provesti analizu ili čak smatrati da je u tom području etalon prešao u višu klasu.

- Najbolji rezultati umjeravanja postižu se u mjernom području 40 – 100 % nazivne sile, što nam govori da bi se u tom području trebao i koristiti ovaj prijenosni etalon.

LITERATURA:

[1] R.S. Figliola, D.E. Beasley: Theory and design for mechanical measurements, John Wiley & Sons, New York, 1991.

[2] EN ISO 376: Metallic materials – Calibration of force proving instruments used for the verification of uniaxial testing machines, 1999.

[3] Ž. Alar: Procjenjivanje nesigurnosti rezultata mjerenja sile, Magistarski rad, Fakultet strojarstva i brodogradnje Sveučilišta u Zagrebu – Zagreb, 2001.

[4] A. Sawla: Guidance for the determination of the best measurement capability of force calibration machines and uncertainty of calibration results of force measuring devices, PTB-Mitteilungen 104 4/94, pp.237-242.

[5] EA-4/02 (EAL-R2): Expression of Uncertainties of Measurements in Calibration, 1997.

10. Savjetovanje o materijalima, tehnologijama, trenju i trošenju
10. Conference on Materials, Processes, Friction and Wear
MATRIB'05, Vela Luka, 23-25.06.2005.

THE INFLUENCE SOME PARAMETARS ON THE QUALITY OF THE RECYCLED PULP

UTJECAJ NEKIH ČIMBENIKA NA KVALITETU RECIKLIRANIH VLAKANACA

Ivana Bolanča, Aleš Hladnik*, Zdenka Bolanča
Faculty of Graphic Arts, Zagreb, Croatia
*Institute of Pulp and Paper, Ljubljana, Slovenija

Abstract: The influence of the following variables: the voltage of the photoreceptor drum in printing, activity of the ageing process of prints, the influence of the basic weight of the printing substrate, particular phases of the recycling process and the felt and the screen side of handsheet on the effectiveness of the recycling process of the digital offset prints Indigo and on the quality of the recycled fibers has been observed in this work.

According to the phases of the recycling process the brightness was measured and the spot size, ink spot number and the ink area of the residual ink on the handsheets were evaluated by means of the image analysis. For observing the quality factors of the handsheet obtained from the fibers of the recycling process of different series of samples the Pareto analysis was used. The investigation results show that higher voltage of the photoreceptor drum used in printing for production of prints for recycling (-600V), higher basic weight of the printing substrate (280 g/m^2), usage of the non aged prints in the deinking flotation process and the application of the deinking process lead to smaller number of the residual particles of ElectroInk on handsheet after flotation, which contributes to greater quality of the recycled fibers.

Key words: recycled prints, printing conditions, basic weight, ageing of prints, image analysis, Pareto analysis

Sažetak: U radu je praćen utjecaj: napona temeljnog bubnja u tisku, djelovanje procesa starenja otisaka, utjecaj gramature tiskovne podloge, pojedine faza samog procesa reciklacije, te pustene i sitove strane laboratorijskog lista. na efikasnost reciklacije otisaka digitalnog ofsetnog tiska Indiga, odnosno na kvalitetu vlakanaca podvrgnutih deinking flotaciji.

Prema fazama procesa reciklacije mjerena je bjelina i procijenjen je broj, veličina i površina zaostalih čestica na listu, pomoću slikovne analize. Za praćenje čimbenika kvalitete lista formiranog iz vlakanaca procesa reciklacije različitih serija uzoraka korištena je Paretova analiza. Rezultati istraživanja pokazuju da viši napon temeljnog bubnja korišten u tisku pri izradi otisaka za reciklaciju (-600V), viša gramatura tiskovne podloge (280 g/m^2), korištenje ne starenih otisaka u procesu deinking flotacije i primjena deinking procesa dovode do manjeg broja zaostalih čestica ElectroInka na laboratorijskom listu poslije flotacije, što doprinosi većoj kvaliteti recikliranih vlakanaca.

Ključne riječi: reciklirani otisci, uvjeti tiska, gramatura, starenje otisaka, slikovna analiza, Paretova analiza

INTRODUCTION

For evaluation of the quality of the recycled pulp and the effectiveness of ink removal, optical parameters, such as brightness, luminance and color can be applied [1]. Frequently encountered parameter to determine the optical quality is the spectral reflectance factor R_{457} used as a measure of brightness. However, this procedure has certain limitations, e.g. the measurement includes only the blue area of the visible spectrum between the wavelengths of 400 and 510 nm. That is why this parameter does not always relate well with visual assessment [2, 3]. In addition, spectral reflectance factor is not only affected by the number of residual ink specks, but also by their size [4, 5].

A more effective means of quantifying residual ink is by measuring the light absorption in the near-infrared part of the spectrum (800 to 1300 nm). The development of the *effective residual ink concentration* – ERIC – by Jordan and Popson has provided a tool to determine how much the ink specks population is impacting brightness of the pulp [6, 3]. The ERIC value is based on the absorption of infrared light at 950 nm as measured by reflectance and depends on the amount of light scattering due to the sample fiber. This method is used when the particles are invisible to the naked eye, i.e. when their size is smaller than 10 μm.

The particles whose diameter is between micro and macro area and the invisible ones, have smaller influence on brightness of the recycled fibers compared to those being smaller than 10 μm [7]. It is important to study the transition from the invisible area into the visible one and to understand the underlying mechanisms as the process conditions influence the product properties. In the determined conditions in the process and agents for the removal of ink, the agglomerations can be formed which will have smaller influence on brightness and which will increase the effectiveness of the particle removal [8,9].

Image analysis systems are useful for recording optical inhomogeneities. These are dirt specks including ink particles in lab handsheets or in paper producing an optical contrast to the sheet background. With this method, the number, diameter and area of the residual dirt particles in visible, macroscopic area can be determined. Many authors have studied the techniques of the image analysis [10, 11].

In this paper, results of investigation of dirt particles size distribution in lab handsheets before and after deinking flotation process of digital offset prints Indigo using image analysis software systems and brightness are presented. As the influential factors on the residual ElectroInk particles on handsheet the following ones have been observed: voltage of the photoreceptor drum in printing, activity of the ageing process of prints, the influence of the basic weight of the printing substrate, particular phases of the recycling process and felt and screen sides of handsheet. Statistical techniques such as factorial design and Pareto chart were used to interpret the finding.

EXPERIMENTAL

The digital offset printing machine Indigo E-Print 1000+ was used for printing. The voltage levels on the photoreceptor drum studied were - 300 V and - 600 V. The test form used in printing contained areas of tonal values ranging from 0 to 100% coverage in steps of 10% for CMYK colours.

Printing substrates were the mat fine art papers of 200, 250 and 280 g/m2 (gsm) basis weight. The printed samples underwent the alkaline deinking flotation process [12]. The handsheets were made using a laboratory sheet former, according to standard TAPPI method T 205.

Brightness was determined on the handsheets after disintegration and after flotation by using the standard method ISO 2469.

Optical unhomogeneity was assessed by means of image analysis. In general, the principle of this method is the usage of the difference in contrast between the particles of dirt specks and the substrate. The image obtained by a flat-bed scanner is digitally converted into pixels

whose size depends on visibility field and the image depends on the scanner resolution. Identification of the dirt specks is based on the differences in gray values. The value between 0 and 255 is given to each pixel in accordance with its reflectance. The image segmentation converts the digitalized gray value image of the camera to a binary, black-and-white, image. In this way all the pixels with the gray value above the determined threshold value are identified as the dirt specks and they get the value 1 in the binary image. Pixels with gray values below the threshold are considered as background. The image analysis ends in measuring the dirt particles and in producing the data output.
Dirt particle analysis procedure is presented in Figure 1.

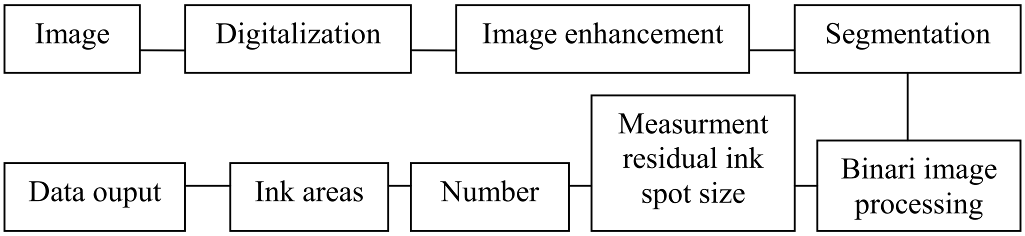

Figure 1: Dirt particle image analysis procedure.
Residual ink particles size (area) and number were assessed with image analysis-based software systems: Spec*Scan (Apogee System). Spec*Scan system utilizes a flat-bed scanner Epson Perfection 2400 Photo to digitize image, its resolution was set to 600 dpi. Three lab handsheet samples for each combination of settings were scanned on both sides. Size intervals were defined according to TAPPI methods T 213 and T 437. Threshold value (100), white level (75) and black level (65) were chosen after comparing computer images to handsheets.

Factorial design

We wanted to examine effects of several variables on efficiency of floatation deinking so we performed experiments according to a standard 2^5 factorial design scheme with randomized runs varying each of the factors at two levels. Factors studied were as follows:

1. Artificial ageing (AGEING): without (S0) / with (S1)
2. Printing drum voltage (VOLTAGE): 300 V (N0) / 600 V (N1)
3. Basis weight (BASISWT): 200 gsm (G0) / 280 gsm (G1)
4. Floatation deinking process (DEINK): before (F0) / after (F1)
5. Handsheet side (PAPSIDE): bottom (P0) / top (P1)

Data on the following eight parameters related to number and size of dirt particles as obtained by image analysis software were recorded:

1. Total number of specks (NOS_T)
2. Number of specks larger than 0,04 mm^2 (NOS_L4)
3. Number of specks smaller than 0,04 mm^2 (NOS_S4)
4. Total area of specks (TSA_T)
5. Average area of specks (ASA_T)
6. Area of specks larger than 0,04 mm^2 (SA_L4)
7. Area of specks smaller than 0,04 mm^2 (SA_S4)
8. Grayscale brightness (GSB)

RESULTS AND DISCUSION

Residual ink size, ink number, ink areas and brightness of handsheet before and after flotation of the non aged and aged prints of the Indigo, made on the paper with the same basic weight in relation to the size of the photoreceptor drum voltage in printing in preparation of samples for analysis are presented in table 1 and 2.

Table 1 The influence of the size and surface of the ElectroInk particles on the handsheet brightness before and after flotation of the non aged Indigo prints made on the paper of the same grammage (200g/m^2) in relation to the voltage size in printing (-300 V - 600 V)

Non aged Indigo prints		Total number of particles	Number of particles >0,04 mm^2	Number of particles <0,04 mm^2	Total particle surface mm^2	Particle surface >0,04 mm^2	Particle surface <0,04 mm^2	Brightness %
200g/m^2 voltage -300V	Before flotation	1748	397	1351	79,146	62,067	12,385	81,9
	After flotation	1725	389	1336	74,452	62,067	12,385	83,1
200g/m^2 voltage -600V	Before flotation	1011	155	856	169,326	163,082	6,244	83,2
	After flotation	731	151	580	112,046	107,518	4,529	85,9

The investigation results show that the handsheet made after disintegration of Indigo prints obtained at higher voltage contain 48,2% smaller number of ElectroInk particles and have 53,3% greater surface covered by particles in relation to the handsheet obtained by processing the prints made at lower voltage in printing. The proportional relationship among the particles and brightness can be noticed. On the other hand the macro particles contribute to the optical inhomogeneity of handsheet. In this case only the small brightness gain is noticed, which points at the weak efficiency of the performed process, because the particles do not correspond in size and shape to those ones which can be successfully detached by flotation

In table 2 the results for earlier described sample series are described with the only difference that in this case the prints were natural aged before deinking flotation.

Table 2 Influence of the size and surface of the ElectroInk particles on the handsheet brightness before and after flotation of aged Indigo prints made on paper of the same basic weight (200g/m^2) in relation to the voltage size in printing (-300 V, -600 V)

Aged Indigo prints		Total number of particles	Number of particles >0,04 mm^2	Number of particles <0,04 mm^2	Total surface of particles mm^2	Surface of particles >0,04 mm^2	Surface of particles <0,04 mm^2	Brightness %
200g/m^2 voltage -300V	Before flotation	2547	499	2048	90,103	70,280	19,823	80,7
	After flotation	2015	481	1792	81,095	64,407	16,688	81,2
200g/m^2 voltage 600V	Before flotation	1313	217	1096	211,773	203,556	8,217	80,8
	After flotation	1063	202	861	151,180	144,87	6,310	82,9

The investigation results show that by the disintegration of the aged prints the total number of particles on handsheet increases somewhat more (32,8%) during processing the prints made at higher voltage in relation to the higher voltage (23,1%). By processing the aged prints the surface coverage of the handsheet by ElectroInk particles increases, which contributes to the decrease of brightness in both cases.

With regard to the complexity of the system and great number of different variables and data, the experimental design in accordance to the 2^5 factorial sheme is applied. Pareto analysis is applied which includes the construction of the specific diagram. In the analysis, the starting point is the principle according to which the sample distribution is not unique but asymmetric one and originates from smaller number of samples in most cases.

Similar information including the mentioned parameters contain Pareto chard. The result of a series of controls p= 0,05 marked limits points at 95% probability, which means that the influence is significant. The sign of the individual activity determines the mark of its positive or negative influence on the determined parameter.

Higher voltage of the printing drum used in printing for production of prints for recycling VOLTAGE (600V), higher basic weight of the printing substrate BASISWT (280 gsm), usage of the non aged prints in the process of deinking flotation, AGEING and the deinking process itself DEINK- all of them lead to lower (NOS_T) figure 2.

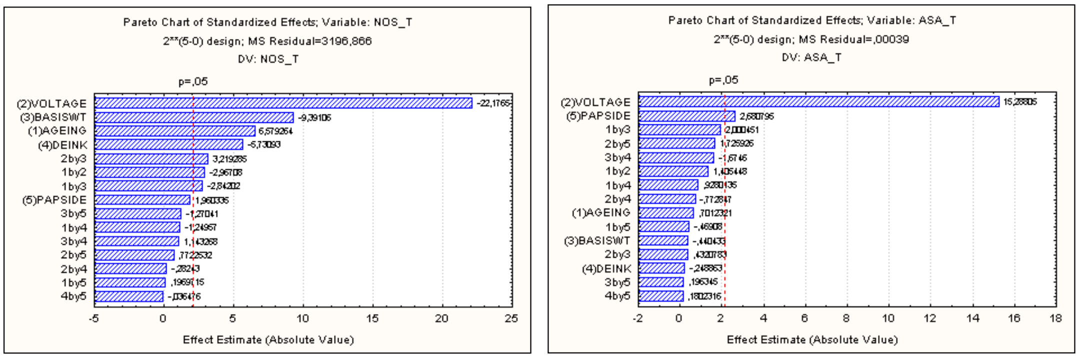

Figure 2 Pareto chart for the total particle number (NOS_T) (right) and average particle size (ASA_T) (left)

In comparison to the voltage of the printing drum, the influences of other factors are very low. With lower voltage of the printing drum VOLTAGE (300V) the average surface of ElectroInk particles on the sheet formed from the fibers from the observed recycling process (ASA_T) is significantly lower, as presented in figure 2

Pareto diagram for the brightness of the grey scale, figure 3 shows that greater basic weight of the printing substrate used in printing the sample for deinking flotation BASISWT (280gsm) is joined to greater brightness GSB.

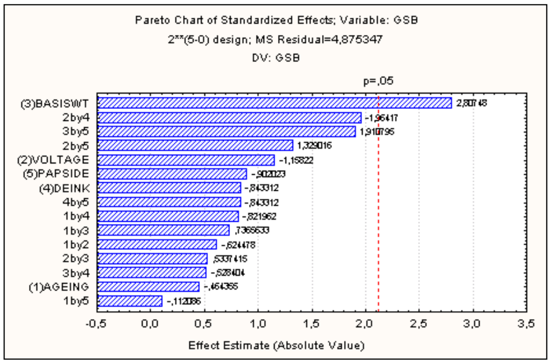

Figure 3 Pareto diagram for the brightness of the grey scale (ASA_T)

4. CONCLUSION

Based on the investigation results of the influence of the conditions in digital offset Indigo printing (-300 V,-600V), the basic weight of the printing substrate (200, 250 and 280g/m^{2}‘), phases of the deinking flotation and formation of lab handsheet (felt and screen side) on the number and the size of the residual ElectroInk particles on handsheet one can conclude the following:

Higher voltage of the printing drum used for production of prints for recycling, higher basic weight of the printing substrate, usage of the non aged prints in the process of deinking flotation and the deinking process itself lead to smaller number of particles on handsheet.

Because when using the higher voltage in printing, the macro particles are present on handsheet after disintegration, which cannot be successfully removed by flotation, the optical inhomogeneity of the substrate has the additional influence on the quality of the recycled fibers

REFERENCE:

[1] N. Pauler, Paper Optics, AB Lorentzen & Wettre, Östervala, 1998, pp. 2-8

[2] N. Dubreuil, How Does the Presence of Optical Brighteners?: in Recycled Fibres Affect Paper Optical Properties, Progress in Paper Recycling 3(3), 1994, pp. 92-96

[3]S.J.Popson; D.D. Malthouse, P.C. Robertson; The Application of Brightness, Whiteness, and Color measurements to Color Removal in Recycling –A TAPPI Press Anthology of Published Papers, Abubakr S.(Ed)., TAPPI Press, ISBN 0-89852-339-7 Atlanta, 1997, pp. 13 19

[4] J.K. Borchard, The effects of kneading on pulped office papers. Part 1. Brightness and particle size studies, Progress in Paper Recycling 6 (3), 1997, pp. 29-38

[5] S.A.F. Julien; E.P.G. Tourtollet B. Perrin, Advanced deinking supervision and control using new on-line sensors, PTS-Deinking Symposium, Munich, 1998, pp. 58-64

[6] B.D. Jordan, S.J. Popson, Measuring the Concentration of Residual Ink in Recycled Newsprint, 2nd Research Forum on Recycling, CPPA, Ste-Adele, Quebec, 1993, pp. 153-169

[7] D.R. Hynes, Measuring Ink Content: from Pulper to Deinked Pulp, Proceedings on TAPPI Recycling Symposium, 2000, pp. 672-691

[8] L. Göttsching, H.J. Putz. K. Renner,. Beeinflussung von Druckfarbenpartikelgrösse und –verteilung beim Deinken von Altpapier, aiF- Report No 8126, Department of Paper Science and Technology, Darmstadt,Germany,1999, pp.10-14

[9] R.J. Trepanier, T. Oksanen, The effect of coating components and fillers in the deinking of paper. Image analysis and microscopic investigations. Proceedings on TAPPI Recycling Symposium, TAPPI Press, 1995, pp .269-275

[10] L. Göttsching, and H. Pakarinen, Recycled Fiber and Deinking, FPEA and TAPPI, Jyväskylä, 2000, pp. 132-148

[11] R.J. Trepanier, B.D. Jordan, N.G. Nguyen, High magnification image analysis with novel background reflectance technique for measuring residual inks in sheets J. Pulp Pap. Sci. 23 (3) 1997. J. pp. 129-136

[12] Z. Bolanča, D. Agić, I. Bolanča, Chemical Deinking of Non-impact Prints, Acta Graphica, 14,(1,2) 2002, pp.1-10

[9] B.Lozo, Z.Bolanča, I.Bolanča, D.Modrić, Recycled Paper – the Influence of Digital Prints, Drvna industrija, 53 (4) 2002 pp. 203-210

10. Savjetovanje o materijalima, tehnologijama, trenju i trošenju
10. Conference on Materials, Processes, Friction and Wear
MATRIB'05, Vela Luka, 23-25.06.2005.

CHARACTERISTICS OF THE RECYCLED PULP IN THE FUNCTION OF THE SURFACTANTS

KARAKTERISTIKE RECIKLIRANE CELULOZE U FUNKCIJI POVRŠINSKO AKTIVNIH TVARI

Zdenka Bolanča; Željka Barbarić Mikočević; Ivana Bolanča Mirković,
Faculty of Graphic Arts, Zagreb, Croatia

Abstract: The conventional and the most used process in paper recycling is deinking flotation. The separation criterion in the process is based on different wetting of the surface of ink particles, fillers, coating pigments, binders (hydrophobic ones) which adhere to the air bubbles and detach in the form of froth in relation to the cellulose fibers (hydrophilic ones) which stay in suspension. In order to achieve the described surface properties, it is possible to use the whole series of chemical which include liquid fatty acids, soaps, synthetic surfactants which can be non-ionic, cationic and anionic ones.
The influence of the surfactants of different chemical composition on some optical properties and the size distribution of the residual particles on lab handsheets in different phases of the recycling process of offset prints are presented in this article.

Key words: deinking flotation, surfactants, recycled fibers, optical properties, image analysis

Sažetak: Konvencionalni i najviše korišteni postupak pri reciklaciji papira je deinking flotacija. Kriterij separacije u procesu zasniva se na različitom vlaženju površina čestica boje, punila, pigmenta premaza, veziva (hidrofobna), koji se prihvačaju za mjehuriče zraka i izdvajaju u obliku pjene, u odnosu na celulozna vlakna (hidrofilna) koja ostaju u suspenziji. Glavna faza u flotaciji ja adhezija odnosno prihvačanje mjehurić- čestica, koje je kontrolirano površinsko aktivnim tvarima. Da bi se postigla opisana površinska svojstva moguće je koristiti cijeli niz kemikalija koji uključuje: tekuće masne kiseline, sapune, sintetske površinko aktivne tvari, koje mogu biti neionske, kationske i anionske.
U ovom radu prikazuje se utjecaj površinsko aktivnih tvari različitog kemijskog sastava na neka optička svojstva i distribuciju veličine zaostalih čestica na laboratorijski izrađenom listu u različitim fazama procesa reciklacije ofsetnih otisaka.

Ključne riječi: deinking flotacija, površinsko aktivne tvari, reciklirana vlakanca, optička svojstva, slikovna analiza

INTRODUCTION

Conventional and the most used process in paper recycling is deinking flotation. Printing ink detaches from the cellulose fibers in deinking process, they are removed in flotation. Flotation is the method which uses different surface properties for separation. Hydrophobic particles of ink adhere to air bubbles and are transported by thrust forces to the surface, while the hydrophilic cellulose fibers stay in the water phase. Froth is formed on the boundary liquid/air and it contains the ink particles, fillers, coating pigments, stickies and binders.

Important factors of the surface chemistry which is active on deinking are: chemical composition of fillers (calcite, clays, zeolites0, pH, temperature, water hardness, surfactant chemicals, gas type and gas flow rate, hydrodynamics in flotation cells, bubble shape and bubble size, size of ink particles and the degree of hydrophobicity of ink particles[1-5].

Surfactant chemicals which are usually used in the process are fatty acids, soaps or synthetic surfactants.

Long chain fatty acids in the presence of Ca ions and hot deinking process cause hydrophobic agglomeration of the ink particles, which can easily be removed by the stream of air bubbles in the flotation cell[6]. This process has proved to be highly selective, economical and yielding good ink removal and minimal fibre loos. The removal of stickies (solvent adhesives, hot melt adhesives, dispersion adhesives, coating binders) from prints is important as well as removing the ink[7].

When the fatty acids are used in the process they are usually the mixture of stearic acid, palmitic and oleic acids. The change in the composition of surfactants chemicals can influence on the froth quantity in the flotation cell, on selectivity of the ink removal and the quantity of reject [8]. Good frothing in the flotation cell can be achieved by using the determined portion of the non saturated fatty acids in the mixture in accordance with the iodine number in the area 10-25 [9.]

A combination of soap and synthetic nonionic surfactants is often used in form of a fatty acid emulsion. In order the system acts as the efficient flotation agent, if the process water is soft, calcium ions have to be present which are added in form of lime milk.

If the first stage in the reaction between soap, calcium ions and ink is the adsorption of the soap to the ink particles one can question the positive effect of non ionic surfactants. The goal of the emulsion is to hydrophilize the ink particles, and this has a negative effect on the adsorption of soap to the ink particles and thus the flotation efficiency.

Anionic synthetic surfactants have not the broaden usage because of their solubility in water which can contribute to the quality decrease of process water and to appearance of great froth quantity which can cause great loss of fibers in the flotation process. The main disadvantage of the cation types is the possibility of binding to the fibers which leads to the loss in the process. The usage of some non ionic surfactants such as ethoxylated nonylphenols is decreased in recent years because of the formation of toxic phenole in their biological disintegration[10].

The influence of the surfactants of different chemical composition on some optical properties and the size distribution of the residual particles on lab handsheets in different phases of the recycling process of offset prints are presented in this article.

EXPERIMENTAL

The offset printing machine MAN Roland was used for printing. The test form used in printing contained areas of tonal values ranging from 0 to 100% coverage in steps of 10% for CMYK colours.

Printing substrate was the coated paper of 120 g/m^2 basis weight. Offset colour with greater portion of mineral oil was used in printing. The printed samples underwent the alkaline deinking flotation process[11].

In the phase of sample soaking, deinking chemicals (1% hydrogen peroxide, different types of surfactants of different mass portions, 0,2 % DTPA, 1% sodium hydroxide and 1% sodium silicate) were added. The consistency is 10% in regard to the dry substance. A good mixing action was achieved; the pulping stage was continued for 45 minutes. Suspension was diluted to 0,6 % pulp consistency. The concentration of calcium ion was 80 and 200 ppm. The flotation time was eight minutes. The handsheets were made using a laboratory sheet former. In the disintegration phase the suspension temperature was changed in the interval from 30-60^0C

The handsheets were made using a laboratory sheet former, according to standard TAPPI method T 205.

Brightness was determined on the handsheets after disintegration and after flotation by using the standard method ISO 2469.

Residual ink spot size, ink spot number and ink areas were assessed with image analysis software Spec*Scan. This software is a windows based system utilizing a scanner to digitize image. Threshold value (100), white level (75) and black level (65) were chosen manually after comparing computer images to handsheets. Particles size intervals were present with the software according to TAPPI standard methods T 213 and T 437.

RESULTS AND DISCUSION

The influence of surfactant chemical of different composition (non ionic, fatty acid, non ionic and fatty acid) and temperature of suspension in the area of 30-60^0C on brightness of handsheet after recycling is presented in figure 1.

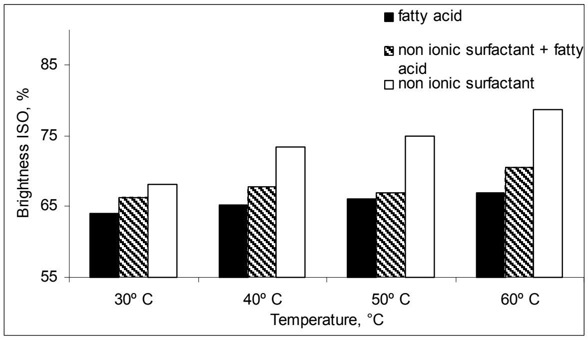

Figure 1: Temperature influence on handsheets brightness after flotation

The investigation results show that the temperature increase of the suspension results in the increase of handsheet brightness. In the theoretical presentation it is visible that great number of factors can influence the flotation. However, the temperature increase can have positive influence on the particle detachment from the fibers. Except that, different influences on brightness are noticed in relation to the type of the used surfactant chemicals. The greatest temperature influence is in the case of the usage of non ionic surfactant. It was noticed that the influence on brightness by using the fatty acid will depend on the addition of calcium chloride and sodium silicate in the disintegration phase. By adding the mentioned chemicals and by increasing the temperature, considerable influence on the increase of handsheet brightness can be noticed; however, flotation recovery is decreased.

As the contribution to the explanation of the mechanism of ink particle detachment from the fibers and observing the coverage of the handsheet surface by the particles in all the phases of deinking flotation, the method of image analysis was used. In figure 2 in the process of deinking flotation, non ionic surfactant was used.

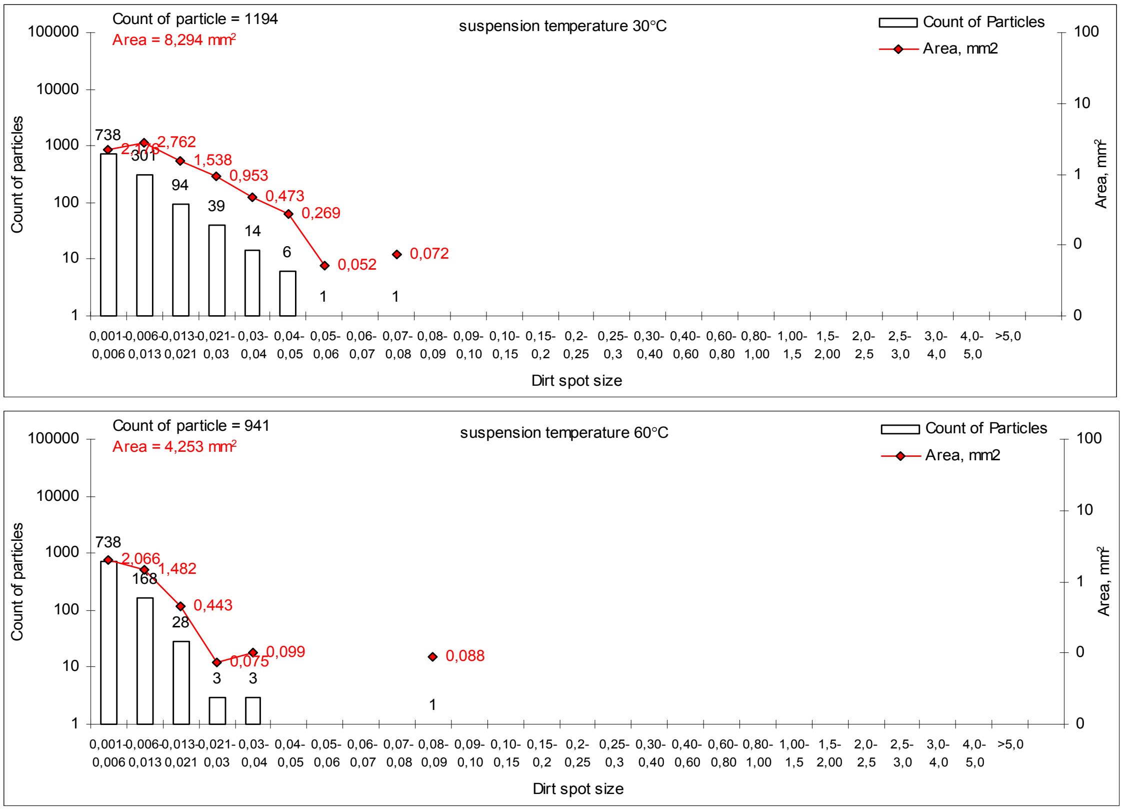

Figure: 2 Total number and size of particles on handsheet after flotation of the offset prints in dependence on temperature –non ionic surfactant

As it is seen from the presentation, the temperature increase of the suspension on the laboratory sheet decreases the total number of offset ink particles for 44,8%, while the total surface is decreased for 34,8%. General characteristic of the particle size distribution is the division of particles within the lowest classes less than 0,04 mm^2 which influences the brightness of handsheet, and which has no greater influence on the optical non-homogeneity of the handsheet surface visible to the eye.
The influence of temperature of suspension on the size and the number of ink particles on handsheet after deinking flotation of the system in which fatty acid was used as surfactant is presented in figure 3.

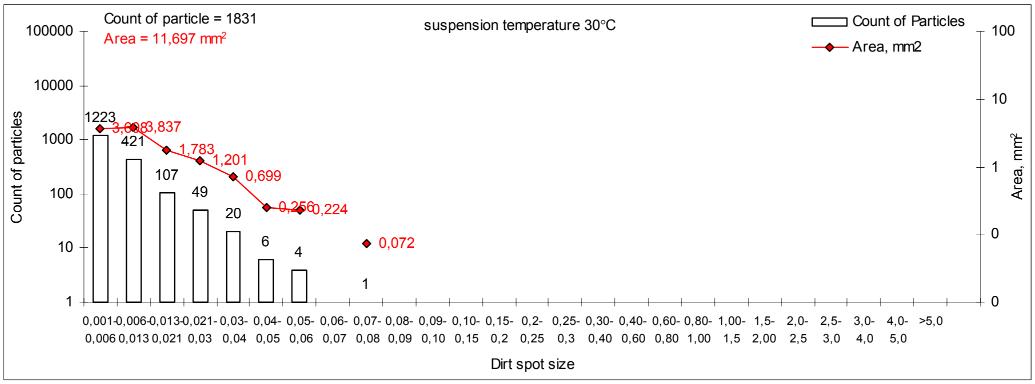

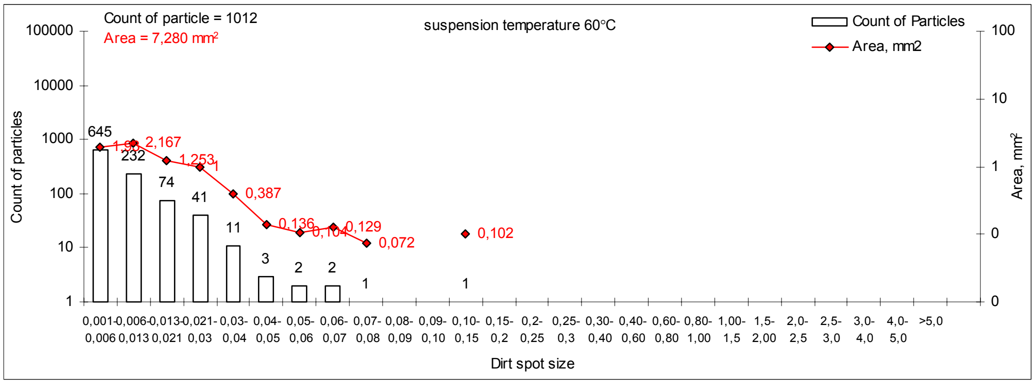

Figure 3: Total number and size of particles on handsheet after flotation of offset prints in dependence on suspension temperature –surfactant fatty acid (concentration of calcium ions 200 ppm).

By changing the temperature of suspension during the recycling of offset prints when using the fatty acid as surfactant smaller influence on the size of the handsheet surface covered by particles in relation to the non ionic surfactant is noticed. The number of particles on handsheet is thus decreased for 9,0%, and the surface for 24% by increasing the temperature of suspension under the same other conditions.

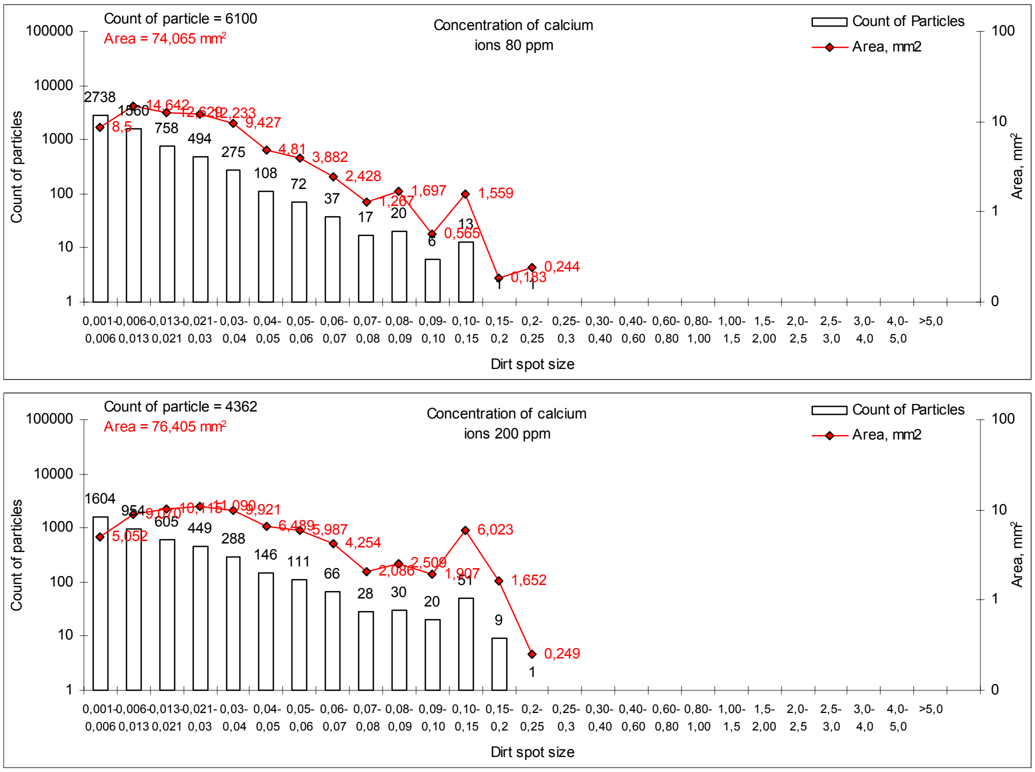

Figure 4: Total number and size of particles on handsheet after flotation of offset prints in dependence on concentration of calcium ions–surfactant fatty acid

Total number and size of particles on handsheet after disintegration of the offset prints at equal suspensions temperature and the presence of fatty acids in relation to different concentration of calcium ions is presented in figure 4.

The difference between the system containing the non ionic surfactant and fatty acid is that, that the system with the application of non ionic surfactant is insensitive to the presence of calcium ions in relation to the process of deinking flotation in which the fatty acids are used as surfactant. When the content of sodium salts of fatty acid is too high it can cause the appearance of small ink particles which cannot be removed successfully by flotation, but too high water hardness can decrease the efficiency of ink removal. Too high addition of fatty acid contributes to the loss of fibers in the process because of entrapment. The used level of calcium ion concentration of 200 ppm (total number of particles < 0,04mm^{2}is 3900, and the surface is 45,247mm^2, the total number of all the particles is 76,405mm^2, in relation to 80ppm calcium ions: the total number of particles < 0,04mm^2 is 5825, and the surface is 57,430mm^2, the total surface of all the particles 74,065mm^2), is enough for transferring the fatty acids into the calcium salts and successful detaching of ink from the system.

CONCLUSION

The investigation results show that the removal of ink is more efficient by increasing the temperature of the suspension in relation to the used surfactants. The flotability is increased with the presence of calcium ions with the application of fatty acid, probably because of the precipitation of calcium salt on the surface of the ink particles. Pulp brightness and particle number and area are used evaluation parameters of efficiency of ink removal.

References

1. Amand F. J. S., Hydrodynamics of deinking flotation, Int. J. Min. Proc. 56(14)(1999) 277-316
2. Hunold M., Krauthauf T., Muller J, .Putz H.J., Effect of air volume and air bubble size distribution on flotation in injector aerated deinking cells J.Pulp Pap. Sci. 23(12)(1997) 3555-3560
3. Carrasco F., Pelach M.A., Mutje P., Deinking of high quality offset paper: influemce of consistency, agitation speed, and air flow ratei the flotation stage, Tappi J. 82 (3) (1999) 125-129
4. Garmer A.E.,Heindel T.J., The effect of fibre type on bubble size, J.Pulp Pap. Sci .26(7)(20009266-269
5. Attard P., Thermodynamic analysis of bridging bubbles and a quantitative compararison with the measured hydrophobic attraction, Langmuir 16(10) (2000) 4455-4466
6. Hynes R.D., Evaluation of fatty acid carryover in North American newsprint deinking mills in: 4th Reaserch Forum on recycling, quebec, Canada,1997
7. Larsson P., Deinking chemistry in: Göttsching, L; Pakarinen (Eds). Papermaking Science and Technology, Fapet Oy, Tappi, Helsinki, 2000. 240-265
8. Ben Y., Doriss G. M., Chemical changes in linseed oil under repulping and flotation conditions, CPPA 4th Research Forum on Recycling Proceedings CPPA, Montreal 1997, 269-277
9. Johansson B., Colloidal chemistry of ink particles agglomeration and flotation, LIC. Thesis, Department of pulpand paper chemistry and technology, Royal Institute of Technology, Stockholm,1997
10. Johansson B., Pugh R.J., Alexandrova L., Flotation deinking studies using model hydrophobic particles and nonionic dispersants, Colloid Surf. A: Eng. Asp. 170(2-3) (2000) 217-229
11. Z. Bolanča, D. Agić, I. Bolanča, Chemical Deinking of Non-impact Prints, Acta Graphica, 14, 2002, vol 1-2, pp.110

10. Savjetovanje o materijalima, tehnologijama, trenju i trošenju
10. Conference on Materials, Processes, Friction and Wear
MATRIB'05, Vela Luka, 23-25.06.2005.

STRUCTURAL ANALYSIS OF AL ALLOY 5083 CAST BY VERTICAL DC PROCESS

STRUKTURNA ANALIZA AL SLITINE 5083 LIJEVANE VERTIKALNIM DC POSTUPKOM

N. Dolić1), K. Terzić1), J. Prgin2), A. Markotić1), F. Unkić1)

1)Metalurški fakultet Sveučilišta u Zagrebu
Aleja narodnih heroja 3
44 000 Sisak
Republika Hrvatska

2)TLM d.d.
Narodnog preporoda 12
22 000 Šibenik
Republika Hrvatska

Abstract: Microstructural analysis of alloy 5083 cast by vertical DC process has been performed by metallographic analysis of casted samples. Grain size has been assessed by semi-automatic methods. Morphology of different phases and distribution of elements in some phases have been assessed by selective etching and scanning by electron microanalysis of separated phases ''in situ''. Obtained results are base for connection between microstructural and process parameters of cast billet of alloy 5083.

Key words: Al - Mg alloy, as – cast structure, grain size

Sažetak: Mikrostrukturna analiza slitine 5083 lijevane vertikalnim DC postupkom provedena je metalografskom analizom lijevanih uzoraka. Određena je veličina zrna poluautomatskim metodama. Selektivnim nagrizanjem i scanning elektronskom mikroanalizom izlučenih faza „in situ“ utvrđena je morfologija i raspored elemenata po pojedinim fazama. Dobiveni rezultati osnova su povezivanja mikrostrukturnih i procesnih parametara lijevanih blokova slitine 5083.

Ključne riječi: Al – Mg slitina, lijevana struktura, veličina zrna

INTRODUCTION

Metallographic analysis has been performed on Al–slabs of alloy 5083 casted on reconstructed and modernized line for casting by vertical DC («direct–chill») process in TLM Casthouse in Šibenik. This process and its variants are practically only methods for manufacturing of slabs and billets. Manufacturing of quality castings in the shape of slabs and billets plays important role for the quality of the final product [1]. First, it is important by casting of semi-products to meet certain criterions of cleanliness, homogeneity of chemical composition, microstructural, mechanical and technological properties. Assurance of small-grained, uniformed structure of slabs and billets is conducted by control of process parameters of pouring and by inoculation of melt by shooting $AlTi_5B$ wire (0,2 - 1,0 kg/t), which finally leads to obtaining of valid products with uniform distributed intermetal phases and with good mechanical and operating properties.

Exemination of microstructure is one of main aids in valuation of alloys and products by assessment of influence of production variables and thermal processing as well as by analysis of defects causes and premature rejection of the products [2]. Small-grained structure with the grain size from 0,2 to 1,0 mm is important quality request of slabs casted by DC process [1].

Alloy 5083 belongs to hard wrought, non - treatable aluminium alloys with Mg, which are dignified by small thickness, high mechanical properties and resistance to corrosion in the usual and marine/sea atmosphere. Alloys of series 5000 often contain other elements like Mn, Cr i Ti, which role is to increase tensile strength and to imporove special properties like resistance to corrosion, weldability and others [3]. Al alloys from this series dedicated to plastic deformation, which are used in industry, usually do not contain more than 5% of Mg because each increase of its contain leads to decrase of stability of alloy, especially under the influence of increase temperature.

The purpose of this paper is to quantify average grain size of Al-alloy 5083 by some of verified metallographic methods and by SEM analysis ascertain the distribution of elements by separete phases.

EXPERIMENTAL PART

Samples for experimental part of the paper have been taken from cross-section, „slice“ of 30 mm thickness, cut at the beginning of the Al-slabs casted by vertical D.C. process. Dimensions of the section of casted slab are 1430x520 mm.

Samples have been cut in water-cooled device for cutting, after which they have been mounted (samples have to be in the form of small roller of 30 mm diameter) and put into mass [4,5]. Used mass is Varidur 20 on the basis of methylmetacrilate, which polimerizated on cold. Grinding of samples has been conducted automatically under the sqirt on series of abrasive paper of grit sizes 120, 240, 400, 600, starting with the roughest to the finest. Grinding under the squirt has this advantage: water removes pieces dropped out from abrasive paper and metal surface, whereby the grinding process accelerates and decreases the possibility of emergence of rough groove on grinded surface [6]. Polishind has been perforemed on appropriate cloth (Microcloth) by water solution of alumina (Al_2O_3) granulation of 0,3 μm on the same device as for the grinding. Polished surface has to be large enough to provide measurement on at least five areas by necessary magnification.

After the polishing it has been passed to etching of the samples [7]. Sample for metallographic examination has been electrolyticlly etched (anodized) by Barker's anodization solution consisted of 4-5 ml HBF_4 in 200 ml H_2O. Anodising or anodic oxidation is an electrolytic process for depositing an oxide film on the metal surface that is epitaxial to the underlying grain structure, which allows observe of microstructure of grains under polarized light (plus sensitive tint) [2]. The resulting interference colors are a function of the anodic film thickness, which depends on the anodising voltage, the solution and the and / or structure present in the specimen.

Metallographic examinations of samples have been conducted on metallographic microscope with digital camera and system for automatic image editing («AnalySIS Materials Research Lab»), with magnification of 100 times. «AnalySIS Materials Research Lab» is the part of «Soft Imaging System» series of software package for research of materials structure.

For determination of average grain size, relatively mean number of grains per unit area comparison procedure has been used [8], and semiautomatic method for determining average grain size by intercept length method and semiautomatic method for determining average grain size by intercept count method [9].

Due to identification of alloy 5083 phases, sample has been, after its preparation, etched with water solutions of HF (0,5 ml HF in 100 ml distilled H_2O) [10]. SEM analysis of etched sample has been conducted by scanning electron microscope JEOL JSM-5610 equipped with Energy Dispersive Spectrometer (EDS and XRF SYSTEMS Inc.500). By the analysis voltage of 20 kV has been used.

RESULTS OF EXEMINATION

Examinated melt has mark 4280 and its chemical composition is presented in the table 1.

Table 1: Chemical composition of examinated alloy 5083

Melt No.	Chemical composition of alloy 5083, [%]									
	Cu	**Mn**	**Mg**	**Si**	**Fe**	**Cr**	**Zn**	**Be**	**Ti**	**Na**
4280	0,01	0,51	4,30	0,15	0,42	0,09	0,005	0,0037	0,025	0,0006

Due to improvement of hardness and other tensile characteristics, majority of Al-Mg alloys contains supplements of iron, chromium, manganese or titanium, separately or in combination, in total amount from 0,25 to 1 %, table 1. Besides of Mg which precipitates most often in the shape Mg_2Al_3 on the borders of grains, in microstructure most likely appears iron-rich complex phases like $(Fe,Cr)_2Mg_3Al_{18}$ and/or $(Fe,Mn)Al_6$ type, and silicon-rich phases [11].

1. DETERMINING AVERAGE GRAIN SIZE

By anodising of examinated sample 5083 by Barker's etch and observation under polarized light with the supplement of sensitive tint filter, obtained is good resolution of the grain like different shades of matching colors, image 1. Operator by him self regulates colors until he gets the best resolution between different colored grains so he could be able to distinguish the grains precise and without doubt.

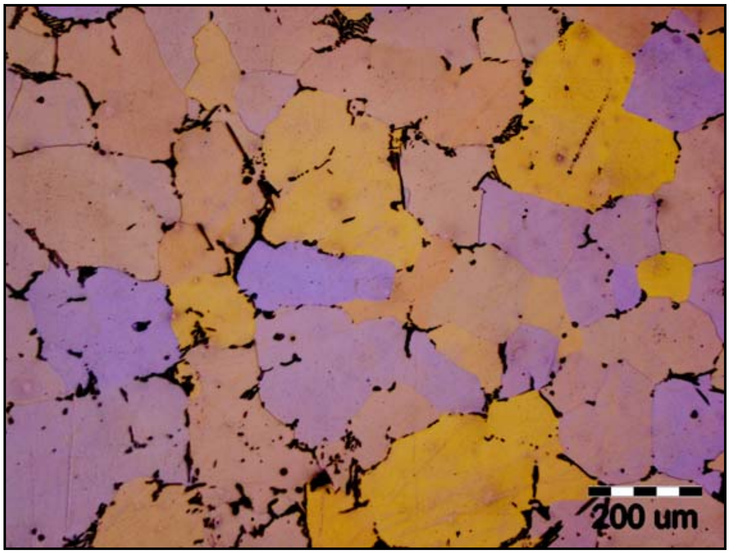

Fig 1 Microstructure of sample of Al alloy 5083 etched by Barker's etch observed with polarized light (plus sensitive tint filter), by magnification 100 x

On the sample etched like that, the average grain size has been assessed (G), relatively number of grains per unit area by following methods:

a) Determining average grain size by comparison method

The comparison procedure does not require counting of either grains, intercepts, or intersections but involves comparison of the grain structure to a series of graded images, either in the form of a wall chart plastic overlays, or an eyepiece reticle [8]. On the samples etched by Barker's etch comparison method has been conducted with 8 comparated images, where the grain size G has been assessed as a whole number, table 2.

Table 2: Results of measurement conducted by comparison method and semi-automatic method for determining average grain size by intercept length method and determining average grain size by intercept count method on the sample etched by Barker's etch.

Reagent	**Comparison method**		**The intercept length method**		**The intercept count method**	
	Grain number/mm^2	**G - number**	**Grain number/mm^2**	**G - number**	**Grain number/mm^2**	**G - number**
Barker	31,00-62,00	2 - 3	54,20	2,79	49,85	2,67

The measurement has been conducted on 10 different, randomly chosen details and the value of G-number had been going from 2 to 3, relatively from 31,00 to 62,00 grains/mm^2. According to the literature quotations, it seems that there is a declination in the valuation of average grain size by comparison method, i.e. specific grain size is bigger then the real one for approximately ½ to 1 [8].

b) Semi-automatic method for determining average grain size by the intercept length method (intercept procedure [8])

Software places reticule for examination, which consists of several parallel, linear horizontal lines (scanning lines) with the interspace bigger than the diameter of clear average grains, through photographic or "live" image, without shift. Operator manually defines interceptions of grain boundaries along scanning line, considering the beginning and the end of each grain, while the grains which are intersected by the border of exterminated surface do not take into consideration. This procedure repeats while at least 500 lengths of intercepts are measured so that the result could be statistical justified [9]. Software automatically calculates average intercept length, $\bar{l}$ [μm], from which, by linear approximation (table 2, [9]) the average number of grains per unit area form measured *n* areas $\overline{N_A}$ [number of grains/mm^2] or *G–number* could be calculated. Results of the measurements are given in table 2, which presents that the G-number assessed by this semi-automatic method is 2,79, calculated on the grain number/mm^2, $\overline{N_A}$ =54,20.

c) Semi-automatic method for determining average grain size by the intercept count method (circular intercept procedures, Abrams three-circle procedure[8])

Because the software for automatic analysis of the image does not recognize grain boundaries which are not completely closed, manually reconstruction of grain boundaries has been conducted. On that way assessed image reticule for examination has been used and it consists of 3 concentric and equally interspaced circles of 500 mm length. Repeat the analysis until at least 500 intercepts length of grain boundaries are counted on 5 or more randomly chosen fields.

Number of intercept length grain boundaries and determination of grain size G have been conducted automatically. Software for each of randomly chosen fields calculates number of intercept length grain boundaries and G-number from which, by approximation, (table 2, [9]) assesses $\overline{N_A}$, table 2. Table 2 points that conducted results of grain size calculation, relatively grain size/mm^2 with two semi-automatic methods of measurements on the samples etched with Barker's etch, are mutual similar (the intercept length method : $\overline{N_A}$ =54,2 zrna/mm^2, G=2,79; the intercept count method: $\overline{N_A}$ =49,85 zrna/mm^2, G=2,67). That points out the credibility of those two methods of measurement and confirmation that those two methods are useful for examination of samples etched with Barker's etch.

2. ANALYSIS OF PRECIPITATED "IN SITU" PHASES

Image 2 presents microstructure of alloy 5083 sample, etched in HF which has been observed by optical microscope with 500 x magnification. From the image is visible that in microstructure dominate two precipitated phases which are different by morphology and color – one is brighter and in the shape of Chinese script and other darker and has improper plate shape.

The differences between those two phases are clearly visible by observing of pictures made with the aid of scanning electronic microscope at the magnification of 750 x, image 3. Both phases are homogeneous, relatively homogeneities are not assessed inside phases although some phases coincidence, which refers to the fact that precipitation of those phases entered in different phases of solidification and cooling of the sample, relatively slab.

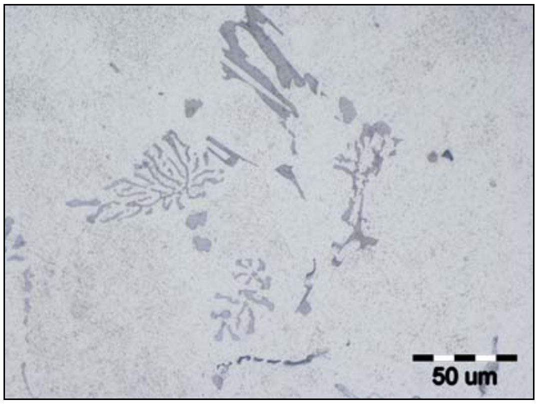

Fig. 2 Microstructure of Al alloy 5083 sample etched with HF, by magnification of 500 x

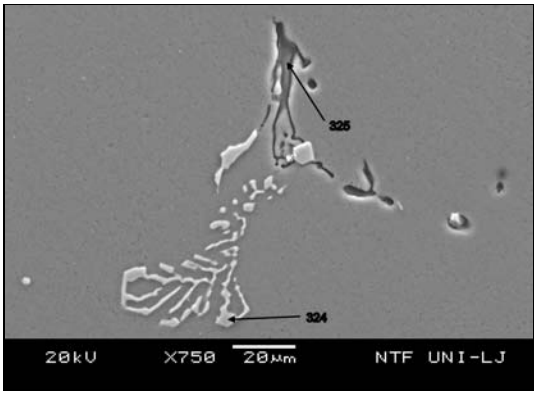

Fig 3 SEM micrograph of Al-alloy 5083 sample etched with HF, by magnification of 750 x

Analysis on details 324 and 325, marked on image 3, has been made by Energy Dispersive Spectrometer (EDS). On the following images SEM micrograph (figures 4a and 5a), as well as its matching EDX spectrums (figures 4b and 5b) has been presented.

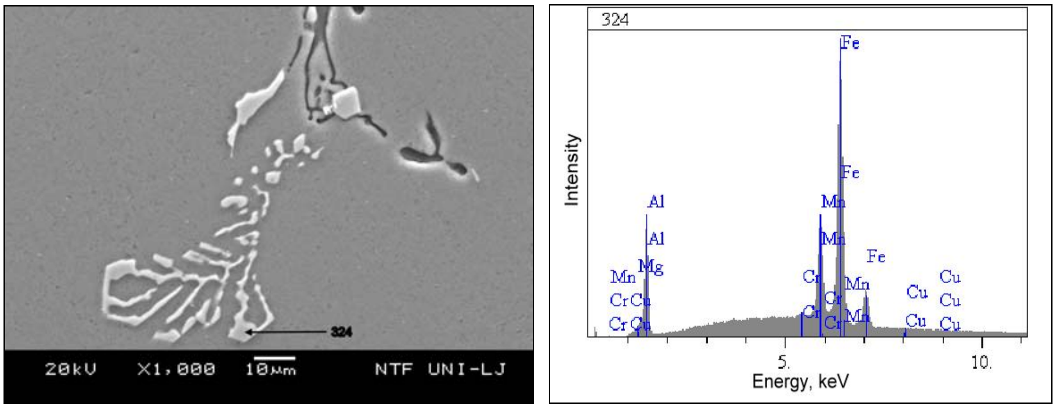

Fig. 4 a) SEM micrograph of Al-alloy 5083 sample, by magnification of 1000 x
b) EDX spectrum of Al-samples (detail 324)

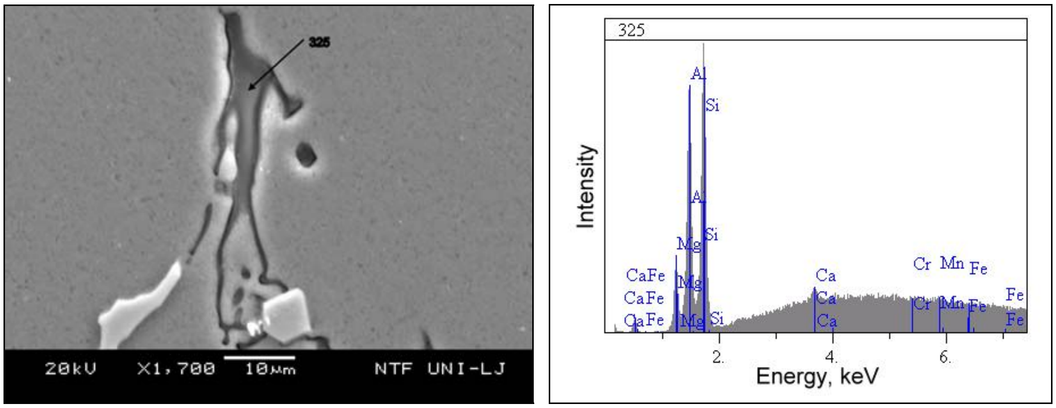

Fig 5 a) SEM micrograph of Al alloy 5083 samples, by magnification of 1700 x
b) EDX spectrum of Al-samples (detail 325)

Results of EDS analysis of details 324 and 325 have been given in table 3 in quantitative form.

Table 3: Chemical composition of chosen details 324 and 325 Al-alloy 5083 samples, wt. %

Detail	**Al**	**Mg**	**Cr**	**Mn**	**Fe**	**Cu**	**Si**
324	12,321	1.366	0,492	16,851	19,110	0,226	-
325	29,714	7,093	0,674	1,944	0,640	1,650	50,236

From the chemical analysis of observed phases conducted by energetic spectrometry, it could be assumed that the dark phase (detail 325) has improper plate shape type $Al_8FeMg_3Si_6$. Chemical analysis of brighter phase of the shape of Chinese script (detail 324) refers that it is most likely about phase type $(Fe,Mn,Cr)_2Mg_3Al_{18}$.

CONCLUSION:

1. Semi-automatic intercept length method, relatively intercept count method on the sample etched with Barker's etch has given almost identical values of grain size and number of grains per unit area (table 2).
2. Electrolytic etch (anodisation) with Barker's etch and observation of samples by polarized light, with the supplement of sensitive tint filter, gives good resolution of color contrast of different grains.
3. Use of software package for automatic assessment of grain size reconstruction of grain boundary was not possible.
4. Grain comparison method gives repeatability and reproducibility of estimation in the range from ± 1 number of grain size (table 2), what is in accordance with literature quotation [8].
5. In metal matrix complex intermetal phases have been precipitated and they differ by morphology and chemical composition.
6. On the base of EDS analysis of alloy 5083 sample etched with HF, it could be assumed that in the case of examination of dark phase of improper plate shape (detail 0325) is about the silicon rich phase of type $Al_8FeMg_3Si_6$. Chemical analysis of brighter phase, which is in the shape of Chinese script (detail 0324), refers that it is most likely about phase type $(Fe,Mn,Cr)_2Mg_3Al_{18}$.

LITERATURE:

[1] Dietrich G, Altenpohl, Aluminium: Technology, Aplications, and Environment, The Minerals, Metals & Materials Society (TMS), Pennsylvania, 1999.
[2] http://www.aluminium.org/education/TALAT/index.htm
[3] I. Duplančić: Obrada deformiranjem, Interna skripta, Fakultet elektrotehnike, strojarstva i brodogradnje, Split, 2004.
[4] «Standard Terminology Relating to Metallography», E 7 – 03, American National Standard Institute/ASTM,2003.
[5] «Standard Guide for Preparation of Metallographic Specimens», E 3 – 01, American National Standard Institute/ASTM, 2001.
[6] L. Stuparević, B. Stuparević, Metalografija, Nauka, Beograd, 2000.
[7] «Standard Practice for Microetching Metals and Alloys», E 407 – 99, American National Standard Institute/ASTM, 1999.
[8] «Standard Test Methods for Determining Average Grain Size», E 112 – 96, American National Standard Institute/ASTM, 2000.
[9] «Standard Test Methods for Determining Average Grain Size Using Semiautomatic and Automatic Image Analysis», E 1382 – 97, American National Standard Institute/ASTM, 1997.
[10] Małgorzata Warmuzek, ASM Handbook, Volume 9, Metallography and Microstructures, ASM International, Materials Park, Ohio, 2004.
[11] John E. Hatch, Aluminum, Properties and Physical Metallurgy, American Society for Metals, Metals Park, Ohio, 1988.

Remark: The Study is prepared under the complex project “Upgraded Casting Process of Slabs/Billets in Hard Wrought Alloys”, (TP – 02-0124-04, HITRA – TEST).

10. Savjetovanje o materijalima, tehnologijama, trenju i trošenju
10. Conference on Materials, Processes, Friction and Wear
MATRIB'05, Vela Luka, 23-25.06.2005.

PHASE CHANGE MATERIAL PERFORMANCE IN A NOVEL LOW ENERGY COOLING HEATING AND DAYLIGHT SYSTEM (LECVHAD)

PART III: FULL SCALE EXPERIMENTAL CHARACTERISATION AND FEASIBILITY STUDY

Anthony J. Farrell*, Brian Norton, and David Kennedy
*Corresponding author: Anthony.Farrell@dit.ie Ph: (+353) (01) 402 3000

Dublin Institute of Technology,
Faculty of Engineering,
Bolton Street,
Dublin 1, Ireland

Abstract :A novel Low Energy Cooling Heating Ventilation And Daylight (LECHVAD) system has been developed that provides ventilation of hot or cold air, and daylight to large-scale building developments. The thermal applications of the ventilation system are controlled using state of the art Latent Heat Thermal Storage (LHTS) to provide cool or heat energy. The storage is achieved using a *phase change material* (PCM). Phase change materials have proved useful in the past, for both heating and cooling applications, but as a result of excessively high or low melting temperatures (60°C or 8°C) were only suitable for applications about those temperatures, such as solar thermal energy storage or for cooling of electronic circuits.

More recently however, PCMs that melt at temperatures of 17 and 18 degrees Celsius have become available and may thus be applicable for thermal comfort applications that require cooling or heating of outdoor air to the melting temperature range. This paper presents the results of full scale experimental characterisation studies into the use of a commercially available PCM with a melting temperature of 17 degrees Celsius suitable for cooling and heating air in ventilation systems. The effective cooling or heating capacity is reported and the suitability of such systems is discussed. Areas for further research are identified and recommendations from this research are proposed.

Keywords: Phase change materials, latent heat thermal storage systems, PCM freezing phase, low energy cooling.

Acknowledgements
The author gratefully acknowledges the financial support from the DIT through their TERS funded Sustainable Energy Research Group (SERG).

1. Introduction

Conventional air conditioning systems heat and cool air using finned tube heat exchangers. The heat is exchanged from/to the incoming air stream to/from a heat exchange medium within the tubes. Water is a conventional form of heat exchange medium, which is heated using water boilers, and cooled using cooling towers and/or vapour compression refrigeration plant. Gravity flow Heat pipes provide a greater heat transfer rate because of their latent heat qualities and consist of no mechanical plant or equipment except for a rotary motor to change the tilt angle for gravity flow of the refrigerant (such as a compressor or evaporator). Further, because of the enhanced heat transfer rate, heat pipes produce significantly less air flow resistance and consequent fan power requirement for a given air flow rate. Heat pipes therefore provide the potential for substantial energy savings in air conditioning systems and consequent reductions in energy supply dependency and CO_2 emissions to the environment. This is a key driver of the European Energy Performance of Buildings Directive (Anon. 2002).

Heat pipes are conventionally used for hot air recovery whereby one portion of the heat pipe (the evaporator) is placed in a hot air stream (kitchen exhaust air) and the other portion (the condenser) is placed in a cold air stream (cool incoming air). The heat pipe therefore transfers the heat energy from the hot air stream to the cold air stream thereby heating the cold air stream and minimising heating energy requirements therein. Heat pipes in this arrangement cannot therefore provide cooling of hot incoming air (evaporation action on heat pipe) since the exhaust air stream will be at least equal to the incoming air temperature, which is greater than the condensing temperature of the refrigerant. This paper proposes the use of phase change material in place of the conventional exhaust air stream and therefore to provide both heating (from a melted PCM state) and cooling (from a frozen PCM state) of cool or hot incoming air respectively. A conventional heat pipe heat exchanger is experimentally characterised for this application and the capacity or efficiency in terms of duration heating or cooling is derived for the maritime climate of the U.K. and Ireland. A baseline reference supply condition, as required by a low energy displacement ventilation system, of 18 and 20 degrees Celsius is selected for summer (cooling) and winter (heating) operation respectively,

2. Experiments

2.1. Background

An industrial standard horizontally mounted heat pipe heat exchanger was set up in a ventilation circuit as shown in Figure 1. The airside portion of the heat exchanger was 1m square and the energy storage (PCM) side 1.6m long by 1m wide as derived from PCM analysis, the volume of which formed the subject of part II of this paper (Farrell *et al.* 2004). The PCM side was modified and fitted with a base and was filled with PCM. Each surface of the PCM side was then insulated and wrapped with food wrap or ‘cling film’ to form an airtight enclosure. The heat exchanger was mounted on a frame that rotated up to five degrees about a fulcrum at the air duct wall. The supply air was ducted to the top of the heat pipe from a lab window opening fitted with a fan (0.5kg/s) and was fitted with a 5kW air element heater to simulate summer maximum temperature conditions. The air was supplied to the room from a duct connected below the heat pipe. Temperature sensors were located at the inlet and outlet planes to and from the heat exchanger enclosure.

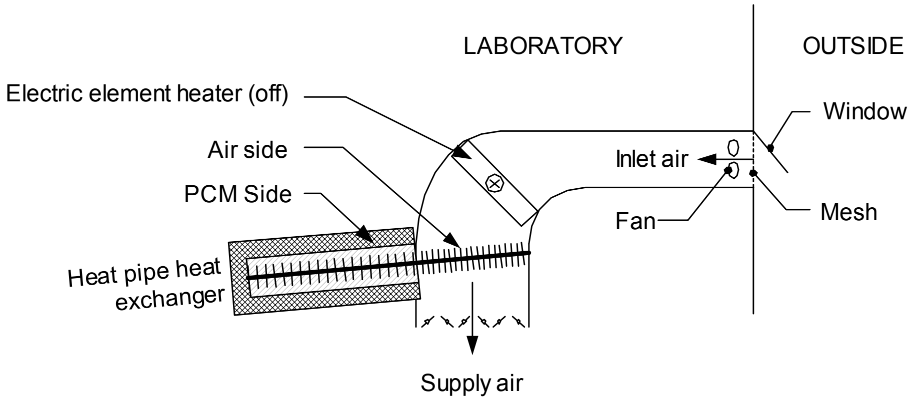

Heating experiment

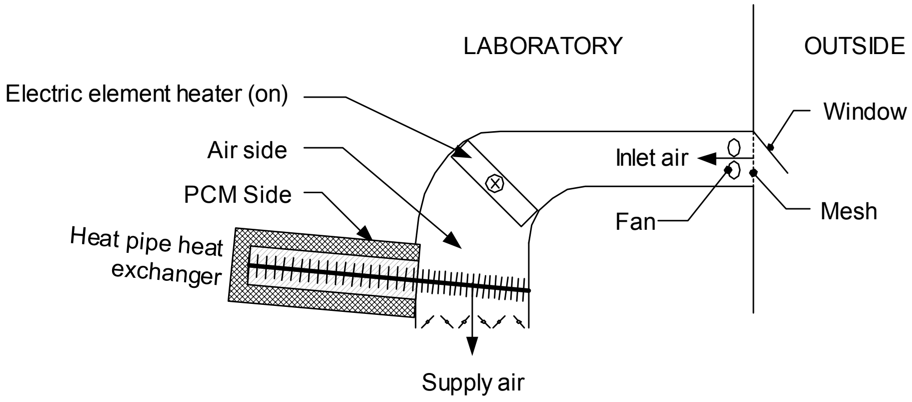

Cooling experiment

Figure 1. Heat pipe heat exchanger PCM experiments for heating (top) and cooling (bottom) operation

2.2 Heating experiment

The PCM was brought to a completely melted state by providing a hot air stream over the evaporator section, which was set by tilting the PCM side five degrees upwards. The melted state was achieved when heat transfer to the PCM became negligible, i.e. the PCM state was liquid and sensible heat exchange was taking place to bring the PCM toward the temperature of the oncoming hot air stream. When this state was achieved the heat exchanger angle was reversed such that the air stream side now became the condenser with the condenser air stream side tilting five degrees upwards. At this point the temperature sensors began logging, the air heater was turned off, and cool outdoor air was supplied. The supply air temperature was logged for a period of 9 hours heating (working day).

2.3 Cooling experiment

The PCM was brought to a completely frozen state by the heating experiment. The frozen state was achieved when heat transfer to the PCM became negligible, i.e. the PCM state was solid and sensible heat exchange was taking place to bring the PCM toward the temperature of the oncoming cool air stream. At this point the heat exchanger angle was reversed to the original heating angle with the PCM side tilting five degrees upwards. Hot air was introduced from outside and the sensors began logging. The supply air was logged for a period of 9 hours cooling (working day).

3. Results and Analysis

Figure 2. presents the results from the heating experiment. The PCM provides sufficient heat to meet the desired supply condition of 18 degrees Celsius for one hour thereby providing an equivalent of 100 per cent savings on the heating system for that period. The PCM begins to enter its frozen state thereafter where sensible heat exchange begins to take place and therefore heating effect reduces. The PCM continues to provide some 20 per cent savings on the heating system for a further three hours maintaining a supply air condition of 15 degrees Celsius, dropping to some eight per cent savings for the remaining five hours in phase with the outdoor temperature profile. The system therefore provides a resultant heating energy savings between 22 and 100 per cent between nine and one hours of operation respectively. Table 1. presents the system energy savings for system durations from one to nine hours.

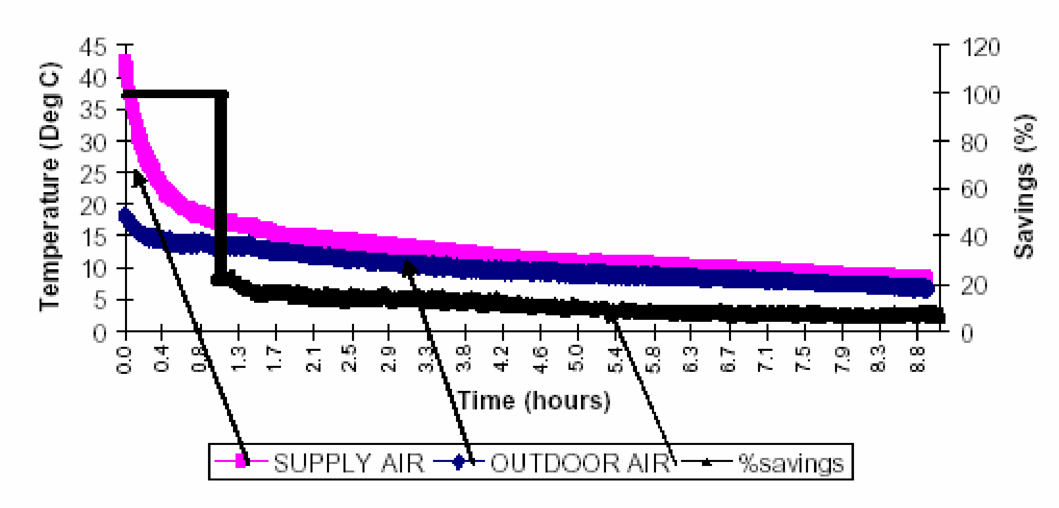

Figure 2. Heating experiment results

Heating duration (d)	1	2	3	4	5	6	7	8	9
Energy savings (%)	100	20	20	20	8	8	8	8	8
Resultant savings (%) *f*(d)	100	60.00	46.67	40.00	33.60	29.33	26.29	24.00	22.22

Table 1. Summary of heating energy savings relative to system operating duration

Figure 3. presents the cooling experiment results. Unlike the heating experiment, the cooling potential from PCM is far greater. The PCM provides sufficient cooling energy storage to meet the desired supply condition of 20 degrees C for the complete cooling duration of nine hours thereby eliminating the requirement of a conventional cooling system. The system is thus 100 per cent efficient for the given duration.

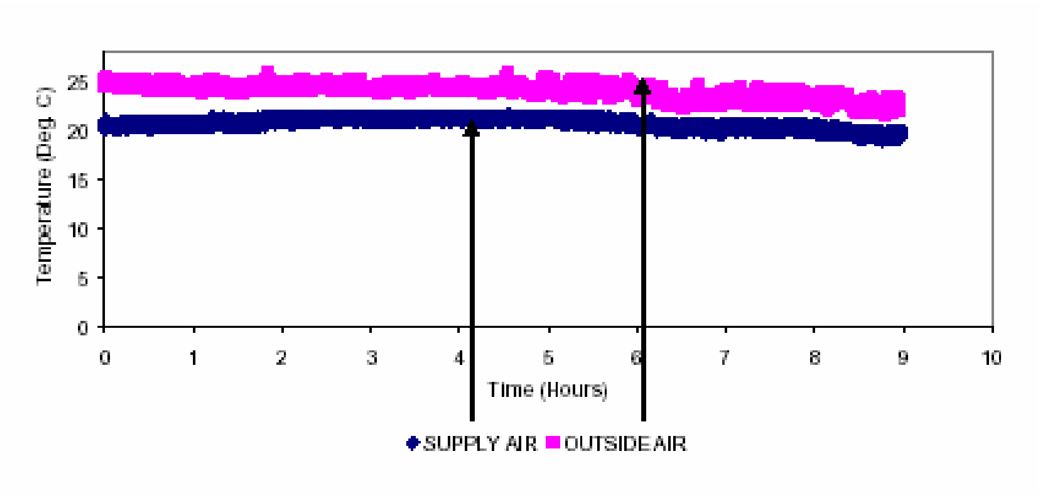

Figure 3. Cooling experiment results

4. Discussion

The system operating duration is a fundamental component of the system efficiency and performance. Further, the temperature difference between the outdoor and supply air will ultimately determine suitability of the system and its application. It was observed during the experiments that the cooling operation performance increased significantly with increased outdoor temperature. For e.g. with an outdoor temperature of 40 degrees Celsius, the supply condition was approximately 30 degrees Celsius, a 100 per cent performance increase, but nevertheless, still supplying air greater than the desired condition of 20 degrees Celsius. This effect could not be tested under heating conditions, as outdoor temperatures throughout the experimental period did not drop below 5 degrees Celsius; however, if the effect observed recurred under heating application, the operating efficiency and associated energy savings presented in Table 1. would increase substantially. The PCM melting temperature appears to range through some four degrees Celsius. During the cooling period when the PCM was in the melting cycle, a mean supply air at a condition of 20 degrees Celsius was recorded and therefore suggests that this is the melting point temperature. During the heating operating period, the freezing cycle, the PCM maintained a supply air condition for some three hours at 15 degrees Celsius (with varying outdoor air temperature below this value) and energy savings of some 20 per cent, after which the supply temperature profile matched the outdoor air at just 8 per cent energy savings. The PCM freezing temperature is therefore approximately 15 degrees Celsius.

5. Conclusion

A conventional heat pipe heat exchanger was modified for use of PCM as the heat recovery component *and* the cooling supply component of an air conditioning system. A PCM with a melting temperature of 17 degrees Celsius was used although the actual melting range proved higher at approximately 20 degrees Celsius during cooling operation (melting cycle) and 15 degrees Celsius during the heating operation (freezing cycle) and concurs with part II of this paper. The laboratory test conditions provide an average supply air temperature of 12 and 25 degrees Celsius over a nine-hour duration for the heating and cooling experiments respectively.

During the melt cycle (summer operation), it was observed that a 100 per cent increase in system energy performance was permissible when the outdoor air temperature approached double the reference temperature of 25 degrees Celsius. The system provides 100 per cent cooling energy savings for maritime climates since the PCM can be brought to the frozen state, prior to the cooling period, at nighttime when the mean average outdoor temperature remains below the melting temperature of 20 degrees Celsius.

The system provides heating energy savings of between 22 and 100 per cent over an operating period of nine and one hours of operation respectively, based on a maximum temperature difference of five degrees between the supply air and outdoor air condition. The Heating cycle may have significantly increased the system energy savings where greater temperature differentials are experienced as was observed with the melting cycle. It is therefore recommended that the further research consider greater temperature differentials of at least 10 degrees Celsius be considered in future heating experiments to identify the consequent impacts on energy efficiency and system performance.

6. References:

Anon. (2002) 'Directive 2002/91/EC of the European Parliament and of the Council of 16 December 2002 on the energy performance of buildings', *Official Journal of the European Communities,* **L 1**, pp 65 – 71.

Farrell, A.J. and Kennedy, D.M. (2004) 'Phase Change Material performance in a novel Low Energy Cooling Heating And Daylight system (LECVHAD), PART II: The freezing phase', *MATRIB 2004 conference on Materials and Tribology, Vela Luka, Croatia, June 2004.*

METODE KARAKTERIZACIJE TANKIH PREVLAKA

METHODS OF CHARACTERISATION OF THIN LAYERS

Krešimir Grilec
Faculty of Mechanical Engineering and Naval Architecture
Ivana Lučića 1, 10000 Zagreb, Croatia
kgrilec@fsb.hr

Remigiusz Michalczewski
Institute for Terotechnology (ITeE)
K. Pulaskiego 6/10, 26-600 Radom, Poland
michalcz@itee.radom.pl

Sažetak: U radu su opisane neke od metoda za analizu materijala, a koje se najčešće koriste za karakterizaciju tankih prevlaka. Dan je kratki opis tih metoda, te su prikazani neki rezultati mjerenja na primjeru ZrO_2 sol-gel prevlaka nanešenih na čeličnu podlogu tehnikom uranjanja.

Ključne riječi: debljina prevlake, prionjivost prevlake, topografija površine, nanotvrdoća

Abstract:. In this paper some methods of characterization of materials are described, especially methods for characterization of thin layers. Some results of analyzing ZrO_2 sol-gel layers are also presented.

Key words: layer thickness, layer adhesion, topography, nanohardness

1. UVOD

Karakterizacija tankih prevlaka može se provesti brojnim tehnikama. Prema [1], najvažnija svojstva prevlaka su: prionjivost, debljina, hrapavost, otpornost koroziji, karakteristike trenja i trošenja, tvrdoća, porozitet, sastav, zaostala naprezanja i struktura..

2. MJERENJE DEBLJINE PREVLAKE

Postoji više metoda za određivanje debljine prevlaka, ali malo njih je moguće koristiti pri mjerenju vrlo tankih prevlaka (svega nekoliko μm). Jedna od tih metoda je metoda slobodne kugle (slika 1 i 2).

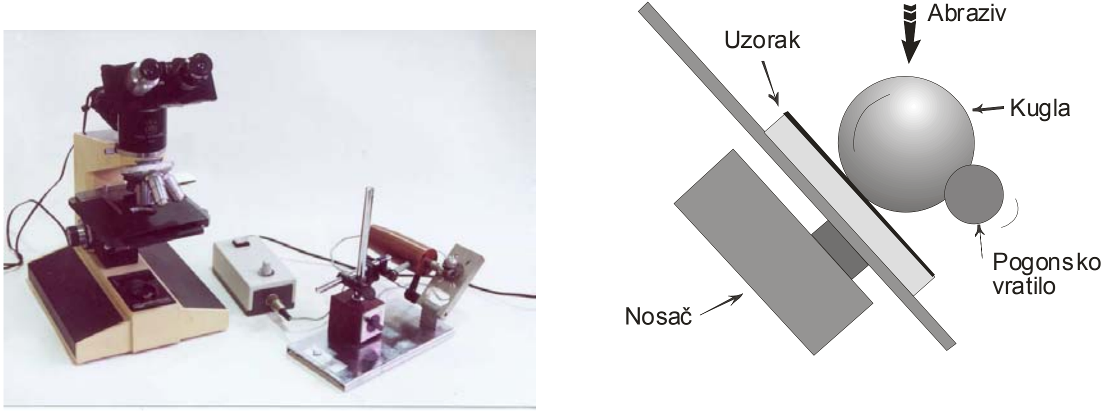

Slika 1 – Uređaj za mjerenje debljine prevlake metodom slobodne kugle, [2]

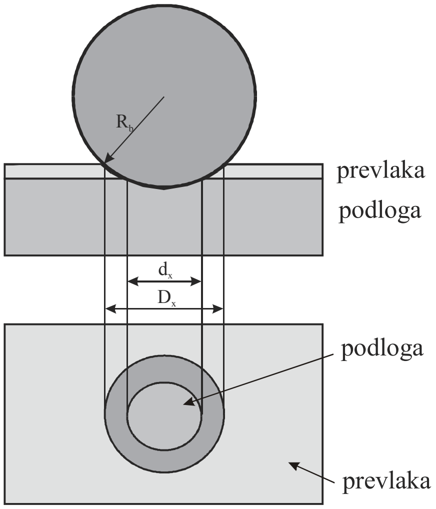

Debljina prevlake može se izračunati prema sljedećem izrazu:

$$x = \sqrt{R_b - \left(\frac{d_x}{2}\right)^2} - \sqrt{R_b - \left(\frac{D_x}{2}\right)^2}$$

Slika 2 – Određivanje debljine prevlake

3. TOPOGRAFIJA POVRŠINE

Najjednostavniji uređaj za analizu topografije površine je profilometar. Profilometar osim standardnih karakteristika hrapavosti površine (navedeni na slici 3), može iscrtati i topografiju površine. Kod vrlo glatkih površina za analizu topografije može se koristiti mikroskop atomske sile (atomic force microscope, AFM). Na slici 4 prikazana je topografija površine ZrO_2 sol-gel prevlake.

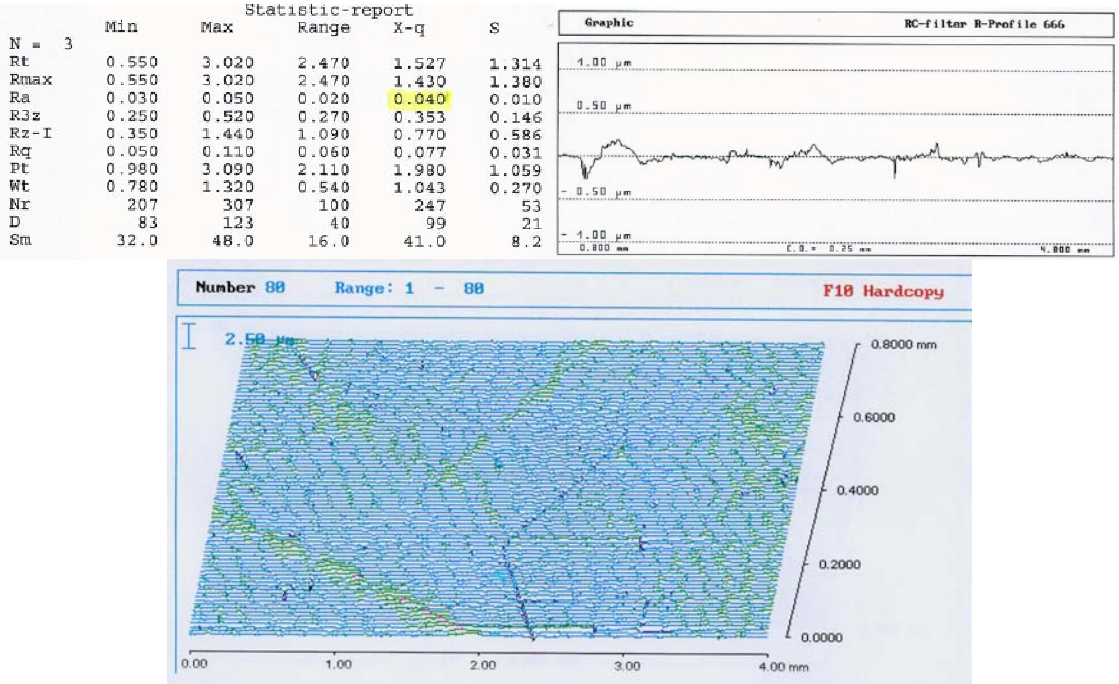

Statistic-report

N = 3	Min	Max	Range	X-q	S
Rt	0.550	3.020	2.470	1.527	1.314
Rmax	0.550	3.020	2.470	1.430	1.380
Ra	0.030	0.050	0.020	0.040	0.010
R3z	0.250	0.520	0.270	0.353	0.146
Rz-I	0.350	1.440	1.090	0.770	0.586
Rq	0.050	0.110	0.060	0.077	0.031
Pt	0.980	3.090	2.110	1.980	1.059
Wt	0.780	1.320	0.540	1.043	0.270
Nr	207	307	100	247	53
D	83	123	40	99	21
Sm	32.0	48.0	16.0	41.0	8.2

Slika 3 – Karakteristike hrapavosti i topografija površine ZrO_2 sol-gel prevlake, analizirane na profilometru T-2000

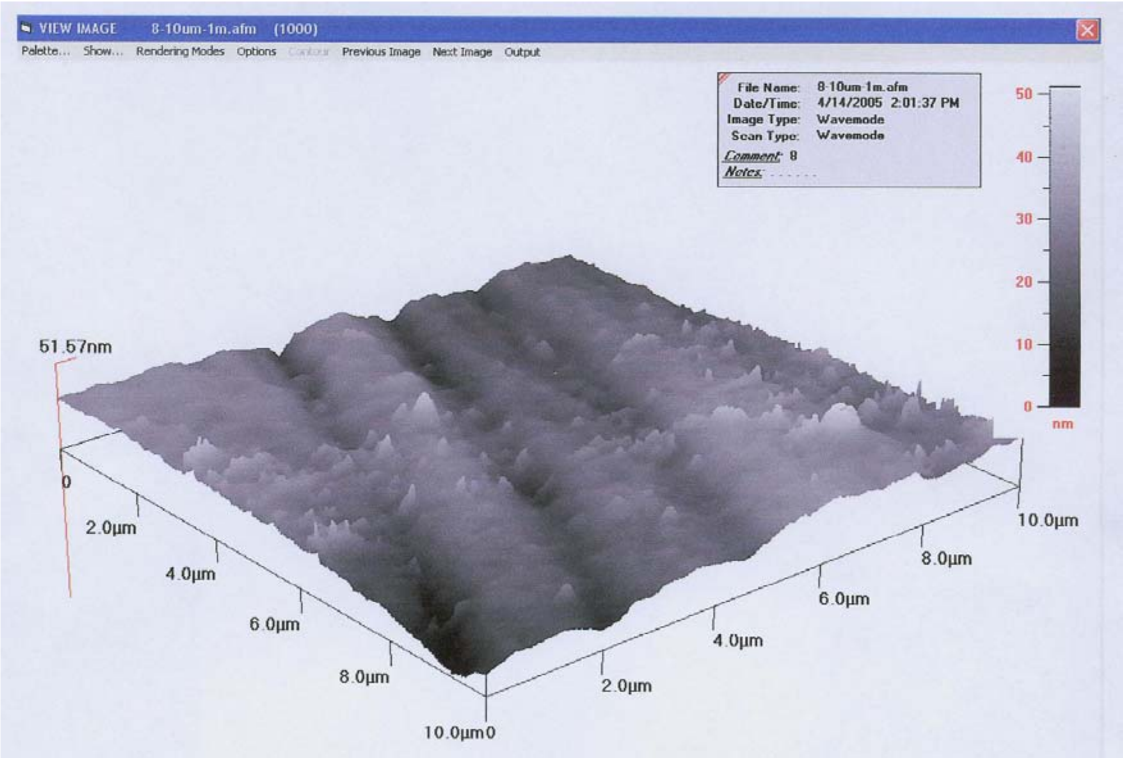

File Name: 8-10um-1m.afm
Date/Time: 4/14/2005 2:01:37 PM
Image Type: Wavemode
Scan Type: Wavemode
Comment: 8
Notes: ......

Slika 4 - Topografija površine ZrO_2 sol-gel prevlake, analizirana na mikroskopu atomske sile (AFM)

4. ODREĐIVANJE SADRŽAJA KEMIJSKIH ELEMENATA

Za određivanje sadržaja kemijskih elemenata u materijalu može se koristiti više različitih metoda, a za analizu prevlaka najinteresantnije su one koje omogućuju praćenje sadržaja kemijskih elemenata u ovisnosti o udaljenosti od površine. Na slikama 5 i 6 prikazana je energijska disperzna spektrometrija (Energy dispersive spectrometer, EDS) kod koje je dana kvalitativna analiza sadržaja kemijskih elemenata unutar određenog površinskog sloja (mnogo veće debljine od debljine same prevlake), a na slikama 7 i 8 optičko emisijska spektrometrija (Glow discharge optical emission spectroscopy, GDOES) kod koje je prikazan profilni raspored sadržaja prisutnih kemijskih elemenata.

Slika 5 – Energijski disperzni spektrometar, EDS (u kombinaciji sa scanning elektronskim mikroskopom, SEM), [3]

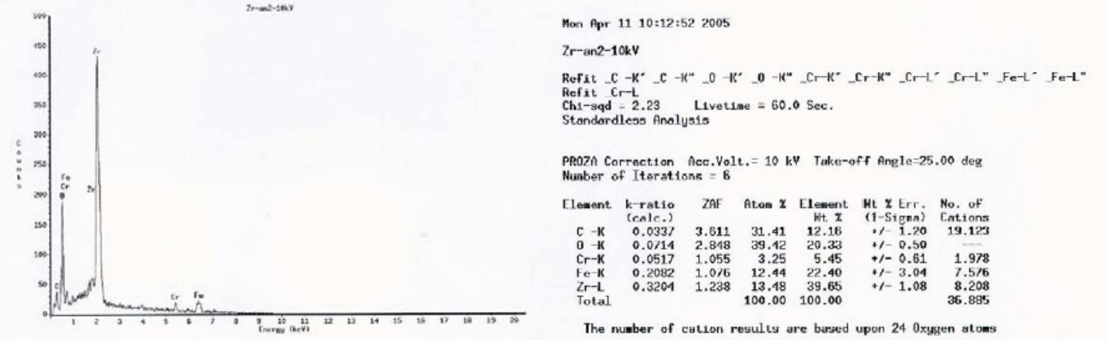

```
Mon Apr 11 10:12:52 2005

Zr-an2-10kV

Refit _C -K' _C -K" _O -K' _O -K" _Cr-K' _Cr-K" _Cr-L' _Cr-L" _Fe-L' _Fe-L"
Refit _Cr-L
Chi-sqd = 2.23     Livetime = 60.0 Sec.
Standardless Analysis


PROZA Correction  Acc.Volt.= 10 kV  Take-off Angle=25.00 deg
Number of Iterations = 6

Element  k-ratio    ZAF    Atom %  Element  Wt % Err.  No. of
         (calc.)                    Wt. %   (1-Sigma)  Cations
  C -K   0.0337   3.611    31.41    12.16   +/- 1.20   19.123
  O -K   0.0714   2.848    39.42    20.33   +/- 0.50     ---
  Cr-K   0.0517   1.055     3.25     5.45   +/- 0.61    1.978
  Fe-K   0.2082   1.076    12.44    22.40   +/- 3.04    7.576
  Zr-L   0.3204   1.238    13.48    39.65   +/- 1.08    8.208
  Total                   100.00   100.00              36.885

   The number of cation results are based upon 24 Oxygen atoms
```

Slika 6 – Kvalitativna analiza kemijskih elemenata u ZrO_2 sol-gel prevlaci i osnovnom materijalu, provedena na energijskom disperznom spektrometru, EDS

Slika 7 - Optičko emisijski spektrometar (GDOES), [3]

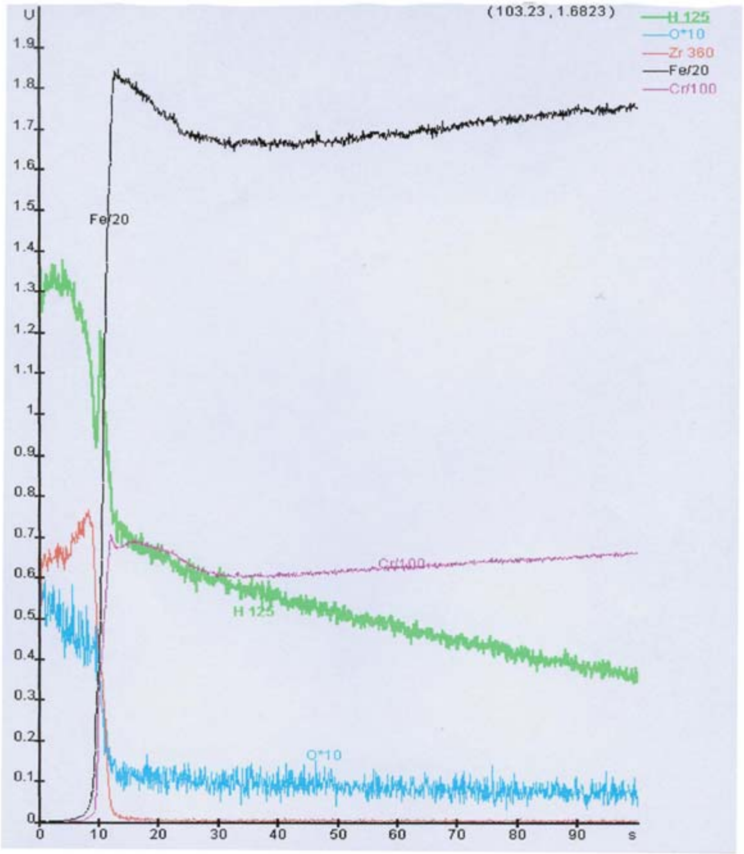

Slika 8 – Sadržaj kemijskih elemenata u ZrO_2 sol-gel prevlaci i osnovnom materijalu, analiziran na optičko emisijskom spektrometru, EDS

5. PROINJIVOST PREVLAKE

Najčešća metoda za mjerenje prionjivosti prevlake je tzv. "scratch test". Kod ove metode se utiskivač Rockwell tipa povlači preko površine prevlake konstantnom brzinom i kontinuiranim porastom sile utiskivanja. Mjera za prionjivost su sile kod kojih se javljaju prve pukotine u prevlaci, zatim djelomično odlamanje prevlake te potpuno odvajanje prevlake sa površine osnovnog uzorka. Uređaj je prikazan na slici 9, tipičan izgled brazde ("scratch") na slici 10, a izgled izvještaja prilikom ovog ispitivanja na slici 11.

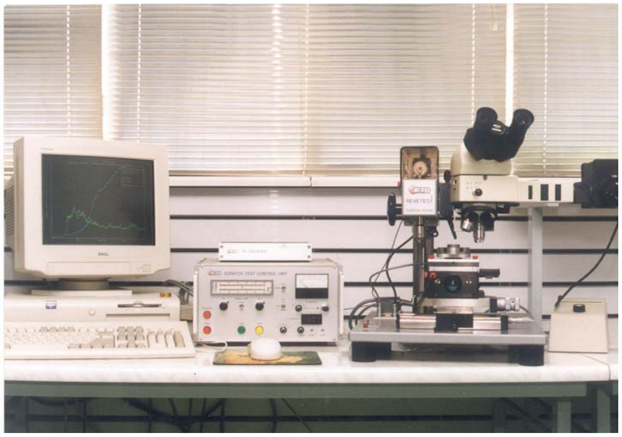

Slika 9 – Uređaj za brazdanje ("scratch tester")

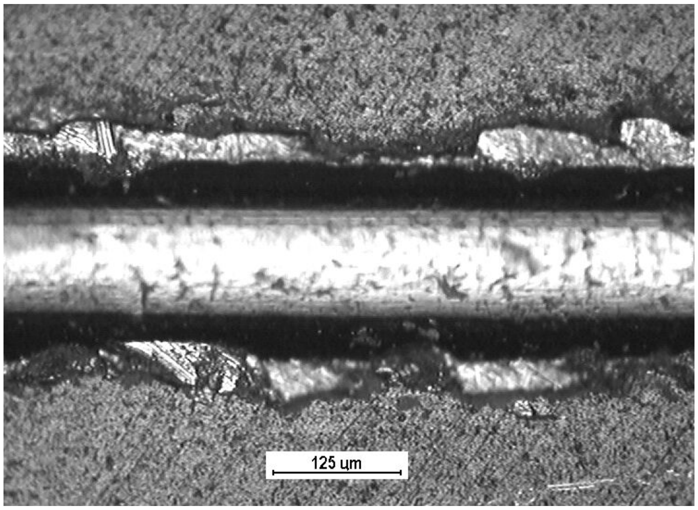

Slika 10 – Izgled brazde prilikom "scratch testa"

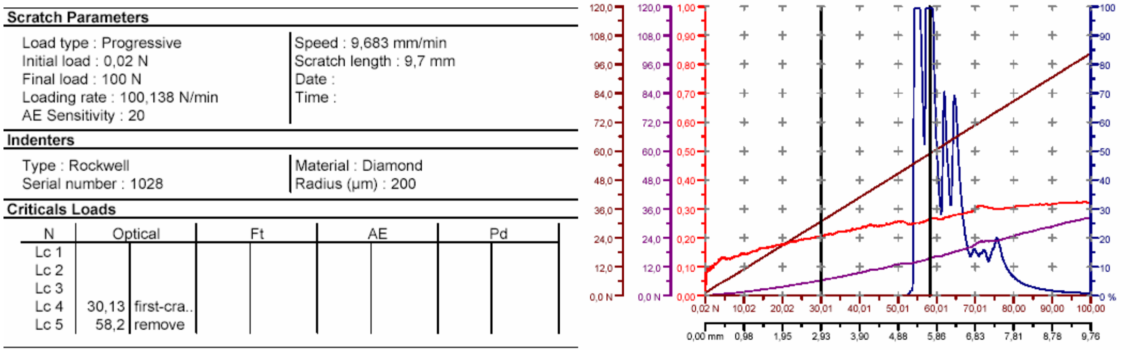

Scratch Parameters

Load type : Progressive
Initial load : 0,02 N
Final load : 100 N
Loading rate : 100,138 N/min
AE Sensitivity : 20

Speed : 9,683 mm/min
Scratch length : 9,7 mm
Date :
Time :

Indenters

Type : Rockwell
Serial number : 1028

Material : Diamond
Radius (µm) : 200

Criticals Loads

N	Optical		Ft		AE		Pd	
Lc 1								
Lc 2								
Lc 3								
Lc 4	30,13	first-cra..						
Lc 5	58,2	remove						

Slika 11 – Izvještaj za "scratch test" ZrO_2 sol-gel prevlake

6. Nanotvrdoća i modul elastičnosti

Za određivanje tvrdoće vrlo tankih prevlaka, opterećanja koja se koriste kod korištenja mikrotvrdomjera su prevelike budući da podloga utječe na rezultate mjerenja. Zbog toga za prevlake koristimo nanotvrdomjere koji koriste još manja opterećenja. Na slici 12 prikazan je nanotvrdomjer tvrtke CSEM.

Slika 12 - Nanotvrdomjer CSEM NHT

Za razliku od mikrotvrdomjera nanotvrdomjeri koriste utiskivač tipa Berkovich (trostrana piramida). Ovi tvrdomjeri prikazuju ovisnost dubine prodiranja utiskivača u ovisnosti o trenutnom opterećenju. Osim toga pružaju i informaciju o modulu elastičnosti ispitivanog materijala. Tipičan izvještaj o mjerenju nanotvrdoće prikazan je na slici 13.

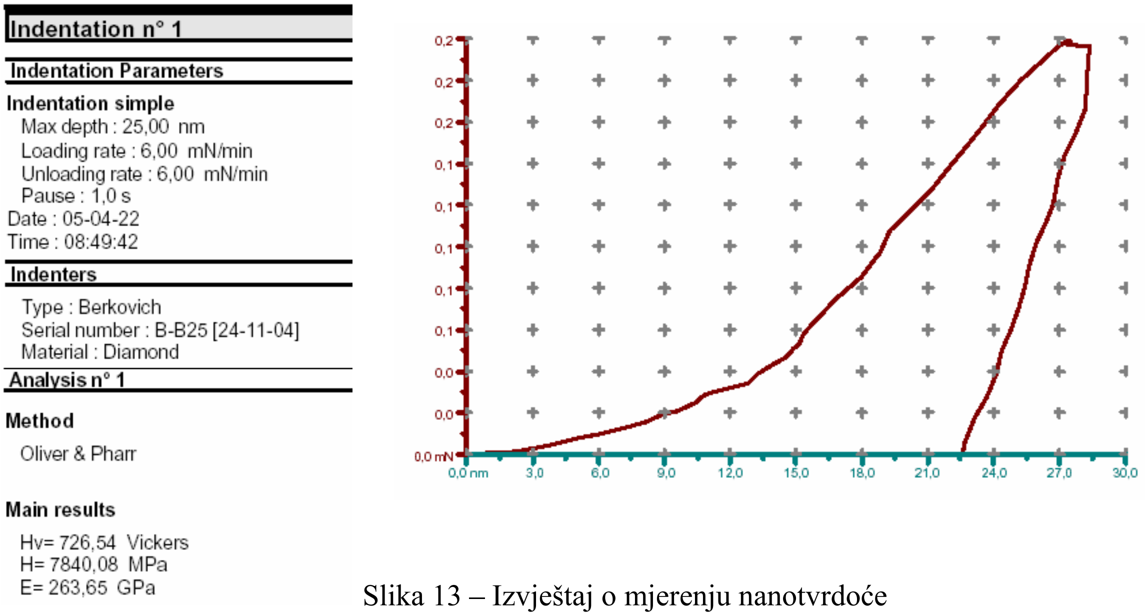

Indentation n° 1

Indentation Parameters

Indentation simple
Max depth : 25,00 nm
Loading rate : 6,00 mN/min
Unloading rate : 6,00 mN/min
Pause : 1,0 s
Date : 05-04-22
Time : 08:49:42

Indenters

Type : Berkovich
Serial number : B-B25 [24-11-04]
Material : Diamond

Analysis n° 1

Method

Oliver & Pharr

Main results

Hv= 726,54 Vickers
H= 7840,08 MPa
E= 263,65 GPa

Slika 13 – Izvještaj o mjerenju nanotvrdoće

ZAKLJUČAK

Postoje brojne tehnike kojima je moguće provesti karakterizaciju prevlaka. Na izbor tehnike koju ćemo koristiti utječe više čimbenika od kojih je jedan i dostupnost uređaja za karakterizaciju.

LITERATURA

[1] K. Holmberg, A. Matthews, "Coatings Tribology", Elsevier, Amsterdam – London – New York – Tokyo, 1994
[2] Z. Schauperl, "Utjecaj tvrdoće podloge na trajnost tankih tvrdih prevlaka", doktorska disertacija, FSB, Zagreb, 2000.
[3] http://www.itee.radom.pl/english/tribologia.htm

10. Savjetovanje o materijalima, tehnologijama, trenju i trošenju
10. Conference on Materials, Processes, Friction and Wear
MATRIB'05, Vela Luka, 23-25.06.2005.

COPARISON OF SURFACE ROUGHNESS OF DENTAL CERAMICS BEFORE AND AFTER ACID MEDIUM EXPOSURE

USPOREDBA HRAPAVOST DENTALNE KERAMIKE PRIJE I NAKON IZLAGANJA KISELOM MEDIJU

Marko Jakovac[1], Sanjin Mahović[2], Lidija Ćurković[2], Jasenka Živko-Babić[1]

[1]School of Dental Medicine, University of Zagreb, Zagreb, Croatia
[2]Faculty of Mechanical Engineering and Naval Architecture, University of Zagreb, Zagreb, Croatia

Abstract: Dental ceramics are considered to be chemically inert. However, influence of oral cavity could change its surface roughness. The aim of this study was to investigate the surface roughness before and after acid medium exposure of two different types of dental ceramics. The samples were made of feldspathic ceramic and glass-ceramic. The roughness of each sample was measured on three spots before and after exposure to 4 % solution of acetic acid.

The results showed that only feldspathic ceramic had significant difference in surface roughness after acid exposure.

The results in this study were very similar to those found in literature. The main reason for different reaction to acid medium is different microstructure of glass- and feldspathic ceramic. It could be concluded that glass-ceramic had better inertness to acid exposure and therefore it is more biocompatible then feldspathic ceramic.

Key words: dental ceramics, surface roughness.

Sažetak: Dentalna keramika smatra se kemijski inertna. Međutim, utjecaj oralne sredine mijenja njenu površinsku hrapavost. Cilj ove studije bio je ispitati promjenu površinske hrapavosti dvije vrste keramika nakon izlaganja kiselom mediju. Uzorci su bili izrađeni od glinične i staklo- keramike. Površinska hrapavost svakog uzorka mijerena je na tri mijesta prije i nakon izlaganja 4 % otopini octene kiseline.

U rezultatima je dobiveno da je samo glinična keramika pokazala značajnu promijenu površinske hrapavosti nakon izlaganja kiselini.

Ovi rezultati se poklapaju s onima nađenim u literaturi. Razlog različitoj reakciji na kiselom mediju je u različitoj mikrostrukturi glinične i staklokeramike. Može se zaključiti da staklokeramika zbog svoje inertnost biokompatibilnija od glinične keramike.

Ključne riječi: dentalna keramika, površinska hrapavost.

Intoduction

There are several *in vitro* studies of chemical behavior of dental materials. For this purpose the artificial saliva and distilled water are the most used media (1,2,3). But, the acid media, for example hydrochloride acid (4) and acetic acid (5, 6) are used for faster degradation and longer prediction of chemical behavior of dental ceramic. The investigation with media with lower pH is suitable for cases when patients have some gastric problems. The ISO standard 6872 (6) also suggest acid (4 % acetic acid) as media for chemical degradation of dental ceramic. The acetic acid is the most used acid in household. The pH value of that acid (2, 4) is similar to same refreshing drinks, fruits and to pH values measured in places under plaque accumulation in oral cavity. Acetic acid is weak organic acid but enough corrosive to glass (7). Therefore, acetic acid has been used in this study.

By influence of oral cavity, the surface of dental ceramic could change its roughness. Therefore, the ceramic properties, for example excellent esthetics, inertness to different media, good biocompatibility, low accumulation of dental plaque and good mechanical properties are in doubt (8).

The aim of this study was to investigate the surface roughness before and after acid exposure of two different types of dental ceramics.

Materials and methods

The samples were made of feldspathic ceramics - sample A (Vitadur Alpha, Vita-Zahnfabrik, Bad Säckingen, Germany) and glass-ceramic - sample C (IPS Empress 2- apatite ceramic, Ivoclar-Vivadent, Schaan, Liechtenstein). One sample for each material in platelet-form, with dimensions 10 x 10 x 2 mm, was made according to manufacturers' instructions. The samples were glazed over the whole surface to imitate the actual restorations from dental laboratories as close as possible. Then, samples were washed with distilled water in the ultrasonic bath (UltraSonic Bath Model 1510 DTH, Electron Microscopy Sciences, Hatfield, USA) (ISO 3696), dried in the sterilizer (Instrumentaria, Zagreb, Croatia) at 150 ± 5 ºC for 4 hours. The roughness of each sample was measured on three spots by means of Perthometer S&P 4.5, (Feinprut Perthen GmbH, GOETTINGEN, Deutschland). After that, every sample was transferred to a plastic polypropylene (PP) flask with 25.0 mL of 4 % acetic acid (CH_3COOH). Samples were completely immersed into the solution. Afterwards, flasks were transferred to thermostatic shaking assembly (Innova 4080 Incubator-Shaker, Herisau, Switzerland) at 80 ºC, 200 rpm, for 16 hours. Then, the samples were removed from the flasks, washed and dried. The roughness was measured again.

Results and Discussion

The parameters measured on samples surface were:
R_a – Arithmetical mean deviation (Figure 1)
W_t – Waviness depth (Figure 1)
R_k – Core roughness depth (Figure 2)
R_{pk} – Reduced peak height (Figure 2)
R_{vk} – Reduced valley depth (Figure 3)
A_1- Material filled profile peak area (Figure 3)
A_2 – Lubricant filled profile valley (Figure 4)
M_{r1} – Material component relative to peaks (Figure 4)
M_{r2}- Material component relative to valleys (Figure 5)

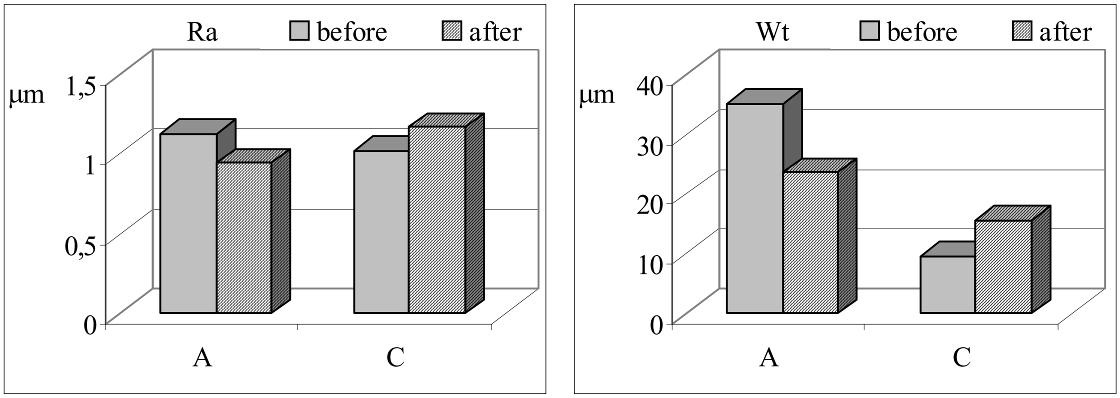

Figure 1. Values of arithmetical mean deviation (Ra, µm) and waviness depth (W_t, µm) *of feldspathic ceramic (sample A) and glass-ceramic (sample C) before and after immersion in 4 % solution of acetic acid.*

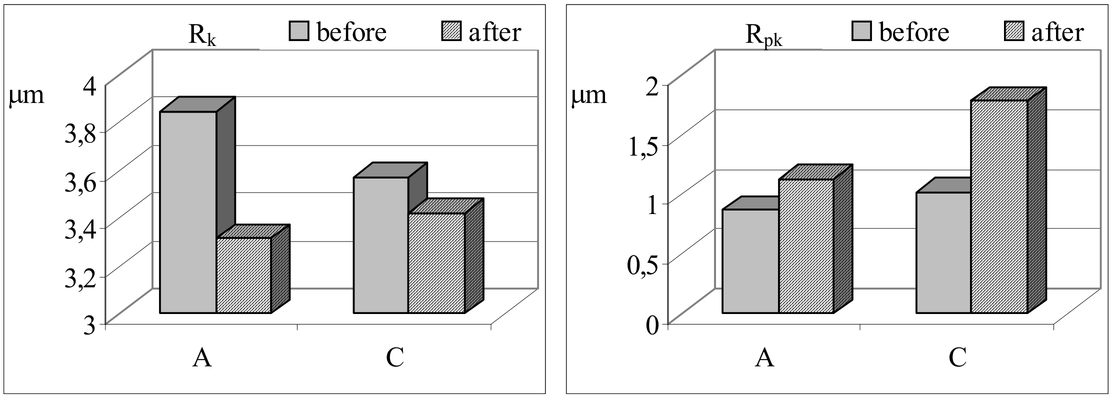

Figure 2. Values of core roughness depth (R_k, µm) and reduced peak height (R_{pk}, µm) of feldspathic ceramic (sample A) and glass-ceramic (sample C) before and after immersion in 4 % solution of acetic acid.

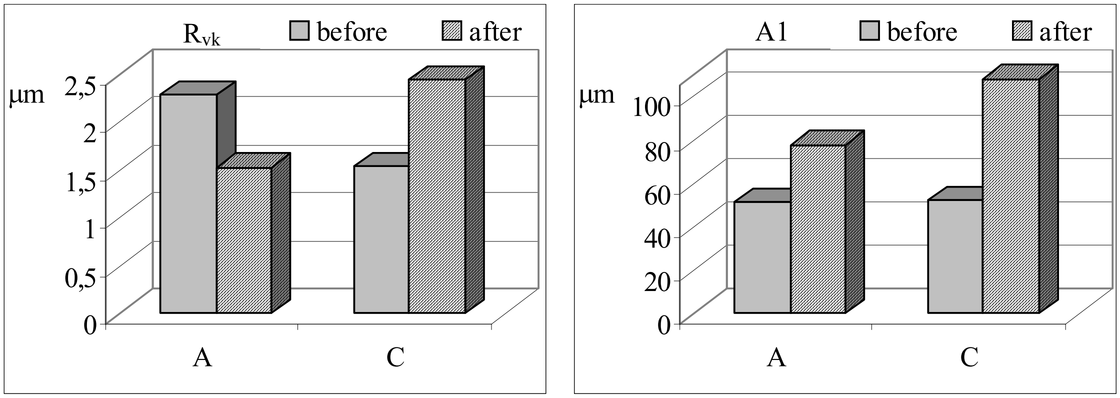

Figure 3. Values of reduced valley depth (R_{vk}, µm) AND material filled profile peak area (A_1, µm) of feldspathic ceramic (sample A) and glass-ceramic (sample C) before and after immersion in 4 % solution of acetic acid.

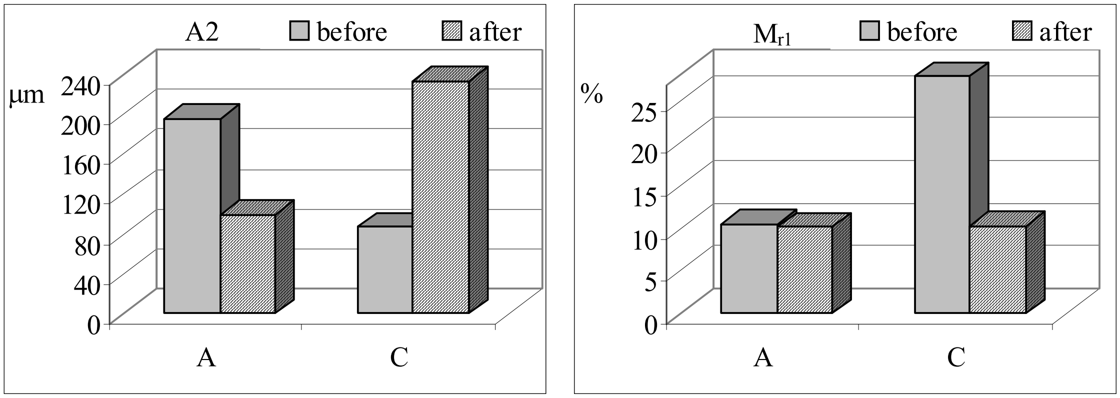

Figure 4. Values of lubricant filled profile valley (A_2, μm) and material component relative to peaks (M_{r1}, %) of feldspathic ceramic (sample A) and glass-ceramic (sample C) before and after immersion in 4 % solution of acetic acid.

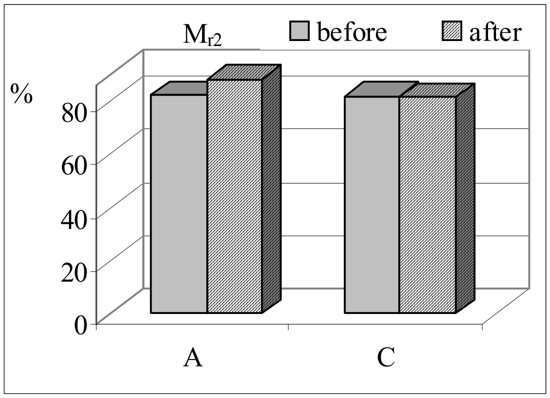

Figure 5. Values of material component relative to valleys (M_{r2}, %) of feldspathic ceramic (sample A) and glass-ceramic (sample C) before and after immersion in 4 % solution of acetic acid.

The results (Figs 1-9) showed that only feldspathic ceramic had significant difference in surface roughness after acid exposure.

For most different dental ceramics chemical degradation cause surface roughness and subsequently wear of antagonistic tooth or restorative material, increase of plaque accumulation, weaken its structure by causing the critical ions exchange on surface and cause more sensibility of dental ceramic to further chemical degradation (7).

The results obtain with this study are in correlation to our previous investigation of chemical stability of ceramic materials (9). In that study samples of glass-ceramic were chemically more stabile than samples of feldspathic ceramic. Millding at all. (7) investigated surface roughness of dental ceramics and had similar results to results found in this study. They also found that only feldspathic ceramic showed statistical differences of surface roughness caused by chemical degradation. That result was explained by differences in composition and microstructure of feldspathic ceramic and glass-ceramic. It is presumed that leucite crystals, with small dimensions, have major role for better chemical stability of glass-ceramic.

The investigations on ceramics with micro crystals or without any crystals showed minimal or no increase of surface roughness after acid exposure. It was found that some of that ceramics showed even glazing of their surface. In general, it was presumed that high fusion feldspathic ceramic are more chemically stabile than they with low fusion temperature. However, recent studies do not support this theory and proof equal chemical stability of high and low fusion ceramics. Modern low fusion ceramics have small leucite or mulite crystals for structure strengthening (10). Latest glass- and hydrothermal-ceramics are materials without crystals, smoother and softer than traditional ceramics (11).

Chemical inertness and biocompatibility are associated and very important for dental materials. Therefore, it could be concluded that glass-ceramic is more biocompatible then feldspathic ceramic. This conclusion however does not exclude use of feldspathic ceramic for dental purposes because the period of emersion in acid was long and feldspathic ceramic has some clinical advantages.

Literature

1. Kappert H F, Knode H, Schultheiss R., Festigkeitsverhalten der In-Ceram Keramik bei mehanischer und thermischer Wechsellast im Kunstspeichel, Dtsch Zahnärztl Z 1991; 46: 129-131.
2. Kedici SP, Aksut AA, Kilicarslan MA, Bayramoglu G, Gokdemir K., Corrosion behaviour of dental metals and alloys in different media, J Oral Rehabilit, 1998; 25: 800-808.
3. Risito C, Lüthy H, Loeffel O, Schärer P., Chemische Löslichkeit und Festigkeit von Niedrigschmelzenden Dentalporzellanen, Schweitz Monatschr Zahnmed, 1995; 105: 611-616.
4. Živko-Babić J, Ćurković L, Ivaniš T, Pandurić J, Borić D., Chemical stability of Feldspatic and Hydrothermal Ceramics, The Proceeding of 24th Annual Conference EPA 2000, Groningen, 2000, p93.
5. American National Standard/ American Dental Association, Specification No. 69. Dental ceramics, Chicago: Council on Dental Materials, Instruments and Equipment, 1991.
6. ISO 6872 International Standards for Dental Ceramics, International Organization for Standardization, Geneva, Switzerland, 1995.
7. Milleding P, Wennerberg A, Alaeddin S, Karlsson S, Simon E., Surface corrosion of dental ceramics in vitro, Biomater, 1999; 20: 733-746.
8. Anusavice K. J., Degradability of Dental Ceramics, Adv Dent Res, 1992; 6: 82-89.
9. Jakovac M, Živko-Babić J, Ćurković L, Aurer A., Measurement of ion elution from dental ceramics, J Europ Ceram. Soc, 2005; in press.
10. Esquivel JF, Chai J, Wozniak W.T., The physical properties of low-fusing porcelains for titanium, Int J Prosthodont, 1996; 9: 563-571.
11. Komma O., Hydrothermal dental ceramic systems, Rosbach, Germany: Ducera Dental GmbH, 1993.

10. Savjetovanje o materijalima, tehnologijama, trenju i trošenju
10. Conference on Materials, Processes, Friction and Wear
MATRIB'05, Vela Luka, 23-25.06.2005.

MANUFACTURE OF NEAR NET SHAPED 3-DIMENSIONAL COMPONENTS FOR INDUSTRIAL APPLICATIONS

David M. Kennedy and Donal Brosnan

Faculty of Engineering
Dublin Institute of Technology
Bolton Street
Dublin 1
Ireland.
David.kennedy@dit.ie

Abstract:

The development of near net shape 3-Dimensional products for industrial applications has been one main goal for Manufacturing Industries over the last few decades. Processes such as polymer blow moulding and its various stages of development, glass forming, extrusion, forging, centrifugal and sand casting, bulge forming and vacuum forming are typical processes that have contributed to this development. Current practices centre on Surface coatings, Rapid Prototyping, laser forming and nanotechnology manufacture of complex 3-D shapes and assemblies.

The work described in this paper is a new and highly efficient and cost effective technique for producing 3-Dimensional thin walled shapes by using compressed gases to form and shape molten materials in a mould or die. A number of rectangular and cylindrical shapes have been produced to prove the concept and it proves to be successful in manufacturing near net shaped 3-D components of industrial standard.

1. Introduction

Numerous methods of producing near net shapes from raw materials have been developed over the years. Raw Materials of glass, plastics and metals are been formed by complex processes which include glass blowing, polymer blow moulding and some casting techniques for raw metals.

In glass forming, such as bottle making, the molten glass is formed in a mould by the aid of air pressure, and the semi molten glass takes up the shape of the desired mould. Any waste is removed by cutting or grinding. For more delicate and craft type work, the glass is shaped by expert blowers and cut to specified patterns and designs before completion. Advances in this craft area has seen the introduction of Computer Numerically Controlled equipment to machine the patterns into the glass, thus speeding up the process and eliminating the craft work from the process.

Mass production of polymer components has from its inception, been high volume and almost perfect near net shape 3-dimensional construction. Materials development and novel manufacturing methods are a core activity of Engineering, especially in relation to developing strong collaborations with industries and SME's, and new company start ups.

Presented here is a novel method which will seek to gain the most optimum way of shaping materials at minimum costs to near net shape and will provide valuable research and development information to apply the process to industrial applications.

2. Near Net shape Manufacturing Processes:

Some manufacturing techniques for producing near net shapes such as hollow cylindrical sections have been in existence for over a century. These include processes such as centrifugal casting and sand casting using internal cores to make a hollow shell. Typical products made from these techniques include pump casings, engine casings and tubular pipes. Processes such as extrusion, forging, fabrication and complex machining techniques are also in use whereby raw materials are shaped from solid stock or from metal sheets. Normally the manufacturing process will be determined by the type of materials used, the costs involved and the skills available. Other established processes are glass blowing of glassware components and products.

More recently, bulge forming processes have been developed to re shape tubular sections for new applications.

The application of compressed air to forming polymeric materials is well established and the most common application involves blow moulding for manufacturing plastic containers from vehicle fuel tanks to simple containers and bottles. Advances in producing near net 3-dimensional shapes from raw materials have been developed over the past decades. These include injection moulding, extrusions, casting and centrifugal casting, rotational blow moulding, vacuum forming, and more recently, rapid prototyping which is a generic term for a wide range of forming processes from polymers and metals, on a layered basis.

In order to decide if a product can be made in one or more parts, the following needs to be defined as outlined by Boothroyd and Dewhurst [1].

1. does a part have to move relative to adjacent parts?
2. does a part have to be made of a different material to other parts, and
3. should it be separate to allow for assembly of other parts.

Designing components for ease of manufacture is not necessary today due to the sophisticated machinery and technology available. Even parts that move relative to other parts such as a spring can be incorporated into adjacent components through the use of advanced manufacturing technology and modern engineering materials. This means products that once consisted of a number of parts can be made in one piece. This is shown in Figure 1. which is a polymer part for a food mixing machine. It consists of one single part that was initially made from 20 pieces including small springs, nuts, bolts and washers. The spring is now part of the product. Designs emerging from such processes are quality in nature and easier to produce, therefore reducing time to market. 3-D manufacturing should be fully utilised to improve production, improve tolerances and reduce costs.

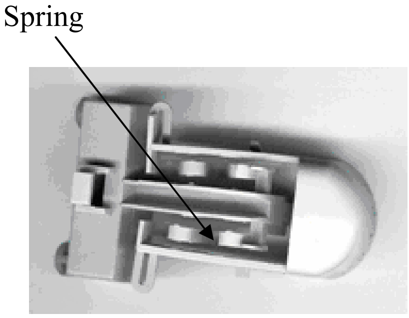

Figure 1. Complex designs and manufacture of multiple functions into one product.

Figure 2. shows elastomeric and metallic components, mass produced for use in the automobile industry. The polymer components are injected moulded at high speeds by an expensive tooling and manufacturing process while the crank shaft is manufactured by a forging process to near net shape and then finish machined.

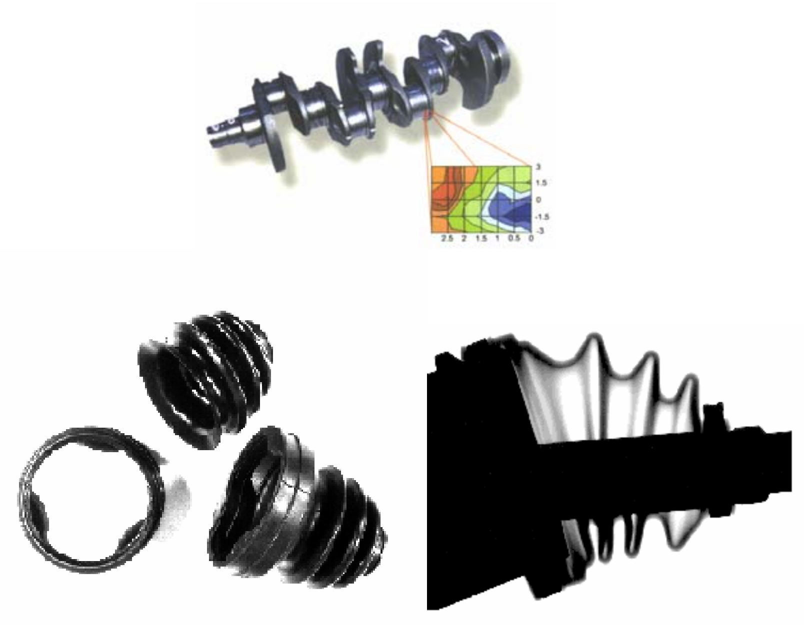

Figure 2. Net shape components for the automobile industry.

Figure 3. shows a basic but typical method of manufacturing a component for a particular application. In this design, eight parts are associated with the product, four bolts, one base, two uprights and a machined cross bar. This product through further research and development can be reduced down to two parts.

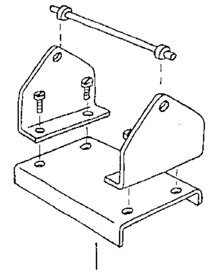

Figure 3. Multi part assemble.

3. Air Forming Process

Air forming of components is a new method (developed by the primary author) of producing cylindrical and hollow metallic parts to near net shape using compressed air. It consists of injecting and directing compressed air into a mould containing a molten material. Under air pressure, the molten material will take the shape of the internal mould and also create an internal cavity in the product. This process is similar to glass forming where glass blowers “blow” air into semi molten glass through a tube, thus creating a hollow cylindrical shape. The wall thickness of the components can be controlled by utilising the correct air pressure and volume. The variable that determine the quality and shape of the components include:

i. material cooling rates.
ii. gas pressure employed
iii. gas velocity and volume
iv. compressed gas direction.
v. type of compressed gas used (standard air or inert gas).

The main advantage of the process includes the speed of forming, low cost of forming and elimination of the need for an internal core. This can have significant labour savings and reduce the time to market. The process is highly advantageous to decorative castings and artwork such as statues, busts, and castings requiring low strength properties. Of particular use is in the casting of pump and motor casings and housings. A broad range of engineering materials can be used in this process. Innovative methods of manufacturing products in a cost effective and efficient manner forms the main theme of this research work.

The research work proposed here involved producing near net shape hollow-section components by applying compressed air or gas to casting technology.

By pouring molten material into preformed moulds and simultaneously injecting compressed air from the base or top of the mould, a hollow component can be produced. The molten materials will take the shape of the internal mould wall and the compressed air will create an internal cavity. The size and shape of this cavity will be determined by the air pressure and air flow rate employed at the time, producing 3-D objects to a variety of shapes, based on the internal mould design.

Initial studies and tests on a 350mm by 60mm by 50mm rectangular shaped mould have shown some basic but promising results. The main advantage of this technique is that it can form complex shapes and it can be applied to a broad range of metals and alloys, especially those that are difficult to machine. It also represents a low cost, rapid manufacturing process over conventional methods and produce components to near net shape.

From initial tests conducted at the Faculty of Engineering at DIT Bolton Street, the process was optimised in terms of air pressure and volume and this will now kllead to industrial collaboration. These industries will include casting companies, pressure die casting organizations and companies involved in extrusion processes.

The research work focused on forming shapes from different alloys and metals and developing greater complexity in shapes.

The stages in the air forming process are shown in Figure 4.

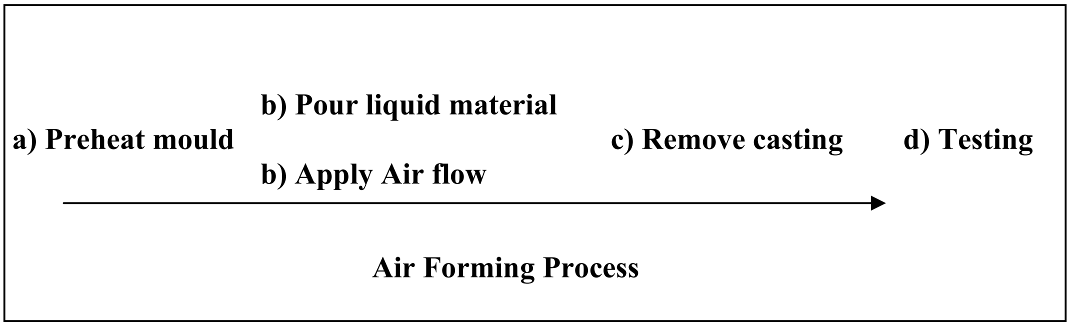

Figure 4. Air Forming Process

4. Results of Air forming Process

Initially a simple tapered mould was produced from steel. This contained an air pipe as shown in Figure 5. On pouring the molten material into the preheated mould, the air pressure through the air pipe was increased until such time as the pressure was adequate to force the molten material to rise up the mould wall and take the shape of the mould cavity. The mould was preheated to approximately 200 degrees Celsius in a simple tempering oven prior to pouring. The molten material was forced by air pressure to completely cover the internal surface of the mould.

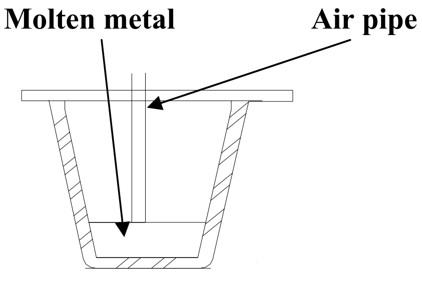

Figure 5. Air Forming Mould

Figure 6 shows the initial test conducted on molten aluminium in a steel cavity using an air pressure of 2.5 Bar. This high pressure produced a 400mm high cylindrical vessel of cross section shown in the figure. Figure 7. shows the external surface of the formed casting. Figure 8. shows the wall thickness of a simple cavity produced by the air forming process. The thick base is an indication that air pressure was not adequate to produce a uniform wall thickness around the surface of the mould. It is noticeable that at the top part of the casting, the wall thickness is uniform and in the order of 0.5mm in thickness. This thickness was repeated on a number of samples produced during the experimentation phase of the work and verifies that the process works effectively with the correct air pressure and air volumes employed.

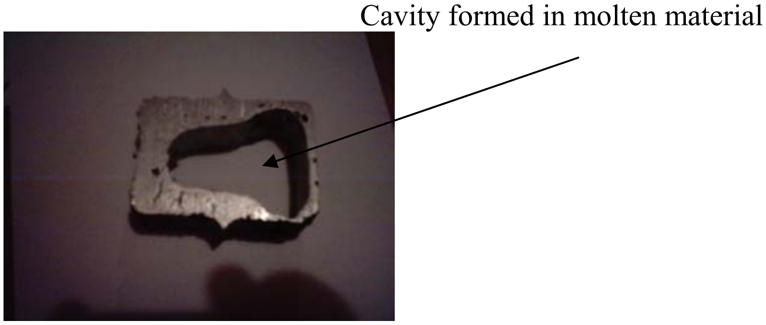

Figure 6. 65mm X 45mm cross section air formed aluminium sample.

Figure 7. External wall of air formed product

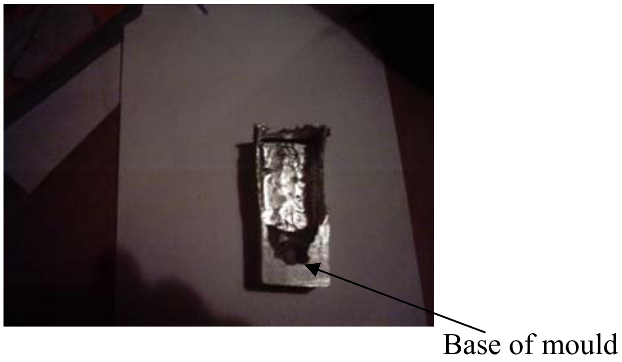

Figure 8. Cavity produced by air forming process

5. Conclusions

The research work proposed here incorporates a new approach to product manufacture and has relevance to a wide range of manufacturing industries involved with castings, injection moulding, tooling, extrusions and 3-D forming.

The main research aspects to this project include the design and manufacture of suitable moulds to investigate the feasibility of producing near net shape components by air forming molten metals. The application of different gases, air pressures and air volume along with air direction have improved the initial tests undertaken. The level of porosity produced in the air forming process will be of major interest to manufacturing processes. The material types suitable for this process including nobel, exotic alloys and traditional metals. Future work will concentrate on mathematical modelling using different air pressures, flow rates and material densities in relation to the mould size to produce different wall thicknesses.

This project will lead to the development of a new manufacturing process for producing hollow components that are currently made by other methods. The applications to mechanical/manufacturing industries in Ireland and abroad are significant and the forming technique proposed will offer an economic and cost effective method of production over other processes.

A products basic design determines how it is made and what it will cost to produce. A suitable design process takes account of manufacture, assembly and materials to improve product quality, reduce costs and time to market. Almost 80 to 90% of the product quality and cost are determined at the design stage and not at the manufacturing stage, yet only 5% or less of the costs are invested in design. As this process is a relatively simple one to control, changes are easier to make and therefore quality and manufacturing parameters can be optimised.

References

[1] G. Boothroyd & P. Dewhurst, Less is more, more or less, Manufacturing Engineer, November 1989.

PROVJERA REZULTATA EKSPERIMENTALNIH ISTRAŽIVANJA METODOM KONAČNIH ELEMENATA

TEST RESULTS OF EXPERIMENTAL RESEARCH USING FINITE ELEMENTS METHOD

Tomislav Mrčela, Elektrotehnički fakultet Osijek
Kneza Trpimira 2b, Osijek, Hrvatska
fax ++385 31 224 605
e-mail: mrcela@etfos.hr,

Antun Pintarić, Elektrotehnički fakultet Osijek
Kneza Trpimira 2b, Osijek, Hrvatska
Tel. ++385 31 224 689
e-mail: Antun.Pintaric@etfos.hr,

Nenad Šešić, Klinički bolnički centar Zagreb

Sažetak: U radu je prikazano numeričko ispitivanje prilikom uvođenja nove metode kod rješavanja prijeloma dugih kostiju metodom osteosinteze. Uporabom novih paket programa simulirano je novo stanje naprezanja kod osteosintetičke kosti uz upotrebu koštanog cementa (Polymethylmetacrylat PMMA). Metoda konačnih elemenata kod uvođenja novih materijala u sanaciju loma dugih kostiju u cijelosti se pokazala kao zadovoljavajuća metoda s kojom možemo na pouzdan način riješiti koncentratore naprezanja u samom spoju osteosinteze Ovom metodom možemo razvijati nove oblike vijaka i pločica za potrebe sanacije kod loma kostiju.

Ključne riječi: metoda, konačni elementi, ekspriment.

Abstract: This paper presents a numerical testing while introducing a new method when solving long bone fractures using osteosynthesis method. A new strain condition on osteosynthetic bones with the use of bone cement (Polymethylmetacrylat PMMA) was simulated by the application of new programme packages. Introducing new materials when healing long bone fractures, the finite elements method has proved to be a very satisfactory method with which we can safely solve strain concentrators in the osteosynthesis junction. With this method, we can develop a variety of new screw and plate shapes for the demands of bone fracture healing.

Key words: method, final elements, experiment.

1. Uvod

Metoda konačnih elemenata numerička je metoda nezaobilazna u matematičko-tehničkim proračunima. Zbog vrlo složenih zahtijeva, u biomehanici postaje gotovo najvažniji alat računanja. Naime, primjena klasičnih diferencijalnih jednadžbi moguća je samo kod jednostavnih proračunskih modela. Za složene mehaničke probleme s kojima se susrećemo u biomehanici, koriste se približne metode u koje spada i metoda konačnih elemenata. Njenu praktičnu primjenu omogućio je razvitak računalne tehnologije početkom druge polovice dvadesetog stoljeća, a samu ideju diskretizacije kontinuiranog sustava postavio je A. Hrenikoff 1941.

2. Osnovne metode.

Suvremena mehanička analiza naprezanja danas koristi tri osnovne grupe metoda koje nisu konkurentne, a istodobno se isprepleću i nadopunjuju. Rezultati jednih služe kao podaci drugima, uz preduvjet pravilnog tumačenja i odabira. Primjerice, analitičkom metodom određen je tip između glavice vijka i utora pločice i kod standardne i kod modificirane osteosinteze s koštanim cementom. Poznavanjem ove bitne činjenice možemo definirati mehaničke preduvjete (constraints) u metodi konačnih elemenata. Rezultati metode konačnih elemenata daju kritična mjesta najvećih naprezanja na koja u eksperimentalnim metodama postavljamo mjerne trake. S druge strane nakon izvršenih eksperimentalnih istraživanja metoda konačnih elemenata daje osobito vrijednu mogućnost da izmjerene vrijednosti provjerimo na računalnim modelima. U tom slučaju u proračun metode konačnih elemenata unosimo na mjernim uređajima izmjerene vrijednosti modula elastičnosti (E) objekta istraživanja ili iz literature poznate module elastičnosti.

Eksperimentalne metode
- *fotoelasticimetrija*
- *tenzometrija*
- *optičke metode*

Numeričke metode
- *metoda konačnih elemenata*
- *metoda konačnih volumena*

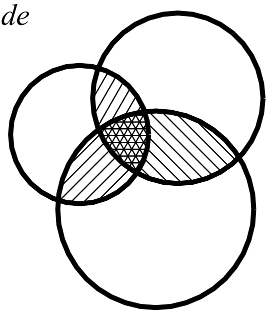

Analitičke metode
koriste jednostavne mehaničke modele,
sa jasnom matematičkim osnovom za :
- *znanost o čvrstoći materijala*
- *teoriju elastičnosti ...*

Kada je mehanički problem odviše složen (primjerice kost) za analitičko matematički izračun koriste se približne numeričke metode, a to je upravo slučaj u metodi konačnih elemenata. Metoda konačnih elemenata daje vjerodostojnu potvrdu eksperimentalnih istraživanja pod uvjetom da je pravilno odabran model proračuna i njegovi elementi.

Temeljni preduvjet u stvaranju numeričkog modela objekta istraživanja predstavlja njegova diskretizacija. Objekt istraživanja diskretizacijom se podijeli na konačan broj pravilnih geometrijskih oblika (konačni elementi) na kojima se mogu izvršiti precizni matematički izračuni. Na slici broj 1 prikazana je mreža konačnih elemenata kortikalnog vijka.

Analitičkom metodom problemi se raščlanjuju na jednostavne mehaničke modele, koji se mogu dobro matematički opisati, a točnost im ovisi o dobrom odabiru (podudarnosti) geometrijskog modela i objekta istraživanja. Ovdje prikazani modeli odgovaraju različitosti standardne osteosinteze pločicom i vijcima i modificirane osteosinteze pločicom i vijcima uz dodatak koštanog cementa u području vrata vijka, odnosno dijela vijka koji se nalazi u prvom kortikalisu.

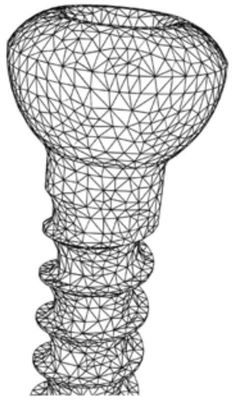

Slika broj 1

Preneseno s tehničkog modela na istraživani problem (slika broj 2), događanja u osloncima odgovaraju kontaktu glavice vijka i pločice u standardnoj osteosintezi, odnosno jednom kuglastom zglobu. Kontaktni spoj (kuglasti zglob) glavice vijka i pločice ostvaren je kružnim spojem glavice vijka i ruba otvora pločice, a rotacijska čvrstoća ovog spoja ovisi o veličini pritezne sile vijka F_v i koeficijentu trenja (μ) metala o metal. Kako je pritezna sila vijka F_v ograničena deset puta manjom čvrstoćom kortikalne kosti od metala (implantata), a koeficijent trenja metala o metal je izrazito nizak trenje je kao mehanizam učvršćenja nedovoljno. Iz tog razloga je potrebito oblikom materijala postići uklještenje. U istraživanom postupku ovo se postiže koštanim cementom koji potpuno popunjava prostor vrata vijka i otvora pločice kao na slici 4 c. Na taj način pločica i vijak djeluju poput jednog krutog tijela (SP – statična površina).

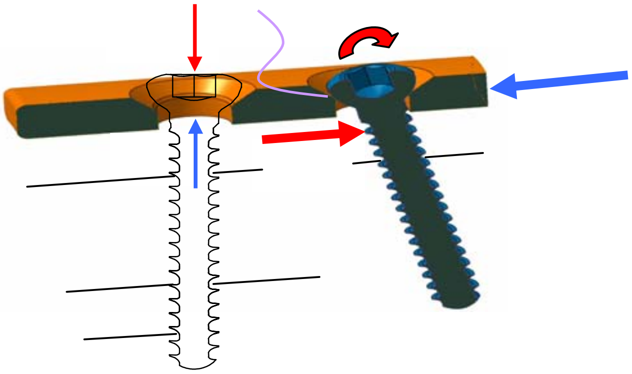

Slika broj 2

Slika 3 prikazuje tehniku i značajke standardne osteosinteze:

a/ "3D solidni model" standardne osteosinteze goljenične kosti pločicom i vijcima.
b/ na 3D presjeku se uočava da je zbog lučnog oblika pločice moguće ostvariti samo rubni crtasti kontakt LK između pločice i kosti, gdje se prenose aksijalna opterećenja kod pritezanja vijkom i kod torzijskih opterećenja kosti.

c/ na detalju 3D presjeka je glavica vijka G, cirkularna površina CP1 kontakta pločice i glavice, zatim cirkularne površine CP2 pločice i glavice, koje nakon osteosinteze ovdje ne prenose bitna kontaktna opterećenja (vezivno tkivo), te konačno navojne površine NP vijka u kosti.

Slika 4 prikazuje tehniku i značajke modificirane osteosinteze:

a/ Računalno modeliran "3D solidni model" osteosinteze goljenične kosti poboljšan koštanim cementom , koji se sastoji od proksimalnog i distalnog dijela kosti KP i KD, pločice P, a između pločice i kosti nalazi se koštani cement – Polymethylmetacrylat PMMA, prikazan kako izviruje na krajevima pločice. Na slici 3 područje koštanog cementa ostaje prazno (ono se tijekom cijeljenja popuni vezivom).

b/ na 3D presjeku uočava se da koštani cement (PMMA) popunjava sveukupan
prostor između kosti i pločice,

c/ na dijelu 3D presjeka prikazana je glavica vijka G, cirkularna površina CP1 kontakta pločice i glavice vijka, cirkularne površine CP2 kontakta pločice s koštanim cementom i kontakta glavice vijka s koštanim cementom, te konačno navojne površine vijka u kosti (NP).

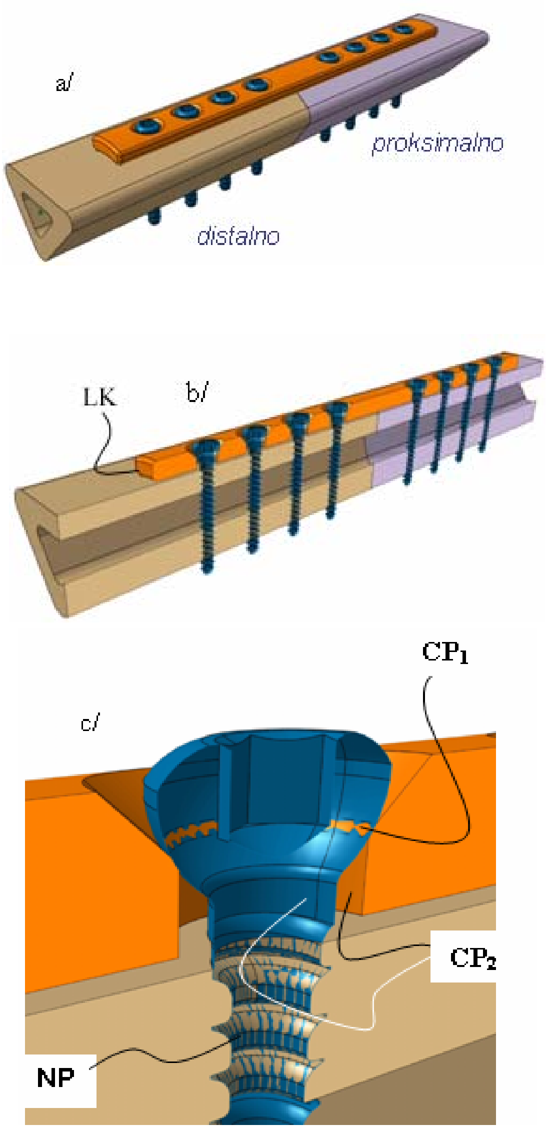

Slika broj 3

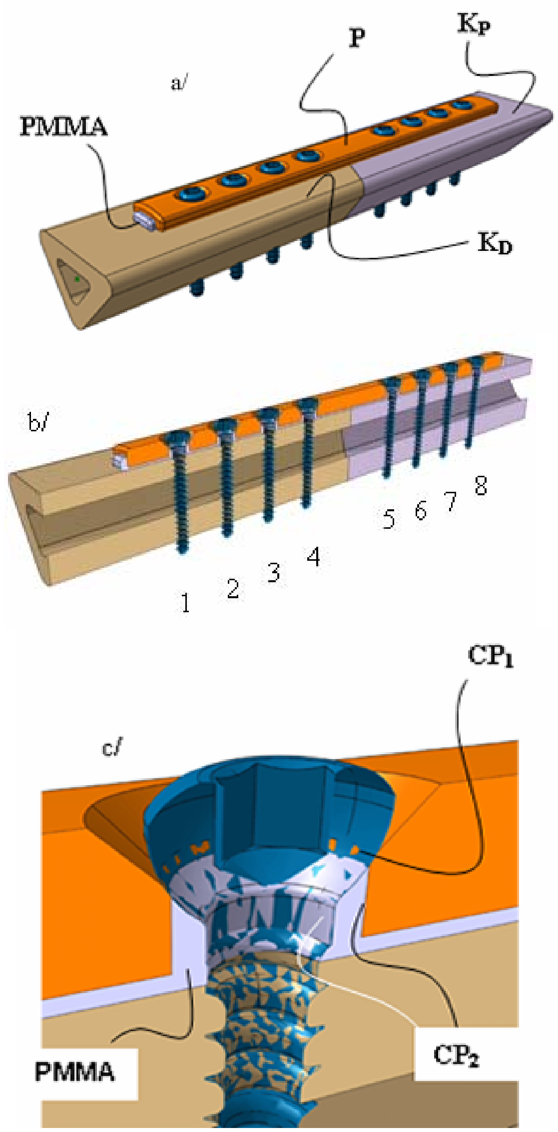

Slika broj 4

3. Računalni programi

Praktična primjena metode konačnih elemenata zahtijeva poznavanje različitih računalnih programa:

1. PREDPROCESOR je računalni program u kojem se definiraju geometrijski i mehanički uvjeti. U istraživanju otpornosti standardne i modificirane osteosinteze na mehanički stres korišten je programski paket 5 CATIA V5 R13, - CAD (Computer Aided Design) Fakulteta strojarstva i brodogradnje Sveučilišta u Zagrebu. U ovom programskom paketu provedeni su slijedeći postupci (slika broj 5 a, b i c):

3D Modeliranje pojedinačnih dijelova, njihovo spajanje u cjelinu međusobnim površinama i rubovima koji se moraju geometrijski podudarati, primjerice, površina vrha spirale navoja kosti odgovara istima u kortikalnom vijku. Dimenzije kortikalnog vijka navedene su iz međunarodnog standarda ISO 5835 6 po kojem je izrađen prikazani 3D solidni model kao i negativ oblika – navojne rupe u kostima.

Generiranje mreže (meširanje) podjela je volumena tijela u 3D mrežu koju provodi računalo, pri čemu je u računalo unesen zadani tip elemenata (primjerice tetraedarske), veličine njihove lokalne mreže (LM) u područjima gdje očekujemo veća naprezanja (primjerice 0,2 mm u području vrata vijka i otvora pločice). Važno je iste veličine mreže pridodati odgovarajućim kontaktnim površinama. Prikaz mreže možemo po potrebi prikazati ili sakriti.

Definiranje rubnih uvjeta (constraints) predstavlja postupak kojim određujemo opterećenje (aksijalne sile Fax i momenta M) i mogućih gibanja (primjerice klizni spoj, rotacija oko određene osi i slično) temeljem analitičke analize problema. U oba slučaja (sa i bez koštanog cementa) spoj vijka i kosti je na osam mjesta čvrsti spoj (ČS), dok su klizni spojevi (KS) između crtastog kontakta pločice i kosti. Slučaj s koštanim cementom ima dodatne čvrste spojeve cirkularnih površina CP2 vrata vijka, koštanog cementa i otvora pločice. Oba slučaja imaju klizni spoj s prednaprezanjem (KSsP) između koštanih ulomaka, te cirkularnih površna CP1 glava vijaka i otvora pločice.

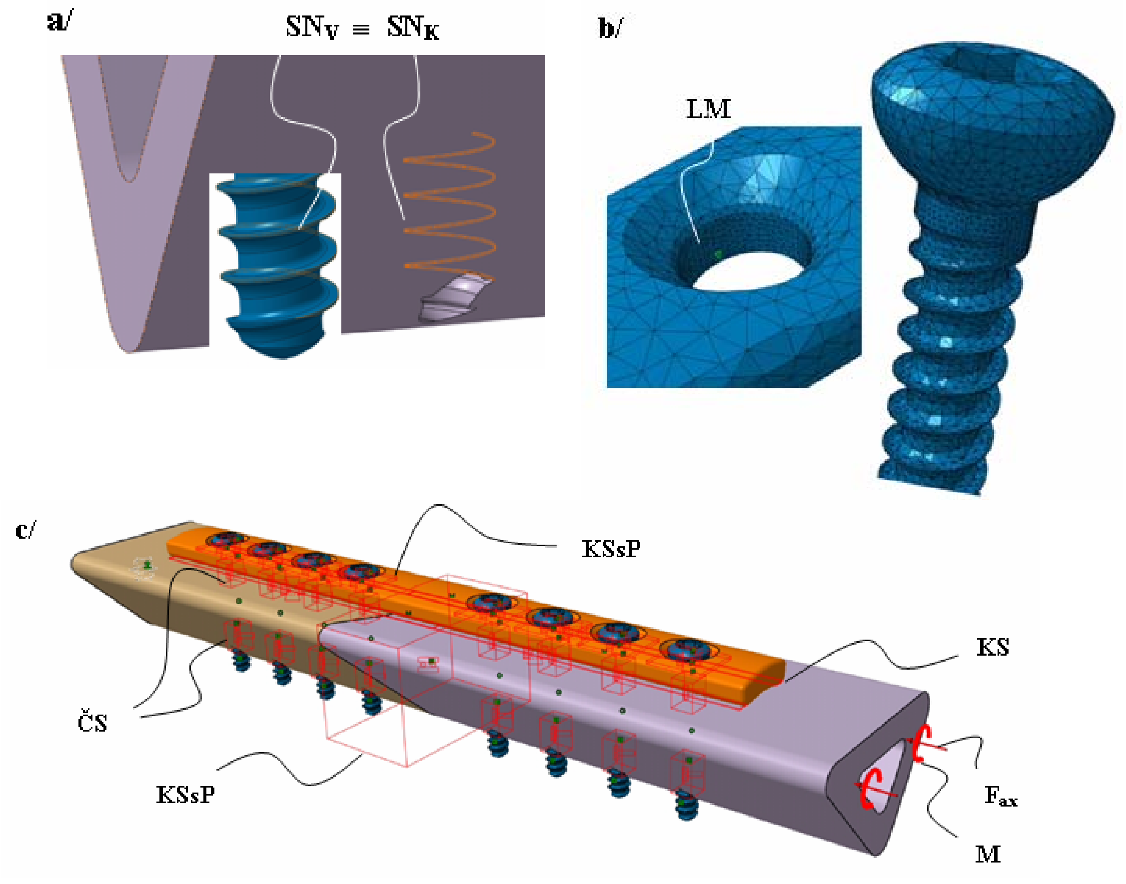

Slika broj 5

2. SOLVER je programski paket (matematički procesor) koji automatski preračunava u računalo unsene postavke i uvjete u trajanju od dijela sekunde do više dana što ovisi o veličini problema (broju elemenata, rubnim uvjetima), jačini računala i definiranom računalnom programu. Korišteni program 7 ABAQUS 6.4 kao solver, jedan je od trenutačno najkvalitetnijih u području numeričke analize krutih i elastičnih materijala, a hardwareska baza je HP radna stanica klase C.

3. POSTPROCESOR je dio programa (CATIA) koji prikazuje rezultate proračuna Solvera na različite načine (u bojama, presjecima i dinamički) što je razvidno iz prikaza na slici 7.

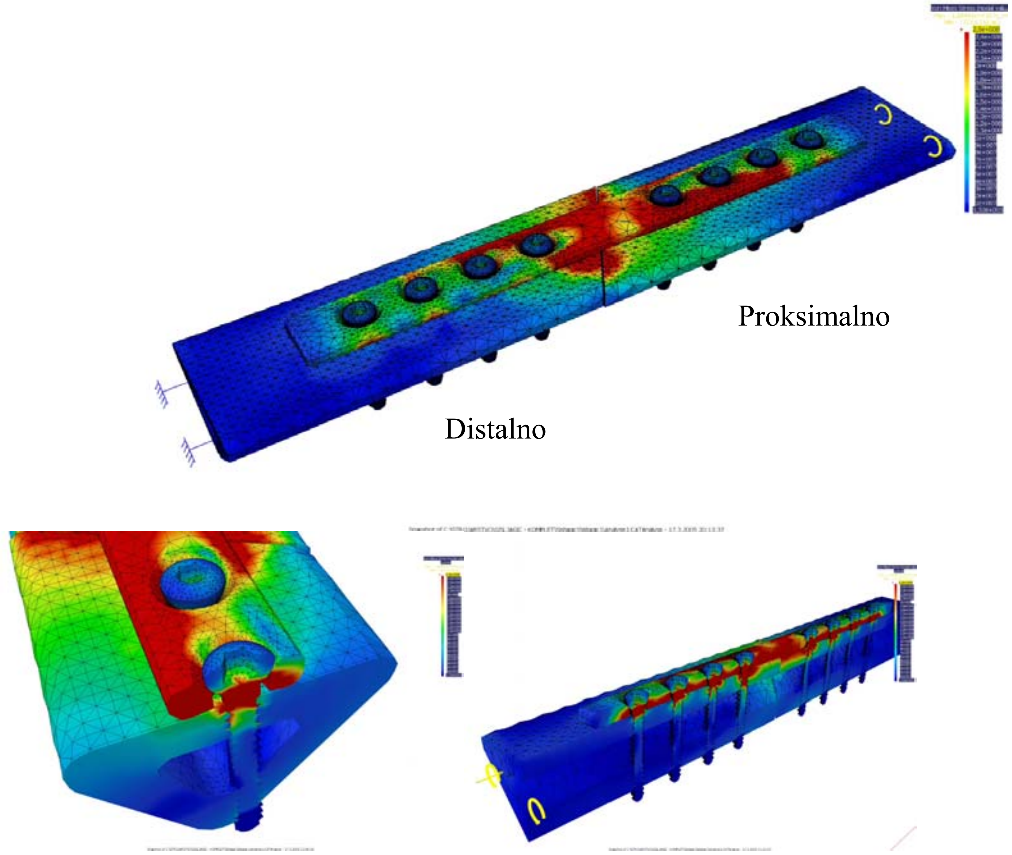

Slika broj 6

Računalni model kosti izrađen metodom konačnih elemenata na slici 7 daje prikaz kirurški zbrinutog kosog loma goljenične kosti tehnikom standardne osteosinteze koji je istodobno opterećen aksijalnom silom - Fax=1000 [N] i momentom - M = 30 [Nm]. Moment torzijske sile (M) prikazan je žutom zaokruženom strelicom i on djeluje u smjeru kazaljke sata na cijelu površinu "proksimalnog" kraja goljenične kosti. U metodi konačnih elemenata to je računski jednako kao da postoji daljnji kontinuitet kosti. Isto vrijedi za "distalnu" površinu kraja goljenične kosti (plave grabljice), koja se na modelu kosti prikazuje kao jedina statična površina (SP) prostora zadanog modela, ali se matematički proračunava kao da se dalje nastavlja.

4. Zaključak:

Pod različitim uvjetima statičkog i dinamičkog opterećenja, računalni model kosti u rezultatu daje prikaz stupnja naprezanja u svakom pojedinom dijelu računalnog modela. Veličina naprezanja iskazana je različitim bojama. Crvena boja predstavlja područja najvećih naprezanja, a plava boja područja najmanjih naprezanja. Uz svaki računalni model kosti pridružena je gradacijska tablica koja sukladno intenzitetu pojedine boje označava veličinu naprezanja dijelova računalnog numeričkog modela kosti u [Pa]. Kako se različiti intenziteti naprezanja obično iskazuju u [MPa], to su i sile naprezanja u gradacijskoj tablici iskazani u [MPa]. Primjerice, oznaka +007 u gradacijskoj tablici označava naprezanje od 10 [MPa], oznaka +008 označava 100 [MPa], oznaka +009 označava 1000 [MPa] slika broj 6.

5. Literatura:

1. Tizard A.: An introduction to computer-aided engineering - McGraw-Hill 1994.
2. Farin G.: Curves and surfaces for computer aided geometric design –Academic Press, New York 1990.
3. Mantyla M.: M introduction to solid modelling, -Computer science Press, Rockvilte 1988.
4. Spirakos C.C.: Finite element modelling in engineering practice, - W. Virginia University press, Morgantown 1994.

10. Savjetovanje o materijalima, tehnologijama, trenju i trošenju
10. Conference on Materials, Processes, Friction and Wear
MATRIB'05, Vela Luka, 23-25.06.2005.

UTJECAJ SIGMA FAZE U DUPLEKS ČELIKU NA OTPORNOST NA ABRAZIJSKO TROŠENJE

Vera Rede, Sanja Šolić
Fakultet strojarstva i brodogradnje
Ivana Lučića 5
10000 Zagreb

Sažetak: Dupleks čelici zbog izvanredne kombinacije mehaničkih i antokorozijskih svojstava nalaze sve širu primjenu u različitim područjima. Svojstva dupleks čelika posljedica su specifične strukture sastavljene od podjednakih udjela ferita i austenita. Ako se ovaj izbalansirani odnos naruši te ako se u mikrostrukturi pojave precipitati sigma faze, što se realno može dogoditi npr. pri zavarivanju, kvare se i mehanička i korozijska svojstva ovog materijala. U radu je istraživan utjecaj pojave i povećanja volumnog udjela sigma faze na otpornosti na abrazijsko trošenje dupleks čelika, kvalitete X2CrNiMoN 22 5 3 (Wst.-Nr. 1.4462). Za potrebe eksperimenta osnovni materijal je toplinski obrađen žarenjem na temperaturi 800°C. Varirano je vrijeme držanja na temperaturi žarenja: 1, 2 i 3 sata. Na uzorcima je provedena kvalitativna i kvantitativna analiza mikrostrukture, mjerenje mikro- i makrotvrdoće te ispitivanje otpornosti na abrazijsko trošenje. Dobiveni rezultati ukazuju na značajan utjecaj sigma faze na otpornost materijala prema abraziji.

Ključne riječi: mikrostruktura, dupleks čelici, sigma faza, otpornost na abraziju, tvrdoća

Abstract: Due to their extraordinary combination of mechanical and anti-corrosion properties, duplex steels are widely used in various fields of application. These properties are consequence of specific structure composed of ferrite and austenite in equal volume shares. If this balanced relation is disturbed, and if in microstructure appear sigma phase precipitants, which can realistically be expected, e.g. by welding, then the mechanical properties and corrosion resistance are damaged.
The aim of investigation was to establish the influence of appearance and increase of sigma phase volume shares, on resistance to abrasion wear of duplex steel, grade X2CrNiMoN 22 5 3 (Wst.-Nr. 1.4462). In the experimental part of the work raw material was annealed at 800°C over the period of: 1, 2 and 3 hours. On the specimens the microstructure was qualitatively and quantitative analysed, micro- and macrohardness, and resistance to abrasion wear were tested. The results which were obtained indicate significant influence of the sigma phase to resistance on abrasion wear.

Key words: microstructure, duplex steels, sigma phase, resistance to abrasion, hardness

1. Uvod

Feritno austenitni dupleks čelici oblikovani su tako da im se struktura sastoji od 50% ferita i 50% austenita. Ako se u strukturi uz ferit i austenit pojave i neke druge strukturne tvorevine (karbidi, nitridi, sigma faza, Chi faza, Lavesova faza, α' faza i neke druge) narušava se optimalna fazna ravnoteža što dovodi do snižavanja žilavosti i korozijske postojanosti. Odlučujući utjecaj na mikrostrukturu dupleks čelika ima kemijski sastav i režim toplinske obrade. Opasnost od nastanka nepoželjnih faza povećava se povećanjem udjela legirnih elemenata pa je posebno izražena kod super dupleks čelika (DSS).

Sve neželjene strukturne tvorevine mogu se, prema temperaturi na kojoj nastaju, svrstati u dva temperaturna područja, slika 1. Na slici je strelicama naznačeno kako pojedini legirni elementi djeluju na kinetiku nastanka nabrojanih faza.

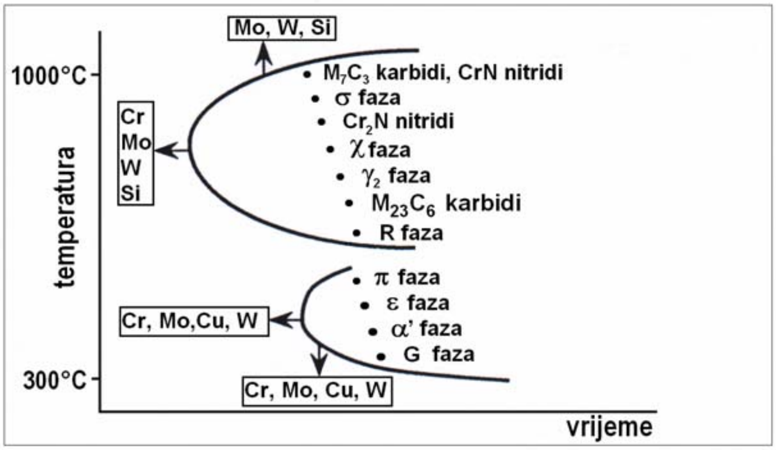

Slika 1 – Shematski prikaz tipičnih precipitacija u dupleks čelicima, [1]

σ-faza je kromom bogata, tvrda i krhka, nemagnetična intermetalna faza koja nastaje zadržavanjem dupleks čelika na temperaturi između 560 i 980ºC. Sklonost nastanku σ-faze raste s povećanjem sadržaja kroma i molibdena, pri čemu molibden ima 4 do 5 puta veći utjecaj od kroma. I svi drugi α-geni elementi potiču stvaranje sigma faze. Sigma faza nastaje eutektoidnom pretvorbom ferita, ferit prekristalizira u sigma fazu i austenit, (α → σ + γ). Sigma faza primarno se formira na faznim granicama ferit/austenit i odatle se dalje širi u ferit. Model nastanka i rasta sigma faze prikazan je na slici 2.

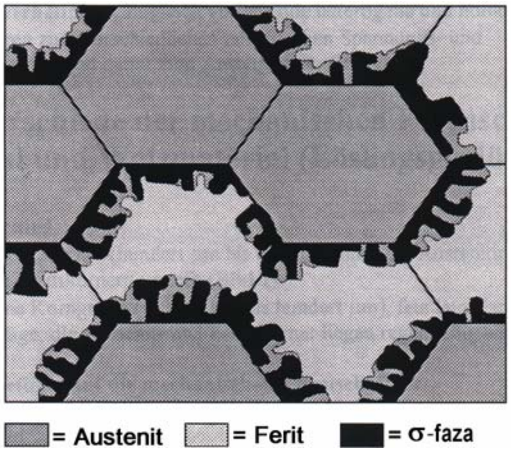

Slika 2 – Model nastanka i rasta sigma faze, [2] Tvrdoća sigma faze je oko 940 HV (68 HRC). Već vrlo male količine izlučene σ-faze značajno utječu na pad žilavosti i istezljivosti. Prisutnost sigma faze može povisiti makrotvrdoću dupleks čelika do 450 HV50, [3]. Sigma faza značajno smanjuje korozijsku postojanost dupleks čelika.

Namjera ovog rada je da prikaže kakav utjecaj sigma faza, tj. povećanje njezinog volumnog udjela u mikrostrukturi dupleks čelika, ima na tvrdoću te na otpornost na abrazijsko trošenje.

2. Materijal i eksperimentalna procedura

Kao probni materijal za predviđeno istraživanje poslužio je standardni dupleks čelik oznake 1.4462 (X2 CrNiMoN 22 5 3) isporučen u obliku valjane ploče iz koje su uzeti svi potrebni uzorci. Kako je struktura valjane ploče izrazito usmjerena posebno se pazilo da svi uzorci budu uzeti iz istog smjera s obzirom na smjer valjanja.

Isporučenom materijalu proizvođač jamči kemijski sastav predočen tablicom 1.

Tablica 1 - Kemijski sastav materijala za istraživanje zajamčen od isporučitelja materijala

	Sadržaj elementa u % mase								
	C	Ni	Cr	Mn	Si	P	S	N	Mo
najmanje		4,50	21,00					0,10	2,50
najviše	0,030	6,50	23,00	2,00	1,00	0,035	0,015	0,22	3,50

Uzorci su toplinski obrađeni u peći sa zaštitnom atmosferom argona. Sva tri uzorka su žarena na istoj temperaturi, 800°C, kako bi se u osnovnoj feritno-austenitnoj strukturi izazovalo formiranje sigma faze. Varirano je vrijeme žarenja od 60 do 180 minuta:

- uzorak «**I**» grijan je na 800°C u trajanju od 60 minuta i hlađen na zraku,
- uzorak «**II**» grijan je na 800°C u trajanju od 120 minuta i hlađen na zraku,
- uzorak «**III**» grijan je na 800°C u trajanju od 180 minuta i hlađen na zraku.

Uzorak koji nije toplinski obrađen i koji predstavlja osnovno stanje nosi oznaku «**O**».

U okviru planiranog istraživanja provedena je kvalitativna i kvantitativna analiza mikrostrukture na svim uzorcima, izmjerena je tvrdoća te ispitana otpornost na abrazijsko trošenje metodom ″suhi pijesak- gumeni kotač″ prema normi ASTM G 65-94, [4].

Oblik i veličina uzoraka nalaze se na slici 3 a uzorci spremni za ispitivanje na slici 4.

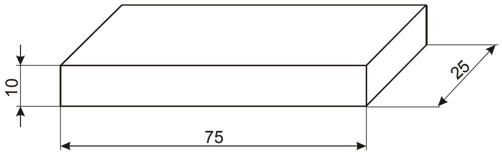

Slika 3 – Oblik i veličina ispitnih uzoraka

Slika 4 – Ispitni uzorci prije ispitivanja

3. Rezultati

Rezultati ***kvalitativne analize mikrostrukture*** prikazani su na slikama 5, 6, 7 i 8, [5]. Mikrostruktura osnovnog materijala izazvana je nagrizanjem sredstvom LB I, prema [6]. Uzorci I, II i III nagrizani su u Murakami otopini, prema [7].

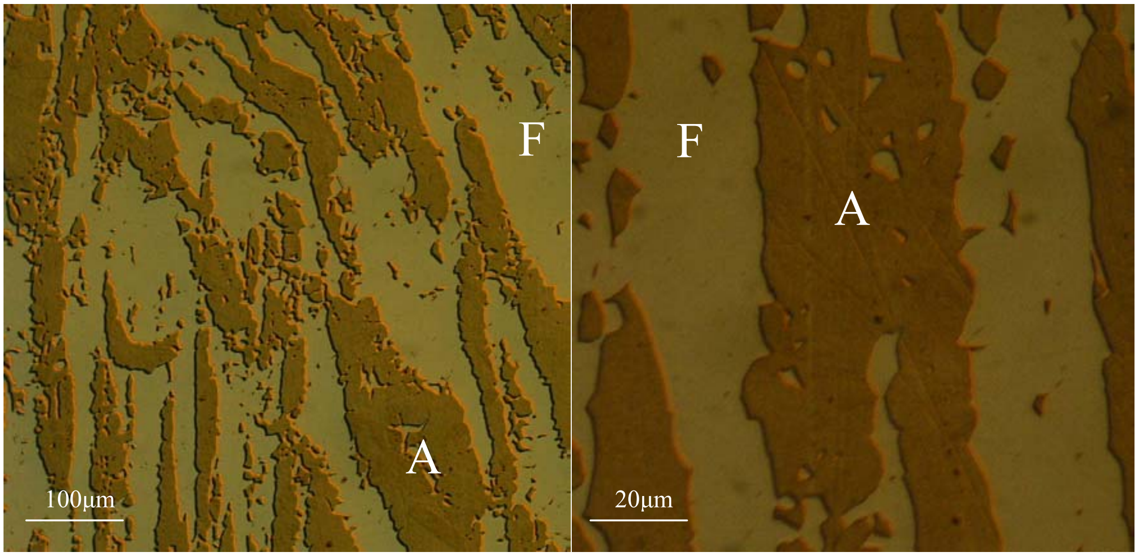

Slika 5 – Mikrostruktura osnovnog materijala, uzorak **O,** površinski presjek. Struktura se sastoji od podjednakih udjela ferita i austenita.

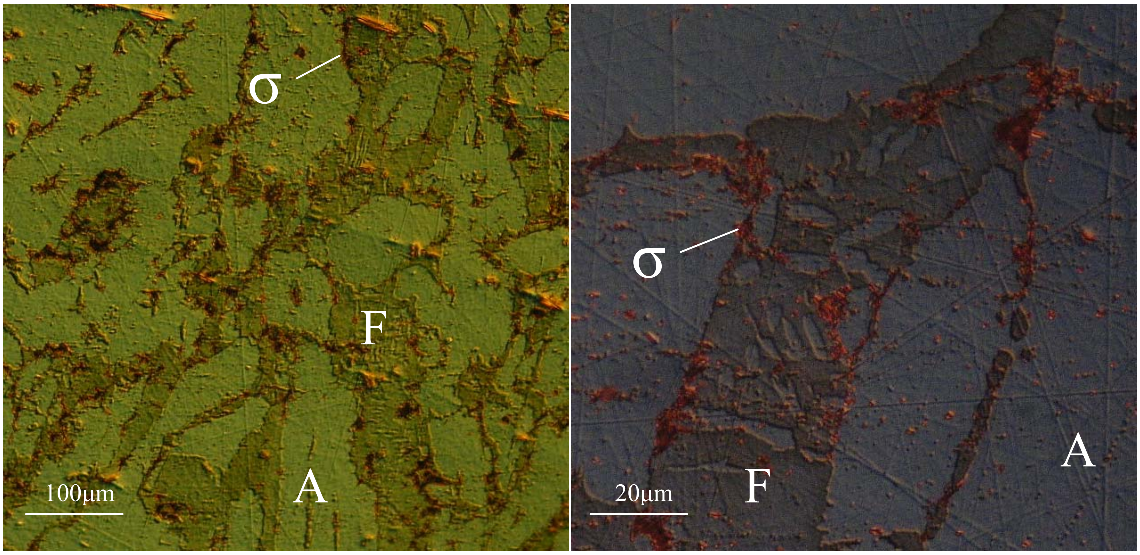

Slika 6 – Mikrostruktura uzorka **I** (TO: 800°C/60'), u površinskom presjeku, sastoji se od austenita, ferita i sigma faze koja nastaje na faznim granicama i širi se dalje u ferit. Udio ferita se smanjuje a raste udio austenita u odnosu na osnovni, toplinski neobrađeni materijal.

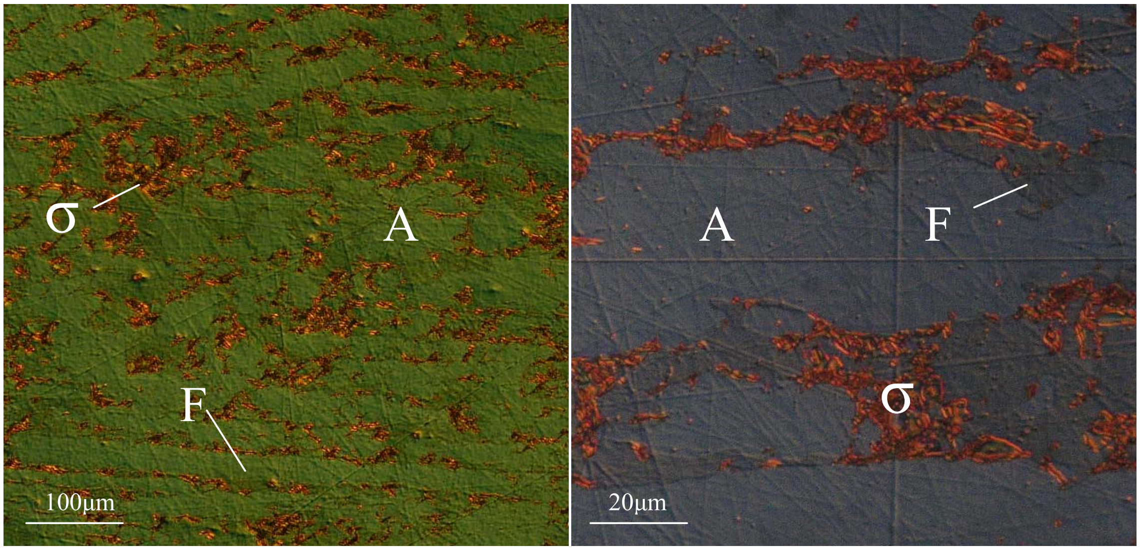

Slika 7 – Mikrostruktura uzorka **II** (TO: 800°C/120'), površinski presjek, sadrži više austenita i sigma faze te manje ferita od uzorka I.

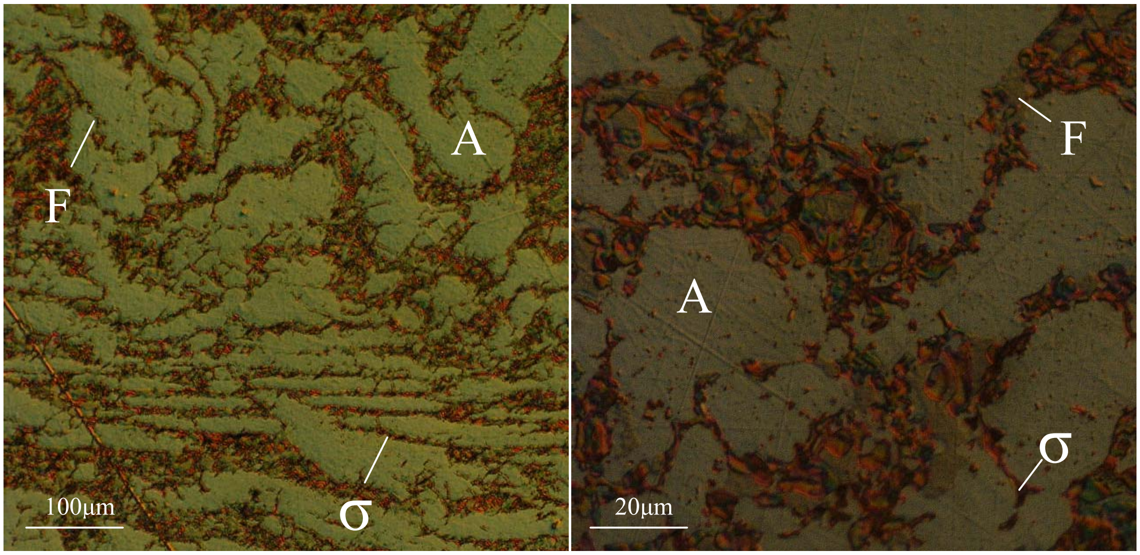

Slika 8 – Mikrostruktura uzorka **III** (TO: 800°C/180'), površinski presjek, sadrži vrlo malu količinu ferita, više austenita i sigma faze nego kod uzorka II.

Kvantitativno određivanje volumnih udjela pojedinih strukturnih faza provedeno je pomoću automatiziranog sustava za analizu slike. Srednje vrijednosti od 10 mjerenja prikazane su u tablici 2.

Tablica 2 – Rezultati mjerenja volumnog udjela faza kvantitativnom analizom slike

Uzorak		**Volumni udio faza u %**		
oznaka	**stanje**	**austenit**	**ferit**	**sigma faza**
O	osnovno stanje	50	50	0
I	žaren na 800°C/60'	68	26	6
II	žaren na 800°C/120'	78	12	10
III	žaren na 800°C/180'	81	6	13

Tvrdoća ispitnih uzoraka izmjerena je Vickersovom metodom pri sili od 10·9,81 N (HV10), 0,2·9,81 N (HV0,2) i 0,02·9,81 N (HV0,02).
Srednje vrijednosti od 10 mjerenja po uzorku nalaze se u tablici 3.

Tablica 3 – Rezultati mjerenja tvrdoće

UZORAK	**HV10**	**HV0,2**		**HV0,02**	
		ferita	**austenita**	**ferita**	**austenita**
O	257	289	280	293	287
I	240	272	267	382	376
II	264	393	317	437	407
III	309	392	378	498	479

Rezultati ispitivanja *otpornosti na abrazijsko trošenje* metodom "suhi pijesak/gumeni kotač" prikazani su tablicom 4 i dijagramom na slici 9. Na svakom uzorku provedena su po tri ispitivanja uz opterećenje silom F=130N. Gubitak mase mjeren je nakon 2000 okretaja gumenog kotača.

Tablica 4 – Rezultati ispitivanja otpornosti na abrazijsko trošenje

Uzorak	**Srednja vrijed. gubitka mase, g** (za 2000 okr.)
O	**0,2227**
I	**0,2420**
II	**0,2653**
III	**0,2950**

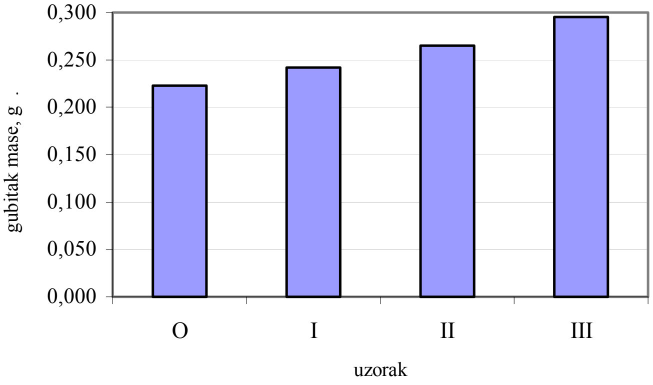

Slika 9 - Gubitak mase za uzorke O, I, II i III

4. Diskusija

Analiza mikrostrukture pokazala je da precipitati sigma faze primarno nastaju na faznim granicama ferit/austenit i odatle dalje rastu u ferit. Udio sigma faze povećava se s vremenom žarenja tako da je uzorak I, žaren 1 sat, imao najmanji a uzorak III, žaren 3 sata, najveći volumni udio ove faze. Nastajanjem sigma faze raspada se ferit pa se njegov volumni udio rapidno smanjuje, pogotovo poslije prvog sata, s 50 na 26%. Istodobno raste udio austenita.
Promjena volumnih udjela austenita, ferita i sigma faze u ovisnosti o vremenu žarenja prikazana je dijagramom na slici 10.

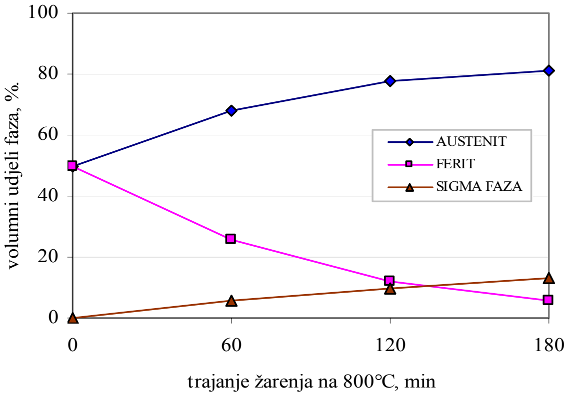

Slika 10 – Utjecaj vremena žarenja na 800°C na volumne udjele ferita, austenita i sigma faze

Rezultati mjerenja *makro* i *mikrotvrdoće* jasno pokazuju da tvrdoća raste povećanjem udjela sigma faze. Povećanje makrotvrdoće nije samo posljedica porasta udjela sigma faze već i porasta tvrdoće austenitne i feritne faze koje nastupa žarenjem na 800°C. Utjecaj povećanja udjela sigma faze na tvrdoću HV10 i mikrotvrdoću HV0,2 i HV0,02 prikazan je na slici 11.

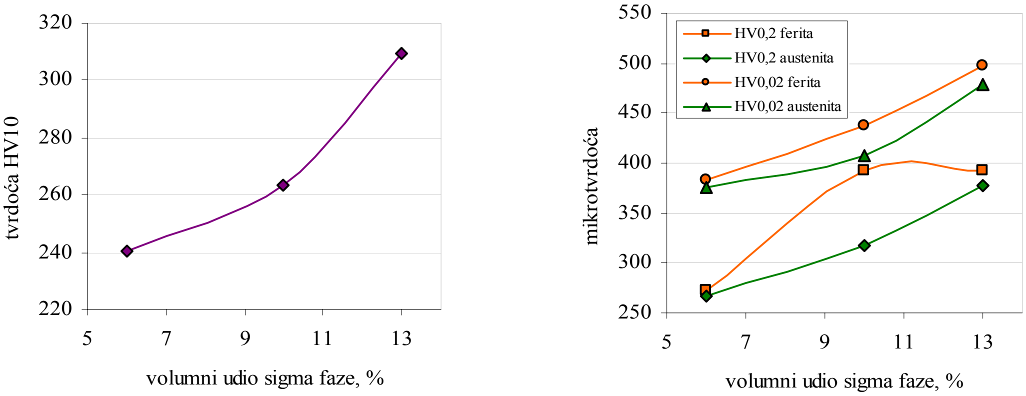

Slika 11 – Utjecaj udjela sigma faze na tvrdoću HV10 i mikrotvrdoću HV0,2 i HV0,02

Rezultati ispitivanja *otpornosti na abrazijsko trošenje* izraženi su gubitkom mase što je prema normi ASTM G 65-94 dopušteno za usporedbu rezultata kod uzoraka čija se gustoća materijala ne razlikuje.

Utjecaj sigma faze na abrazijsko trošenje prikazan je dijagramom na slici 12. Sigma faza koja se pri žarenju formira na granicama između feritnih i austenitnih zrna, i čiji se udio u mikrostrukturi povećava s vremenom žarenja, smanjuje otpornost materijala na abrazijski mehanizam trošenja. Ovakav utjecaj na trošenje je dosta neočekivan s obzirom na povećanu tvrdoću uzoraka sa sigma fazom i činjenicu da se povećanjem tvrdoće redovito povećava i otpornost na trošenje[8]. Razjašnjenje ove kontradikcije moglo bi, s jedne strane, biti u činjenici da se istodobno s povećanjem sigma faze smanjuje udio ferita a povećava udio austenita, koji je najzastupljenija ali i najmekša od ove tri faze. S druge pak strane, nazočnost sigma faze u strukturi jako utječe na pad žilavosti, pa premda je kod abrazijskog trošenja stupanj opasnosti od umora materijala nizak, može se pretpostaviti da povećana krhkost ima određeni utjecaj na dobivene rezultate.

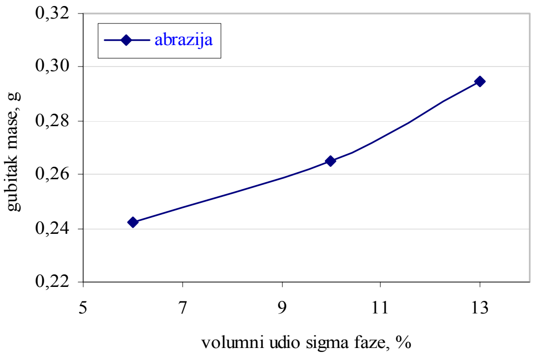

Slika 12 – Utjecaj rasta udjela sigma faze na gubitak mase pri abrazijskom trošenju

5. Zaključak

Na kraju istraživanja može se istaknuti sljedeće:

- Žarenjem dupleks čelika na 800°C mijenja se njegova osnovna struktura sastavljena od ferita i austenita u omjeru 50:50. Na faznim granicama ferit-austenit stvaraju se precipitati sigma faze i odatle dalje rastu u ferit. Dolazi do raspada ferita, njegov udio u mikrostrukturi se smanjuje a istodobno se povećava udio austenita. Nabrojane promjene su intenzivnije ako je vrijeme žarenja dulje.
- Žarenje na 800°C izaziva porast tvrdoće to veći što je duže vrijeme žarenja. Uzrok tome je porast udjela sigma faze u mikrostrukturi dupleks čelika te istodobni porast udjela austenita i smanjenje ferita. Mikrotvrdoća austenita, HV0,2, također se povećava duljim žarenjem.
- Otpornost na abrazijsko trošenje smanjuje se povećanjem udjela sigma faze u mikrostrukturi. Ovakav utjecaj je dosta neočekivan zato što sigma faza povisuje tvrdoću, ali se može objasniti istodobnim velikim smanjenjem duktilnosti te ostalim promjenama u mikrostrukturi koje su direktno povezane s nastankom sigma faze (porast udjela austenitne i smanjenje udjela feritne faze).

Literatura:

[1] Charles, J.: *Super Duplex Stainless Steel: Structure and Properties*, Duplex Stainless Steels Conf. Proc., Vol 1, Les Editions de Physique, Les Ulis Cedex, 1991.

[2] Reick,W.: *Kaltumformung und Rekristallisation eines rostbeständigen, ferritisch austenitischen Duplex-Stahles,* Werkstoff-Kolloquium Duplex-Stähle, Bochum, 1994.

[3] Pohl,M., Ibach,A., Lange,K.-H.: *Gefüge und Gebrauchseigenschaften von Super-Duplexstählen,* Prakt. Met., 28, str 333-349, 1991.

[4] ASTM G 65-94, Standard Test Method for Measuring Abrasion Using the Dry Sand/Rubber wheel Apparatus (1994.), originally published as G 65-80

[5] Rede,V.: *Utjecaj mikrostrukture zavara dupleks čelika na otpornost prema trošenju - disertacija,* Fakultet strojarstva i brodogradnje Sveučilišta u Zagrebu, Zagreb, 2004.

[6] E.Weck, E.Leistner: *Metallographische Anleitung zum Farbätzen nachdem Tauchverfahren, Teil II: Farbätzmittel nach Beraha und ihre Abwandlungen,* Deutscher Verlag für Schweißtechnik (DVS) GmbH – Düsseldorf, 1983.

[7] A.Schrader: *ÄTZHEFT - Verfahren zur Schliffherstellung und Gefügeentwicklung für die Metallographie,* Berlin, 1957.

[8] Ivušić,V.: *Tribologija,* Hrvatsko društvo za materijale i tribologiju, Zagreb, 1998.

10. Savjetovanje o materijalima, tehnologijama, trenju i trošenju
10. Conference on Materials, Processes, Friction and Wear
MATRIB'05, Vela Luka, 23-25.06.2005.

NUMERICAL SIMULATION OF SQUAT PHENOMENA ON RAIL

G. Fajdiga, B. Zafošnik, J. Kramberger, M. Šraml and J. Flašker

University of Maribor
Faculty of Mechanical Engineering,
Smetanova ul. 17, 2000 Maribor
Slovenia

Abstract

Rail dark spot defect, also termed squat failure or shelling, is a rolling contact fatigue failure which occurs frequently on high speed traffic railway rails. It is one of the most dangerous rail failures. The rail dark spot defect is strongly dependent on loading conditions, material of contacting parts, surface roughness, etc. The theories of contact mechanics and fracture mechanics are widely used to understand this complex phenomenon. The main goal of this research is to develop a computational model for simulation of the complete material fatigue process in rail-wheel contact, starting from the micro-structural changes in the material, subsequent crack initiation and its propagation. Therefore the computational model is divided into two main parts: Contact Fatigue Crack Initiation Model and Contact Fatigue Crack Propagation Model.

The results of such a unified model enable a computational estimation of probable number of load cycles that a wheel-rail system can sustain before development of the initial crack in the rail and the number of load cycles required for a crack to propagate from initial to critical length, when the final fatigue failure (squat) can be expected to occur.

Keywords: rail, crack initiatian and propagation, squat, computational analysis

1 Introduction

Repeated railway wheel–rail rolling contacts cause a nonproportional multiaxial stress–strain response in the rail. This causes fatigue damage to the rail, which in the first place leads to the initiation of cracks that originate either on the surface or subsurface of the rail. There are many parameters that have a significant influence on the crack initiation and propagation of the crack (geometry of the rail and the wheel, loading of the wheel, traction forces, residual stress field in the rail, train velocity, traffic density, weather conditions etc.). Each of these demands increases rail Rolling Contact Fatigue (RCF) damage, raises maintenance costs and affects railway traffic safety. To prevent the future demands from resulting in catastrophic rail failures, it is urgent to conduct such investigations that identify and suggest improvements for the rails available today. Over the last 20 years, rail failures have been increasing, especially failures involving rolling contact fatigue. One of them is rail dark spot defect, which is usually termed as a "squat" and a "shell" in the literature [7], Fig. 1.

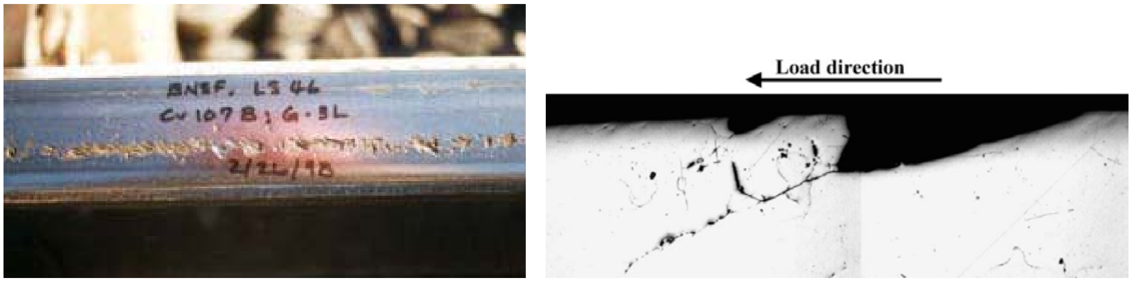

Figure 1: RCF damage of rail [3].

The main goal of this study is to simulate the squat phenomena. It has been considered that the squat is caused by RCF. Contact fatigue damage can be defined as a kind of damage caused by changes in the material microstructure which result, initially, in crack initiation and then in crack propagation, under the influence of time-dependent rolling and/or sliding contact loads. The two phases of the contact fatigue process are generally referred to as (i) Contact Fatigue Crack Initiation (CFCI) and (ii) Contact Fatigue Crack Propagation (CFCP).

2 Theoretical models

2.1 Contact Fatigue Crack Initiation (CFCI)

Comprehensive model for CFCI of mechanical elements should consider the time history of applied contact loads, in particular their range of variation. The rolling-sliding contact loads, typical for mechanical elements such as wheels and rails, gears, rolling bearings etc., are generally stochastic, due to the character of contact parameters. For a description of a general case of contact loading, one has to estimate average normal and tangential contact forces for computational determination of surface and subsurface contact stresses. Normal contact forces can be appropriately determined by applying the Hertzian contact theory [6], while the tangential frictional forces are explained by the Coulomb friction law [6]. The stress loading cycle for each observed material point (x_i, y_i) on or under the contact surface can be computationally determined by applying the contact loading conditions in a moving fashion along the contact area (Fig. 2). This procedure enables a realistic description of a stress cyclic loading in the time domain due to rolling and/or sliding contact conditions. A finite or boundary element method can be used for this purpose.

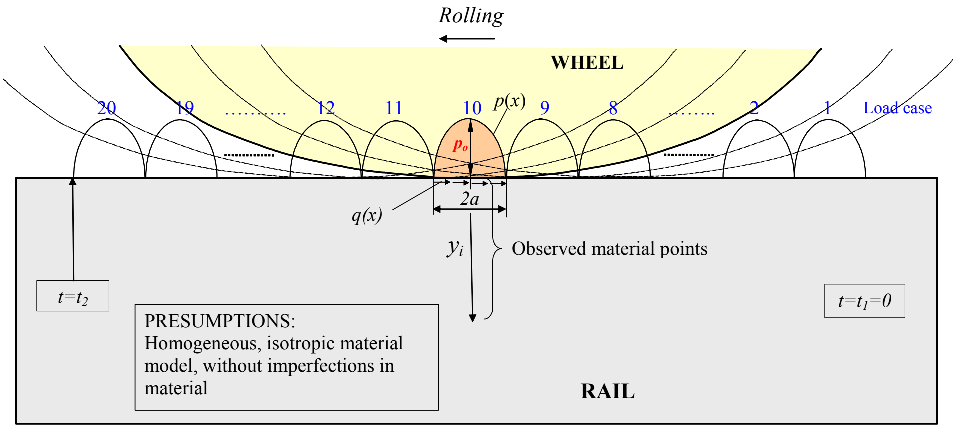

Figure 2: Determination of contact loading cycle [4].

When the stress loading cycles are determined, fatigue analysis for each observed material point can be performed. The methods for fatigue analysis are most frequently based on Coffin-Manson relation between deformations, stresses and number of loading cycles and are usually modified to fit the nature of the stress cycle, e.g. repeated or reversed stress cycle [10]. The number of loading cycles required for fatigue crack to appear, can be determined with the strain-life method ε-N, where the relationship between the specific deformation increment $\Delta\varepsilon$ and the number of loading cycles N is fully characterized with the following equation [10]:

$$\frac{\Delta\varepsilon}{2}=\frac{\sigma_a}{E}+\frac{\Delta\varepsilon_p}{2}=\frac{\sigma'_f}{E}(N)^b+\varepsilon'_f(N)^c, \tag{1}$$

where σ_f' is the fatigue strength coefficient, b the strength exponent, ε_f' the fatigue ductility coefficient and c the fatigue ductility exponent. In the above equation, N needs to be replaced with $2N$ for reversed stress cycle (one cycle is two reversals). The strain-life method ε-N is not an ideal model for fatigue damage initiation analysis at the microstructural level since the micro-crack initiation in crystal grains and dislocation theory are not taken into account. However, it has been established that fatigue damage initiation can be represented by transition of a certain number of loading cycles before the first actual fatigue damage occurs in the assumed initial homogenous state of material [10]. Thus, the ε-N method represents a very useful method for determination of the initial fatigue damage, which is located at the material point with the largest stresses, where fatigue damage initiation is most probable in the time domain.

2.2 Contact Fatigue Crack Propagation (CFCP)

A theoretical model, which is illustrated in Fig. 3, forms a base for the numerical model, used in the work reported here. Theoretical model consists of a two dimensional surface-breaking crack in a half-space, length a, and inclined at an arbitrary angle β to the surface. The surface of the half-space is repeatedly traversed by a Hertzian contact distribution, with a contact half-width b_H, and maximum pressure p_0. The load moves over the surface of the half-space from right to left (under these conditions the crack would be expected to grow) [2]. The contact area is also subjected to a distribution of tangential traction, with the maximum value q_0. The simulation of the surface initiated crack propagation is considered in addition the influence of the lubricant on the crack propagation. In the presented model the hydraulic pressure mechanism [2] has been adopted, where the lubricant is driven into the crack by contact loading pressure and keeps the crack faces separated by its pressure, thus implying increased mode I and II separation at the crack tip due to additional normal pressure and lack of friction between crack faces [2]. In the computational procedure the lubricant pressure inside the crack is simply approximated with a uniform pressure distribution along the crack faces [2]. The level of lubricant pressure is equal to the current pressure determined at the crack mouth, *i.e.* the pressure depends on the contact pressure distribution position in respect to the crack mouth. Figure 3b illustrates crack face pressure determination and distribution for two consecutive contact loading configurations.

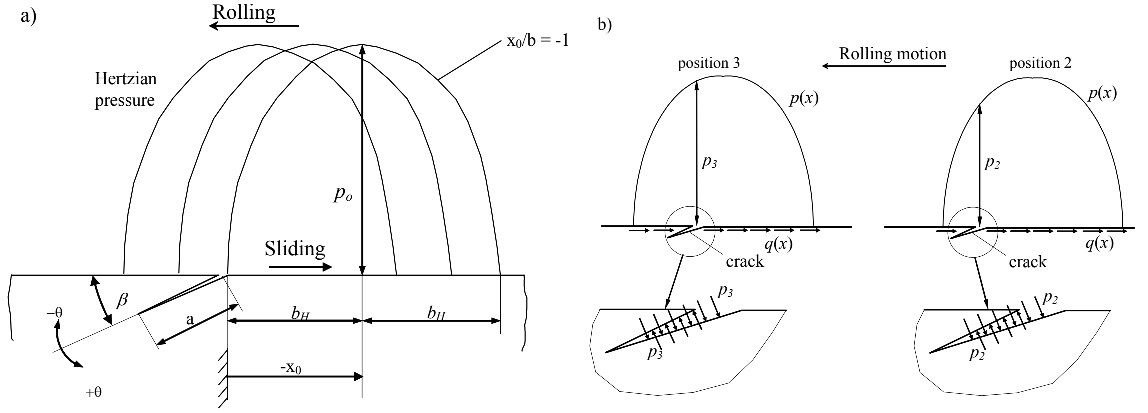

Figure 3: Simulation of moving contact a) for hydraulic pressure mechanism b).

2.2.1 Maximum Tangential Stress (MTS) criterion for determination of crack propagation angle

According to Erdogan and Sih [9], the crack extension starts along the radial direction in the plane perpendicular to the direction of the greatest tension. In this direction tangential stress $\sigma_{\theta\theta}$ is maximum and the shear stress $\tau_{r\theta}$ is zero.

The tangential stress around the crack tip, in polar co-ordinates, can be written for pressurised crack as [11]:

$$\sigma_{\theta\theta}(\theta,r)=\frac{1}{\sqrt{2\pi r}}\cos\frac{\theta}{2}\left[K_I\cos^2\frac{\theta}{2}-\frac{3}{2}K_{II}\sin\theta\right]+T\sin^2\theta-\sigma_{xx}^c\sin 2\theta+\sigma_{yy}^c\cos^2\theta. \qquad (2)$$

The angle θ_0 at which the crack will propagate could be determined from

$$\left.\frac{\partial \sigma_{\theta\theta}}{\partial \theta}\right|_{r=r_c} = 0 \Rightarrow \theta = \theta_0 . \tag{3}$$

Rearranging the solution from eq. 3 gives the following expression:

$$\left[K_{\mathrm{I}} \sin\theta_0 + K_{\mathrm{II}}\left(3\cdot\cos\theta_0 - 1\right)\right] - \gamma \sin\frac{\theta_0}{2}\cos\theta_0 + \delta\frac{1}{\cos\frac{\theta_0}{2}}\cos 2\theta_0 = 0 . \tag{4}$$

where:

$$\gamma = 16\left(\left(T - \sigma_{yy}^{c}\right)\sqrt{2\pi r_c}\right)/3 \text{ and } \delta = 16\left(\sigma_{xx}^{c}\sqrt{2\pi r_c}\right)/6 . \tag{5}$$

Equation (4) describes a generalized MTS criterion for the determination of crack propagation angle, when the crack surfaces are loaded with constant internal pressure.

A physical length scale r_c presents the distance ahead of the crack tip where the fracture process starts. The distance r_c is a material parameter, which is very difficult to determine. It is assumed that the r_c is contained in the region of constrained yielding [8]. In case of cyclic loading for plane strain conditions r_c is determined with:

$$r_c = \frac{1}{6\pi}\left(\frac{K_{Ic}}{2\cdot\sigma_{pl}}\right)^2 , \tag{6}$$

where K_{Ic} is plane strain fracture toughness and σ_{pl} is yield stress.

3 Simulation of rail damage

3.1 Simulation of a wheel-rail contact

The purpose of a wheel–rail contact analysis is to determine the maximal contact pressure between the wheel and the rail. A contact patch is developed at the area where the wheel contacts the rail. The size and shape of this contact patch can be calculated from the loading conditions, the material properties and the geometry of the wheel and the rail in this region. The input data for the 3D wheel-rail numerical model are shown in Tab. 1.

Table 1: Input data for 3D numerical model of rail-wheel.

Wheel geometry [4]	***Rail geometry [4]***	***Young's modulus E [GPa]***	***Poisson ratio ν***	***Wheel-rail position h [mm]***	***Coeff. of friction***	***Static axle loading - locomotive [t/axle]***	***Static axle loading – coach [t/axle]***
UIC 510-2	***60 E1***	***206***	***0.29***	***76.044***	***0.1***	***22***	***12***

Pressure ellipses as a consequence of the wheel-rail contact considering friction forces are shown in Fig. 4. The maximal contact pressure is 1133 MPa for the locomotive loading and 907 MPa for the coach loading. Squats are defects which usually occur in the rolling direction. Therefore the crack initiation and propagation is simulated with 2D numerical models. The actual 3D wheel-rail contact problem is transformed into its generalised 2D model with Hertzian theory [6] (see Fig. 1 and Fig. 2).

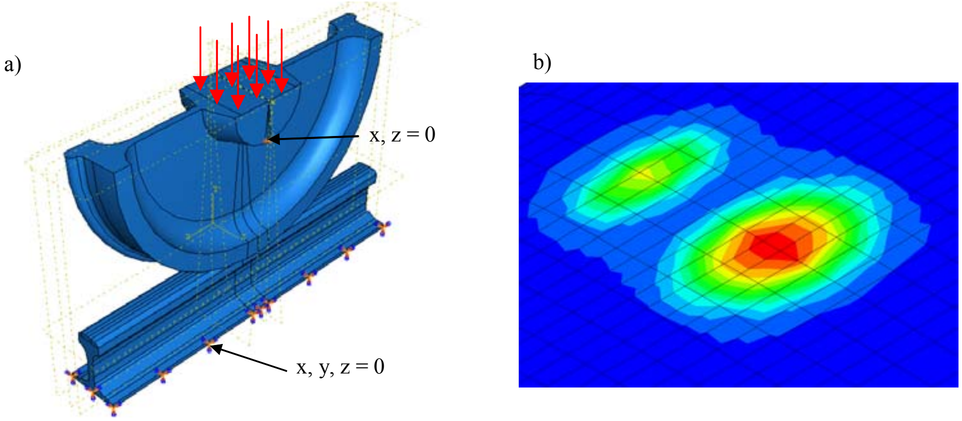

Figure 4: Boundary conditions a) and pressure ellipses for wheel-rail contact b).

3.2 Numerical Model of CFCI

In this paper only the theoretical prediction of crack initiation was considered. The fatigue life model described in Section 2.1 is based on the strain life method. Once a local stress or strain-time history has been established using Finite Element Analysis (FEM) the fatigue analysis method could be applied. Furthermore, material properties are introduced as "material fatigue data" from tests [4] for the rail made from 300 HB. The material parameters used in analysis are: exponent of material strength b = -0.15, fatigue ductility exponent c = -0.62, fatigue ductility coefficient ε_f'= 0.71, fatigue strength coefficient σ_f'= 2050 MPa, material strength coefficient K' = 2168 MPa and material hardening exponent n'=0.24. The strain life approach is preferred over S-N method even in high cycle application, due to its less scatter-prone materials data. The assumption that has been made at fatigue life models is the following: the models are uni-axial, which means that just one principal stress occurs in one direction (single stress vector). Using applied relationship between the specific deformation and the number of loading cycles for fatigue damage initiation, (Eq. 1), the position of the initial fatigue damage and the number of required stress cycles can be determined. Previously described theory for fatigue crack initiation is implemented in the fatigue analysis program FE-safe [5] which was used for computational estimation of the number of cycles for crack initiation. Simulation of the moving load was performed for 1 locomotive (4 wheels) and 6 passenger coaches (6 times 4 = 24 wheels), see Fig.5.

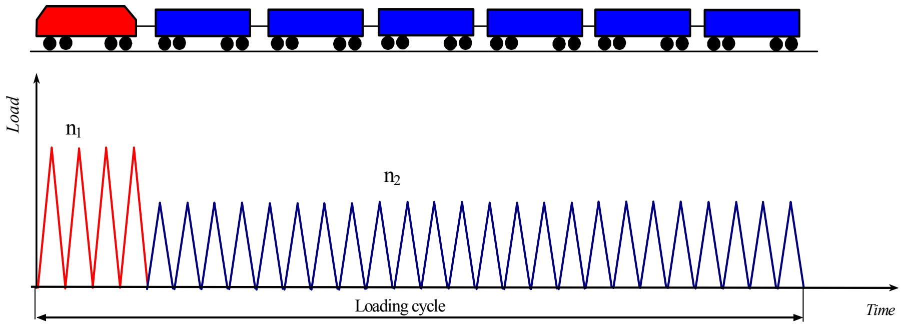

Figure 5: Block loading with two different load amplitudes for locomotion and passenger coaches.

The coefficient of friction was μ=0.1 and the roughness of the rail surface was R_a = (0.25÷0.6) µm. Fatigue lives (output as $\log_{10}$ Live) are shown as a contour plot of damage regions (Fig. 6).

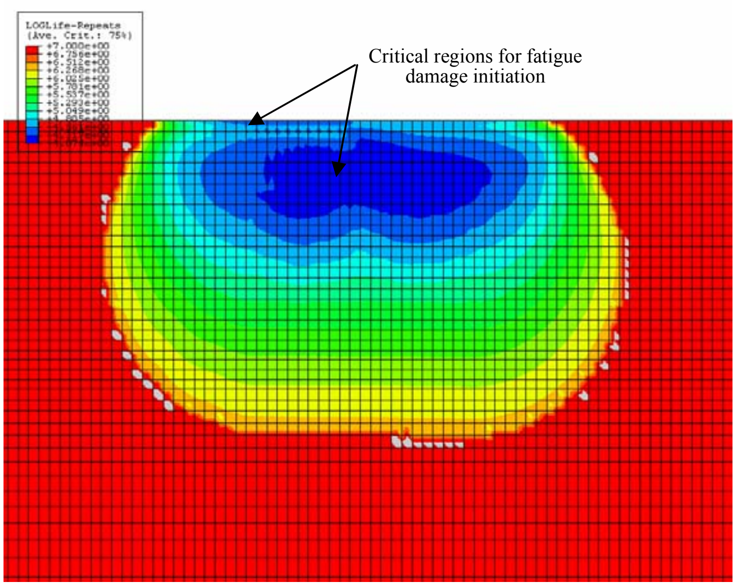

Figure 6: Damage analysis (log scale), N_i=1.18·10^4.

It is obvious, that the critical damage appears in the two places, under the contact surface and at the contact surface (N_i=1.18·10^4 cycles), see Fig. 6.

3.3 Numerical Model of CFCP

In order to investigate the effect of the moving contact on the stress field around the crack tip, five loading configurations have been considered for a hydraulic pressure mechanism (Fig.2) [2]. All configurations have the same normal *p(x)* and tangential *q(x)* contact loading distributions, which are applied at different positions with reference to the crack mouth (Fig.2). The Hertzian contact pressure distribution $p(x)$ and the half-length of the contact area

b_H = 8,97 mm were estimated using previous contact analysis and the Hertzian contact theory. The tangential loading $q(x)$ has been determined using Coulumbus law [6]. The orientation and length of the crack follow from the metallographic examination of initial squat cracks appearing in rails [3, 7]. The initial length of the crack is equal to a_o = 150 µm, with the initial inclination angle towards the contact surface equal to β = 20°. Due to unavailable material parameters for analysing the fatigue crack growth, crack increments were assumed to be equal to Δa = 15 µm. Plane strain fracture toughness K_{Ic} of 1075,2 $MPamm^{1/2}$ and yield stress σ_{pl} of 710 MPa (assuming no cyclic hardening or softening) were considered in the analyses.

Eight rectangular quarter-point finite elements were used around the crack tip to simulate $r^{-1/2}$ stress singularity and $r^{1/2}$ displacement variation at the crack tip. The rest of the model was discretized with standard quadrilateral isoparametric elements. Stress intensity factors K_{I} and K_{II} and the T-stress were calculated using interaction integral method [1]. Kink angles were calculated with different MTS criterion which takes into account the influence of the stress intensity factors and/or T-stress and/or fluid pressure on the crack surfaces.

The results on Fig. 7 are given in terms of a relative position of the loading case with respect to the half-contact width b_H for two crack lengths: initial crack length a_0 = 150 µm and extended crack length a_1 = 165 µm, which corresponds to the extension for 15 µm of the initial crack.

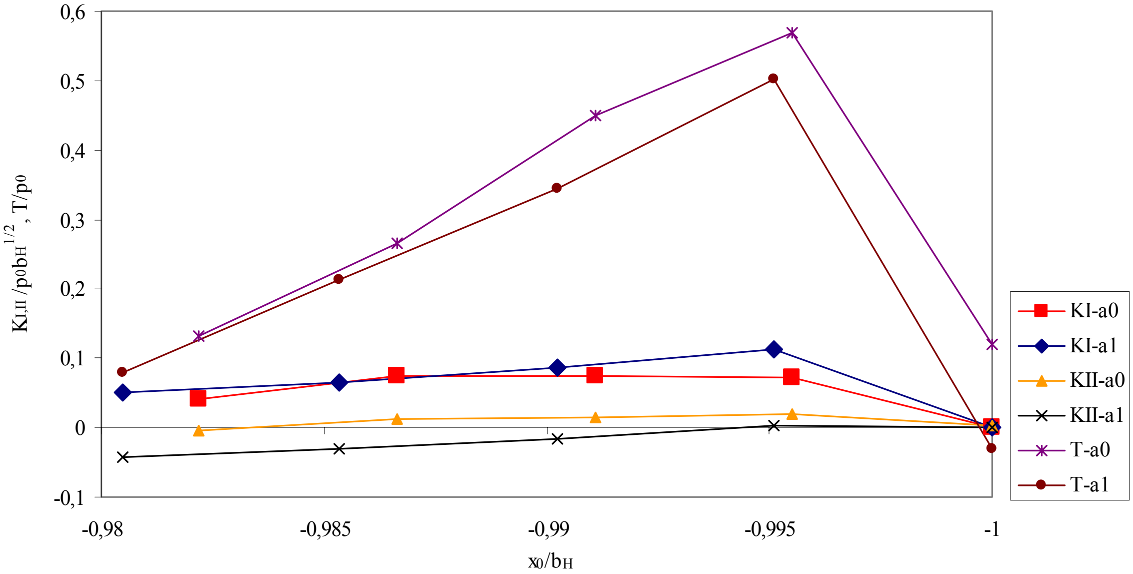

Figure 7: Stress intensity factors K_I, K_{II} and T-stress fracture parameters.

From Fig. 7, it can be seen that the stress intensity factor K_{I} increases when load moves over the crack mouth (x_0/b_{H} > -1). It achieves a maximum at load case IV for initial crack length and at load case II for kinked crack. After this, load case K_{I} decreases.

The load case I cause minimum and the load case II maximum value of the stress intensity factor K_{II} for the initial crack and kinked crack. After this load case K_{II} decreases.

When the load moves over the crack mouth, positive T-stress occurs for both cracks and achieves maximum for load case II. Smaller values of the T-stress for kinked crack are caused by higher compressive stress around the crack tip, because the tip of kinked crack is nearer to the free surface, than the tip of the initial crack.

Variation of the kink angle determined by MTS criteria is summarised in Fig. 8. Results obtained using only stress intensity factors K_{I} and K_{II} are marked with "cl". When the T-stress is also considered in the formulation, results are marked with "T", whereas "g" mark denotes the generalized criteria.

Results on Fig. 8 show that the highest kink angle occurs for the load case I. This load case is not critical, because the crack is not loaded with the internal pressure. When other load cases are observed, the largest kink angle is determined with the generalized MTS criterion. The smallest kink angle is determined when classical MTS criterion is used. Experimental results [3, 7] show that the kink angles of squat crack in the rail are very large. It can be concluded that the *T*-stress has big influence on the crack propagation in rails and therefore they should be considered in analysis. The largest crack propagation angles are estimated with generalized MTS criterion, which better corresponds with available experimental data [3, 7].

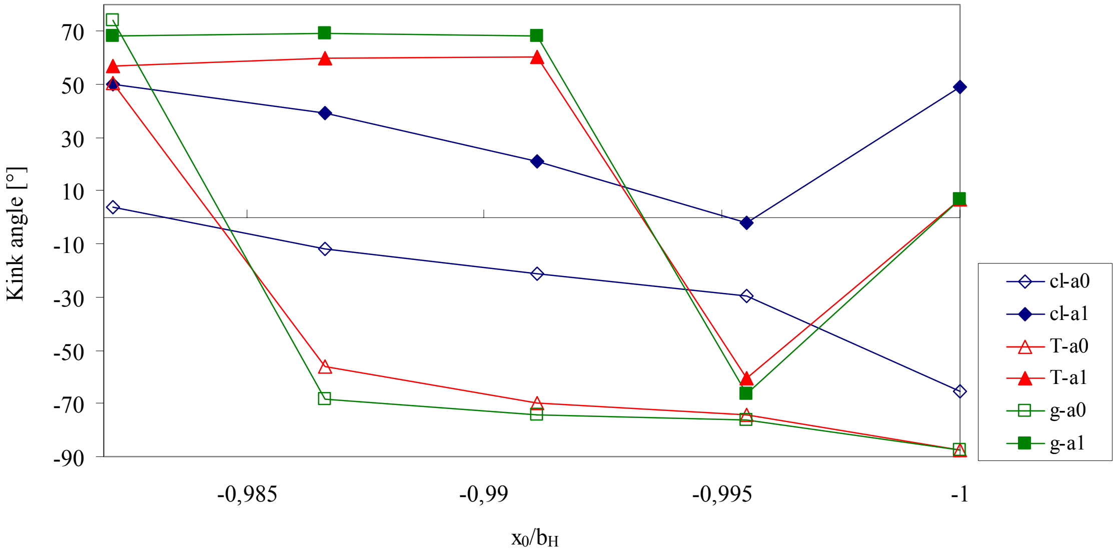

Figure 8: Kink angle determined with different fracture parameters.

4 Concluding remarks

The paper presents a computational simulation of squat phenomena in rail tracks as a consequence of the rolling contact fatigue. The total service life of a rail under the fatigue loading until a squat appears can be divided into the period required for the crack initiation and the period needed for its propagation until the final surface failure-squat appears. Therefore the computational model presented in this paper is divided into two main models: (i) CFCI model based on the modified ε-N method and (ii) CFCP model based on the MTS criterion, which takes into account the influence of stress intensity factors and/or T-stress and/or internal pressure. Squats are generally 3D defects where main crack propagation is observed in the rolling direction. Therefore the crack initiation and propagation was analysed using 2D numerical models. In both computational models the data for the 300 HB material were used. With the CFCI model the critical damage locations were determined under and on the contact surface, in the range of N_i=1.18·10^4 loading cycles. Regarding to our results and the available experimental results [3, 7] the initial micro crack is assumed to appear on the surface. Results obtained from the CFCP model shows that the initial surface crack propagates to the contact surface. Comparison with the available experimental results of crack propagation in rails [3, 7] indicates that the most comparable results are for the case when *T*-stress and internal pressure are included. If combined with appropriate short fatigue crack growth theories, the results of computations can be used to predict the service life (loading cycles) required for development of squats.

References

[1] Abaqus Version 6.4. Online Documentation, Generated: 2003.

[2] Bower A. F., (1988): "The influence of crack face friction and trapped fluid on surface initiated rolling-contact-fatigue cracks", *Journal of Tribology*, Vol. 110, pp. 704–711.

[3] Donzella G., Faccoli M., Ghidini A., Mazzu A., Roberti R., (2004): "The competitive role of wear and RCF in a rail steel", *Engineering Fracture Mechanics,* Vol. 72, pp. 287–308.

[4] Fajdiga G., Zafošnik B., Šraml M., Kramberger J., Flašker J., (2004): "HIPERTRACK-Final report about the ULJ rolling-contcact fatigue simulation activities".

[5] Fe-safe Works Version 5. User's Manual, Generated: 2003.

[6] Johnson, K.L., (1985): "Contact mechanics", *Cambridge University Press*.

[7] Kaneta M., Matsuda K., Marukami K. and Nishikawa H. (1998): "A Possible Mechanism for Rail Dark Spot Defects", *Transaction of the ASME*, Vol.120, pp. 304-309.

[8] Larsson, S. G. and Carlsson, A. J., (1973): "Influence of non-singular stress terms and specimen geometry on small-scale yielding at ctack tips in elastic-plastic materials", *Journal of Mech. Physics Solids*, Vol 21, pp. 263-277.

[9] Sih, G. C., (1974): "Strain Energy Density Factor Applied to Mixed-Mode Crack Problems", *International Journal of Fracture*, Vol. 10, pp. 305–321.

[10] Suresh, S., (1998): "Fatigue of materials", *Cambridge University Press* (Second Edition), Cambridge.

[11] Zafošnik, B., (2004): "Energy model for prediction of surface crack propagation on gear flanks", Doctoral dissertation (in Slovene language), Maribor.

.

10. Savjetovanje o materijalima, tehnologijama, trenju i trošenju
10. Conference on Materials, Processes, Friction and Wear
MATRIB'05, Vela Luka, 23-25.06.2005.

INFLUENCE OF COOLING INTENSITY (SECTION THICKNESS) ON MICROSTRUCTURE PROPERTIES AND HARDNESS OF VERMICULAR CAST IRON

UTJECAJ INTENZITETA HLAĐENJA (DEBLJINE STJENKE) NA MIKROSTRUKTURNA SVOJSTVA I TVRDOĆU VERMIKULARNOG LIJEVA

Z. Glavaš[1], Š. Majstorović[2], K. Terzić[1], F. Unkić[1]

[1] Faculty of Metallurgy, University of Zagreb
Aleja narodnih heroja 3, 44000 Sisak
Republic of Croatia

[2] Foundry „ Dalit Corp.“ d.d.
S. i A. Radića 46, 43500 Daruvar
Republic of Croatia

Abstract:

Production of vermicular cast iron by method of exact addition of alloy for melt treatment based on Mg is difficult due to very narrow range of residual Mg, which is often less than ± 0,001%, what is difficult to obtain due to process's variables. Microstructure of vermicular cast iron is highly sensitive to the section thickness of casting, relatively cooling intensity, which requests optimizing and strict control of production parameters with the purpose of obtaining requested properties of vermicular cast iron castings.

In this paper influence of cooling intensity on obtained microstructure properties and hardness of casting of vermicular cast iron have been analyzed. It has been ascertained which increase of cooling intensity results in high proportion of nodular graphite and pearlite in microstructure and increases hardness of vermicular cast iron.

Key words: vermicular cast iron, microstructure properties, nodularity, hardness

Sažetak:

Proizvodnja vermikularnog lijeva metodom točnog dodatka legure za obradu na bazi Mg otežana je vrlo uskim područjem količine rezidualnog Mg, često manjem od ± 0,001%, što se s obzirom na varijable postupka teško postiže. Mikrostruktura vermikularnog lijeva izuzetno je osjetljiva na debljinu stjenke odljevka, odnosno intenzitet hlađenja, što zahtijeva optimiziranje i strogu kontrolu proizvodnih parametara u cilju postizanja traženih svojstava odljevaka od vermikularnog lijeva.

U okviru ovog rada analiziran je utjecaj intenziteta hlađenja na postignuta mikrostrukturna svojstva i tvrdoću odljevaka od vermikularnog lijeva. Ustanovljeno je da povećanje intenziteta hlađenja rezultira višim udjelom nodularnog grafita i perlita u mikrostrukturi te porastom tvrdoće vermikularnog lijeva.

Ključne riječi: vermikularni lijev, mikrostrukturna svojstva, nodularnost, tvrdoća

1.0. INTRODUCTION

Vermicular cast iron is kind of cast iron whose main characteristic is excretion of graphite in so called vermicular or compacted shape according to HRN EN ISO 945:2002 (“Cast iron – Designation of microstructure of graphite”) [1]. According to this standard, vermicular graphite is specified by shape III. Designation of this material is base on HRN EN 1560:1997 (“Founding – Designation system for cast iron”). Vermicular cast iron possesses wide use due to its favorable combination of properties, first in automotive industry for building engine block and head, parts of brake system, pressure clutch plate, etc.

Production methods of vermicular cast iron are based on precisely addition of alloy which contains compacting elements (Mg, Ce) or addition of alloy which contains compacting elements (Mg, Ce) and non compacting elements (Ti, Al etc.) [2, 3]. Treatments of melt with alloy which contains Mg besides addition of non compacting elements (Ti) considerably make easy production process of vermicular cast iron. At the same time, Ti remarkably decreases machinability of castings and influence on contamination of returned material what makes production of nodular cast iron considerably hard within same foundry [4]. Due to this weakness, more and more used method in practice is method based on precisely addition of alloy which contains Mg. Disadvantage of this method is very tight range of residual Mg, often less than ± 0,001% [5], what is hard to obtain regarding process variables (treatment temperature, content of S and O in melt). Crystallization of graphite is not controlled only by residual Mg but also by dissolve oxygen and nitrogen and oxides and silicates present in melt. Those facts make process control of production of vermicular cast iron distinctly complex.

To obtain acceptable microstructure and mechanical properties of vermicular cast iron (max. 30% nodular graphite, without lamellar graphite) [5] special attention should be dedicated to [4-7]:

- the metallurgical state of base iron (nucleation state of melt, quantity of dissolved oxygen and nitrogen, content and type of oxides, sulphides, silicates, nitrides etc., carbon equivalent, content of S and Mn etc.),
- process parameters (structure of charge materials, stay time in furnace, preheating of ladle, treatment temperature, velocity of melt tapping from furnace, place of strike of stream melt in ladle, preparation of reaction chamber and quantity of steel cover),
- type and quantity of alloy for treatment (best results in practice show alloys for treatment with exactly balanced contents of Mg and elements of rare earths (RE)),
- inoculation of melt (small change in quantity of addition of inoculant could be increasing share of nodular graphite in microstructure),

Cooling intensity has considerable influence on microstructure properties of vermicular cast iron, first of all on share of nodular graphite in microstructure. Therefore, optimization of process parameters (addition of alloy for treatment and addition of inoculant) is requested.

In this paper influence of section thickness of casting (cooling intensity) on microstructure properties and hardness of vermicular cast iron has been analyzed.

2.0. EXAMINATION METHODOLOGY

Examinations have been performed in foundry “Dalit Corp.” d.d. in Daruvar. Vermicular cast iron melts have been made in induction furnaces capacity of 250 kg/charge. Treatment of base melt has been performed by "sandwich" method. Each melt has been divided on 5 equal parts and treated separately by various quantities of treatment alloy and inoculants. From treated melt test samples have been casted (step wedge test block) in mold made of green sand mixture due to examination of influence section thickness on share of nodular graphite in microstructure. Altogether, 27 melts have been made and casted. Metal charge for production of vermicular cast iron consists from returned material, special pig iron with low content of Mn and steel scrap. Treatment of base melt has been performed by alloy with exactly balanced ratio Mg and RE (rare earth), well-know as CompactMag® (5-6% Mg, 44-48% Si, 5-7% RE, 1,8-2,3% Ca, max. 1,0% Al). Inoculation of melts has been performed by foundry grade FeSi and special evaluate inoculant which contains Ba (Foundrisil®).

Chemical content of melt has been made on spectrometer ARL 3460. Metallographic examination of samples prepared by standard technique has been performed by light metallographic microscope with digital camera (OLYMPUS GX 51) and image analysis system (AnalySIS® Materials Research Lab).

3.0. EXAMINATION RESULTS AND DISCUSSION OF RESULTS

The goal of performed examination was to examine how change of cooling intensity, i.e. casting thickness, influences on obtained microstructure properties of vermicular cast iron.

Addition of alloy for treatment were in range from 0,3 – 0,35 wt%. Addition of inoculants in ladle were until 0,3 wt%. By variation of quantity and type of inoculants and alloy for treatment it has been tried to ascertain their influence on residual content of Mg, formation of carbides and share of nodular graphite in microstructure. Postinoculation, i.e. inoculation in stream was applied during the casting on some melt in quantity to 0,15 wt%. Treatment temperatures of melt were in range from 1500 – 1525°C.

Step wedge tests blocks have been made by casting of melt in mold made of green sand mixture. Figure 1 shows shape and dimensions of step wedge test block.

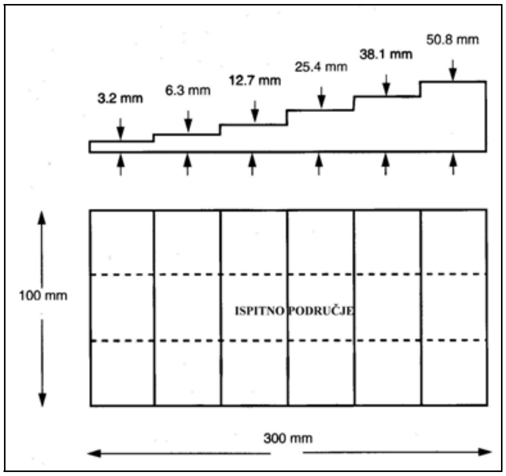

Figure 1. Step wedge test block

Step wedge test block has 6 ”steps” of various thickness which simulate casting thickness. By taking of test samples from step wedge test block and their metallographic analysis, influence of section thickness, i.e. cooling intensity on microstructure properties of vermicular cast iron could be examined. The highest cooling`s velocity, i.e. the highest cooling intensity has section of smallest thickness.

Examples of obtained results for one of analysed melt are shown in table 1 and 2. Table 1 shows chemical content of melt 1L2. Table 2 shows results of metallographic and hardness examination of the samples with various thicknesses made from step wedge test block.

On each test sample 5 optical micrographs have been made in order to of properly determination of the nodularity and share of ferrite in microstructure. In microstructure carbides and phosphide eutectic had not been observed.

Table 1. Chemical composition of treated melt 1L2 (CompactMag® = 0,3%, Foundrisil® = 0,30% (in ladle))

	C, %	Si, %	Mn, %	P, %	S, %	Mg, %	Cr, %	Ni, %	Cu, %	Sn, %	Ti, %	Al, %
1L2	3,56	2,72	0,393	0,024	0,008	0,008	0,030	0,030	0,114	0,010	0,012	0,005

Table 2. Nodularity and share of ferrite in microstructure and hardness of examinated samples from step wedge test block (melt 1L2)

Section thickness, mm	Nodularity, %	Ferrite, %	Hardness HB 2,5/187,5/15
3,2	90,00	46,83	222
6,3	55,00	67,16	191
12,7	29,00	75,29	172
25,4	26,00	82,34	167
38,1	25,00	82,66	163
50,8	23,00	76,33	157

From table 2 it is visible the influence of section thickness on share of nodular graphite in microstructure of the samples. In thin section (3,2 and 6,3 mm), due to highest cooling`s velocity and highest degree of undercooling, mechanism of spiral growth of graphite (in *c* direction) is dominated. That results with high share of nodular graphite in microstructure, especially in section thickness 3,2 mm.

From table 2 it is visible that with increase of section thickness decreases hardness of vermicular cast iron. Figure 2 shows dependence of hardness on section thickness.

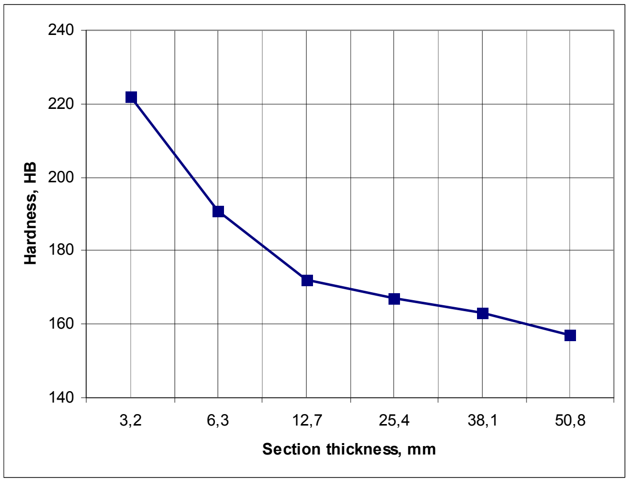

Figure 2. Dependence of hardness on section thickness of vermicular cast iron (melt 1L2)

Figure 3a – 3c show optical micrographs of examined samples from step wedge test block (melt 1L2).

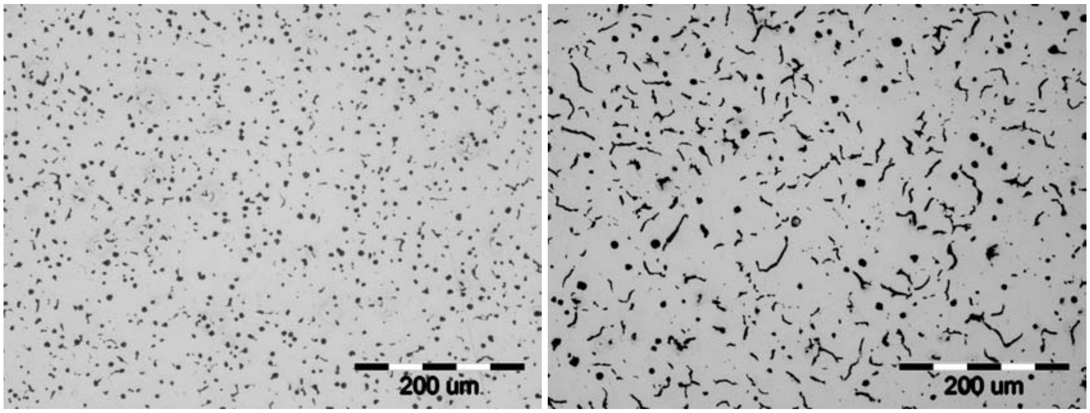

a) b)

Figure 3a. Optical micrographs of microstructure of samples from step wedge test block (melt 1L2), no etched: a) section 3,2mm, b) section 6,3 mm

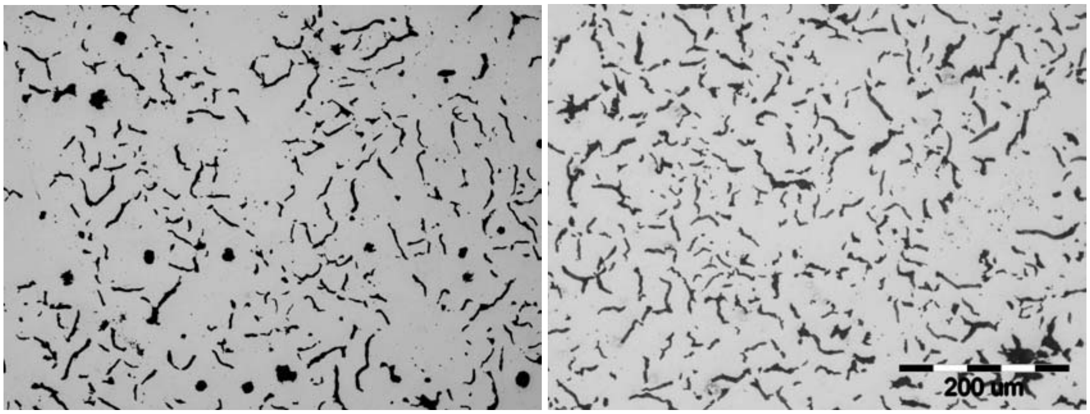

a) b)

Figure 3b. Optical micrographs of microstructure of samples from step wedge test block (melt 1L2), no etched: a) section 12,7mm, b) section 25,4 mm

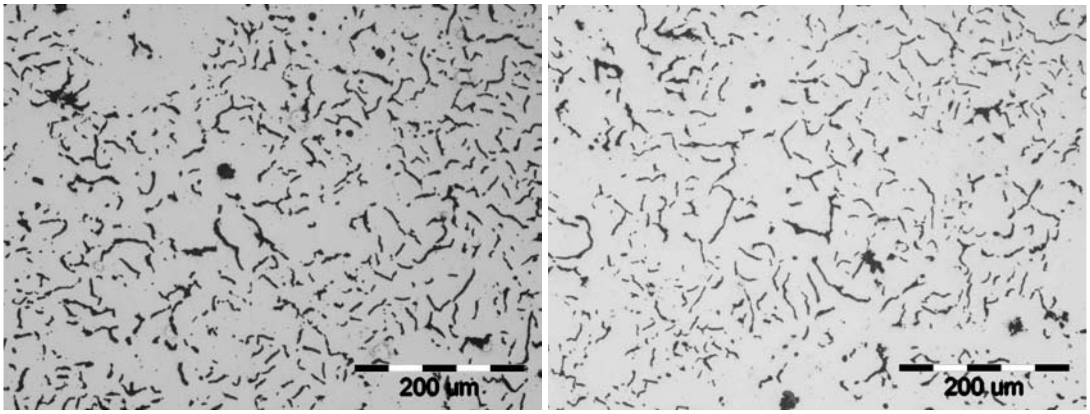

a) b)

Figure 3c. Optical micrographs of microstructure of samples from step wedge test block (melt 1L2), no etched: a) section 38,1 mm, b) section 50,8 mm

Besides of residual content Mg, which is of course the most important parameter which influences on share of nodular graphite in microstructure of vermicular cast iron, high influence has mode of inoculation (in ladle or in melt stream) and quantity of inoculant addition. By decrease of inoculant quantity, i.e. moderate inoculation, share of nodular graphite in microstructure could be decreased. On melts inoculated with 0,1 wt% Foundrisil® in ladle, without inoculation in stream, share of nodular graphite is decreased on ~ 85% in microstructure of section thickness 3,2 mm, i.e. on ~ 40% in microstructure of section thickness 6,3 mm. All melts have residual content of Mg in range of 0,007 – 0,010%.

4.0. CONCLUSION

Based on performed examination of influence of cooling intensity on obtained microstructure properties and hardness of casting of vermicular cast iron the following is ascertained:

- due to susceptibility of vermicular cast iron on casting section thickness, i.e. cooling intensity, toward the share of nodular graphite in microstructure, low residual content of Mg inside very narrow limit is requested, as well as moderate inoculation of melt which has to prevent formation carbides and retention acceptable nodularity. In section thickest (3,2 mm) it is very hard to obtain acceptable nodularity due to high cooling`s velocity, i.e. high degree of undercooling which determine mode of graphite crystal growth.
- for castings with distinctly changeable section thickness (for example: engine blocks) or thin section (for example: cylinder liner) except of quantity of residual Mg and type, quantity and place of inoculation, special attention is required for metal charge material and possible quantity of elements which generate carbides (Mn, Cr, V, Ti etc.),
- hardness of vermicular cast iron decreases with increase of section thickness. That is related to decrease of share of pearlite in microstructure,
- it is possible to continue the examination by application of other alloys for melt treatment which are available on market. Assigned results should be compared.

5.0. LITERATURE

[1] Državni zavod za normizaciju i mjeriteljstvo, HRN EN ISO 945:2002, Zagreb, 2002.
[2] C.M. Ecob, C. Hartung, An Alternative Route for the Production of Compacted Graphite Irons, Foundry Trade Journal 177(2003)3600, 6-11.
[3] F. Unkić, I. Popović, R. Dmitrović, Utjecaj titana i aluminija na dobivanje i mehanizam skrućivanja lijevanog željeza s vermikularnim grafitom, Livarstvo 5(1990)2, 35-43.
[4] R.V. Sillén, Process Control Methods for Production of Castings in Compacted Graphite Iron, The 66th World Foundry Congress, Casting Technology 5000 Years and Beyond, Foundrymen`s Association of Turkey, editor: Kubilay Dal, 1017-1030, Istanbul, Turska, 6-9 september 2004.
[5] S. Dawson, Controlling the Production of Compacted Graphite Iron, Modern Casting, 88 (1998)12, 38-41.
[6] M. Lampić, Eine neue Chance für Gußeisen mit Vermiculargraphit, Giesserei, 79(1992)21, 872-878.
[7] M. Lampič, Kontrola procesa pri taljenju in modifikaciji litega železa s posebnim pogledom na litino z vermikularnim grafitom, Zbornik referatov 34. livarskega strokovnega posvetovanja, Društvo livarjev Slovenije in Katedra za livarstvo, metalurgija, Univerza v Ljubljani, urednik: M. Trbižan, 186-212, Portorož, 27. 29. maj 1993

FRAKTOGRAFSKA ANALIZA NISKOLEGIRANOG Cr-Mo-Nb ČELIKA NAKON ELEKTROLUČNOG ZAVARIVANJA POD PRAHOM

FRACTOGRAPHIC ANALYSIS OF LOW ALLOYED Cr-Mo-Nb STEEL AFTER SUBMERGED ARC WELDING

Mirko Gojić[1], Boro Mioč[2] i Ladislav Kosec[3]

[1] Metalurški fakultet Sisak, Aleja narodnih heroja 3, 44103 Sisak, Hrvatska
[2] TIM TOPUSKO, Tvornica istegnutih metala, d.o.o., Školska bb, 44415 Topusko, Hrvatska
[3] Naravoslovnotehniška fakulteta, Univerza v Ljubljani, Aškerčeva 12, 1000 Ljubljana, Slovenija

[1] Faculty of Metallurgy, University of Zagreb, Aleja narodnih heroja 3, 44103 Sisak, Croatia
[2] TIM TOPUSKO, Company of extended metals, Ldt., Školska bb, 44415 Topusko, Croatia
[3] Faculty of Natural Sciences and Enginnering, University of Ljubljana, Aškerčeva 12, 1000 Ljubljana, Slovenia

Sažetak:

U radu su prikazani rezultati fraktografske analize prijelomnih površina ostataka uzoraka nakon ispitivanja mehaničkih svojstava i udarne radnje loma zone taljenja niskolegiranog Cr-Mo-Nb čelika nakon EPP zavarivanja. Ispitivanja su provedena pretražnim elektronskim mikroskopom (SEM) opremljenim sustavom za energetsko disperzijsku (EDS) analizu. Utvrđeno je da su prijelomne površine karakterizirane sitnojamičastim duktilnim prijelomom. Iniciranje prijeloma odvijalo se na međupovršinama karbid/metalna osnova i uključak troska/metalna osnova. Zapažena su i područja krhkog transkristalnog prijeloma.

Ključne riječi: niskolegirani čelk, EPP zavarivanje, prijelomna površina

Abstract: In this work the results of fractrographic analysis of fracture surfaces of samples after tensile testing and impact energy of weld metal for low-alloyed Cr-Mo-Nb steel after submerged arc welding are shown. Tests were carried out using scanning electron microscopy (SEM) equipment with device for energy dispersive spectrometry (EDS) analysis. It was was found that fracture surfaces characterized by ductile fracture. Also the field of brittle transgranular fracture are observed. Initiation of the failure was at interfaces carbide/matrix and nonmetallic inclusion slag/matrix, respectively.

Key words: low-alloyed steel, submerged arc welding, fracture surface

UVOD

Uporaba niskolegiranih zavarljivih toplinski otpornih čelika vrlo je raširena na energetskim postrojenjima [1]. Zavareni čelični proizvodi iz ovih čelika najčešće se izrađuju u obliku limova i cijevi. Mikrostruktura im je feritno-perlitna (ako su normalizirani) ili bainitna (ako su kaljeni i popušteni). Među niskolegiranim čeličnim proizvodima koji se koriste u termoenergetskim postrojenjima, kemijskim i procesnim postrojenjima najčešće se koriste čelici legirani molibdenom, te molibdenom i kromom [2].

Molibden i krom stvaraju karbide koji usporavaju puzanje, povećavaju prokaljivost i otpornost na popuštanje [3]. Osim toga krom pozitivno utječe na povećanje mehaničkih svojstava, istezljivosti i oksidacijske otpornosti. Mikrolegiranje niskolegiranih čelika ima ulogu usitnjenja zrna što se pozitivno odražava na parametre plastičnosti (istezanje, kontrakcija, žilavost).

Često tijekom uporabe niskolegiranih čelika za kemijska i procesna postrojenja može doći do neočekivanih prijeloma. Zato je nužno poznavati fraktografsku analizu prijelomnih površina nakon ispitivanja mehaničkih svojstava zavarenih spojeva [4, 5].

EKSPERIMENTALNI DIO

Lim debljine 18 mm iz niskolegiranog Cr-Mo-Nb čelika (tablica 1) pripremljen je u obliku X-spoja za zavarivanje. Predgrijavanje ploča 1000x300x18 mm provedeno je kod temperature 190°C. Korijen zavara provaren je netaljivom elektrodom pod zaštitom plina (TIG postupak) uporabom DCMS-IG elektroda promjera 2,4 mm. Postupkom elektrolučnog zavarivanja pod zaštitom praha (EPP postupak) provedena je popuna zavarenog spoja u 11-17 prolaza uporabom S2CrMo1 elektrode promjera 2 mm kod brzine zavarivanja 0,45 m/min. Nakon mehaničkih ispitivanja provedena je analiza prijelomnih površina pretražnom elektronskom mikroskopijom (SEM) uz uporabu sustava za energetsko disperzijsku analizu.

Tablica 1. Kemijski sastav osnovnog metala, mas. %

C	Mn	P	S	Si	Mo	Al	Cr	Ni	Cu	Nb
0,07	1,40	0,016	0,003	0,46	0,45	0,04	1,42	0,49	0,09	0,06

REZULTATI I DISKUSIJA

Budući da elektrolučni postupak zavarivanja pod prahom spada u postupke zavarivanja taljenjem tijekom zavarivanja u zoni taljenja dolazi do miješanja osnovnog i dodatnog materijala (elektrode). Iz kemijskog sastava zone taljenja (tablica 2) vidljivo je da je on sličan kemijskom sastavu osnovnog metala (tablica 1).

Tablica 2. Kemijski sastav zone taljenja, mas. %

C	Mn	P	S	Si	Mo	Al	Cr	Ni	Cu	Nb
0,09	1,43	0,012	0,003	0,62	0,47	0,03	1,19	0,14	0,08	0,015

Ispitivanje prijelomnih površina provedeno je na standardnim uzorcima koji su stanjeni u području zavarenog spoja. Ispitivanje udarne radnje loma provedeno je

Charpyevom metodom na standardnim uzorcima 10x10x55 mm s V-zarezom dubine 2 mm u sredini zone taljenja kod sobne temperature.

Iz mikrofraktografija pokazanih na slikama 1 i 3 vidljivo je da nakon ispitivanja udarne radnje loma postoje područja miješanog prijeloma osnovnog materijala. Međutim primaran je transkristalni prijelom kojeg karakteriziraju ravne površine. Prijelom je započinjao na međupovršini karbid/metalna osnova (slika 2). Iz usporedbe prijelomne površine kod istog povećanja (18x) zapaženo je da je nakon zavarivanja došlo do smanjenja kontrakcije uzoraka (za oko 32%) zone taljenja (slika 4) u odnosu na osnovni materijal.

Prijelomne površine zone taljenja primarno karakterizira sitnojamičasti prijelom (slike 5 i 7). Unutar sitnih jamica (0,3-3 μm) prisutni su karbidi (slika 6). Zapaženo je i da prijelom započinje oko kompleksnog uključka troske (slika 7).

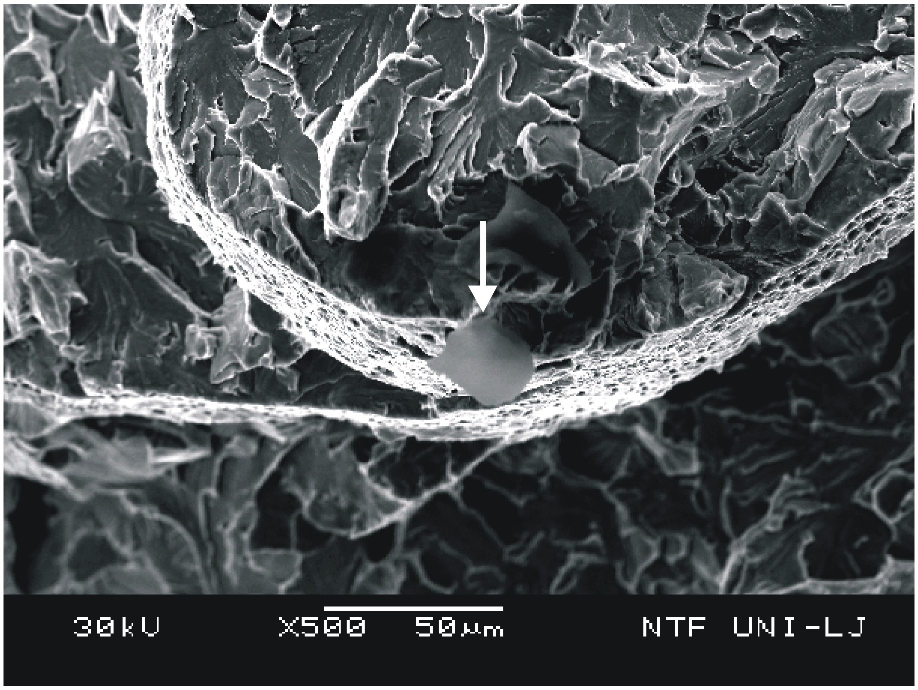

Slika 1. SEM mikrofraktografija osnovnog materijala nakon ispitivanja udarne radnje loma (22 J) kod povećanja 500x, I pozicija

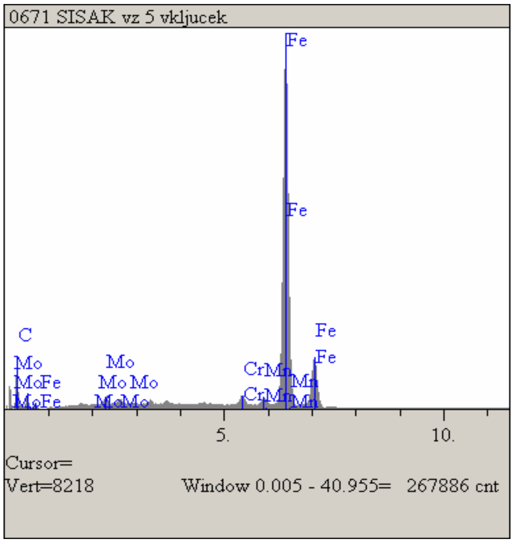

Element	Linija	Intenzitet (c/s)	Mas. %
C	K_α	60,48	24,831
O	K_α	21,67	3,798
Cr	K_α	28,81	0,785
Mn	K_α	18,49	0,531
Fe	K_α	1191,83	68,943
Mo	K_α	14,09	1,113
Ukupno			100,000

Slika 2. EDS spektar karbidne čestice označene strelicom na slici 1

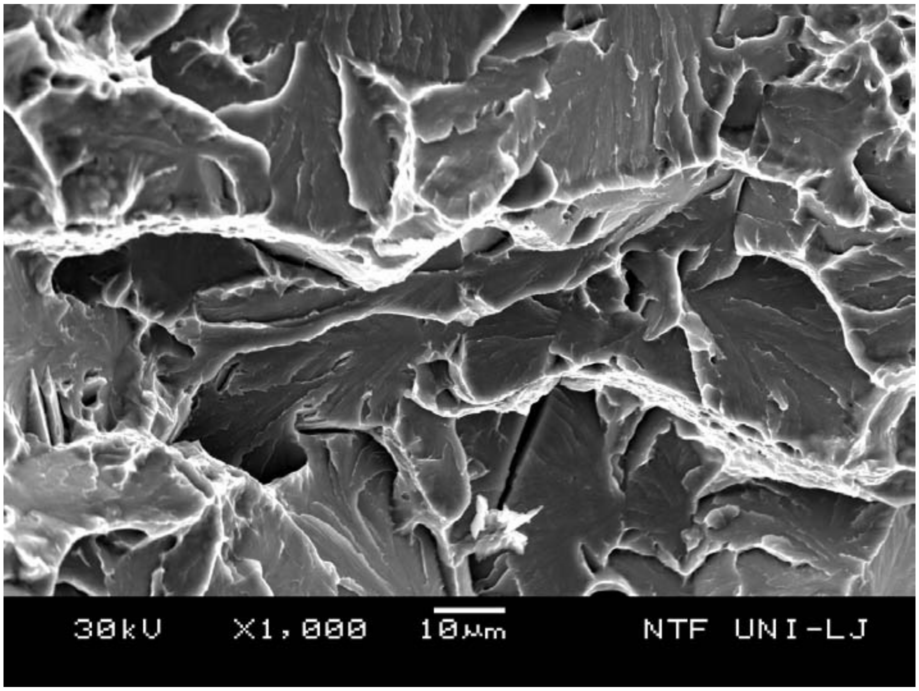

Slika 3. SEM mikrofraktografija osnovnog materijala nakon ispitivanja udarne radnje loma (22 J) kod povećanja 1000x, II pozicija

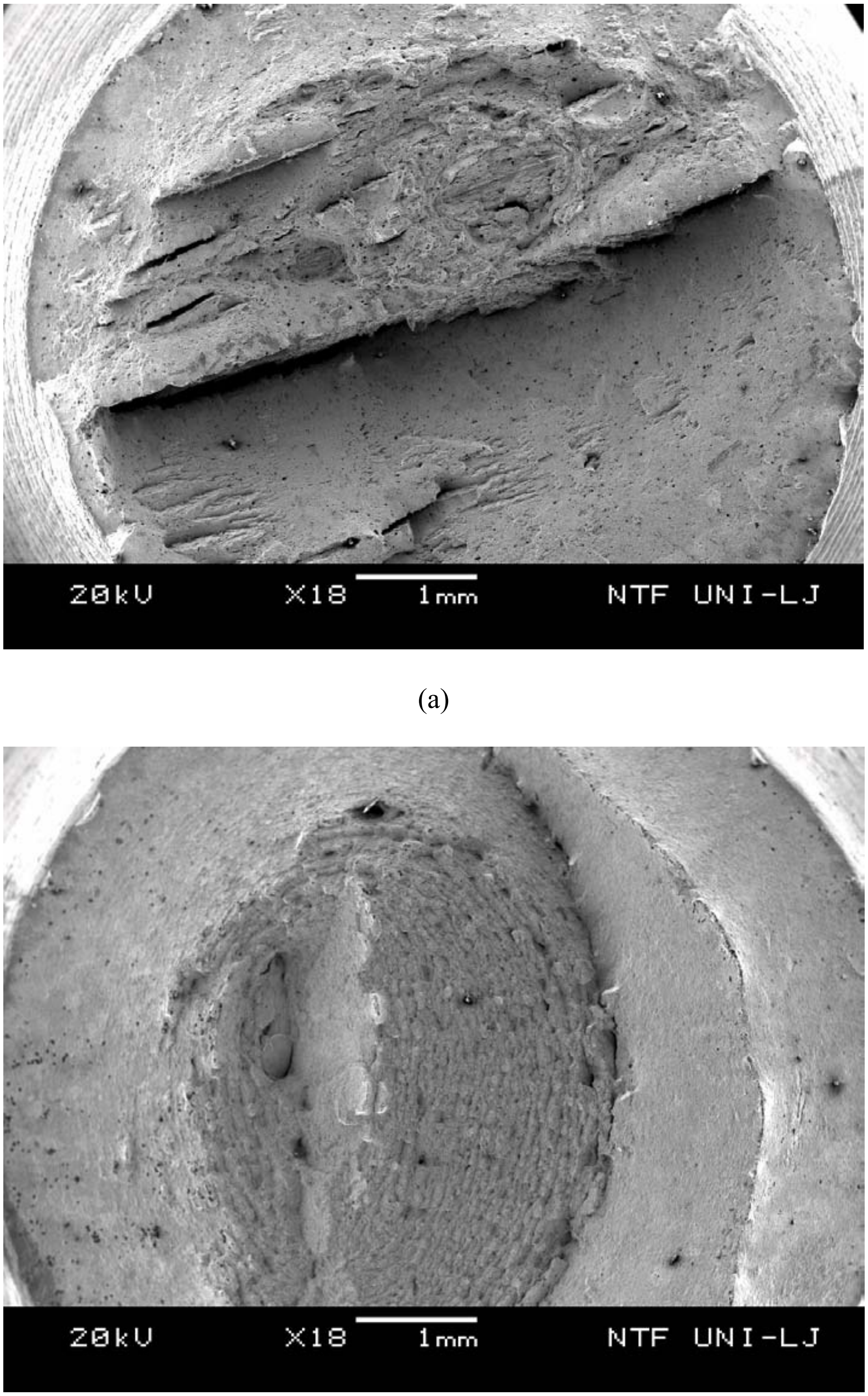

(a)

(b)

Slika 4. SEM mikrofraktografija osnovnog materijala (a) i zone taljenja (b) uzoraka nakon ispitivanja vlačne čvrstoće kod povećanja 18x

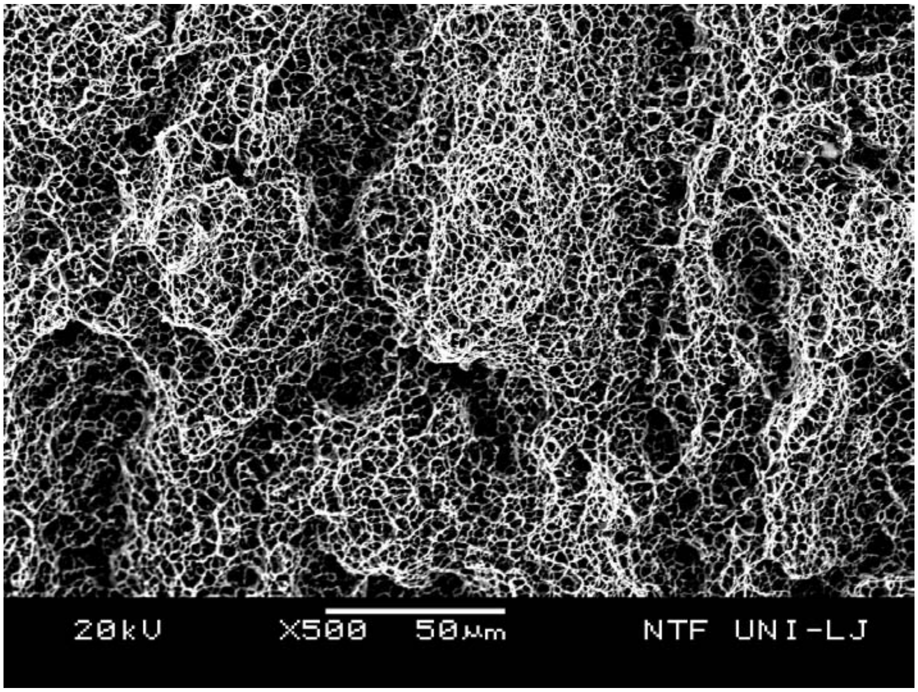

(a)

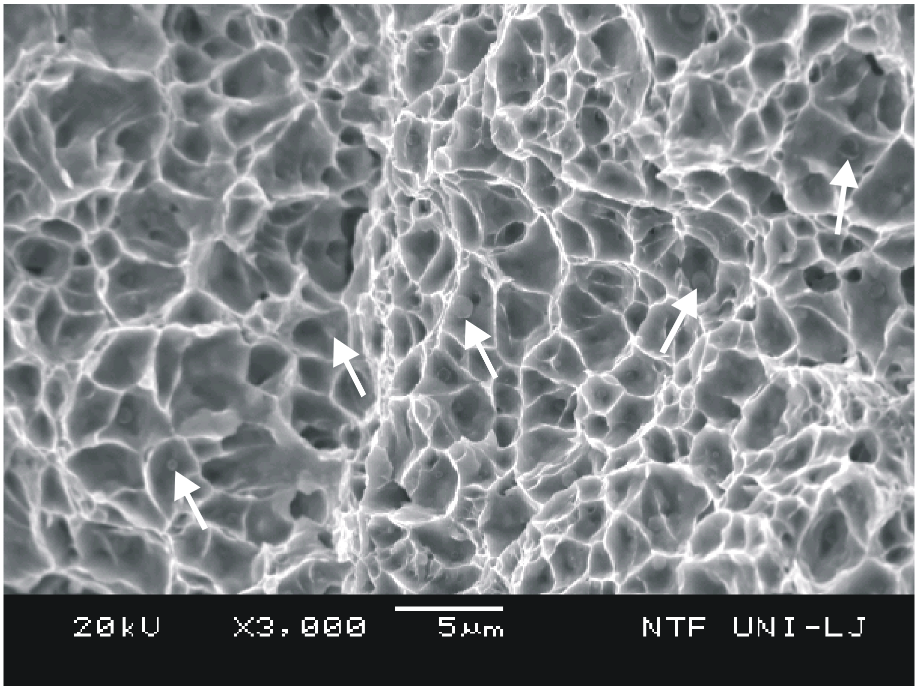

(b)

Slika 5. SEM mikrofraktografija zone taljenja kod različitih povećanja uzoraka nakon ispitivanja vlačne čvrstoće, a – 500x, b – 3000x

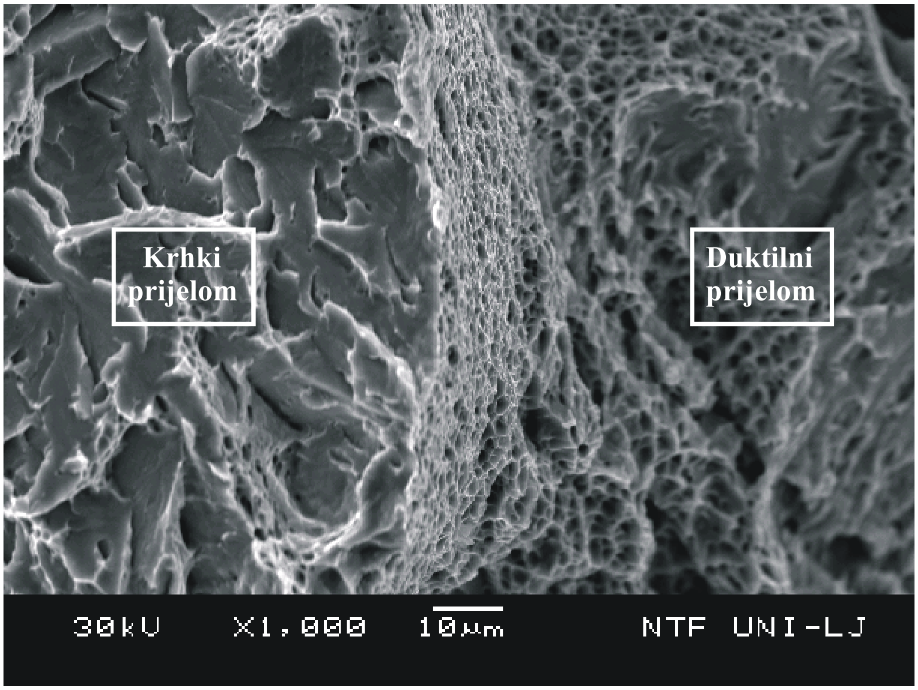

(a)

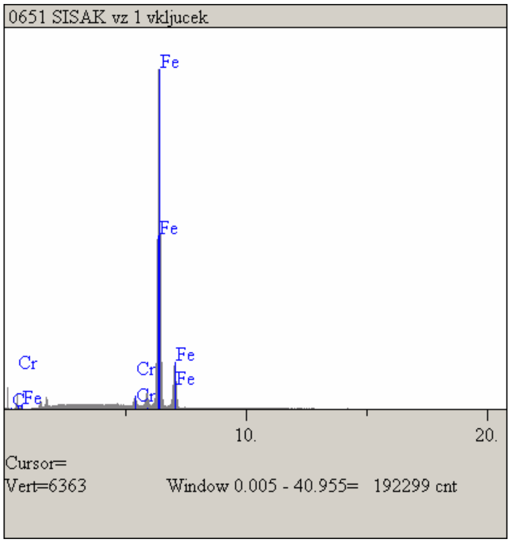

Element	Linija	Intenzitet (c/s)	Mas. %
C	K_α	0,37	0,358
Cr	K_α	25,51	1,023
Fe	K_α	927,66	98,619
Ukupno			100,000

(b)

Slika 6. SEM mikrofraktografija (a) s odgovarajućim EDX spektrom (b) čestica u jamicama plastičnog prijeloma uzoraka nakon ispitivanja udarne radnje loma (91 J)

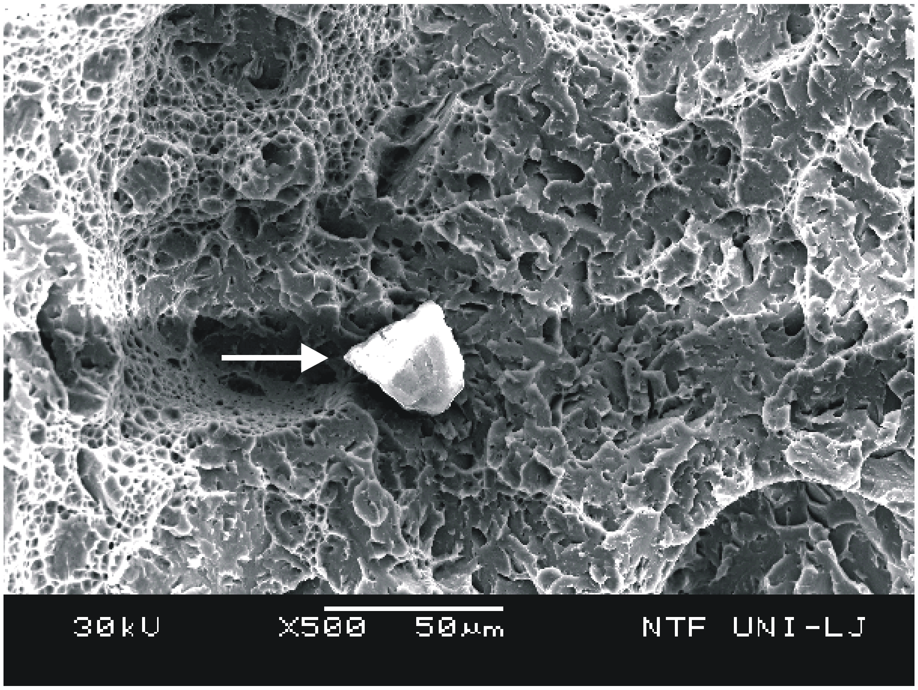

(a)

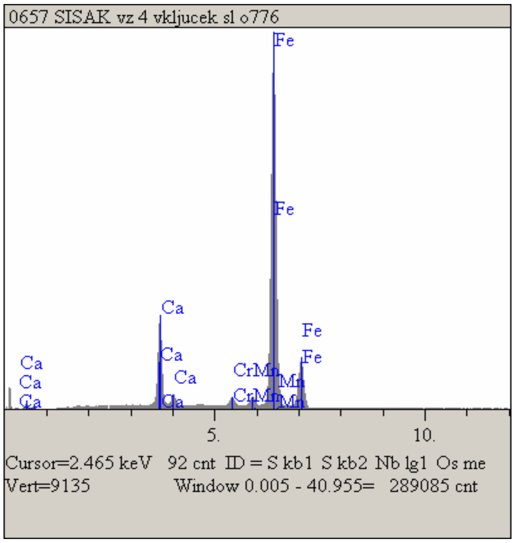

Cursor=2.465 keV 92 cnt ID = S kb1 S kb2 Nb lg1 Os me
Vert=9135 Window 0.005 - 40.955= 289085 cnt

Element	Linija	Intenzitet (c/s)	Mas. %
O	K_α	14,02	2,383
Ca	K_α	264,23	9,623
Cr	K_α	26,94	1,002
Mn	K_α	27,69	1,098
Fe	K_α	1314,98	85,895
Ukupno			100,000

(b)

Slika 7. SEM mikrofraktografija (a) s odgovarajućim EDS spektrom uključka (b) na prijelomnoj površini uzorka nakon ispitivanja udarne radnje loma (44 J), povećanje 500x

ZAKLJUČAK

Na temelju provedenih istraživanja prijelomnih površina može se zaključiti sljedeće:

- Prijelomne površine osnovnog materijala karakterizira primarno krhki transkristalni prijelom.
- Zonu taljenja nakon mehaničkih ispitivanja karakterizira primarno sitnojamičasti duktilni prijelom s veličinom jamica od 0,5 do 3 μm.
- Zapaženo je da prijelom započinje na međupovršinama karbid/metalna osnova ili uključak troske/metalna osnova.

LITERATURA

1. M. Gojić, L. Kosec, D. Pinotić, Mikrostruktura 2.25Cr - 1Mo čeličnih cijevi prije i nakon zavarivanja, Zbornik 2. međunarodnog znanstveno-stručnog savjetovanja SPECIJALNI POSTUPCI I PROIZVODI U TEHNICI ZAVARIVANJA, DTZ – Sl. Brod, 19-21.11.2003, Slavonski Brod, str. 149-158.
2. R. C. Thomson, H. K. D. H. Bhadeskia, *Materials Science and Technology* **10** (1944) 3, str. 205-208.
3. T. Filetin, F. Kovačiček, J. Indof, Svojstva i primjena materijala, Fakultet strojarstva i brodogradnje, Zagreb, 2002.
4. S. Ahila, V. M. Radhakrishnan, S. R. Iyer, *Journal of Materials Science Letters* **12** (1992) 16, str. 1296-1298.
5. M. Gojić, L. Kosec, *ISIJ International* **37** (1997) 4, str. 412-418.

THERMAL BEHAVIOUR OF THERMOPLASTIC POLYURETHANE /POLYPROPYLENE BLENDS

Emi Govorčin Bajsić & Vesna Rek
Faculty of Chemical Engineering and Technology, P.O.Box 177, Zagreb, Croatia
e-mail:egovor@marie.fkit.hr

Abstract:
The melting and crystallization behaviour of blends consisting of thermoplastic polyurethane (TPU) and an isotactic polypropylene (i-PP) have been investigated by differential scanning calorimetry (DSC). Glass transition temperature was also measured by DSC to estimate the compatibility of the blends. Blends of different ratios of TPU/PP were produced by melt mixing using a Haake Record 90 twin –screw extruder. The investigation indicated that the total degree of crystallinity of the blends increases with the increase in the PP content. The melting peaks of the blends shifted to a higher temperature as the PP content was increased. The crystallization temperature of the PP decreases with increasing TPU content and a new crystallization peak appears. The crystallization of PP is obviously hindered by the presence of TPU and/or the mechanism of crystallization changes with composition. The glass transition temperature of the PP phase could not be detected by DSC. The Tg value of the TPU phase in the blends increases with increasing PP content, it may be assumed that the TPU/PP system is partially miscible.

Key words: polymer blends,thermoplastic polyurethane, DSC,crystallinity, compatibility.

Ključne riječi: polimerne mješavine, termoplastični poliuretan, diferencijalna pretražna
Kalorimetrija, kristalnost, kompatibilnost.

1.INTRODUCTION

Thermoplastic polyurethane (TPU) is an important class of elastomers that has found many novel and specialized applications where high mechanical and chemical performances are prerequisites. They are known for their good mechanical strengths, wear and tear resistance, and low-temperature elasticity [1,2]. TPUs are linear segmented copolymers, composed of micro-phase separated hard and soft segments. The hard segment domains, consisting of a diisocyanate extended with a short chain diol or diamin are distributed in the soft segment matrix which containing either polyesters or polyethers glycols. The hard segments are held together by hydrogen bonds, which form physical crosslinks these physical crosslinks are thermally labile at melt temperatures. Blending of polymers has been the subject of intensive research in both academic and industrial laboratories. The main goal of blending is modification of mechanical properties, improvement of impact strength at low temperatures, in particular abrasion resistance and, last but not least, improvement of processability[3]. Polymer blends are intimate mixtures of different commercially available polymers with no covalent bonds between individual component polymers [4]. Properties of the resulting materials may be tailored to meet requirements of customers or expectations of specific new applications with satisfactory balance of a wide range of material properties and costs [5]. The final materials are mostly characterized by combinations of the useful properties of the components of the polymer blend, superior to those of single polymers.It is well known that morphologies of a partially miscible polymer blend depend on its composition, morphology and preparation conditions.

Polyolefins may be blended with TPUs to reduce TPU's cost and improve TPU's thermal stability,mechanical properties and processing performance. On the other hand, TPU is blended with polyolefin to improve polyolefin's properties. Polypropylene (PP) belongs to the family of polyolefins, it is a vinyl polymer having hydrogen atom substituents $(\text{-}H_2C\text{-}CH_2)_n$ or $(H_2C\text{-}CRH\text{-})_n$. The idea of selecting PP as the second component comes mainly because of its ease of processing, chemical resistance, high melting point which giving high temperature stiffness, good rigidity and heat resistance and relatively low cost [6-8]. PP, as a dispersed phase in a TPU/PP blend can improve the physical properties of the blend.
The object of this work is the study of the thermal behaviour of pure thermoplastic polyurethane (TPU), pure polypropylene (PP) and their blends TPU/PP.

2. EXPERIMENTAL

Materials and preparation

Polyurethane (Desmopan 300) was commercial product of Bayer, Germany.It is a polyester-type TPU with hard segment formed by the addition of butanediol to diphenyl methane-4-4'-diisocyanate (MDI). Isotactic polypropylene (Novolen 1100 N, MFI= 12 g/ 10 min)) was supplied by BASF, Germany.
The pure polymers and TPU/PP blends were prepared in a Haake Record 90 twin-screw extruder. The temperatures of the four zones of the extruder were 170,180,180 and 200 °C, respectively. The screw speed was adjusted to 60 min $^{-1}$. The samples used for the measurements were prepared by pressing the extruded granules in a hydraulic press at 220°C.

Table 1. Composition of the studied samples

Sample	1	2	3	4	5	6	7
TPU/%	0	20	40	50	60	80	100
PP/%	100	80	60	50	40	20	0

Differential scanning calorimetry (DSC)

The thermal analysis of the pure components (TPU and PP) and TPU/PP blends was carried out using a Du Pont DSC 2910 Differential Scanning Calorimeter (TA Instruments, USA).Glass transition temperature of the samples was determined as follows: the samples were heated to 200°C at a heating rate of 20°C and maintained at his temperature for 10 min in order to eliminate any previous thermal history and then cooled to -100°C and maintained for 1 min and then heated to 250°C. Melt temperatures and crystallinity temperature of the samples were determined as follows: samples were heat-treated at 200 °C for 10 min to eliminate the thermal history, and then cooled down to 25°C at cooling rate of 10 °C/min and maintained at this temperature 1 min after that the samples were heated to 250°C.

3. RESULTS AND DISCUSSION

Figure 1 shows the DSC curve of the pure TPU. On this curve, the glass transition temperature (Tg) of the soft segment of TPU is at -41.1°C, the melting point is at 159.3 °C [9, 10]. One exothermic peak appears at about 70 °C, indicating the presence of the crystalline portion of TPU. The DSC thermogram of the pure PP is shown in Fig. 2. The DSC curve of PP shows one sharp endothermic peak at 162.2 °C which indicating melting of PP and exothermic peak at 118.4 °C which represents the crystalline phase in PP. The Tg of the PP phase cannot be determined by DSC.

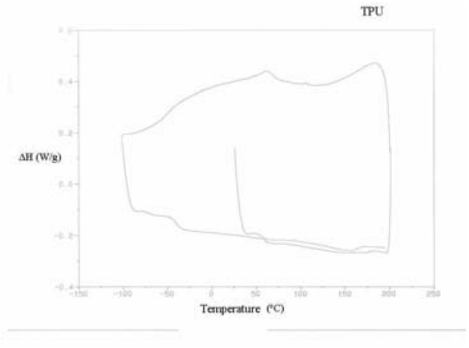

Figure 1. *DSC thermogram of pure TPU*

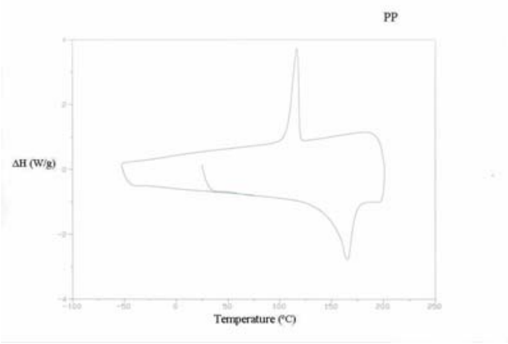

Figure 2. *DSC thermogram of pure PP*

The Tg of the TPU phase increases with increasing PP content of the blend indicating limited miscibility of the TPU and PP (Fig.3) .

DSC cooling and heating curves illustrating melting and recrystallization behaviour of the pure TPU, pure PP and TPU/PP blends are shown in Figs. 4 and 5 .What was noticed from the results is that the positions of the endotherm (Tm) and exotherm (Tc) peaks had shifted, depending of the blend ratio.

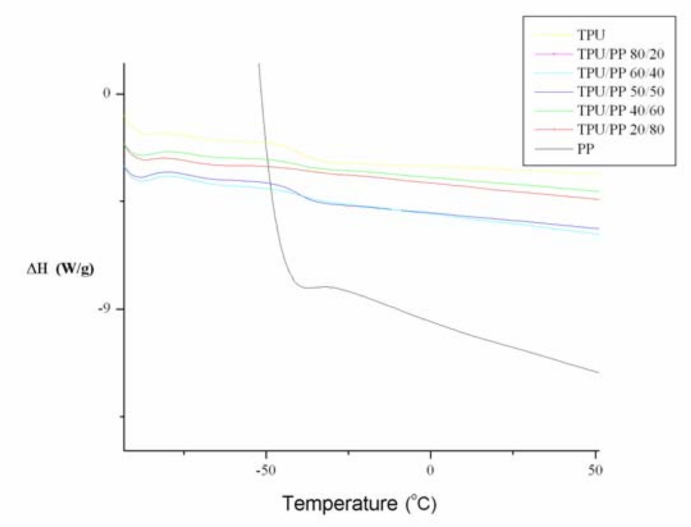

Figure 3. *The T_g of the pure components and TPU/PP blends*

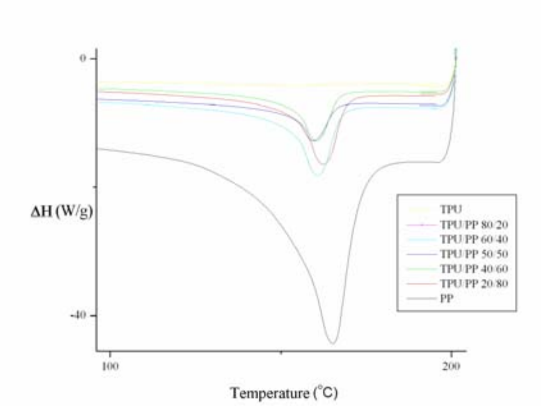

Figure 4. Me*lting behaviour of the pure components and TPU/PP blends*

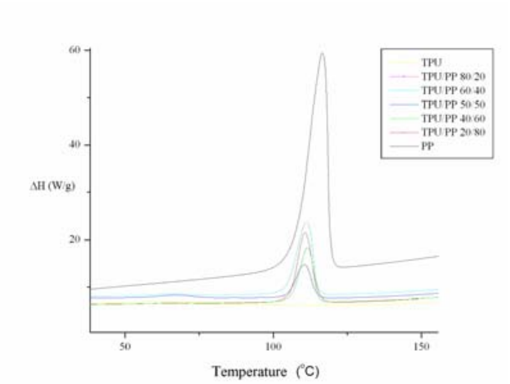

Figure 5. *Crystallization behaviour of the pure components and TPU/PP blends*

Note that as the PP content was increased in the blends, the melting peak of the polymer blends and the crystalline peaks of PP shifted to a higher temperature. The crystallization temperature of PP decreases with increasing TPU content. The crystallization of PP is obviously hindered by the presence of TPU and/or the mechanism of crystallization changes with composition. This behaviour was explained by a change in the mechanism of nucleation [11,12]. However, limited solubility may also lead to the observed decrease of crystallization temperature, since crystallization from solution starts at a lower temperature than from melt [13,14]. The thermal properties of the TPU/PP blends are summarized in Table 2.

Table 2. Physical properties of pure components and TPU/PP blends

Sample	T_{g1}/ ºC	T_m/ ºC	T_{c1}/ ºC	T_{c2}/ ºC	ΔH_c J/g	ΔH_m J/g
TPU/PP 100/0	-41,1	135,7	72,6	-	-	7,38
TPU/PP 80/20	-40,8	157,9	71,5	111,3	24,85	34,35
TPU/PP 60/40	-38,9	159,1	70,7	112,4	26,71	36,39
TPU/PP 50/50	-40,2	159,2	69,9	110,8	41,12	52,15
TPU/PP 40/60	-39,1	159,1	70,1	112,3	47,13	48,02
TPU/PP 20/80	-35,7	160,8	69,9	112,4	75,32	75,83
TPU/PP 0/100	-	162,5	-	118,4	96,91	103,2

Thermal parametars such as melting temperature (Tm) and the entalpy of crystallization (ΔH_c) of the studied samples are plotted as a function of composition (Fig. 6). They reveal chenges in morphology and in the amount of the crystalline fraction of the PP phase. It can be shown that the ΔH_m and T_m increase with increasing PP content. These results indicate some interaction of the components in the blends [15].

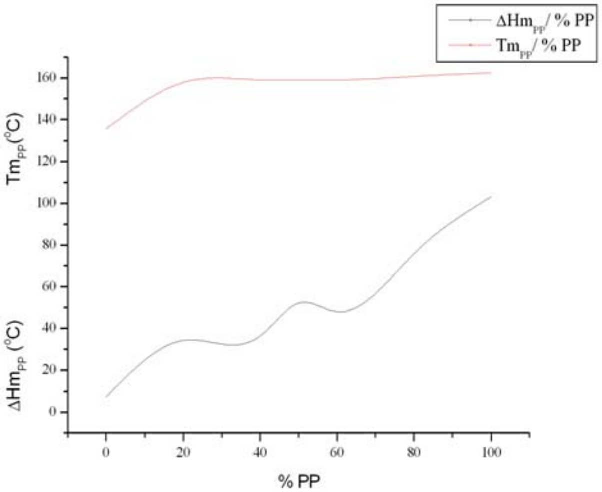

Figure 6. *Composition dependence of the melting characteristics of TPU/PP blends*

4. CONCLUSIONS

The T_g of the TPU phase increases with increasing PP content of the blend indicating limited miscibility of the TPU and PP. The ΔH_m and T_m increase with increasing PP content. These results indicate some interaction of the components in the blends.As the PP content was increased in the blends, the melting peak of the polymer blends and the crystalline peaks of PP shifted to a higher temperature.This behaviour was explained by a change in the mechanism of nucleation

5. REFERENCES

1. Domininghaus H. Plastics for engineers: materials, properties, applications. Munich: Hanser, 1988.

1. Walker BM, Rader CP. Handbook of thermoplastic elastomers, chap. 7. New York: Van Nostrand Reinhold, 1988.
2. N.C. Billingham, O.J. Hoad, F. Chenard and D.J. Whiteman. *Macromol. Symp.* 115 (1997)203–214.
3. F.P. LaMantia. *Angew. Makromol. Chem.* 216 (1994)45–66.
4. LaMantia FP. In: Halim Hamid S, Amin MB, Maadhah AG, editors. Handbook of polymer degradation. New York: M. Dekker, 1992. p. 95–126.
5. B. Lotz, J.C. Wittmann and A.J. Lovinger *Polymer* 37 (1996) 4979.
6. J. Varga *J Mater Sci* **27** (1992), p. 2557.
7. P. Jacoby, B.H. Bersted, W.J. Kissel and C.E. Smith *J Polym Sci Part B: Polym Phys* 24 (1986) 461.
8. R.W. seymour, S.L. Cooper, Macromolekules, 6 (1973) 48.
9. JT Koberstein, I Gancarz, TC Clark , J Polym. Sci, Polym. Phsy 24, (1986)2487.

10. B. Pukauszky, F. Tudos, A. Kallo, G. Bidor, Polymer, 30 (1989) 1399.

11. Ghijesels, N. Groesbeek, C.W. Yip, Polymer, 23 (1982) 1913.

12. J.K. Shah, L. E. Lakti, Ind. Eng. Chem. Prod Res. Dev. 12 (1973) 304.

13. Wunderlich, Macromolecular Physic: Cristal Nucleation, Growth, Annealing,vol 2, Academic Press, New York, 1967, 304.

14. C.P. Papadopoaloa, N.K. Kalfoglou, Polymer, 39 (1998) 7015.

10. Savjetovanje o materijalima, tehnologijama, trenju i trošenju
10. Conference on Materials, Processes, Friction and Wear
MATRIB'05, Vela Luka, 23-25.06.2005.

ENGINEERING SURFACES FOR EXTENDED LIFE

Maurice Grech
UNIVERSITY OF MALTA
FACULTY OF ENGINEERING
Department of Metallurgy and Materials Engineering

Abstract:

The demands and constraints imposed by today's engineering components can be quite intimidating. Machine parts may be required to be strong, tough, light, easily machinable, have high wear and corrosion resistance and satisfy many other physical, mechanical, electric, magnetic, optical, financial and esthetic requirements. Not surprisingly, such specific requirements frequently cannot be met by a single material, thus leading to the surface engineering design methodology. The natural sequence involved in the manufacture of components using surface engineering procedures include: the assessment of properties and design requirements, the selection of a material on the basis of bulk properties such as strength, toughness, ductility and density, and finally the selection of an overlay coating or surface modification technique which satisfies demands such as enhanced friction, wear and corrosion resistance and other surface characteristics. In this respect the bulk material and the surface can be considered as forming a composite material with properties unattainable in either the base or surface material alone.

In this lecture the major surface engineering technologies are reviewed namely:, plasma nitriding, carburizing, nitrocarburizing, induction hardening, shot peening, ion implantation, physical vapour deposition, chemical vapour deposition, thermal spraying and electro and electroless deposition. These techniques are discussed from aspects including processing method, coating/modified surface thickness, surface characteristics and properties as well as material and plant requirement.

Various applications are discussed and reference is made to a number of case studies involving among other TiN coatings applied using a PVD process, laser melting, laser transformation hardening and ion implantation. The author shows how these and other surface treatments serve to minimize costs by extending tool life, reducing machine down time and improving productivity. The writer demonstrates how these techniques simultaneously help improve the quality of the finished part and add value to the product.

The author highlights processes that are environmentally friendly and compares these to variants and/or other processes that involve the use of toxic materials. Attention is drawn to the fact that the competitiveness of traditional processes such a electroplating will be gradually eroded by the requirement to pass on additional health and safety and environmental control costs to the customer. The increasing financial and political pressures would encourage the uptake of environmentally friendly processes such as those involving vacuum, lasers, plasmas and ion beams.

10. Savjetovanje o materijalima, tehnologijama, trenju i trošenju
10. Conference on Materials, Processes, Friction and Wear
MATRIB'05, Vela Luka, 23-25.06.2005.

TRIBOLOGICAL BEHAVIOUR OF HARD WEAR RESISTANT LAYERS AT HIGH TEMPERATURES

Jiří Hájek[a]
Antonín Kříž[b]
Petr Beneš[c]
[a] ZČU Plzeň, Univerzitní 22, 306 14 Plzeň, ČR, hajek@kmm.zcu.cz
[b] ZČU Plzeň, Univerzitní 22, 306 14 Plzeň, ČR, kriz@kmm.zcu.cz
[c] ZČU Plzeň, Univerzitní 22, 306 14 Plzeň, ČR, beenndy@seznam.cz

Abstract

The contribution deals with study of tribological behaviour of thin film – substrate systems during the “PIN-on-DISC“ test. As experimental material were chosen hard, wear resistant layers CrAlSiN (nanocomposite), TiAlSiN (multilayer), AlTiN (with adhesive layer TiN). Thin layers were deposited on HSS substrates X82WMoCrV654. The experiment was taken under different temperatures in range from 20°C to 700°C. As counterparts were chosen ceramic materials Al_2O_3, Si_3N_4. The results show good resistance of all systems against wear at room temperature. However, there is a significant change in tribological properties of systems during the thermal load. Contribution also includes the attention to problems, which may distort measurement results and to which is important to pay attention during the test.

Keywords*:* ”PIN-on-DISC“, friction, wear, CrAlSiN, AlTiN, TiAlSiN

1. PREFACE

Nowadays there is transition from conventional cutting methods (with use of procedural liquid at lower speed) to high-speed dry cutting. That sets higher demands on cutting tools with thin layers. During cutting process noticeable thermal stress of tools and layer arises and influence of thermal treatment (up to 700°C) on tribological properties of thin layer-substrate system is investigated.

2. EXPERIMENTAL MATERIAL

On substrate from high-speed steel X82WMoCrV654 were deposited three various types of PVD layers. These are AlTiN, TiAlSiN, CrAlSiN.

Heat treatment of used specimens:

1. Hardening from 1200°C, cooling in oil.
2. Tempering twice at 560°C.
3. Tempering for the third time at 570°C, cooling in air.

Thin wear resistant layers were deposited on substrates by the PVD low-voltage arc evaporating in vacuum. Deposition temperature did not exceed 500°C, so the substrate was not thermally influenced.

3. TRIBOLOGICAL EXPERIMENT

Tribological experiment was provided on high temperature tribometer (CSEM INSTRUMENTS) by "PIN-on-DISC" method. "PIN" was a ball. Analysed was friction coefficient and character of failure of thin layers. Wear of "PIN" ball was also monitored by Light microscopy.

3.1 Wear resistance of thin layer - substrate system at room temperature

To learn the system's resistance was used "PIN-on-DISC" test with following parameters:

F [N]	r [mm]	v [cm/s]	n [number of cycles]	"PIN" ball
10	8	20	12 000	Al_2O_3

In figure 2 are illustrated courses of friction coefficient of all analysed layers at friction against "PIN" ball from Al_2O_3.

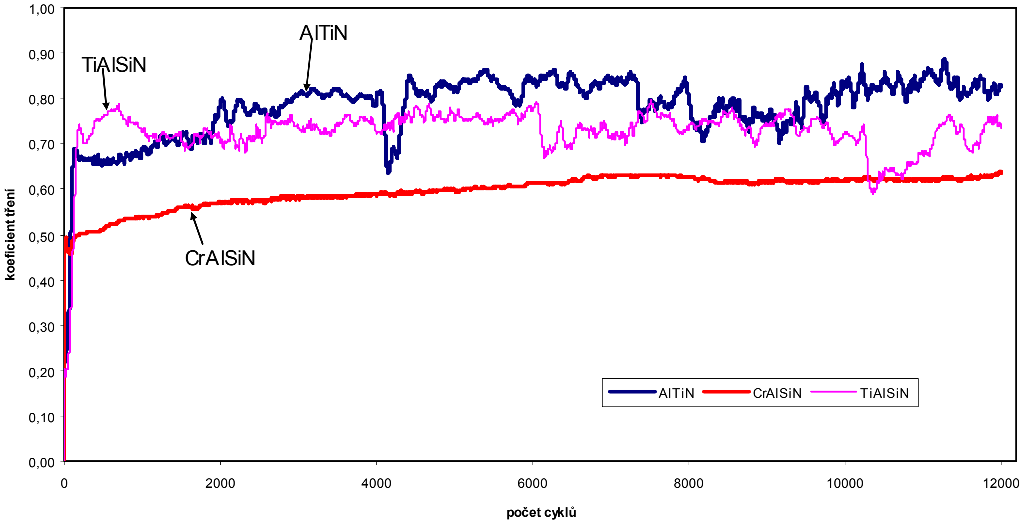

Fig. 2- Courses of friction coefficients, „PIN“-Al_2O_3, F = 10N, r = 8mm, T = 20°C, n = 12 000 cycles.

From results of friction coefficient and the state of tribological track is evident, that against hard Al_2O_3 ball most wear resistant layer is CrAlSiN. This resistance is evident for example from course of friction coefficient, which does not show strong deviation of friction coefficient values. This is probably caused by absence of pulled-out elements from layer in the tribological track. By AlTiN and TiAlSiN layers is wear of "PIN" ball covered by transfer layer. This layer inhibits contact of "PIN" ball with surface of thin layer [1]. These layers are strongly adhesively connected with the ball surface. By CrAlSiN layer this phenomenon did not arise. From this it is possible to conclude, that with increasing adhesive - cohesive properties of these layers, possibility of transfer layer generation declines. Transfer layer is composed from debris from thin layer - substrate system, which with influence of simultaneous high contact pressure in the contact of "PIN" ball and arisen frictional heat step by step weld on surface of the ball.

Production of adhesive sticked elements on "PIN" ball is related to presence of acoustic emission. Strong acoustic emission was registrated by AlTiN layers (from 9300 cycles). By TiAlSiN layer was registrated only weak acoustic emission. Experiment by CrAlSiN proceeded without any acoustic emission. Resulting from that it is possible to come to a conclusion, that acoustic emission is evocated by the presence of adhered elements on "PIN" ball. Resulting from microscope observation, the most wear resistant layer against Al_2O_3 ball is layer CrAlSiN. Damage of this layer is only slight. By this layer and also by TiAlSiN, there was no substrate exposure.

3.2 Resistance of system thin layer - substrate at thermal influence

Layers were during tribological experiments exposed to temperatures 500°C and 700°C. These temperatures correspond to cutting temperatures (fig. 3). It is also necessary to consider the changes of substrate hardness and hardness of thin layer in dependence on temperature.

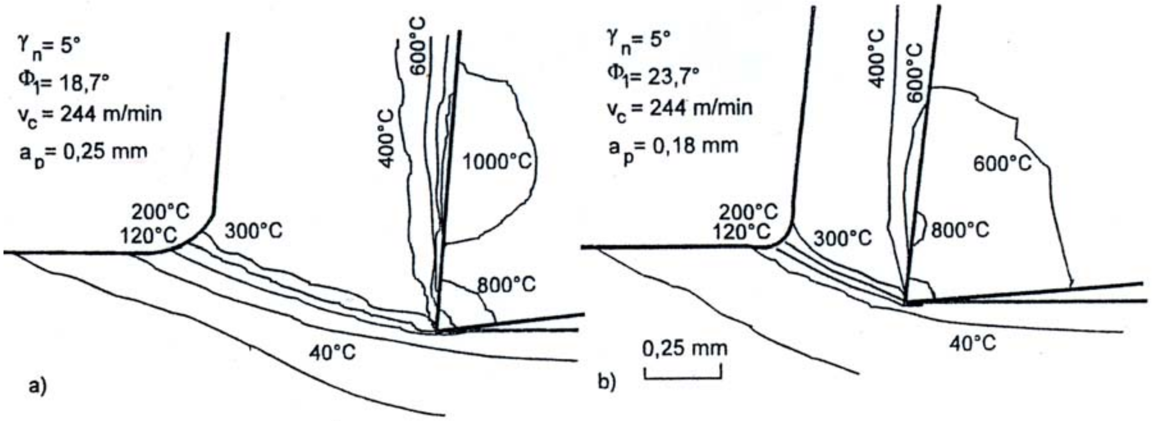

Fig. 3 –Temperatures during machining

Tay *et.al*

At high temperature experiments was used only the ball from Si_3N_4. Parameters of high temperature measurements are in table 1.

F [N]	r [mm]	v [cm/s]	Temperature [°C]	n [number of cycles]	"PIN" ball
2	4	10	700	3 500	Si_3N_4
	2	5	500	3 500	Si_3N_4

3.3 Layer AlTiN

From figure 4 is noticeable difference in friction coefficient at 500°C, which was higher, than at 700°C. At 500°C there are evident two increases of friction coefficient values. Friction coefficient at 700°C is stationary. Higher friction coefficient at 500°C is probably caused by adhesive wear. During this test the oxidation of wear debris creates the compact unit - glaze. It is probable that the time to the glaze creation is connected with increasing friction coefficient. After its creation only slight wear appears. This claim confirms the fact, that the wear of "PIN" ball is very low. At 700°C is friction coefficient influenced by thick oxidised film, whose plasticity at 700°C is lower than at 500°C, which may result in decrease of friction coefficient [1].

At 500°C were found in the wear track areas with plastic deformation of thin layer. At 700°C this phenomenon was not registered. Surface of the track after tribological experiment at 500°C is coated by oxidised film. This oxidised film is created by mixture of debris from thin layer and oxidised Al_2O_3 film. Oxidised film does not contain elements from "PIN" ball. At 500°C stayed in the track on several places undamaged layer AlTiN of original thickness. The substrate revealed at 700°C in the middle of the track.

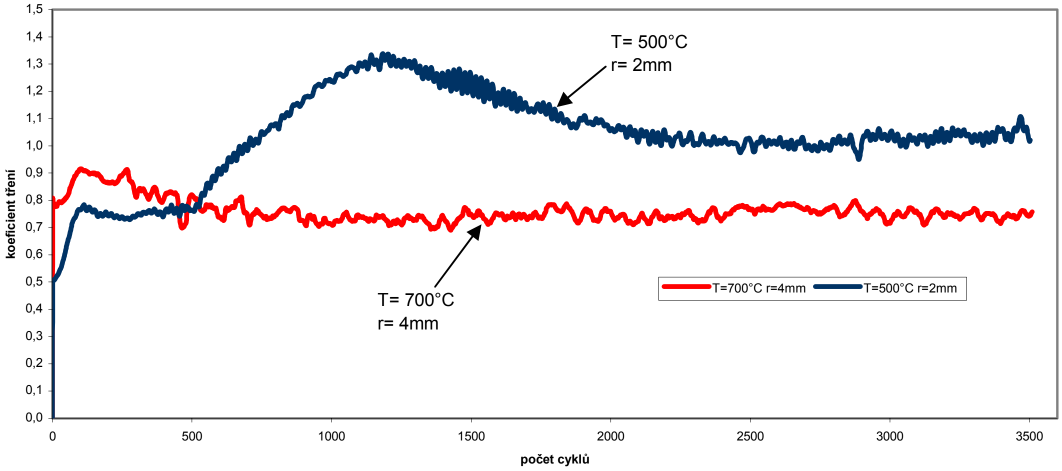

Fig. 4- AlTiN - courses of friction coefficients, T= 500°C, 700°C, F= 2N

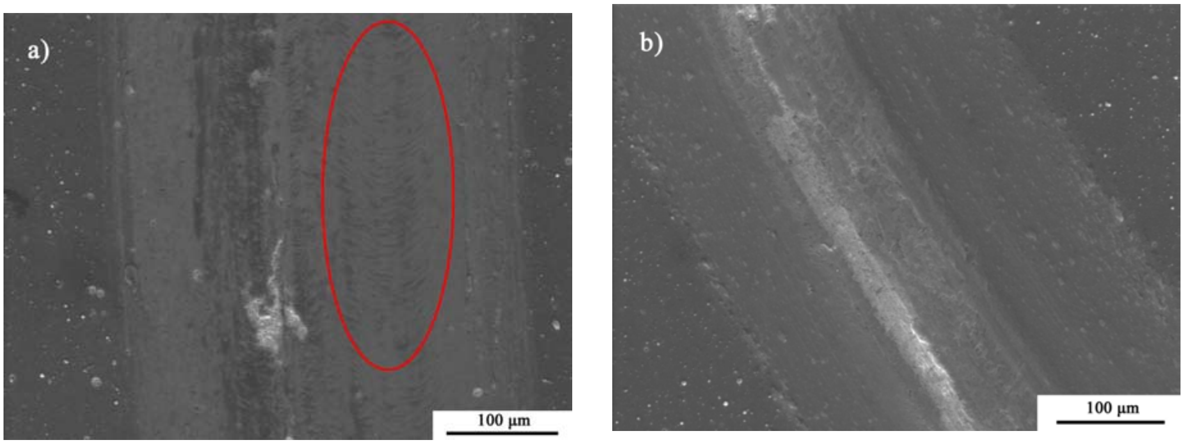

Fig. 5 – Wear tracks from SEM: a) T= 500°C with marked area of " plastic flow of the layer" (not cleaned) b) T= 700°C (not cleaned)

Calottes grinded in individual wear tracks confirm, that at 500°C there was no exposure of the substrate, while at 700°C there was complete damage of the layer.
At 500°C only very small wear of "PIN" ball appeared. Spot, which was created on the "PIN" ball at 700°C, had irregular shape. At its margin of the spot is caught small debris from the layer [1], [2].

3.4 TiAlSiN

Friction coefficient also in this case was higher at 500°C than at 700°C. At 500°C happens similar phenomenon as in the case of layers AlTiN (creation of "glaze"), but in case of TiAlSiN there is no such a high ploughing of "PIN" ball in the thin layer. This documents the SEM analysis. It is possible to think, that even microhardness of thin layer TiAlSiN is at these temperatures higher than microhardness of AlTiN layer. At thermal stress of 700°C there is frequent failure of oxidised film, thereby "PIN" ball gets in the contact with thin layer and marked deviation of friction coefficient follows.

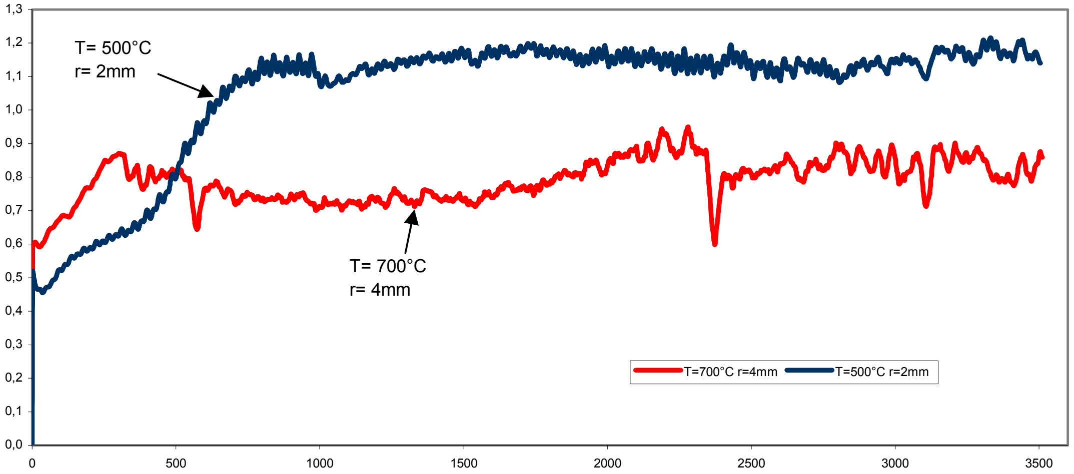

Fig. 6 – TiAlSiN - courses of friction coefficients, T= 500°C, 700°C, F= 2N

At temperature 500°C is wear track covered by oxidised layer throughout whole perimeter. Track is created by debris from damaged thin layer and from oxidised film. This oxidised film is very fast adhesively connected with TiAlSiN layer. Resulting from calotest at 500°C substrate was not revealed. From margins of calotte it is possible to come to a conclusion, that the penetration depth of "PIN" ball to the layer is minimal. At 700°C substrate was exposed in the middle of the wear track. Total exposure of substrate was only in a narrow zone of the track. In experiment at 500°C there was only slight wear of "PIN" ball compared to the test at 700°C, when the wear is higher. After test at 700°C stayed on the margin of the spot high amount of fine debris from the layer. Irregular spot with noticeable relief was created at this temperature.

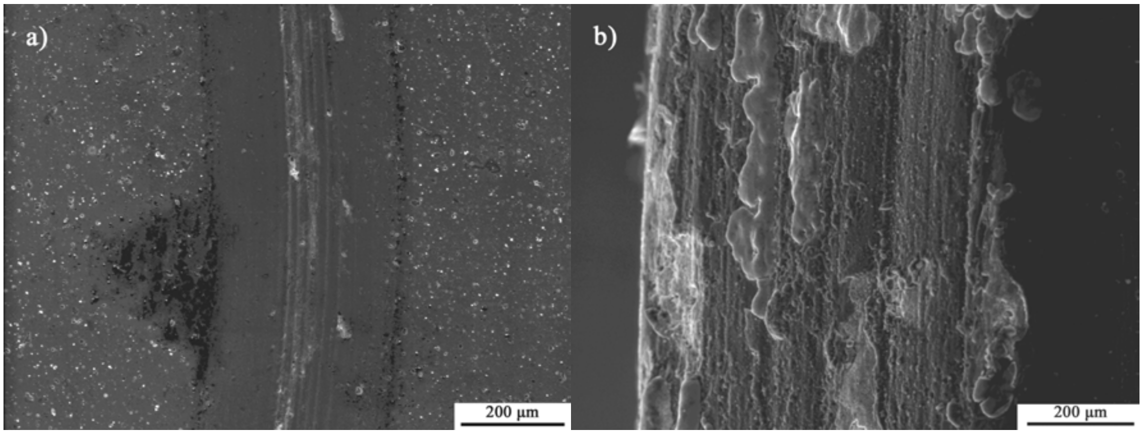

Fig.7 – Wear tracks from SEM: a) T= 500°C (cleaned) b) T= 700°C (cleaned)

3.5 CrAlSiN

Resulting from fig. 7 friction coefficient is at temperature 700°C lower than at 500°C. However differences between friction coefficients are smaller than by other layers. During thermal exposition of CrAlSiN layer creates on its surface highly efficient oxidised protective layer Cr-Al-O, which prevents further oxidation of the layer [3]. Due to this reason at temperature 700°C no noticeable thermal degradation proceeds. That is why at temperatures 20°C, 500°C a 700°C by CrAlSiN layer there are only slight differences in friction coefficient values.

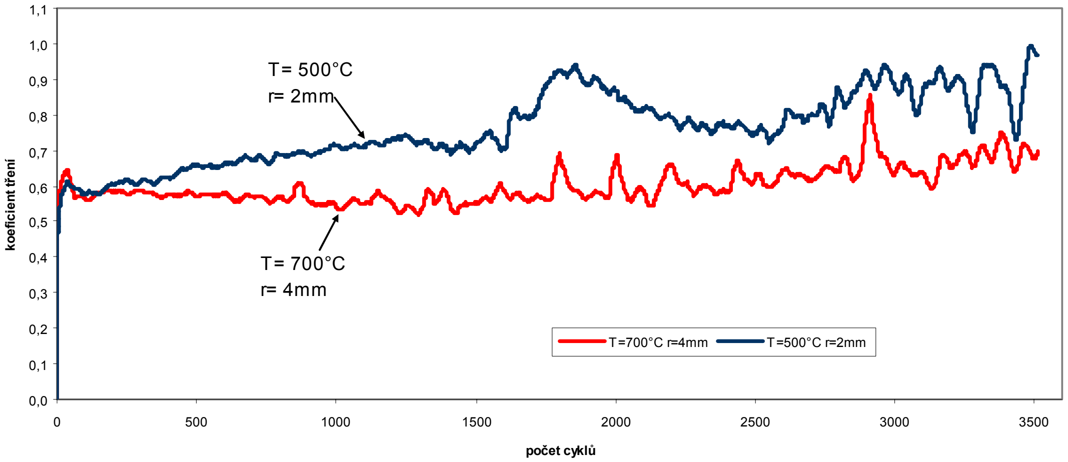

Fig. 8 - CrAlSiN- courses of friction coefficients, T= 500°C, 700°C, F= 2N

Wear depth is by both tracks minimal. Resulting from calottes, there was no substrate exposure at any temperature.

Wear spots of "PIN" balls have almost circular shape and their surface is plane without any noticable abrasive ploughing.

CONCLUSION:

Undertaken experiments are connected with previous ones, in which the tribological properties of systems with thin layers TiN, TiAlN were investigated [4]. Obtained results show significant influence of silicium on tribological properties, but above all replacement of titanium by chromium seems to be really revolutionary, because layer CrAlSiN proves several times higher wear resistance. Also generation of oxidised barrier Cr-Al-O at these layers is highly efficient. In cases of TiAlSiN and AlTiN generated thermal barrier was not so effective. Part of the experiment was also the comparison of tribological properties at normal temperatures whereas the samples were before the tribological test thermally loaded. Results show that at temperatures above 500°C thin layer loses markedly its adhesion to substrate. Up to which certain point it is, will be the subject of further research.

Text of this contribution and the presentation will be available at website http://www.ateam.zcu.cz.

This contribution was solved under the support of PhD. grant. 921/2005/G1 and post-PhD. grant 106/03/P092

LITERATURE:

[1] Stachowiak G. W., Batchelor A. W., „Engineering tribology"
[2] P. Panjan, B. Navins, M. Cekada, A. Zalar, „Oxidation behaviour of TiAlN coatings sputtered at low temperature", Vacuum 1999
[3] H. Ohnuma , N. Nihira , A. Mitsuo, K. Toyoda , K. Kubota , T. Aizawa „Effect of aluminum concentration on friction and wear properties of titanium aluminum nitride films", Surface and Coatings Technology 2004
[4] Hlomberg, K. – Matthews, A., „Coating tribology, Netherlands", 1998.
[5] ASM Handbook, Volume 18, „Friction, Lubrication and Wear Technology", 1992
[6] www.shm-cz.cz
[7] Kříž, A., „PIN-on-DISC" tribological test", Metal 2004, Hradec nad Moravicí

10. Savjetovanje o materijalima, tehnologijama, trenju i trošenju
10. Conference on Materials, Processes, Friction and Wear
MATRIB'05, Vela Luka, 23-25.06.2005.

APPENDIX TO THE STUDY OF THERMAL CONDITION BY PROCESS OF GRINDING

PRILOG STUDIJI TERMIČKOG STANJA PRI OBRADI BRUŠENJEM

Mr. sci. Lutvo Haznadarević
Univerzitet „Džemal Bijedić“ u Mostaru, Mašinski fakultet
Univerzitetski kampus bb
BiH – 88104 Mostar

Dr. sci. Krsto Mijanović
Međunarodni forum „Bosna“ Sarajevo
Ferhadija 30/III
BiH – 71000 Sarajevo

Abstract:

A generated thermal energy from subject of processing is becoming coolant, means of rinsing and lubrication (**SHIP**) by the process of grinding. Grindstone consumption and its pore blockage are reducing grindstone stability and its processing quality is making worse. A grindstone pore blockage causes shavings' and mechanical particles of SHIP. Explorations of a tensional condition in the layer surface are very important to dynamic load parts in a presence of higher temperature.

This work gives results of exploration of SHP's means influence on mechanical and physical conditions, and indexes of condition's efficacy.

Key words: cooling, lubrication, friction, and consumption.

Sažetak:

Pri obradi brušenjem generirana toplinska energija iz predmeta obrade, strugotine i brusa prelazi u sredstvo za hlađenje, ispiranje i podmazivanje (SHIP). Trošenje brusa i začepljenost pora brusa smanjuje njegovu postojanost i pogoršava kvalitetu obrade. Čestice strugotine i mehaničke čestice iz SHIP-a uzrokuju začepljenost pora brusa. Istraživanja napregnutog stanja u površinskom sloju naročito su značajna za dijelove koji su dinamički opterećeni uz prisutnost povišene temperature.

U radu su dati rezultati istraživanja utjecaja sredstava SHP-a na mehanička i fizička stanja kao i indeksi efikasnosti stanja.

Ključne riječi: hlađenje, podmazivanje, trenje, trošenje.

1. INTRODUCTION

The process of grinding develops in a combination of cutting and friction, and that is the reason of the warmth quantity development. Undesirable developments appear on the grinding area as a consequence of that, such as burning up, tempering, micro crack, tension of layer surface, and consumption of the sawn surface of grindstone, as well. This warmth, which is developed mainly by friction, can be affected by:

- ☐ Forming a stable lubricated wedge, that reduce a level of friction
- ☐ Cleaning and rinsing of the sawn surface of grindstone
- ☐ Cooling of sawn grindstone and processing surface, than taking warmth away.

SHIP is taking the warmth away, that is developing itself intensively during a grinding, but it (*SHIP*) is making this temperature lower by the effect of lubrication of *SHIP*. Practice shows that great percentage of the problems connected with the quality of the ground surface emerge because of bad *SHIP* choice, its insufficient quantity or bad wire solution.

This work gives results of exploration of *SHIP* quality by grinding in a more efficacious manner.

2. THE INFLUENCE OF TERMAL PROCESSES ON ELEMENTS OF THE PROCESS-SYSTEM

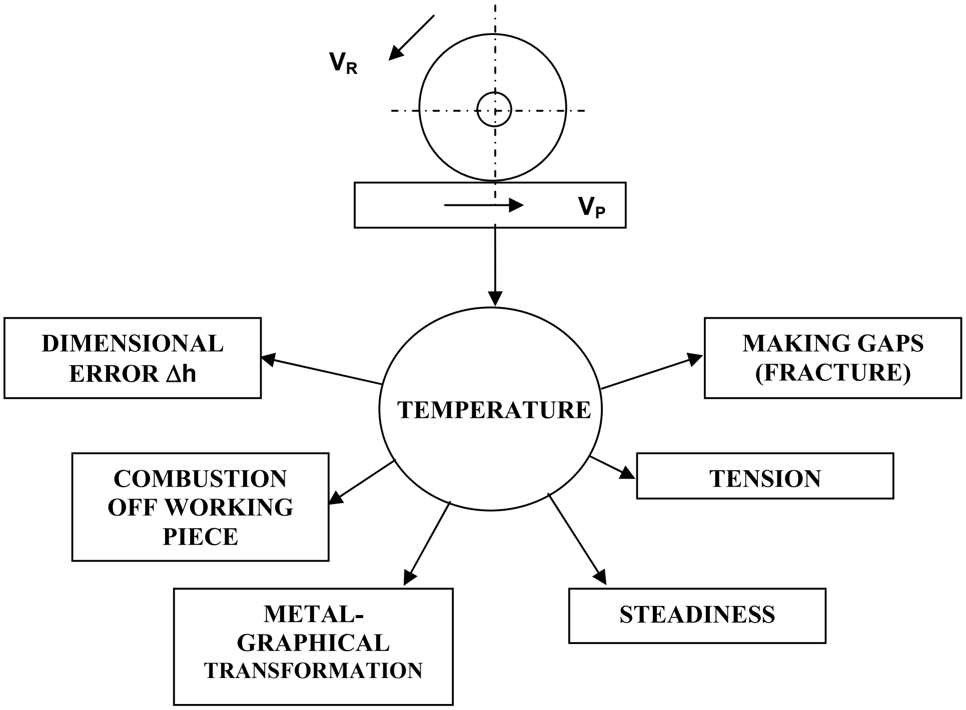

Picture No 1. The heat-thermal influence on the ground surface

Thermal processes effects on subject of processing and tools in the sawn area during the grinding. Experiments are necessary for the exploration of the process of grinding, and mathematical data processing. Usage of the modern equipment for precise measuring of output parameters of the processes of grinding and usage numerical methods (MPK for example) give us a chance for a discovering the indicators that are able to make the process of grinding optimal in a more efficacious manner.

The goal of process is the enlargement of the grindstone steadiness, extension of *SHIP* duration for its usage with achievement of gratifying quality process.

The influence of thermal processes on the grindstone can be controlled by grindstone steadiness. The grindstone failures by grinding in a more efficacious manner are the result of:

- ☐ Abrasion of grindstone grain;
- ☐ Pore blockage of grindstone;
- ☐ Non-achievement of precise construction.

A proportion of the middle temperatures can be used as a criterion for a technical/technological score of *SHIP* characteristics:

$$I_\theta = \frac{\theta_{m0}}{\theta_{mk}} \tag{1}$$

Where is:

θ_{m0} - The mean temperature by the basic *SHIP* cooling;

θ_{mk} - the mean temperature by the new *SHIP* cooling.

Index of SHIP efficacy in a way of characteristic of lubricant compute in accordance with the pattern:

$$I_F = \frac{F_{20}}{F_{2x}} \tag{2}$$

Where is:

F_{20} - The total resistance to the grinding in a more efficacious manner by the basic *SHIP* cooling;

F_{2x} - the total resistance to the grinding in a more efficacious manner by the new *SHIP* cooling.

3. ANALYSIS OF THE BACKWARD INTERNAL TENSIONS

The backward tensions by the grinding processing grow from thermal and mechanical load. This process is described by the system of the harnessed equations of thermal-plasticity [7].

$$\begin{gathered} C\left[tr \cdot \ddot{T}(M,t) + \dot{T}(M,t)\right] + 3K_\alpha\left[tr \cdot \dot{T}(M,t)\dot{U}_{i,i}(M,t) + tr \cdot T(M,t)\ddot{U}_{i,i}(M,t) + T(M,t)U_{i,i}(M,t)\right] = \\ = \lambda \cdot \nabla^2 \cdot T(M,t) + tr \cdot q_v(M,t) + q_v(M,t) \end{gathered} \tag{3}$$

$$G \cdot \nabla^2 \cdot U_i(M,t) + \left(K + \frac{G}{3}\right) \cdot U_{j,ji}(M,t) + f_i^{\circ}(M,t) = \\ = \rho \cdot \ddot{U}_i(M,t) + 3K_\alpha T,i(M,t) \tag{4}$$

Where is:

$M = x, y, z$,
t – Time [s],
∇^2 - operator,
tr – time of making inroads of thermal energy waves,
α - coefficient of expansion,
U – moving.

With the initial and border conditions in [7]. Treating material characteristics depend on the temperature, in the presence of the grindstone grains dynamic activity. (Picture No. 2.).

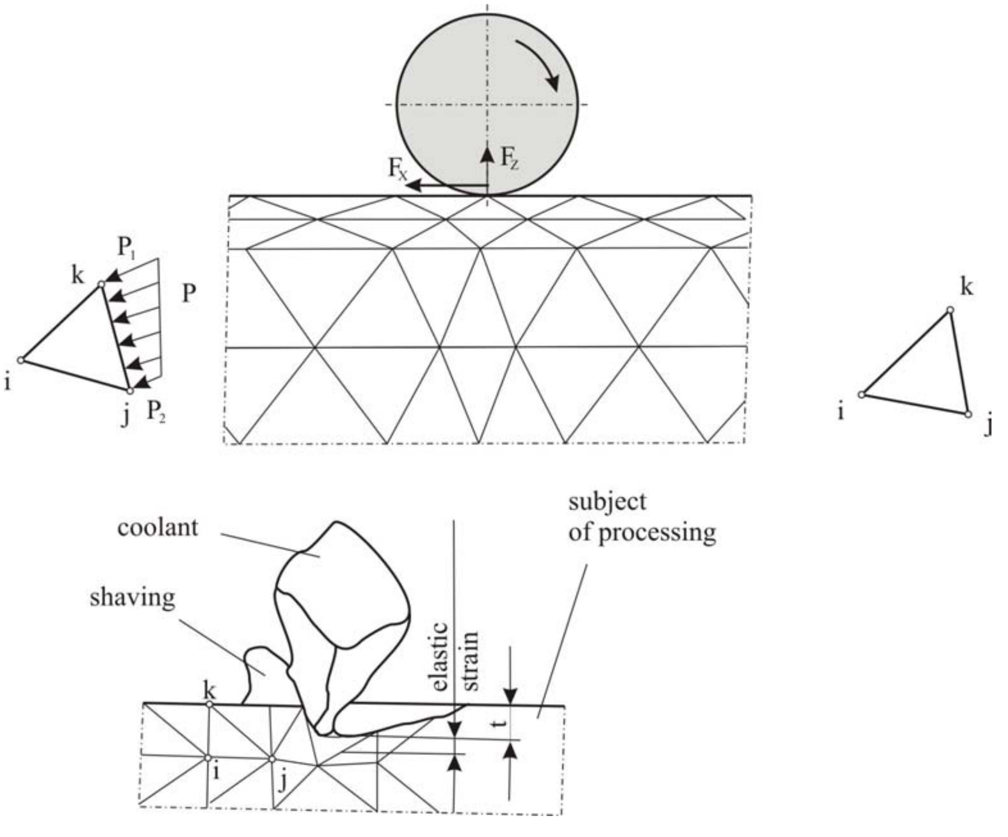

Picture No 2. Illustration of the grinding processing and division of the sawn area on the final elements

Considering that is $\frac{\chi}{\left[\frac{1+\chi+4G}{3K}\right]} << 1$ possible situation in which (1) and (2) variation methods can be used for the purpose of getting the shape of functionale:

$$I(U_i)=\int_F \left\{ \begin{matrix} K(M)\left[U_{k,k}(M)-3\varepsilon^{(T)}(M)\right]^2/2+G(M)\left[U_{k,k}^2(M)-U_{k,k}(M)U_{l,l}(M)\right]+ \\ G(M)\left[U_{1,2}(M)+U_{2,1}(M)\right]^2/2-f_i^{\circ}(M)U_i(M) \end{matrix} \right\} dF - \int_{r'} P_i^{\circ}(N)U_i(N)d\Gamma_i \qquad i,\ k,\ l=1,\ 2,\ 3 \tag{5}$$

Which is appropriate for the usage of the final elements' method. The term for the linear equations system is being given by organizing functionale.

$$[K]\{U\}=\{P\} \tag{6}$$

Where is:

$[K]$- Hard matrix,

$\{U\}$- moving vector,

$\{P\}$- vector of power.

Temperature field is defined iteratively [4] in a time interval $\Delta t = 0{,}001\ s$.

$$\left([K]+\frac{2}{\Delta t}[e]\right)\{T\}=\frac{2}{\Delta t}[C]\{T\}_0-\{F\} \tag{7}$$

Where is:

$[K]$ - Matrix of conductivity,

Δt – iterative move.

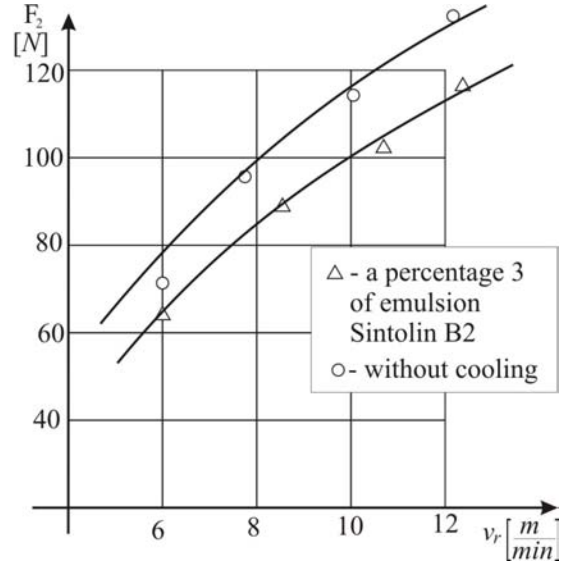

Picture No 3. The grinding power depending on a way of cooling –without cooling and 3% emulsion

Estimate results are concerning to backward inner tensions made by grinding of the tempered steel Č. 4751 by the grindstone 2B 54 10V SWATY. Dependence of the sawn resistance, in relation to processing factors, is defined and reads as follows:

$$F_x = 89 \cdot Vr^{0,235} \cdot t^{0,735} \cdot b^{0,662} \; [N]$$
$$F_z = 113 \cdot Vr^{0,470} \cdot t^{0,74} \cdot b^{0,492} \; [N] \tag{8}$$

These magnitudes of the sawn resistance were being needed for the estimate of the temperature fields (for defining the thermal fluks power $q = \frac{F_x \cdot v}{M \cdot A}$ and mechanical loads that are obtained on the basis of the equation $P = \frac{F_z}{A}$).

Here it is A – intersection of the grindstone contact and the working subject.

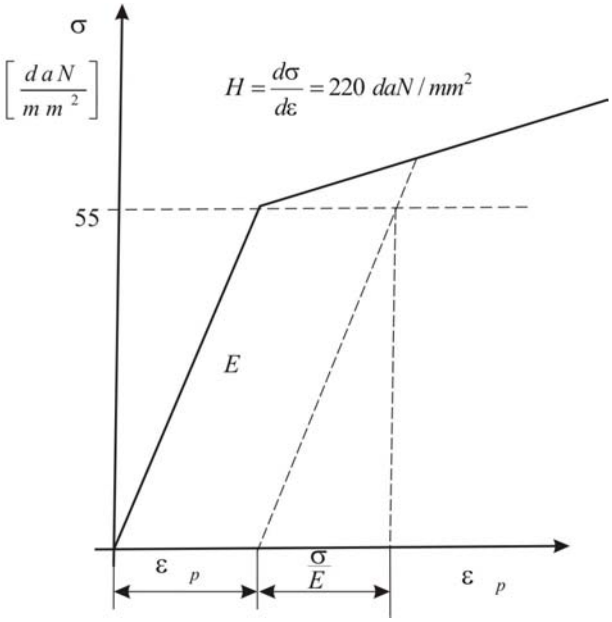

Picture No 4. Characteristic curve for the plastic flowing estimate

Special tools do hardness measuring in the layer surface, and tensional magnitudes are estimated by magnitude of hardness.

4. CONCLUSION

Following claims are given from the foregoing text:

- Measured results of the backward tensions are placed in the same zone in relation to estimated temperature backward tensions, and they are with the same omen, too
- Magnitudes of resistance are reduced by the usage of coolant that has positive effect on the sawn temperature falling off and the backward temperature tensions, as well. The temperature falling off and tensional decrease can be achieved by the intervention made on a grindstone and by making an additional development.
- This shows that backward inner tensions can be specified by the process of grinding in a relative simple way if its the sawn resistance and thermal condition of the subject areas in crops are known.

LITERATURE

[1] D. Vukelja, *Termodinamika rezanja*, Monografija IAMA (2), Beograd, 1970.

[2] A. Mišković, *Analiza naponskog stanja u reznim elementima alata metodom konačnih elemenata*, Doktorska disertacija, Strojarski fakultet, Mostar, 1972.

[3] E. Marozov, G. Nikislav, *Metod konečnih elementov v mehanike razrušenia*, Moskva, „Nauka“, 1980.

[4] L. J. Segerlind, *Applied finite element analysis*, John Wiley & Sons, New York, 1978.

[5] K. Kozo, E. Hirochi, *Analysis of the structure and thermil residuol stres in the mashi red surfoce loyer by grinding*, Tons. Jop. Inst. Metods 1972., 13 No6 412-418.

[6] Zbornik, *Naučnie osnovi progresivnoj tehnologiji*, Moskva, Mašinostroenie, 1982.

[7] V. S. Zarubin, *Priklodnie zadači termopročnosti elementov konstrukcije*, Moskva, Mašinostroenie, 1985.

[8] H. Parkus, *Instrationere Warmespannungen*, Wien, Sprilger-Verlog, 1959.

[9] A. Mišković, D. Vukelja, *Prilog studiji toplinskog stanja i zaostalih naprezanja pri brušenju*, Zbornik radova 21. Savjetovanje proizvodnog strojarstva Jugoslavije, Opatija, 1987.

10. Savjetovanje o materijalima, tehnologijama, trenju i trošenju
10. Conference on Materials, Processes, Friction and Wear
MATRIB'05, Vela Luka, 23-25.06.2005.

MEHANIZMI TROŠENJA I OBLICI ISTROŠENOSTI KANALA CIJEVI TOPNIČKOG ORUŽJA

Mirko Jakopčić

Zapovjedništvo za izobrazbu i obuku HKoV
Časnička škola
Zagreb, Ilica 256 B
e-mail: mjakopc@yahoo.com

Sažetak: U ovom su radu analizirani mehanizmi trošenja koji djeluju na cijev topničkog oružja, te su prikazani oblici istrošenosti cijevi.

Proces opaljenja predstavlja složen tribološki proces, jer njegovim odvijanjem nastaju višestruki mehanizmi trošenja: adhezija, abrazija, erozija, trobokorozija i umor površine. Tribološki proces dovodi do trošenja cijevi i do stanja njezine istrošenosti. Duž kanala cijevi se uočavaju razni oblici istrošenosti: korozijska nagrizenost, pobakrenost, okrznuti bridovi i polja, spljoštena polja, rascijepljenost polja i žlijebova, odsmicanost boka polja, podignutost polja i otkinutost polja.

Istrošenost cijevi uzrokuje promjenu balističkih značajki oružja, pa stupanj istrošenosti treba pratiti redovnim pregledima i mjerenjima.

Ključne riječi: cijev, trošenje, istrošenost, adhezija, abrazija, erozija, tribokorozija, umor površine

Abstract: This paper describes the wear mechanisms which act on the artillery weapons barrel and shows the barrel wear forms.

The firing process is a complex tribological process, because he effects different wear mechanisms: the adhesion, the abrasion, the erosion, the tribocorrosion and the fatigue. The barrel is worn by the complicated tribological process, so the various wear forms appear all along the bore: corroded and copper-plated bore surface, grazed the edges and the lands, flattened lands, cleft lands and grooves, sheared land sides, erect lands and broken lands.

The barrel wear influences to the change of the weapon ballistic parameters, so the wear level of the barrel must be determined by the regular surveys and measurements.

Key words: barrel, wear, adhesion, abrasion, erosion, tribocorrosion, fatigue

1 UVOD

Prilikom kretanja kroz cijev, projektil se svojim centrirajućim i vodećim prstenom oslanja o površinu kanala cijevi. Zbog mase projektila i njegovog kretanja, na dodirnim se površinama kanala cijevi i prstenova projektila stvara pritisak i sila trenja klizanja. Pritisak i sila trenja su naročito visoki kod oružja s ožlijebljenom cijevi, gdje se vodeći prsten projektila utiskuje u profil žlijebova i polja kanala cijevi. U tom slučaju polja kanala cijevi predstavljaju rezni alat koji oblikuje profil vodećeg prstena odvajanjem čestica materijala.
Navojni žlijebovi prisiljavaju projektil da prilikom pravocrtnog kretanja kroz cijev ujedno i rotira oko svoje uzdužne osi. Pri tome projektil normalnom silom $\mathbf{F_N}$ djeluje na radnu bočnu površinu žlijebova kanala (sl. 1).
Točka **A** predstavlja hvatište svih sila, a nalazi se u središtu boka polja. Iz te je točke pod kutom uvijanja žlijeba α usmjerena sila trenja $\boldsymbol{\mu}\mathbf{F_N}$.
Vodeći prsten je od čistog elektrolitičkog bakra ili od mjedi, čije se čestice prilikom kretanja projektila odvajaju i mikrozavaruju na čeličnu površinu kanala cijevi. To je proces pobakrivanja cijevi.

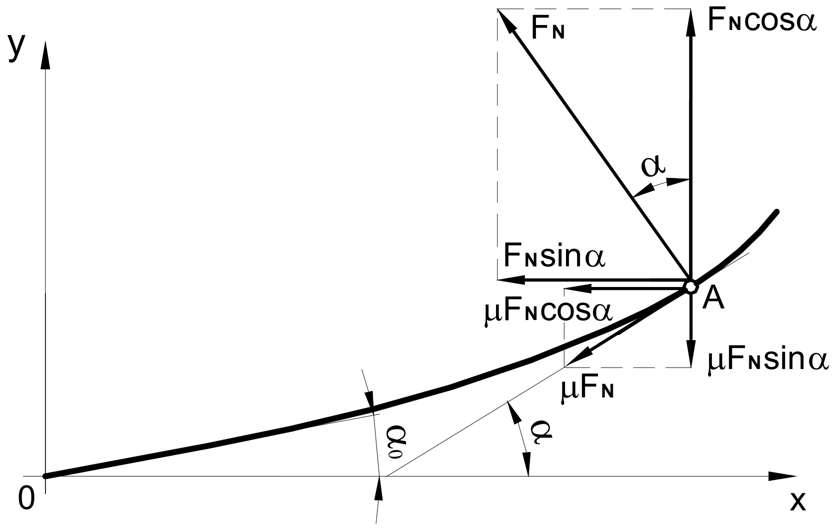

Slika 1 – Sile kojima cijev oružja djeluje na vodeći prsten pri kretanju projektila [1]

Barutni su plinovi složenog kemijskog sastava i sadrže CO, CO_2, H_2O, H_2 i N_2, koji su vrlo agresivni za materijal cijevi. Osim toga, u njima su sadržane i krute čestice: čestice čađe i zrnca neizgorjelog baruta. Zbog snažne turbulencije barutnih plinova, ove čestice bombardiraju površinu kanala cijevi, mehanički djeluju na nju i odnose čestice materijala s mikroneravnina površine. Osim toga, zbog kretanja vrlo velikom brzinom, ove se čestice zabijaju u površinu materijala i stvaraju žarišta razvoja korozije.
Toplina koja se oslobađa prilikom izgaranja barutnog punjenja zagrijava cijev i barutne plinove. Temperatura površinskih slojeva kanala cijevi može dosegnuti nekoliko stotina, pa čak i do 1000 °C. To uzrokuje promjenu strukture materijala i njegovih mehaničkih svojstava. Poslije svakog opaljenja zatvarač otvara cijev, pa dolazi do prostrujavanja okolnog hladnog zraka kroz cijev, što može dovesti do spontanog pougljičenja i zakaljenja površinskih slojeva kanala cijevi.

Osim toga, cijev se nejednoliko zagrijava po presjeku, pa vanjski hladniji slojevi ne dopuštaju toplinsko rastezanje unutarnjih zagrijanih slojeva. Zbog toga se prema površini kanala cijevi stvaraju sve veća toplinska naprezanja, koja nakon većeg broja opaljenja dovode do pojave površinskih mikropukotina.
Prema svemu navedenom, proces opaljenja, uz okolnu atmosferu, imaj složeno mehaničko, toplinsko i kemijsko djelovanje na cijev topničkog oružja, što rezultira nastankom mehanizama trošenja cijevi.

2 MEHANIZMI TROŠENJA CIJEVI TOPNIČKOG ORUŽJA

Kao posljedica djelovanja projektila na cijev pri opaljenju oružja, zajedno s djelovanjem barutnih plinova, razvijene topline, čestica gareži i baruta, te atmosfere, nastaju sljedeći mehanizami trošenja cijevi: **abrazija, adhezija, umor površine** i **tribokorozija** [2]. Svi ovi mehanizmi tijekom trajanja procesa opaljenja istodobno djeluju na cijev.

2.1 Abrazija

Abrazija predstavlja trošenje materijala mikrorezanjem, koje je izazvano tvrdim česticama ili tvrdim izbočinama. Pri tome dolazi do mikrorezanja abrazivom geometrijski nedefinirane oštrice.
Abrazija cijevi topničkog oružja izazvana je trenjem klizanja vodećeg i centrirajućeg prstena projektila po površini kanala cijevi. Materijal prstena je mekši od abradirane površine, pa se tu radi o nultoj abraziji. Abraziju cijevi izaziva i abrazivna erozija česticama gareži i zrncima baruta, kada ove čestice velikom brzinom i pod malim kutom udaraju o površinu kanala cijevi

2.2 Adhezija

Adhezija nastaje pri trenju klizanja, kada materijal prelazi s jedne tarne plohe na drugu tijekom njihovog relativnog gibanja. Budući da se kod adhezije stvaraju mikrozavareni spojevi, materijali koji nisu skloni mikrozavarivanju tribološki su kompatibilni i pogodni za rad u paru. Pri vrednovanju tribološke kompatibilnosti čistih metala, tribološka kompatibilnost željeza i bakra je loša, a željeza i cinka izrazito loša [3]. To pokazuje da je materijal cijevi tribološki loše kompatibilan s bakrom i mjedi, od kojih se izrađuje vodeći prsten projektila.
Klizanjem vodećeg prstena po površini kanala cijevi nastaje adhezijski spoj čestica mjedi ili bakra s česticama čelika, te dolazi do pobakrivanja cijevi. Tu se zapravo adhezijski troši vodeći prsten. Međutim, zbog pobakrivanja površine kanala cijevi i naknadne elektrokemijske korozije cijevi, razgrađuje se i materijal same cijevi.

2.3 Umor površine

Umor površine predstavlja odvajanje čestica s površine uslijed cikličkih promjena naprezanja. Oštećenje koje se uočava na površini ima oblik rupice (pitting).
Umor površine u cijevi topničkog oružja nastaje kao posljedica višestrukih naprezanja: pritiska na dodirnim površinama projektila i cijevi, pritiska barutnih plinova i koncentracije naprezanja u korijenu polja. Također, kod veće istrošenosti cijevi javlja se zračnost između centrirajućeg prstena projektila i kanala cijevi, pa dolazi do klaćenja projektila i udaranja njegovog centrirajućeg prstena po poljima, što izaziva udarna opterećenja i trajne deformacije polja. Umor površine cijevi nastaje i zbog udarne erozije, kada čestice gareži i neizgorjelih zrnaca baruta velikom brzinom i pod velikim kutom udaraju o površinu kanala cijevi.

2.4 Tribokorozija

Tribokorozija ili tribokemijsko trošenje je mehanizam trošenja koji nastaje kao posljedica kemijske ili elektrokemijske reakcije materijala s okolišem. Osnovni kriterij za otpornost materijala na tribokoroziju je kemijska pasivnost materijala u određenom mediju.

Tribokoroziju cijevi topničkog oružja uzrokuju kemijske i elektrokemijske reakcije materijala cijevi s barutnim plinovima, čađi i s nataloženim česticama bakra ili mjedi, te kemijska reakcija materijala s okolnom atmosferom.

3 TROŠENJE I ISTROŠENOST CIJEVI

Proces trošenja dovodi do stanja istrošenosti cijevi. Tragovi trošenja javljaju se na površini kanala cijevi, ali i u dubljim slojevima materijala, mijenjajući oblik, izgled i dimenzije profila kanala cijevi, te homogenost strukture materijala cijevi. Najvažniji pokazatelji stupnja istrošenosti cijevi su:

- povećanje kalibra cijevi;
- produženje barutne komore;
- promjene stanja površine kanala cijevi;
- broj izvedenih opaljenja iz cijevi u usporedbi s balističkim životom cijevi;
- savijenost cijevi [4].

U praksi je utvrđeno da se proces trošenja cijevi ne odvija jednakim intenzitetom duž cijele površine kanala cijevi (sl. 2).

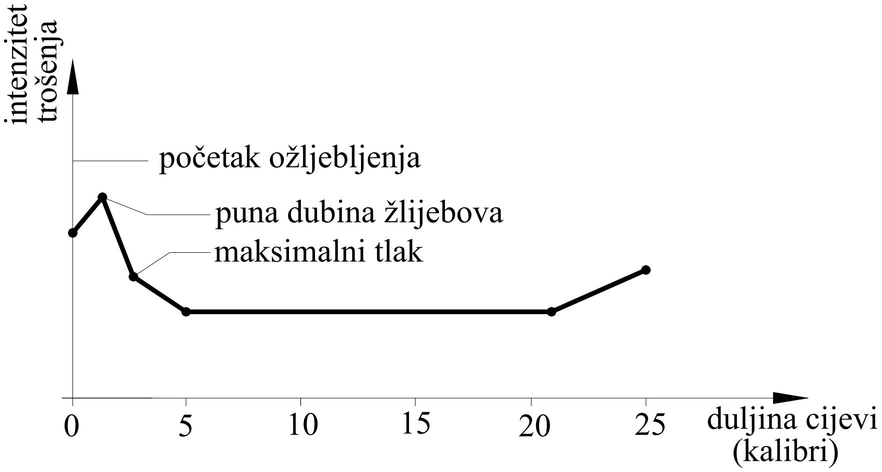

Slika 2 – Dijagram trošenja cijevi [4]

Trošenje cijevi je najintenzivnije na prijelaznom konusu i početnom dijelu ožljebljenja, gdje su najveći dodirni pritisci i trenje između vodećeg prstena i cijevi. Tu se zapažaju i prvi tragovi trošenja: površina cijevi postaje matirana, što predstavlja finu mrežu kratkih i plitkih prskotina. Povećanjem broja opaljenja, prskotine se povećavaju i sve više orijentiraju u smjeru kretanja projektila. Prskotine se naročito produbljuju u podnožju polja, te se oblikuju u pukotine koje mogu postići dubinu do jednog, pa čak i do dva milimetra. Takvo polje se može lako odlomiti po manjoj ili većoj dužini.

Intenzitet trošenja dalje pada, do mjesta gdje se postiže najveći tlak barutnih plinova. Nakon toga intenzitet trošenja je konstantan, a prema ustima cijevi opet raste. Uzrok tome je veliko vrtložno strujanje barutnih plinova i lošije centriranje projektila u tom dijelu cijevi, kao i djelovanje vrtložnih užarenih plinova na taj dio kanala cijevi nakon izlaska projektila iz cijevi.

Istrošenost cijevi ima za posljedicu pogoršanje balističkih značajki oružja. Sposobnost cijevi da izdrži predviđeni broj opaljenja, a da pri tome njezina balistička kvaliteta ne padne ispod dopuštenih vrijednosti, naziva se **balistički vijek** ili **život cijevi**.

4 OBLICI ISTROŠENOSTI CIJEVI

Tragovi trošenja cijevi nisu prisutni samo na mjestima najveće istrošenosti, već se uočavaju duž cijele površine kanala cijevi. Ti su tragovi s promjenjivom gustoćom razmješteni po površini, a predstavljaju različite oblike istrošenosti cijevi kao što su:

- korozijska nagrizenost cijevi;
- pobakrenost cijevi;
- okrznuti bridovi polja;
- spljoštenost polja;
- cijepanje polja i žlijebova;
- smicanje boka polja;
- podignuto polje;
- otkinuto polje.

4.1 ***Korozijska nagrizenost cijevi*** uočava se u obliku tamnih točkica ili mrlja različite veličine i gustoće, ovisno o stupnju nagrizenosti (sl. 3). Sam početak korozijskog djelovanja uočava se već nakon nekoliko opaljenja u obliku mat zamagljenih površina. Ta su mjesta ujedno žarišta daljnjih korozijskih procesa.

Slika 3 – Korozijska nagrizenost cijevi [5]

Na slici 3 prikazana je korozijska nagrizenost početnog dijela ožljebljenja cijevi, do koje je došlo djelovanjem barutnih plinova visoke temperature. Na tom je mjestu, uz zagrijavanje materijala, djelovanje korozije najintenzivnije.

Prema normi DIN 53210, nagrizenost korozijom razvrstana je u šest stupnjeva: od R_0 kao početnog stanja nove cijevi, do R_5 kao stanja najvišeg stupnja nagrizenosti.

Potpuna i objektivna ocjena stupnja nagrizenosti cijevi korozijom nije jednostavna, pa se ona u pravilu izvodi komisijski.

4.2 ***Pobakrenost cijevi*** može se uočiti već nakon stotinjak opaljenja. Na početku ožljebljenog dijela cijevi pojavljuju se nepravilne mrlje, slične tragovima korozije.
Intenzitet pobakrivanja nije jednolik, kako po dužini cijevi, tako ni po poljima i žlijebovima, što prikazuje dijagram na slici 4.

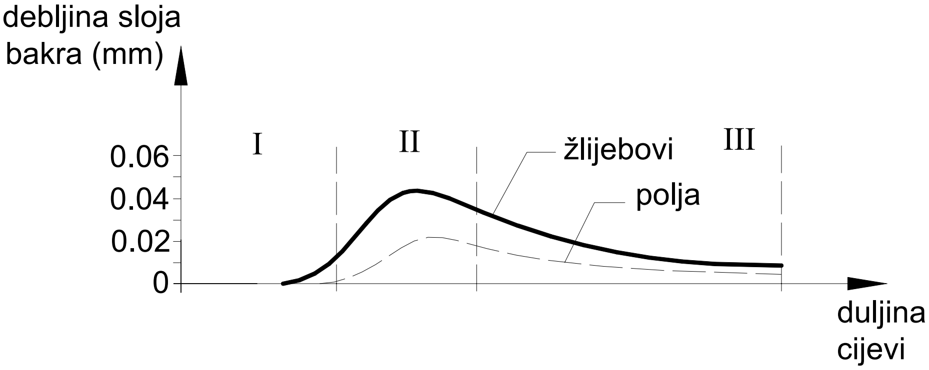

Slika 4 – Intenzitet pobakrivanja cijevi topničkog oružja [1]

Naslage bakra mogu se primijetiti na oko dva do tri kalibra od početka ožlijebljenja cijevi, nakon čega se intenzitet pobakrivanja naglo povećava prema sredini cijevi. Približavanjem prema ustima cijevi, pobakrivanje je sve slabije i postaje jedva vidljivo.
Iz prakse je poznato da su tragovi bakra izraženiji u žlijebovima nego na poljima kanala cijevi. Pobakrivanje je također jače pri korištenju vodećih prstena od čistog bakra, nego kod onih od mjedi.
Koncentrirano taloženje bakra na nekim mjestima dovodi do promjene oblika poprečnog profila kanala cijevi, a i do smanjenja kalibra. Odbakrivanje cijevi provodi se kemijskim postupkom.

4.3 ***Okrznuti bridovi polja*** (sl. 5) nastaju kao posljedica neposrednog djelovanja suhog trenja između materijala cijevi i vodećeg prstena projektila, uz dodatno djelovanje plinske erozije. Na samim bridovima polja dolazi do pada čvrstoće materijala cijevi i do otkidanja njegovih čestica. Polja se postupno zaobljuju na bridovima, s većim zaobljenjem na vodećem bridu.
Ovaj se oblik trošenja dopušta sve dok kalibar cijevi ostaje u propisanim granicama.

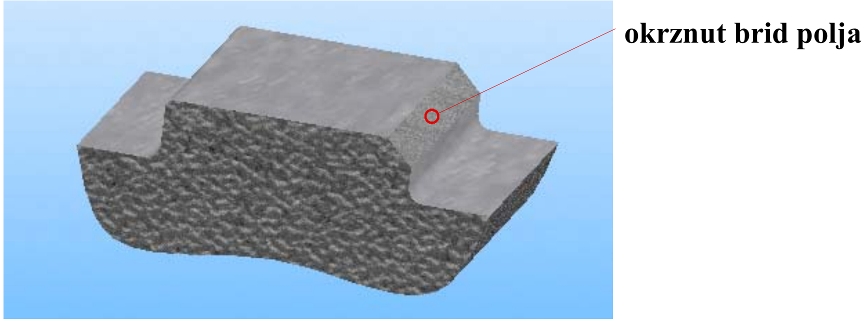

Slika 5 – Okrznut brid polja

4.4 ***Spljoštenost polja*** najčešće nastaje kao posljedica stvaranja velike zračnosti između centrirajućeg prstena projektila i cijevi, zbog čega se projektil pri kretanju klati. Nastaje pojava slična kovanju: projektil udara centrirajućim prstenom po poljima, čime nastaju trajne deformacije na bridovima i cijeloj površini polja. Bridovi se spuštaju, a time se spušta i cijelo polje (sl. 6). Daljnjom uporabom cijevi dolazi do pojave odcjepljenja i otpadanja ruba polja u obliku trake.

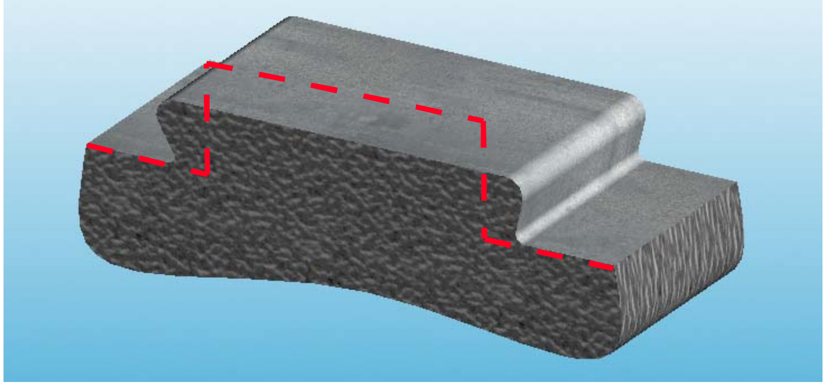

Slika 6 – Spljošteno polje

4.5 ***Cijepanje polja i žlijebova*** nastaje kao posljedica umora materijala cijevi toplinskim naprezanjima i spontanim zakaljivanjem površinskih slojeva kanala cijevi. Postojeće sitne naprsline se progresivno proširuju u obliku lokvi kod krhkih čelika, te u obliku uzdužnih rascjepa kod žilavih čelika (sl. 7).

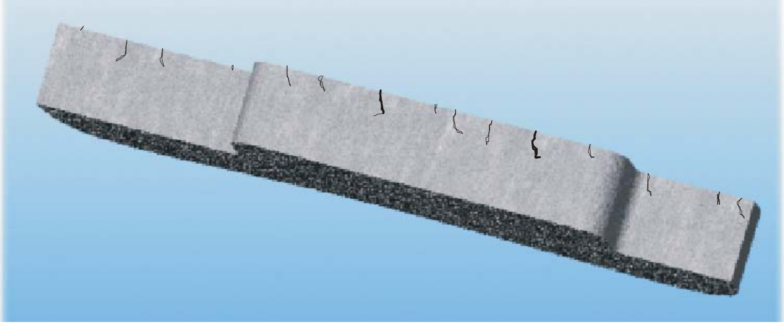

Slika 7 – Cijepanje polja i žlijebova u obliku uzdužnih rascjepa

Dugotrajno naprezanje dovodi do pojave otkidanja vodećeg brida spljoštenog polja, a prskotine koje se nalaze ispod brida dalje se šire u rascjepe, što dovodi do otkidanja polja u cijelosti.

4.6 ***Smicanje boka polja*** nastaje kao posljedica koncentracije naprezanja u dnu polja, prvenstveno na radnom boku polja i progresivnog razvoja prskotina u unutrašnjosti polja. Kada se jedna prskotina spoji s dvije ili više drugih prskotina, oblikuje se naprslina koja se

proširuje u dubinu ili prema površini. Djelovanjem bočne sile vodećeg prstena dolazi do koncentracije naprezanja i do pojave smicanja radnog boka polja (sl. 8).
Spajanjem pukotina na radnom boku polja s pukotinama na neradnom boku, ispod površine žlijeba, te bočnim djelovanjem sile vodećeg prstena, dolazi do smicanja polja.

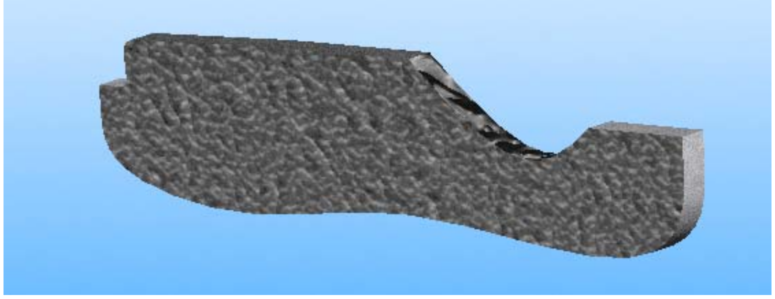

Slika 8 – Odsmicani radni bok polja

Uočena je pojava da smicanje boka polja, smicanje polja i otkidanje polja nastaje na početku ožlijebljenja cijevi, a ovi oblici trošenja jače su izraženi na gornjoj površini kanala cijevi.

4.7 ***Podignuto polje*** nastaje kao posljedica progresivnog proširivanja prskotina u pukotine ispod polja, kada su krajevi pukotine iznad ravnine žlijeba (sl. 9).
Podignuto polje je potencijalno žarište dubinske korozije, jer se u njega može nakupiti znatna količina produkata izgaranja. Progresivnim razvojem pukotine podignuto polje može otpasti kao odsmicani radni bok ili odsmicano polje.

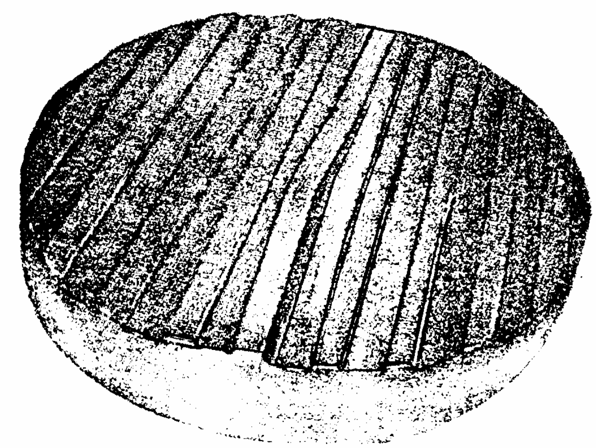

Slika 9 – Podignuto polje [6]

4.8 ***Otkinuto polje*** nastaje kao posljedica umora materijala cijevi, pa se javlja i kod naprezanja koja su niža od granice razvlačenja materijala. Inicijalna pukotina umora materijala najčešće nastaje kod podignutog polja, na površini radnog boka polja u razini

žlijeba. Pukotina se širi prema unutrašnjosti materijala i dovodi do otkidanja polja bez vidljive plastične deformacije.
Otkidanje polja zbog umora materijala je neugodna pojava, jer nastaje bez prethodno vidljive plastične deformacije, čak i kod vrlo duktilnih materijala cijevi.

5 ZAKLJUČAK

Prilikom opaljenja oružja u njegovoj se cijevi odvija složen tribološki proces, koji rezultira nastankom višestrukih mehanizama trošenja. Djelovanjem projektila, barutnih plinova i barutnog punjenja, cijev je izložena adhezijskom, abrazijskom, erozijskom i trobokorozijskom trošenju, te umoru površine. Odvijanjem trošenja cijevi, duž njezinog kanala se uočavaju razni oblici istrošenosti: korozijska nagrizenost, pobakrenost, okrznuti bridovi i polja, spljoštena polja, rascijepljenost polja i žlijebova, odsmicanost boka polja, podignutost polja i otkinutost polja. Istrošenost cijevi dovodi do promjene balističkih značajki oružja.
Tragovi trošenja javljaju se na površini kanala cijevi, ali i u dubljim slojevima materijala. Najvažniji pokazatelji stupnja istrošenosti cijevi su: povećanje kalibra cijevi, produženje barutne komore, promjene stanja površine kanala cijevi; broj izvedenih opaljenja iz cijevi u usporedbi s balističkim životom cijevi, te savijenost cijevi. Trošenje cijevi je najintenzivnije na prijelaznom konusu i na početnom dijelu ožljebljenja, gdje su najveći dodirni pritisci i trenje između vodećeg prstena i cijevi.
Istrošenost cijevi dovodi do pada kvalitete balističkih značajki oružja, pa treba stalno pratiti stupanj njezine istrošenosti.

6 LITRERATURA

[1] M. Jakopčić, "Otpornost na trošenje cijevi topničkih oružja", disertacija, Fakultet strojarstva i brodogradnje Sveučilišta u Zagrebu, Zagreb, 2002.

[2] M. Jakopčić, "Temeljne značajke tribološkog procesa u cijevi topničkog oružja", Zbornik MATRIB '99, 111-118, ISBN 953-96038-4-6, Trogir, 1999.

[3] E. Rabinowicz, "Gaps in our knowledge of friction and wear", Materials Technology, New York, 1976.

[4] M. Jakopčić, "Osnove topničkog naoružanja", Hrvatsko vojno učilište "Petar Zrinski", Zagreb, 1996.

[5] http://www.corrosion-doctors.org/Hot Corrosion/Hot.htm

[6] P. Jacić, "Osnovi održavanja sistema naoružanja III", Visoke vojnotehničke škole KoV, Zagreb, 1988.

LIGHT-WEIGHT STRUCTURAL DESIGN USING OF METALLIC FOAMS

Jaroslav Jerz, František Simančík, Roman Florek, Martin Nosko
Institute of Materials and Machine Mechanics SAS, Bratislava, Slovak Republic

Abstract:

Structural applications of metallic foams are considerably limited by a fact, that they are not able to withstand high tensile stresses. This drawback can be very efficiently overcome via strengthening of tensile loaded surface skin with various reinforcements. Components made from reinforced metallic foams, such as foamed panels, sandwiches, complex 3-D-parts, foamed hollow profiles as well as castings with foamed cores, possess enormous future potential for applications where lightweight combined with high stiffness and acceptable manufacturing costs is of prime interest.

Excellent stiffness-to-weight ratio of the foam combined with unique crash absorption capability and strength of reinforcements provide enormous potential for application of reinforced foams in lightweight load bearing structural parts. The significant features ensured from the improvement of the reinforced metallic foam product's properties are highlighted and the most promising industrial applications are suggested with respect to recent technological state of the art in this contribution.

Key words: metallic foams, aluminium foam, light-weight design

INTRODUCTION

The main objective of the development of advanced material technologies for light-weight design is to promote the desired properties of modern machines, vehicles or structural components. This progress is usually achieved by:

- technologies improving material properties (e.g. increasing of the purity of magnesium alloys to avoid surface corrosion),
- technologies where the material has an additional function (e.g. combination of reduced manufacturing costs and enhanced damping properties using foamed cored castings),
- technologies qualifying a material for a new application and leading to a substitution of materials (e.g. replacing aluminium profiles by reinforced aluminium foam profiles in order to increase their stiffness-to-weight ratio),
- technologies reducing process steps and improving the properties of the component (e.g. production of highly porous complex 3-D-castings with reinforced surface by injection moulding of liquid metal foam).

The contribution to improve mechanical property-to-weight ratio achieved by modern technologies of advanced material production is of prime importance. Moreover, the economical and ecological aspects must also be considered during selection of manufacturing process. In this respect, notable achievements made by advanced materials include:

- reduction of energy consumption through light-weight material design,
- improvement of crash energy absorption through optimized deformation behaviour,
- reduction of costs of ownership through using of ecologically harmless and corrosion resistant materials,
- improvement of safety through using of non-inflammable materials, which do not evolve toxic fumes in a fire,
- maintaining the original appearance and function throughout the lifetime of the structural components through corrosion resistant material combinations,
- enhancement of ergonomical parameters, e.g. comfort and handling performance with light-weight components.

The performance of a structural component is limited by the properties of the material of which it is made, and by the shapes to which the material can be formed. Performance may mean strength for a given weight, for instance, or stiffness for minimum cost, or fatigue life, or thermal resistance, or safety, while meeting certain design requirements.

Performance is often limited by a combination of material properties. For example the best material for a light, stiff tie (a tensile strut) is that with the greatest value of the specific stiffness E/ρ (E is the Young's modulus and ρ is the density). In other modes of loading, the performance-maximising criterion or 'performance index' can be more complicated [4]. The best material for a light stiff beam, for instance, is that with the largest value of $E^{1/2}/\rho$. Other design objectives lead to other performance indices. Some examples of performance indices, covering mechanical design for standard design cases can be found in Table 1.

Table 1: Typical performance indices for material design (Stiffness- and strength limited design at minimum mass).

Function and constraints	**Maximize**
Tie (tensile strut) - stiffness, length prescribed; section area free	E/ρ
Beam - loaded in bending; stiffness, length, shape prescribed; section area free	$E^{1/2}/\rho$
Panel - loaded in bending; stiffness, length, width prescribed; thickness free	$E^{1/3}/\rho$
Tie (tensile strut) - stiffness, length prescribed; section area free	σ_f/ρ
Beam - loaded in bending; load, length, shape prescribed; section area free	$\sigma_f^{2/3}/\rho$
Panel - loaded in bending; stiffness, length, width prescribed; thickness free	$\sigma_f^{1/2}/\rho$

E - Young's modulus, ρ - density, σ_f – failure strength

Nowadays, development of light-weight structural materials pays special attention to the field of metallic foams, due to their unusual combination of high stiffness and low density, which cannot be effectively achieved by using of any conventional structural material. However, insufficient ability of the foam to resist excessive tensile stresses in critically exposed surfaces of load-bearing components can initiate premature fracture of the component. That is why the foam is usually combined with bulk materials into sandwiches, foam-core castings, etc. The main role of the foam is to be a filler or space holder that increases inertial moments of initially hollow cross section. In order to use metallic foams for structural application the foamed component should have an own load-bearing ability, without need to combine them with relatively heavy and expensive bulk components. The using of aluminium foams partially reinforced by proper reinforcements (wires, meshes, stretched steel sheets, etc.) in the most exposed surface is the best approach how to extend the application potential of metallic foams for light-weight structural design.

REINFORCED ALUMINIUM FOAMS FOR STRUCTURAL APPLICATIONS

The cellular structure of natural load-bearing solids (wood, bone) provides very good tool for highest stiffness and buckling resistance at minimum weight. This knowledge leads to the development of artificial cellular materials for applications where light-weight plays a primarily role. Aluminium is potentially interesting candidate for cell-wall material, because of its low density, good ductility, fair corrosion and heat resistance, moderate melting temperature, environmental compatibility and easy recycling. However, the main obstacle for use of aluminium foams in structural applications is their insufficient ability to resist excessive tensile stresses in critically exposed surfaces of load-bearing components. For this reason is the foam for structural applications usually combined with bulk materials into sandwiches, foam-core castings (**Fig. 1**), etc. The typical role of the foam in this case is to be a filler or space holder, which increases inertial moments of initially hollow cross section.

Fig. 1 *Foamed-core casting*

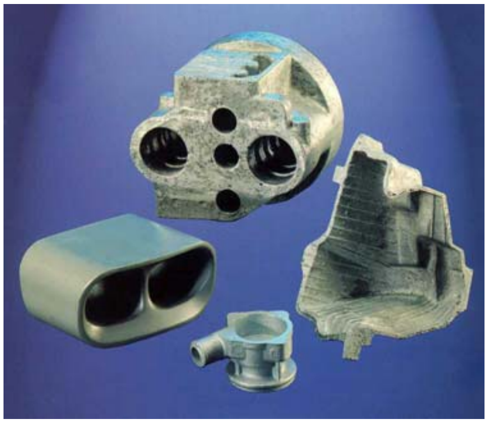

Fig. 2 *Complex-shaped structural components prepared by injection moulding of Al foam*

The most promising technology for production of aluminium foams is the method utilizing foamable precursor material made by powder metallurgical route, because of its high shape and alloy flexibility and relatively low costs for manufacturing of complex 3D-shaped structural foam components (**Fig. 2**). This method enable to reinforce foamed structural parts by metallic elements (e.g. wires woven into meshes, stretched steel sheets etc.) in tensile loaded surfaces (**Fig. 3**). Tensile stresses, that usually cause yielding or even fracture of aluminium foam component, can be overtaken by reinforcement. If the yield strength and the elasticity modulus of the reinforcement are sufficiently high, the problem of premature catastrophic failure is eliminated, because the critical tensile stresses are transferred onto reinforcing element embedded in the foam surface.

The aim of this contribution is to suggest a way for proper use of reinforced aluminium foam, to discuss achieved benefits and suggest potential applications.

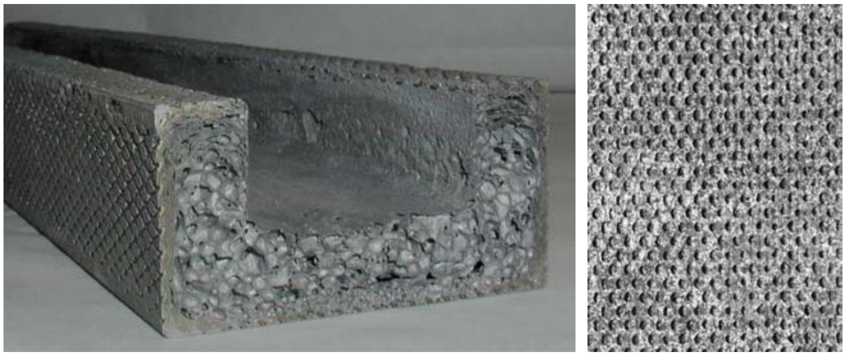

Fig. 3 *Lightweight U-beam made of aluminium foam - outer surface layer is reinforced with stretched steel sheet (right – detail of reinforced surface)*

MANUFACTURING OF REINFORCED ALUMINIUM FOAMS

The powder metallurgical technique for aluminium foam manufacturing, comprises foaming of the precursor prepared by compacting of powdered aluminium with foaming agent (e.g., TiH_2 powder) by cold isostatic pressing followed by hot extrusion. The obtained precursor of various shapes (rods, wires, open profiles) possesses gas tightly sealed particles of foaming agent within metallic matrix. The pore forming hydrogen is evolved during melting of aluminium matrix from admixed foaming agent. If the precursor is inserted in a suitable mould before foaming, foam follows the shape of mould cavity. Subsequent rapid solidification of the foam enables to obtain solid foam with dense surface skin and cellular inner structure.

The reinforced aluminium foams can be prepared similarly by (**Fig. 4**):

- foaming in the mould,
- injection of foam into the mould.

If the reinforcement, such as stainless stretched steel sheet or other mesh, net or woven textile made from metal or ceramic, is placed in the foaming mould together with foamable precursor, the foam infiltrates the reinforcement during foaming or flows around it. If surface of the foamed part or profile is reinforced in proper way, the large part of tensile load can be carried by reinforcement and the remaining forces within the foam volume are mainly compressive, thus preventing creation and growth of fatigue breakage emerging from the surface of foamed parts.

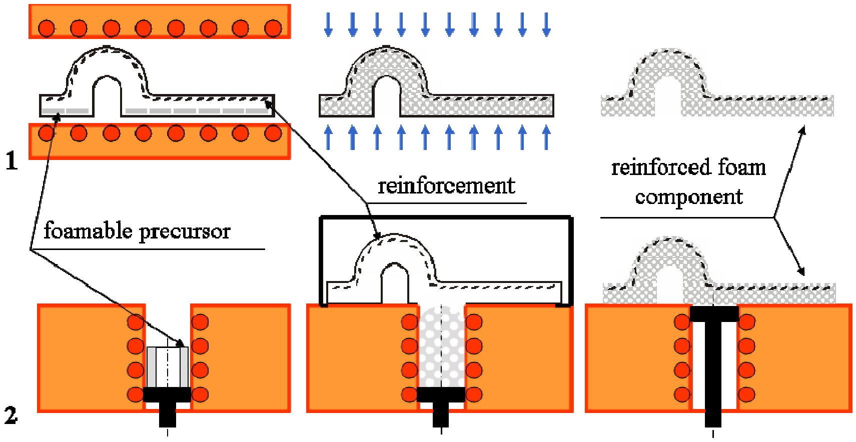

Fig. 4 *Manufacturing methods of reinforced aluminium foam*
(1 - foaming in the mould, 2 - injection of foam into the mould)

MECHANICAL PROPERTIES OF REINFORCED ALUMINIUM FOAMS

The bending tests were performed on U-beams (**Fig. 3**) made of AlSi12 foam (70 × 35 × 400 mm, thickness 15 mm). As can be seen in **Fig. 6**, significant improvement of bending stiffness and strength without any weight increase was attained for U-beams reinforced with stainless stretched steel sheet and the problem of premature catastrophic failure during bending was removed as well. The reinforced U-beams failed in buckling and did not break during bending tests. Therefore, if the aluminium foam is used for purpose of structural applications, it will be necessary to reinforce at least the tensile loaded surface of foamed part. Additionally, the reinforcement has stabilizing effect during foaming. It prevents liquid foam from collapsing thus allowing higher final porosity of the foam. That is why the apparent density of foamed U-beam without reinforcement is comparable with reinforced one. Moreover, the reinforced foamed U-beam as well as any other foamed structural part has an excellent ability to absorb impact energy. The use of reinforced foam is very suitable for this purpose, because the required level of deformation can be relatively easy tailored by proper selection and placement of reinforcements. This possibility is demonstrated in Fig. 6c. In this case the beam was reinforced only locally in bottom part, allowing upper part to deform in compression at moderate loads. After densification of upper foam part the beam deforms in bending, finally achieving the same bending strength as it was in a case of fully reinforced beam.

detrimental failure without visible plastic deformation

considerable plastic deformation, no visible fracture

squeezing of upper part without excessive bending, no fracture

Fig. 5 *Bending of U-beams made of AlSi12 foam (a - no reinforcements, b - whole surface reinforced, c - locally reinforced with stretched steel sheet (bottom surface))*

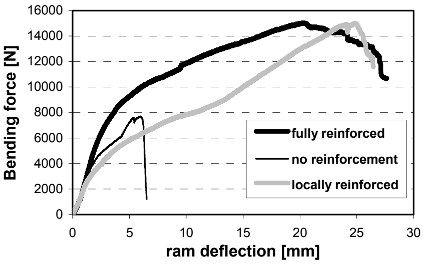

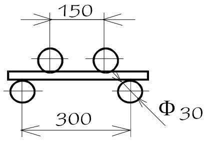

Fig. 6 *Comparison of plain foam U-beam with fully and locally reinforced U-beam response to 4-point bending, all of similar outer geometry (70 × 35 × 400 mm, thickness 15 mm) and weight (500 - 520 g).*

APPLICATIONS OF REINFORCED ALUMINIUM FOAMS

Reinforced aluminium foams owing to easy manufacturing allowing the reasonable production costs can be successfully used in light-weight constructions, crash energy absorbers, machine parts with request to enhanced vibration damping and sound absorption as well as panels created thermal barriers and noise attenuators. They are very attractive for transport industry, especially for light-weight stiff body structures of future cars, busses, trains, ships, aeroplanes, cableways, etc. They can be in the future even successfully used for novel 3D-shaped frameless shell structures of cars, where excellent performance (stiffness, strength, passive safety) is expected at minimum weight. Because of their excellent corrosion resistance, non-inflammability and the fact, that they do not evolve toxic fumes in a fire, they can be utilized also as decorative material for design applications, e.g. for passenger cabins in ships, dividing walls in airplanes, buses, trains, cinemas, theatres, supermarkets, etc.

CONCLUSIONS

The possibility to use the reinforced aluminium foam for structural applications was demonstrated. The reinforcements ought to be placed to the foam surface according to the way of expected loading, preferably at tensile loaded side of the foam. The manufacturing method makes possible to reinforce the foamed part also selectively according to the expected load only in weakest points, which enables to improve bending stiffness, strength, plasticity, energy absorption capacity, fracture toughness and damage tolerance of foamed component without significant weight or cost increase. Moreover the reinforcements increase the thickness of surface skin, prevent liquid foam from collapsing, simplify joining of foamed parts and enable limited shaping after foaming process.

ACKNOWLEDGEMENTS

The financial support of Alulight International GmbH., Ranshofen, Austria is greatly appreciated.

REFERENCES

[1] Simančík F., Rajner W., Laag R.: "Alulight - Aluminum foam for lightweight construction", SAE Tech. Paper Series 2000-01-337, Warrendale: SAE, Inc., 2000, p. 31.
[2] Kováčik J., Simančík F., Jerz J., Tobolka P.: "Reinforced aluminium foams". In: Proc. of Int. Conf. "Advanced Metallic Materials", 5-7.11.2003, Smolenice, Slovakia, p.154-159.
[3] Simančík F., Rajner W., Laag R.: "Reinforced Alulight for structural use". In: Processing and properties of Lightweight Cellular Metals and Structures (TMS Annual Meeting), Seattle, February 17 – 21, 2002, p. 25.
[4] Ashby M.F.: "Materials selection in mechanical design." Pergamon Press, Oxford, 1992.
[5] Simančík F., Florek R., Tobolka P.: "Reinforced aluminium foam profiles". In *Powder metallurgy 2004, Viedeň, 17-21.10.2004*. Shrewsbury: EPMA, 2004, p. 47-48.
[6] Jerz J.: Foamed Aluminium and Aluminium Alloys Prepared by Powder Metallurgy, PhD thesis, TU Vienna, 1995.

GAS PRESSURE INFILTRATION OF COPPER INTO POROUS CARBON/GRAPHITE BODIES

Juraj KORÁB
Institute of Materials and Machine Mechanics, Slovak Academy of Sciences, Račianska 75,
831 02 Bratislava 3, Slovak Republic

Ľubomír ŠTEFKE
Elektrokarbon Topoľčany, joint stock company, Tovarnícka 412, 955 22 Topoľčany,
Slovak Republic

Abstract: In the paper cooperation between both research and industrial subject on production of copper impregnated carbon/graphite materials is described and properties of sliding contacts for trolleybuses are analysed. The contacts were the first ones that were prepared by the Institute of Materials and Machine Mechanics of the Slovak Academy of Sciences for the Elektrokarbon Topoľčany, joint stock company. The technology used was the gas pressure infiltration. Some important properties of sliding contacts were measured and analysed e.g. the weight gain the electrical resistivity, bending strength and hardness. They were also tested in real conditions - mounted on the trolley poles. Test results showed that the copper carbon/graphite material has properties fulfilling requirements of the producer and potential customers. The material showed better properties in different weather conditions in comparison to other types of sliding materials e.g. antimony and organic resin infiltrated contacts.

Keywords: gas pressure infiltration, copper, carbon, graphite, sliding contacts

Introduction

Gas pressure infiltration of molten metals into porous bodies is very progressive technology for preparation of different types of metal matrix composites (MMCs). One of the industrial applications is the antimony-carbon/graphite material that is used in pumping industry (sealing rings). Another well-known application is the Cu-carbon/graphite sliding contact, which found application in different fields e.g. for electric trains (pantograph heads), trolley buses (they are mounted to the end of trolley poles) and as carbon brushes for electrical rotating machines. The technology is very competitive in comparison with other MMC production routes. It involves many aspects from physics, surface chemistry, metallurgy, graphite chemistry and composite mechanics.

In Slovakia the only company that commercially produces contact materials by using the gas pressure infiltration technology is Elektrokarbon Topoľčany, joint stock company. Its main products are different carbon/graphite materials, carbon brushes and carbon/graphite-antimony composites. In 2002 the company decided to introduce a new product on a market: the Cu-carbon/graphite composite (Cu-C MMC), made by gas pressure infiltration for application in trolley busses and trains.

The Institute of Materials and Machine Mechanics of the Slovak Academy of Sciences (IMMM) has been working for several decades in the field of gas pressure infiltration. It gained sufficient knowledge in both based and industrial research with focusing on analysis of different types of MMCs e.g. Mg-Li and Al-based matrix reinforced with both ceramic (Saffil) and carbon fibres and infiltration of copper into porous bodies. The institute not only performed a lot of development and optimisation but also helped the Elektrokarbon to produce first volumes of Cu-C MMCs for new customers.

Cooperation description

In the frame of the cooperation between the IMMM and the Elektrokarbon Topoľčany, the work was concentrated on infiltration of porous carbon/graphite pre-forms with dimensions of $20 \times 15 \times 102$ mm^3 for sliding contact applications (in trolleybuses). Annual production in 2004 was about 5000 pieces. In the future it is planned to produce up to 10 000 pieces due to increased number of customers. That is why it will be necessary to move the production to the Elektrokarbon and the IMMM will be responsible only for research work.

Experimental

From the beginning of cooperation very large number of pieces were going to be infiltrated and that is why it was necessary to design a suitable holder. It could allow infiltrating as much pieces as possible in one infiltration trial. The holder had to be strong enough to bear 12 kg load of infiltrated contacts and should withstand high temperature of molten copper. Except the holder the production optimisation comprised such parameters such as infiltration pressure and temperature. The main aim of optimisation was to:

1. decrease costs to an acceptable level
2. increase the product quality

Properties of infiltrated sliding contacts e.g. electrical conductivity, wear resistance and strength depend mainly on amount of metal that is infiltrated into a porous graphite skeleton. To infiltrate copper into graphite is usually difficult due to poor wettability between these two constituents. Large wetting angle ($\vartheta > 90^o$) gives rise to the negative capillary pressure that occurs in pores $p_k < 0$, this means that metal is pushed out from pores. However, when external pressure P_e is used it overcomes this capillary pressure and liquid metal can enter pores. It is obvious that whole pore volume cannot be filled because for very small pores with diameter $r_e \to 0$ external pressure has to be very large $p_e \to \infty$ [1]. From the previous text is obvious that with increasing infiltration pressure increases copper volume that pores can contain.

Infiltration quality

Infiltration quality can be assessed from the amount of copper that was infiltrated into porous body. It is usually characterised by a weight gain X_m [%]:

$$X_m = \left(1 - \frac{m_1}{m_2}\right).100\% \qquad (1)$$

where m_1 and m_2 represents sample weights before and after infiltration, respectively. The higher is weight gain the better is the quality of infiltration.

Sample preparation

In the frame of the work different types of carbon/graphite pre-materials were infiltrated but main volume represented trolleybus sliding contacts. They were developed and produced at the company Elektrokarbon Topoľčany (Fig.1). A traditional production technology comprised following steps:

- mixing of basic ingredients (natural graphite, coke, black carbon and pitch) and homogenisation
- extrusion of homogenised blend to a required shape
- firing at 1050 °C – 1150 °C
- machining to a final shape

Fig. 1 Carbon/graphite raw material, which was copper infiltrated at the IMMM. In front at left side one can see a trolleybus sliding contact with length of 102 mm. Longer pieces (l = 275 mm) represent a shortened version of sliding contacts for electric trains.

Infiltration technology procedure

Gas pressure infiltration of molten copper into graphite bodies was performed in the large autoclave of the IMMM (Fig.2) and can be described in several points:

1. a special holder containing carbon / graphite pre-material is placed inside - to the upper part of the autoclave
2. copper is heated at low vacuum, $p_{vac.} = 80 - 100$ Pa, to the melting temperature
3. holder immersion to molten metal at a suitable temperature, $T \approx 1200\ ^{o}$C

4. then follows inert gas introduction
5. short infiltration period, $t = 120$ s, at pressure $p_e \approx 5$ - 6 MPa
6. holder withdrawal from the melt
7. cooling and gas deflating
8. holder removal and sample cleaning

Fig. 2 A semi-production autoclave at the IMMM SAS. Crucible dimensions: ∅ 310 mm x 550 mm.

Optimisation of infiltration time

With regard to technical possibilities of the equipment the infiltration was performed at two different temperature cycles. In the first one samples were immersed in the copper melt at 1200 ^{o}C and then 10 min long dwell followed. In the second temperature cycle samples were infiltrated immediately after they were put into the copper. The aim of this procedure was to compare if longer pre-heating in the molten metal might have any influence on the quality of infiltrated contacts / on volume of copper in the pores.

Optimisation of infiltration pressure

Different infiltration pressures were used in order to optimise production costs. Infiltration trials started at lower pressure, 4 MPa, and later on the infiltration pressure was increased up to 6.5 MPa.

RESULTS

Structure of carbon/graphite pre-materials

The average porosity of the carbon/graphite material was measured by the Archimedes method and was in the range from 20 to 25 vol. %. Pore distribution analysis was not measured but later on detailed research will be carried out in this field. Some contacts contained larger cracks that developed during firing when some organic material evaporated from the material volume. They were visible in the cross-section and their dimensions were 1 – 4 mm in length. Basic properties of non-infiltrated contacts were measured at the Elektrokarbon Topoľčany. Their average values are summarised in Table 1 – column (1). In the column (2) properties of the competitive material are presented. They indicate that both materials are similar although production routes were supposed to be slightly different.

Table 1 Basic properties of carbon/graphite pre-material produced at Elektrokarbon (1) and at one competitor (2). Both materials are designed for trolleybus application.

	(1)	(2)
specific electrical resistivity [μΩm]	25 - 35	*35 – 40 [2]*
hardness HRB 10/100	90 –110	
density [g.cm^{-3}]	1.55 – 1.75	*1.55 – 1,65 [2]*
bending strength [MPa]	min. 20	*33 - 45 [2]*
porosity [%]	20 – 25	

Influence of infiltration time on quality of the composite

Four groups of contacts were compared (trial No.183, with 10 min. pre-heating period; No. 80; 184 and 185 – no pre-heating) in order to analyse influence of infiltration time. Material infiltrated in the trial No.183 was heated at 1200 °C in molten copper for 10 minutes before the gas pressure was applied. It was expected that due to longer time of immersion the inner temperature of contacts would increase in comparison with other temperature cycles. It is known that at higher temperature the wetting angle between copper and graphite is lower. Then pores with smaller diameter should have been filled with copper and the material infiltrated in the trial No.183 was expected to contain more copper [3]. Other infiltration trials performed without this pre-heating period should have presented lower weight gain. However, from Figure 3 one can see no difference between different temperature cycles. This can also demonstrate the average weight of infiltrated pieces calculated for each trial (78,3 g; 78,2 g; 78,1 g and 76,7 g, for infiltration trails No. 183; 180; 184 and 185, respectively).

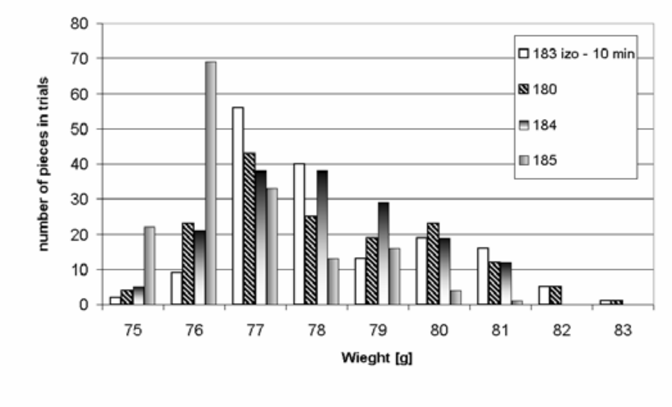

Fig. 3 Comparison of sliding contacts (weight after infiltration), which were infiltrated in different temperature cycles. In the trial No. 183 sliding contacts were pre-heated 10 min. at 1200 oC (183 izo – 10 min). In other trials temperature cycle was shorter - without pre-heating period (180, 184 and 185)

Influence of infiltration pressure on quality of the composite

In Figure 4 dependence of sliding contact weight on infiltration pressure is presented. According to theory it can be observed that with increasing pressure copper volume in carbon/graphite skeleton increases – sliding contacts show higher weight. However, one can see quite large dispersion of results. This is due to non-homogeneous structure of the pre-material that contained some cracks and due to other factors that might influence the infiltration process e.g. temperature gradient in the crucible, pressure variations; melt flow and turbulent environment in the autoclave during infiltration. From the experience the optimum pressure appeared to be in the range from 6 to 7 MPa when the Cu-C MMC could achieve high weight gain at low infiltration costs. Although the autoclave is able to work at 10 MPa (best results), however, it should be pointed out that in this case the gas consumption would be extremely high.

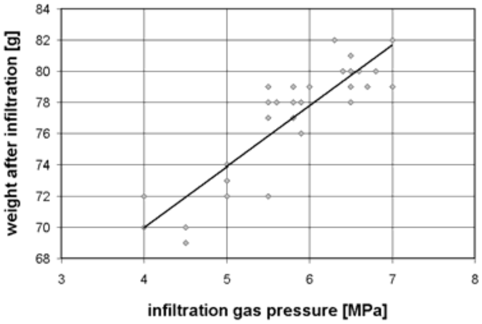

Fig. 4 Dependence of weight gain on infiltration pressure for Cu-impregnated carbon/graphite sliding contacts. The starting weight of contacts was 56 – 57 g. The line represents the linear trend line obtained from measurements.

Measurement of physical properties

Basic physical properties of Cu-carbon/graphite contacts were measured at the company Elektrokarbon Topoľčany. Measured were hardness, bending strength, compressive strength and electrical resistivity (Table 2).

Table 2 Results of basic physical properties for sliding contacts for trolleybuses impregnated with organic resin, antimony and copper. Added are properties obtained of one large European sliding contact producer.

	Elektrokarbon			***competitor***
	Impregnation with organic resin	Impregnation with antimony	**Impregnation with copper**	
Density [g/cm^3]	1.6-1.7	2.3-2.7	2.1-2.3	*2.4 –2.5*
Specific el. resistivity [μΩm]	30-35	10-15	2-5	*10 - 15*
Brinell hardness HRB 10/100	100-120		110-125	
Brinell hardness HRB 5/150	80-100	100-110	95-97	
Bending strength [MPa]	20-25	50-55	55-65	*55 – 70*
Strength in compression [MPa]	30-45		140-180	

They were obtained for different composite materials – for those ones impregnated with antimony, organic resin and copper. From the table it can be concluded that the copper-infiltrated material presents much lower electrical resistivity than older products. Bending strength is at the same level to that for the antimony-infiltrated material and much higher that gives impregnation with organic resin. Interesting is a comparison of hardness values that are at the same level for all types of composites. In the case of Cu – carbon/graphite MMC it can be explained according to observations in [4] where authors found that there is no copper in the thin outer layer of the composite (approximately 0.5 mm). That is why the value does not represent the hardness of the composite but of the carbon/graphite pre-material. This fact can be supported by hardness comparison values from Table 1 and Table 2.

Outside testing in trolleybuses

Infiltrated sliding contacts were mounted to a current collector heads that were placed at the end of trolley poles in trolleybuses. Tests in real conditions in different transport companies in Slovak and Czech republics were performed. From results of these tests the Elektrokarbon Topoľčany can conclude that the Cu – carbon/graphite material:

- is suitable for rainy and winter conditions: in comparison to materials infiltrated with antimony and organic resin it achieved lifetime by 15 – 20 % and by 80 – 120 % longer, respectively
- in dry and summer time it presented higher lifetime than the antimony and organic resin infiltrated materials, however the ratio "lifetime / price" was not so competitive

Importance of cooperation for Elektrokarbon Topoľčany:

The technology of copper infiltration was optimised at the IMMM SAS for production of new types of products. It enabled the Elektrokarbon, joint stock company to:

- introduce new and competitive copper-infiltrated products to the market
- strengthen the position on Slovak and Czech markets with sliding contacts for trolleybuses
- spread its activities to western and eastern countries e.g.:
  1. *France* – tests of trolleybus sliding contacts were successfully finished in two transport companies
  2. *Switzerland* – Elektrokarbon was allowed to test its products in two transport companies
  3. *Poland* – became a new business partner in the field of sliding contacts
- define technological and technical conditions that are required for design and development of a new autoclave for Elektrokarbon (production of sliding contacts for trains with dimensions of 1200 mm x 60 mm x 30 mm)
- development of new contacts based on other than copper matrix, e.g. magnesium and aluminium

Literature:

[1] Schweighofer, A. and Kúdela S.: Research report of the Institute of Materials and Machine Mechanics, Slovak Academy of Sciences, Bratislava, Slovak republic, 1979, (in Slovak)

[2] Schunk Kohlenstofftechnik – a company leaflet, Industrial and Traction Technology, Carbon Sliding Strips for Pantographs and Trolley Pole Systems,

[3] Krcho, S.: Study of transport phenomena in carbon /graphite skeleton infiltrated composites, PhD.Thesis, Slovak University of Technology, Bratislava, Slovak academy of sciences, Slovak republic, 1987 (in Slovak)

[4] Harmady, J.: Influence of microstructure on mechanical properties of infiltrated material, Master Thesis, Slovak Technical University Bratislava, Faculty of mechanical engineering, 1980, (in Slovak)

10. Savjetovanje o materijalima, tehnologijama, trenju i trošenju
10. Conference on Materials, Processes, Friction and Wear
MATRIB'05, Vela Luka, 23-25.06.2005.

MIKROSTRUKTURNA I FAZNA ANALIZA TROSKI NEHRĐAJUĆEG ČELIKA

THE MICROSTRUCTURE AND PHASE ANALYSIS OF STAINLESS STEEL SLAGS

Stjepan Kožuh[1], Mirko Gojić[1], Jakob Lamut[2]

[1] Metalurški fakultet, Sveučilište u Zagrebu, Aleja narodnih heroja 3, 44103 Sisak, Hrvatska
[2] Naravoslovnotehniška fakulteta, Univerza v Ljubljani, Aškerčeva 12, 1000 Ljubljana, Slovenia

[1] Faculty of Metallurgy, University of Zagreb, Aleja narodnih heroja 3, 44103 Sisak, Croatia
[2] Faculty of Natural Sciences and Enginnering, University of Ljubljana, Aškerčeva 12, 1000 Ljubljana, Slovenia

Sažetak: U radu su prikazani rezultati mikrostrukturne (SEM) i fazne (XRD) analize skrutnute troske dobivene pri proizvodnji visokolegiranih nehrđajućih čelika vakuumskim (VOD) postupkom. Detaljno je analizirana troska nastala nakon oksidacije ugljika. Tijekom perioda oksidacije ugljika dolazi do nastanka kromovog oksida Cr_2O_3 koji vezan s oksidom željeza stvara kromit $FeO{\cdot}Cr_2O_3$. Provedenom analizom je uz $FeO{\cdot}Cr_2O_3$ u trosci utvrđena prisutnost $MnO{\cdot}Cr_2O_3$, $MgO{\cdot}Cr_2O_3$ i kompleksnog spinela $(FeO{\cdot}MnO{\cdot}MgO){\cdot}Cr_2O_3$. Prosječni sadržaj Cr_2O_3 u trosci iznosi 25-40 %, dok u kromitu može biti Cr_2O_3 iznad 70 %. Zbog nastalih kromita takve troske su slabo tečljive, tj. tjestaste (kašaste). Krom se iz troske može ponovno vratiti u metalnu talinu dodatkom reducensa, najčešće ferosilicija ili aluminija.

Ključne riječi: troska, nehrđajući čelik, kromit, SEM analiza, XRD analiza

Abstract: In this work the results of SEM and XRD analysis of solid slags at industrial production of high alloy stainless steel by Vacuum Oxygen Decarburization (VOD) technological route are shown. Particularly was analysed of slag taken after oxidation of carbon. During reduction of the carbon the chromium oxide content Cr_2O_3 is formed and it is bound with iron oxide forming chromite $FeO{\cdot}Cr_2O_3$. By analysis was found that is beside $FeO{\cdot}Cr_2O_3$ in the slag presence of $MnO{\cdot}Cr_2O_3$ and $MgO{\cdot}Cr_2O_3$ phases. The $(FeO{\cdot}MnO{\cdot}MgO){\cdot}Cr_2O_3$ type complex spinel was formed. Average content of Cr_2O_3 in slags is 25-40 %, while in chromite is above 70% Cr_2O_3. Because formed chromite such slags were slightly liquid or doughy (mushy). Chromium can again from slag in heat come back, usually with addition substance for reduction (ferro-silicon or aluminium).

Key words: slag, stainless steel, chromite, SEM analysis, XRD analysis

UVOD

Nehrđajući čelici predstavljaju skupinu visokolegiranih čelika kod kojih je krom glavni legirajući element [1]. U nehrđajućim čelicima minimalan sadržaj kroma iznosi 10,5 mas. %. Pored kroma, ovisno o vrsti čelika, mogu biti prisutni i ostali legirajući elementi kao što su npr. Ni, Mo, V itd. Zbog svog kemijskog sastava nehrđajući čelici se ističu izvanrednom korozijskom otpornošću, postojanošću kod visokih temperatura te dobrim mehaničkim svojstvima (povoljan odnos čvrstoća/masa) i kod izrazito niskih temperatura.

U početku su se nehrđajući čelici proizvodili samo u elektrolučnoj peći. Međutim, oksidacija ugljika u elektrolučnoj peći dovodila je do neželjene oksidacije kroma.

Postupci koji se danas koriste za proizvodnju nehrđajućih čelika uglavnom se sastoje od dvije faze. U elektrolučnoj peći provodi se taljenje uloška (čelični otpad, ferolegure i ostale sirovine). U relativno kratkom vremenu dobiva se rastaljena metalna talina. Odugljičenje taline provodi se u drugom agregatu najčešće uz primjenu argona i kisika (AOD – eng. Argon Oxygen Decarburization) ili vakuuma (VOD – eng. Vacuum Oxygen Decarburization). Uvođenje AOD postupka predstavljao je veliki doprinos u proizvodnji nehrđajućih čelika. Osim pojeftinjenja proizvodnje u AOD konvertoru poboljšana je i kvaliteta čelika. Zato je AOD danas dominantan postupak (oko 70 %) za proizvodnju nehrđajućih čelika [2].

Pri proizvodnji nehrđajućih čelika značajnu ulogu ima troska jer i ona sudjeluje u odvijanju kemijskih reakcija. Pri oksidaciji kod proizvodnje nehrđajućih čelika krom oksidira uz oslobađanje topline i pritom nastaju CrO, Cr_2O_3 i CrO_3. Ponašanje oksida kroma u metalurškoj trosci veoma je kompleksno zbog njihovog visokog tališta i različitih stupnjeva oksidacije kroma. Stupanj oksidacije kroma u trosci ovisi o kemijskom sastavu i temperaturi troske te parcijalnom tlaku kisika. Kod procesa izrade čelika u kojima nastaje kisela troska krom oksidira u CrO, a kod bazičnih troski krom oksidira u Cr_2O_3. Ako Cr_2O_3 nije reduciran u trosci mogu nastati kompleksni spineli tzv. kromiti. Na kraju oksidacije (kad su postignuti vrlo niski sadržaji ugljika u metalnoj talini) mogu nastati različiti kromiti, npr. $FeO{\cdot}Cr_2O_3$, $MnO{\cdot}Cr_2O_3$, $MgO{\cdot}Cr_2O_3$, $CaO{\cdot}Cr_2O_3$. Navedeni kromiti imaju vrlo visoku temperaturu taljenja (> 2000°C) pa mogu prouzročiti pojavu tjestasto-kašaste, odnosno krute troske. Kod takvih troski površina (kora) je skrutnuta, a ispod kore je tanak sloj tekuće troske koja je pretežno sastavljena od kalcijevih silikata [3].

Redukcija u trosku oksidiranih elemenata kao što su krom, željezo, mangan može se postići dezoksidacijom troske, čime se smanjuje sadržaj kisika u trosci te razaraju kromiti [4]. Dezoksidacija troske se provodi uglavnom dodatkom ferosilicija i aluminija. Dezoksidacija troske prihvatljiva je samo u onim slučajevima kada je nizak sadržaj fosfora, budući bi se u suprotnom i fosfor reducirao (vratio iz troske u čelik).

Nove tehnologije proizvodnje nehrđajućih čelika uključuju djelotvorno odugljičenje s minimalnom oksidacijom kroma. To se postiže primjenom novog tipa koplja za upuhivanje kisika odozgo radi poboljšanja porasta temperature i naknadnog izgaranja primjesa u početnom stadiju upuhivanja, upuhivanjem kisika razrjeđenog s dušikom u kombinaciji s vakuumskim otplinjavanjem te upuhivanjem dušika kod proizvodnje niskougljičnih nehrđajućih čelika [5].

EKSPERIMENTALNI DIO

U radu su prikazani rezultati analize nekoliko uzoraka troske dobivene pri proizvodnji nehrđajućih čelika. Kemijski sastav nehrđajućih čelika kod čije je proizvodnje uzeta troska za analizu naveden je u tablici 1.

Tablica 1. Kemijski sastav nehrđajućih čelika, mas. %

Čelik	C	Si	Mn	$P_{max.}$	$S_{max.}$	Cr	$Cu_{max.}$	Ni	$Al_{max.}$	$Sn_{max.}$	Mo	Ti
AISI 304 (1.4301)	0,04-0,06	0,30-0,75	1,40-1,80	0,04	0,003	18,00-18,50	0,50	8,00-9,00	0,015	0,03	-	-
AISI 316Ti (1.4571/73)	max. 0,04	0,30-0,75	1,40-1,80	0,04	0,003	16,50-17,00	0,50	10.50-11,00	0,015	0,03	2,00-2,30	max. 0,30
AISI 316L (1.4404/35)	max. 0,03	0,30-0,75	1,40-1,80	0,04	0,003	16,50-17,00	0,50	10,00-10,50	0,015	0,03	2,00-2,30	-
AISI 321 (1.4541)	max. 0,04	0,30-0,75	1,40-1,80	0,04	0,003	17,00-17,50	0,50	9,00-9,50	0,015	0,02	-	max. 0,30
AISI 301 (1.4310)	0,09-0,12	0,30-0,75	1,40-1,80	0,04	0,003	16,50-17,00	0,50	7,00-7,50	0,015	0,03	-	-

AISI – American Iron Steel Institute

Uzorci troske uzimani su kod različitih perioda procesa proizvodnje nehrđajućih čelika. Detaljnije je analizirana troska nastala nakon perioda oksidacije primjesa. Mikrostrukturna analiza uzoraka troske provedena je skenirajućom elektronskom mikroskopijom (SEM), a fazna identifikacija rendgenskom difrakcijskom analizom (XRD). Prije analize uzorci krute troske samljeveni su u praškasti oblik.

SEM analiza je provedena pomoću pretražnog elektronskog mikroskopa Jeol JSM-5610 EDS IXRF systems Inc. 500 koji omogućava energetsku x-ray spektrometriju. Napon ubrzanja elektrona iznosio je 10 kV. Praškasti uzorci troske su prije SEM analize zaliveni u odgovarajuću plastičnu masu te su napareni ugljikom radi postizanja električne provodljivosti. Fazna identifikacija praškastih uzoraka provedena je metodom X-ray difrakcije uz sljedeće uvjete snimanja: CuK_{α} zračenje, napon 40 kV, struja 20 mA, brzina snimanja 2,5°/min, područje snimanja kuta difrakcije (2θ) od 20 do 70°. Dobiveni difrakcijski spektar analiziran je metodom usporedbe s JCPDS podacima [6].

REZULTATI I DISKUSIJA

Nastajanje troske odvija se tijekom oksidacije željeza i prisutnih primjesa (Si, Mn, P…). Troska je lakša od željeza i pliva na površini metala. Uz produkte oksidacije primjesa (SiO_2, MnO, P_2O_5, Cr_2O_3) glavni izvori troske su i produkti erozije vatrostalne obloge peći (MgO, Cr_2O_3), nečistoće unesene punjenjem, pomoćni materijali i oksidansi. Brzina prijelaza sastojaka troske u homogenu tekuću otopinu ovisi o temperaturi taline, sastavu troske, intenzitetu miješanja taline, dodatku troskotvoraca itd.

Rastaljene su troske po prirodi ionske otopine jer se sastoje od pozitivno nabijenih iona (kationi) i negativno nabijenih kompleksnih silikatnih, aluminatnih i fosfatnih iona (anioni). Kationi prisutni u trosci su Fe^{2+}, Fe^{3+}, Mn^{2+}, Ca^{2+}, Mg^{2+}, Cr^{2+}, Cr^{3+} i dr., dok su anioni O^{2-}, S^{2-}, SiO_4^{4-}, PO_4^{3-} itd. Mineraloška analiza krutih troski pokazala je da su u troskama prisutni brojni različiti minerali (silikati i aluminosilikati, spineli, jednostavni oksidi i ostali minerali) [7]. Međutim, navedeni minerali utvrđeni su samo u troskama nakon skrućivanja, dok su struktura i sastav rastaljenih troski nedovoljno poznati.

Troska bogata s kromovim oksidima nastaje za vrijeme proizvodnje nehrđajućih čelika, tj. tijekom taljenja u elektrolučnoj peći i odugljičenja u AOD ili VOD agregatu.

Na slikama 1a i 2a prikazana je mikrostruktura uzoraka troske u struji sekundarnih elektrona, uzete nakon perioda oksidacije primjesa tijekom industrijske proizvodnje nehrđajućih čelika. Slike 1b i 2b prikazuju energetsko disperzijski spektar (EDS) nekih od označenih mjesta (kromit i kalcij silikatna osnova) na slikama 1a i 2a. U tablicama 2 i 3 navedeni su rezultati EDS analize u kvantitativnom obliku. Rendgenogrami uzoraka troske nakon oksidacije i redukcije u VOD agregatu prikazani su na slikama 3 i 4.

Može se primijetiti (slika 1a i 2a) da troska nastala nakon oksidacije taline sadrži značajan udio kromovog oksida raspoređenog u kalcij-silikatnoj osnovi. Sadržaj Cr_2O_3 iznosi na pojedinim pozicijama čak oko 77 % (tablice 2 i 3). Kemijski sastav troske nastale pri proizvodnji nehrđajućih čelika pokazuje da se troske uglavnom sastoje od sljedećih oksida: FeO, MnO, MgO, CaO, SiO_2, Cr_2O_3, Al_2O_3. Stoga se može pretpostaviti da se troske nastale pri proizvodnji nehrđajućih čelika sastoje od kompleksnih spinela $(FeO \cdot MnO \cdot MgO) \cdot Cr_2O_3$, a ne od pojedinačnih kromita (npr. $FeO \cdot Cr_2O_3$).

XRD analiza troske dobivene poslije oksidacije taline potvrdila je rezultate EDS analize. Rendgenogram troske prikazan na slici 3 pokazuje da se troska sastojala uglavnom od $MgO \cdot Cr_2O_3$. Poslije redukcije sastav troske se promijenio. Osnovna komponenta troske poslije redukcije bio je gehlenit – $2CaO \cdot Al_2O_3 \cdot SiO_2$ (slika 4). Također, poslije redukcije u trosci su zapaženi i kromiti. U odabranom primjeru prikazanom na slici 4 to je bio $MgO \cdot Cr_2O_3$ koji je ostao nereduciran u trosci.

Rafinacija taline troskom odvija se tako da se određeni sastojci raspodijele između metala i troske. Raspodjela i prijelaz tih sastojaka iz jedne u drugu fazu posljedica su odvijanja kemijskih reakcija na međufaznoj granici troska/metal, te gibanja reaktanata i produkata reakcija kroz granični sloj.

Oksidacijska sposobnost troske očituje se u njenom transferu kisika. Rastaljena metalna talina sadrži najviše željeza, te ostale primjese koje su više ili manje plemenitije od željeza. Tijekom rafinacije plemenitije primjese se sporije oksidiraju od željeza. Pri interakciji metala i troske Fe-oksid (FeO) je glavni oksidans, a tome pridonosi i trovalentno željezo (Fe_2O_3).

Budući da u metalnoj talini željeza ima daleko više od ostalih primjesa kisik prvo reagira s željezom:

$$[Fe] + [O] \rightarrow (FeO) \qquad (1)$$

Sadržaj Fe-oksida u trosci u određenim momentima može biti znatan (ponekad do 50%). Željezni se oksid u troskama otapa kao Fe^{2+} i Fe^{3+}. Odnos Fe^{2+}/Fe^{3+} ovisi o temperaturi, potencijalu kisika i sastavu troske.

Uz željezo veoma brzo se oksidira i mangan. Pritom može nastati MnO_2, Mn_2O_3, Mn_3O_4 i MnO. Od navedenih oksida mangana jedino je MnO stabilan kod visokih temperatura. Oksidacija mangana može se prikazati kao:

$$[Mn] + [O] \rightarrow (MnO) \qquad (2)$$

ili

$$[Mn] + (FeO) \rightarrow (MnO) + [Fe] \qquad (3)$$

Krom kao glavni legirajući element također oksidira. Kod bazičnih procesa izrade čelika krom oksidira uz oslobađanje topline:

$$2[Cr] + 3(FeO) \rightarrow (Cr_2O_3) + 3[Fe] \qquad (4)$$

Model odugljičenja koji navodi N. Kikuchi et al. [5] pokazuje da prilikom odugljičenja postoje tri područja na kojima dolazi do odvijanja reakcija: slobodna površina taline, međupovršina troska/metal i područje pri dnu mlaza upuhanog kisika. Reakcija na slobodnoj površini taline kontrolirana je prijenosom ugljika i kisika na međupovršini plin/metal. Dio upuhanog kisika reagira s ugljikom, a preostali kisik oksidira krom stvarajući kromov oksid koji se absorbira u sloju troske.

Ukoliko Cr_2O_3 nije reduciran nastaju kompleksni spineli, tj. spojevi kromovog oksida s ostalim oksidima (FeO, MnO, MgO, CaO):

$$(FeO) + (Cr_2O_3) \rightarrow (FeO)\cdot Cr_2O_3 \qquad (5)$$

$$(MnO) + (Cr_2O_3) \rightarrow (MnO)\cdot Cr_2O_3 \qquad (6)$$

$$(MgO) + (Cr_2O_3) \rightarrow (MgO)\cdot Cr_2O_3 \qquad (7)$$

$$(CaO) + (Cr_2O_3) \rightarrow (CaO)\cdot Cr_2O_3 \qquad (8)$$

Za svaku od reakcija (1-8) moguće je izračunati konstantu ravnoteže. Tako npr. za reakciju (4) konstanta ravnoteže iznosi:

$$K = \frac{a_{(Cr_2O_3)}}{a_{[Cr]}^{2} \cdot a_{(FeO)}^{3}} \qquad (9)$$

Budući da realne troske sadrže mnogo komponenti proračuni konstante ravnoteže su prilično složeni jer nema prevelikog broja podataka o aktivitetima komponenti. Problem se pojednostavljuje pretpostavkom da je troska idealna ionska otopina, pa se aktiviteti komponenti troske izjednačavaju s njihovim ionskim udjelima.

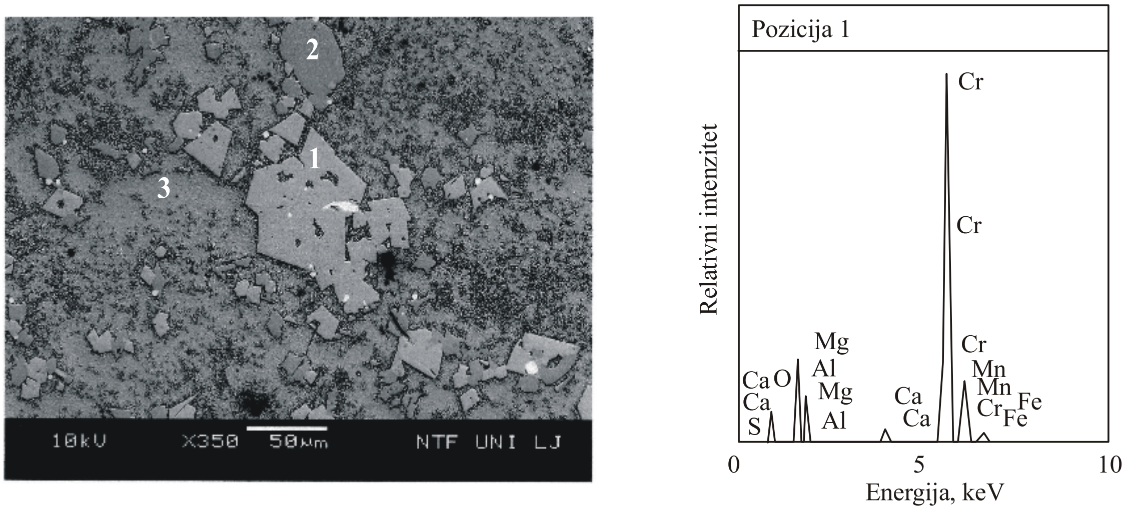

(a) (b)

Slika 1. Mikrosnimak uzorka troske 733 (a) i energetsko disperzijski spektar uzorka troske 733 - pozicija 1 (b)

Tablica 2. Kemijski sastav pojedinih područja označenih na slici 1a, mas. %

Pozicija	FeO	MnO	MgO	CaO	SiO_2	Cr_2O_3	Al_2O_3
1	0,60	2,99	11,38	0,87	0,15	77,47	6,55
2	0,88	7,01	57,52	0,94	0,36	30,52	2,77
3	0,01	4,05	3,65	52,92	23,29	2,14	13,94

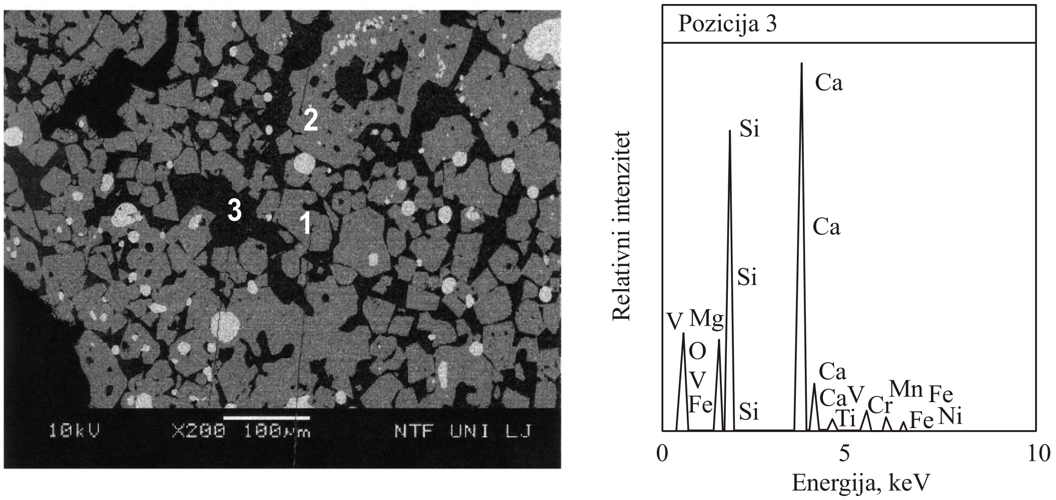

(a) (b)

Slika 2. Mikrosnimak uzorka troske 96 (a) i energetsko disperzijski spektar uzorka troske 96 - pozicija 3 (b)

Tablica 3. Kemijski sastav pojedinih područja označenih na slici 2a, mas. %

Pozicija	FeO	MnO	MgO	CaO	SiO_2	Cr_2O_3	Al_2O_3
1	14,84	3,61	1,34	2,16	-	75,98	2,07
2	14,51	3,83	1,28	1,94	-	75,66	2,77
3	-	-	-	46,27	38,32	5,52	9,89

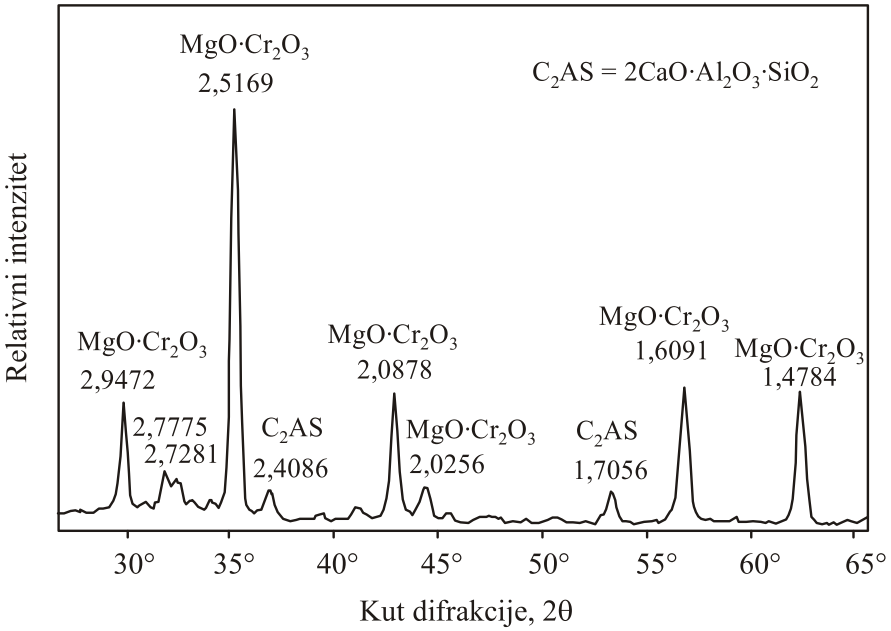

Slika 3. Rendgenogram troske nakon oksidacije taline u VOD agregatu

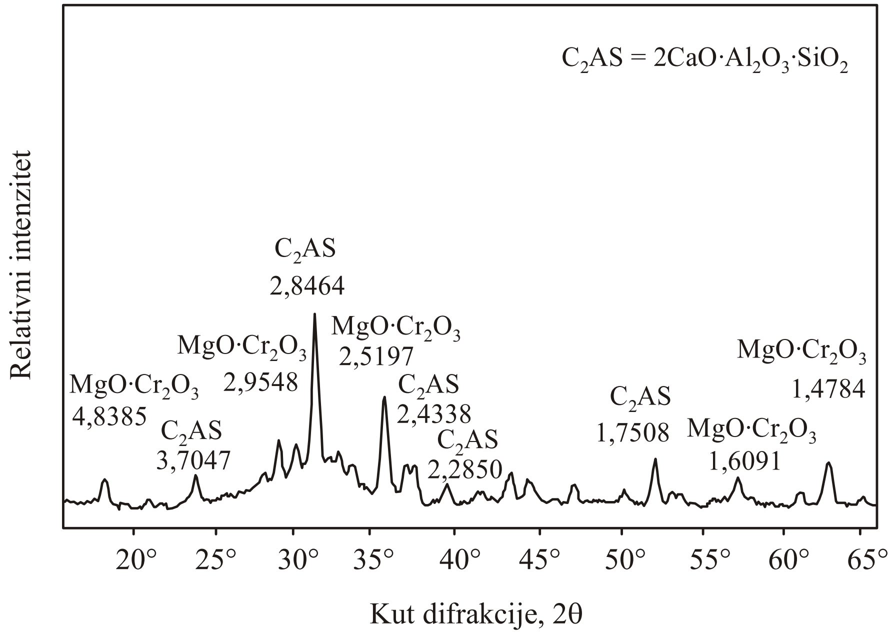

Slika 4. Rendgenogram troske dobivene poslije redukcije Cr_2O_3 u VOD agregatu

ZAKLJUČAK

Na temelju provedenih ispitivanja nekoliko različitih uzoraka troske dobivene pri proizvodnji nehrđajućih čelika može se zaključiti sljedeće:

- SEM analiza kromita u trosci pokazuje da sastav nastalog kromita ne odgovara čistom $FeO \cdot Cr_2O_3$ već se dobije kompleksni spinel.
- Kod proizvodnje nehrđajućih čelika nakon perioda oksidacije taline u trosci je prisutan veliki udio Cr_2O_3 (do 77 %). Osim Cr_2O_3 nastaju i FeO, MnO i MgO.
- Oksidacijom nastali oksid kroma (Cr_2O_3) s ostalim oksidima stvara spojeve: $FeO \cdot Cr_2O_3$, $MnO \cdot Cr_2O_3$, $MgO \cdot Cr_2O_3$, $CaO \cdot Cr_2O_3$, koji tvore kompleksni spinel $(FeO \cdot MnO \cdot MgO) \cdot Cr_2O_3$.
- Zbog ekonomičnosti postupaka izrade nehrđajućih čelika potrebno je trosku koja sadrži velik udio Cr_2O_3 reducirati pomoću aluminija i/ili ferosilicija. Nakon redukcije glavna komponenta u trosci više nije spoj koji se sastoji od Cr_2O_3 i ostalih oksida već gehlenit ($2CaO \cdot Al_2O_3 \cdot SiO_2$). Pritom mogu biti prisutni i nereducirani kromiti, ali u znatno manjoj mjeri.

LITERATURA

1. Heinen, K.H., Elektrostahl Erzeugung, Vereins Deutscher Eisenhüttenleute, VDEh, Düsseldorf, 1977.
2. International Stainless Steel Forum [online], International Iron and Steel Institute / International Stainless Steel Forum, 2003, <www.worldstainless.org>
3. Juhart, M., Peter, M., Koch, K., Lamut, J., Rozman, A., *Stahl und Eise*n **121** (2001) 9, str. 35-41.
4. Görnerup, M., Lahiri, A.K., *Ironmaking and Steelmaking* **25** (1998) 4, str. 317-322.
5. Morishita, H., Nakai, K., Kikuchi, N., Millennium Steel, Steel Publishing, London, 2003, str. 108-113.
6. Search Manual for Selected Powder Diffraction Data for Metals and Alloys, ed. by S. Weissman, JCPDS International Centre for Diffraction Data, Pennsylvania, Swarthmore, 1978.
7. Gojić, M., Kožuh, S., Kosec, L., *Acta Metallurgica Slovaca* **10** (2004) 1, str. 285-290.

ČETIRI RAZINE LABORATORIJSKOG ISPITIVANJA TISKARSKIH BOJA

FOUR LEVELS OF PRINTING INKS LABORATORY TESTING

V. Kropar-Vančina, D. Babić, S. Jamnicki
Grafički fakultet Sveučilišta u Zagrebu,
Getaldićeva 2,
10000 Zagreb

Sažetak: Razvoj tiskarskih boja uvjetovan je naglim razvojem grafičke tehnologije pa je potrebno poboljšati već postojeće, a istodobno formulirati nove boje. Učinkovita formulacija tiskarskih boja temelji se, prvenstveno, na dobrom poznavanju sastavnica tiskarskih boja i laboratorijskom ispitivanju boja koje se obavlja na četiri razine. Prva razina ispitivanja tiskarskih boja je ispitivanje sastavnica tiskarskih boja. Na drugoj razini ispituju se svojstva tiskarske boje, a na trećoj laboratorijski otisci otisnuti s ispitivanim bojama. Potpuno suhi otisci ispituju se na četvrtoj razini ispitivanja. U sklopu ovog rada opisane su sve razine laboratorijskih ispitivanja konvencionalnih tiskarskih boja kao i njihovih karakteristika.

Ključne riječi: laboratorijsko ispitivanje, osiguranje i kontrola kvalitete, svojstva tiskarskih boja, tiskarska boja.

Abstract: Development of printing inks follows the extensive development of printing processes. Existing formulations of inks are improved and new formulations are invented almost every day by a dedicated team working in the industry. This can be achived by laboratory testing of all raw materials on delivery during the first level of testing. The second level of testing is testing of produced inks and the third level is based upon testing of laboratory prints. Testing of printed and completly dry prins is conducted during the last or fourth level of laboratory testing. In this work four levels of laboratory testing of printing inks for conventional printing processes are described.

Key words: ensurance of quality, laboratory testing, printing ink, properties of printing inks, quality control.

1 UVOD

Zadnjih desetak godina u grafičkoj proizvodnji karakterizira izraziti razvoj tehnologije. Sukladno tome mijenjaju se i svojstva tiskarskih boja jer se na tržištu pojavljuju tiskarski strojevi sve boljih mogućnosti odn. performansi. Dobar i kvalitetan tisak uvjetovan je, prvenstveno, tehnikom tiska, konstrukcijom tiskarskog stroja, brzini otiskivanja, tiskovnom formom, tiskarskom bojom, tiskovnom podlogom i ostalim uvjetima.

"Zahtjevi" koji se postavljaju na tiskarske boje su mnogobrojni, a osiguranje i kontrola kvalitete boja temelji se na ispitivanjima tijekom formulacije, proizvodnje, tiska i uporabe otisaka. Ispitivanja obavljaju proizvođači boja, ali i tiskari kako standardnim tako i empirijskim metodama. Tiskarske boje su kompleksni disperzni sustavi koji se prema konzistenciji dijele na pastozne ili guste te tekuće rijetke ili fluidne, a prema tehnikama tiska na boje za konvencionalne i digitalne tehnike tiska (NIP).

Ispitivanja tiskarskih boja provode se na četiri razine, a to su:

1. ispitivanja sastavnih dijelova tiskarskih boja (pigmenata, veziva, dodataka itd.),
2. ispitivanja samih tiskarskih boja (ispitivanja viskoznosti, tečljivosti, ljepljivosti boja),
3. ispitivanja laboratorijskih otisaka (brzina sušenja i sljepljivanje otisaka, izbor optimalne kombinacije tiskarske boje i tiskovne podloge),
4. ispitivanja gotovih suhih otisaka (različite otpornosti otisaka ovisno o njihovoj uporabi).

2 OPĆI DIO

TISKARSKE BOJE su složeni koloidni i/ili molekularni disperzni sustavi sastavljeni od: pigmenta i/ili bojila, punila, veziva (ulja, smola/polimera, otapala), sušila/sikativa i različitih dodataka. Boje se formuliraju za različite tehnike tiska, a u sklopu pojedine tehnike razlikuju se prema vrsti tiskarskog stroja, tiskovnoj podlozi i brzini otiskivanja. U osnovi boje se dijele se na pastozne ili guste i tekuće, rijetke ili fluidne. [1-5]

PIGMENTI su krute kemijski čiste tvari koje daju obojenje tiskarskim bojama, a o njima ovise reološka i druga svojstva tiskarskih boja kao npr. opacitet, transparentnost, svjetlostalnost, otpornost na toplinu, kemikalije, vodu itd.

Pigmenti su netopljivi u vodi i/ili vezivima u kojima se raspršuju/dispergiraju i s kojima se trebaju dobro močiti te tvoriti koloidne disperzije.

Razlikujemo prirodne i umjetne, anorganske i organske, akromatske (bijele, crne) i kromatske (obojene), amorfne i kristalne, optičke (kolorante) i specijalne (magnetske, fluorescentne) pigmente.

Osnovne karakteristike pigmenata su: veličina, raspodjela veličina čestica i oblik čestica, pokritnost, izdašnost, svjetlostalnost, tekstura i ostala svojstva.

BOJILA su krute tvari (organski spojevi) koje daju (kao i pigmenti) obojenje tiskarskim bojama, a za razliku od pigmenata bojila se, uglavnom, otapaju u otapalu/otapalima s kojima tvore molekularne disperzije "čiste" prozirne otopine.

Bojila su zbog finog molekularnog disperziteta: sjajna, velike izdašnosti i transparentna pa se rabe za višebojni tisak s procesnim bojama (CMYK).

Zbog jednoznačne klasifikacije i identifikacije 600 pigmenata i 8000 bojila se označavaju šifrom prema Colour Indexu (CI) koji propisuju Society of Dyers and Colourists (GB) i American Association of Textile Chemists and Colorists (USA). [6,7]

PUNILA ili POMOĆNI PIGMENTI su krute anorganske tvari prirodnog ili umjetnog podrijetla koja djelomično zamjenjuju skupe pigmente (smanjuju cijenu) i mijenjaju reološka svojstva tiskarskih boja. Punila su netopljiva u vodi i/ili vezivima u kojima se raspršuju i s kojima se trebaju dobro močiti. Uljne disperzije punila su manje ili više prozirne, a vodene su neprozirne. [6-8]

VEZIVA su tekuće tvari (uglavnom smjese ulja, smola/polimera i otapala) s kojima se pigmenti moče i u kojima se pigmenti raspršuju tvoreći homogene smjese odn. disperzije.

Vezivo kovencionalne tiskarske boje: nosi pigment kroz prijenosne mehanizme tiskarskih strojeva, osigurava prijenos boje na tiskovnu podlogu i veže boju na tiskovnu podlogu.

Vezivo daje tiskarskoj boji: reološka svojstva (viskoznost, tečljivost), sušiva svojstva i pogodnost za tisak. Odabir veziva uvjetovan je tehnikom i vrstom tiskarskog stroja, brzinom otiskivanja i tiskovnom podlogom.

Vezivo (po sastavu) može biti viskozna tekuća tvar (različita ulja), otopina smole/polimera u organskom otapalu, otopina smole/polimera u ulju ili vodena emulzija smole/polimera s vodom. [6,7,9]

Veziva tiskarskih boja:

ULJA su viskozne tekuće tvari koje se prema podrijetlu dijele na biljna, životinjska, mineralna i umjetna, a prema sušivosti na sušiva, polusušiva i nesušiva (sušivost ulja proporcionalna je nezasićenosti odn. broju dvostrukih kovalentnih veza u molekuli). [4,6]

Veziva tiskarskih boja:

SMOLE su viskozni tekući ili amorfni kruti organski spojevi relativno velike molekularne mase, a dijele se na: prirodne, modificirane i umjetne. Smole tiskarskim bojama poboljšavaju adheziju, čvrstoću, savitljivost i sjaj suhog otiska. [5,7]

Veziva tiskarskih boja:

OTAPALA ili solventi su tekući organski spojevi koji otapaju smolu/smole odn. polimere tiskarskih boja i zadržavaju smolu/polimer u stabilnoj otopini tijekom proizvodnje, skladištenja i tiska do sušenja otiska, a nakon otiskivanja otapalo treba što brže ispariti osim otapala koja služe kao omekšivači tvrdih filmova otisaka koji u suhom filmu zaostaju neodređeno vrijeme.

Rabe se otapala niskih (Tv do 100 °C), srednjih (Tv od 100 do 150 °C) i visokih vrelišta (Tv do 225 °C), koja se brzo, srednje i sporo isparavaju odn. suše, a najvažnija svojstva otapala su jakost otapala i brzina isparavanja otapala.

Otapala su otrovna, zapaljiva (osim kloriranih ugljikovodika), a često i eksplozivna pa se u pogonima ugrađuju rekuperatori odn. uređaji pomoću kojih se pare otapala kondenziraju i vraćaju u tisak ili proizvodnju boja. [1,5,7]

SUŠILA ili sikativi su tvari koje ubrzavaju sušenje tiskarskih boja koje se suše oksipolimerizacijom na tiskovnim podlogama odn. sušenje otisaka, a po kemijskom sastavu su oleati, rezinati i naftenati, kobalta, mangana i olova. Sušenje katalizira metalni, a topljivost sušila u vezivu određuje kiselinski ion. Brzinu sušenja tiskarske boje određuje vrsta i količina sušila, temperatura i udjel vlage, a temelj katalize je tvorba aktivnog, elementarnog ili nascentnog kisika. Samo optimalne količine sušila ubrzavaju sušenje otisaka tiskarskih boja. [1,7-9]

DODATCI poboljšavaju određena svojstva tiskarskih boja ili otklanjaju nepoželjne pojave u tisku. Dodatci tiskarskih boja su: voskovi, ulja, masti, antioksidansi, sapuni, mirisi. [2,5,7-9]

3 LABORATORIJSKO ISPITIVANJE TISKARSKIH BOJA

U današnje vrijeme formuliraju se nove tiskarske boje s kojima se mogu dobiti kvalitetni otisci bez problema u tisku. Osnova uspješne formulacije tiskarskih boja su temeljna i temeljita ispitivanja sastavnica tiskarskih boja koje se isporučuju i testiraju tijekom formulacije i proizvodnje boja. Rezultati ispitivanja i istraživanja uspoređuju se s numeričkim preporukama/standardima ili se rabe kvalitativni testovi koji uključuju vizualnu procjenu boje i kontrolu tiska, a uglavnom se procjenjuju navlake boja. [4-10]

PRVA RAZINA LABORATORIJSKOG ISPITIVANJA TISKARSKIH BOJA: ISPITIVANJE SASTAVNICA TISKARSKIH BOJA

Sastavnice tiskarskih boja treba ispitivati kako bi bili sigurni kako njihova kvaliteta odgovara kvaliteti standarda koja je ugovorena s dobavljačem. Ispituju se pigmenti, bojila, ulja, smole, otapala, sušila i dodatci odn. sve sastavnice potrebne ili rabljene za formulaciju tiskarske boje. PIGMENTI se, uglavnom, ispituju nakon dispergiranja u vezivu. Ako je pigment dispergiran u uljnom vezivu, ispituje se adsorpcija ulja jer vezivo mora dobro močiti pigment, a adsorpcija ulja izravno određuje viskoznost i tečljivost boja. Ako adsorpcija ulja nije odgovarajuća boja nije konzistentna. Ispitivanje adsorpcije ulja svodi se na određivanje količine standardnog ulja potrebne za potpuno močenje 100 g ispitivanog pigmenta.
Vlažnost i hlapljivost pigmenta definira lakoću dispergiranja pigmenta u vezivu. Vlažnost i eventualna hlapljivost pigmenta određuju se sušenjem pigmenta, do kostantne mase, u električnom sušioniku pri temperaturi od 105 °C. Gubitak mase proporcionalan je udjelu vlage i hlapljivosti ispitivanog pigmenta.
Otpornost pigmenta ispituje se nakon dispergiranja pigmenta u vezivu koje se najviše rabi za pojedine tehnike tiska odn. nekom standardnom vezivu. Ispitivanje se može modificirati ako pigment nije kompatibilan sa standardnim vezivom. Uobičajeno je ispitivati otpornost pigmenta na otisku otisnutom sa standardnim vezivom, a to je offsetno vezivo koje se, ipak, ne rabi za ispitivaje pigmenata fleksografskih, sitotiskarskih i boja za duboki tisak. Nakon dispergiranja pigmenta u odgovarajućem vezivu, finoća disperzije se uspoređuje sa standardnim uzorkom odn. standardnom bojom na grindometru (slika 1) kako bi bili sigurni da se s minimalnim mljevenjem može dobiti kvalitetna disperzija. Zatim se određuju viskoznost i tečljivost boje, a rezultati se uspoređuju sa standardom.

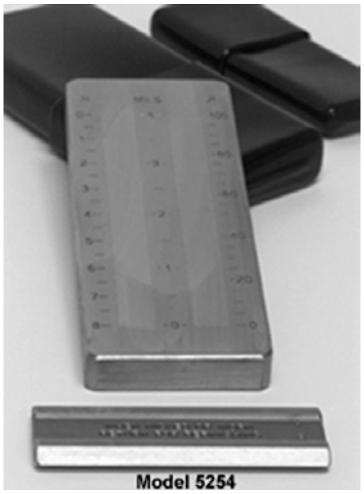

Slika 1 - Grindometar

Jakost i ton boje pigmenta može se procijeniti na osnovi navlake (slika 2) i navlake standardne boje za puni ton i smjesu s transparentnom bijelom bojom u omjeru 20:1 kad se odeđuje relativna jakost boje pigmenta i razlike u čistoći uzoraka. Za ispitivanje sjaja i otpornosti priprema se laboratorijski otisak, a ispitivanje se obavlja kada se otisak osuši. U prvom slučaju lakše je odrediti ton, a drugi pokus pokazuje relativnu jakost boje pigmenta i razlike u čistoći uzoraka. Za ispitivanje sjaja i otpornosti priprema se laboratorijski otisak, a ispitivanje se obavlja kada se otisak osuši. [4,8]

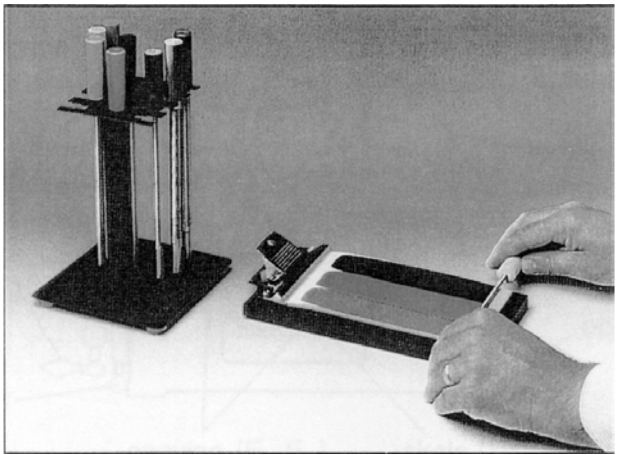

Slika 2 - Štapovi Handcoatera i izradba navlaka boja

BOJILA se ispituju slično kao i pigmenti. Bojilo se ispituje nakon otapanja, kao što se pigment ispituje nakon dispergiranja u vezivu, a kako se radi o molekularnoj otopini mora se provjeriti stabilnost otopine odn. ispitati dolazi li do taloženja bojila tijekom skladištenja. [7]

SMOLE treba, kao i sve druge sastavnice tiskarskih boja, kontinuirano kontrolirati odn. ispituje se svaka nova pošiljka smole koju isporučuje dobavljač.

Ispituje se kiselost smole, jer ona može utjecati na: topljivost, postojanost otopine, tečljivost, mogućnost otiskivanja, sjaj i močenje pigmenta raznim oblicima smola. Kiselost se određuje titracijom sa standardnom alkalnom otopinom.

Lužnatost smole također treba odrediti jer hidroksilne skupine koje se nalaze u smoli mogu bitno utjecati na: topljivost, viskoznost otopine, otpuštanje otapala, netopljivost u vodi, sušenje reaktivnih sustava, močenje pigmenata, transparentnost i tečljivost boje. Lužnatost smole se određuje opetovanim miješanjem s anhidridom octene kiseline,hidrolizom preostalog anhidrida i titracijom s lužinom.

Kako je poznato da smole zbog svog kompleksnog sastava omekšavaju unutar nekog temperaturnog intervala ispituje se i raspon tališta određene smole. Veći raspon tališta znači: manju topljivost, veću viskoznost otopine, tvrđi film boje i brže otpuštanje otapala. Za određivanje raspona tališta rabe se dva uređaja - uređaj s kuglicom i prstenom te uređaj s kapilarom.

Topljivost smole ispituje se izravno otapanjem smole u odgovarajućem otapalu. Reprezentativni uzorak smole iz nove pošiljke i uzorak standardne smole otapaju se u odgovarajućem otapalu i dobivenim otopinama izmjeri se viskoznost. [6-9]

OTAPALA koja sadrže tiskarske boje su tekući spojevi određene tehničke čistoće ili smjese naftnih destilata odn. smjese alifatskih i aromatskih ugljikovodika. Ispitivanjem treba utvrditi je li rabljeno odgovarajuće otapalo te je li udjel nečistoća unutar dozvoljenih granica.

Ispitivanja uključuju instrumentalne analize s infarcrvenom spektroskopijom ili plinsko - tekućinskom kromatografijom, no takva oprema nije svima dostupna. Stoga se rabe klasične metode za određivanje raspona temperatura vrelišta, gustoće i plamišta, a rezultati mogu ukazati na prisutnost neprihvatljive razine nečistoća.

Veći udjel aromatskih spojeva u komercijalnim naftnim ugljikovodicima povećava: topljivost, miris, toksičnost i tendenciju ka bubrenju gumenih valjaka ili navlaka. Dva testa koja se rabe za određivanje udjela aromatskih spojeva su "anilinska točka" i "kauri-butanol vrijednost".

Ostala ispitivanja koja se rabe u nekim slučajevima su određivanja: udjela vode (Karl Fisher metoda), indeks loma, udjela sumpora (naftnih proizvoda) i subjektivno ispitivanje mirisa. [6]

DODATCI se ispituju tijekom primješavanja u tipične formulacije i uspoređivanje tako dobivenih uzoraka sa standardnim uzorkom. Kod nekih materijala ispitivanje se može nadopuniti ili zamijeniti infracrvenom spektroskopijom. [5-7]

DRUGA RAZINA LABORATORIJSKOG ISPITIVANJA TISKARSKIH BOJA:
ISPITIVANJE KVALITETE TISKARSKIH BOJA TIJEKOM I NAKON PROIZVODNJE

Svrha ispitivanja kvalitete tiskarske boje tijekom proizvodnje je dokazati kako je boja dobro formulirana i kako odgovara standardu. Ispitivanja kvalitete boja mogu se podijeliti na: kratkotrajna ispitivanja tijekom procesa proizvodnje i dugotrajna ispitivanja koja se provode nakon proizvodnje, ali prije isporuke naručiocu.

Većina kratkotrajnih ispitivanja gustih/pastoznih i rijetkih/fluidnih boja provodi se čim boja počne dolaziti s disperzijskog mlina. Ispitivanja koja se provode su: određivanje stupnja disperziteta, tečljivost, jakost, ton, transparentnost i sjaj tiskarske boje.

Dispergiranje se najčešće provjerava navlakom uzorka boje i standardne boje na grindometru (slika 1) iako neki proizvođači rabe sofisticirane video mikroskope. Tek kada je postignuto odgovarajuće dispergiranje ispituju se tečljivost i viskoznosti boje. Kod gustih boja tečljivost i gustoća boje određuju se povlačenjem boje pomoću "špahtle" na staklenoj ploči iako mjerljive rezultate možemo dobiti samo instrumentalnom analizom npr. Larayevim viskozimetrom (slika 3). Procjena tečljivosti rijetkih fluidnih boja obavlja se pomoću istjecajne čaše kao što su Zahn (slika 4) i Ford čaše. [7-10]

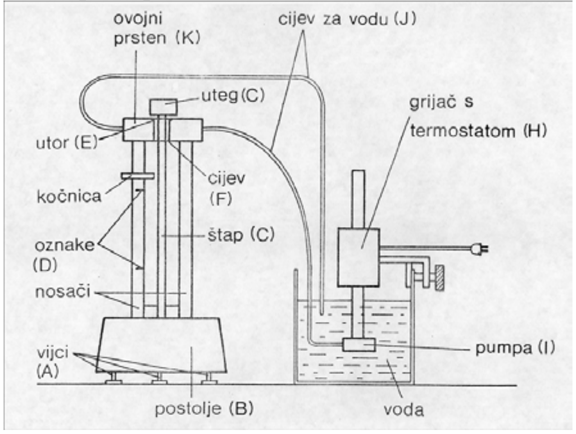

Slika 3 - Laray viskozimetar za pastozne boje

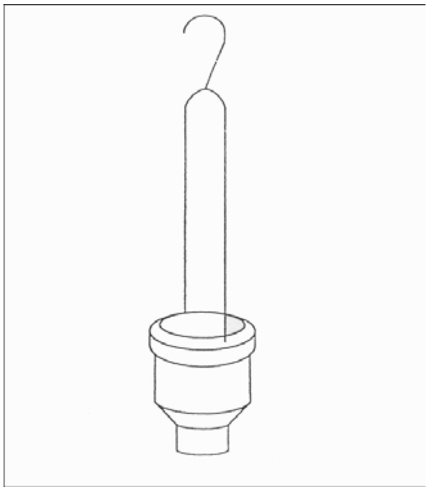

Slika 4 - Zahn istjecajna čaša za tekuće boje

Svojstvo ljepljivosti boje procjenjuje se utiskivanjem boje prstom na ploču, no mjerljivi rezultati dobivaju se samo instrumentalnim mjerenjem.
Iako se navlaka boje može rabiti za ispitivanje tona, izdašnosti i transparentnosti boje, za boje za duboki tisak znatno se više rabe "štapovi" Handcoatera (slika 2) i laboratorijski Aniloks valjci za fleksografske boje (slika 6) koji su jednostavniji za uporabu, a daju pouzdanije rezultate. Nakon ispitivanja tona i izdašnosti boje između miješanja i mljevenja, dobro je ispitati svojstva gotovih izmješanih boja. Navlaka boje se uspoređuje s navlakom standardne boje, nakon čega slijedi ispitivanje boje razrijeđene s bijelom bojom i priprema laboratorijskih otisaka. [5-7]

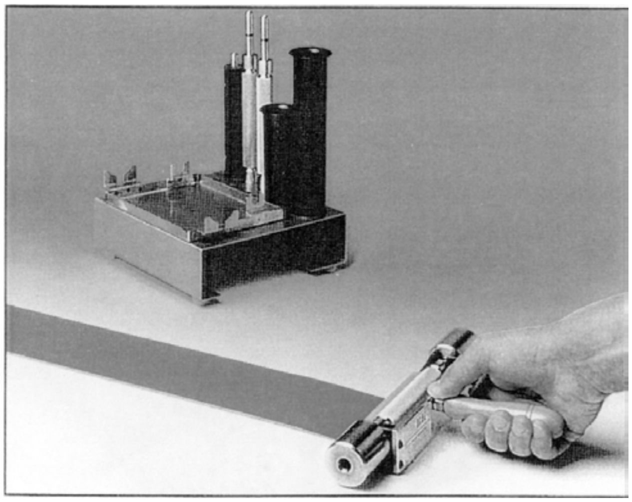

Slika 6 - Laboratorijski Aniloks valjci za ispitivanje tekućih boja

Mnoge tiskarske boje prolaze kroz završnu fazu miješanja tek nakon dodavanja dodataka za sušenje, voskova itd. Nakon miješanja, a prije pakiranja, provode se dugotrajna ispitivanja: brzine početnog sušenja, brzine sušenja i čvrstoće osušenog sloja boje, prašenja boje i neka specijalna ispitivanja. [1-3,5]

TREĆA RAZINA LABORATORIJSKOG ISPITIVANJA TISKARSKIH BOJA: ISPITIVANJE KVALITETE TISKARSKIH BOJA

Sušenje pastoznih ili gustih offsetnih i knjigotiskarskih boja može se odvijati u jednom ili dva stupnja ovisno o mehanizmu sušenja boja kao što su npr: "quickset", oksidacijsko i UV sušenje. Offsetne boje suše se uglavnom "quickset" mehanizmom pa se prvo ispituje brzina prihvaćanja/početnog sušenja boje. Laboratorijsko ispitivanje uključuje pripremu laboratorijskih otiska ispitivane i standardne boje, nakon čega se otisci stave na neotisnuti papir licem prema dolje pa ih zatim pomoću IGT-A2 (slika 5) uređaja za ručno otiskivanje treba otisnuti u određenim vremenskim intervalima. Kako se na neotisnutom papiru dobivaju sve "slabiji" kontraotisci lako je usporediti kvalitetu ispitivane boje s kvalitetom standardne boje. [9,10]

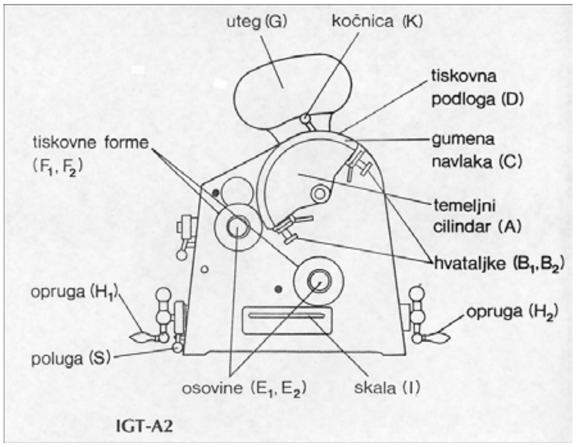

Slika 5 - IGT-A2 uređaj za laboratorijsko otiskivanje pastoznih boja

Ako treba odrediti vrijeme sušenja (engl. dry) koje je različito od vremena prihvaćanja (engl. set), ukoliko se otiskuje na neupojnim podlogama ili ako se ispituje stabilnost boje na tiskarskom stroju onda boju treba razvaljati na staklenu ili metalnu ploču i strugati iglom sve dok se glatki trag u boji ne pretvori u suhi "izgrebani" trag boje. [7-10]

Nadalje se obavljaju laboratorijska otiskivanja kojima se mogu simulirati uvjeti tiska. Najviše se rabe IGT (slika 5) i Prüfbau uređaji za laboratorijsko ispitivanje. Prüfbau uređaj sastoji se od dijela za razribavanje boje, dva seta valjaka tako da se istodobno mogu ispitati dvije boje te agregata za tisak gdje se mogu mijenjati brzina i tlak otiskivanja. [9,10]

Interakcija tiskarske boje s otopinom za vlaženje ispituje se na uređaju kao što je npr. "Litho Tester". Sustav od tri valjka s jednim valjkom uronjenim u posudu s otopinom za vlaženje sadrži razdvojene valjke koji se mogu močiti s dvije boje. Moguće je postići prekomjerno emulgiranje ili kapanje u otopinu, također je moguće izmjeriti količinu vode koju boja emulgira. Na uređaju se može vidjeti preveliko emulgiranje ili probijanje pigmenta u otopinu za vlaženje.

Brzinu sušenja fluidnih tiskarskih boja moguće je ispitati pomoću grindometra na kojem se istodobno ispita i usporedi nova boja sa standardnom bojom. Relativna brzina sušenja može se odrediti prstom na različitim debljinama filma na grindometru. Iako tekuće boje karakterizira niska viskoznost ipak može doći do taloženja pigmenta. Uzorak nove "šarže" ispituje se nakon što nova boja odleži (miruje) 48 sati. [6-9]

Pjenjenje boja na osnovi vode ispituje se mućkanjem boje i standardne boje pa se stupanj pjenjenja nove boje komparira sa standardnom bojom s kojom nije bilo problema u tisku. Kod boja na osnovi vode mjeri se i pH pH-metrom, a pH boje mora biti unutar dozvoljenih granica jer se prekisele boje teško odn. sporo suše, a lužnate su nestabilne. [6,7]

Laboratorijski uređaji za ispitivanje fleksografskih boja i boja za duboki tisak služe za određivanje svojstava nove pošiljke i usporedbe sa svojstvima standardne boje, no oni nisu praktični za rutinske kontrole u tisku. Zato bi bilo poželjno laboratorijsko ispitivanje uvijek potvrditi pokusima u komercijalnom tisku. Kontrolni otisci s fleksografskim bojama i bojama za duboki tisak, u pravilu se izrađuju pomoću Handcoatera, malih laboratorijskih uređaja za otiskivanje kao što je npr. K-uređaj ili ručnim Aniloks valjcima (slika 6). Pri svakom tisku pa tako i laboratorijskom važno je da je viskoznost boje optimalna. [8-10]

ČETVRTA RAZINA LABORATORIJSKOG ISPITIVANJA TISKARSKIH BOJA: ISPITIVANJE GOTOVIH SUHIH OTISAKA

OTPORNOST OTISAKA NA OTIRANJE - ispituje se tako da se otisak licem prema dolje postavi na neotisnutu tiskovnu podlogu nakon čega se obavi otiranje pri određenom tlaku, a broj otiranja treba dogovoriti. Za ispitivanja rabi se PIRA uređaja za ispitivanje otpornosti otiska na otiranje (slika 7). Za svako ovakvo ispitivanje otisci moraju biti potpuno suhi.

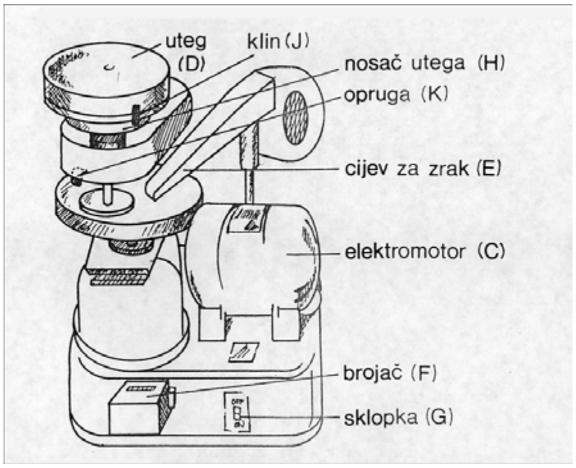

Slika 7 - PIRA uređaj za ispitivanje otpornosti otisaka na otiranje

OTPORNOST OTISAKA NA SAVIJANJE - kvalitativno ispitivanje obavlja se savijanjem otiska za 180º, a zatim se lagano zagrebe noktom po pregibu, no za preciznije određivanje treba rabiti PIRA uređaj za ispitivanje otpornosti prema savijanju.

OTPORNOST OTISAKA NA SAVIJANJE - kvalitativno ispitivanje obavlja se savijanjem otiska za 180º, a zatim se lagano zagrebe noktom po pregibu, no za preciznije određivanje treba rabiti PIRA uređaj za ispitivanje otpornosti prema savijanju.

PRIJANJANJE I FLEKSIBILNOST OTISAKA - ispitivanje se uglavnom obavlja pomoću ljepljive trake. Standardna ljepljiva traka određene duljine stavlja se na otisak i zagladi prstom. Zatim se polako povlači natrag do polovice svoje duljine prije nego što se ostatak brzo prihvati. Otisak i ljepljivu traku treba pregledati kako bi se utvrdio eventualni prijelaz boje. Iako je samo ispitivanje brzo i jednostavno, treba paziti da traka ne ostane na otisku, jer bi sastavnice ljepila trake omekšale otisak. Ispitivanje fleksibilnosti otiska obavlja se tako da se otisak drži između palca i kažiprsta obje ruke, a razmak treba biti pola incha. Zatim se savija 10 puta prije nego se ispituje je li nešto boje uklonjeno.

SLJEPLJIVANJE OTISAKA - ispituje se stavljanjem otiska u dodir s poleđinom sličnog otiska, odmah nakon sušenja, koji se zatim stavlja pod hidraulični čekić i tlak od 0,125x10^5 do 2,000x10^5 Pa. Ispitivanje se može obaviti pri sobnoj, ali i pri povišenim temperaturama. Sam postupak se provodi pomoću FOGRA blok uređaja (slika 8).

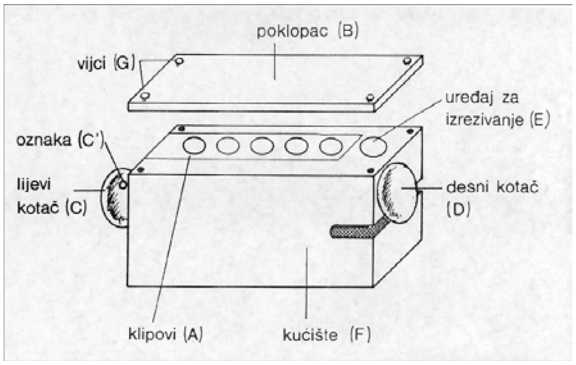

Slika 8 - FOGRA blok za ispitivanje sljepljivanja otisaka

KEMIJSKA STABILNOST OTISAKA - uključuje ispitivanja otpornosti na: sapun, detergent, lužinu, kiselinu, vosak, sir, jestiva ulja i masti, začine, vodu i otapala.
SVJETLOSTALNOST ili SVJETLOSTABILNOST OTISAKA - za ispitivanje se rabi skala "plave vune" (skala svjetlostalnosti pigmenata), a rezultati se iskazuju kao brojčane vrijednosti od 1 do 8, gdje je 1 vrlo slaba, a 8 odlična svjetlostabilnost. U nekim slučajevima svjetlostalnost ne bi smjela biti manja od 4.
OTPORNOST OTISAKA NA TOPLINU - procjenjuje se "ponašanje" otisaka pri različitim temperaturama. U limotisku gdje se otisci suše u peći, otisak se može "peći" 5 minuta pri 150 ºC ili dvije min pri 230 ºC kako bi se simulirali uvjeti proizvodnje. Pečene ili nepečene ploče se uspoređuju kako bi se vidjelo postoje li promjene u boji, čvrstoći ili sjaju otiska.
OTPORNOST OTISAKA NA DUBOKO SMRZAVNJE - određuje se stavljanjem otiska u duboko smrzavanje 24 sata, a zatim se otisak vadi i savija. Nakon toga stavlja se u vodu sobne temperature na dva sata prije ponovnog savijanja. U obje faze ne bi se smjelo ukloniti više od 5% boje.
LAMINIRANJE I LAKIRANJE OTISAKA - ako se otisak laminira, lakira ili premazuje treba ispitati moćenje sloja boje ljepilom, lakom ili premazom kako bi se postigla optimalna adhezija u sloju. Nakon sušenja otisak se laminira određenim lakom, ljepilom ili premazom. Uspoređuje se otisak i laminirani otisak nakon jednog i 7 dana kako bi vidjeli prodire li boja u laminat ili je došlo do promjene boje otiska laminacijom.
MIRISI I ŠTETNE TVARI - ispituju se u bojama koje se rabe za prehrambenu amblažu jer ne smiju sadržavati mirise kako ne bi došlo do kontaminacije sadržaja ambalaže. Uzorci otiska za ispitivanje, standardnog otiska i neotisnute podloge zapečaćuju se u posebne spremnike bez mirisa i skladište jedan sat pri 50 ºC. Nakon otvaranja spremnika provjerava se ima li zaostalog mirisa, nakon čega se otisci vrate u spremnik, opet zapečate, a zatim se ponovno ispituju pri sobnoj temperaturi. Ne bi trebalo biti vidljive razlike između neotisnte podloge i otisnutih uzoraka odn. otisaka. [4-10]

4 RASPRAVA I ZAKLJUČCI

Tiskarske boje su vrlo kompleksni disperzijski sustavi koji moraju imati definirana i namjenom određena fizikalna i kemijska svojstva. Od proizvđača tiskarskih boja traže se formulacije boja za određene tehnike tiska, iako u sklopu pojedine tehnike tiska postoje značajne razlike u svojstvima boja kao i svojstvima tiskovne podloge, vrsti tiskovne forme, brzini tiska itd.
Danas je proizvodnja tiskarskih boja standardizirana pa se uvijek mogu dobiti boje istih karakteristika, ali tiskarske boje ipak treba ispitati prije tiska konkretne naklade.
Sastavnice tiskarskih boja uglavnom ispituju proizvođači boja što je istodobno i prva razina ispitivanja tiskarskih boja. Isto tako proizvođači temeljito ispituju svaku proizvedenu tiskarsku boju prije isporuke naučiocu.
U sklopu tiskara također se ispituju svojstva tiskarskih boja prije i tijekom tiska u labortoriju i pogonu, pa se u drugu razinu ispitivanja tiskarskih boja ubrajaju sva ispitivanja boja koja obavljaju proizvođači boja i tiskari.
Treća razina ispitivanja boja obavlja se u kontrolnim i istraživačkim laboratorijima kako bi bili sigurni da kvaliteta boje odgovara specificiranoj odn. kako bi se iznašle nove formulacije tiskarskih boja. Za ova ispitivanja rabe se navlake boja i laboratorijski otisci.
Gotovi suhi otisci ovisno o konačnoj uporabi moraju imati određena svojstva i/ili otpornosti (engl. end use properties) pa se u sklopu četvrte razine ispitivanja obavljaju određivanja uporabnih vrijednosti otisaka.

5 LITERATURA

1. R. M. Romano and F. J. Romano (Eds.), The GATF Encyclopedia of Graphic Comunications, GATF Press, Pittsburgh, 1998.

2. G. A .Stevenson, Graphic Arts Encyclopedia, McGraw Hill, New York, 1991.

3. F. Mesaroš, Grafička enciklopedija, Tehnička knjiga, Zagreb, 1971.

4. C. H. Williams, The Printer's Ink Handbook, Maclean Hunter Ltd, Hertfordshire, 1992.

5. N. R. Eldred and T. Scarlett, What the Printer Should know about Ink, GATF; Pittsburgh, 1990.

6. R. E. Todd, Printing Inks, Pira International, Leatherhead, 1994.

7. B. Thompson, Printing Materials, Science and Technology, PIRA, Leatherhead, 2004.

8. J. P. Crouch, Flexography Primer, GATF Press, Pittsburgh, 1998.

9. V. Vančina, Predavanja iz predmeta: Tiskarske boje, Grafički fakultet Sveučilišta u Zagrebu, akad. god. 2004./2005.

10. V. Vančina i M. Mikota, Materijali u grafičkoj proizvodnji - boje, priručnik za vježbe, Grafički fakultet Sveučilišta u Zagrebu, Zagreb, 1992.

THE OPTIMIZATION OF HYDROXYAPATITE SOL-GEL PROCESSING FROM TRIETHYL PHOSPHATE

OPTIMIZACIJA PROCESA SOL-GEL SINTEZE HIDROKSILAPATITA IZ TRIETILFOSFATA

Stanislav Kurajica, Emilija Tkalčec and Juraj Šipušić
Faculty of Chemical Engineering and Technology, University of Zagreb, Marulićev trg 20, HR-10000, Zagreb, Croatia

Abstract

Hydroxyapatite, $Ca_{10}(PO_4)_6(OH)_2$, is suitable material for various biomedical applications due to a good compatibility with the human organism and strong bonding to the bone, of which is primary constituent. Hydroxyapatite is extensively studied with regard to synthesis, characterisation and applications. Sol-gel synthesis routes are of special interest, due to advantages gained through this technique.

Hydroxyapatite powders were prepared by sol-gel method using triethyl phosphate, $PO(OC_2H_5)_3$, and calcium acetate, $Ca(CH_3COO)_2$, as initial compounds, and water as solvent. In order to accelerate low hydrolysis rate of triethyl phosphate, hydrogen peroxide (H_2O_2), phosphoric acid (H_3PO_4), ammonia solution (NH_4OH) and 2-propanole (C_3H_7OH), were used in course of synthesis. The gels were aged and dried under different conditions: slow aging/drying at room temperature, rapid drying in oil bath at 75°C and decomposition in electrical furnace at 500°C were performed. The evolution of crystal phases after thermal treatment has been detected and characterized by powder X-ray diffraction. The influence of added agents and aging and drying conditions to relative hydroxyapatite quantity have been investigated and compared. The crystallization path was investigated by simultaneous DTA/TGA analysis. It has been established that the crystallization of hydroxyapatite in investigated samples is always accompanied with crystallization of additional crystal phases, CaO being the most prominent among them. It was found that the most effective agent in promoting the hydrolysis of triethyl phosphate is phosphoric acid. The presence of H_3PO_4 during the synthesis influences the triethylphosphate hydrolysis mechanism. Rapid aging in oil bath at 75°C yields best results providing enough time and energy for reaction. Treatment of crystallized samples with hydrochloric acid turned out to be effective method of undesired calcium phases removal.

Keywords: DSC/TGA, Hydroxyapatite, Sol-gel, Triethyl phosphate, XRD.

Ključne riječi: DSC/TGA, Hidroksilapatit, Sol-gel, Trietil fosfat, Rendgenska difrakcija.

Introduction

Hydroxyapatite (HAP) ceramics are suitable materials for many medical applications (1). Hydroxyapatite, $Ca_{10}(PO_4)_6(OH)_2$, is primary constituent of human hard tissues and the structure of artificially prepared HAP is the same as that of the HAP of natural bone. HAP, because of its good compatibility with human organism and strong bonding to the bone, has find different applications as, e.g., for artificial tooth roots, filler of bone defects, bioactive coatings etc (2). Due to a poor mechanical properties HAP cannot be used as a load bearing material, on the other hand, due to a strong bioactive properties HAP coating on metallic or ceramic prosthesis can drastically accelerate the integration of the implant (3). A major use of HAP coatings is on titanium alloy implants (tooth implants and hip prosthesis). The surface of titanium alloy is tipically coated with HAP to gain bioactive properties for the purpose of long-term fixation to human hard tissues. Current techniques of HAP coating onto metallic substrates include plasma spraying, electrophoretic deposition, biomimetic and dip-coating.

HAP has been prepared in various ways in the last few years (solid-state reaction, co-precipitation, hydrothermal method and the sol-gel route). During the last decade, the sol-gel process proved its suitability for the processing of HAP powders, films or bulk forms. The sol-gel processing technique affords greater control over the formation of phases, high product purity, homogeneous composition and lower processing temperatures. Significantly lower crystallization temperature of the HAP coating reduce the possibility of metal substrate oxidation (4). Another advantage of the sol-gel route is its applicability for surface coating through dip coating technique (4). The mayor limitations in its applications have been due the drawbacks associated with hydrolysis of phosphates (5) and the high cost of the raw materials. Because of volatility and of the low hydrolysis rate of the alkoxy phosphorous compounds, an exact stoichiometry of sol-gel HAP is difficult to achieve (6).

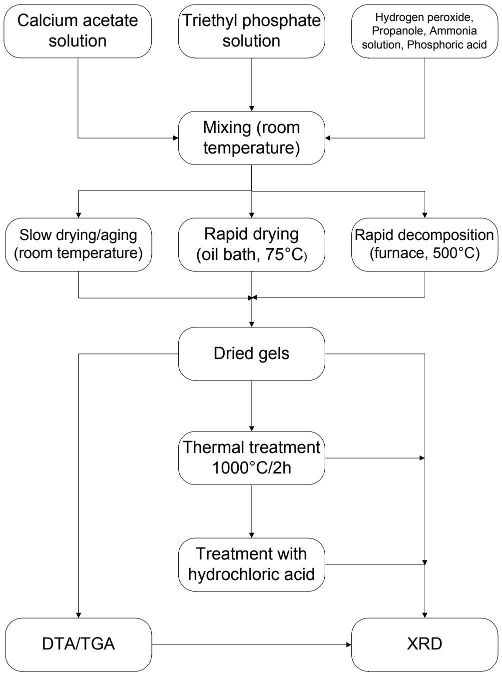

Fig. 1. Flowchart of samples preparation & characterisation.

The triethyl-phosphate (TEP), as well as organo-phosphates generally, has been concerned as inconvenient precursor for the sol-gel synthesis due to extremely slow rate of hydrolysis (7,8). Recently there were some successful attempts of sol-gel synthesis of HAP using TEP (4,9-18). Some attempts were made in order to enhance the rate of organo-phosphates hydrolysis (19,20) or to overcome slow TEP hydrolysis rate by formation of colloidal gel (12,13).

The aim of the present work was to synthesize HAP powders using sol-gel route with simple procedures and relatively inexpensive chemicals. The effectiveness of various agents in accelerating hydrolysis of triethyl-phosphate (TEP) has been evaluated as well as different aging/drying conditions. The crystallization path was also investigated.

Experimental

The precursors used in investigation were triethyl phosphate, $PO(OC_2H_5)_3$ (Fluka), and calcium acetate hydrate, $Ca(CH_3COO)_2 \times H_2O$ (Aldrich), as initial compounds, and water as solvent. 0.04175 mol of calcium acetate was dissolved in 25 ml of water, after 1h the solution of 0.025 mol of TEP in 25 ml of water was added dropwise to TEP solution in order to attain stoichiometric Ca/P molar ratio of 1.67. No agent was added to first sol batch, 10 ml of: 30% of hydrogen peroxide (H_2O_2) was added to second sol batch, 25% ammonia solution (NH_4OH) to the third and 2-propanole to the fourth. To fifth batch 85% phosphoric acid (H_3PO_4) was added but the quantity of TEP was reduced in order to remain stoichiometric Ca/P molar ratio and to adjust TEP/H_3PO_4 molar ratio to 1. The mixtures were placed on magnetic stirrer, and sols were stirred vigorously for 24h at room temperature. Prepared sols were divided in three equal parts. One part was dried and aged at room temperature for 2 months, second was dried in oil bath at 75°C for 2 days and third was placed in electrical furnace at 500°C for 1h.

Prior to thermal treatment samples were examined by X-ray diffraction (Philips PW 1710) as well as simultaneous DTA/TGA analysis (Netzsch STA 410). Thermal treatments were carried out in electrical furnace by heating the samples at a rate of 10°Cmin^{-1} until 1000°C, followed by 2h soaking period at this temperature. The evolution of crystal phases after thermal treatment has been detected and characterized by X-ray diffraction. Semi-quantitative comparison of hydroxyapatite quantity in each sample was conducted by computer integration of XRD peak areas for HAP, CaO and $Ca(OH)_2$ (several peaks for each phase were used). In order to remove undesired calcium phases the thermally treated powders were stirred in 0.05 M and 0.1 M HCl solution, and further filtered. Flowchart of samples preparation and characterisation is shown in Fig. 1.

Results and discussion

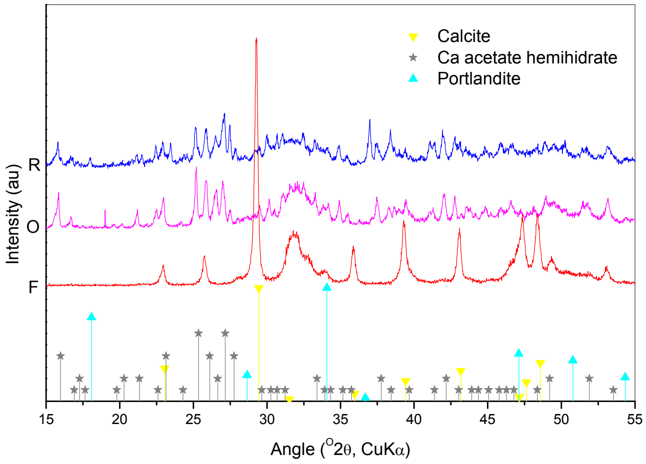

Fig. 2. XRD patterns of TEP/H_3PO_4 powder after: R) drying at room temperature, O) drying/aging in oil bath at 75°C and F) rapid decomposition in furnace at 500°C.

In the course of synthesis no precipitation was observed, the gelling was observed during the drying and ageing process. Samples dried and aged in oil bath gelled in a less than 24h, while this process was much slower for samples kept at room temperature. None of the gels after drying regime was completely amorphous. Figure 2. shows the XRD measurements of HAP gel obtained with phosphoric acid addition as example. As can be seen, calcium acetate phase is dominant in samples dried at room temperature and oil bath while in sample treated in furnace calcite peaks are the most intense. Judging by the XRD patterns the process of polycondensation was only partial. The majority of calcium precursor precipitated in the course of drying and ageing process, which inhibited the formation of homogeneous gel. TEP hydrolysis was far from complete. Kordas and Trapalis (9,10) suggested that in this process just part of ethyl groups are removed and consequently the condensation is just partial. This leads to difficulties in achieving the exact gel stoichiometry. Further stoichiometry disturbance is due to a volatility of TEP (21).

The attempts were made in order to overcome the limitations of the extremely slow rate of hydrolysis of phosphate esters by addition of various agents. Hydrogen peroxide, propanole, ammonia solution and phosphoric acid were employed. The hydrogen peroxide effectiveness for hydrolysis rate acceleration has been demonstrated with organo-phosphoric pesticides (19). Basic aqueous solutions of sodium perborate $NaBO_3$ has proven effective in enhancing hydrolysis due to the dissociation of perborate ion to form hydrogen peroxide (20). As can be seen in Fig. 3 some increase in HAP quantity has been obtained. This could be explained by greater reactivity of HOO^- toward phosphoric esters compared with OH^- (20).

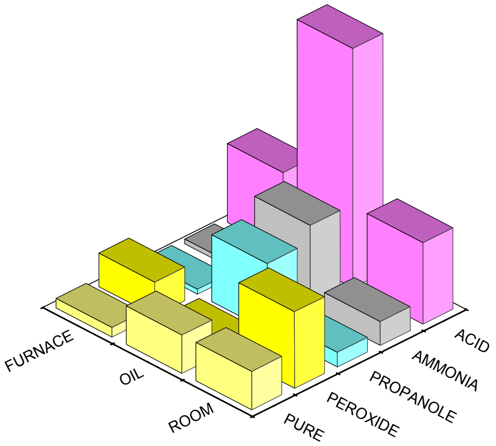

Figure 3. Relative ratios of HAP and other calcium compounds calculated from XRD peak intensities.

The addition of propanole yield increase of HAP quantity only in sample dried in oil bath (Fig. 3). The difficulties associated with the slow TEP hydrolysis rate were thus overcome by formation of colloidal gel (9,10,12,13). The effects of TEP immobilization in colloidal gel diminish with drying process. Although the polymeric gel has not been obtained, according to Hsieh NMR study (14) some calcium ions are incorporated in oligomeric phosphate. Partial formation of stable complex prevents complete precipitation of calcium acetate hydrates and loss of TEP.

It is known that the hydrolysis rates of organo-phosphate esters are enhanced in basic conditions. According to our results only sample dried in oil bath showed some increase in HAP quantity (Fig. 3).

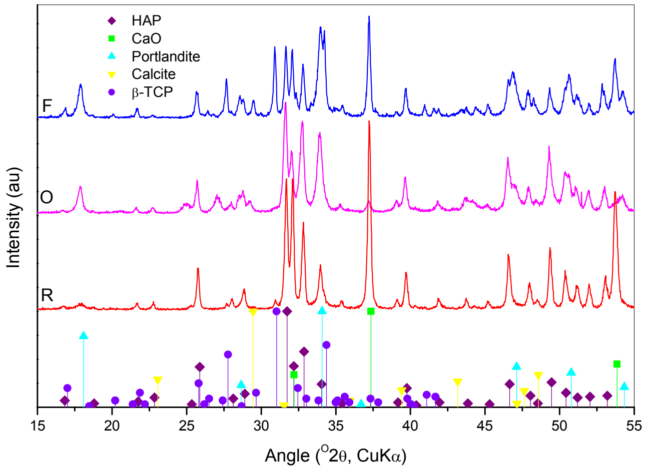

Figure 4. XRD patterns of TEP/H_3PO_4 powders calcined at 1000°C. R) sample dried at room temperature, O) sample dried/aged in oil bath at 75°C and F) sample rapidly decomposed in furnace at 500°C.

Phosphoric acid has an extremely rapid reaction rate leading to precipitation of the calcium phosphate rather than hydrolysis (12). Nevertheless phosphoric acid has also been successfully used in the course of HAP synthesis via sol-gel technique (22). Combining TEP and phosphoric acid as phosphor precursors gave best results (Fig. 3). Some authors (21) concern that the addition of acid influences the mechanism of hydrolysis enabling hydrolysis at each ethyl group, which leads to efficient condensation process. Some initial interactions of TEP and phosphoric acid have also to be considered.

The thermal processing involved in HAP sol-gel synthesis route includes thermal decomposition of the gel in order to carry out expulsion of residual organics, gaseous products and water molecules so as to get desired ceramics. The drying, aging and thermal processing of the gel could be conducted in different conditions: at room temperature, moderate temperature mostly between 60 and 90°C (4,9,10,16,23) as well as by rapid calcinations at 500°C (11,16,17).

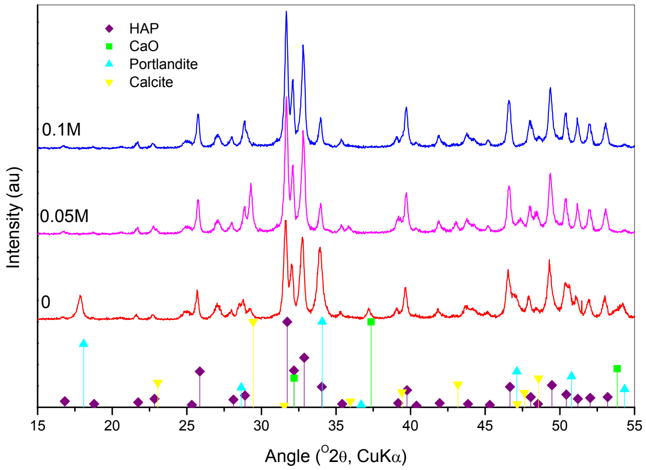

Figure 5. XRD patterns of TEP/H_3PO_4 powders dried/aged in oil bath at 75°C and calcined at 1000°C. 0) sample not treated with HCl, 0.05M) and 0.1M) samples treated with 0.05M HCl and 0.1M HCl.

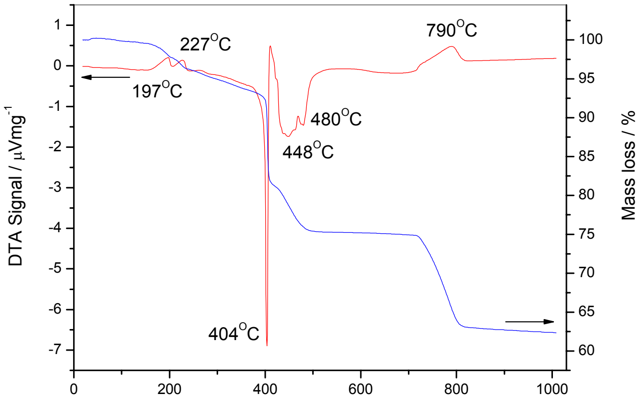

Figure 6. DTA and TGA trace for TEP/H_3PO_4 powder dried/aged in oil bath at 75°C.

As can be seen in Fig. 3 the drying process carried out in oil bath at 75°C yielded best results. Although rapid calcination is claimed to enable avoiding of carbonaceous residues that inhibit HAP nucleation and lead to a lower crystallization temperature (16) in course of this process vigorous combustion reaction was observed leading to formation of undesired calcium compounds. On the other hand, slow evaporation of solvent in oil bath enabled prolonged intimate precursor contact, providing time and energy for process.

Even with the combination of TEP and prosphoric acid completely pure HAP can't be obtained (Fig. 4). Reports to date on the sol-gel derived HAP using triethyl phosphate indicate that synthesis of HAP is always accompanied by secondary calcium phases (9-18). It was shown that such phases could be eliminated by stirring the powder in hidrocloric acid solution followed by filtration (12). Water soluble calcium chloride is thus washed away leaving behind the hydroxyapatite phase. Fig. 5 illustrate the efficiency of this procedure. Mixing of appropriate amounts of crystallized sample, obtained combining TEP and phosphoric aicid as precursors, and 0.1 M hydrochloric acid resulted with pure HAP.

Due to a complex nature of the sol-gel technique, characterization of the products formed at various stages of processing is of extreme interest. Therefore the dried TEP/H_3PO_4 gel was studied using thermal analyses techniques of differential thermal analysis (DTA) and thermogravimetric analyses (TGA). The DTA/TGA traces, obtained at a heating rate of 10°Cmin^{-1} are shown in Fig 6. Slight mass loss observed at low temperatures can be attributed to evolution of moisture present in the system. Two endothermic effects observed arround 200°C, accompanied with mass loss are due to the decomposition of calcium acetate hydrates. A sharp exothermic peak at approximately 400°C is a consequence of the collapse of the gel and burning off the evolved organics. The TGA trace in this temperature area is characterised with the significant and rapid mass loss. This process is followed by group of exothermic peaks between 400 and 500°C, accompanied by further loss in mass but at slower rate. According to XRD results, this group of peaks is associated with the HAP crystallization as well as the majority of the sideway calcium compounds. Some amount of calcium compounds is formed prior to this temperature, probably as a product of calcium acetate decomposition process. The last event on DSC/TGA traces is the decomposition of calcium carbonate.

Conclusion

Hydroxyapatite was sintesized using sol-gel route with calcium acetate and triethyl phosphate as precursors. In order to overcome the limitations of the extremely slow rate of TEP hydrolysis, hydrogen peroxide, propanole, ammonia solution and phosphoric acid were employed. The combination of TEP and phosphoric acid as phosphor precursors yielded best results, owning to the acid influence on the mechanism of hydrolysis.

The gels were aged and dried under different conditions: slow aging/drying at room temperature, rapid drying in oil bath at 75°C and decomposition in electrical furnace at 500°C were performed. The drying process carried out in oil bath at 75°C yielded best results due to a prolonged intimate precursor contact and sufficient time and energy for process.

The formation of hydroxyapatite occurs at relalatively low temperature of about 500°C. Hydroxyapatite synthesized using TEP as precursor is always accompanied by secondary calcium phases. Such phases could be eliminated by stirring the powder in 0.1M hydrocloric acid solution, followed by filtration.

References

1. R. H. Doremus, J. Mat. Sci., 27 (1992) 285.
2. L. L. Hench, J. Am. Ceram. Soc., 74 (1991) 1487.
3. G. Willmann, Brit. Ceram. Trans. 95 (1996) 212.
4. L. Guo and H. Li, Surf. Coat. Technol., 185 (2004) 268.
5. J. Livage, P. Barboux, M. T. Vanderborre, C. Schmutz and F. Taulelle, J. Non-Cryst. Solids 147/148 (1992) 18.
6. T. Brendel, A. Engel and C. Russel, J. Mat. Sci: Mater. Med., 3 (1992) 175.
7. J.-C. Schroter, A. Cardenas, M. Smaihi and N. Hovnanian, J. Sol-Gel Sci. Tech, 4 (1995) 195.
8. M. Zaharescu, A. Vasilescu, V. Badescu and M. Radu, J. Sol-Gel Sci. Tech, 8 (1997) 59.
9. Kordas and C. C. Trapalis, J. Sol-Gel Sci. Tech, 9 (1997) 17.
10. G. Kordas and C. C. Trapalis, J. Sol-Gel Sci. Tech, 9 (1997) 305.
11. H. K. Varma, S. N. Kalkura and R. Sivakumar, Cer. Intl. 24 (1998) 467.
12. A. Jillavekantesa and R. A. Condrate sr., J. Mat. Sci., 33 (1998) 4111.
13. A. Jillavekantesa D. T. Hoelzer and R. A. Condrate sr., J. Mater. Sci., 34 (1999) 4821.
14. M.-F. Hsieh, L.-H. Perng, T.-S. Chin and H.-G. Perng, Biomaterials, 22 (2001) 2601.
15. M. Manso, M. Langlet, C. Jimenez and J. M. Martinez-Duart, Intl. J. Inorg. Mater., 3 (2001) 1153.
16. M.-F. Hsieh, L.-H. Perng and T.-S. Chin, J. Sol-Gel Sci. Tech., 23 (2002) 205.
17. M. Manso, S. Ogueta, P. Herrero-Fernandez, L. Vasquez, M. Langlet and J. P. Garcia-Ruiz, Biomaterials 23 (2002) 3985.
18. M. Manso-Silvan, M. Langlet, C. Jimenez, M. Fernandez and J. M. Martinez-Duart, J. Eur. Ceram. Soc., 23 (2003) 243.
19. C. Quian, P. F. Sanders, J. N. Seiber, Bull. Environ. Contam. Toxicol., 35 (1985) 682.
20. M. D. David and J. N. Seiber, Environm. Pollut., 105 (1999) 121.
21. K. Itatani, K. Iwafune, F. Scot Howell, M. Aizawa, Mater. Res. Bull., 35 (2000) 575.
22. K. Hwang, J. Song, B. Kang and Y. Park, Surf. Coat. Tech. 123 (2000) 252.
23. A. Beganskiene, O. Didko, R. Sirutkaitis and R. Giraitis, Mat. Sci., 9 (2003) 383.

SANS STUDY OF THE PRECIPITATES PHASES MICROSTRUCTURAL EVOLUTION IN INCONEL 738 SAMPLES SUBMITTED TO DIFFERENT AGEING TREATMENTS

V. T. Lebedev Petersburg Nuclear Physics Institute, Gatchina, St. Petersburg, Russia
vlebedev@pnpi.spb.ru

M. Rogante Rogante Engineering Office, NDT, Contrada San Michele, n. 61, P. O. Box 189, 62012 Civitanova M., Italy, engineering@interfree.it

Abstract
Ni-based superalloys, due to their high strength together with good oxidation and corrosion resistance, offer various application possibilities, mainly in high temperature environment, such as turbo-machinery industry (jet engines, pump bodies and parts, rocket motors, etc.).
Inconel 738 belongs to modern Ni-based superalloys adopted at high temperatures in aggressive environments, and it has found applications over a very wide range of temperature. Small angle neutron scattering (SANS) is a useful tool for materials characterisation in the nanoscale range (10Å-1000Å). The same technique has been adopted for the investigation of Inconel 738 samples submitted to different annealing temperatures and ageing times, in order to study the precipitates phases' microstructural evolution and obtain useful information on the material behaviour.

Keywords: SANS; Inconel 738; ageing; precipitates.

1. Introduction

Ni-based superalloys, due to their high strength together with good oxidation and corrosion resistance, offer numerous application possibilities, mainly in high temperature environment, for instance in turbo-machinery industry (jet engines, pump bodies and parts, rocket motors, etc.).

The crucial parameters for the stability of such alloys at high temperatures are yield stress, high elastic modulus and low thermal expansion coefficient [1, 2], and excellent mechanical properties result also from their two-phase structure and grain boundaries strengthening by carbides. The high temperature stability and deformation behaviour strongly depends on changes of microstructure caused by complex operating thermo-mechanical conditions [1, 3].

Inconel 738 belongs to modern Ni-based superalloys adopted at high temperatures in aggressive environments. Jet engine turbine components and stationary gas turbine components make use of this alloy for its high-temperature strength and oxidation resistance. It is also used in liquid-fuelled rockets for cryogenic tanks. It suffers from strict vulnerability to high-pressure H embrittlement, and such susceptibility has limited its application in rocket components. Temperatures appreciably below the aging temperature are not likely to modify the microstructure. The temperature dependence of density follows thermal expansion; hence it is inversely proportional to three times the linear thermal expansivity.

Ni-based superalloys turbine buckets for power plants, e.g., are generally working in very rigorous conditions, i.e. centrifugal loads, an extremely high temperature (800-1000 °C) of the gas, high temperatures gradients, and vibrations. Such environment can involve a risk of material failure associated to events like creep, high cycle fatigue, thermal fatigue and corrosion.

2. Method

Many different techniques allow materials characterization in the nanoscale range (10Å-1000Å). Small Angle Neutron Scattering (SANS) have the advantages of being non-destructive and of providing information with high statistical accuracy due to the averaging over a macroscopic sample volume. The sample, due to the non-destructivity, can be measured any number of times after more using or heat-treating. The small absorption of neutrons, in particular, consents in many cases the investigation of centimetre thick material. In SANS experiments, as in other diffraction investigations, one measures the scattered intensity I(q), as a function of the direction of scattering, if the elastic scattering dominants in the interaction of the neutron and nuclei, the vector q corresponding to the momentum transfer. The low limit ($qR_g<1$) behaviour of scattering intensity can be written with the Guinier expresses for all shape of non-interacting scatterers:

$$I(q) = \phi K^2 V^2 \exp\left(-q^2 R_g^2\right) \qquad (1)$$

where R_g is the radius of gyration of each individual scatterer, K is the contrast, V is the total volume and Φ is the concentration of scatterers. An important feature of this equation is that R_g can be determined even if $I(q)$ is known only in arbitrary units. In the large q region of scattering, the signal due to the interface between each scatterer and the embedding medium dominates the intensity. The Porod law can describe this behaviour:

$$I(q) = \left(2\pi K^2 \Sigma\right) q^{-4} \qquad (2)$$

where Σ is the total area of the interface per unit volume of sample. The limit of Porod law is qR>4 [4, 5]. Some earlier SANS studies of thick samples [6, 7] and on real turbine buckets [8] have shown the measurement feasibility and useful information on the microstructure, complementary to those obtained by TEM and SEM, where a very small area of the sample can be probed, thus resulting in a reduced statistical significance.

32. Experimental, results and discussion.

Inconel 738 samples submitted to different annealing temperatures and ageing times have been considered, as listed in table 1, for the SANS investigation of the precipitates phases microstructural evolution, in order to obtain useful information on the material behaviour.

Sample	Ageing time, h	Annealing temperature, °C
1	1000	800
2	3000	800
3	6000	800
4	1000	900
5	3000	900
6	6000	900
7	as received	

Table 1 - Inconel 738 samples list.

The measurements were performed by using the V12 double crystal diffractometer with bent crystals of HMI, Berlin [9]. The main applications of the same instrument are: SANS study of porous materials (hydrating cement paste, rocks, coal), inhomogeneous metallic alloys, particles (polymers, ceramics) and material inhomogeneities from 30 nm to 30 μm; investigations of neutron optical components (refractive index gratings, holographic gratings); investigations of reflection from surfaces; study of diffraction and refraction at magnetic domains.

Such instrument adopts two perfect Si crystals cylindrically bent with the axis perpendicular to the scattering plane, and an asymmetrically cut crystal-analyzer. The equivalent momentum transfer is:

$$Q = \frac{2\pi \cdot x}{\lambda \cdot R_2 \cdot \sin(2\Theta_B)} \tag{3}$$

where x is the distance from the centre of the intensity distribution for $Q = 0$, and R_2 is the radius of curvature of the second crystal. A double crystal diffractometer with bent crystals allows collecting simultaneously the whole spectrum by a linear position-sensitive detector, and that to tune the angular resolution as well as luminosity by the bending of crystals. It allows, moreover, for the operation in the medium Q-range and to overlap the Q-gap between conventional SANS instruments and Bonse-Hart cameras. Figure 2 represents the layout of the considered instrument.

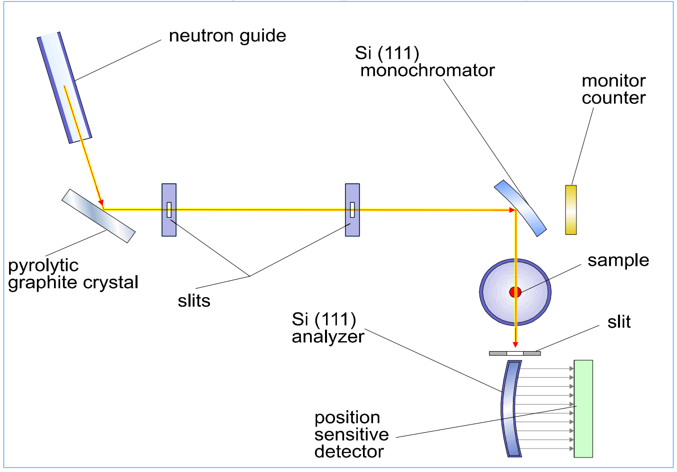

Fig. 2 - Layout of the V12 double crystal diffractometer with bent crystals of HMI, Berlin.

The incident neutron beam is deflected to the diffractometer by a pyrolytic graphite pre-monochromator. The neutron beam, monochromatized by the Bragg diffraction at monochromator, enters the end face of an asymmetrically cut analyzer crystal and propagates along its longest edge. The analyzer crystal reflects the neutron beam only in the case the scattered beam fulfils the Bragg-condition. By changing the curvatures of the monochromator and the analyzer within a rather wide range, it is possible to modify both the resolution (monochromator) and the Q-range available (analyzer).

The investigated samples were 10x10x2 mm^3 plates. The instrumental unit was displaced in order to obtain $q_{max} = 8.6 \cdot 10^{-2}$ nm^{-1}. The data analysis was performed using the model of homogeneous spheres (radius R=10-1000 nm) scattering independently. The regularization procedure gives the distribution D(R) of volume fraction of spheres as a function of their radius (Fig.3, with reference to the thermal treatment at 800°C by 250, 1000, and 3000 h).

At the time **t**=250h we observe the characteristic zones in scatterers distribution: a wide low-size zone, R_1=10-100nm, and a fraction, R_2~300nm. The intermediate time t=1000h leads to the annihilation of low-size defects while the volume fraction of larger defects remains practically the same. On the other hand, the long-time treatment produces defects is the range R=10-400nm. Except of the growth of low-size, R_1=10-100nm, and large-size, R_2=300nm, particles we observed the appearance of middle objects, R_3~150 nm (Fig.3). The temperature 800°C appears favourable for the growth of small (R_1=10-60nm) and middle-size (R_3~150nm) precipitates. In order to understand the peculiarities of structural transformations we used the increased temperatures, 850°C and 900°C, keeping annealing time (Figs. 4 and 5).

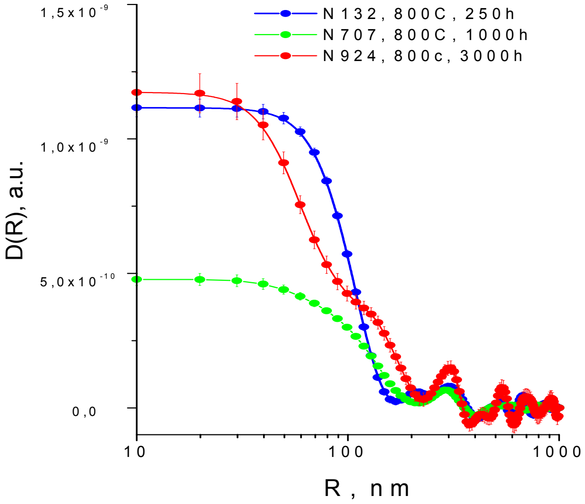

Fig.3 - Volume fraction of scatterers D(R) vs. radius R (thermal treatment at 800°C by 250, 1000, 3000 h).

At 850°C the small-size defects (R_1=10-100nm) disappear but the larger ones, R=150-400nm, grow progressively and form the zone $R_{2\text{-}3}$ =150-400nm (Fig.4). We have checked the effects of short-time treatment t=250h and performed the experiment on the 2nd sample confirmed the data on the 1st sample (Fig.5).

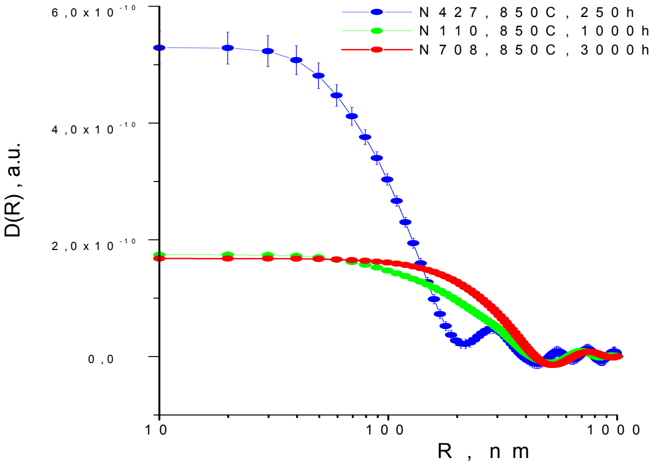

Fig. 4 - Volume fraction of scatterers D(R) vs. radius R, (thermal treatment at 850°C by 250, 1000, 3000 h).

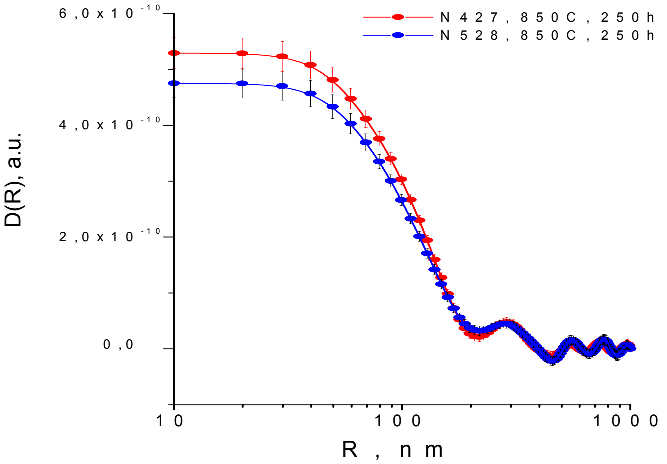

Fig.5 - Volume fraction D(R) vs. radius R, (thermal treatment at 850°C by 250, used).

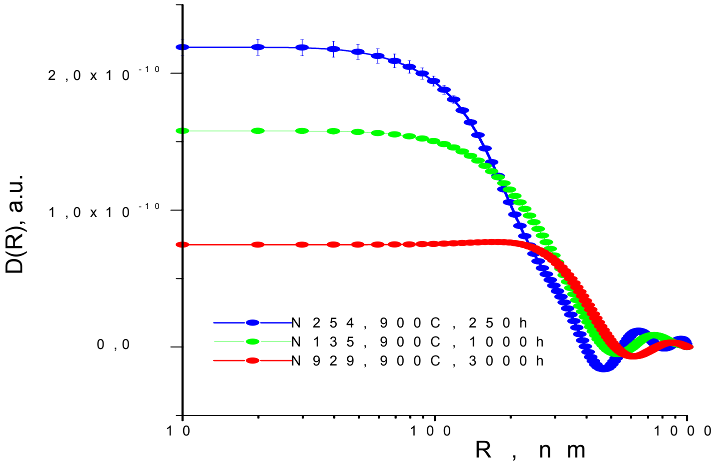

Fig.6 - Volume fraction D(R) vs. radius R: (thermal treatment at 900°C by 250, 1000, 3000 h).

Conclusion

Inconel 738 samples submitted to different annealing temperatures and ageing times have been investigated by SANS in order to study the precipitates phases' microstructural evolution and obtain useful information on the material behaviour. Summarizing the effect of thermal treatment at 800-900^{o}C, the heating up to 900^{o}C shifts of precipitates size to higher magnitudes from R~10-300nm to R~10-600nm. At 900^{o}C the volume fraction distribution becomes uniform up to 300 nm. Thus, the large scale objects, R~200-300 nm, provide the volume part by factor 2 higher than that for small particles, R~10-100nm. On the other hand, at 800^{o}C low-size fractions (R=10-100nm) includes ~90 % of the total volume of precipitates and the entities, R~200-300 nm, have a minor content ~10%.

Acknowledgements

EC is acknowledged for the substantial support for access to the BENSC facilities.

References

[1] T. Khan, P. Caron, High Temperature Materials for Power Engineering 1990, Part II, eds. E. Bachelet et al., Kluwer Academic Publisher, Dodrecht, The Netherlands (1990) 1261-1270.

[2] R.V. Curtis, R.N. Ghosh, M. McLean, Creep and Fracture of Engineering Materials and Structures, The Institute of Materials, London (1993) p. 199.

[3] J. Zrník, Influence of thermal and stress loading on the structure of nickel superalloys, Habilitation Thesis, Department of Material Sciences, Technical University in Košice, Slovakia (1990) 15-22.

[4] Lecture Notes on Neutron Scattering Introductory Course to ECNS'99, Ed. G. Kádár and L. Rosta, Budapest, 1999.

[5] O. Glatter, O. Kratky: Small Angle X-ray Scattering, Academic Press, 1982.

[6] P. Strunz, J. Zrník, R. Gilles, A. Wiedenmann, Physica B. (2000). **276-278**, 890-891.

[7] P. Strunz, P.Lukáš, P. Mikula, J. Šaroun, E. Keilová, J. Kočík, Acta Physica Hungarica. (1994). **75**, 279.

[8] V. Marinčák, P. Strunz, J. Šaroun, V. Ryukhtin, P. Lukáš, L. Cassì, G. F. Ceschini, M. Rogante, Non-destructive SANS investigation of IN 738 turbine blades after high-temperature operation, Int. Conf. ICM9, Geneva, Switzerland, May 25-29 2003, Book of abstracts, p. 165.

[9] Neutron-Scattering Instrumentation at the Research Reactor BER II, ed. T. Robertson, H. A. Graf, R. Michaelsen, P. Vorderwisch, Berlin Neutron Scattering Center, Hahn-Meitner-Institut, Berlin, May 1996.

10. Savjetovanje o materijalima, tehnologijama, trenju i trošenju
10. Conference on Materials, Processes, Friction and Wear
MATRIB'05, Vela Luka, 23-25.06.2005.

STRUKTURNA SVOJSTVA KOKSOVA

STRUCTURAL PROPERTIES OF COKES

M. Legin-Kolar, A. Rađenović
University of Zagreb, Faculty of metallurgy
Aleja narodnih heroja 3, 44000 Sisak, Croatia

Sažetak:

Struktura koksova ovisi o kemijskom sastavu sirovine za koksiranje i toplinskoj obradbi proizvedenih koksova.

U radu su ispitani kristalografski parametri i morfologija površine naftnog i metalurškog koksa nakon toplinske obradbe do 2400°C. Razlike u kristalografskim parametrima prate promjene u morfologiji površine koksova.

Osim u metalurgiji, prema dobivenim rezultatima ispitani koksovi bi se mogli rabiti za proizvodnju konstrukcijskih materijala.

Ključne riječi: sirovina za koksiranje, koks, temperatura, kristalografski parametri, morfologija površine

Abstract

The structure of cokes depends on the chemical composition of the coking feedstock and on the temperature treatment of produced cokes.

This paper deals with the investigation of crystallographic parameters and surface morphology of petroleum and metallurgical cokes after heat treatment to 2400°C. Differences in crystallographic parameters of the cokes also become manifest through their surface morphology. On the basis of obtained results, investigated cokes could be useful and suitable, not only in metallurgy but also for the manufacture of construction materials.

Key words: coking feedstock, coke, temperature, crystallographic parameters, surface morphology

UVOD

Koksovi spadaju u krhke materijale, ali koji se zbog svojih raznovrsnih dobrih svojstava mogu rabiti kao sirovina pri izradi i mehanički vrlo opterećenih elemenata. Oni sve manje zastaju za tradicijskim materijalima, naročito pri visokim temperaturama ili u agresivnoj sredini. Kako se krhki materijali ne mogu plastično deformirati, oni se lome na sebi svojstven način tj. tako da naglo pucaju na mjestima slučajnih strukturnih pogrešaka. Stoga je važan parametar čvrstoće (konstrukcije materijala) morfologija koksova, orijentacija slojeva, veličina kristalita, općenito njihova struktura koja se odgovarajućom toplinskom obradom može i poboljšati. Nepravilnosti u geometriji strukture i različitim stupnjem kristalne sređenosti dati će materijale različitih svojstava: od vrlo krhkih i poroznih do žilavih, tvrdih ali laganih «super» materijala koji uspješno mogu zamijeniti mnoge već dobro poznate materijale |1-3|.

U radu su prikazani rezultati ispitivanja strukturnih parametara naftnog i metalurškog koksa koji govore o njihovoj uporabljivosti kao sirovine za mnoge ugljične materijale.

EKSPERIMENTALNI RAD

U eksperimentalnom dijelu rada dobiveni su podaci o veličini kristalita (L_c) te međuslojnog razmaka (d_{002}) oba koksa, kao i utjecaj vremena zagrijavanja na ove karakteristike. Ispitana je također i morfologija koksova prije i poslije toplinske obradbe da se utvrdi primjenjivost pojedinog uzorka za daljnju uporabu kao sirovine za konstrukcijske materijale.

Uzorci

Osnovne karakteristike sirovine za koksiranje iz koje su dobiveni ispitani koksovi prikazane su u tablici 1. Ispitivanja strukturnih parametara i morfologija koksova provedena su na dva uzorka istog naftnog koksa (NK) i dva uzorka istog metalurškog koksa (MK) čije su karakteristike prikazane u tablici 2. Ovi uzorci veličine zrna 0,2 mm, zagrijavani su pri 1200, 1600, 2000, 2400°C u vremenu od 2 i 4 sata brzinom od 10°C/min. Toplinska obradba je provedena u grafitnim lončićima u visokotemperaturnoj peći «Astro» - tip 1000 - 3050 FP u atmosferi argona.

Tablica 1. Osnovne karakteristike sirovina za koksiranje

Karakteristike	Atmosferski ostatak	Pirolitički ostatak	Ugljen
Gustoća, kgm^{-3}	935	1050	983
Ugljik, %	84	88	87
Sumpor, %	0,85	0,25	1,01
Aromati, %	48	86	-
Asfalteni, %	0,36	5,7	-
Isparljive tvari, %	-	-	24,1
Pepeo, %	0,08	0,01	7,54

Analiza uzoraka

Veličina kristalita (L_c) i međuslojni razmak (d_{002}) određeni su metodom difrakcije X-zraka (Cu Kα zračenje) s čistim grafitom kao unutarnjim standardom na «Philips» - Norelco strukturnom rendgenu. Morfologija površine uzoraka ispitana je na Scanning - elektronskom mikroanalizatoru JXA - 50 A firme «Joel». Nakon poliranja koksnih površina provedena je i oksidacija kromatnom kiselinom te je nanesen tanki sloj bakra da se održi vodljivost elektrona.

Tablica 2. Osnovne karakteristike uzoraka koksova

Karakteristike	Naftni koks (NK)			Metalurški koks (MK)		
	NK_1	NK_2	srednja vrijednost	MK_1	MK_2	srednja vrijednost
Gustoća, kgm^{-3}	2090	2130	2,11	1890	1920	1900
Isparljive tvari, %	0,16	0,18	0,17	11,35	10,81	11,08
Sumpor, %	0,71	0,77	0,74	0,78	0,83	0,80
Pepeo, %	0,19	0,16	0,17	6,82	6,87	6,84

REZULTATI I DISKUSIJA

Rezultati ispitivanja kristalografskih parametara (veličina kristalita, L_c i međuslojnog razmaka, d_{002}) naftnog i metalurškog koksa prikazani su na slikama 1 i 2. Uzorci su temperaturno obrađeni pri 1200, 1600, 2000 i 2400°C u vremenu od 2 i 4 sata uz brzinu zagrijavanja od 10°C/min.

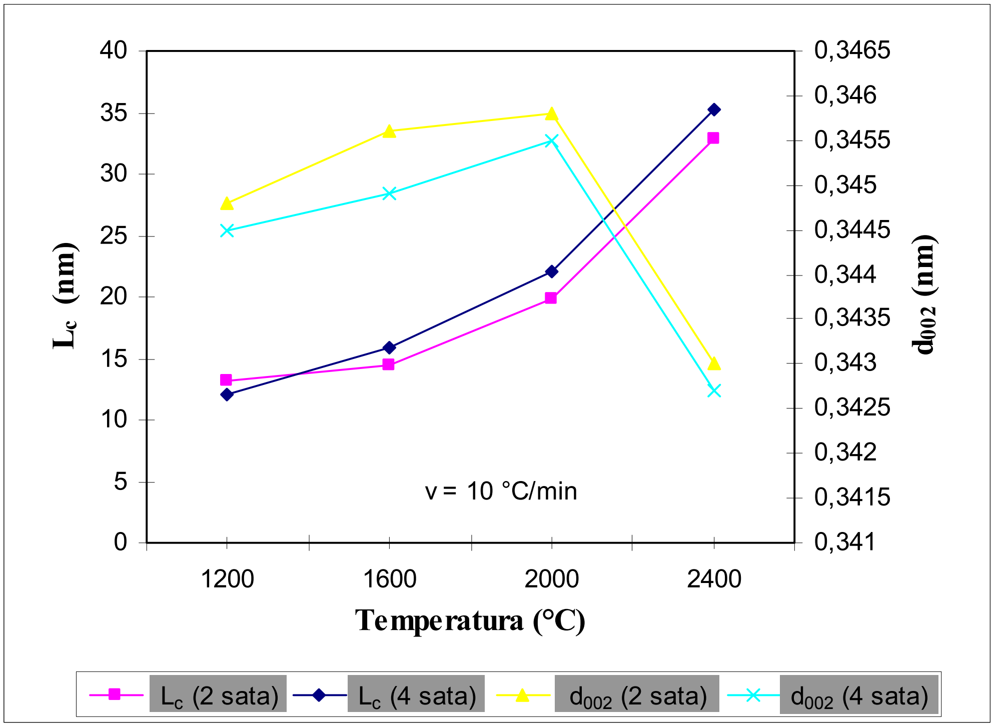

Slika 1. Utjecaj temperature i vremena zagrijavanja na veličinu kristalita (L_c) i međuslojnog razmaka (d_{002}) naftnog koksa (NK)

Za razliku od sirovine za dobivanje naftnog koksa, ugljen za koksiranje ima veće udjele sumpora i anorganskih sastojaka koji se koncentriraju u pepelu ugljena odnosno metalurškog koksa. Iz tablice 2 je vidljivo da metalurški koks sadrži 6,48 % pepela za razliku od naftnog koksa koji ima svega 0,17 % pepela. Dobiveni rezultati pokazuju da, bez obzira na vrstu koksa, porastom temperature zagrijavanja dolazi do gotovo linearnog povećanja veličine kristalita, L_c (slike 1 i 2). Ipak, do značajnijeg porasta veličine kristalita dolazi iznad 2000°C kao posljedice znatnijih promjena u strukturi, što je u skladu s ranijim istraživanjima nekih ugljičnih materijala |4, 5|. Ustanovljeno je da toplinska obradba između 1300 - 1800°C utječe na proces stvaranja kristalita. Tek iznad 1800°C (faza kristalizacije) dolazi do znatnijeg porasta veličine kristalita uslijed spajanja manjih u veće ranije orijentirane kristalite.

Rezultati dobiveni provedenim ispitivanjima ukazuju na određene razlike u strukturnim svojstvima ispitanih koksova o kojima ovisi njihova uporaba. Na svojstva koksa, pored ostalog, utječu vrsta i sastav sirovine za koksiranje |6|. Određene razlike u fizikalno-kemijskim karakteristikama ispitanih koksova izravna su posljedica razlika u svojstvima sirovine za njihovu proizvodnju.

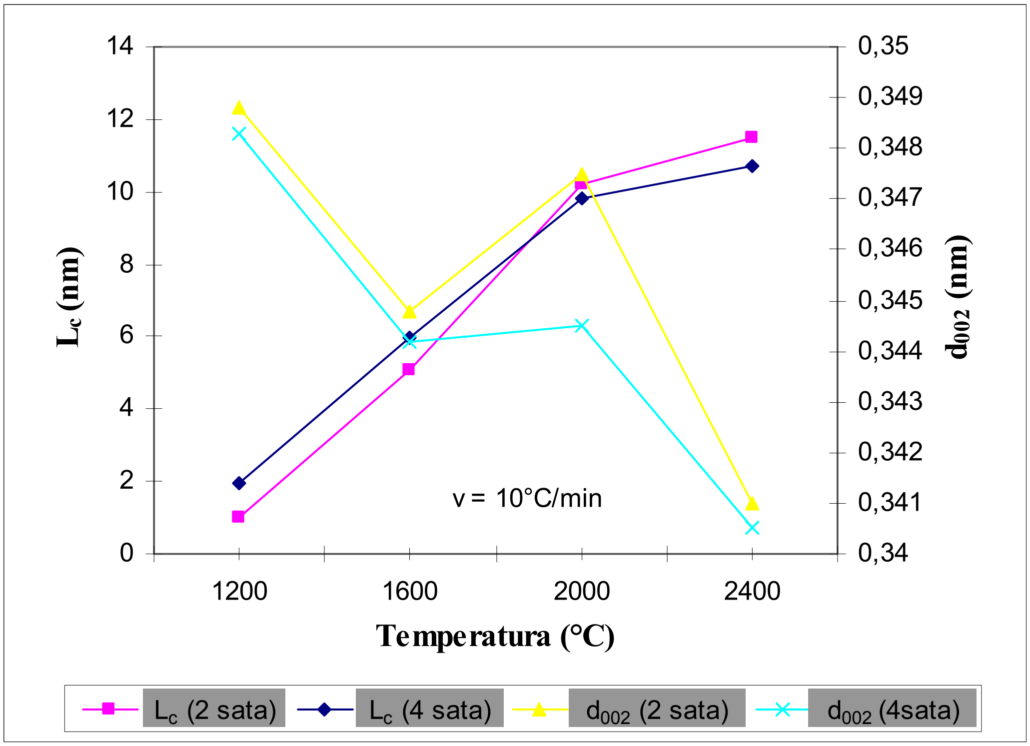

Slika 2. Utjecaj temperature i vremena zagrijavanja na veličinu kristalita (L_c) i međuslojnog razmaka (d_{002}) metalurškog koksa (MK)

Metalurški koks je proizveden postupkom koksiranja ugljena, a naftni koks koksiranjem smjese sastavljene od ostataka prerade nafte (atmosferski i pirolitički ostatak) čije osnovne karakteristike su prikazane u tablici 1. Oba koksa proizvedena su industrijski.

Prisutnost aromatskih ugljikovodika (naročito veći udjel u pirolitičkom ostatku) te neznatan sadržaj asfaltena u sirovini doprinose promjenama do kojih dolazi u procesu primarne karbonizacije uključujući stvaranje mezofaze |7, 8|. Obzirom na ulogu i značaj mezofaze, ona se smatra intermedijarom između tekuće faze i anizotropnog koksa.

Podaci o sadržaju isparljivih tvari također su različiti jer ih naftni koks sadrži 0,17 %, a metalurški koks 11,08 % što je također posljedica različitog sastava sirovina za koksiranje. Veći sadržaj isparljivih tvari u metalurškom koksu doprinjeo je njihovom naknadnom izdvajanju tijekom toplinske obrade što je utjecalo i na narušavanje njegove strukture.

Duže vrijeme zagrijavanja, pri istim temperaturama i pri istoj brzini, doprinjelo je porastu veličine kristalita kod oba ispitana koksa. Iz slika 1 i 2 također je vidljivo da naftni koks ima veće kristalite u odnosu na metalurški koks bez obzira na uvjete ispitivanja. Najveća vrijednost za L_c od 3,5 mm je postignut za naftni koks nakon 4 sata zagrijavanja pri 2400°C brzinom od 10°C/min.

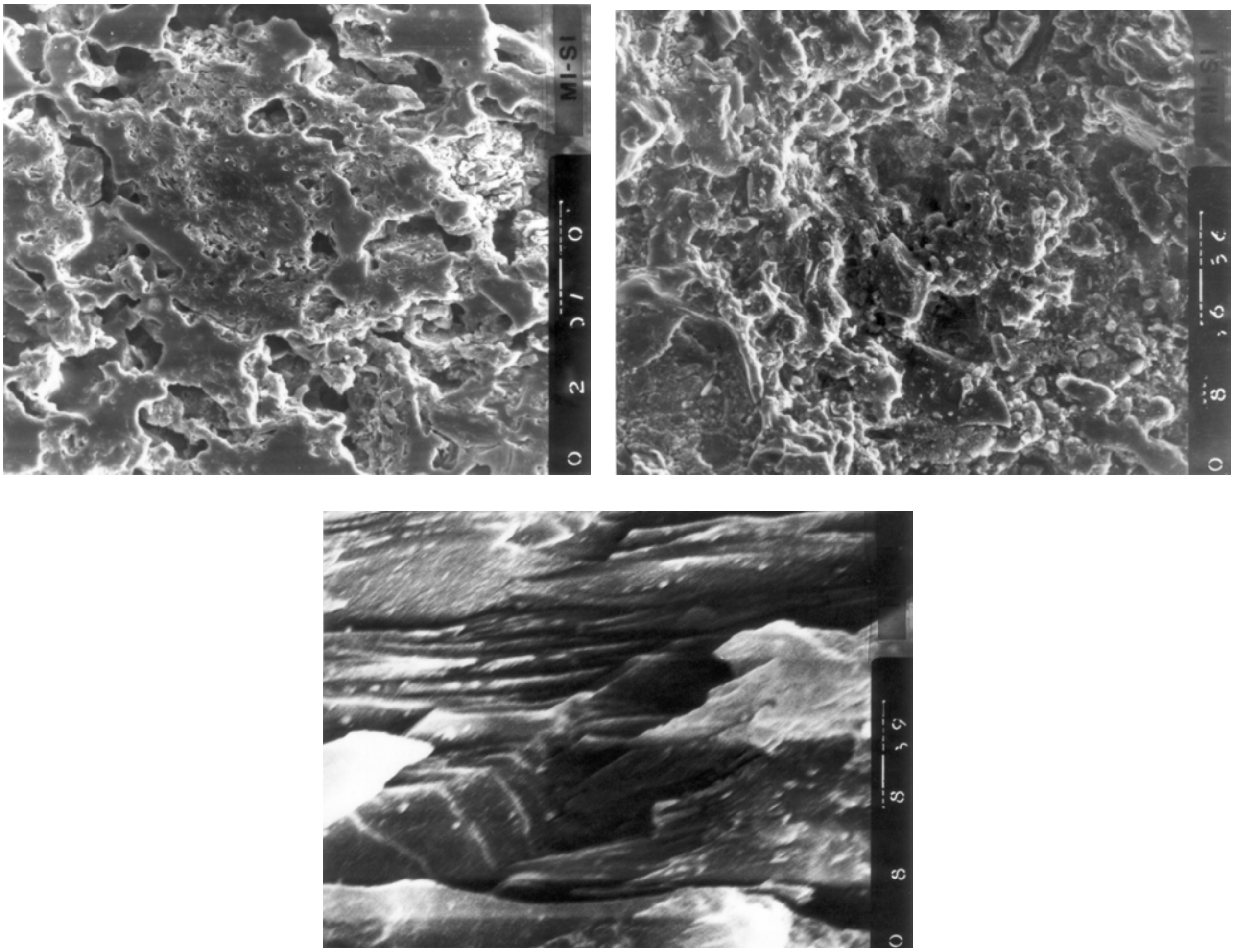

Slika 3. SEM mikrofotografije površine metalurškog koksa

a) prije toplinske obrade, 150x
b) nakon zagrijavanja na 1200°C, 150x
c) nakon zagrijavanja na 2400°C, 1500x

Ispitivanja međuslojnog razmaka d_{002} pokazala su nepravilniju promjenu s porastom temperature obradbe ispitanih koksova. Ipak, može se uočiti da porastom temperature dolazi do smanjenja međuslojnog razmaka oba koksa iako je ta promjena nepravilnija u odnosu na promjenu veličine kristalita (slika 1 i 2). Ova nepravilnost se odražava kao porast međuslojnog razmaka pri 1600 i 2000°C za naftni koks (slika 2) odnosno pri 2000°C (slika 2) za metalurški koks. Pojava se može objasniti istovremenim izdvajanjem anorganskih sastojaka, a posebno sumpora iz koksa. Uslijed toga dolazi do izvjesnog narušavanja slaganja i usmjerenosti strukturnih elemenata što se daljnjim zagrijavanjem, pri višim temperaturama, ponovo uspostavlja.

Morfologija površine metalurškog koksa prije i nakon zagrijavanja na 1200°C i 2400°C u vremenu od 2 sata prikazane su na slici 3. Iz slike 3a vidljivo je da mikroteksturu ovog koksa prije toplinske obradbe predstavlja srednjezrnati mozaik uz djelomičnu poroznost. Nakon toplinske obradbe pri 1200°C uzorka istog koksa nisu primijećene gotovo nikakve promjene u morfologiji površine (slika 3b). Uočavaju se jedino promjene u manjem broju i izgledu pora čiji rubovi postaju zaobljeniji. Tek zagrijavanje na temperaturu od 2400°C dovodi do znatnijih promjene morfologije površine metalurškog koksa. Dio sitnih zrna mozaika se povećava, a dio zrna mozaika se transformira u izdužene oblike slične lamelama tako da mikrotekstura ovog koksa postaje mješovita. Za razliku od metalurškog koksa, morfologija površine naftnog koksa predstavljena je većim lamelarnim područjima te sitno i srednje zrnatim mozaikom.

Slika 4 prikazuje morfologiju površine naftnog koksa nakon toplinske obradbe na 2400°C. Vidljiva je dobro izražena slojevita struktura kao posljedica paralelne orijentacije lamela u obliku listića, a područja jednake anizotropije su relativno mala.

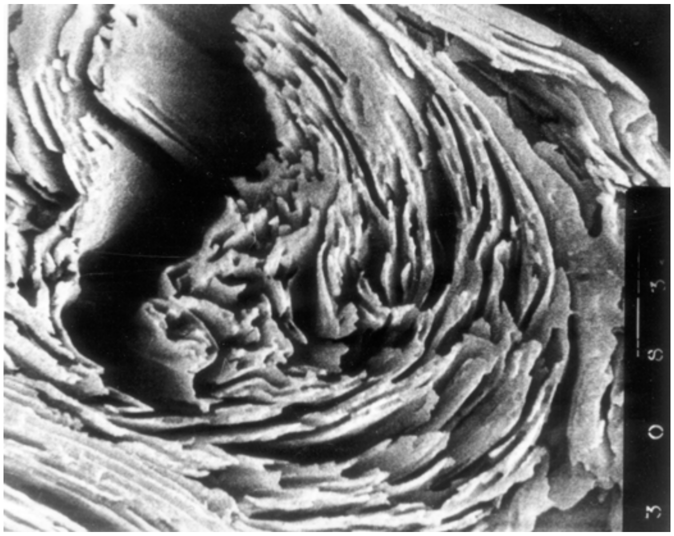

Slika 4. SEM mikrofotografija površine naftnog koksa (NK$_2$) nakon zagrijavanja na 2400°C, 3000x

Ispitani naftni koks je korišten kao punilo za proizvodnju anoda kod dobivanja aluminija.. Ugljična anoda u elektrolitičkoj ćeliji za dobivanje aluminija ima ulogu vodiča kroz koji prolazi istosmjerna struja koja uz pomoć drugih kemijskih sredstava pomaže rastvaranje glinice. Obzirom da su po visini anode različite temperature, ona mora imati dobre mehaničke osobine da ne dolazi do pucanja i odvajanja pojedinih dijelova anoda u kupku čime bi se poremetio strujni tok. Stoga takva anoda treba biti dovoljno kvalitetna, a što ovisi i o naftnom koksu koji je (uz smolu katrana kamenog ugljena kao veziva) punilo i sirovina za dobivanje anoda.

Budući da udio anoda u cijeni koštanja aluminija iznosi i preko 20 %, vrlo je važna sistematska kontrola i poboljšanje njezine kvalitete, a time i istraživanja karakteristika naftnog koksa čija svojstva znatno utječu na kvalitetu anode.

Koks kao punilo treba imati što manje metalnih primjesa i sumpora da se spriječi onečišćenje taljevine i pojava pukotina na anodama uslijed njihovog naknadnog izdvajanja. Strukturne karakteristike koksa kao što su prisutne strukturne jedinice u morfologiji površine koksnih zrna i poroznost, utječu na intenzivnost interakcije punila i veziva o kojima ovise svojstva ugljičnih anoda.

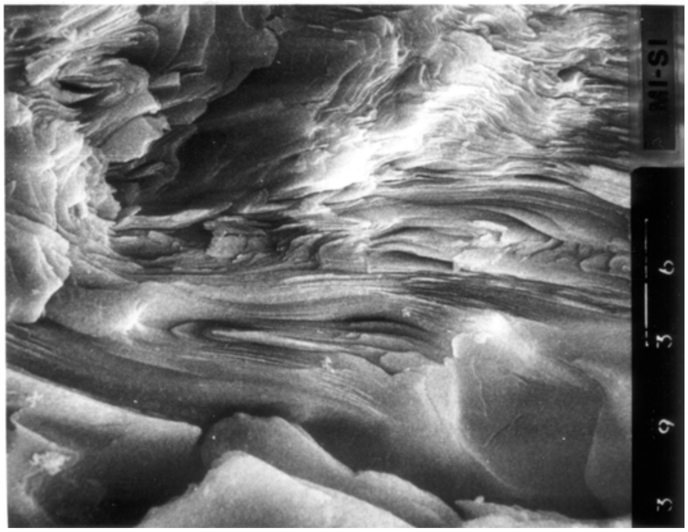

Slika 5. SEM mikrofotografija površine anode (punilo-NK$_2$), 1500x

Obzirom na veliki sadržaj aromata (96 %) i mali sadržaj asfaltena (0,30 %) u smoli katrana kamenog ugljena poboljšava se morfologija anoda povećanjem temperature pa su rezultati ispitivanja bili očekivani. Slika 5 prikazuje površinu anode s ispitanim naftnim koksom kao punilom i smolom katrana kamenog ugljena kao vezivom. Vidljiv je veliki udjel ravnih i cilindričnih lamela što omogućuje izuzetno dobru povezanost osnovnih komponenti tako da ih je teško razlikovati na mikrofotografiji.

ZAKLJUČAK

Rezultati provedenih ispitivanja su pokazali da strukturna svojstva koksa ovise o sastavu sirovine za koksiranje i uvjetima naknadne toplinske obradbe. Strukture metalurškog i naftnog koksa nakon toplinske obradbe pri visokim temperaturama postaju slične. Ipak, toplinskom obradbom naftnog koksa proizvedenog iz smjese atmosferskog i pirolitičkog ostatka preradbe nafte dobiveni su bolji pokazatelji strukturnih svojstava u odnosu na metalurški koks. Posebno se ističe veličina kristalita od 35,1 nm te razvijene lamele u mikrostrukturi nakon 4 sata zagrijavanja naftnog koksa na 2400°C.

Ova ispitivanja su pokazala da bi se, osim u metalurgiji, naftni i metalurški koksovi sličnih karakteristika mogli rabiti i u proizvodnji konstrukcijskim materijala.

LITERATURA

1. M.A. White, Properties of Materials, Univ. Press, Oxford, 1999.
2. H. Marsh, E.A. Heintz, F. Rodriguez-Reinoso, Introduction to Carbon Technologies, University of Alicante, Alicante, 1997.
3. T.D. Burchnell (Ed.), Carbon Materials for Advanced Technologies, Pergamon Press, Oxford, 1999.
4. Legin-Kolar, M., Rađenović, A., Ugarković, D.: Fuel **78** (1999) 1599
5. Q. Zhang, X. Wa, A. Feng, M. Shi, Fuel Procc. Technol. **86** (2004) 1
6. D.W. Van Krevelen (Ed.) Coal, Elsevier, Amsterdam, 1993.
7. Greinke, R.A., in Thrower P.A. (Ed.), Chemistry and physics of carbon, vol. 24, Marcel Dekker, New York, 1994.
8. P. Torregrosa-Rodriquez, M. Martinez-Escandell, F. Rodriquez-Reinoso, H. Marsh, C. Gomez de Salazar, E. Romero Palazon, Carbon **38** (2000) 535

10. Savjetovanje o materijalima, tehnologijama, trenju i trošenju
10. Conference on Materials, Processes, Friction and Wear
MATRIB'05, Vela Luka, 23-25.06.2005.

OPTIČKI ASPEKTI DIGITALNOG TISKA NA ADHEZIVNIM MEDIJIMA

OPTICAL ASPECTS OF THE DIGITAL PRINTING ON ADHESIVE MEDIA

Igor Majnarić[1], Maja Brozinčević, Stanislav Bolanča[1]
Grafički fakultet Zagreb, Getaldićeva 2

Sažetak: Etikete danas spadaju u jedane od najzastupljenijih grafičkih proizvoda. Za tisak etiketa do nedavno se koristila isključivo tehnika ofsetnog tiska. Zbog prednosti personalizacije u tisku taj posao postepeno preuzima digitalni tisak. Danas se nastoji za tisak etiketa koristiti elektrofotografska digitalna tehnologija koja je brza, ali i zagrijava tiskovnu podlogu. U ovom radu se želi istražiti kako struktura i boja tiskovne podloge, te ljepljiva pozadina samoljepljivih materijala za tisak etiketa dijeluje na kvalitetu reprodukcije i optički izgled proizvoda. Za tisak se koristilo 7 tiskovnih podloga za samoljepljive etikete, karakterističnih grupa materijala. Mjerenjem se obuhvatio spektrofotometrijsko mjerenje u L*a*b* sustavu s konstrukcijama gamuta, ΔE s obzirom na konvencionalni ofset po cijelom području rastertonskih vrijednosti, balans sivog, relativni tiskarski kontrast (K$_{rel}$), te prostorno konstruiranje rasporeda boja u Mullenovom tijelu boja. Na temelju poznatih činjenica i naših ispitivanja mjerenjem bez razaranja, određuju se granice prihvatljivosti kvalitete za digitalni tisak samoljepljivih etiketa.

Ključne riječi: Samoljepljivi materijali, elektrofotografski digitalni tisak, spektrofotometrija, denzitomtrija, L* a*b*, gamuti reprodukcije.

Abstract: Labels belong today to the most representative graphic products. For printing on labels the offset printing techniques was exclusively used recently. Because of the advantage of personalization in printing, this work is taken over by the digital printing technique, especially by Ink Jet, because there is no heating of the printing substrate in this printing technique. Today the electrophotographic digital technology is used for label printing. It is much quicker but it warms up the printing substrate. The task of this work is to find out how the structure and the colour of the printing substrate as well as the adhesive back side of the self-adhesive materials for label printing influence the quality of the reproduction and the optical view of the product. Seven printing substrates for self-adhesive labels, of the characteristic material groups were used for printing. Measuring comprised the spectrophotonmetric measurement in L*a*b* system with the gamut constructions, ΔE with regard to the conventional offset on the whole area of screen value, grey balance, relative printing contrast (K$_{rel}$) and space construction of the colour arrangement in the Mullen colour body. Based on the known facts and our investigations the limits of acceptability of the quality for digital printing of self-adhesive labels were determined using the technique of electrophotographic digital printing on the determined characteristic groups of the printing substrates.

Key words: self-adhesive materials, electrophotographic digital printing, spectrophotometry, densitometry, L*a*b*, reproduction gamut.

1. UVOD

Potrošnja i proizvodnja samoljepljivih medija je kao i kod papira u stalnom porastu. Razvojem novih materijala i ljepila omogućilo je proizvodnju raznih grafičkih proizvoda kao što su: naljepnice raznih namjena (poštanske, promocijske, deklaracijske, vinske, igraće, kartonske…). Mogućnost otiskivanja samoljepljivih materijala s novim tehnologijama digitalnog tiska nije u potpunosti istražen. Nameću se istraživanja interakcija između tiskarskog bojila i tiskarske podloge, to jest komparacije kvalitete digitalnih otiska u odnosu na konvencionalni način otiskivanja.

2. TEORIJSKI DIO

Presudni čimbenici koji utječu na kvalitet tiska su: tiskarski stroj, odgovarajuće bojilo, tiskovna forma i tiskovna podloga. Do unazad nekoliko godina za tisak grafičkih proizvoda uglavnom je korištena tehnika ofsetnog tiska. Ofset koristi stalnu aluminijsku tiskovnu formu koja ima hidrofilne i hidrofobne povrπine, te se prije otiskivanja prvo vlaži vodom, te obojava uljnom bojom (1). Nanešeno bojilo se najprije prijenosi na ofsetnu gumu sa koje se uvijek isti motiv reproducira na tiskovnu podlogu. Svojom kvalitetom, brzinom, i velikim brojem tiskovnih podloga namjenjena je proizvodnjih srednjih i visokih naklada (2).

Digitalni tisak kao način umnožavanja u posljednjih 10 godina ima sve značajniju ulogu u tiskarstvu. Digitalni tisak svojim mogučnostima omogućuje tisak često ponavljanih niskih naklada uz mogućnost personalizacije(3). Najpoznatije digitalne tehnike otiskivanja su elektrofotografija i Ink Jet. Elektrofotografski tisak pri radu koristi 7 osnovnih faza (nabijanje, osvjetljavanje, razvijanje, prijenos, fuziranje i čišćenje), pri čemu je bojilo prah ili tekućina (4). Elektrofotografski način otiskivanja tekućim bojilima omogućava tisak u visokoj rezoluciji i kvaliteti koja je veoma slična klasičnoj tehnici ofseta. Jedan takav elektrofotografski digitalni sustav je HP Indigo kojeg karakterizira indirektni naćin otiskivanja, rezolucija od 812 do 2460 dpi, i specijalno ElectroInk bojilo (5).

Samoljepljivi mediji su višeslojni materijali koji se sastoje od površinskog sloja, ljepljivog sloja, sloja za lakše odljepljivanje i podloge (slika 1). Samoljepljivi materijali debljine su od 50 do 290 µm, odnosno gramature od 65 do 285 g/m2.

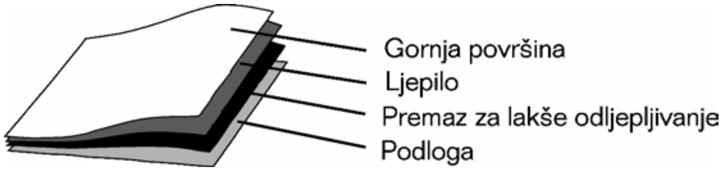

Slika 1. Prikaz samoljepljivih materijala

Površinski sloj samoljepljivog materijala može biti od raznih materijala a najčešće je to papir. Od papira obično su to bezdrvni bijeli ofsetni papir, obojeni bezdrvni papiri, i višestruko premazani papiri(6). Često je površina prethodno laminirana sa mekim vinilnim filmom prilagođenim za ofsetni tisak, sintetičkim papirom rađenog od gustog polietilena, celuloznim acetatskim filmom i etilenskim filmom.

Površinski sloj obrađen je tako da upije pastasto bojilo zajedno sa viškom tekućine za vlaženje. Premazivanjem površine samoljepljivog medija sa pigmentiranim premazima postiže se veća refleksija ulaznog svijetla na podlogu, gdje otisnuto bojilo dijeluje kao filtar smanjujući indeks reflenktancije i pojačavajući optički kontrast (7).

Ljepljivi sloj bitno određuje funkcijonalnost grafičkog proizvoda. Odabirom odgovarajućeg tipa ljepila postiæžu se različito kvalitetne adhezije samoljepljivog materijala. Ovisno o ljepljenoj podlozi, klimatskim uvjetima u kojima etikete egzistiraju, kao i o primjenjenom ljepilu, samoljepljivi materijali dijele se na: permanent, removable, supertack i deep freeze. “Permanent” samoljepljivi mediji posjeduju veliku početnu snagu ljepljenja, te su pogodna za ljepljenje na glatke površine. Odljepljivanjem površinski otisnuti sloj se obavezno uništava. Postavljen zahtjev za “Removable” samoljepljive medije je da se skidanjem površinski sloj ne oštećuje, čime je osiguran veći broj ponovljenih ljepljenja. ”SuperTack” samoljepljivi mediji imaju visoku adhezivnu moć, što je osnovni preduvijet za ljepljenje teško ljepljivih i neravnih površina. ”Deep freeze” specijalni samoljepljivi mediji namjenjeni su za ljepljene podloga koje su izložene niskim temperaturama (8).

Za uspješnost tiska podloga samoljepljivih materijala vrlo je važna. Njenom debljinom omogućava se besprijekoran transport samoljepljive tiskovne podloge po tiskarskom stroju. Neposredno prije ljepljenja podloga se skida. Lagano skidanje osigurano je specijalnom perforacijom podložnog sloja (horinzotalna ili vertikalna), kao i njenom površinom koja je premazana s glatkim pigmentiranim premazom.

Korištenjem ne razarajuće spektrofotometrije i denzitometrije moguće je analizirati površinsku obojenost otisnute tiskovne podloge, što ima za cilj optičko praćenje kvalitete reprodukcije. Vrijednost obojenja otiska definira se u L*a*b* kolornom sustavu koji je predstavljen sa kromatskim vrijednostima a*b* i svjetloćom L*. Denzitometrijom se određuje akromatska apsorpcijska moć otisnute boje na tiskovnoj podlozi, čime se u tisku aproksimativno izražava debljina nanosa bojila. Mjerenjem relativnog tiskovnog kontrasta poromatra se uspješnost reprodukcije punog polja i 3/4 polja (70-80% RTVa) koji je najosjetljiviji na povećanje nanosa boje (9).

Konstrukcijom, otiskivanjem i mjernjem specijalne tiskovne forme (sadrži 387 polja u bojama suptrktivne sinteze u međusobnim varijacijama od 5%), moguće je konstruirati trodimenzionalni gamut reprodukcije za bilo koju tiskarsku tehniku kao i pripadajuću tiskovnu podlogu (10).

Izračunavanjem razlike u obojenju (ΔE) za 100% otisnute primarne procesne boje (CMYK), kao i njihovih kombinacija (RGB), moguće je uočiti odstupanja i kvantificirati ih. Standardna formula CIE ΔE_{94} je 2001. godine modificirana, te je sada u primjeni CIE ΔE_{2000} koja bolje opisuje razlike u obojenju u plavom području (11). Određivanjem relativnog tiskarskog kontrasta, odrediti će se najveća moguća moć reproducibilnosti, a time i najveća kvaliteta grafičkog proizvoda. Aparativne metode lišene su subjektivnih emocija, te je važno ocjeniti kako vizualni izgled etikete ocjenjuju stvarni konzumenti. To je izvedivo tzv. metodom standardnog promatraća.

3. EKSPERIMENT

Za potrebu istraživanja formirana je specijalna tiskovna forma koja sadrži standardne ISO i ECI elemente. Osim toga tiskovna forma sadrži i CMYK rasterske stepenaste klinove u rasponu od 10% do 100% RTVa i stupnjem razlikovanja od 10%. U tiskovnu formu je implementirana i standardizirana višebojna ilustracija, koja služi za vizualnu ocjenu kvalitete reprodukcije.

Otisci etiketa napravljeni su na digitalnom ofsetnom stroju HP Indigo. Tiskarski stroj je četvorobojan i kalibriran neposredno prije otiskivanja proba. U istraživanju korištene su 7 samoljepljivih tiskovnih podloga koje se razlikuju po površinskoj obradi, vrsti ljepila i skidajućoj podlozi. Prije upotrebe samoljepljive podloge izrezane su na standardni format A3, i njihove karakteristike dane su u tablici 1.

Tablica 1. Karakteristike FASSON samoljepljivih tiskovnih podloga korištnih u istraživanju

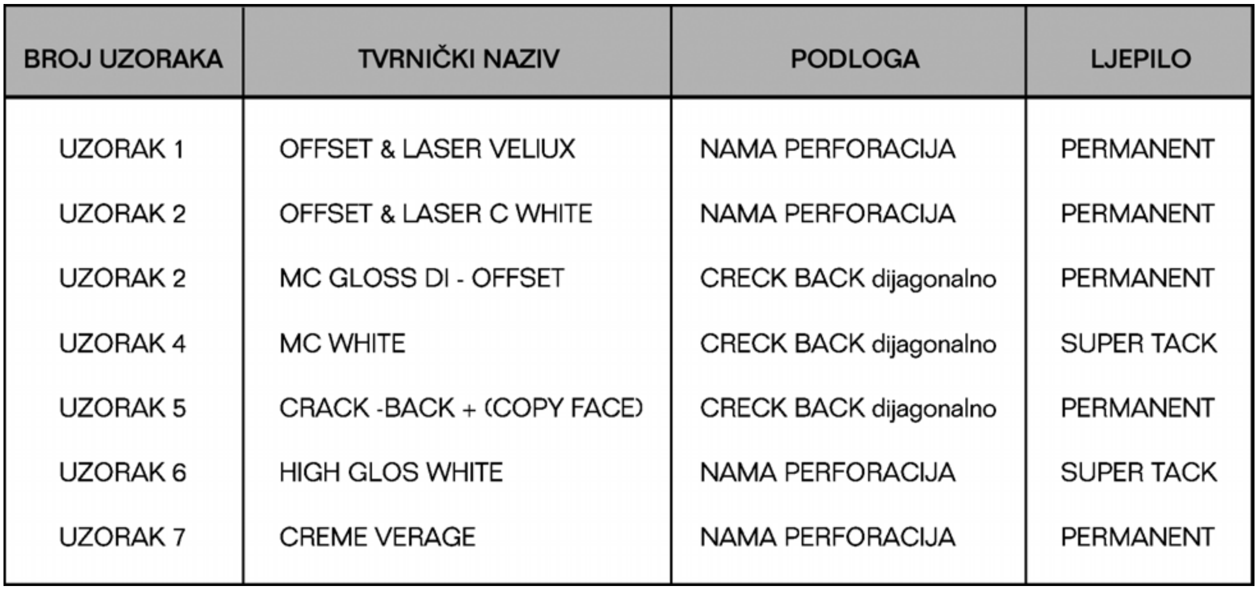

BROJ UZORAKA	TVRNIČKI NAZIV	PODLOGA	LJEPILO
UZORAK 1	OFFSET & LASER VELIUX	NAMA PERFORACIJA	PERMANENT
UZORAK 2	OFFSET & LASER C WHITE	NAMA PERFORACIJA	PERMANENT
UZORAK 2	MC GLOSS DI - OFFSET	CRECK BACK dijagonalno	PERMANENT
UZORAK 4	MC WHITE	CRECK BACK dijagonalno	SUPER TACK
UZORAK 5	CRACK -BACK + (COPY FACE)	CRECK BACK dijagonalno	PERMANENT
UZORAK 6	HIGH GLOS WHITE	NAMA PERFORACIJA	SUPER TACK
UZORAK 7	CREME VERAGE	NAMA PERFORACIJA	PERMANENT

Dobiveni otisci na digitalnom stroju komparirani su sa ofstnim otiskom koji je otisnut na papiru za umjetnički tisak MagnoStar 135 g/m2 u skladu sa ISO normom 12647/3. Za spektrofotometrijsko mjerenje otisaka korišten je spektrootometar X-rite DTP 41 koji zajedno s programom Monaco Profiler daje L*a*b* vrijednosti za 387 polja. Konačni prikaz trodimenzionalnog gamuta prikazan je u aplikaciji Monaco Gamut Works. Iz dobivenih L*a*b* vrijednosti izračunata je i razlika u obojenju (ΔE) po formuli CIE ΔE2000 za puna polja primarnih boja (CMYKRGB) kao i za 50% rastertonsku vrijednost.

Denzitometrijska mjerenja otisnutih klinova izvršena su dezitometrom X-rite Swatch Book koji radi zajedno uz aplikaciju ColorShop 4.2. Na temelju njih izračunat je i relativni tiskovni kontrast. Na samom kraju je izvršena i vizualna ocjena kvalitete reprodukcije od strane 24 ispitanika.

4. REZULTATI I DISKUSIJA

Rezultati spektrofotometrijskih mjerenja prikazani su na slikama 2 i 3. U njima su konstruirani gamuti HP Indiga i standardnog ofsetnog otiska (pod kutevima gledanja od 0°, 90°, 180° i 270° za sve vrijednosti svjetloća), kao i presjeci gamuta za svjetloću L*=50. Prostorni volumeni prikazani su histogramskom obliku na slici 4.

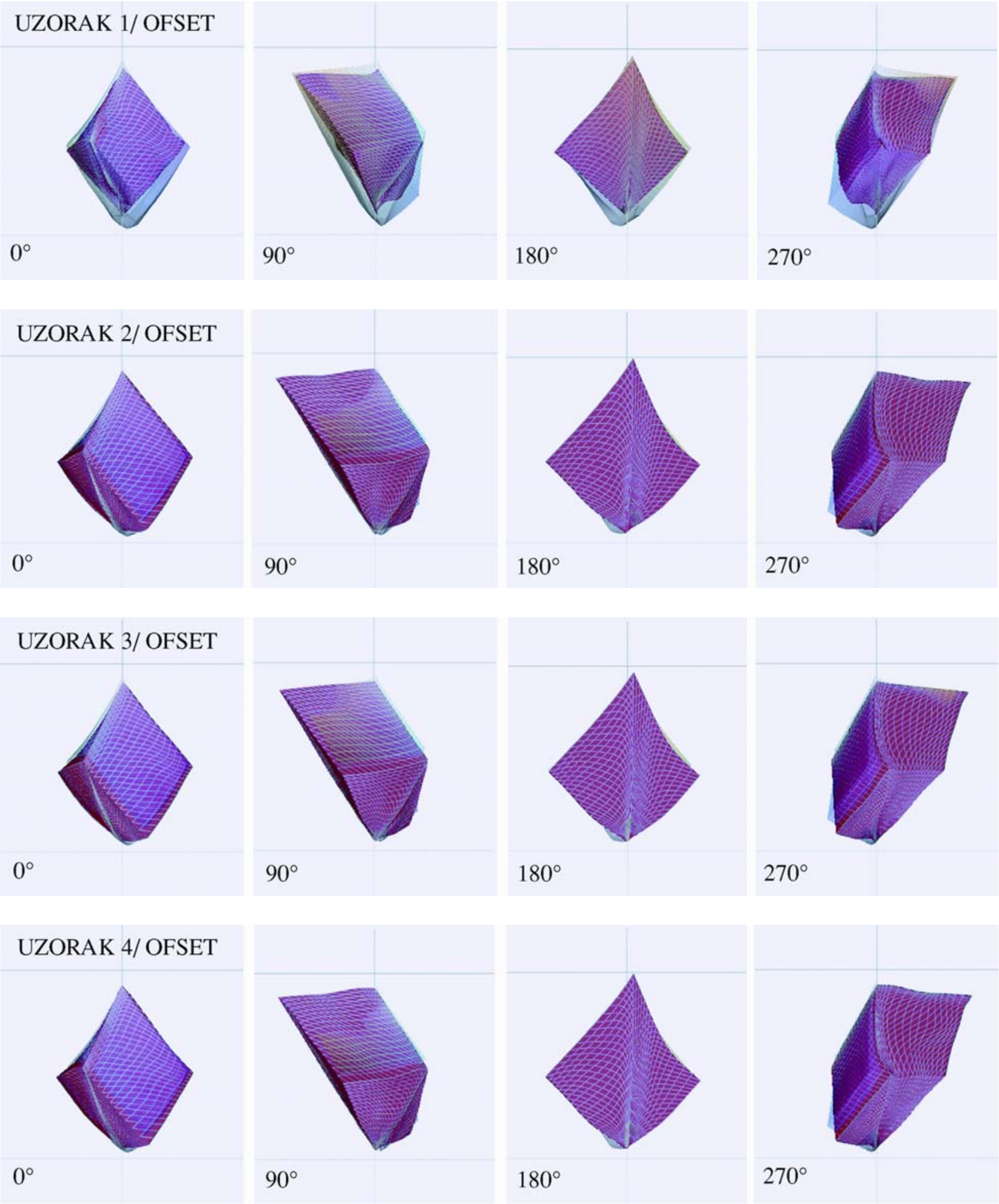

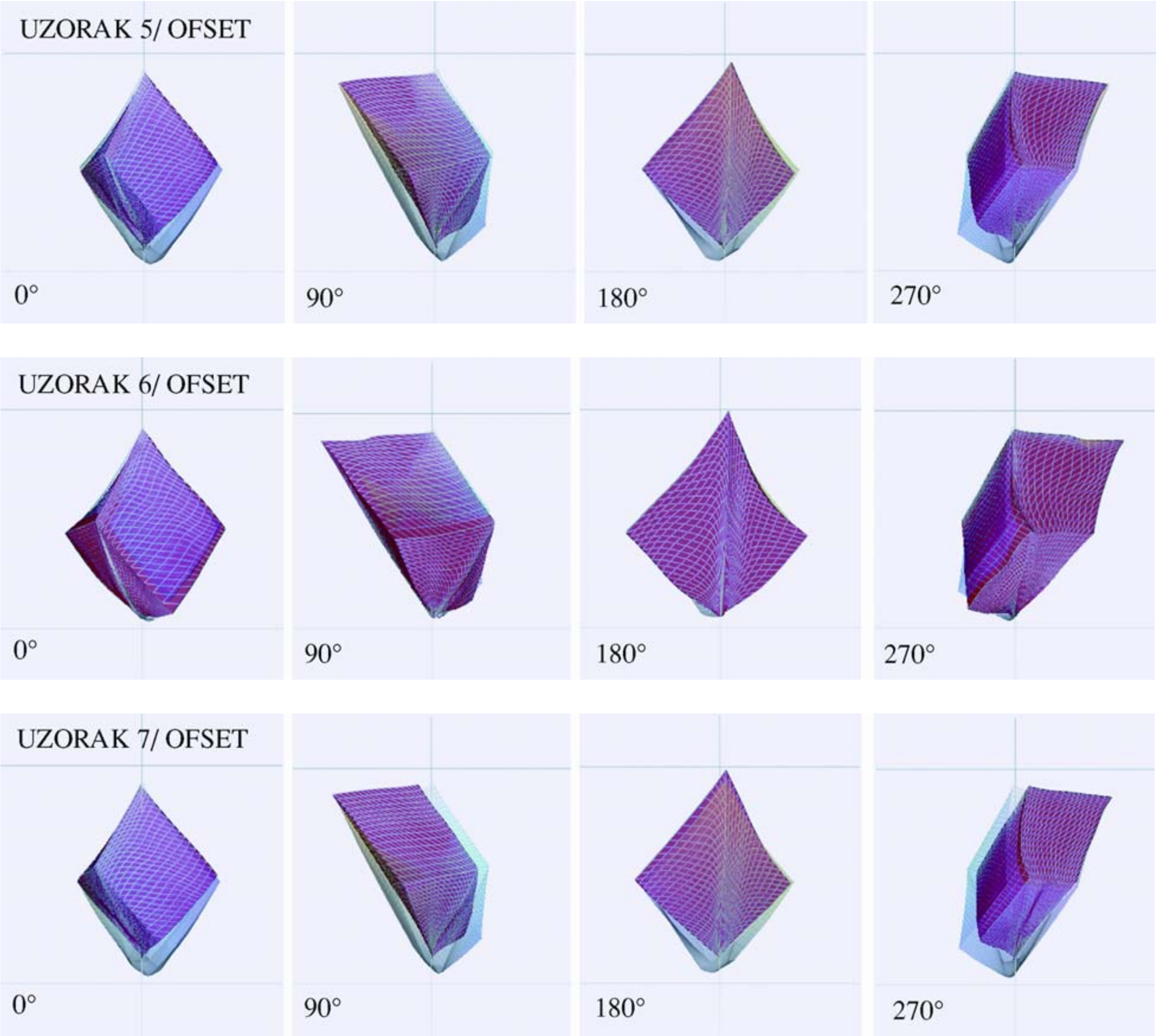

Slika 2. Gamuti reprodukcija HP Indiga i klasićnog ofseta na samoljepljivim medijima i standardnom papiru za umjetnički tisak

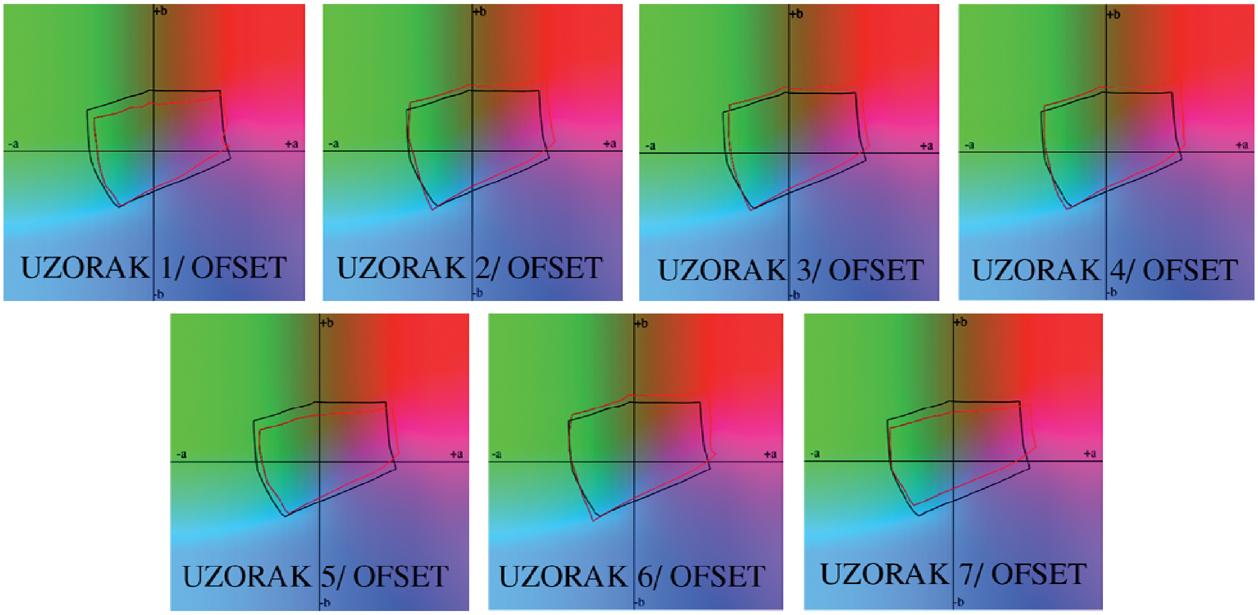

Slika 3 Kromatske vrijednosti a*b* Indigo otisaka i ofsetnog standarda pri svjetloći L*=50

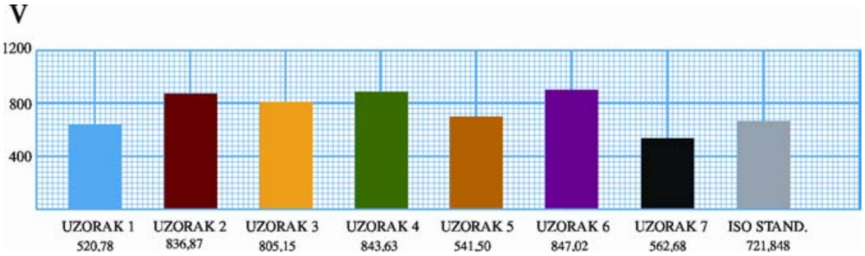

Slika 4. Histogram volumena za samoljepljive uzorke

Rezultati pokazuju da otisci na ”Hight Gloss White” samoljepljivom papiru (uzorak 6) daje najveći raspon obojenja (V=847,02) i bolju reprodukciju od standardnog ofseta. Kvalitetna reprodukcija uoćena je i kod otiskivanja ”MC White (uzorak 4), ”Offset Laser MC White (uzorak 2) i “MC Gloss DI-Of (uzorak 3), koji su neznatno veći od standarda. Ostali samoljepljivi materijali “Crème Verge (uzorak 7), ”Creck-Beck +” (uzorak 5) i ”Offset Vellux Mat” (uzorak 1) reducirani su u odnosu na ofsetni otisak. Iz ovoga je vidljivo da kvaliteta površinskog sloja igra presudnu ulogu pri postizanju kvalitetnog otiska, te što je refleksija i glatkoća izraženija reprodukcija samoljepljivog materijala je bolja.

Oscilacije u obojenju ofsetnog otiska i otisaka na samoljepljivim materijalima promatrane su u punim tonovima, kao i u rasterskom području od 50%, za CMYK i RGB boje. Rezultati su prikazani na slikama 5 i 6.

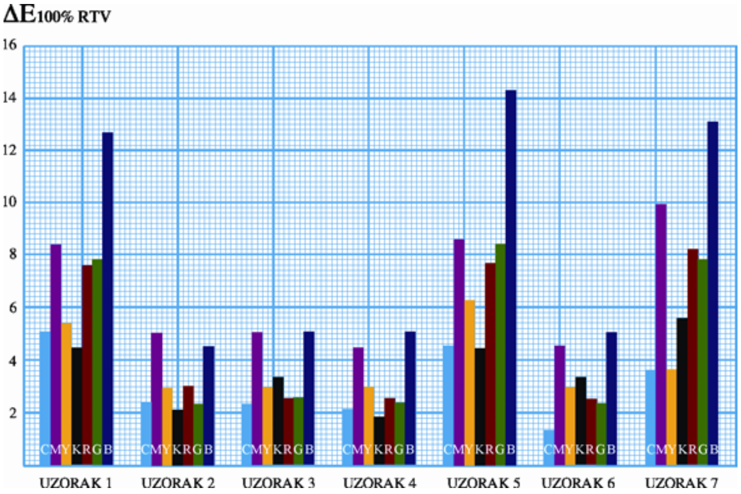

Slika 5. Razlika obojenja ΔE za pune tonove između standardnog ofsetnog otiska i indigo samoljepljivih otisaka

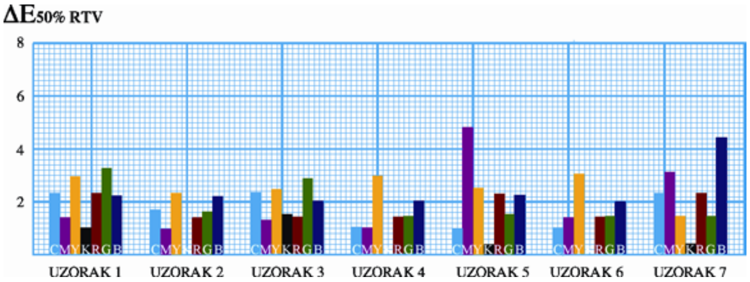

Slika 6. Razlika obojenja ΔE za pune tonove između standardnog ofsetnog otiska i indigo samoljepljivih otisaka

Za pune tonove kod svih samoljepljivih medija najveće oscilacije uočene su pri reprodukciji ljubičasto plave boje, pri čemu se posebno ističu “Creck Back +” (ΔE=14,33), ”Crème Verge” (ΔE=13,12) i ”Offset Laser Velux Mat” (ΔE=12,74). Ostali mediji su usklađeni s prosječnom oscilacijom oko ΔE=2,50.

Pri reprodukciji rastera razlika obojenja između referentnog ofsetnog uzorka i Indigo otisaka na samoljepljivim medijima vrlo je ujednačena. Na svim uzorcima uočava se promjena u tonovima koja se dobivaju reprodukcijom žute. Srednja vrijednost razlike u obojenju æute je ΔE=2,5 te jedino kod ”Crème Verge” materijala (uzorak 7) je najbliža ofsetu (ΔE=1,4). Najveći ekstremi su kod ”Crack-Back +” (uzororak 5) za magentu ΔE=9,8 i “Crème Verge” (uzorak 7) za ljubičasto-plavu ΔE=4,4.

Denzitometrijom se mjeri apsorpcija sa otisnutog sloja bojila, te vrijednošću punog tona i 70% rastertonskog polja izračunavamo relativni tiskarovni kontrast K_{rel}. Što je vrijednost relativnog tiskovnog kontrasta viša kvaliteta otisaka je bolja (slika 7).

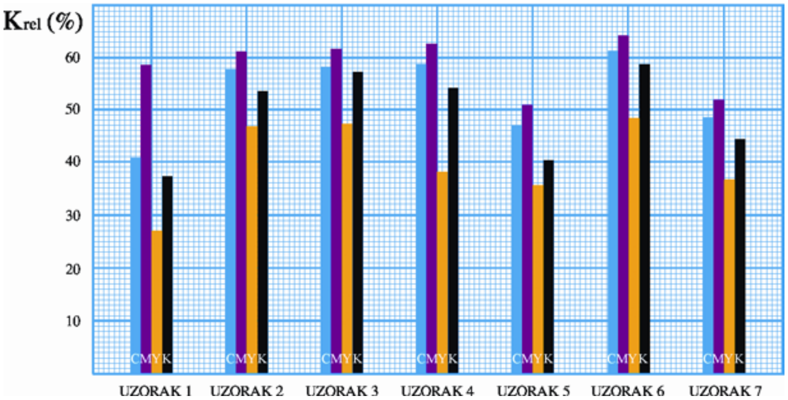

Slika 7. Relativni tiskovni kontrasti za HP Indigo otiske na samoljepljivom materijalu

U svim uzorcima najbolje se reproducira magenta, cijan, crna i na kraju žuta. Lošu reprodukciju žute možemo zahvaliti lošoj pigmentaciji i vodljivosti HP ElectroInka, što je zamjećeno i u drugim radovima (2,11). Samoljepljivi ”High Gloss White” meterijal najbolje se reproducira te kod njega kontrast iznosi K_c=61,6 K_m=64,2 K_y=48,1 I K_k=58,6. Vizualnom ocjenom također su se potvrdila aparativna mjerenja (tablica 2).

Tablica 2. Vizualna ocjena digitalnih otisaka na samoljepljivom papiru

Uzorci	Vellux mat	MC white (sjajni)	MC Gloss	MC white3	Crack-Back	High Gloss white	Creme Verge
Ocjene ispitanika	2	5	4	3	3	4	1
	3	4	5	3	4	5	3
	2	4	5	2	4	5	3
	1	4	4	1	3	5	1
	2	3	4	4	3	5	4
	1	3	3	3	1	5	4
	3	5	5	2	3	3	2
	3	4	4	4	3	5	2
	2	3	3	3	3	4	2
	2	3	4	3	5	5	1
	3	5	5	4	3	5	2
	5	4	4	3	3	4	2
	2	3	3	2	3	4	1
	2	3	4	3	4	5	1
	2	3	3	4	3	5	2
	2	4	3	3	3	4	1
	2	4	3	4	3	4	4
	2	5	3	3	4	5	4
	3	5	4	3	5	5	4
	2	3	3	3	2	4	1
	3	2	4	3	3	3	1
	3	4	5	4	4	5	4
	2	3	4	3	4	5	4
	2	4	3	4	3	4	1
Prosjek	2,33	3,75	3,85	3,08	3,29	4,5	2,29

Promatraći su najbolje ocjenili također ”High Gloss White” samoljepljivi otisak sa prosječnom ocjenom 4,5 ”MC Gloss DI-OF (3,83) i ”Offset Laser MC White” (3,75). Vizualna ocjena ne slaže se kod materijala ”Creck-Back +” i ”Crema Verge”. Iako “Crème Verge” materijal ima bolju vrijednost relativnog tiskovnog kontrasta (K_{rel}=45,2), vizualno je ocjenjen najlošije s prosječnom ocjenom 2,29, dok kod ”Crack Back+” koji ima lošiji kontrast (K_{rel}=43,5) vizualno je bolje ocjenjen (prosječnom ocjenom3,29). Žutost podloge u ovom slučaju utječe na cjelokupni vizualni dojam otiska, što mjerni uređaji naravno ne perceptira.

5. ZAKLJUČAK

Iz ovog rada nameću se slijedeći zaključci:

- elektrofotografskim digitalnim tiskom sa tekućim tonerom moguće je postići veoma kvalitetnu reprodukciju.
- prostorni gamuti HP Indigo samoljepljivih otisaka ”High Gloss White”, ”Offset Laser MC White” , ”MC White” i ”MC Gloss White” u odnosu na referentni ofsetni otisak izvrsno se otiskuju i potpunosti zadovoljavaju. Ostali samoljepjivi materijali (Crème Verage, Creck Back+ i Offset Laser Vellux) na žalost ne zadovovoljavaju.
- Njaviše oscilacije u obojenju kod svih materijala uočene su kod reprodukcije punih tonova ljubičasto-plave boje, dok pri reprodukciji rastera najviše oscilira žuta.
- Vizualnom ocjenom potvrđne su uglvnom denzitometrijska aparativna mjerenja. Jedina oscilacija je uoćena kod žuto obojenog Crème Verge samoljepljivog materijala, kod kojeg vizualna ocjena odudara od vrijednosti relativnog kontrasta, Time se potvrđuje da je vizuala metoda vrlo važna pri određivanju kvalitete grafičkih proizvoda.

LITERATURA

1.M.R. Luo, G. Cui, B. Rigg; The Development of the CIE 2000 Colour-Difference Formula: CIE DE2000, COLOR research and application, 26 (2001). 340 - 349.
2. U.Chatow, R. Samuel, Digital Labels printing, Proccedings of 19th International Conference on Digital Printing Technologies, 2003, 476 - 481.
3. S. Bolanča, Glavne tehnike tiska,Acta Graphica, Zagreb, 1997.
4. S. Bolanča, Suvremeni ofset, ©kolska Knjiga , Zagreb,1991.
5. B. Drannan, Indigo E-print, Adams-Harmon Graphic Press, Chichago 1998.
6. I. Majnarić, Kvaliteta digitalnih otisaka uvjetovana starenjem tiskovne podloge, Magistarski rad, Zagreb, 2004.
7. H. Kiphan. Hand Book of Print Media, Springer, Berlin, 2001.
8. H. M. Fenton, J. F. Romano, On Demand Printing, The Revolution in Digital and Costomised Printing, Pretince Hall, PTR, New Yersy, 1998.
9.F. Grum , C.J. Bartleson, Colour Measurment, Academic Press, New York, 1987,
10. W. Walenski, Das Papier das Buch, Verlag Beruf + Schule, 1994.
11. I. Majnarić, I. Bolancć, Z. Bolanća, M. Milković, Condition in Digital Printing of Packaging on Print Quality, IS&T Production Printing Conference, Amsterdam 2005.

10. Savjetovanje o materijalima, tehnologijama, trenju i trošenju
10. Conference on Materials, Processes, Friction and Wear
MATRIB'05, Vela Luka, 23-25.06.2005.

SAVOJNA SVOJSTVA PROFILA OD ALUMINIJSKE PJENE

BENDING PROPERTIES OF ALUMINIUM FOAMS PROFILES

Dr.sc. Gojko Marić[1)] gojko.maric@fsb.hr
Ivan Kramer, dipl.ing.[1)] ivan.kramer@fsb.hr
Mr.sc. Željko Alar[1)] zeljko.alar@fsb.hr

1) Faculty of Mechanical Engineering and Naval Architecture
University of Zagerb
I. Lucica 5, 10000 Zagreb, Croatia

Sažetak: Kao što je već dobro poznato, metalne pjene su porozni, ćelijasti materijali s vrlo nejednolikom strukturom. Upravo ta struktura značajno utječe na njihova mehanička svojstva. Glavni cilj ovog rada bio je ispitivanje savojnih svojstva različitih profila napravljenih od aluminijske pjene s zatvorenim ćelijama. Pri tome su varirani oblik profila i gustoća. Prvi korak bio je izrada profila od aluminijske pjene postupkom plinom oslobođenih čestica rastvorenih u polučvrstoj fazi (Alulight postupak). Svi profili imaju jednaku površinu presjeka i jednaku duljinu. Za samo ispitivanje koristila se metoda savijanja u tri točke. Ispitivanjem su dobivene vrijednosti savojne sile koja također ovisi o obliku profila i gustoći. Kao krajnji rezultat pokazano je kako savojna svojstva profila od aluminijske pjene ovise o njihovom obliku i gustoći.

Ključne riječi: aluminijske pjene, profili, savojna svojstva

Abstract: It is well known that metal foams are porous, cellular materials with very nonuniform structure. In fact, that structure significantly affects metal foams mechanical properties. Main goal of this paper was testing of bending properties of the various profiles made from aluminium foam with closed cells. During the testing next parameters were varied: shape of the profile and foam density. The first step was the production of aluminium foam profiles with Gas releasing during melting of solid foamable precursor (Alulight) process. Cross section area and length of the profiles are equal. The three point bending method was used for investigation. With this testing were obtained bending forces which also depend on shape of the profile and foam density. As a final result the effect of the aluminium foam profiles shape and density on bending properties was presented.

Keywords: aluminium foams, profiles, bending properties

1. UVOD

Metalne pjene spadaju u skupinu novih i visokoporoznih metalnih materijala. Prema strukturi one se dijele na dvije osnovne vrste: metalne pjene s zatvorenim i otvorenim ćelijama. Danas su najzastupljenije aluminijske pjene s zatvorenim ćelijama. Postoji nekoliko razloga zašto metalne pjene nisu još uvijek šire zastupljene u različitim granama industrije, a to su: nepravilna struktura može u velikoj mjeri utjecati na svojstva gotovog proizvoda, gustoća nije jednoliko raspoređena po cijelom volumenu komada, u komadu postoje zone s različitim veličinama pora, stijenke ćelije često sadrže više ili manje pukotina. U ovom se radu željelo ispititi kako oblik i gustoća različitih profila od aluminijske pjene s zatvorenim ćelijama utječu na savojna svojstva.

2. PROIZVODNJA PROFILA OD ALUMINIJSKE PJENE

Prvi korak je bila proizvodnja profila različitih oblika. Profili su proizvedeni tzv. Alulight postupkom. Aluminijska pjena nastaje uslijed oslobađanja plina tijekom zagrijavanja prekursora. Prekursor je poluproizvod koji nastaje miješanjem prahova aluminijske legure i 0,5-1% dodatka koji pospješuje pjenjenje (najčešće je to TiH_2). Nakon toga se mješavina hladno kompaktira i ekstrudira na temperaturi 400-480°C. Prilikom zagrijavanja na temperaturu nešto višu od tališta aluminija dodatak oslobađa plin koji uzrokuje stvaranje pjene. Pjena je stabilizirana zbog postojanja sitnih čestica oksida. Kako bi se dobio točno određeni oblik profila cijeli proces se odvija u čeličnim kalupima. Proizvedena su tri različita profila: kvadratni profil (**K**), T-profil (**T**) i I-profil (**I**). Svi profili su napravljeni od pjene legure **AlSi10**. Slika 1 prikazuje dimenzije poprečnog presjeka profila.

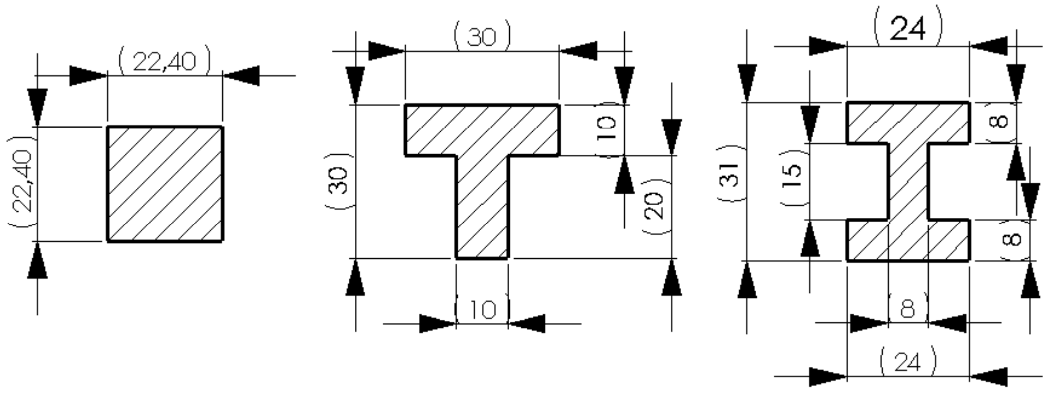

Slika 1. Dimenzije poprečnih presjeka profila.

Dimenzije su odabrane tako da svi profili imaju jednaku površina presjeka koja iznosi oko 500 mm^2. Duljina profila iznosi 200 mm. Ukupno je proizvedeo šest profila.

Slika 2 prikazuje kretanje temperature u peći prilikom proizvodnje profila od aluminijske pjene. Kalup se stavlja u peć koja je zagrijana na temperaturu 710-740°C. Nakon toga dolazi do opadanja temperature do otprilike 640-660°C i daljnjeg laganog rasta do 700°C. Vrijeme držanja kalupa u peći iznosi 600-840 sekundi.

Tablica 1 sadrži slijedeće podatke o profilima: mase, poroznost i vrijeme proizvodnje.

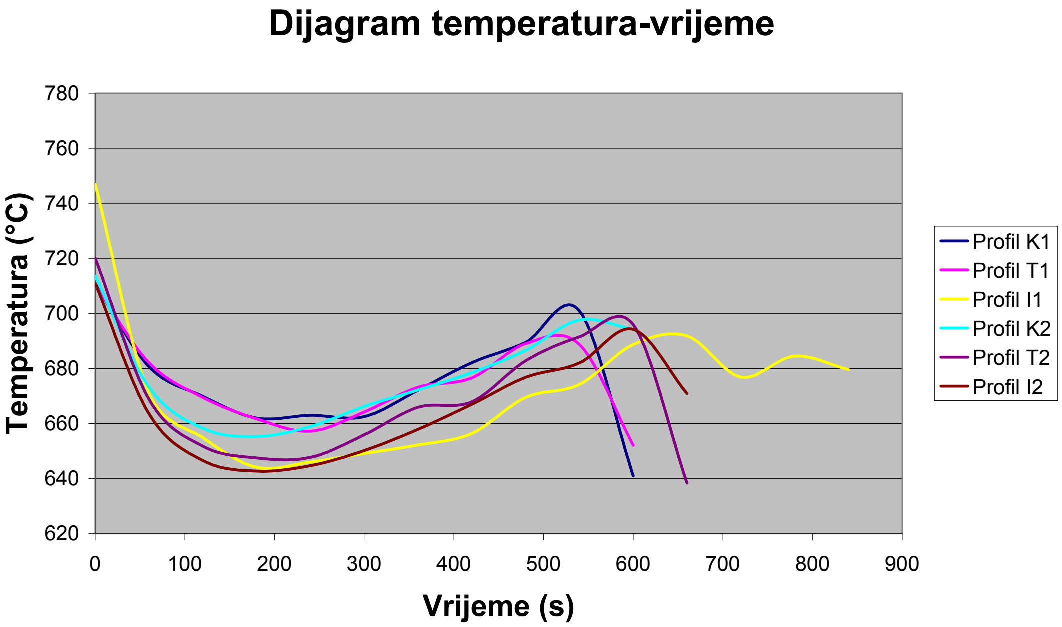

Slika 2. Dijagram temperatura-vrijeme prilikom proizvodnje profila u peći.

Tablica 1. Masa, poroznost i vrijeme proizvodnje profila od aluminijske pjene.

Profil	Masa	Poroznost	Vrijeme proizvodnje
K1	56,50 g	79,07 %	600 s
T1	58,10 g	78,48 %	600 s
I1	71,00 g	73,70 %	840 s
K2	82,50 g	69,44 %	660 s
T2	47,70 g	82,33 %	720 s
I2	88,90 g	67,07 %	660 s

Na slijedećoj slici se vide profili proizvedeni od pjene legure AlSi 10.

Slika 3. Profili od aluminijske pjene.

3. ISPITIVANJE SAVOJNIH SVOJSTAVA

Ispitivanje savijanjem provedeno je u Laboratoriju za ispitivanje mehaničkih svojstava (LIMS) FSB-a u skladu s normom DIN EN ISO 7438. Za ispitivanje primjenjen je uređaj slijedećih specifikacija:

- proizvođač: ZWICK, Njemačka;
- tip: ZD 50;
- mjerno područje: 0 – 5 kN;
- klasa: 1.

Temperatura okoline pri ispitivanju je bila u granicama 20±2°C. Primjenjena je metoda savijanja u tri točke pri čemu je razmak oslonaca bio 100 mm. Svi profili su opterećivani savojnom silom pomoću istog trna te konstantnom brzinom opterećivanja. Tijekom ispitivanja praćene su vrijednosti sile i progiba. Na slici 4 su dijagramski prikazani rezultati ispitivanja ovisnosti između sile savijanja i progiba za svaki profil. Ovdje je potrebno napomenuti da je ispitivanje teklo do maksimalne sile savijanja.

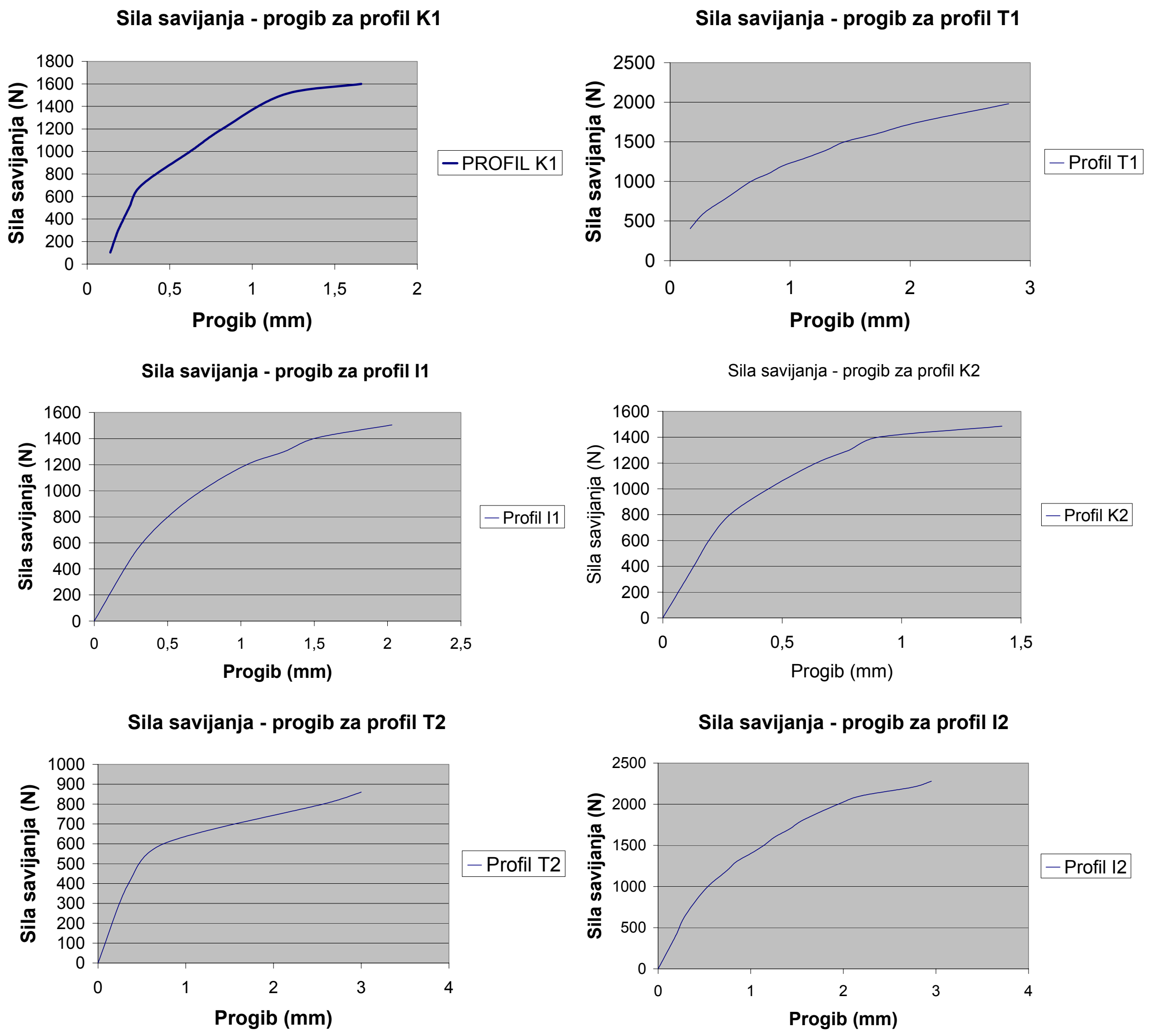

Slika 4. Odnos sile savijanja i progiba za sve profile.

Slika 5 prikazuje I profil na kidalici i na njoj je vidljiv početak loma na vlačno opterećenoj zoni.

Slika 5. Početak loma I profila.

Slika 6 prikazuje presjeke profila na kojima je došlo do loma.

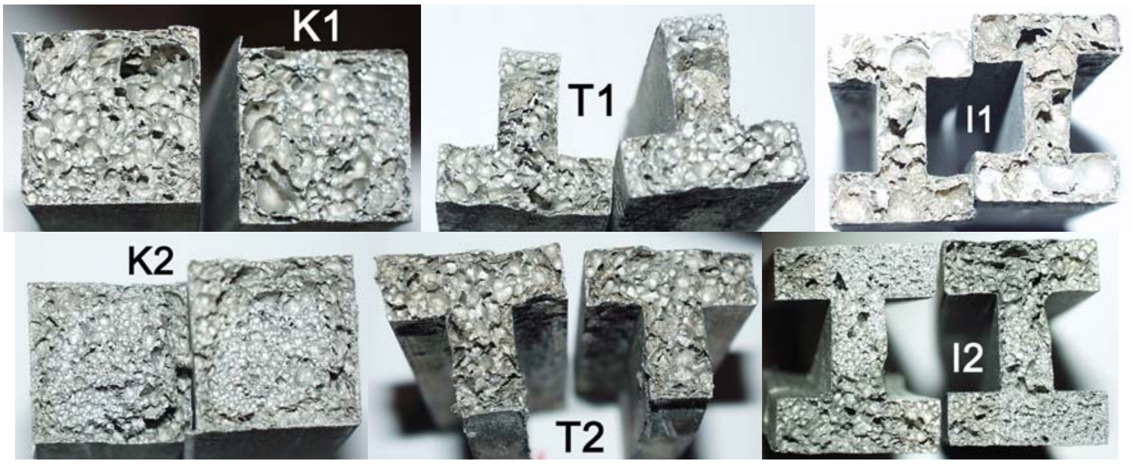

Slika 6. Prijelomne površine profila.

4. ZAKLJUČAK

- temperature pri kojima se proizvode profili od aluminijske (AlSi10) pjene kreću se u rasponu 660-710°C. Vremena proizvodnje se kreću u rasponu 600-840 sekundi. Pri tome je vrlo teško povezati oblik profila, poroznost i vrijeme proizvodnje. U slučaju kvadratnog profila vrijeme proizvodnje komada manje poroznosti je više, dok je u slučaju T i I profila to je obrnuto.
- savojna ispitivanja u 3 točke su pokazala kako je najveća sila savijanja od 2280 N postignuta u slučaju I profila s poroznošću 67,07%. Nakon toga slijedi T profil s poroznošću 78,48% i silom 1980 N, K profil s poroznošću 79,07% i silom 1600 N, I profil s poroznošću 73,70% i silom 1550 N, K profil s poroznošću 69,44% i silom 1485 N i T profil s poroznošću 82,33% i silom 860 N.

- vidljivo je veliko rasipanje vrijednosti maksimalne sile savijanja. Ukoliko promatramo svaki oblik profila posebno vidi se kako K profil veće poroznosti ima bolja savojna svojstva, T profil veće poroznosti ima lošija savojna svojstva i I profil veće poroznosti ima lošija svojstva.
- ako promatramo sve profile najbolja svojstva ima T profil, a nakon njega je I profil dok najlošija svojstva ima K profil.
- kao što je već i prije napomenuto raspored gustoće i veličine pora u profilima je vrlo nejednolika. Ukoliko je u zoni savojnog opterećenja veća poroznost pretpostavlja se kako će taj uzorak imati lošija savojna svojstva.
- potrebna je izrada većeg broja uzoraka kako bi se dobila nešto detaljnija slika o savojnim svojstvima aluminijskih pjena.

5. LITERATURA

1. T. Filetin, I. Kramer, G. Marić: Metalne pjene, Hrvatsko društvo za materijale i tribologiju, Zagreb, 2003
2. M.F. Ashby, A.G. Evans, N.A. Fleck, L.J. Gibson, J.W. Hutchinson, H.N.G. Wadley: Metal foams: a design guide, Butterworth-Heinemann, Woburn, USA, 2000.
3. F. Simančik, J. Kovačik, N. Minarikova: Bending properties of foamed aluminium panels and sandwiches, MRS Symposium Proceedings (Ed. by. D.S. Schwartz, D.S. Shih, A.G. Evans and H.N.G. Wadley, Vol. 521, Materials Research Society, Warrendale, Pennsylvania, 1998., p. 91
4. L.J. Gibson, M.F. Ashby: Cellular solids: structure and properties (Second Ed.), Cambridge University Press, Cambridge, 1997.

10. Savjetovanje o materijalima, tehnologijama, trenju i trošenju
10. Conference on Materials, Processes, Friction and Wear
MATRIB'05, Vela Luka, 23-25.06.2005.

ISTRAŽIVANJE ODNOSA KAKTERISTIKA GAMUTA I INTENZITETA DOŽIVLJAJA KVALITETE REPRODUKCIJE

RESEARCH OF RELATIONSHIP OF GAMUT CHARACTERISTICS AND EXPERIENCE INTENSITY OF QULITY REPRODUCTION

N. Mrvac*, M. Milković, I. Zjakić***
* Faculty of Graphic Arts, University of Zagreb, Getaldićeva 2, 10000 Zagreb
** Graphic Institution of Croatia, Radnička cesta 210, 10000 Zagreb

Sažetak: Različiti mediji, koje u svakodnevnom životu koristimo za distribuciju informacija, posjeduju ograničenja, koja se odnose na set informacija koje mogu obuhvatiti i prezentirati. Vizualni mediji limitirani su količinom informacija o boji (i njenim karakteristikama) koje mogu prikazati. Isto vrijedi i za medije koje koristimo u procesu grafičke reprodukcije (skeneri, digitalne kamere, zasloni računala, razni pisači, digitalni i klasični tiskarski strojevi).

Sukladno tome na intenzitet doživljaja kvalitete grafičke reprodukcije utječe niz parametara među kojima su u prvom redu parametri vezani uz karakteristike gamuta.

Ovim radom ustanovljeno je da su vizualne ocjene kvalitete otisaka u korelaciji s određenim karakteristikama gamuta, čime je potvrđena direktna veza između doživljaja kvalitete grafičke reprodukcije i karaketristika gamuta.

Ključne riječi: gamut, prostor boja, otisak, grafička reprodukcija

Abstract: Different media, used in everyday life for the information distribution have limitations that refer to the information set which they can comprise and present. Visual media are limited by the information quality about colour and its characteristics which they can present.

The same refers to the media which we use in the process of the graphic reproduction (scanners, digital cameras, monitors, different printers, digital and classic printing machines).

According to that the intensity of experience of graphic reproduction is influenced by a series of parameters among which there are first of all the parameters connected to the gamut characteristics.

It is found out in this work that visual evaluations of print quality are in correlation with the defined gamut characteristics which proves the direct connection between the quality experience of the graphic reproduction and the gamut characteristics.

Key words: gamut, colour space, print, graphic reproduction

1. Uvod

Tijekom povijesti točnost reprodukcije boja u većini slučajeva temeljila se na metodama koje su uglavnom bile zasnovane na metodama pokušaja i pogreške. Situacija se u tom smislu počela mijenjati tek u ovom stoljeću napretkom znanosti i tehnologije, što je konačno rezultiralo napretkom raznih tehnologija prikaza i reprodukcije originala i njegovih boja.

Reprodukcija originala u boji, prema današnjim CIE interpretacijama, jest proces koji uključuje četiri osnovna elementa: karakterizaciju medija, modeliranje izgleda boje, poboljšanje slike i mapiranje gamuta. Prva dva navedena elementa procesa grafičke reprodukcije (karakterizacija medija i modeliranje izgleda boja) bila bi u načelu dovoljna za reprodukciju originala u boji kada bi mediji bili u mogućnosti reproducirati uvijek isti set i opseg boja te kada proces grafičke reprodukcije ne bi uključivao kategoriju koju nazivamo namjera poboljšanja slike (vjernost, točnost, ugoda, dizajnerski zahtjevi i sl.). S obzirom da to u realnoj grafičkoj proizvodnji uglavnom nije čest slučaj nužno je odrediti proceduru (algoritam) prevođenja gamuta (sveukupni opseg informacija o boji).

Kako bi se u čim većoj mjeri prevladale razlike između raspona boja koje se mogu dobiti s obzirom na različite medije te kako bi se proces grafičke reprodukcije u čim većoj mjeri standardizirao CIE komisija je 2001. godine definirala četiri osnovne metode renderiranja boja koje između ostalog sadrže i definirane procedure mapiranja gamuta.

Sukladno navedenome određeni su i ciljevi ovog rada koji su orijentirani prema tome kako bi se u čim većoj mjeri razjasnili i odredili međuodnosi procedura mapiranja gamuta te konačnog doživljaja intenziteta kvalitete grafičkog proizvoda.

2. Teoretski dio

2.1. Pojam gamuta

Različiti mediji, koje u svakodnevnom životu koristimo za distribuciju informacija, posjeduju ograničenja, koja se odnose na set informacija koje mogu obuhvatiti i prezentirati. Vizualni mediji, limitirani su količinom informacija o boji koje mogu prikazati.

Isto vrijedi i za medije koje koristimo u procesu grafičke reprodukcije (skeneri, digitalne kamere, zasloni računala, razni pisači, digitalni i klasični tiskarski strojevi). Taj navedeni ograničeni skup informacija o boji za dani mediji, definiran je kao pojam koji nazivamo gamut. Matematički opis pojma gamuta u grafičkoj reprodukciji (na otisku) dan je sljedećim relacijama:

Ako je Ω_{CIE} opseg numeričkih vrijednosti u određenom selektiranom području CIE prostora boje i ako je Ω_{otisak} numerički opseg kontrolnih vrijednosti boje medija, tada set:

$$G = \{ t \in \Omega_{CIE} \mid \exists c \in \Omega_{otisak} \ za \ kojeg \ vrijedi \ F_{ured.}(c) = t \}$$

određuje gamut navedenog uređaja (medija). Slično je i kada se radi o komplementarnom skupu:

$$G^c = \{ t \in \Omega_{CIE} \mid \nexists c \in \Omega_{otisak} \ za \ kojeg \ vrijedi \ F_{ured.}(c) = t \}$$

gdje definiramo boje koje se nalaze izvan gamuta *Gc* navedenog uređaja (medija).

Oznaka $F_{ured.}$ predstavlja funkciju koja vrši transformaciju iz zavisnog prostora boje uređaja/ medija u CIE prostor boja, oznaka *t* predstavlja informaciju o boji u CIE prostoru, a oznaka *c* predstavlja njezinu transferiranu vrijednost u zavisnom prostoru boja uređaja/medija.

Boje koje su unutar G^c (boje izvan gamuta), a ne mogu se reproducirati na mediju/uređaju, moraju se smjestiti unutar gamuta, koji dani uređaj/medij može prikazati. Taj postupak smještanja boja iz jednog gamuta u drugi gamut različite veličine (opsega i karakteristika) naziva se mapiranje gamuta. Za boje koje su unutar gamuta provodi se mapiranje između kontrolnih vrijednosti uređaja/ medija i CIE prostora boje.

2. 2. Mapiranje gamuta

Kod reprodukcijskog procesa u grafičkoj tehnologiji, gamut originala (scene ili skenerskog predloška) u pravilu je različit (veći) od gamuta otiska odnosno reprodukcije, što izravno dovodi do zaključka da se pojedine boje originala neće moći reproducirati na otisku. Metoda preslikavanja (dodjeljivanja) pojedinih informacija o boji iz jednoga gamuta u drugi (manji ili veći) gamut naziva se mapiranje gamuta.

Ciljevi mapiranja gamuta mogu se u osnovi sažeti u težnji osiguravanja korespondentnosti sveukupnoga doživljaja boja između dva gamuta (originala i reprodukcije), uz kompenzaciju nejednakosti u veličini, obliku i položaju boja između gamuta originala i njegove reprodukcije. Razlike između gamuta, za koje se prilikom postupka mapiranja mora osigurati korespodentnost u sveukupnom doživljaju mogu biti u: veličini (opsegu) između dvaju gamuta, obliku opsega (obliku granica gamuta) te lokaciji tih gamuta unutar uniformiranog CIE prostora boja.

Uzmemo li u obzir jednu od definicija pojma “slika” koji kaže da je slika neke prirodne scene u osnovi njezin korespondirajući dvodimenzionalni vizualni stimulus (podražaj), sastavljen od elementarnih objekata (pixela ili rasterskih točkica), koji su svaki za sebe definirani veličinom, te vlastitom informacijom o boji, tada analizirajući osobine ljudskoga vizualnog sustava (koji je u osnovi nelinearan) možemo zaključiti sljedeće: ukoliko se informacije o boji elementarnih objekata slike (pixela ili rasterskih točkica) sveukupno u malom iznosu pomaknu (izmijene) u odnosu na original, ali se ujedno zadrže istovjetni međusobni unutarnji odnosi (relacije) između informacija o boji tih elementarnih objekata na slici, reprodukcija će zadržati doživljajna svojstva gotovo identična orginalu.

Iz navedenoga, jasno se očituje jedna od nelinearnih karakteristika ljudskoga oka koju svakodnevno upotrebljavamo na grafičkim otiscima, temeljena na činjenici da je za naš naučeni vizualni sustav, prilikom promatranja slike neke scene, važniji međusobni odnos (relacije između boja (informacija o boji elementarnih objekata) prisutnih na slici, nego njihove precizne vrijednosti (točnost u odnosu na orginal).

U daljnjim istraživanjima ljudskoga vizualnog sustava, potvrđena je teza koja tvrdi da je ljudski doživljaj koji ocjenjuje odstupanja reprodukcije od originala manji kada se svim elementarnim objektima (pixelima i rasterskim točkicama) na slici, informacija o boji promijeni jednolično, u istom iznosu u određenom smjeru (smjeru tona, smjeru zasićenja ili smjeru svjetline), negoli kada se samo malom broju elementarnih objekata, informacija o boji promijeni u istom iznosu ali nasumično (u različitim smjerovima tona, zasićenja ili svjetline) [1].

Nadalje, nelinearnost se ljudskog vizualnog sustava naročito očituje u percepciji kod odnosa između intenziteta i svjetline, te u percepciji između različitih raspona tonova (gamuta) različitih primara koji generiraju pojam iste scene ili slike.

Nelinearnost u odnosu između intenziteta (koji predstavlja broj fotona koji dospijevaju do osjetilnih stanica oka) i svjetline (koja je ustvari osjećaj odnosno doživljaj koji se generira u našemu mozgu na osnovi različitih intenziteta) je takva da npr. kada se za dvostruko poveća intenzitet nekoga svijetla, ljudski mozak to ne percipira kao dvostruko svjetlije, odnosno nema linearnog odnosa između intenziteta i svjetline.

Slično se događa i kod različitih gamuta koji predstavljaju istovjetnu sliku ili scenu. Naš mozak u mnogo slučajeva neće percipirati, barem ne značajno, razliku između dvaju različitih

gamuta koji predstavljaju istu scenu (original i reprodukcija), ako je proces mapiranja gamuta iz većeg u manji proveden na jedan od ispravnih načina. Sve prethodno navedeno upućuje na činjenicu, da transfer (konverzija) informacija o boji, iz većeg gamuta u manji, na ispravan i sustavan način (ispravnom tehnikom mapiranja), može rezultirati time da reprodukcija i original imaju vrlo sličan doživljaj prikaza u ljudskom mozgu.
Analiziravši prethodno opisano, jasno je da mnogi parametri utječu na ispravno mapiranje gamuta, jedne veličine u gamut, druge veličine. Međutim, određeni broj dolje navedenih ciljeva koji se žele ostvariti u procesu mapiranja, a koji će omogućiti maksimalnu korespondenciju između orginala i reprodukcije, mogli bi se izdvojiti kao najvažniji [7]:

- *očuvanje odnosa unutar krivulje reprodukcije akromatskih tonova*
- *očuvanje kontrasta (odnosa između svijetlih i tamnih tonova)*
- *minimaliziranje pomaka tona*
- *povećanje zasićenja je dozvoljeno, ali i poželjno*

2.3. Namjera prikaza boje

Namjera prikaza boje je željeni odnos između informacije boje u originalnom i reprodukcijskom mediju. Budući da postoje brojna rješenja u međumedijskoj reprodukciji, različite namjere kod reprodukcije mogu biti praćene različitim mapiranjima gamuta. Najčešće namjere su točnost i ugodnost, ali je moguće definirati i druge specifične zahtjeve. Na osnovi prethodnih dviju klasifikacija, a s ciljem standardizacije, 2001. godine ICC je definirao i standardizirao četiri osnovna načina mapiranja gamuta s obzirom na namjeru (točnost) prikaza informacije o boji te ih nazvao sljedećim imenima:

- *Perceptualno*
- *Relativno kolorimetrijsko*
- *Saturacijsko*
- *Apsolutno kolorimetrijsko*

Pojam namjere prikaza boje (color rendering intent) odnosi se na postupak prevođenja (mapiranja) gamuta originala u gamut reprodukcije, ovisno o namjeri na koji se način (kojom točnošću i sa kojim karakteristikama) žele reproducirati boje u gamutu reprodukcije.

2.3.1. Perceptualno renderiranje

Perceptualno renderiranje je s obzirom na tip mapiranja gamuta linearna kompresivna tehnika, sa smjerom mapiranja orijentiranim prvenstveno prema svjetlini, a zatim prema kromatičnosti i tonu. Kod perceptualnog renderiranja sve boje originalnog gamuta prevode se tako da postanu dio gamuta reprodukcije, odnosno komprimiraju se tako da u potpunosti ili gotovo u potpunosti stanu u gamut reprodukcije. Takvim prevođenjem, sve boje originalnoga gamuta, pa čak i one koje su se istovjetne mogle prevesti u reprodukcijski gamut, izmijenjene su na izlazu, međutim os svjetline (raspon od najsvjetlijeg do najtamnijeg), kao i međusobni odnos između tonova su sačuvani, odnosno zadržani su relativni odnosi među njima.
Kod perceptualnoga renderiranja, točnost kolorimetrijskih karakteristika boje, izmijenjena je u korist ukupnog perceptualnog doživljaja, koji se temelji na zadržavanju relativnoga odnosa među bojama, pa s aspekta točnosti reprodukcije, perceptualna metoda zadovoljava kriterije ekvivalentne ili korespondirajuće reprodukcije.

2.3.2. Saturacijsko renderiranje

Saturacijsko renderiranje je s obzirom na tip mapiranja gamuta kombininacija nelinearne kompresivne i odrezujuće tehnike, mada se u pojedinim područjima koja se nalaze uz granice gamuta primjenjuje i ekspanzivna tehnika. S obzirom na smjer mapiranja, saturacijsko renderiranje orijentirano je isključivo prema kromatičnosti.

Kod saturacijskog renderiranja, sve boje koje nisu dio gamuta reprodukcije obično se preslikavaju u najbliže korespondirajuće boje istog zasićenja, dok svjetlina i ton mogu biti promijenjeni. Boje koje se nalaze unutar granica reprodukcijskog gamuta, pomiču se prema granicama gamuta kako bi se dodatno povećalo zasićenje.

Kolorimetrijska točnost između originala i reprodukcije, kod saturacijskog renderiranja može čak u određenim slučajevima biti i zadržana, ali nije prioritet. S obzirom na točnost, saturacijska metoda ima odlike koje se u određenoj mjeri traže kod preferirane (željene) reprodukcije.

2.3.3. Relativno kolorimetrijsko renderiranje

Relativno kolorimetrijsko renderiranje je, s obzirom na tip mapiranja gamuta, odrezujuća tehnika kombinirana u pojedinim područjima sa linearnom kompresivnom, a s obzirom na smjer je simultana trodimenzionalna, s posebnim algoritmima orijentiranim prema svjetlini.

Kod relativnog kolorimetrijskog renderiranja, sve boje koje pripadaju gamutima i originala i reprodukcije ostaju nepromijenjene. Boje koje nisu dio gamuta reprodukcije, mapiraju se u najbliže boje iste svjetline (ovisno o crnoj i bijeloj točki), ali različitog zasićenja, koje se nalaze na granicama gamuta reprodukcije.

Mapiranje više različitih boja različite svjetline u jednu vrijednost svjetline, koje se provodi u području izvan gamuta reprodukcije, uzrokuje poremećaje (gubitak vrijednosti) na osi svjetline, pa je za relativno kolorimetrijsko renderiranje karakteristično da reprodukcije mogu izgledati tamnije. Međutim, metoda relativnog kolorimetrijskog renderiranja pokušava navedene probleme umanjiti točnom reprodukcijom crne i bijele točke.

S obzirom na točnost, relativnoj kolorimetrijskoj metodi renderiranja boja najbliža je kolorimetrijska reprodukcija.

2.3.4. Apsolutno kolorimetrijsko renderiranje

Apsolutno kolorimetrijsko renderiranje, s obzirom na tip mapiranja, također je odrezujuća tehnika kombinirana s linearnom kompresivnom, a s obzirom na smjer je simultana trodimenzionalna. Kod apsolutnog kolorimetrijskog renderiranja, sve boje koje pripadaju gamutima i originala i reprodukcije ostaju nepromijenjene. Boje koje nisu dio gamuta reprodukcije, mapiraju se u najbliže boje različitog zasićenja, koje se nalaze na granicama gamuta reprodukcije. Osim što dolazi do gubitka tonova i svjetline u području izvan gamuta reprodukcije, kod apsolutnog kolorimetrijskog renderiranja javlja se i drugi problem vezan uz akromatsku os svjetline, a odnosi se na različite vrijednosti crne i bijele točke na gamutu originala i gamutu reprodukcije.

Kod “cross-media” reprodukcije, koja se odvija u procesu gra. čke proizvodnje, gdje imamo aditivne (grafička priprema) i suptraktivne medije (tisak), dolazi do problema vezanog uz crnu i bijelu točku [6].

Aditivni mediji odnosno njihovi primari ne mogu utjecati na predefinirane vrijednosti crne točke (fosfori bez podražaja), a suptraktivni mediji na vrijednost bijele točke (boja tiskovne podloge). Navedeno uzrokuje da se svi odnosi između tonova i svjetlina na slici ne mijenjaju u ovisnosti o bjelini podloge, što rezultira netočnim prikazivanjem svijetlih tonova.

3. Eksperimentalni dio

U istraživanju, su korišteni otisci izrađeni na dvije vrste kolor strojeva za digitalni tisak, koji svoje principe rada temelje na suhom, odnosno tekućem (ink-jet) toneru. Otisci izvedeni suhim tonerom, producirani su na Xerox DocuColor 2060 stroju za digitalni tisak, upravljanim Xerox EFI Fiery workflow-om, u sklopu kojeg je i aplikacija za rastriranje (RIP), te aplikacija za CM (Xerox EFI ColorWise Pro CMS).

Otisci izvedeni tekućim tonerom, producirani su na Canon W2200 stroju za digitalni tisak, upravljanim Heidelberg MetaDimension workflow-om, u sklopu kojega je također i aplikacija za rastriranje, te aplikacija za upravljanje bojama (Heidelberg Meta Dimension CMS). Oba stroja su za vrijeme provedbe procesa istraživanja bila redovito održavana i u potpunosti u ispravnom radnom stanju.

Za provedbu procesa otiskivanja, kao tiskovna podloga korišten je za oba stroja istovjetan materijal - višestruko obostrano premazani sjajni papir za umjetnički tisak, visokoga stupnja bjeline (izraženo u CIE L*a*b* vrijednostima: L* = 95.8, a* = 0.2 i b* = 0.3), gramature 135 g/m^2, formiran na veličinu 350 x 480 mm.

Papir je prije provedbe procesa otiskivanja bio u istovjetnoj prostoriji klimatiziran u periodu od 48 sati, na zadane ambijentalne uvjete (temperatura 23^0 C, relativna vlažnost zraka 55%).

Bojila odnosno toneri, koji su upotrebljavani prilikom otiskivanja, nose oznake Xerox 13R90142, odnosno Canon BC1302.

Testna forma dizajnirana je na poseban način iz standardnih ISO i ECI kako bi se dobili uzorci na kojima je moguće izmjeriti gamut te koji mogu poslužiti za vizualna ispitivanja. Kreirana je u aplikaciji Adobe Photoshop, u tri različita modela boja (RGB, CMYK i Lab) koji se mogu koristiti za potrebe grafičke proizvodnje. Sve varijante zapisane su (pohranjene) u TIF formatu (Taged Image File Format), sa razlučivošću od 600 tpi.

Svaka varijanta testnog uzorka otisnuta je na stroju za digitalni tisak na principu suhoga tonera (Xerox DC2060) i na stroju za digitalni tisak na principu tekućega tonera (Canon W2200). Otisci su izrađeni u istovjetnim klimatskim uvjetima, pri čemu je radna temperatura u prostoriji iznosila 23^0 C, a relativna vlažnost zraka 55%. Otisci su na oba stroja za digitalni tisak izrađeni s istovjetnom razlučivošću od 600 tpi. Oba stroja bila su kalibrirana opisanim metodama, i u ispravnom stanju.

Prilikom otiskivanja, svaka od testnih formi renderirana je sa svakom od definiranih standardnih metoda: perceptualnom, saturacijskom, relativnom kolorimetrijskom i apsolutnom kolorimetrijskom.

Navedenim postupkom otisnuto je 12 različitih uzoraka, na svakom od digitalnih tiskarskih strojeva (3 prostora boja x 4 metode renderiranja), odnosno ukupno 24 različita uzorka. Naklada svakog od uzoraka iznosila je 10 otisaka (radi statističke točnosti prilikom procesa mjerenja). Nakon otiskivanja, izrezivanjem su razdvojeni dijelovi namijenjeni za vizualnu i instrumentalnu analizu.

Instrumentalna analiza, odnosno mjerenje kalibriranim spektrofotometrom izvedeno je na svakom od 12 uzoraka u punoj nakladi. Na osnovi dobivenih vrijednosti, u aplikaciji ColorOpen, prvo je izvedena konverzija CIE XYZ veličina u CIE L*a*b*, kako bi se u navedenom trodimenzionalnom unificiranom prostoru boja omogućilo konstruiranje i prikazivanje gamuta danih uzoraka.

Za potrebe mjerenja spektrofotometrom te konverzicju CIE XYZ vrijednosti u CIE L*a*b* vrijednosti, korištena je Heidelbergova aplikacija ColorOpen.

Iz CIE L*a*b* veličina, u X-Rite-ovoj aplikaciji "Monaco Gamut Works", konstruiran su gamuti za svaki od uzoraka te je izračunat volumen svakoga od gamuta, izražen u CCU veličinama. (CCU - Color Cubic Units) za CIE L*a*b* prostor boja. Također su u istoj aplikaciji definirana područja boja izvan gamuta reprodukcije, a koja se nalaze unutar gamuta originala te područja u kojima je .E* > 1.

Nakon tiska uzorci su pripremljeni za vizualno ocjenjivanje. S obzirom na varijable imali smo sve zajedno 24 uzorka. Svi uzorci bili su obrezani na iste dimenzije identično u margo. Od tako pripremljenih uzoraka odvojeni su setovi od po četiri uzoraka (za svaku metodu renderiranja, za svaki prostore boje, te za dva različita tipa digitalnog tiska).

Zadatak svakog ispitanika sastojao se u tome da razvrsta četiri otisnuta uzorka prema kvaliteti od najboljeg prema najgorem. Najboljem otisku, dodjeljuje ocjenu 4, a posljednjem 1. Ispitanici su uvijek razvrstavali otisnute uzorke istog prostora boja i otisnute na istom tiskarskom stroju.

Za sve ispitanike određeni su uvjeti rasvjete, ne idealni već dnevno svijetlo i umjetna rasvjeta kako bi odgovarali uvjetima realne konzumacije grafičkog proizvoda.

Na taj način je ispitano sveukupno 50 ispitanika. Ispitanici nisu bili vremenski ograničeni prilikom procjene kvalitete otisaka.

4. Rezultati istraživanja

Tablica 1. Prikaz volumena gamuta s obzirom na njihovu veličinu

Dig. tis. stroj.	**Prostor boja**	**Metoda renderiranja**	**Volumen gamuta (CIE L*a*b* CCU)**
W2200	Lab	Perceptualna	293928
W2200	Lab	Saturacijaska	297116
W2200	CMYK	Perceptualna	396992
W2200	CMYK	Saturacijaska	401812
W2200	Lab	Relativna kolorimetrijska	419210
W2200	RGB	Perceptualna	465158
W2200	RGB	Saturacijaska	467058
W2200	CMYK	Relativna kolorimetrijska	553525
W2200	CMYK	Apsolutno kolorimetrijska	578016
W2200	Lab	Apsolutno kolorimetrijska	587851
W2200	RGB	Relativna kolorimetrijska	593611
W2200	RGB	Apsolutno kolorimetrijska	682203
DC2060	Lab	Saturacijaska	728200
DC2060	Lab	Perceptualna	738192
DC2060	CMYK	Perceptualna	751777
DC2060	CMYK	Saturacijaska	756073
DC2060	RGB	Perceptualna	791049
DC2060	RGB	Saturacijaska	792887
DC2060	Lab	Relativna kolorimetrijska	830160
DC2060	CMYK	Relativna kolorimetrijska	838543
DC2060	Lab	Apsolutno kolorimetrijska	849975
DC2060	CMYK	Apsolutno kolorimetrijska	859160
DC2060	RGB	Relativna kolorimetrijska	965570
DC2060	RGB	Apsolutno kolorimetrijska	1038538

Tablica 2. Rezultati normiranih srednjih ocjena vizualnog ocjenjivanja otisaka, s obzirom na pojedinu metodu renderiranja, ovisno o tipu reprodukcije, za dani početni prostor boja i digitalni tiskarski stroj.

Prostor boja/ dig. tis. stroj	**Metoda renderiranja**			
	Perc.	Sat.	Rel. kol.	Aps. Kol.
	Normirana srednja ocjena			
RGB/Xerox DC 2060	1,8	1,8	3,4	2,9
RGB/Canon W2200	1,6	1,7	3,3	3,4
CMYK/DC 2060	2,3	2,5	2,9	2,3
CMYK/Canon W2200	1,6	1,6	3,5	3,4
Lab/Xerox DC 2060	1,9	1,8	3,2	3,1
Lab/Canon W2200	1,3	1,8	3,5	3,4

5. Diskusija rezultata

Analizirajući rezultate utvrđeno je da je u slučaju kada se kao kriterij promatranja uzima tip digitalnog tiskarskog stroja (Xerox DC2060 i Canon W2200), odnosno princip suhog i tekućeg tonera, volumen gamuta kod digitalnih otisaka na principu suhoga tonera, u svim slučajevima (na svim uzorcima), uvijek veći od gamuta otisaka dobivenih tekućim tonerom.

Instrumentalno izračunata razlika u volumenima gamuta za CIE L*a*b* CCU, između dviju navedenih tehnika je tolika da je najmanji gamut izmjeren na otisku nastalom na principu suhoga tonera (V=728200 CIE L*a*b* CCU), još uvijek veći od najvećeg gamuta dobivenog na principu tekućeg tonera (V=682203 CIE L*a*b* CCU).

Daljnje uočljive razlike u veličini gamuta između dviju tehnika digitalnog tiska, pokazuju da je volumen najvećega gamuta izračunat za otisak izveden na principu suhoga tonera (V=1038538 CIE L*a*b* CCU), gotovo 3 puta veći od namanjeg volumena gamuta za otisak izveden na principu tekućega tonera (V=293928 CIE L*a*b* CCU).

Kada, analizirajući rezultate iz instrumentalnih izvora, kao kriterij promatranja uzmemo početni prostor boje originala, koji u procesu grafičke proizvodnje može biti RGB, CMYK ili L*a*b*, uočljive su sljedeće zakonitosti vezane uz odnose volumena gamuta:

Najveći volumen gamuta kod obaju tipova digitalnih tiskarski strojeva, ostvaren je u slučaju, tonera, te uzorci 22 i 10 kod tekućeg tonera), a najmanji volumen gamuta ostvaren je također kod oba tipa digitalnih tiskarskih strojeva, za istovjetni prostor boje, koji je u ovom slučaju bio L*a*b* (uzorci 13 i 14 kod suhog tonera, te uzorci 6 i 18 kod tekućeg tonera). Uzorci (otisci), kojima je početni prostor originala bio CMYK prostor boja, nalaze se s obzirom na veličinu gamuta, u pravilu u središnjem dijelu (između RGB i L*a*b* prostora boja) za pojedini tip digitalnog tiskarskog stroja. Međutim, promatrajući veličine gamuta sva 24 uzorka, na oba digitalna tiskarska stroja, nije moguće u potpunosti egzaktno ustvrditi, koji će prostor boje uvijek dati najveći gamut na otisku. Jer osim za najmanji i najveći volumen gamuta za 24 uzorka, ne postoji egzaktna ponovljivost.

Ukoliko, uz prioritet promatranja, kao drugi selekcijski parametar odredimo metodu renderiranja, tada se dobivaju puno jasniji pokazatelji, s točnije de. niranim utjecajem početnoga prostora boja na volumen gamuta. Prilikom promatranja rezultata, koji opisuju međusobni utjecaj početnoga prostora boje te pojedine metode renderiranja, vidljivo je da za svaku metodu renderiranja, kod digitalnog tiska i na principu suhog tonera i na principu tekućeg tonera, postoji pravilan redoslijed utjecaja početnoga prostora boje originala na volumen gamuta reprodukcije.

Kod svake pojedine metode renderiranja, najveći volumen gamuta na reprodukciji (otisku), ostvaren je upotrebom RGB početnoga prostora boja kod orginala. Najmanji volumen gamuta na otisku, ostvaren je uporabom L*a*b* početnoga prostora boje originala. CMYK prostor boje originala za pojedinu metodu renderiranja, kod oba stroja za digitalni tisak s obzirom na veličinu gamuta koji daje, nalazi se uvijek između veličina gamuta koje daju RGB i L*a*b* početni prostori boja.

Rezultati vizualnih ocjenjivanja, s obzirom na utjecaj pojedine metode renderiranja, za stalni prostor boje, na ukupni doživljaj kvalitete otiska, iako nisu u potpunosti jednaki, pokazuju vrlo slične trendove u veličini ocjene, kao i međusobne odnose s obzirom na primijenjenu metodu renderiranja kod oba tipa otisaka (na principu suhog i tekućeg tonera).

Najbolji rezultati, odnosno najviše ocjene ostvarene su na oba tipa digitalnih tiskarskih strojeva (za stalni prostor boje) primjenom kolorimetrijskih metoda renderiranja (apsolutna i relativna metoda), dok su značajno niže ocjene dane otiscima generiranim perceptualnom i saturacijskom metodom. Iznimka su jedino rezultati prikazani ocjene dane za otisak izveden suhim tonerom (DC2060) i CMYK početnim prostorom boje, gdje su ocjene dodijeljene saturacijskoj metodi veće u odnosu na ocjene dodijeljene preostalim metodama renderiranja.

6. Zaključak

Ovim radom ustanovljeno je da su vizualne ocjene kvalitete otisaka u korelaciji s određenim karakteristikama gamuta, čime je potvrđena direktna veza između doživljaja kvalitete grafičke reprodukcije i karaketristika gamuta.

Također ustanovljeno je da je volumen gamuta kod digitalnih otisaka na principu suhoga tonera, u svim slučajevima (na svim uzorcima ispitivanim u ovome radu), uvijek veći od gamuta otisaka dobivenih tekućim tonerom. Da je utjecaj kombinacije pojedine metode renderiranja s pojedinim početnim prostorom boje na veličinu gamuta, puno izraženiji kod uzoraka otisnutih tekućim tonerom, nego kod uzoraka otisnutih sa suhim tonerom.

Kod svakog pojedinoga početnoga prostora boja, najveći izračunati volumen gamuta na otisku, kod oba tipa strojeva za digitalni tisak, ostvaren je upotrebom apsolutne kolorimetrijske metode renderiranja, potom, relativne kolorimetrijske metode renderiranja, zatim saturacijske i na kraju perceptualne metode renderiranja. Dobivena odstupanja od navedenih pravila za L*a*b* početni prostor boja kod stroja za digitalni tisak na principu suhoga tonera upućuju na potrebu provedbe daljnjih istraživanja za dani slučaj.

7. Literatura

1. Braun G.J., Fairchild M.D., Gamut Mapping for Pictorial Images, TAGA Procedings, Vol. 9, 1999., 420-432.
2. Kipphan H., Handbook of Print Media, Springer Verlag, Heidelberg , 2001.
3. Milković M., Studij gamuta grafičkih otisaka, Magistarski rad, Grafički fakultet Sveučilišta u Zagrebu, Zagreb 2004.
4. Morovic J., Luo R.M., The Fundamentals of Gamut Mapping: A Survey, Color & Imaging Institute, Darby, UK, 2002., 1-36
5. Viggiano M., Wang J., A Comparison of Algorithms for Color Matching Between Media of Different Luminance Ranges, TAGA Procedings, Vol.2, 1992., 959-974.
6. Woslki M., Allebach J.P., Bouman C.A., Gamut Mapping, Squeezing the Most out of Your Color System, 2nd IS&T / SID Proceedings, Color Imaging Conference, 1994., 89-92.

10. Savjetovanje o materijalima, tehnologijama, trenju i trošenju
10. Conference on Materials, Processes, Friction and Wear
MATRIB'05, Vela Luka, 23-25.06.2005.

UTJECAJ KOVARINE NA KVALITETU PRIVREMENE ZAŠTITE ČELIČNIH BEŠAVNIH CIJEVI

EFFECT OF SCALE ON THE QUALITY OF TEMPORARY PROTECTION OF SEAMLESS STEEL TUBING FROM CORROSION

Vjera Novosel – Radović, Mirjana Lončar, Nikol Radović*, Milka Balen
Željezara Sisak, Sisak, Hrvatska
*Geodetski fakultet Sveučilišta u Zagrebu, Zagreb, Hrvatska
nradovic@geof.hr

Sažetak: Istražen je utjecaj kovarine na kvalitetu izvedbe postupka pripreme zaštite toplo valjane čelične bešavne cijevi od korozije. Za istraživanje su uporabljene toplo valjane bešavne cijevi (dimenzije 73 x 5.5 mm, kvalitete N – 80) tretirane postupkom dekapiranja i/ ili žarenja i/ ili pjeskarenja. Uporabljeni uzorci cijevi su istraženi u obliku pločica, 10 x 10 mm ili praha (dobivenog mehaničkim skidanjem kovarine sa površine cijevi). Uzorci su mjereni tehnikom brojenja i filma na uređaju za difraktometriju, tipa Philips uz uporabu CoK_α zračenja ili pretražnom elektronskom mikroskopu. Dobivene rentgenske slike su analizirane metodom komparacije uz uporabu JCPDS podataka. Metodom vanjskog standarda određen je maseni udio faze: Fe_3O_4, αFe_2O_3 i FeO a njihova raspodjela po površini cijevi koeficijentom standardne devijacije i korelacije.

Uzorci cijevi malih vrijednosti koeficijenata standardne devijacije ukazali su na dobru korozijsku opstojnost i prekrivanje površine cijevi uporabljenim premazom na osnovi silikonskih smola.

Ključne riječi: bešavna cijev, kovarina, privremena zaštita

Abstract: An investigation was conducted to find out how the scale on the tube surface could affect the quality of temporary protection from corrosion. Hot-rolled seamless steel tubes (size Φ 73×5.5 mm, class N-80) which had undergone treatment by pickling, heating and/or sand blasting were used for analysis. Samples were collected from pieces of the tubes cut into 10×10 mm plates, and from the powder obtained by scraping the scale off the tube surface. The methods applied were the counting technique using a Philips counter diffractometer with $\mathrm{CoK}\alpha$ radiation and scanning electron microscopy. Analysis of X-ray powder patterns was based on comparison with ICPDS data. The external standard method was used to determine Fe_3O_4, αFe_2O_3 and FeO phase concentrations. The distribution of the phases alongside the tube surface was expressed in terms of standard deviation coefficients. The tube samples that had low standard deviation coefficients were taken to indicate high corrosion resistance and good-quality silicious resin coating of the tube surface.

Key words: seamless tube, scale, temporary protection

UVOD

U fazi skladištenja i/ili eksploatacije čelične, bešavne cijevi su izložene procesu korozije[1]. Za smanjenje njena utjecaja, površina cijevi se prekriva tankim filmom sredstva za privremenu zaštitu od korozije[2]. Ona po svojoj prirodi mogu biti organske ili anorganske prirode. Neka od njih služe isključivo za privremenu zaštitu od korozije (prevlaka na osnovi cinka ili bitumenskih smola), dok druge uz zaštitu površine povečavaju njenu tvrdoći i otpornost na mehaničko trošenje. Nastali film određene debljine jednoliko prekriva površinu, brzo se suši i prema potrebi lako uklanja sa površine cijevi. Prije nanošenja premaza površina cijevi određenog stupnja hrapavosti trebala bi biti čista[3]. U praksi često to nije slučaj. Uz neravnine, ogrebotine i pukotine nalazi se film i/ ili nakupine kovarine, neodređene veličine i oblika neravnomjerno raspoređene po površini cijevi. Za njihovo uklanjanje sa površina cijevi upotrebljavaju se različite metode. Površina cijevi se tretira brušenjem i/ ili kemijski i/ ili toplinski i/ ili pjeskarenjem[4]. No, i nakon toga prisutni film i/ ili nakupine kovarine ostaju i izravno utječu na kvalitetu nastalog filma premaza. U ovom radu istražen je utjecaj kovarinena uspješnost prekrivanja toplovaljane bešavne cijevi uporabom sredstava za njihovu privremenu zaštitu od korozije.

EKSPERIMENT

Za istraživanje uporabljeni su model uzorci, pripremljeni iz toplo valjanih bešavnih cijevi, dimenzije 73 x 5.51 mm, tipa N – 80. Površine cijevi svih uzetih uzoraka za istraživanje su jednoliko prekriveni filmom kovarine i/ ili slojastih slagalina različite debljine, slika 1.

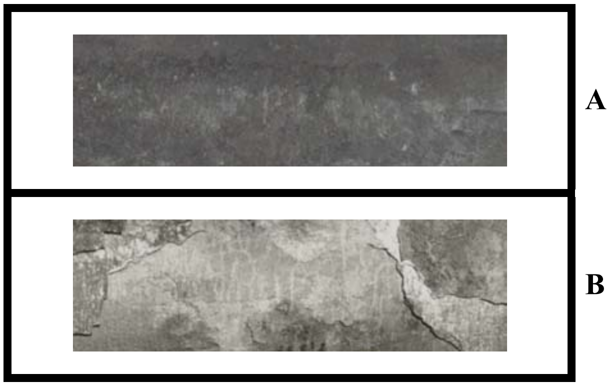

Slika 1. Snimka površine uzorka toplovaljane bešavne cijevi prekrivene filmom kovarine: A – jednoliko i/ ili B – u obliku slojastih slagalina po cijeloj dužini uzorka cijevi

Uporabom metoda rentgenske difrakcije određen je kvalitativni fazni sastav prosječnih/ separiranih uzoraka kovarine. Za istraživanje, uzorci su uzimani mehaničkim skidanjem kovarine uzduž cijele površine cijevi. Separirani uzorci uziani su sukcesivno unutar jednog uzorka na 10 različitih mjesta. Uzeti uzorci usitnjavani su u mehaničkoj drobilici, 5 minuta uz dodatak alkohola. Uzorci su dodatno usitnjavani i homogenizirani u WC priključku mlina za usitnjavanje i homogenizaciju, tipa Spex. Usitnjeni i homogenizirani uzorci su snimani tehnikom brojenja na uređaju za difraktometriju, tipa Philips uz uporabu CoK_α zračenja. Mjerenjem integralnog intenziteta difrakcijske linije refleksa: 220 od Fe_3O_4, 104 od $\alpha\ Fe_2O_3$ i 200 od FeO metodom vanjskog standarda[6] određen je maseni udio faze: Fe_3O_4, $\alpha\ Fe_2O_3$ i FeO. Kvalitativni fazni sastav kovarine po njenoj debljini filma kao i raspodjela filma prevlake silikonske smole određen je također metodom rentgenske difrakcije, tehnikom filma uporabom Debye Scherrer kamere i svjetlosne mikroskopije. Prije nanošenja prevlake silikonske smole sa površine istraživanih uzoraka uklonjen je prisutni film kovarine. Nakon odmaščivanja pojedinog uzorka uporabom organskog otapala trikloretilena i/ ili benzina uzorci su tretirani kemijski, toplinski i pjeskarenjem. Za kemijsko tretiranje uporabljena je svježe pripremljena sulfatna kupelj (200 g/ l H_2SO_4) uz dodatak inhibitora kiselinske korozije (0.5 g/ l), temperature 60ºC u vremenu 15 minuta. Svaki kemijski tretirani uzorak ispran je vodom, sušen i toplinski tretiran 15 minuta na 920ºC u komornoj peći te pjeskaren na uređaju Sandmaster, 60S. Uspješnost uklanjanja kovarine sa površine pojedinog uzorka cijevi istražen je uporabom pretražnog elektronskog mikroskopa, tipa Joel u snopu sekundarnih elektrona pri povečanju 200 X. Uporbom istog istražena je površina filma nastalog nanošenjem zaštitnog sredstva silikonske smole u snopu odbijenih elektrona, pri povećanju 50 X, 500 X i 1500 X.

REZULTATI I DISKUSIJA

Dobiveni rezultati istraživanja utjecaja kovarine na kvalitetu nastalog filma nanošenjem sredstava za privremenu zaštitu silikonske smole upućuju na njenu utjecaj. Razlog tome su zapažene velike razlike u masenom udjelu faza: α Fe_2O_3, Fe_3O_4 i FeO po debljoni filma kovarine te prosječnom uzorku pojedinog uzorka.

Rezultati kvalitativne fazne analize kovarine po debljini filma, slika 2. upućuju na njenu slojevitost. Tako na mikrosnimci uzorka kovarine cijevi 2 zapažena su tri sloja, gornji α Fe_2O_3, srednji od Fe_3O_4 i donji FeO, ali uz prisutnost inkluzija faze Fe_3O_4 nastale pri postepenoj međufaznoj transformaciji. Na analogna zapažanja upućuju Kim i Szpunar[7] te Chen i Yuen[8].

Prisutni slojevi međusobno se razlikuju u debljini, tvrdoći (prema Moh's faza Fe_3O_4 ima najveću tvrdoću 6.5) i topivost u sulfatnoj kupelji. Na promjenjivost broja slojeva u pojedinom istraživanom uzorku filma kovarine, kao i njihove debljine upućuju rezultati kvantitativne fazne analize, slika 3. Prema slici 3. istraživani uzorci: 1, 2, 4, 5, 7, 8, 10 film kovarine čine *tri* sloja. Unutar njih maseni udio faze α Fe_2O_3 se mijenja od 3.08 do 19.28 %, Fe_3O_4 od 20.5 do 86.27 % i FeO od 8.25 do 76.24 %. U ostalim uzorcima: 6 i 9 film kovarine čini *dva* sloja, različitih debljina: deblji sloj faze Fe_3O_4 – 91.50 % i tanji sloj α Fe_2O_3 – 9.03 %. U uzorku 9 deblji sloj čini taza α Fe_2O_3 – 88.94 % a tanji Fe_3O_4 – 10.21 %. U uzorku 3 film kovarine čini samo faza Fe_3O_4 uz neznatnu prisutnost faze: α Fe_2O_3 i/ ili FeO (u masenom udjelu manjem od 1%). Na ova zapažanja kao i promjene prisutnih slojeva te njihove debljine unutar pojedinog istraživanog uzorka filma upućuju rezultati kvantitativen fazne analize separiranih uzoraka unutar svakog istraživanog uzorka kovarine, slika 4.

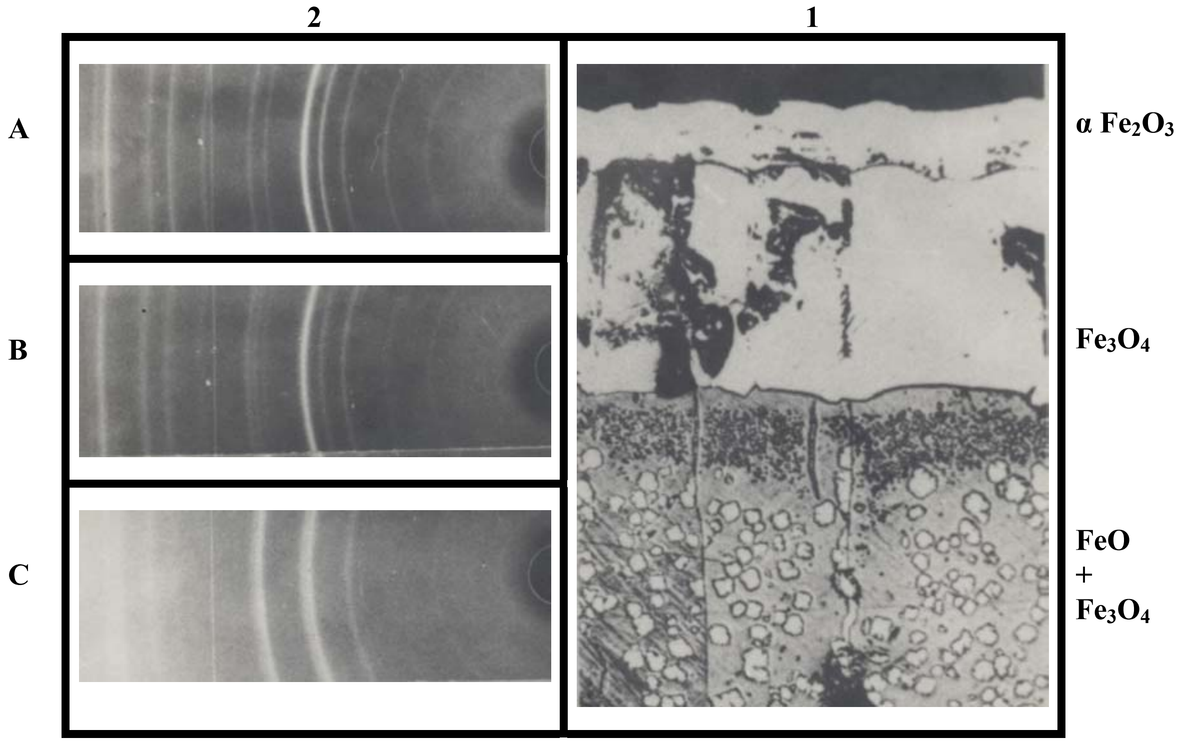

Slika 2. Mikrosnimka - **1** i difrakcijska slika - **2** filma kovarine po slojevima: **A** – gornji, **B** – srednji i **C** – donji sloj.

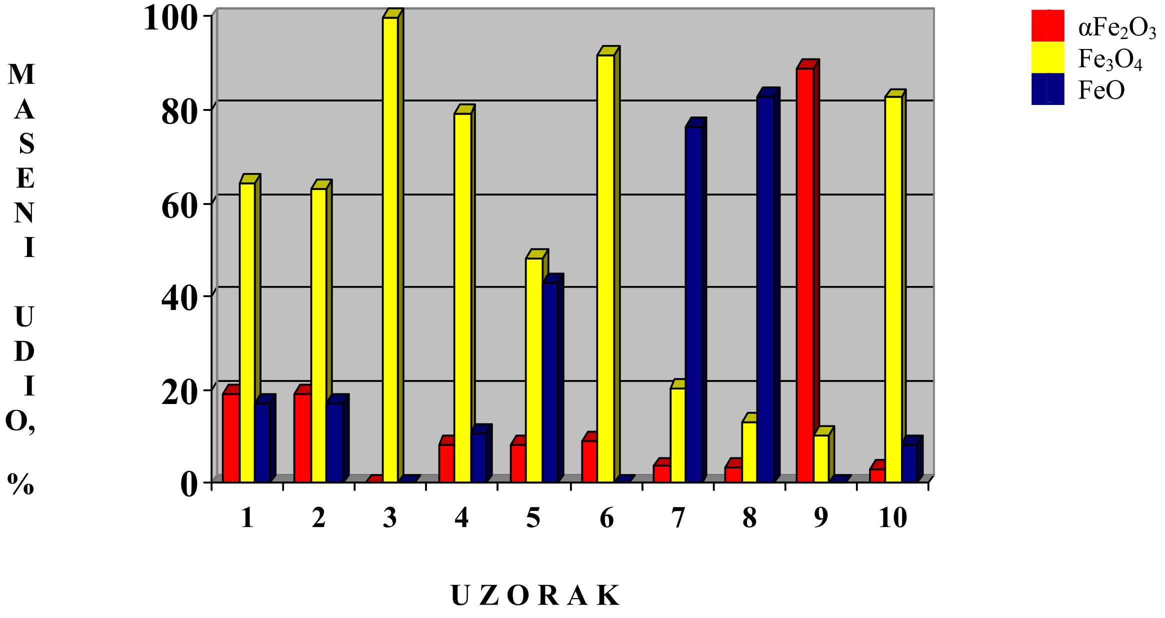

Slika 3. Rezultati kvantitativne fazne analize istraživanih uzoraka kovarine.

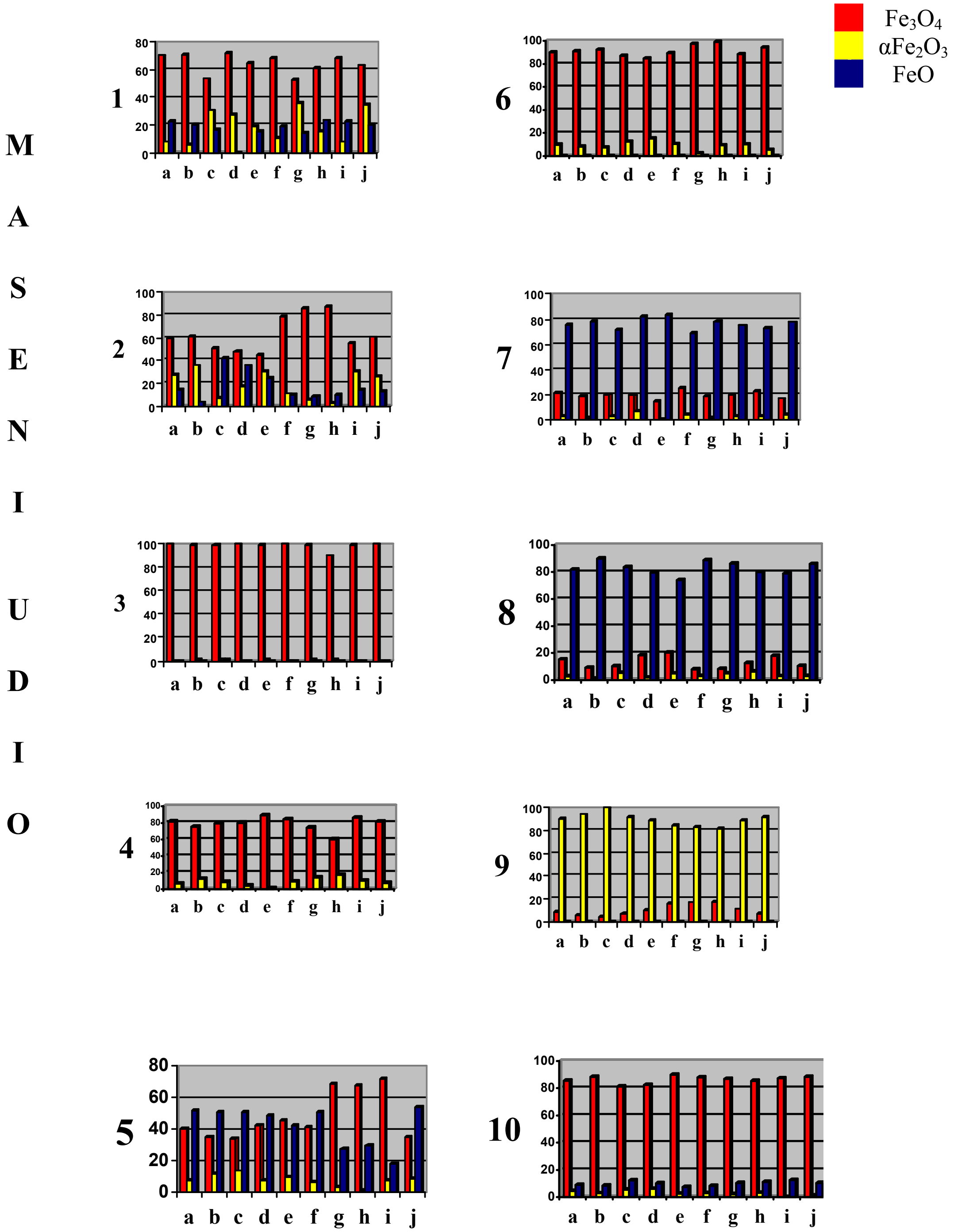

Slika 4. Histogrami promjene masenog udjela faze: α Fe_2O_3, Fe_3O_4 i FeO unutar istraživanog uzorka kovarine: 1, 2, 3, 4, 5, 6, 7, 8, 9, 10 na mjestu: a, b, c, d, e, f, g, h, i, j.

Zapažene razlike u masenom udjelu faze: α Fe_2O_3, Fe_3O_4 i FeO izražene su njima izračunatim vrijednostima standardne devijacije, σ i koeficijenta varijance, Σ^9. Uporabom ovih vrijednosti može se unaprijed predskazati uspješnost uklanjanja filma kovarine uporabljenim postupkom tretiranja površine cijevi. Tako u uzorku 2 različitih vrijednosti, σ

(α Fe_2O_3 – 11.94 %, Fe_3O_4 – 17.12 % i FeO – 12.67 %) i vrlo visokih vrijednosti Σ (α Fe_2O_3 – 62.71 %, Fe_3O_4 – 27.15 % i FeO – 73.26 %) tijekom postupka tretiranja površine, film kovarine djelomično se istanji, ali uz izrazitu prisutnost nakupina, 6. One nastali film nanešenog sredstva za privremenu zaštitu od korozije, čine isprekidanim, neujednačene debljine i uzrokom su pojave korozije, slika 7. Prema rezultatima rentgenske analize prisutne nakupine čine ostaci sloja faze Fe_3O_4 (uz neznatnu primjesu ostalih faza) koji niti uporabom postupka pjeskanja se u cijelosti nisu uklonili sa površine cijevi. Nasuprot tome u uzorku kovarine 3, gotovo jednakih vrijednosti σ i Σ 0.12/ 0.13 % uporabljenim postupkom tretiranja površine film se postepeno istanjuje i homogeno prekriva površinu cijevi, slika 6B. Film nanešenog sredstva za privremenu zaštitu od korozije, homogeno prekriva cijelu površinu cijevi, slika 7. koja na zabilježenom rentgenogramu se bilježi u obliku difuznog debyevskog prstena.

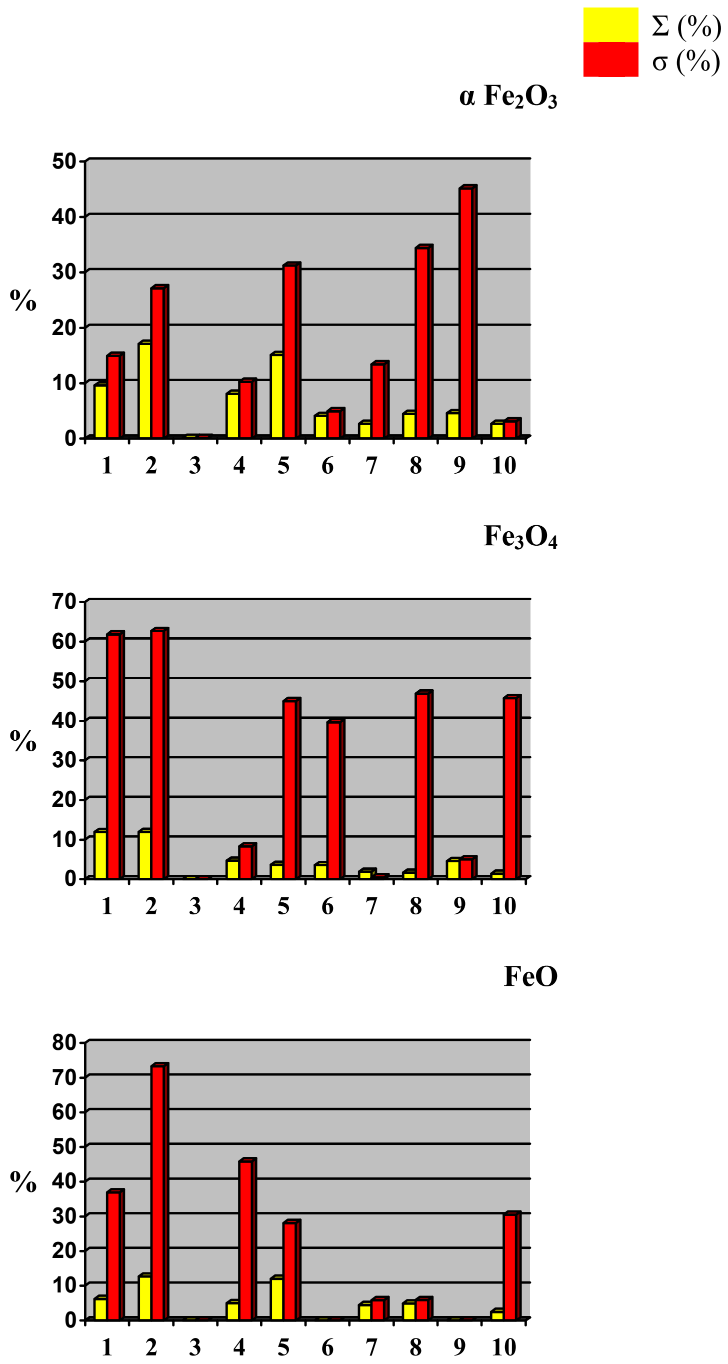

α Fe_2O_3

Fe_3O_4

FeO

Slika 5. Histrogram standardne devijacije, σ i koeficijent korelacije Σ unutar pojedinog istraživanog uzorka filma kovarine.

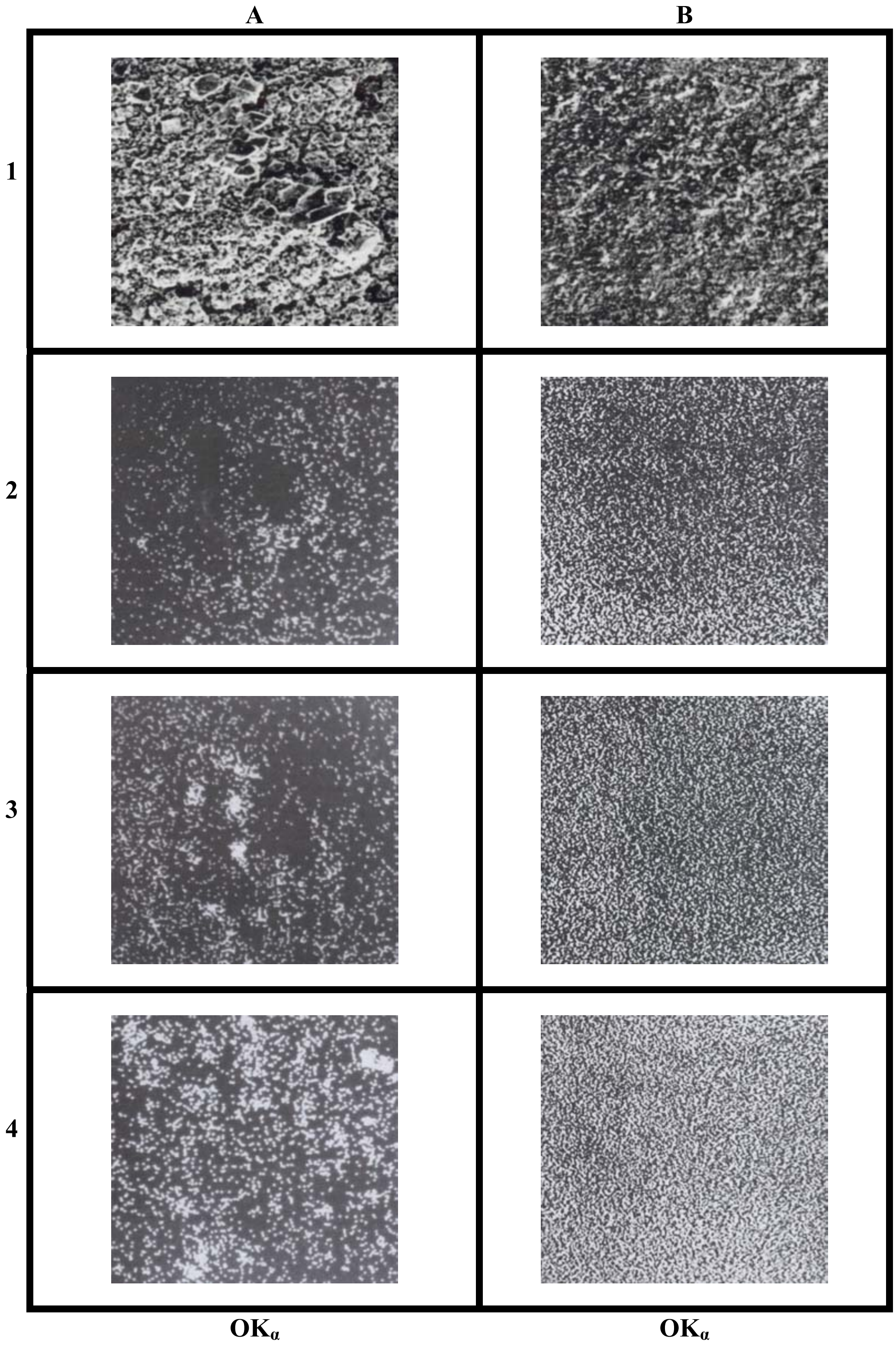

Slika 6. Elektronska snimka površine toplo valjane cijevi **A** – **2** i **B** – **3**, u snopu sekundarnih elektrona, **1** – povećanje 200 X, snimci karakterističnog rentgenskog zračenja OK$_\alpha$: nakon tretiranja površine: **2** – sulfatnj kupelji, **3** – toplinski i **4** – postupkom pjeskarenja.

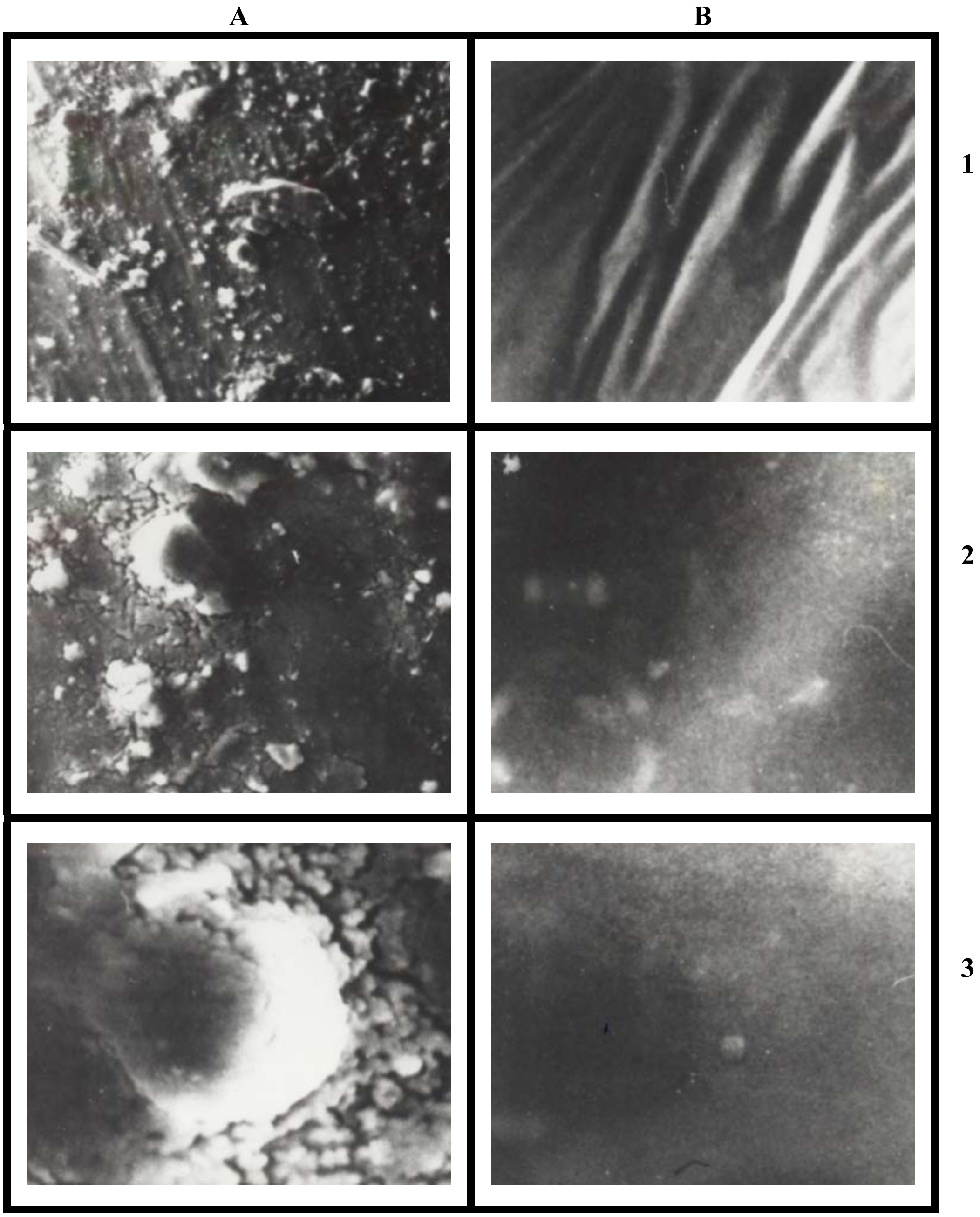

Slika 7. Elaktronski snimci površine uzorka toplo valjane bešavne cijevi **A** – **2** i **B** – **3** nakon nanošenja preparate za privremenu zaštitu, u snopu odbijenih elektrona, pri povećanju **1** – 50 X, **2** – 500 X, **3** – 1500 X.

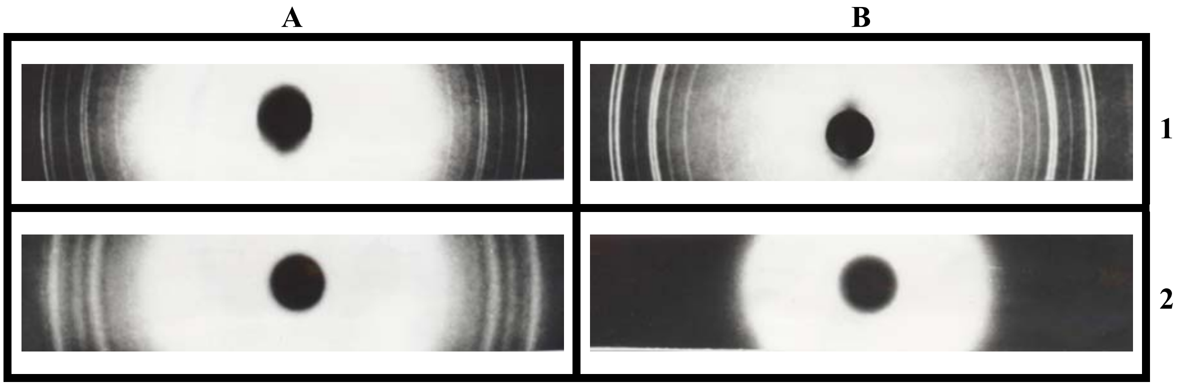

Slika 8. Rentgenogrami uzorka **A – 2** i **B – 3** površine toplo valjane bešavne cijevi: 1A – 2 i 1B – 3 prije i nakon nanošenja preparata za privremenu zaštitu površine cijevi: 2A – 2 i 2B – 3.

ZAKLJUČAK

Uporabom metoda rentgenske difrakcije i pretražne elektronske mikroskopije su analizirani uzorci filma kovarine toplo valjane bešavne cijevi. Dobiveni rezultati analize i izračunate vrijednosti σ i Σ upučuju na nehomogenu raspodjelu debljine slojeva faza: α Fe_2O_3, Fe_3O_4 i FeO unutar istraživanih uzoraka filma kovarine, mogućnost uklanjanja filma kovarine uporabljenim postupcima tretiranja površpine, te uspješnost kvalitete izvođenja privremene zaštite od korozije.

Samo u slučaju niskih vrijednosti σ i Σ, koje su gotovo jednake, elektronkski snimci i rentgenogrami filma (nastalog nanošenjem sredstava za privremenu zaštitu od korozije) upućju na njegovo jednoliko prekrivanje površine cijevi. Nasuprot tome, kod visokih vrijednosti σ i Σ, velike međusobne razlike, elektronski snimci i rentgenogrami upućuju na nepotpuno prekrivanje površine cijevi (uporabljenim sredstvom za privremenu zaštitu), te isprekidanost filma preostalim filmom kovarine (i nakon tretiranja površine) u obliku većih/ manjih nakupina nepravilnog oblika.

LITERATURA

1. H. Uhlig, R. W. Revie, *Corrosion and Corrosion Control*, John Wiley & Sons, New York, 1985.
2. N. D. Tomašov, *Teorija korozii i zaščiti metalov,* IZD-VO, ANSSSR, Moskva, 1960.
3. N. V. Bogojavleskaja, *Elektrohemičeskaja obrabotka trub,* IZD-VO Mašinostroenie, Moskva, 1970.
4. Travlenie i Obezžirivanie trub od staljev i splavov, IZD – OV Metalurgija, Moskva, 1967.
5. M. Lončar, V. Novosel – Radović, S. Rešković, *Zbirka referata 11. Savjetovanja o zaštiti materijala i industrijskom finišu*, Zagreb 23. – 24. lipnja, 1994., HDZM, 1-8.
6. Novosel – Radović, M. Balen, N. Radović, *Book of Abstract, Third European Powder Diffraction Conference,* Sep. 25. – 28. (1993.), Vienna – Austria, pp. 133.
7. K. Kim, J. A. Szpunar, *Scr. Mater. Eisevier Science*, New York, USA, 2001., 2605– 2610.
8. Y. Chen, W. Y. D. Yuen, *Oxid. Met.* 56(2001) 89 – 118.
9. P. S. Mann, *Introductory Statistics,* John Wiley & Sons, Inc., New York, 2001.

TRIBOLOŠKI ASPEKTI IZVLAČENJA SA REDUKCIJOM DEBLJINE ZIDA

Mirna Nožić
Univerzitet "Džemal Bijedić", Mašinski fakultet
Maršala Tita bb, 88 104 Mostar, BiH

Himzo Đukić
Sveučilište u Mostaru, Strojarski fakultet
Matice Hrvatske bb, 88000 Mostar, BiH

Sažetak:
U radu je analiziran uticaj trenja na vrijednost deformacione sile pri izvlačenju na višestepenim alatima.
Eksperimentalnim putem određene su vrijednosti sile izvlačenja u laboratorijskim i proizvodnim uslovima za višestepene alate sa dva, tri, četiri i pet prstenova.
Računskim putem , pomoću dva izraza za silu, dobivene su vrijednosti sile izvlačenja na višestepenim alatima za različite vrijednosti koeficijenta trenja.

Ključne riječi: trenje, deformaciona sila, duboko izvlačenje, višestepeni alati

1. UVOD

Istraživanja prezentirana u ovom radu usmjerena su na analizu uticaja trenja na vrijednost deformacione sile u procesu dubokog izvlačenja na višestepenim alatima.
Eksperimentalnim putem izvršena je registracija i mjerenje deformacione sile izvlačenja na dvostepenom, trostepenom, četverostepenom i petostepenom alatu u laboratorijskim uslovima i trostepenom, četverostepenom i petstepenom alatu ua proizvodnim uslovima.
Računskim putem, pomoću dva izraza za proračun deformacione sile pri izvlačenju na višestepenim alatima, dobivene su vrijednosti sile izvlačenja za istraživane višestepene alate i različite vrijednosti koeficijenta trenja.

2. ANALITIČKI IZRAZI ZA PRORAČUN DEFORMACIONE SILE PRI IZVLAČENJU NA VIŠESTEPENIM ALATIMA

U dostupnoj literaturi nisu navedeni izrazi za proračun deformacione sile pri izvlačenju na višestepenim alatima sa više prstenova (više od dva).
U radovima E.A.Popova [1] dat je izraz za proračun deformacione sile prilikom izvlačenja kroz dva prstena istovremeno:

$$F = A_2 \cdot k_{2sr} \cdot \frac{b_2}{b_2 - 1}\left[1 - \left(\frac{A_2}{A_1}\right)^{b_2 - 1}\right]\left(1 + \frac{\mu}{b_2 \cdot n_2 \cdot tg\alpha_2}\right) + \mu \cdot \pi \cdot d_2 k_{2sr} \cdot l_2 \left\{1 - \frac{b_2}{b_2 - 1}\left[1 - \left(\frac{A_2}{A_1}\right)^{b_2 - 1}\right]\right\}$$

$$+ \mu \cdot \pi \cdot d_1 \cdot k_{1sr} \cdot l_1 \left\{1 - \frac{b_1}{b_1 - 1}\left[1 - \left(\frac{A_1}{A_0}\right)^{b_1 - 1}\right]\right\} + 2 \cdot \mu \cdot \pi \cdot \cdot s_1 \cdot H \cdot k_{1sr} \qquad [daN] \qquad (1)$$

gdje su:

A_0 – površina poprečnog presjeka pripremka
A_1 – površina poprečnog presjeka obratka nakon prolaska kroz prednji prsten u alatu
A_2 - površina poprečnog presjeka obratka nakon prolaska kroz zadnji prsten u alatu
d_1, d_2 - prečnik prednjeg odnosno zadnjeg prstena za izvlačenje
d - prečnik izvlakača
d_0 – prečnik pripremka
l_1, l_2 - visine zona glačanja prednjeg, odnosno zadnjeg prstena za izvlačenje
H - rastojanje između zona deformisanja prednjeg i zadnjeg prstena za izvlačenje
α_1 – ugao konusa prednjeg prstena u alatu
α_2 - ugao konusa zadnjeg prstena u alatu
s_1 – debljina zida komada nakon prolaska kroz prednji prsten
s_2 – debljina zida komada nakon prolaska kroz zadnji prsten
k_{2sr} - srednja vrijednost specifičnog deformacionog otpora poslije izvlačenja kroz zadnji prsten za izvlačenje
k_{1sr} - srednja vrijednost specifičnog deformacionog otpora poslije izvlačenja kroz prednji prsten za izvlačenje
μ - koeficijent trenja

Koeficijenti b_1 i b_2 računaju se po izrazima:

$$b_1 = \frac{1}{\cos\alpha_1} + \frac{\mu}{\sin\alpha_1} + \frac{\mu}{n_1 tg\alpha_1} \tag{2}$$

$$b_2 = \frac{1}{\cos\alpha_2} + \frac{\mu}{\sin\alpha_2} + \frac{\mu}{n_2 tg\alpha_2} \tag{3}$$

gdje su:

$$n_1 = \frac{d_0 + d_1}{2d} \tag{4}$$

$$n_2 = \frac{d_1 + d_2}{2d} \tag{5}$$

U radu P.Popovića [2] dat je jednostavniji oblik izraza za proračun deformacione sile pri izvlačenju kroz dva prstena, u obliku:

$$F = k_{2sr}\varphi_2\left(1 + \frac{n_2 - 1}{n_2} \cdot \frac{\mu}{\alpha_2}\right) \cdot \left[A_2 \cdot \frac{n_2 \cdot (\alpha_2 + \mu)}{n_2 \cdot (\alpha_2 + \mu) - \mu} - \mu\pi d_2 l_2\right] - k_{1sr}\varphi_1\left(1 + \frac{n_1 - 1}{n_1} \cdot \frac{\mu}{\alpha_1}\right) \cdot \mu\pi d_1 l_1 +$$

$$\mu\pi d_2 l_2 k_{2sr} + \mu\pi d_1 l_1 k_{1sr} + 2\mu\pi s_1 H k_{1sr} \qquad [\text{daN}] \quad (6)$$

Po analogiji sa izrazom (1) može se napisati izraz za deformacionu silu izvlačenja na višestepenim alatima sa n prstenova u obliku:

$$F = A_n \cdot k_{nsr}\frac{b_n}{b_n - 1}\left[1 - \left(\frac{A_n}{A_{n-1}}\right)^{b_n - 1}\right]\left(1 + \frac{\mu}{b_n \cdot n_n \cdot tg\alpha_n}\right) + \mu \cdot \pi \cdot d_n k_{nsr} \cdot l_n\left\{1 - \frac{b_n}{b_n - 1}\left[1 - \left(\frac{A_n}{A_{n-1}}\right)^{b_n - 1}\right]\right\}$$

$$+ \sum_{i=1}^{n-1} \pi \cdot d_i \cdot k_{isr} \cdot l_i\left\{1 - \frac{b_i}{b_i - 1}\left[1 - \left(\frac{A_i}{A_{i-1}}\right)^{b_i - 1}\right]\right\} + 2 \cdot \mu \cdot \pi \cdot \cdot s_i \cdot H_{i+1} \cdot k_{isr} \qquad [\text{daN}] \quad (7)$$

Na isti način, a na osnovu izraza (6) , izraz za deformacionu silu izvlačenja na višestepenim alatima s n prstenova imao bi oblik:

$$F = k_{nsr}\varphi_n\left(1 + \frac{n_n - 1}{n_n} \cdot \frac{\mu}{\alpha_n}\right)\left[A_n \cdot \frac{n_n(\alpha_n + \mu)}{n_n(\alpha_n + \mu) - \mu} - \mu\pi d_n l_n\right] - \sum_{i=1}^{n-1} k_{isr}\varphi_i\left(1 + \frac{n_i - 1}{n_i}\frac{\mu}{\alpha_i}\right)\mu\pi d_i l_i +$$

$$\mu\pi d_n l_n k_{nsr} + \mu\pi d_1 l_1 k_{1sr} + 2\sum_{i=2}^{n-1}\mu\pi d_i l_i k_{isr} + 2\sum_{i=1}^{n-1}\mu\pi s_i H_{i+1} k_{isr} \qquad [\text{daN}] \quad (8)$$

3. REZULTATI EKSPERIMENTALNIH ISTRAŽIVANJA

Eksperimentalna istraživanja obuhvatala su registraciju i mjerenje deformacione sile u procesu izvlačenja na dvostepenom, trostepenom, četverostepenom i petostepenom alatu. U laboratorijskim uslovima, proces izvlačenja izveden je na hidrauličnoj kidalici pomoću eksperimentalnog alata. Dimenzije alata korištenog za istraživanja date su u Tabeli 1.

Dimenzije prstenova za izvlačenje		
Redni broj prstena	Prečnik prstena d (mm)	Ugao konusa α_i (°)
1	13.5	6
2	12.65	8
3	12.20	10
4	11.92	8
5	11.785	8

Tabela 1. Dimenzije prstenova za izvlačenje

Za sve realizovane eksperimente snimljeni su dijagrami zavisnosti deformacione sile od hoda izvlačenja (F-h), sa kojih su očitane srednje vrijednosti sila u karakterističnim tačkama pri deformisanju dna radnog komada i pri deformisanju omotača.
U Tabeli 2. navedene su srednje vrijednosti sila u karakterističnim tačkama za izvlačenja u laboratorijskim uslovima (oznake eksperimenta: E15 – petostepeni alat, E14 – četverostepeni, E13- trostepeni i E12 – dvostepeni) i proizvodnim uslovima (H15 – petostepeni alat, H14- četverostepeni i H13 – trostepeni).

Vrijednosti deformacione sile F (kN)								
Red.br. eksp.	Oznaka eksp.	Pri deformisanju dna komada					Pri defor. omotača	
		Mjerna mjesta						
		1	2	3	4	5	6	7
1	E12	2.47	8.76	-	-	-	9.52	7.58
2	E13	2.42	8.82	17.03	-	-	13.23	8.87
3	E14	2.02	8.39	16.77	21.4	-	15.16	10.65
4	E15	1.94	8.39	16.61	21.13	24.47	14.84	6.77
5	H15	0.18	1.85	6.55	12.50	14.52	8.11	3.32
6	H14	1.06	4.88	10.18	12.86	-	8.63	3.98
7	**H13**	1.85	6.86	10.17	-	-	7.42	0.79

Tabela 2. Vrijednosti deformacione sile u karakterističnim tačkama

4. UTICAJ TRENJA NA VRIJEDNOST DEFORMACIONE SILE IZVLAČENJA NA VIŠESTEPENIM ALATIMA

Na osnovu dimenzija alata datih u Tabeli 1, dobivene su računske vrijednosti sile preko izraza (7) za vrijednost koeficijenta trenja $\mu = 0.06 - 0.15$ za sve realizovane eksperimente. Rezultati su dati u Tabeli 4.

Vrijednost sile izvlačenja						
Broj prstenova	Koeficijent trenja μ					
	0.06	0.08	0.10	0.12	0.14	0.15
2	11.44	13	14.42	15.87	17.27	17.98
3	11.84	14.07	15.43	18.40	20.72	21.86
4	13.09	16.19	18.37	22.20	25.30	26.86
5	13.88	17.77	20.68	25.46	29.25	31.11

Tabela 4. Računske vrijednosti sile izvlačenja na višestepenim alatima (po izrazu 7)

U Tabeli 5. Dati su rezultati proračuna deformacione sile po izrazu (8) za sve realizovane eksperimente i vrijednost koeficijenta trenja μ=0.04 – 0.15.

Vrijednost sile izvlačenja								
Broj prstenova	Koeficijent trenja μ							
	0.04	0.06	0.07	0.08	0.10	0.12	0.14	0.15
2	9,94	11.52	12.28	14.19	14.66	16.14	17.66	18.45
3	10.35	13.05	14.4	15.75	18.42	21.06	23.65	24.95
4	12.43	16.77	18.93	21.10	25.36	29.64	33.84	35.96
5	14.27	20.31	23.31	26.4	30.82	38.16	44.11	47.06

Tabela 5. Računske vrijednosti sile izvlačenja na višestepenim alatima (po izrazu 8)

Na osnovu rezultata datih u Tabeli 4. Urađeni su dijagrami zavisnosti sile izvlačenja od koeficijenta trenja za sve realizovane eksperimente – Slika 1.

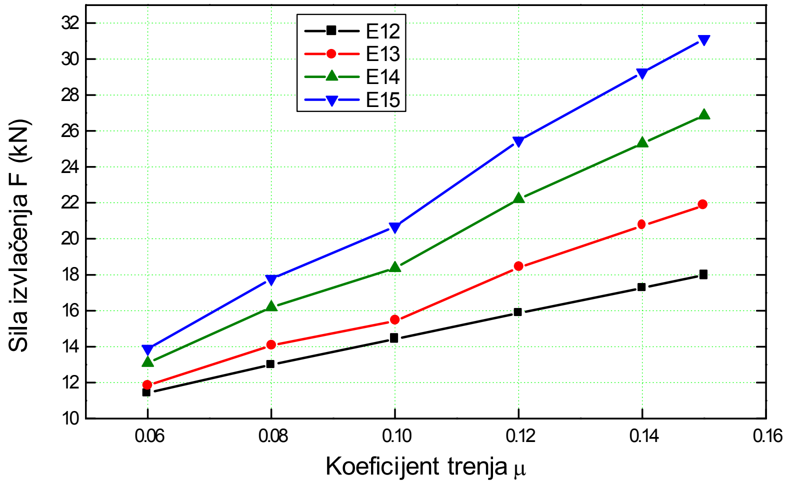

Slika 1. Dijagram zavisnosti sile izvlačenja od koeficijenta trenja

Na Slici 2. Dat je dijagram zavisnosti sile izvlačenja od koeficijenta trenja prema vrijednostima navedenim u Tabeli 5.

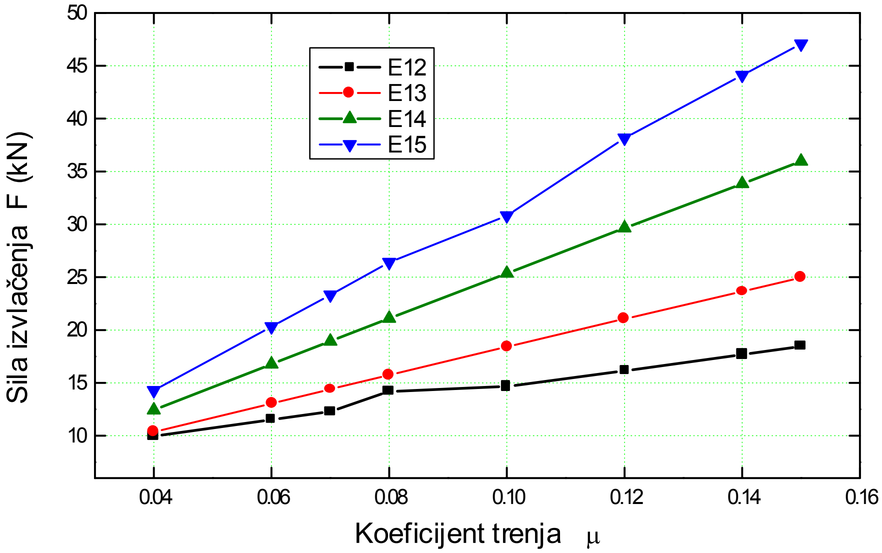

Slika 2. Dijagram zavisnosti sile izvlačenja od koeficijenta trenja

Za analizu uticaja trenja na rast sile izvlačenja na višestepenim alatima urađen je dijagram zavisnosti sile od broja prstenova u višestepenom alatu za vrijednost koeficijenta trenja $\mu = 0.06 - 0.15$ prema podacima iz Tabele 4, Slika 3.

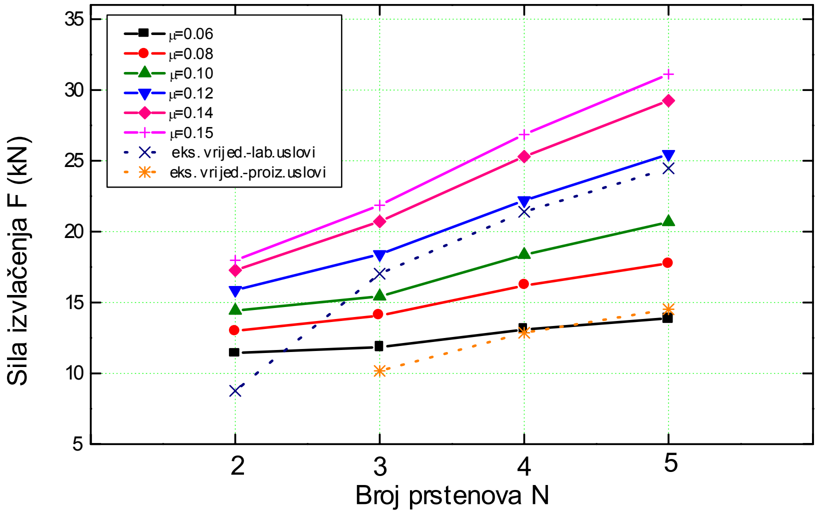

Slika 3. Dijagram zavisnosti sile izvlačenja od broja prstenova u višestepenom alatu za vrijednost koeficijenta trenja $\mu = 0.06 - 0.15$

Krive na dijagramu obiljžene crtkanim linijama predstavljaju eksperimentalne vrijednosti sile izvlačenja na dvostepenom, trostepenom , četverostepenom i petostepenom alatu.

5.ZAKLJUČAK

Računske vrijednosti sile izvlačenja na višestepenim alatima, dobivene po izrazu (7), slažu se sa eksperimentalnim rezultatima dobivenim u proizvodnim uslovima za vrijednost koeficijenta trenja $\mu = 0.06$, što odgovara realnim vrijednostima koeficijenta trenja u proizvodnim uslovima. Zbog uticaja brzine deformisanja eksperimentalne vrijednosti sile izvlačenja u laboratorijskim uslovima su veće u odnosu na proizvodne uslove i slažu se sa računskim vrijednostima sile izvlačenja za $\mu = 0.11$.

5. LITERATURA

[1] E.A.Popov	Osnovi teoriji listovoj štampovki. Mašinostroenie, Moskva, 1968.
[2] P.Popović	Istraživanje i razvoj metoda projektovanj i proračunatehnologije i izrade cilindričnih elemenata metodom dubokog izvlačenja sa redukcijom debljine zida omotača po visini, Završni elaborat, Naučno istraživački projekat, Mostar, 1984.
[3] M.Nožić	Prilog istraživanju pojedinčnog i ukupnog opterećenja višestepenih alata za izvlačenje sa redukcijom debljine zida, Doktorska disertacija, Mostar, 2005.

RECIKLIRANJE TISKANIH PLOČICA

Antun Pintarić, Tomislav Mrčela
Elektrotehnički fakultet Osijek
Kneza Trpimira 2b, Osijek, Hrvatska

Sažetak:
Sve više suvremenih proizvoda sadrži tiskane pločice (PCB - printed circuit board). Karakteristika njihove primjene je minijaturizacija, raznovrsnost materijala i sadržaj opasnih tvari. Rad daje pregled vrsta materijala u tiskanim pločicama. Prikazana su važnija područja primjene tiskanih pločica i tipični potupci izrade. Detaljnije su prikazane metode zbrinjavanja otpadnih tiskanih pločica u svijetu, te pregled mehaničkih, toplinskih i kemijskih postupaka recikliranja.

10. Savjetovanje o materijalima, tehnologijama, trenju i trošenju
10. Conference on Materials, Processes, Friction and Wear
MATRIB'05, Vela Luka, 23-25.06.2005.

ISTRAŽIVANJE ČELIKA API STUPNJA N-80 MODIFICIRANOG KEMIJSKOG SASTAVA

THE INVESTIGATION OF STEEL API GRADE N-80 WITH MODIFIED CHEMICAL COMPOSITION

A. Prelošćan, M. Golja, H. Šprišić*
Metalurški fakultet, Sveučilište u Zagrebu,
Aleja narodnih heroja 3, 44103 Sisak
*FELIS Produkti d.o.o., B. Adžije 19, 44010 Sisak

Sažetak

Ispitivan je čelik API N-80 modificiranog kemijskog sastava, koji je, pored uobičajenog sadržaja vanadija, takoder mikrolegiran s niobijem. Zbog postizanja većeg učinka vanadija i niobija na strukturu i svojstva čelika, ispitivani N-80 ima i povišeni sadržaj dušika.
Tražena mehanička svojstva čelika postignuta su nakon odgovarajuće toplinske obradbe. Mehanizmi boljeg vezanja mikrolegirajućih elemenata povoljno utječu na svojstvo žilavosti. Najbolje rezultate pri tome pokazuju ispitani uzorci čelika u poboljšanom stanju.

Ključne riječi: modificirani čelik N-80, naftne cijevi, mehanička svojstva, poboljšanje

Summary

API steel N-80 chemically modified not only with vanadium, but also with niobium micro alloyed was investigated. In order to achieve a stronger impact of vanadium and niobium on the structure and properties, the investigated steel has a higher content of nitrogen too.
The desired mechanical properties of the steel are realized after the adequate heat treatment. The mechanisms of more efficient bonding of micro alloying elements have favorable impact on quality of notch toughness. The best results are obtained for the investigated samples of steel in quenched and tempered condition.

Key words: modified steel N-80, pipe for petroleum industrie, mechanical properties, quenched and tempered.

UVOD

Čelik kvalitete N-80, kakav se proizvodi u Željezari Sisak za zaštitne cijevi i cijevne spojnice ne zadovoljava uvjetima koji su propisani standardom API Std 5CT, bez toplinske obrade.

Veliki dio svjetskih proizvođača cijevi orijentiran je na proizvodnju cijevi viših kvaliteta (C-75 do C-95 po API standardu), pri čemu se uglavnom primjenjuje toplinska obrada postupkom poboljšanja cijevi po cijeloj dužini.

Postupkom kaljenja postiže se martenzitna mikrostruktura i dovoljna dubina prokaljivosti debelostjene cijevi.

Odgovarajućim popuštanjem nakon kaljenja na temperature ispod 700C postiže se tražena granica razvlačenja i zadovoljavajuća žilavost, te dobra otpornost na koroziju pod naprezanjem i tvrdoća [1-5].

Ispitivanja u ovom radu provedena su na uzorcima bešavnih cijevi dimenzije ϕ244.5x11.99 mm (API $9^{5/8"}$x11,99) u valjanom, normaliziranom i poboljšanom stanju.

Istraživani čelik je modificirani kvalitet N-80 koji pored uobičajenog sadržaja vanadija sadrži i mikrolegirajući element niobij, te povišeni sadržaj dušika.

Modificirani sastav čelika pokazuje bolje rezultate u valjanom, normaliziranom, a naročito u poboljšanom stanju.

TEORIJSKI DIO

Istraživanje i iskorištavanje nafte i zemnog plina jedno je od najvažnijih industrijskih i ekonomskih pitanja današnjice, što potvrđuje i visoka svjetska potražnja za naftnim cijevima.

U novije vrijeme započela su istraživanja i eksploatacija nafte u većim dubinama (preko 5000 m) što zahtijeva korištenje kvalitetnijih cijevi s granicom razvlačenja od 900 do 1000 MPa. Osim toga, u sve većoj se mjeri istražuje podmorje, kao i arktičko područje.

Posebno složeni uvjeti eksploatacije nafte i plina su u korozivnim sredinama zbog utjecaja agresivnih plinova H_2S i CO_2. Daljnja otežavajuća okolnost je ta, što se cijevi nalaze i u uvjetima povišenih radnih temperatura od 220 do 330ºC, odnosno povećanog pritiska i do 100 MPa.

Visoku kvalitetu cijevi za naftnu industriju proizvođači postižu upotrebom čelika visoke čistoće i odgovarajućeg kemijskog sastava, te toplinskom obradom. Razvijeni su postupci za poboljšanje cijevi, koji osiguravaju ravnomjerno kaljenje i popuštanje cijevi s debljinama stjenke do 25,4 mm. Upotrebom defektoskopskih metoda bez razaranja osigurava se potpuno odstranjivanje grešaka na isporučenim cijevima [1, 2].

API (American Petroleum Institut) standard, je danas vodeći standard na području eksploatacije i prerade nafte.

Kvaliteta zaštitnih cijevi (casing) i spojnica (couplings) postiže se proizvodnjom odgovarajuće kvalitete čelika koja se postiže kombiniranjem kemijskog sastava čelika i njegove odgovarajuće toplinske obrade.

Niobij, kao mikrolegirajući element, djeluje na osobine čelika putem izlučenih karbonitrida. Oni se otapaju u austenitu na temperaturi iznad 1300ºC, a tijekom preradbe se izlučuju, blokirajući rast austenitnog zrna. Zbog toga nakon $\gamma \rightarrow \alpha$ preobražaja nastaje sitna feritno perlitna struktura [2, 3].

Vanadij usitnjava primarno austenitno zrno kao jaki karbidotvorac i nitridotvorac. Od mikrolegirajućih elemenata vanadij pokazuje najvišu topivost u austenitu bez obzira na sadržaj ugljika.

Vanadij slično ostalim mikrolegirajućim elementima ima jači afinitet prema dušiku nego ugljiku. Zavisno od sastava čelika i temperature, vanadij može precipitirati kao nitrid, karbonitrid ili karbid. Budući da su vanadij - nitridi i karbonitridi s visokim sadržajem dušika stabilni, da se fino dispergiraju i da su otporni prema okrupnjavanju, nastoji se pospješiti vezanje vanadija s dušikom.

Količina izlučenih vanadijevih precipitata ovisi osim o sastavu čelika i o dimenziji valjanog proizvoda, završnoj temperaturi plastične prerade,te brzini hlađenja poslije prerade [4].

Vanadijevi karbonitridi sadrže veće ili manje količine dušika, što opet ovisi o prisutnosti drugih elemenata i temperaturi žarenja čelika. Utvrđeno je, da čvrstoća čelika raste s porastom količine dušika u karbonitridima.

EKSPERIMENTALNI DIO

Plan pokusa i metode ispitivanja

Planom pokusa predviđeno je ispitivanje uzoraka od zaštitnih cijevi dimenzije ϕ244.5x11.99 mm (API $9^{5/8”}$x11,99) u Valjaonici bešavnih cijevi Željezare Sisak.

Glavni cilj ukupnog istraživanja je da se modificiranim kemijskim sastavom čelika N-80 postignu zadovoljavajuće mehaničke osobine po API standardu.

U odnosu na standardni sastav čelika N-80, modificirani čelik sadrži i mikrolegirajući element niobij, te povišeni sadržaj dušika. Uz istovremeno veći učinak vanadija i niobija u karbidima, nitridima i karbonitridima koji utječu na povećanje granice razvlačenja i povećanje žilavosti.

Na uzorcima bešavnih cijevi dimenzije 244.5x11.99 mm (API $9^{5/8”}$x11,99) provedena su ispitivanja u normaliziranom i poboljšanom stanju. Postignuti rezultati ispitivanja uspoređeni su s propisanim vrijednostima po standardu.

U istraživanju su korištene sljedeće metode ispitivanja:

- Određivanje kemijskog sastava čelika na emisijskom vakuumskom kvantometru ARL-31000 i uređaju za određivanje sadržaja ugljika i sumpora LECO/WR-12.
- Frakcijska analiza dušika i kisika, na automatskom uređaju LECO TC-436.
- Metalografska ispitivanja strukture, na mikroskopu ORTHOLUX, Leitz i kameri Olympus DP 11.
- Izolacija i analiza faza. Elektrokemijska izolacija izvršena je u elektrolitskoj ćeliji po W. Kochu, a maseni udio elementa izmjeren je na spektrometru atomske apsorpcije Perkin Elmer 503. Metoda difrakcije rendgenskih zraka upotrebljena je za određivanje faznog sastava izolata [5].
- Mehanička ispitivanja izvršena su na elektronskoj kidalici INSTRON 1196 prema API Std 5 CT standardu, pri brzina razvlačenja 5 mm/min.
- Ispitivanje žilavosti po Sharpy-u izvršeno je na epruvetama kvadratnog presjeka sa V zarezom.

REZULTATI ISPITIVANJA

Rezultati analize kemijskog sastava čelika N-80 prikazani su u tablici 1.

Tablica 1. Kemijski sastav čelika N-80, maseni %

C	Si	Mn	Cr	Ni	Mo	V	Al	Cu	Sn	P	S	Nb	N
0.33	0.27	1.13	0.10	0.06	0.01	0.16	0.012	0.13	0.008	0.011	0.015	0.042	0.0160

Rezultati frakcijske analize dušika prikazani su u tablici 2.

Tablica 2. Raspodjela dušika u nitridima i karbonitridima

Toplinska obrada	**Količina dušika N % vezana na:**				
	željezo Fe	željezo-mangan Fe-Mn	vanadij V	aluminij-niobij Al-Nb	Ukupan dušik N %
Normalizirano 890ºC/35' zrak	0.0027	0.0095	0.0047	0.0006	0.0175
Poboljšano kaljeno 870ºC/35' ulje popušteno 600ºC/60' zrak	0.0024	0.0088	0.0052	0.0007	0.0171
kaljeno 870ºC/35' ulje popušteno 600ºC/60' zrak	0.0021	0.0085	0.0054	0.0006	0.0166

Rezultati izolacije i analize faza prikazani su u tablici 3 i 4.

Tablica 3. Rezultati izolacije i kvantitativne analize faza

Toplinska obrada	masa izolata %	sadržaj elemenata u izolatu		vezano u spojeve		stupanj vezanja %	
		V %	Nb %	V_V %	Nb_V %	V_V/V_{UK}	Nb_V/Nb_{UK}
Valjano	3.50	2.30	0,59	0.081	0.021	50.63	52.50
Normalizirano 890ºC/35' zrak	3.62	2.73	0.60	0.099	0.022	61.87	55.00
Poboljšano kaljeno 870ºC/35' ulje popušteno 600ºC/60' zrak	3.71	2.76	0.62	0.102	0.023	63.75	57.50
kaljeno 870ºC/35' ulje popušteno 600ºC/60' zrak	3.77	2.74	0.61	0.103	0.023	64.40	57.50

V_V , Nb_V - vanadij vezani, niobij vezani
V_{UK} , Nb_{UK} - vanadij ukupni, niobij ukupni, iz tablice 1

Tablica 4. Kvalitativna analiza izoliranih faza metodom rendgenske difrakcije.

Izolat	Utvrđene faze
karbidi - nitridi	Fe_3C, Fe_2C, NbN, VN, NbC, VC
oksidi	$FeO \cdot Nb_2O_5$, $3Al_2O_3 \cdot 2SiO_2$, $FeO \cdot Al_2O_3 \cdot 5SiO_2$
sulfidi	FeS, MnS

Rezultate metalografskih ispitivanja strukture u normaliziranom i poboljšanom stanju pokazuju slike 1 i 2.

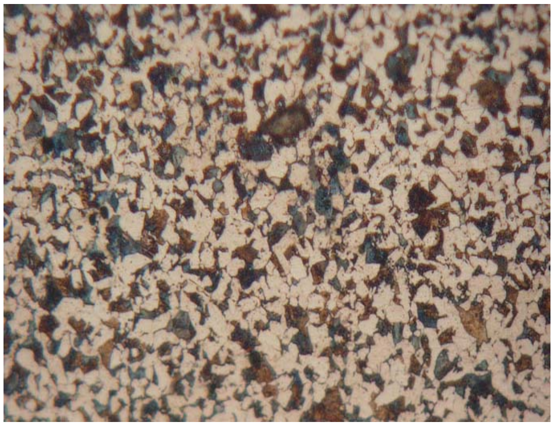

Slika 1. Mikrostruktura u normaliziranom stanju, 890ºC/35 min., nital, 280x

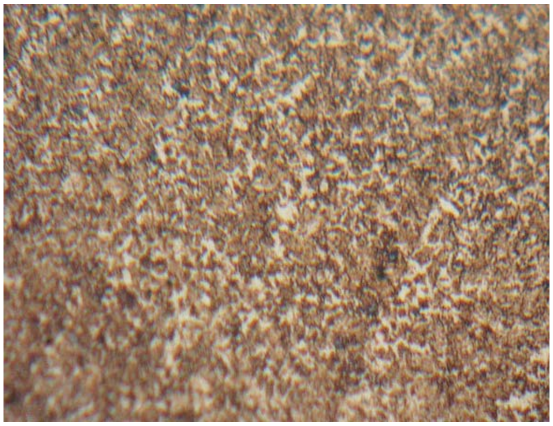

Slika 2. Mikrostruktura u poboljšanom stanju, 870ºC/35 min. kaljeno u ulju i popuštano na 620ºC/60 min., nital, 280x

Rezultati mehaničkih ispitivanja prikazani su u tablici 5.

Tablica 5. Mehanička svojstva u valjanom, normaliziranom i poboljšanom stanju

Mehanička svojstva	granica razvlačenja R_{eh}/MPa		čvrstoća Rm/MPa		istez. A/%	kontr. Z/%
	min.	ispitano	min.	ispit.		
Valjano	552	482	689	733	22.8	59.0
Normalizirano 890ºC/35' zrak	-	566	-	770	25.3	59.9
Poboljšano kaljeno 870ºC/35' ulje popušteno 600ºC/60' zrak	-	743	-	841	19.1	62.2
kaljeno 870ºC/35' ulje popušteno 600ºC/60' zrak	-	719	-	785	21.3	61.5

Rezultati ispitivanja udarne žilavosti KV na 0^0C i tvrdoće HRC u normaliziranom i poboljšanom stanju prikazani su u tablici 6.

Tablica 6. Žilavost KV na 0°C i tvrdoća HRC u normaliziranom i poboljšanom stanju

Toplinska obrada	Žilavost KV, J/cm^2		Tvrdoća HRC	
	min.	ispitano	min.	ispitano
Normalizirano 890ºC/35' zrak	28.75	35.87	22	22.50
Poboljšano kaljeno 870ºC/35' ulje popušteno 600ºC/60' zrak	28.75	77.03	22	22.50
kaljeno 870ºC/35' ulje popušteno 600ºC/60' zrak	28.75	35.87	22	22.50

ZAKLJUČAK

Na temelju provedenih ispitivanja mogu se postaviti slijedeći zaključci:

1. U ispitivanom čeliku API N-80 modificiranog kemijskog sastava, boljim iskorištenjem mikrolegirajućih elemenata mehanizmom boljeg vezanja u karbidima i nitridima, utječe se na bolje mehaničke osobine i žilavost.

2. Rezultati izolacije i analize faza pokazuju da količina izlučenih karbida, nitrida i karbonitrida ovisi o načinu toplinske obrade. Ispitivanjima je utvrđeno da je najmanji stupanj vezanja vanadija u valjanom stanju (50,63%), a najveći u poboljšanom stanju (64,40%). Količina vezanog niobija u valjanom stanju iznosi 0,021%, u normaliziranom 0,022%, a najveća u poboljšanom stanju 0,023%. Ispitivanjem je utvrđeno, da je najmanji stupanj vezanja niobija u valjanom stanju (52,50%), a najveći u poboljšanom stanju (57,50%).

3. Mehanička ispitivanja zatezanjem provedena su na: valjanim, normaliziranim i poboljšanim uzorcima, prema API Std 5CT standardu.
Rezultati ispitivanja uzoraka u normaliziranom i poboljšanom stanju zadovoljavaju propisane vrijednosti.

4. Rezultati žilavosti i tvrdoće u normaliziranom i poboljšanom stanju pokazuju vrlo dobre vrijednosti.

5. Rezultati metalografskog ispitivanja strukture pokazuju da normalizirani uzorci imaju nešto veća zrna u odnosu na poboljšano stanje koji pokazuju izrazito sitno zrno i finu strukturu. Zbog toga poboljšani uzorci čelika imaju bolje mehaničke osobine, a naročito veću žilavost na 0°C.

6. Analizom svih rezultata ispitivanja može se zaključiti da modificirani sastav čelika API N-80 ne osigurava tražene osobine u valjanom stanju.
Potrebne vrijednosti žilavosti i mehaničkih osobina po standardu API Std 5CT postignute su tek nakon normalizacijskog žarenja.
Najbolji rezultati postignuti su ipak na uzorcima u poboljšanom stanju, žilavost KV na 0^0C 109 J/cm^2 i granica razvlačenja $R_{EH} = 751$ MPa.

LITERATURA

1. A.Preloščan, F. Vodopivec, I. Mamuzić: Fine-grained structural steel with controlled hot rolling, Materials and Technology 36 (2002) 5, 181-185.
2. M.Malina, A.Prelošćan, J.Butorac: Tendencije razvoja proizvodnje čeličnih cijevi za naftnu industriju, Metalurgija 24 (1985) 4, 161-167.
3. M.Kornchynsky: Symposium - Low Alloy High - Strength Steels, Nurnberg (1970) 17
4. M.Kornchynsky, J.Pauls: Microalloyed Forginy Steels, SAE International Congress and Exsposition Detroit. Michigan II, (1989)
5. M.Prelošćan, A. Prelošćan, V.Živanović-Magdić: Utjecaj termomehaničke obrade na proces izlučivanja niobija u visokočvrstim konstrukcijskim čelicima, Metalurgija 24 (1985) 1, 29-34.

FRICTIONAL BEHAVIOUR OF GLASS FIBRE REINFORCED POLYMER COMPOSITES

J. Quintelier[1], P. Samyn[1], P. De Baets[1]
[1]Department of Mechanical Construction and Production
Laboratory Soete, Ghent University
St. Pietersnieuwstraat 41, 9000 Ghent, Belgium

Abstract:

Based on the well-known pin-on-disc test rig, a new test-set up has been developed for measuring the wear and friction behaviour of polymer matrix composites online. Instead of the standard composite specimen and steel disc, a rotating composite disc and steel pin is used to be able to have a visible composite wear track.

The material used in this investigation is glass fibre reinforced polyester. This material was produced via the pultrusion process, resulting in a well know structure of the composite disc. A non-woven, and finally the unidirectional fibres follow a top layer. This structural influence has a major importance in the evolution of wear and friction.

Under different loads and speeds, the wear and frictional behaviour of these pultruded composites. A thin film yields a reduction of the frictional force with almost 20%. The reduction disappears when the film is removed, as a result of the change in structure, resulting in a very thin film, which just covers slightly the fibre surface. After this 'removal' of the film as a result of the structure the friction force reaches is old level. Related to the production method, the results of the fibre orientation on the friction force can be shown. Perpendicular fibre orientation yields higher frictional force, parallel results in a lowest friction force. If the friction coefficients of these test are all put in one graph, statements about the influence of fibre orientation, load, speed and underlying structure can be made.

Keywords: Friction, composites, pultrusion, PV-value

INTRODUCTION

The study of wear of polymers in general and polymer based systems in particular is finding increasing citations in literature [1] due to the availability of wider choice of materials, ease of manufacturing, good strength and light weight. An area where their use has been found to be very effective is the situation involving sliding contact wear [2]. The polymer-based materials are preferred in recent years over metal-based counterparts in view of their low coefficient of friction [3] and ability to sustain loads. This has given an impetus to industrial production of the materials, as for instance in the production of bearing components used in automobile industries [4] such as gears, cams, wheels, etc.

However, the deployment of these as components for use in actual service requires good understanding of the processing related structure and its influence on wear and friction. Also the relationship between formulation and performance is not clear and complex problems involving instabilities in the coefficient of friction, excessive wear, vibration, and noise accompany the friction processes of polymer matrix composite materials [5]. A friction process is always accompanied by the development of wear debris, which adheres to the rubbing couple [6]. As a result, a characteristic friction layer (thin film) forms on the surface, and this thin film determines performance [7].

TEST RIG

A new pin-on-disc test rig (Fig. 1) was built in order to be able to monitor the tribological behaviour of composite materials as bearing material. The materials on the most common pin-on-disc set-up [8-11] (composite pin/steel disc) were switched, namely a composite disc and a steel pin were used. This yields the possibility that in one test the influence of the fibre orientation on wear and friction can be investigated by choosing an unidirectional fibre reinforced composite.

The pin (7), made of steel, with a length of 35 mm is hollow at the top, because measuring bending of the pin with strain gauges requires a sufficient strain in the steel pin. Two flat parallel faces close to the contacting surface are places for an accelerometer (see Fig. 1,a) and an acoustic emission sensor. Thermocouples can be placed all over the pin geometry. A ball from a deep groove ball bearing forms the mating surface, or the top of the pin. Thus the pin can be reused, while only the ball has to be replaced.

Characteristics of this test rig are: relative velocities from 10 up to 100 mm/s, a possible normal load up to 1000 N, and the possibility to place additional sensors on the pin (2) for further research.

For the measurement of the wear depth of the wear track, a contactless proximitor (9) is used, providing an estimate of the evolution of the wear depth with time.

For measuring the normal force on the pin a load cell is placed above the pin (1). This load cell is protected by a spring mechanism, which allows pressing directly on the load cell, without damaging this load cell. Another method to measure the normal force on the pin is by measuring the air pressure in the cylinder used as supplier for the normal force. This cylinder is connected via valves to the compressor. The friction force is measured with a load cell (2).

On the rotating disc, magnets (8) are placed, which are used as trigger for the various signals, but are also used to synchronize measured friction and wear signals with the fibre orientation. This type of indication is very reliable, and gives the possibility to calculate the values of the friction force related to a specific orientation (0°, 90°, 180°, 270°).

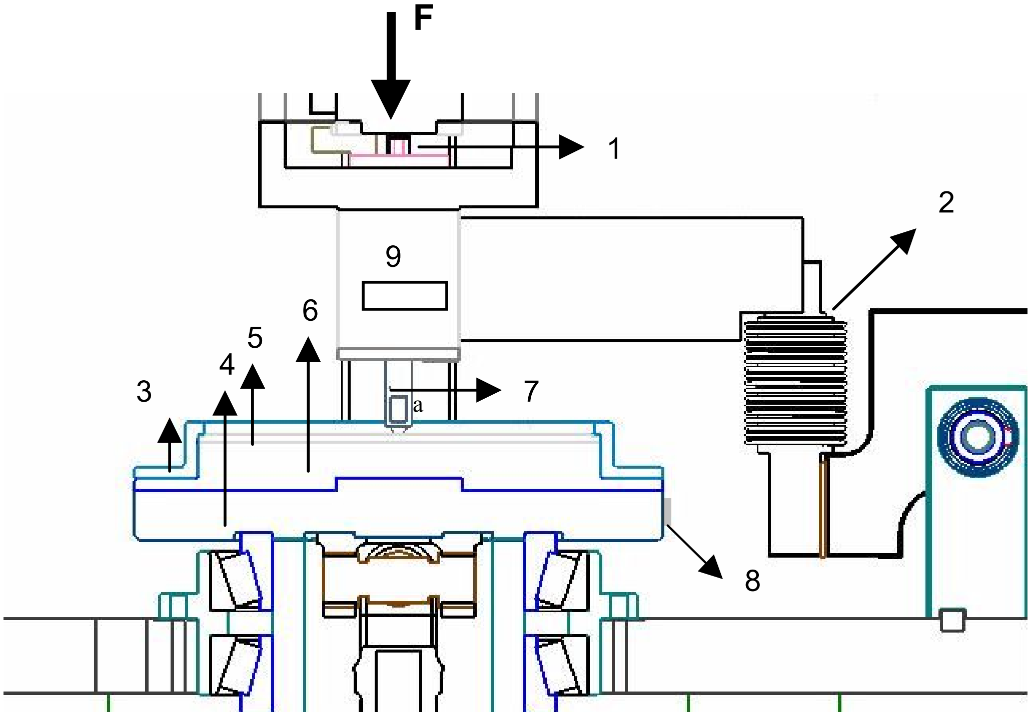

Fig. 1: Pin-on-disc test rig, with (1) normal load cell, (2) friction load cell, (3) ring for keeping the composite disc fixed and in the centre, (4) fixed disc on the test rig, (5) composite disc, (6) removable disc where the composite test specimen is glued on, (7) pin, (8) magnets for triggering, (9) contactless proximitor counter face

On a steel disc (6), the composite disc (5) is fixed with bee wax. Due to high frictional loads this might not prevent rotation of the disc, therefore the disc is kept in place with an external ring (3). This ring not only presses slightly the composite disc onto the steel disc at the edge, but also makes sure that the composite disc stays centered to the rotation, yielding a perfectly circular wear pattern on the disc. This replaceable disc construction is then placed on a fixed disc (4). The whole disc construction rests on two bearings, and is driven by the axis of a reduction unit, which itself is driven by an asynchronous motor through a speed reducer and a timing belt.

MATERIALS AND METHOD

The material used in this investigation is glass fiber reinforced low profile polyester. The material is produced via pultrusion revealing a typical structure (Fig. 2).

The test rig is based on classical Pin-on-Disc, with in this case a composite disc and a steel pin. The discs were cut out larger plates by water jet process.

Tests were performed at different speeds (10 – 40 mm/s) and different loads (100 – 300N, via weights) resulting in different Fv values. Tests were performed for 10.000 rounds of 400mm.

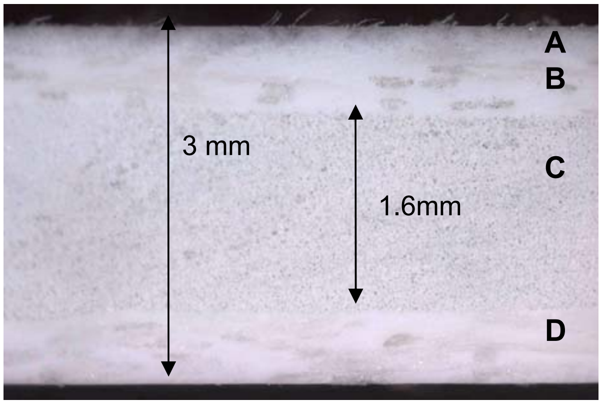

Fig. 2: Cross section of material used

RESULTS AND DISCUSSION

The results on the frictional behavior in function of the Fv value of this material are shown in Fig. 3. The use of Fv instead of the classical Pv can be stated due to the combined wear of pin and disc, and differences in width of the wear track depending on load and speed, as such that a combination of load multiplied by speed yields to almost the same contact area after 10000 rounds. The same Fv value can be the results of a different combination of load and speed, for instance 150N*40mm/s equals 200N*30mm/s. The difference in behavior seen by Fv = 6000 is the result of the structure of the pultruded plates. It can be stated that the higher coefficient of friction in case of 150N (circled in Fig. 3) is the result of not reaching the unidirectional fibers of the pultruded profile (zone C in Fig. 2).

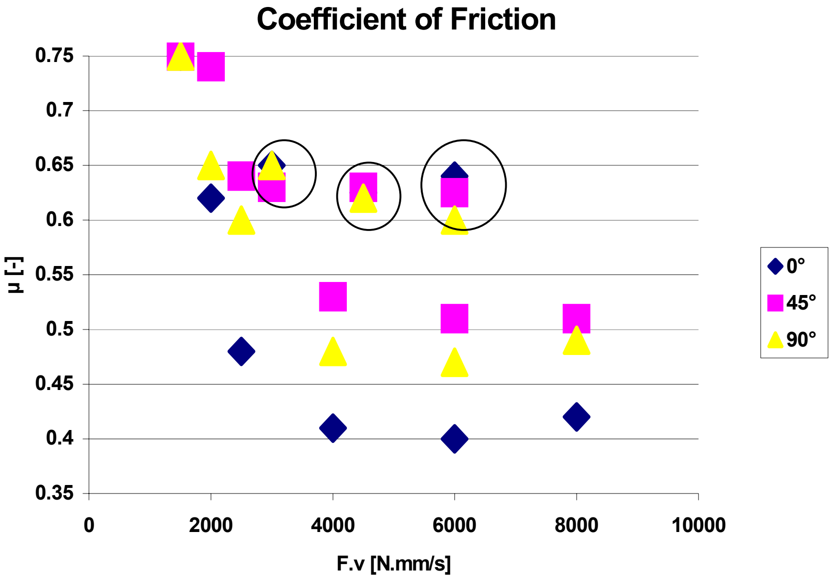

Fig. 3: Coefficient of friction in function of various Fv values

Starting at 200N and higher loads results in reaching the unidirectional fibres after 10.000 rounds and a clear separation of the friction force related to the fibre orientation. This proves the fact that in the case of 150N not the complete thickness of zone B is removed. At Fv = 6000 the case where the normal load equals 150N also shows the beginning of a separation between the fibre orientation. This, in correlation with a clear separation starting with 200N and an Fv of 2000, means that the normal load has a more pronounced influence on the frictional behaviour related to the fibre orientation than the speed. Higher speeds results in lower coefficients of friction after the same distance of sliding.

The separation of the coefficient of friction with fiber orientation yield that an orientation of 45° related to the direction of motion results in the highest coefficient of friction, the parallel orientation in the lowest. Differences between these orientations of 0.13 in coefficient of friction are shown.

The results on the wear behaviour of these materials yield the formation of a thin film onto the wear track, as a result of particles, falling from the edges of the wear track, being pressed against and later on over the composite surface, depending on the normal force and the underlying composite structure. Although this film results in a lowering of the coefficient of friction (up till 20%), this film is not protecting the surface from wearing. Differences in wear mechanisms can be stated, because due to the film deformation the surface is subjected to shear in the film in the direction of movement combined with shear forces parallel to the direction of motion. This results in a stepwise cross section of the wear track, determined by the toughness of the glass fibres. These fibre ends are coming in the zone of contact with the pin and results in wear of the pin.

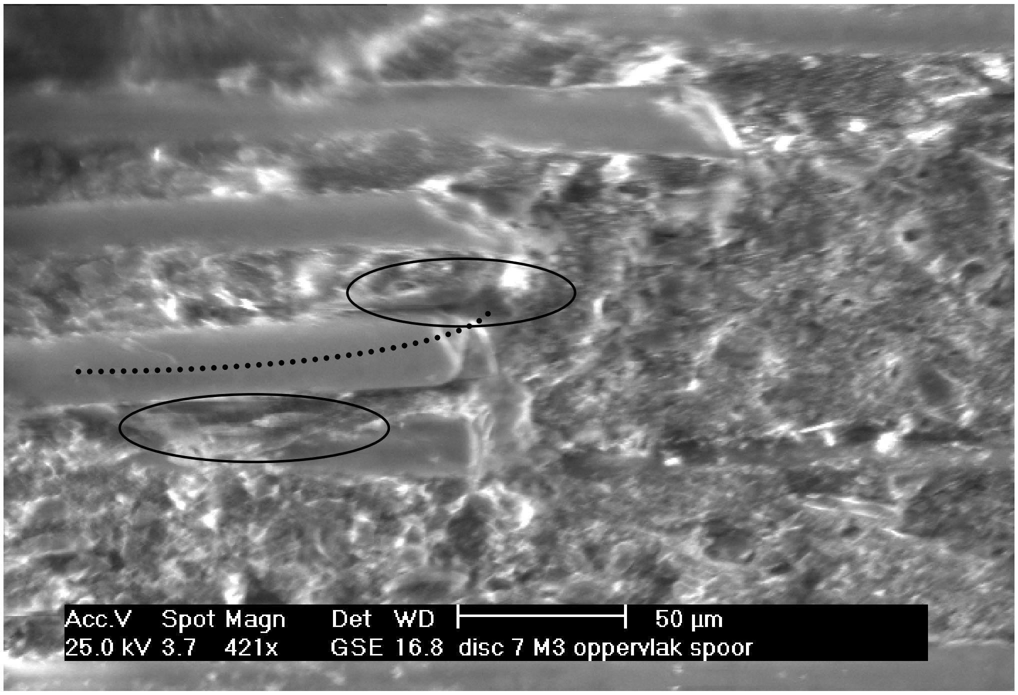

Fig. 4: SEM of the wear track

In Fig. 4 a typical result of the wear surface is shown. The direction of motion is vertical. First of all the end of the fibers is correlated with a deeper zone were the matrix material and the fibers are already removed. Fiber matrix debonding can be seen in the pure polyester zone. The two ellipses on the figure indicate zones of removed material as a result of the movement of the pin. This resulted in the bending of the fiber and ‘wearing’ away of the matrix. The fibers itself are removed after brittle fracture as a result of early bending of the fiber at the edges of the wear track, or as a result of the high contact pressure in the center of this wear track.

CONCLUSIONS

The composite structure plays an important role in frictional behavior of composite materials.

The normal load has more influence than the speed on the frictional behavior.

The 45° fibre orientation yields the highest coefficient of friction, while the parallel orientation the lowest.

REFERENCES

[1] Scott D. Henry, Materials for friction and wear applications, ASM Handbook, ASM International, Materials Park, Pa., U.S.A.,1992

[2] R. Ramesh, Kishore and R.M.V.G.K. Rao, "Dry wear studies on glass-fibre-reinforced epoxy composites" Wear, 89(1983), pp. 131-136

[3] S.K. Biswas and K. Vijayan, "Friction and wear of PTFE — a review" Wear, 158(1992), pp. 193-211

[4] K. Friedrich in K. Friedrich ed., Friction and Wear of Polymer Composites, Composite Materials Series, Vol. 1, Elsevier, Amsterdam, 1986, p. 233.

[5] P. Filip, Z. Weiss and D. Rafaja, "On friction layer formation in polymer matrix composite materials for brake applications" Wear, 252 (2002), pp. 189-198

[6] J. Schön, "Coefficient of friction and wear of a carbon fiber epoxy matrix composite"Wear, 257(2004), pp. 395-407

[7] R.S. Cowan and W.O. Winer in D. Dowson, ed., Proceedings of the 19th Leeds-Lyon Symposium on Tribology, Elsevier, Amsterdam, 1989, pp.631

[8] J. P. Davim, N. Marques, Dynamical experimental study of friction and wear behaviour of bovine cancellous bone sliding against a metallic counterface in a water lubricated environment, Journal of Materials Processing Technology 152 (2004) 389–394

[9] K. Friedrich, J. Flöck, K. Váradi, Z. Néder, Experimental and numerical evaluation of the mechanical properties of compacted wear debris layers formed between composite and steel surfaces in sliding contact, Wear 251 (2001), pp. 1202–1212

[10] R.L. Fusaro, Counterface effects on the tribological properties of polyimide composites, Lubr. Eng. Vol. 42 (1986), pp. 668-676

[11] P. Põdra, S. Andersson, Simulating sliding wear with finite element method, Trib. Int. 32 (1999), pp. 71-81

10. Savjetovanje o materijalima, tehnologijama, trenju i trošenju
10. Conference on Materials, Processes, Friction and Wear
MATRIB'05, Vela Luka, 23-25.06.2005

MATERIALS USED FOR EXTRUSIONS AND FOR INJECTION MOLDING

Prof.dr.Nedžad Repčić
Faculty of Mechanical Engineering
University of Sarajevo
tel. 65 31 92, 65 65 62 fax. 65 30 55
e.mail: repcic@mef.unsa.ba,
Sarajevo,Vilsonovo 9, B&H

Abstract: The homopolymers are available in several viscosity ranges that meet a variety of processing and end-use needs. The higher viscosity materials are generally used for extrusions and for molded parts requiring maximum toughness; the lower viscosity grades are used for injection molding. Elastomer-modified grades offer greatly improved toughness. Properties: Acetal homopolymer resins have high tensile strength, stiffness, resilience, fatigue endurance, and moderate toughness under repeated impact. Properties of low moisture absorption, excellent creep resistance, and high deflection temperature suit acetal homopolymer for close-tolerance, high-performance parts. Long-term behavior in various environments can be predicted from design handbook data. Applications: Automotive applications of acetal homopolymer resins include fuel-system and seat-belt components, steering columns, window-support brackets, and handles. Typical plumbing applications that have replaced brass or zinc components are shower heads, ballcocks, faucet cartridges, and various fittings. Consumer items include quality toys, garden sprayers, stereo cassette parts, butane lighter bodies, zippers, and telephone components. Industrial applications of acetal homopolymer include couplings, pump impellers, conveyor plates, gears, sprockets, and springs. Acrylic thermoplastics are known for their crystal clarity and outstanding weatherability. They are available in cast sheet, rod, and tube; extruded sheet and film; and compounds for injection molding and extrusion. Cell-cast sheet is produced in several sizes and thicknesses. Alkyd molding compounds are based on unsaturated polyester-type resins, which are combined with crosslinking monomers, catalysts, reinforcements, lubricants, and fillers. The formulations are similar to those of thermosetting polyesters but with lower amounts of monomers.But each process may create stresses in different areas. Sometimes, processing conditions are so severe that there is no choice but to redesign the shape and change to a different plastic. Designers used to take little interest in the molding of parts they designed. They sent the drawings to the molder in another department or another company and expected perfect parts to emerge. But design and processing have become so interrelated that this separation can no longer exist if products are to be consistently successful. Molders can usually be relied upon to detect and correct visible problems or readily measured factors such as color, surface condition, and dimensions. Even here, there is the danger that these sources may not be aware of the many compromises a company must make internally among production, engineering, purchasing, and marketing considerations to produce a product that will sell at a profit. Also, a molder might be inclined to recommend the material that works best in his equipment, rather than the best for the application.

Key words: materials, extrusion, injection, molding

INTRODUCTION

The copolymers have an excellent balance of properties and processing characteristics. Melt temperature can range from 182 to 232 °C with little effect on part strength. The resin is available in natural (translucent white) and in a wide range of colors. UV-resistant grades (also available in colors), glass-reinforced grades, low-wear grades, and impact-modified grades are standard. Also available are electroplatable and dimensionally stable, low-warpage grades. Properties: Acetal copolymers have high tensile and flexural strength, fatigue resistance, and hardness. Lubricity is excellent. They retain much of their toughness through a broad temperature range and are among the most creep resistant of the crystalline thermoplastics. Moisture absorption is low, permitting molded parts to serve reliably in environments involving humidity changes. Good electrical properties, combined with high mechanical strength and a UL electrical rating of 100 °C, qualify these materials for electrical applications requiring long-term stability. A new acetal copolymer resin, Ultraform S 1320X-003, is available from BASF Corporation Plastic Materials. It has a combination of high mechanical and heat deflection properties (close to those of acetal homopolymers) and the good thermal stability and processing properties of acetal copolymer resins. The tensile strength, modulus of elasticity, impact strength, heat-deflection temperature, and surface hardness are about 10% higher than those of general-purpose acetal copolymers. The impact-modified acetal copolymer resins have a good balance of toughness and rigidity. Acetal copolymers have excellent resistance to chemicals and solvents. For example, specimens immersed for 12 months at room temperature in various inorganic solutions were unaffected except by strong mineral acids -- sulfuric, nitric, and hydrochloric. Continuous contact is not recommended with strong oxidizing agents such as aqueous solutions containing high concentrations of hypochlorite ions. Solutions of 10% ammonium hydroxide and 10% sodium chloride discolor samples in prolonged immersion, but physical and mechanical properties are not significantly changed. Most organic reagents tested have no effect, nor do mineral oil, motor oil, or brake fluids. Resistance to strong alkalies is exceptionally good; specimens immersed in boiling 50% sodium hydroxide solution and other strong bases for many months show no property changes.Strength of acetal copolymer is only slightly reduced after aging for one year in air at 115 °C. Impact strength holds constant for the first six months, and falls off about one-third during the next six-month period. Aging in air at 82 °C for two years has little or no effect on properties, and immersion for one year in 82 °C water leaves most properties virtually unchanged. Samples tested in boiling water retain nearly original tensile strength after nine months. Applications: Industrial and automotive applications of Celcon acetal copolymer include gears, cams, bushings, clips, lugs, door handles, window cranks, housings, and seat-belt components.Plumbing products such as valves, valve stems, pumps, faucets, and impellers utilize the lubricity and corrosion and hot-water resistance of the copolymer. Mechanical components that require dimensional stability, such as watch gears, conveyor links, aerosols, and mechanical pen and pencil parts, are other uses. Applications for the FDA-approved grades include milk pumps, coffee spigots, filter housings, and food conveyors. Parts that require greater load-bearing stability at elevated temperatures, such as cams, gears, TV tuner arms, and automotive underhood components are molded from glass-fiber-reinforced grades.

ACRYLIC THERMOPLASTICS

Acrylic thermoplastics are known for their crystal clarity and outstanding weatherability. They are available in cast sheet, rod, and tube; extruded sheet and film; and compounds for injection molding and extrusion. Cell-cast sheet is produced in several sizes and thicknesses.

Acrylic sheet cast by the continuous process (between stainless-steel belts) is more uniform in thickness than cell-cast sheet. Cell-cast sheet, on the other hand, which is cast between glass plates, has superior optical properties and surface quality. Also, cell-cast sheet is available in a greater variety of colors and compositions.Cast acrylic sheet is supplied in general-purpose grades and in ultraviolet-absorbing, mirrored, super-thermoformable and cementable grades, and with various surface finishes. Sheets are available in transparent, translucent, and opaque colors. Acrylic film is available in 2, 3, and 6-mil thicknesses, in clear form and in colors. It is supplied in rolls to 1525 mm wide, principally for use as a protective laminated cover over other plastic materials. Injection-molding and extrusion compounds are available in both standard and high-molecular-weight grades. Property differences between the two formulations are principally in flow and heat resistance. Higher molecular-weight resins have lower melt-flow rates and greater hot strength during processing. Lower molecular-weight grades flow more readily and are designed for making complex parts in hard-to-fill molds. Also available are high-impact molding grades, which provide the same transparency and weatherability as the conventional acrylics.

Properties: Acrylic plastics transmit and control light, resist weather, are stable against discoloration, and have superior dimensional stability and an excellent combination of structural and thermal properties. Clear acrylic plastic is as transparent as the finest optical glass. It has a light transmittance of 92%, exceptionally low haze level of approximately 1%, and an index of refraction of 1.49 -- high enough for use in lenses and other optical applications.Colorants produce a full spectrum of transparent, translucent, or opaque colors. Most colors can be formulated for long-term outdoor durability. Acrylics are normally formulated to filter ultraviolet energy in the 360-nm and lower band. Other formulations are opaque to UV light or provide reduced UV transmission. Mechanical properties of acrylics are high for short-term loading. However, for long-term service, tensile stresses must be limited to avoid crazing or surface cracking. The moderate impact resistance of standard formulations is maintained even under conditions of extreme cold. High-impact grades have considerably higher impact strength than standard grades at room temperature, but impact strength decreases as temperature drops. Special formulations ensure compliance with Underwriters' Laboratories standards for bullet resistance. Although acrylic plastics are among the most scratch resistant of the thermoplastics, normal maintenance and cleaning operations can scratch and abrade them. Special abrasion-resistant sheet is available that has the same optical and impact properties as standard grades. Toughness of acrylic sheet, as measured by resistance to crack propagation, can be improved severalfold by inducing molecular orientation during forming. Jet-aircraft cabin windows, for example, are made from oriented acrylic sheet. Acrylic sheet and moldings resist solutions of inorganic acids and alkalies and aliphatic hydrocarbons such as VM&P naphtha, as well as most detergent solutions and cleaning agents. They are attacked, however, by chlorinated and aromatic hydrocarbons, esters, and ketones. Transparency, gloss, and dimensional stability of acrylics are virtually unaffected by years of exposure to the elements, salt spray, or corrosive atmospheres. These materials withstand exposure to light from fluorescent lamps without darkening or deteriorating. They ultimately discolor, however, when exposed to high-intensity UV light below 265 nm. Special formulations resist UV emission from light sources such as mercury-vapor and sodium-vapor lamps. Applications: Cast acrylic sheet is used in aircraft, boat, mass transit, architectural, and protective glazing; internally illuminated outdoor signs, lighting diffusers, and skylights; and product prototypes and demonstration models. Special ultraviolet-absorbing grades are used for document preservation in museums and for various photographic applications. Acrylic film is used as a laminated protective surface on ABS, PVC, or other plastic sheet that is thermoformed into parts requiring resistance to outdoor weathering.

Examples include motorcycle shrouds, recreational-vehicle panels, residential siding, and transformer housings. Acrylic moldings are used for light-control lenses in lighting fixtures, camera lenses, vending-machine parts, and appliance panels, knobs, and housings. Automotive applications include lenses for taillights and parking lights, instrument panels, nameplates, medallions, and dials. A modified molding compound contains an impact modifier to increase toughness. Parts molded from these durable transparent materials include automotive dials, housewares, piano keys, medical instruments, and toys. Specially formulated acrylic sheet is available for deeply formed components such as tub-shower units, which are subsequently backed with glass-fiber-reinforced polyester. Chemical resistance of this sheet is superior to that of conventional sheet. Sheet extruded from the high-impact molding grade is used for signs, thermoformed products, toys, and glass-fiber-polyester-backed components such as camper tops, furniture, and recreational-vehicle bodies.

ALKYD MOLDING COMPOUNDS

Alkyd molding compounds are based on unsaturated polyester-type resins, which are combined with crosslinking monomers, catalysts, reinforcements, lubricants, and fillers. The formulations are similar to those of thermosetting polyesters but with lower amounts of monomers. Alkyds are part of the group of materials that includes bulk-molding compounds (BMCs) and sheet-molding compounds (SMCs). They are processed by compression, transfer, or injection molding. Fast molding cycles at low pressure make alkyds easier to mold than many other thermosets. Alkyds are furnished in granular compounds, extruded ropes or logs, bulk-molding compound, flake, and puttylike sheets. Except for the putty grades, which may be used for encapsulation, these compounds contain fibrous reinforcement. Generally, the fiber reinforcement in rope and logs is longer than that in granular compounds and shorter than that in flake compounds. Thus, strength of these materials is between those of granular and flake compounds. Because the fillers are opaque and the resins are amber, translucent colors are not possible. Opaque, light shades can be produced in most colors, however.Properties: Low-moisture absorption and excellent dimensional stability and electrical properties are the outstanding characteristics of most alkyd molding compounds. For electrical-grade materials, absorption can be as low as 0.5%. Alkyds are relatively low-loss materials, especially the mineral-filled and glass-filled grades.Those containing cellulose may have higher loss characteristics and "drift" with temperature and humidity changes. Molded alkyd parts resist weak acids, organic solvents, and hydrocarbons such as alcohol and fatty acids; they are attacked by alkalies. Glass and asbestos-filled compounds have better heat resistance than the cellulose-modified types. Depending on type, alkyds can be used continuously to 177 °C and, for short periods, to 232 °C. Alkyd molding compounds retain their dimensional stability and electrical and mechanical properties over a wide temperature range. Halogen and/or phosphorus-bearing alkyd molding compounds with antimony trioxide added provide improved flame resistance. Other flame-resistant compounds are available that do not contain halogenated resins.

Many grades are UL-rated at 94V-0 in sections. Flammability ratings depend on specific formulations, however, and can vary from 94HB to V-0. Flammability ratings also vary with section thickness.Applications: High-impact grades of alkyd compounds (with high-glass content) are used in military switchgear, electrical terminal strips, and relay and transformer housings and bases. Mineral-filled grades, which can be modified with cellulose to reduce specific gravity and cost, are used in automotive ignition parts, radio and TV components, switchgear, and small appliance housings. Alkyds with all-mineral fillers have high moisture resistance and are particularly suited for electronic components. Grades are available that can withstand the temperatures of vapor-phase soldering.

ESTERS IN THE ALLYL FAMILY

Esters in the allyl family consist principally of diallyl phthalate (DAP) and diallyl isophthalate (DAIP). Both are used as monomers and as prepolymers, which are readily converted to thermoset molding compounds and resins for preimpregnated glass cloth and paper. Allyls are also used as crosslinking agents for unsaturated polyesters. Compounds based on allyl prepolymers are reinforced with fibers (glass, polyester, or acrylic) and filled with particulate materials to improve properties. Glass fiber imparts maximum mechanical properties, acrylic fiber provides the best electrical properties, and polyester fiber improves impact resistance and strength in thin sections. Compounds can be made in a wide range of colors because the resin is essentially colorless.

Prepregs (preimpregnated glass cloth) based on allyl prepolymers can be formulated for short cure cycles. They contain no toxic additives, and they offer long storage stability and ease of handling and fabrication. Properties such as flame resistance can be incorporated. The allyl prepolymers contribute excellent chemical resistance and good electrical properties. Properties: Allyl molding compounds do not corrode copper or plated inserts or contacts, even in hot, humid environments. Molded parts maintain their high electrical properties at high temperature (to 188 °C for DAP and 205 °C for DAIP) and humidity levels. Allyl materials are also characterized by excellent dimensional stability and resistance to moisture, chemicals, and liquid oxygen. They withstand strong and weak acids, alkalies, and organic solvents, even at elevated temperatures.

Allyl moldings have low mold shrinkage and postmold shrinkage -- attributed to their nearly complete addition reaction in the mold -- and have excellent stability under prolonged or cyclic heat exposure. Advantages of allyl systems over polyesters are freedom from styrene odor, low toxicity, low-evaporation losses during evacuation cycles, no subsequent oozing or bleed-out, and long-term retention of electrical-insulation characteristics. Applications: Diallyl phthalate monomer is used as a nonvolatile crosslinker in polyester compounds to improve properties and handling characteristics. Deflection temperature is raised to 205 °C or higher, dimensional stability and electrical properties are upgraded, and flexural properties are retained for long periods at elevated temperatures. DAP is also used in combination with polyester resin systems for low-pressure decorative laminates. Allylic resins in powder and liquid form are used for coatings and for impregnating materials. Allyl prepolymers are particularly suited for critical electronic components that serve in severe environmental conditions. Chemical inertness qualifies the resins for molded pump impellers and other chemical-processing equipment. Their ability to withstand steam environments permits uses in sterilizing and hot-water equipment. Because of their excellent flow characteristics, diallyl-phthalate compounds are used for parts requiring extreme dimensional accuracy. Modified resin systems are used for encapsulation of electronic devices such as semiconductors and as sealants for metal castings.A major application area for allyl compounds is electrical connectors, used in communications, computer, and aerospace systems. The high thermal resistance of these materials permits their use in vapor-phase soldering operations. Uses for prepolymers include arc-track-resistant compounds for switchgear and TV components. Other representative uses are insulators, encapsulating shells, potentiometer components, circuit boards, and housings. Allyl-based prepregs are used to make lightweight, intricate parts such as radomes, printed-circuit boards, tubing, ducting, and aircraft parts. Another use is in copper-clad laminates for high-performance printed-circuit boards. FEP resin applications include wire and cable insulation for computer and electronic systems, telephone and alarm systems, and business-machine interconnects, FEP resin is also supplied as extruded sheet and film for release surfaces, roll covers, linings for chemical-processing tanks, and piping.

CONCLUSIONS

Melamine and urea are the principal commercial thermosetting polymers called aminos. The amino resins are formed by an addition reaction of formaldehyde and compounds containing NH 2 amino groups. They are supplied as liquid or dry resins and filled molding compounds. Applying heat in the presence of a catalyst converts the materials into strong, hard products. Aminos are used as molding compounds, laminating resins, wood adhesives, coatings, wet-strength paper resins, and textile-treating resins.

The base resin used in urea and melamine molding compounds is water-white and transparent. Translucent and opaque colors are produced by adding pigments and opacifying agents. Cellulose fibers improve strength and dimensional stability and reduce light transmission.

Properties: Moldings made from amino compounds are hard, rigid, abrasion resistant, and have high resistance to deformation under load. They do not impart taste or odor to foods, and they have excellent electrical insulation characteristics. Melamines are superior to ureas in resistance to acids, alkalies, heat, boiling water, and for applications involving wet/dry cycling. Urea and some melamine molding compounds have flammability ratings of 94V-0. Melamines containing alpha cellulose, mineral, or glass fibers have the greatest flame resistance. These materials can be used for appliance parts classified by UL as indirect supports of current-carrying parts. Melamines and ureas are not resistant to strong oxidizing acids or strong alkalies, but they can be used safely with conventional household chemicals such as naphtha and detergents. They are unaffected by organic solvents such as acetone, carbon tetrachloride, ethyl alcohol, heptane, and isopropyl alcohol. Petroleum, paraffin hydrocarbons, gasoline, kerosene, motor oil, aromatic hydrocarbons, and fluorinated hydrocarbons (Freon) have no apparent effect on urea and melamine moldings. Dimensional stability is good, but moldings do swell and shrink slightly in varying moisture conditions. Baking of molded parts accelerates postmold shrinkage and improves dimensional stability, dielectric strength, and dissipation factor.

Applications: Typical applications for cellulose-filled urea resins include circuit breakers, receptacles, and other electrical wiring devices, toaster and other appliance bases, pushbuttons, knobs, handles, piano keys, and camera parts. Cellulose-filled melamine is used principally for dinnerware. Other applications include utensil handles, food-service trays, and housings for electric shavers and mixers. Industrial melamine compounds are used for meter blocks, connector plugs, automotive and aircraft ignition parts, standoff terminals, coil forms, and switch housings. In liquid form, both urea and melamine resins are used as baking-enamel coatings, particleboard binders, and paper and textile treatment materials. Both resins are also used in compounding adhesives. Melamine, the more durable of the two, is waterproof, which qualifies melamine-based adhesives for exterior use. A concentrate is available for Freon-blown-foam wire coating.

REFERENCES

[1] Brown, R.: Handbook of Polymer Testing, RAPRA Technology Limited, 2002.
[2] Culter, J.: Plastics Packaging:Properties, Processing, Applications,RAPRA,2001.
[3] Massey,L.: Permeability Properties of Plastics and Elastomers, England, 2000.
[4] Herman, M.: Encyclopedia of Polymer Science and Technology, Amazon, 1999.
[5] Malloy,R.: Plastic Part Design for Injection Molding , Pergamon press , Oxsford , 2001.
[6] Tres,P.: Designing Plastics Parts for Assembly, England, 2002.
[7] Zweifel, H.: Plastics Additives Handbook, Springer Verlag, 2000.
[8] Catalogues and standards: ISO, EN, DIN, SKF, FAG, SHELL, ASME, SAE, VDI, FAM, INA.
[9] Web sites - http:// www / science / engineering / design / tribology/ plastics

10. Savjetovanje o materijalima, tehnologijama, trenju i trošenju
10. Conference on Materials, Processes, Friction and Wear
MATRIB'05, Vela Luka, 23-25.06.2005.

COMPARATIVE STUDY ON THE FRICTION AND WEAR BEHAVIOUR OF INTERNAL LUBRICATED CAST NYLONS ON A LARGE-SCALE TRIBOTESTER

P. Samyn, J. Quintelier, P. De Baets

Department of Mechanical Construction and Production
Laboratory Soete, Ghent University
St. Pietersnieuwstraat 41, 9000 Gent, Belgium

Abstract

Preliminary small-scale tests on pure and oil-filled cast polyamides show a transition towards lower friction for pure polyamides due to transfer and higher friction for oil-filled polyamides, as the oil diffusion is restricted. On large-scale samples, pure polyamides are prone to heavy stick-slip, which can be reduced by proprietary solid lubricants. Solid (wax) lubricants are more effective in providing stable friction and low wear than oil-filled polyamides, as the latter form thick and brittle transfer films with additional running-in effects after mid-time restart. An increase in sliding temperature however causes a reversible transition towards stick-slip above 50°C. Different catalysers (Na, Mg) influence the stiffness and thermal stability of polyamide, competing for low wear rates and melting.

Keywords: Polyamide, friction, wear, small-scale, large-scale

1. INTRODUCTION

Nylons are widely used plastics, especially as bearing and wear material. Depending on their composition, they cover a wide range of applications with increasing interest in demanding applications where large size sliding parts are required, as e.g. in a crane guidance, resisting wear, abrasion and vibration. Tribological research [1] is however mostly performed on small test specimens, while present study focuses on a practical simulation test for better estimation of the loading capacities and wear rates. The applied contact pressures and pv-values exceed the values cited in literature and the exposure rate of lubricant depends the contact area.

2. EXPERIMENTAL SMALL-SCALE AND LARGE-SCALE TESTING

Both reciprocating small-scale and large-scale test rigs as shown in Figure 1 are used. As a reference, small-tests are performed with a line contact between a polymer cylinder (Ø 5 mm x 12 mm) and a steel plate under 100 N and 200 N normal load and 0.3 m/s sliding velocity. Large-scale tests are performed on polymer plates with sliding area 150 x 150 mm^2 and steel counterfaces measuring 410 x 200 mm^2, under contact pressures between 8 MPa to 150 MPa and a sliding velocity of 0.005 m/s. The surface roughness R_a is approximately 0.2 µm for both test configurations. Test materials include two pure polyamides PA 6 obtained with different catalytic processes, two synthetic oil-filled polyamides and two proprietary solid lubricant filled polyamides obtained by low pressure casting (Table 1). Wear rates are calculated from weight reduction after a drying procedure of 3 hours in a hot-air oven.

Test material		d (g/cm^3)	E (MPa)	HRc	σy (MPa)	ε (%)	HDT (°C)
Pa-Na	pure nylon Na catalysed	1.15	1900	88	55	25	80
Pa-Mg	pure nylon Mg catalysed	1.15	2100	83	60	70	75
PAo1	homogeneous oil dispersion	1.135	1700	82	40	20	75
PAo2	lubricating oil in holes	1.135	1600	85	45	22	75
PAs1	proprietary solid lubricated	1.14	1500	81	50	25	75
PAs2	proprietary solid lubricated	1.11	1450	59	62	10	70

Table 1. Different polyamide grades and their mechanical properties

Large-scale tester	Small-scale tester
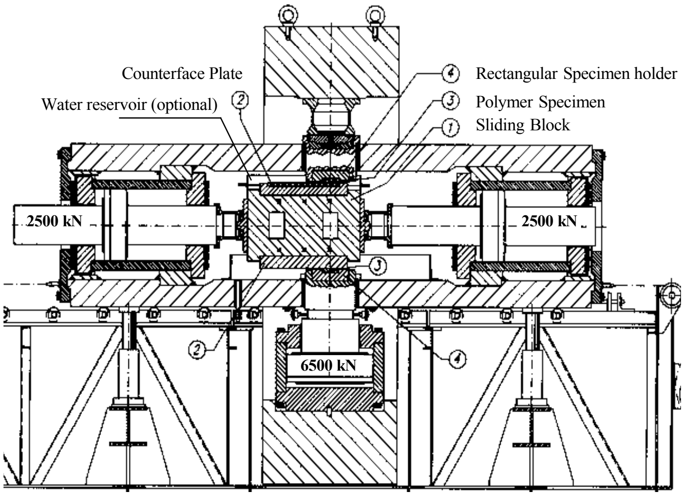	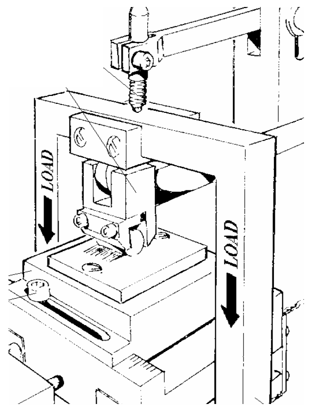

Figure 1. Test-rigs available for large-scale and small-scale specimen tests

3. TEST RESULTS
3.1 Preliminary small-scale tests

The evolution of friction and wear with sliding distance as presented in Figure 2 for pure and oil-filled nylons reveals different transitions. Pure Pa-Na show instable sliding during a running-in period, suddenly dropping to a constant friction value and a continuous increasing wear depth, as correlated to the occurrence of a thick and continuous transfer film. Pa-Mg has higher friction and a stabilised wear depth, while forming a discontinuous flake-like transfer film. The high work of rupture for Pa-Mg compared to Pa-Na definitely contributes to higher sliding resistance and deformation component of friction. Moreover, the lower HDT temperature for PA-Mg contributes to melting and stick-effects. No visual or a very thin transfer film was observed for PAo1, although a strong transition in friction is observed after 250 m sliding distance. The lubricating effect of oil is based on partial diffusion [2] of oil through the polymer bulk to be provided at the sliding interface. Local melting and deformation of the polymer bulk however restricts the oil diffusion and leads to friction values that are identical to the unlubricated Pa-Na. Due to the specific surface structure of PAo2 with lubricant holes, tests could not be performed on small scale geometries.

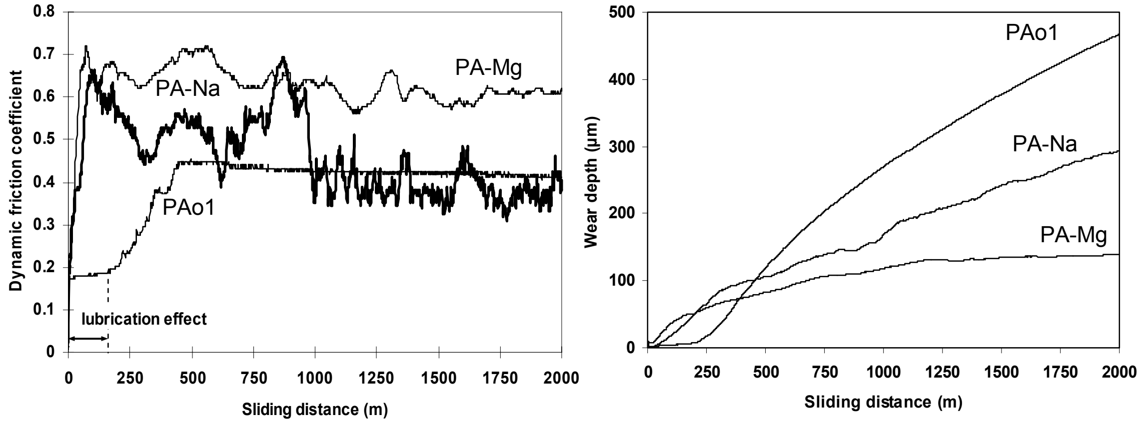

Figure 2. Small-scale friction and wear of pure and oil-filled nylons under 100 N, 0.3 m/s

A summary of average friction and wear rates measured on small-scale tests is given in Table 2, indicating various tendencies under low loads and under high loads. With Pa-Na as a reference, oil as internal lubricant seems more favourable under high loads for reduction in wear rates, while the tougher Pa-Mg provides lower wear rates under low loads. High friction of PAo1 under low loads possibly yields a strong increase in surface temperature and melting explains the high specific wear rates under 100 N compared to 200 N, in combination with reduction in strength after oil lubrication. The lower wear rates for Pa-Mg at low loads is attributed to the higher surface toughness, while melting is observed under 200 N.

	100 N normal load			200 N normal load		
	Friction	Wear rate (mm^3/m)	Specific wear rate (mm^3/Nm)	Friction	Wear rate (mm^3/m)	Specific wear rate (mm^3/Nm)
Pa-Na	0.44	0.0027	$2.72\ 10^{-5}$	0.49	0.0066	$3.29\ 10^{-5}$
Pa-Mg	0.68	0.0009	$9.13\ 10^{-6}$	0.63	0.0226	$11.3\ \ 10^{-5}$
PAo1	0.19 - 0.44	0.0063	$6.35\ 10^{-5}$	0.20 - 0.32	0.0021	$1.04\ 10^{-5}$

Table 2. Friction and wear results for small-scale tests under 100 N and 200 N normal loads

3.2 Pure polyamides under overload conditions

Pure PA-Na and PA-Mg were subjected to large-scale sliding tests in order to investigate the effect of surface plastification and/or melting on friction and wear mechanisms in overload conditions. It is known from general friction models that friction lowers with increasing normal loads, while the interaction with plastification, creep and/or higher sliding temperatures might lead to different transfer. Also the higher contact area compared to small-scale tests changes the wear debris movability. The measurements of friction with sliding distance are shown in Figure 3 and the wear rates for both top and bottom test specimens are calculated in Table 3. Contrasting to transitions on small-scale sliding, a continuous increase in friction with ongoing sliding and the heavy noise during large-scale sliding for PA-Na indicate severe stick-slip. The interaction between polyamide and its transfer film with highly polar molecules explains the unstable sliding. Friction of PA-Mg shows good accordance to PA-Na sliding, as surface plastification in both cases contributes to lower friction compared to small-scale tests. Only at 8 MPa the higher surface toughness induces different trends.

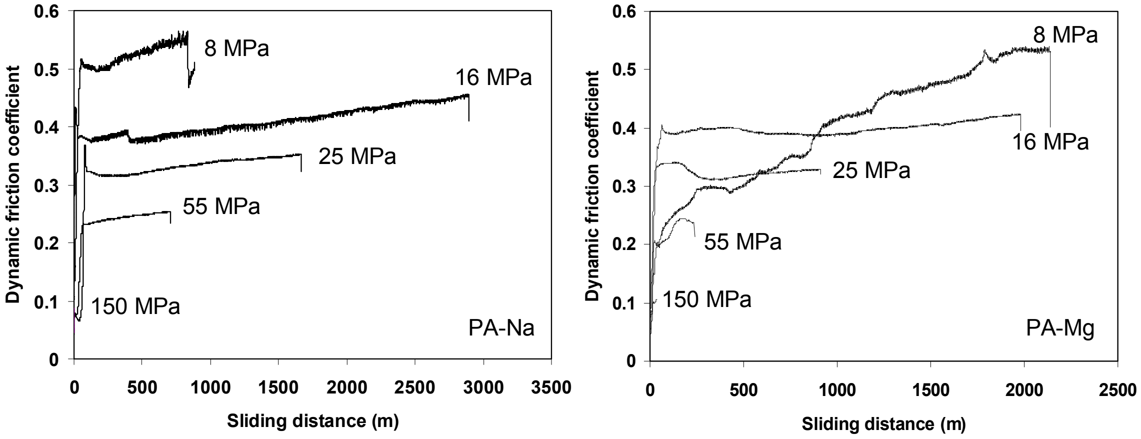

Figure 3. Large-scale friction of pure nylons PA-Na and PA-Mg under 8 MPa to 150 MPa

In accordance with small-scale tests, the wear rates for pure PA-Mg under low loads are below those for pure PA-Na, while overload effects for PA-Mg are more prominent due to observed melting (Figure 4) as implied by its lower heat-deflection temperature (HDT, Table 1). Differences in top and bottom wear rates reflect the influence of relative positioning of the wear sample and its counterface. There is better agreement between weight and thickness measurements for PA-Mg than for PA-Na own to its higher elasticity modulus (Table 1).

Polymer	Contact pressure [MPa]	Steady-state volumetric wear rates (mm^3/m)						Specific wear rate (10^{-6} mm^3/Nm)
		top specimen		bottom specimen		average		
		weight	dim	weight	dim	weight	dim	
PA-Na	8	1.46	2.05	1.74	4.35	1.60	3.32	8.42
	16	9.17	11.6	9.18	10.9	9.18	11.3	24.1
	25	8.35	11.6	9.84	11.5	9.10	11.5	20.5
	55	51.0	75.4	43.0	63.6	47.0	70.0	37.3
	150	Overload after 4 m sliding						
PA-Mg	8	0.88	0.75	1.23	1.14	1.06	0.95	5.57
	16	11.9	11.8	40.6	40.5	26.3	26.2	69.2
	25	69.7	69.8	67.2	67.3	68.4	68.5	122
	55	227	256	200	251	213	253	169
	150	Overload after 35 m sliding						-

Table 3. Volumetric wear rates and specific wear rates for pure polyamides after large-scale testing

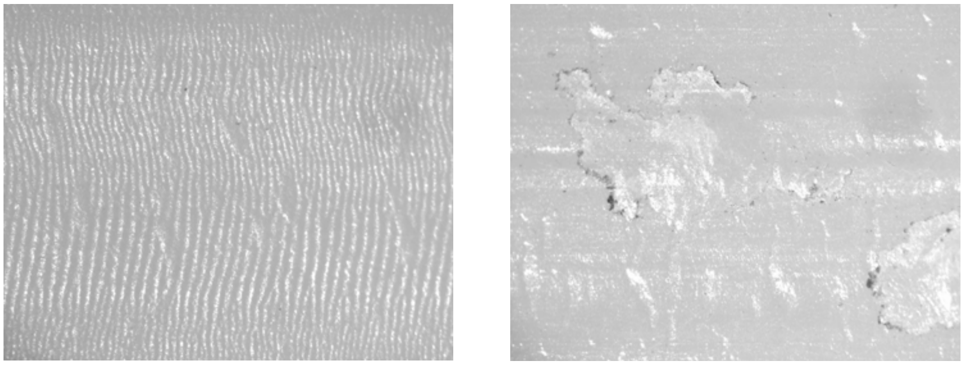

Figure 4. Optical microscopy of PA-Na (stick-slip) and PA-Mg (melting) after large-scale testing under 16 MPa

3.3 Effect of internal oil and solid lubricants under high loads

Solid lubricated polyamides were not small-scale tested, since it was already observed for internally lubricated PET [3] that lubricants become more effective under large-scale sliding. Under working conditions between 10 MPa and 40 MPa, the coefficients of friction and the wear depths are plotted in Figure 5 for pure, oil and solid lubricated polyamides. Each contact pressure was applied for 6 hours, where all nylon types have running-in phenomena during about 30 m sliding. Stick-slip effects are detailed in Table 4, with an indication of the static coefficients of friction at start (μ,s1) and at the reversals (μ,sn) of the sliding motion in relation to dynamic friction (μ,d). Solid (wax) lubricants are the most effective in reducing stick-slip. After a mid-term restart after 3 hours sliding under e.g. 40 MPa, the oil-filled grades again showed high static friction with additional running-in, while it immediately stabilised for solid lubricated nylons. Depending on the type of solids, small peaks in dynamic friction were however observed due to interaction with transfer (Figure 6). Bulk temperatures as measured remain below 35 °C. However an increase from 20 °C to 75 °C for PAs2 reveals gradually higher dynamic (0.06 to 0.09) and static (0.13) friction with a reversible transition at 50 °C towards stick-slip, disappearing after cooling.

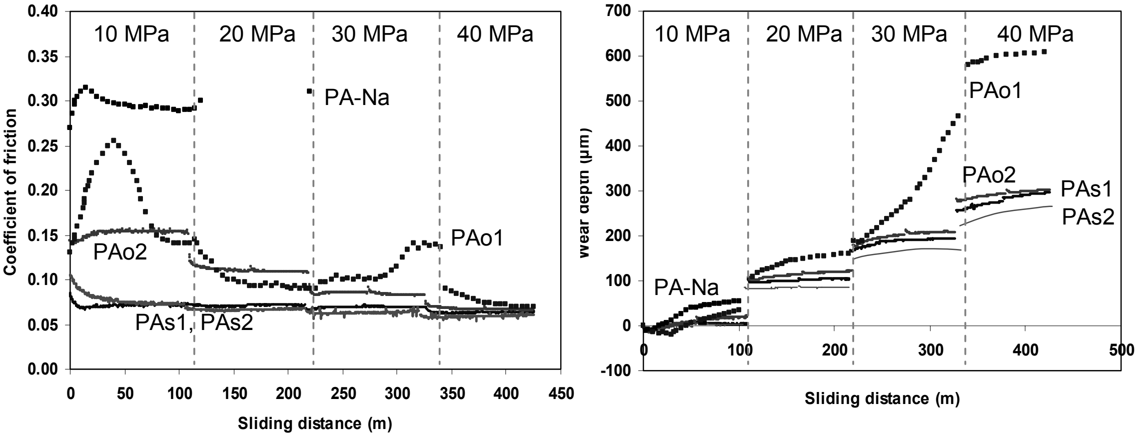

Figure 5. Friction and wear of oil and solid lubricated polyamides during large-scale tests at 10, 20, 30, 40 MPa

	10 MPa			20 MPa			30 MPa			40 MPa		
	µ sl	µ sn	µ d	µ sl	µ sn	µ d	µ sl	µ sn	µ d	µ sl	µ sn	µ d
PA-Na	0.16	0.33	0.30	0.26	-	-	0.28	-	-	-	-	-
PAo1	0.16	0.19	0.23	0.18	0.17	0.08	0.09	0.28	0.13	0.12	0.11	0.06
PAo2	0.24	0.22	0.17	0.22	0.15	0.12	0.15	0.12	0.09	0.11	0.10	0.08
PAs1	0.17	0.12	0.09	0.10	0.09	0.09	0.08	0.08	0.07	0.07	0.07	0.06
PAs2	0.15	0.09	0.09	0.08	0.08	0.07	0.08	0.08	0.07	0.08	0.08	0.07

Table 4. Static and dynamic coefficients of friction during large-scale tests at 10, 20, 30, 40 MPa

The wear rates in Table 5 refer to the entire 24 hours test with different loads and are therefore "overall values" used for a relative material classification. They are based on weight and dimensional measurements immediately after testing (1) and after 1 week recovery (2). According to friction properties, solid lubricants provide the lowest wear rates. Although, the strong reduction in elasticity e.g. for PAs2 causes higher deformation than for PAs1. The dimensional stability for homogeneous oil filled materials (PAo1) is worse than for lubricant holes (PAo2). Transfer (top) and polymer surfaces (under) are shown in Figure 6. The PAo2 forms a thick film that is however brittle with cracks and peeling off. Separate island-like

	Weight reduction (g)	Thickness reduction (mm)		Equivalent wear rate (mm^3/m)		
				Weight	Dimensional	
		(1)	(2)		(1)	(2)
PA-Na*	- 5.10	- 0.25	- 0.20	41.1	52.1	41.6
PAo1	- 8.56	- 0.62	- 0.50	17.4	32.3	26.1
PAo2	- 0.64	- 0.14	- 0.04	1.31	7.29	2.08
PAs1	- 0.24	- 0.05	- 0.03	0.49	2.61	1.56
PAs2	- 0.08	- 0.12	- 0.07	0.17	6.25	3.65

Table . Wear rates for oil and and solid lubricated polyamides under 10 MPa to 40 MPa (* only 10 MPa) depositions occur on the polymer surface besides the lubricant holes. The PAs1 shows coherent transfer in the roughness grooves and softened depositions. The PAs2 surface shows visually degradation, while a very transfer thin film is formed with locally brown coloured wear particles.

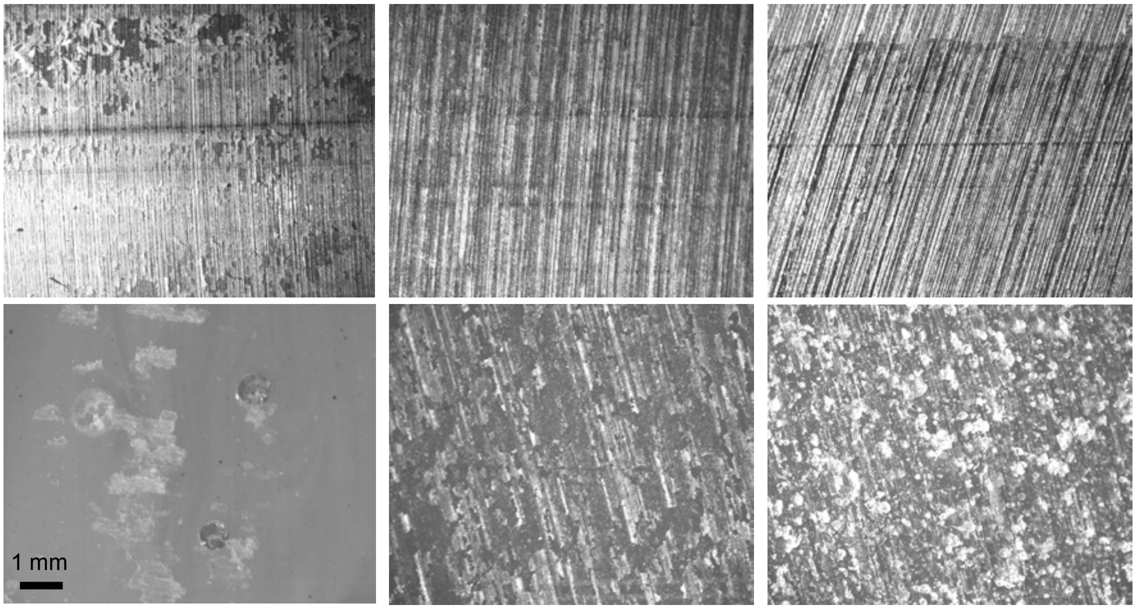

Figure 6. Optical microscopy of PAo2 and Pas1, Pas2 surface and transfer after large-scale testing at 40 MPa

4. CONCLUSIONS

Different behaviour of nylons on small-scale and large-scale test samples was observed, with a transition to stable friction for pure nylon on small-scale and continuous stick-slip on large-scale. Oil lubrication does not exclude stick-slip effects own to thick and brittle transfer, while it is favourably reduced by solid (wax) internal lubricants. An increase in bulk temperature above 50°C however induces against stick-slip.

References

[1] S.C. Kang, D.W. Chung, *Wear* 254 (2003), 103-110
[2] M. Marchetti, H.M. Meurisse, P. Vergne, J. Sicre, M. Durand, *Trib. Letters* 10,3 (2003), 163-170
[3] P. Samyn, J. Quintelier, W. Ost, P. De Baets, G. Schoukens, *Polymer Testing* (2005), in press

NANOSTRUCTURED HIGH STRENGTH ALUMINIUM PROFILES

František Simančík, Martin Balog, Juraj Nagy, Karol Iždinský

Institute of Materials and Machine Mechanics Slovak Academy of Sciences,
Račianska 75, 83102 Bratislava, Slovakia, e-mail: ummssima@savba.sk

Abstract:

Ultrafine-grained metals have attracted enormous interest among scientists because of their extraordinary properties. The current fundamental problem in the scope of world research on this topic is the preparation of fine graded (nanostructured) metallic materials in amounts and thickness, which would enable practical industrial application in machinery and other structures. The paper will review state-of-the-art in the technology for manufacturing of such bulk metals. Various techniques including deep drawing, ball milling, severe plastic deformation (ECAP), rapid solidification, etc. will be presented with respect to structure evolution, structure homogeneity, thermal stability and achieved properties.

Preparation of Al bulk profiles which can be potentially used as a construction material, in applications where high strength at room and elevated temperatures is required, was investigated. A bottom-up route was used, wherein thermally pre-prepared ultra-fine Al based alloy powders and quasicrystalline Al-alloys in the form of melt-spun ribbons (MSR) were consolidated by direct extrusion or modified equal channel angular pressing (ECAP) with an aim to keep the initial grain size in ultrafine grained region and thus obtain unique mechanical properties.

Ultrafine aluminium powder was used as a plasticizer in order to reduce high loads and/or temperatures required for extrusion of MSR. Ultra-fine grained Al matrix composites (MMC) reinforced with aperiodic MSR particles with improved plasticity and fracture toughness were obtained in this way. The nanoscale dispersoids arising on extrusion from broken Al powder oxides provide further strength increase and additionally act as barriers against extensive grain growth at elevated temperatures.

Microstructure of MMC compacts revealed well consolidated pore-free structure with plastically deformed Al powder matrix area reinforced with longitudinally arrayed MSR flakes, which exhibit almost no plastic deformation. Perfect metallurgical bonding without the presence of any third phase was observed on powder-ribbon interfaces. Due to finely dispersed nanooxides in the matrix the microstructure and the mechanical properties of such composite remained almost intact also after annealing at 350 °C for 20 hours. Influence of MSR flake size, powder-to-ribbon ratio, chopping method and processing parameters on the microstructure development and mechanical properties was studied.

Rod profiles with the diameter of 10 mm and the compressive strength up to 800 MPa were successfully extruded. UTS values up to 540 MPa with relatively good ductility (ETF up to 6 %) were achieved. Long exposure at 350°C resulted only in slight decrease of UTS values (5%), what confirmed good temperature stability of the structure.

The results will be compared with previous investigations made on plain MSR and also on plain fine 1 μm Al 99.7 % powder. It will be shown, that the use of both materials in a composite mixture brings additional synergetic effects, while utilising high strength of ribbons, good plasticity of powder and dispersion strengthening due to broken powder surface oxides.

ANALIZA NASTAJANJA I ŠIRENJA PUKOTINA U RADNIM KOLIMA FRANCIS TURBINA

Mikan Slijepac MARTING d.o.o., Nova cesta 171,
Zagreb
Mladen Franz Fakultet strojarstva i brodogradnje, Ivana Lučića 5,
Zagreb

Sažetak: U radu je teoretski i eksperimentalno obrađena problematika vezana za nastanak i širenje pukotina na turbinskim radnim kolima. Posebna pažnja posvećena je uzrocima koji djeluju na nastajanje i brzo širenje pukotina, a koji su vezani za svojstva materijala, djelovanje vanjskih i unutarnjih sila i vode kao radnog medija. U radu su povezani rezultati ispitivanja metodama kontrole bez razarenja (KBR) i rezultati eksperimentalnog ispitivanja uzoraka materijala s primjenom teoretskih metoda.

U eksperimentalnom dijelu rada na uzorcima iz eksploatacije, izvršeno je opsežno ispitivanje mikrostrukture i mehaničkih svojstava materijala iz kojih je određena i lomna žilavost (K_{1C}).

Primjenom rezultata iz eksperimenta, odabranih karakterističnih pukotina i poznatog naprezanja, metodama LEML i NLML mehanike loma izračunate su kritične i dopuštene duljine pukotina.

Na osnovi svih provedenih analiza materijala turbinskih elemenata i rezultata provedenih proračuna metodama mehanike loma utvrđeni su uzroci nastanka i širenja pukotina u eksploatacijskim uvjetima te dane preporuke za sustavno praćenje istih kao i sanaciju turbinskih radnih kola.

Ključne riječi: nehrđajući čelični lijev, mikrosturktura, lomna žilavost, napetosna korozija, širenje pukotina, kritične pukotine

Abstract: The thesis presents theoretical and experimental analysis of the problems related to the occurrence and propagation of cracks on the Francis water turbine rotor runners. Special attention has been paid to the causes which affect the cracks initialization and fast propagation in connection with material properties and the action of external and internal forces, as well as water as the working medium. The thesis combines the results of non destructive (NDT) method test and the results of material experimental testing, accompanied by applicable theoretical methods.

In the experimental part of the thesis, complex testing of microstructure and mechanical properties of material on samples taken from practice were performed, determining also the fracture toughness (K_{1c}).

From the application of experimental results, selected characteristic cracks and known stresses, the calculated critical and allowed length of the cracks were calculated by using LEFA and NLFA fracture mechanics.

Based on all the performed analyses of turbine component materials and calculation results by using fracture mechanics methods, the causes of cracks initialization and their propagation in working conditions have been determined and actions have been recommended for systematic monitoring of the cracks and turbine rotor runner.

Key words: corrosive-resistant steel casting, microstructure, fracture toughness, stress corrosion, cracks progression, critical cracks

1. UVOD

Turbinska radna kola izrađena su tehnologijom lijevanja iz nehrđajućih martenzitnih, martenzitno feritnih i mekomartenzitnih čeličnih ljevova, koji imaju zadovoljavajuću otpornost na koroziju i dovoljno dobra mehanička svojstva za izradu ovih elemenata. Prema stvarnim dimenzijama elementi vodnih turbina pripadaju kategoriji velikih odljevaka u kojima prilikom izrade neminovno dolazi do zaostajanja u materijalu značajnog broja makro nepravilnosti u obliku poroznosti, plinskih mjehurića, segregacija kemijskih elemenata, nemetalnih uključaka, površinskih ulegnuća i pukotina. Veći dio ovih makro nepravilnosti su i dopuštene prema standardnim zahtjevima za velike odljevke. Pored zaostalih makro nepravilnosti postoje i nepravilnosti u mikrostrukturi materijala koje nastaju u procesu toplinske obrade, poglavito kada se radi o elementima strojeva na kojima su debljine stijenki međusobno bitno različite. Odstupanje od željene mikrostrukture očituje se u neravnomjernom rasporedu faza i nepravilnom izlučivanju karbida (tvrde čestice intermetalnih spojeva). Navedene makro nepravilnosti već su same po sebi potencijalne inicijalne pukotine na čijim će vrhovima, pod djelovanjem vanjskih i unutrašnjih sila, nastati koncentracija naprezanja koja može izazvati stabilno ili nestabilno širenje pukotina. Makro nepravilnost ili inicijalna pukotina počet će se stabilno širiti, ako je na njenom vrhu koncentracija naprezanja veća od granične koncentracije kod koje počinje njen rast. Stabilno širenje pukotine odvijat će se tijekom rada sve dok pukotina ne postigne svoju kritičnu duljinu, što znači da je vrijednost faktora intenziteta naprezanja K_I dostigla svoju kritičnu vrijednost i da pukotina ulazi u područje nestabilnog širenja. Proces iniciranja i razvoja pukotina bitno će se ubrzati ako se ostvare uvjeti za pojavu napetosne korozije. Ti uvjeti su vrlo povoljni na mjestima makro nepravilnosti, nehomogene mikrostrukture, površinskim oštećenjima i mjestima najveće koncentracije naprezanja.

Prema najvećem dijelu raspoložive literature, u pravilu se navodi uspješna primjena mehanike loma na materijale koji imaju visoke vrijednosti granice razvlačenja. Vrlo mali broj autora upušta se u praktičnu primjenu ovih metoda na materijale gdje je $K_{IC}/R_e > 1.5$. Za materijale iz kojih su izrađeni analizirani elementi turbina ovaj faktor iznosi $K_{IC}/R_e > 5.7$, što znači, da prema ovom faktoru, sklonost materijala prema krhkom lomu trebala bi biti mala, a kritične duljine pukotina vrlo velike. Prema podacima iz eksploatacije, unatoč očekivanoj velikoj otpornosti materijala prema inicijalizaciji i širenju pukotina, nakon dugogodišnjeg rada na elementima turbina registriran je veliki broj pukotina i njihovo ubrzano širenje. Prema navedenom, uočeni problem proizlazi iz oprečnih činjenica, koje govore da materijal nije sklon pukotinama, a pukotine se javljaju. Razjašnjenje ovog problema je preduvjet da bi se mogla donijeti ocjena pouzdanosti elemenata turbine. Uočeni problem nastojati će se riješiti u ovom radu na osnovi informacija o pojavama pukotina u eksploataciji, rezultata dobivenih u eksperimentu, analizom izgleda i položaja pukotina i poznatog naprezanja u njihovom okolišu.

2. KARAKTERISTIČNI PRIMJERI PUKOTINA NA RADNIM KOLIMA FRANCIS TURBINA

2.1 Površinske pukotine

Na slikama br. 2.1-2 i 2.1-3 prikazan je karakterističan izgled površinskih pukotina na izlaznom bridu lopatica turbinskog radnog kola jedne brzohodne Francis turbine snage 21.3 MW i karakterističan izgled oštećenja površine izazvane erozijom usljed pojave kavitacije.

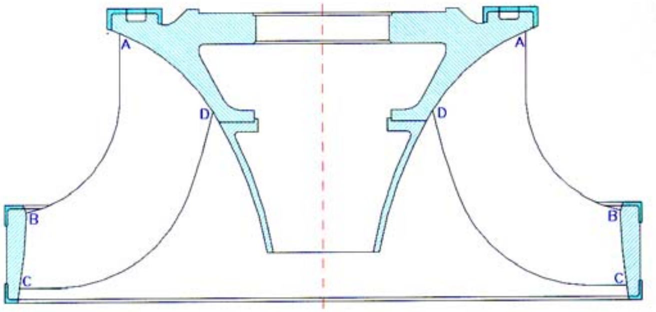

Slika 2.1-1 Presjek radnog kola

Slika br. 2.1-2

Slika br. 2.1-3

3. MEHANIČKA SVOJSTVA I MIKROSTRUKTURA

3.1 Mehanička svojstva

U tablici 3.1-1 prikazane su dobivene srednje vrijednosti mehaničkih svojstava na ispitnim uzorcima koji su uzeti iz poprečnog i uzdužnog smjera u zoni pojave pukotina. U tablici je također prikazan omjer granice razvlačenja $R_{p0.2}$ u odnosu na lomnu čvrstoću R_m.

Tablica 3.1-1 - Srednje vrijednosti rezultata mehaničkih svojstava ispitnih uzoraka iz materijala GX8CrNi13 [9]

Položaj epruvete na lopatici	Smjer	$R_{p0.2}$ N/mm^2	R_m N/mm^2	A_5 %	Z %	Udarna radnja loma KV J		$R_{p0.2}$ / R_m
						20°C	-20°C	
Rukavac	Poprečno	485	677	9,4	18	39,5	28,6	0,716
	Uzdužno	494	707	19,5	29,5	39,9	26,6	0,698
List	Poprečno	482	710	21,8	48	32,5	21,3	0,678
	Uzdužno	481	703	17,7	31,9	35,5	24,7	0,684
Priljevak	Zahtjev DIN 17445/1984	min 440	590-790	≥15	-	27	-	max 0,745

3.2 Osnovna svojstva iz linearno elastične mehanike loma

Prema rezultatima ispitivanja udarne radnje loma KV kod 20°C i -20°C rezultati su ujednačeni, a minimalne srednje vrijednosti dobivene na uzorcima iz eksploatacije su:

$$\overline{KV}_{20^\circ C} = 32.5 \ [J]$$

$$\overline{KV}_{-20^\circ C} = 21.3 \ [J]$$

Prema literaturi [6], eksperimentalno je definiran odnos između udarne radnje loma, KV [J] i lomne žilavosti K_{1C} koji glasi:

$$K_{1C} = 600.4\sqrt{KV} \tag{1}$$

Ova relacija vrijedi uz uvjet da je:

$$KV \ < 50[J] \text{ i } K_{1C} < 5000 \ \left[N/mm^{3/2}\right]$$

Primjenom relacije (1) i prema literaturi [7], u tablici 4.2-1 navedena su osnovna svojstva materijala GX8CrNi13 iz linearno elastične mehanike loma.

Tablica 3.2-1 - Osnovna svojstva iz linearno elastične mehanike loma za materijal GX8CrNi13 [7]

<table>
<tr><td colspan="4">LOMNA ŽILAVOST K_{1C} [N/mm$^{3/2}$]</td></tr>
<tr><td colspan="2">20°C</td><td colspan="2">-20°C</td></tr>
<tr><td colspan="2">$K_{1C} \approx 3400$</td><td colspan="2">$K_{1C} \approx 2800$</td></tr>
<tr><td colspan="4">Parametri brzine propagacije pukotine prema PARIS-ovoj relaciji:
$\frac{dL}{dN} = C(\Delta K)^m$</td></tr>
<tr><td colspan="2">Sredina zrak</td><td colspan="2">Sredina voda</td></tr>
<tr><td>C</td><td>m</td><td>C′</td><td>m′</td></tr>
<tr><td>$3.26 \cdot 10^{-16}$</td><td>3.9</td><td>$>3.26 \cdot 10^{-16}$</td><td>$\cong 3.9$</td></tr>
</table>

gdje su: C, C′, m i m′ konstante materijala [7]

3.3 Mikrostruktura

Materijal: GX8CrNi 13 (W.Nr. 1.4008)
Stanje toplinske obrade: poboljšano
Nagrizanje: elektrokemijski

Metalografska analiza mikrostrukture sa zdravog dijela radnog kola prikazana je na slici 3.3-1, koja predstavlja mikrostrukturu martenzitno-feritnog čelika sa nepovoljno izlučenim feritnom fazom po granici zrna. Oko feritne faze izlučeni su karbidi. U samom zrnu vidljive su granice podzrna na kojima su grupirani i sferodizirani karbidi. Ovakav izgled strukture je nepovoljan zbog oblika feritne faze i položaja izlučenih karbida.

Mikrostruktura snimljena s repariranog dijela ulaznog brida lopatice radnog kola prikazana je na slici 3.3-2, ista predstavlja tipičnu mikrostrukturu koja nastaje kod zavarivanja [8], što se prepoznaje po karakterističnom izgledu feritne faze. Feritna faza je izlučena po granicama zrna i razgranata s izraženim oštrim iglama ferita, a karbidi su grupirani u nizu.

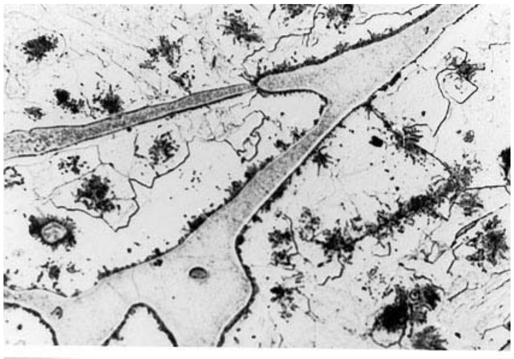

Slika 3.3-1 - U mikrostrukturi je vidljiva izlučena feritna faza po granicama zrna u matici popuštenog martenzita. Na granicama feritne mreže jasno se vide grupirani karbidi u nakupinama. U zrnu su vidljive granice podzrna i grupirani karbidi**.**

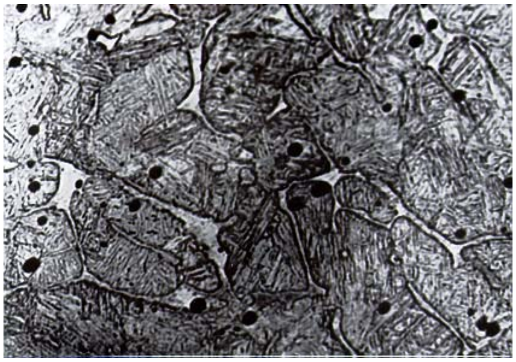

Slika 3.3-2 - Mikrostruktura uzorka s reparirane lopatice (povećanje 60:1). Mikrostriktura se sastoji od matice igličastog martenzita u kojoj je izlučena feritna faza po granicama zrna i razgranata s oštrim vrhovima, a koju okružuju izlučeni karbidi.

4. PRIMJENA MEHANIKE LOMA NA ANALIZU ŠIRENJA PUKOTINA

Praktična primjena mehanike loma na realnim konstrukcijama polazi od toga da u materijalu konstrukcije već postoje makro nehomogenosti tipa pukotina, čije se stanje analizira u polju mehaničkih naprezanja i deformacija.

Sigurnost napregnutih konstrukcija i elemenata strojeva ovisi o stvarnoj početnoj grešci u materijalu koja se može promatrati kao pukotina.

Dijagram na slici 4.-1 prikazuje moguće pukotine u materijalu te stupanj kritičnosti tijekom njezinog razvoja do loma.

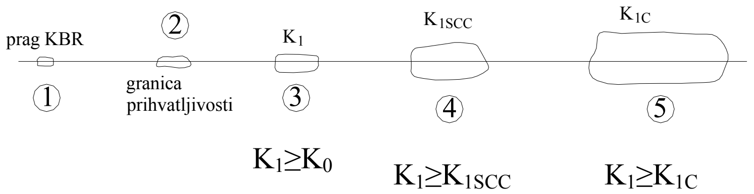

Slika 4.-1- Dijagram karakterističnih veličina pukotine u njezinom razvoju do loma

Značenje točaka u dijagramu:

1- najmanja pukotina koju je moguće registrirati KBR-metodama (kontrolom bez razaranja)
2- dozvoljena veličina pukotine koja ne ugrožava konstrukciju
3- veličina pukotine na kojoj je intenzitet naprezanja (K_1) dovoljan za početak razvoja pukotine
4- veličina pukotine pri kojoj nastaju aktivni mehanizmi napetosne korozije što znači da je intenzitet naprezanja K_{1SCC} (Stress Corrosion Cracking) ostvaren, pri čemu vrijedi da je $K_1 \geq K_{1SCC}$
5- veličina pukotine na kojoj se ostvaruje kritična vrijednost intenziteta naprezanja (K_{1C}), kad vrijedi $K_1 \geq K_{1C}$

Prag KBR-metoda određuje najmanju veličinu greške koja se uz zadovoljavajuću pouzdanost može registrirati.

Granica prihvatljivosti definira veličinu dozvoljene greške koja je uvijek veća od praga KBR-metoda. Istovremeno, granica prihvatljivosti je znatno manja od veličine pukotine na kojoj se postiže koncentracija naprezanja (K_1) koja odgovara početku razvoja pukotine.

Ukoliko se pretpostavi da KBR-metodama nije registrirana pukotina koja je veća od granice za početak razvoja pukotine, ista će se kod radnih naprezanja stabilno razvijati kroz proces plastičnog deformiranja uz koncentraciju naprezanja K_1. Proces razvoja pukotine će se bitno ubrzati ukoliko se ostvare uvjeti za pojavu napetosne korozije, odnosno, kada je žilavost znatno manja (K_{1SCC}). Ukoliko u cijelom periodu razvoja pukotine ista ostane neotkrivena, ili se u eksploataciji razvije zbog bilo kojih slučajnih događaja, pukotina će postići svoju kritičnu veličinu te će dostići faktor K_{1C} kada dolazi do nepredvidivog razvoja pukotine i do loma.

U primjeni mehanike loma važno je utvrditi da li se deformacije i naprezanja u dvoosnom stanju nalaze u području ravninskog stanja naprezanja ili ravninskog stanja deformacija.

Ravninsko stanje deformacija je stanje u kojem su deformacije okomite na ravninu glavnog naprezanja vrlo male, što se javlja u dovoljno debelim presjecima. Dijelovi konstrukcije koji se nalaze u takvom stanju deformacija skloni su krhkom lomu te je moguća primjena linearno-elastične mehanike loma (LEML), odnosno, primjena linearne elastičnosti. Kod ravninskog stanja naprezanja nastalog uslijed opterećenja promatranog dijela konstrukcije, naprezanja su planarno raspoređena. Deformacije kod ovakvog naprezanja imaju troosnu raspodjelu pa lomu prethode deformacije u sve tri osi i nastupa žilavi ili duktilni lom. U tom slučaju se provodi analiza pomoću nelinearne mehanike loma (NLML) za elasto-plastično stanje.

Kriterij na temelju kojeg se određuje sklonost dijela konstrukcije prema krhkom ili žilavom lomu je Irvin-ov uvjet koji je sastavni dio standarda ASTM E 399-81 za analizu pomoću mehanike loma. Prema tom uvjetu vrijedi da je debljina u kojoj se razvija pukotina jednaka:

$$h \geq 2.5 \cdot \left(\frac{K_{1C}}{R_{p0.2}} \right)^2 \tag{2}$$

gdje je:

h [mm] – debljina promatranog dijela
K_{1C} [N/mm$^{3/2}$] – lomna žilavost materijala
R_e[N/mm^2] – granica razvlačenja materijala

Svi dijelovi konstrukcije sa stijenkama debljim od (h) prema relaciji (2) podliježu metodama linearne mehanike loma (LEML), dok dijelovi tanji od (h) prema istoj relaciji podliježu metodama nelinearne mehanike loma (NLML).

Ne ulazeći u detalje mehanike loma, ovdje će se dati neki pojmovi važni za njenu primjenu. Kritična duljina ili dubina pukotina je veličina do koje se pukotina širi stabilno ili relativno sporo u polju promjenjivih naprezanja i deformacija. Kada pukotina dostigne svoju kritičnu veličinu, dolazi do njezinog nestabilnog širenja i loma. Do širenja pukotina može doći i uslijed djelovanja konstantne sile, što je slučaj kada djeluje napetostna korozija, koja se javlja i na radnim kolima Francis turbina.

U području linearne mehanike loma, kritična poluduljina pukotine (a_{kr}), računa se iz relacije:

$$a_{kr} = \frac{1}{M \cdot \pi} \cdot \left(\frac{K_{1C}}{\sigma_n} \right)^2 \tag{3}$$

Ovdje je:
K_{1C} [N/mm$^{3/2}$] – lomna žilavost, koja je karakteristika materijala i njegovog stanja
σ_n [N/mm^2] – normalno naprezanje u okolišu pukotine
M - faktor modifikacije koji ovisi o obliku pukotine te o obliku dijela u kojem je pukotina

Brzina širenja (propagiranja) pukotina definirana se kao prirast njezine poluduljine (da) prema prirastu broja ciklusa (dN). Ovdje je (N) broj cikličkih promjena. Dinamički intenzitet naprezanja izračunat je relacijom:

$$\Delta K = \Delta\sigma \cdot M \cdot \sqrt{\pi \cdot a} \qquad \frac{da}{dN} \tag{4}$$

$\Delta\sigma$ je promjena naprezanja i jednaka je u jednom ciklusu:

$$\Delta\sigma = \sigma_{\max} - \sigma_{\min} \tag{5}$$

Faktor nesimetričnosti naprezanja (R) je jednak:

$$R = \frac{\sigma_{\min}}{\sigma_{\max}} \tag{6}$$

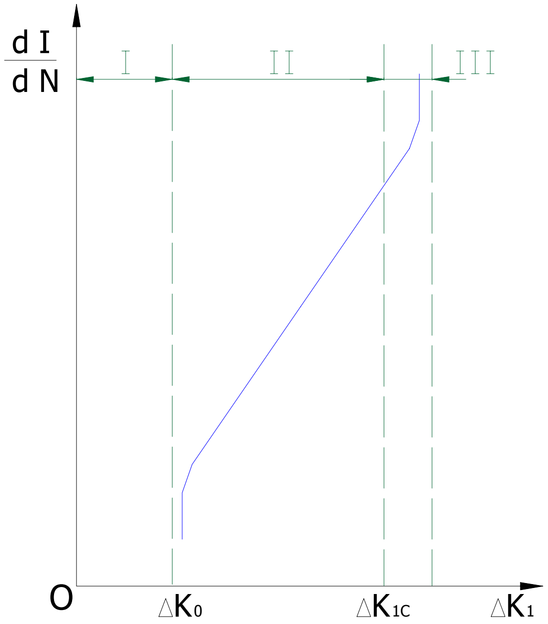

Slika 4.-2 Ovisnost brzine širenja pukotine da/dN o dinamičkom intenzitetu naprezanja ΔK

Krivulja na slici koja se sastoji od linearnog i zakrivljenog dijela, prikazuje u log-log mjerilu porast brzine širenja pukotine. Kao što se vidi, postoje tri (3) karakteristična područja:

I. $\Delta K < \Delta K_0$ – područje u kojem se pukotina neće širiti
II. $\Delta K_0 < \Delta K < \Delta K_{1C}$ – područje stabilnog rasta pukotine
III. $\Delta K < \Delta K_{1C}$ - kritično područje nestabilnog širenja pukotine

Analitička relacija koja povezuje da/dN i ΔK u području stabilnog širenja pukotine (područje II) prema Parisu je sljedeća:

$$\frac{da}{dN} = C \cdot (\Delta K)^m \tag{7}$$

ova relacija u području stabilnog rasta pukotine u izračunima, kroz izvedene formule, dosta dobro se podudara sa stvarnim širenjem pukotina na radnim kolima Francis turbina u eksploataciji, a njezin izvedeni oblik za pogonske cikluse radnog kola je:

$$N_{1,2} = \frac{1}{C \cdot \left(\frac{m}{2} - 1\right) \cdot \left(\Delta\sigma \cdot M \cdot \sqrt{\pi}\right)^m} \cdot \left(a_1^{1-\frac{m}{2}} - a_2^{1-\frac{m}{2}}\right) \tag{8}$$

gdje je:
a_1 – početna duljina pukotine
$a_2 = a_{kr}$ – kritična duljina pukotine
c = $3.26 \cdot 10^{-16}$ - konstanta materijala
m = 3.9 – konstanta materijala
$N_{1,2}$ = broj ciklusa potreban da se pukotina početne duljine a_1 proširi do a_2=a_{kr}

Primjer:

Radno kolo turbine br. 1

σ_n = 210 N/mm^2
a = 160 mm
a_{kr} = 47 mm → LEML [9]
a_{kr} = 119 mm → NEML [9]
a_d = 79 mm $\qquad a_d = \frac{a_{kr}}{1.5}$ - dozvoljena duljina pukotine

Prema izgledu pukotine na slici 2.1.-2, prihvaća se a_{kr} = 119 mm.

Prema Paris-ovoj relaciji (8), broj radnih ciklusa do postizanja kritične duljine pukotine je:

a_1 = 25 mm	a_1 = 25 mm
$a_2 = a_{kr}$ = 47 mm	$a_2 = a_{kr}$ = 119 mm
$\Delta\sigma = \sigma_{max}$ = 210 N/mm^2	
M = 1.2	
160 radnih ciklusa na godinu	
$N_{1,2}$ = 1.98 godina	$N_{1,2}$ = 3.39 godina

Pukotina duljine a=160 mm prema LEML i NLML značajno prelazi svoju kritičnu duljinu.

Stabilno širenje pukotine a_1 iznosi 1.98 godina za a_2=a_{kr}=47 mm, a 3.39 godina kod a_2=a_{kr}=119 mm.
Dobiveni izračuni dobro se podudaraju sa stvarnim širenjem pukotina u eksploataciji.
Radno kolo turbine br. 2

σ_{max} = 75 N/mm^2
σ_{min} = 0

$R=0$
$\Delta\sigma = \sigma_{max} = 75\ \mathrm{N/mm^2}$
$M=1.2$
$a_1 = 45$ mm
$a_2 = a_{kr} = 379$ mm [9]

Broj radnih ciklusa 500 na godinu.

$N_{1,2} = 32.8$ godina

Prema izračunu, registrirana pukotina duljine a_1=45 mm stabilno bi se širila u vremenu dužem od 30 godina. Ovaj dobiveni izračun je matematički, znatno prije dolazi do pojave napetostne korozije i primjene K_{1SCC}.

5. ZAKLJUČAK

➢ Uzrok pojave i širenja pukotina

- Prema rezultatima iz eksperimenta, utvrđeno je da se u zonama s učestalom pojavom pukotina, mikrostrukura materijala GX8CrNi13 sastoji od matice popuštenog martenzita, gdje je po granicama zrna izlučena feritna faza u obliku mreže koju okružuju karbidi u nizu. Ova mikrostruktura je zbog nepovoljno izlučene feritne faze i pada koncentracije kroma u rubnim dijelovima zrna koju okružuju karbidi, sklona inicijalizaciji i širenju pukotina te pojavi napetostne korozije. Tvrde čestice izlučenih karbida su mjesta nagomilavanja dislokacija, gdje zbog slabih veza između matice i karbida nastaju mikropukotine.
- Nakon dugogodišnjeg rada i velikog broja promjena naprezanja, pukotine dostižu svoju kritičnu duljinu kada intenzitet naprezanja K_1 dostiže lomnu žilavost K_{1C} ili K_C ovisno da li su ostvareni uvjeti ravninskog stanja deformacije ili naprezanja $(K_1 \geq K_{1C})$, a dalje se pukotina širi nestabilno do loma.
- Nakon dugogodišnjeg rada znatno se povećava broj mjesta s inicijaliziranim pukotinama, jer tijekom rada dolazi do površinske degradacije materijala u svim pojavnim oblicima, s velikim brojem koncentratora naprezanja, na kojima istovremeno počinje razvoj velikog broja pukotina, koje sada imaju ubrzan razvoj zbog povoljnosti međusobnog spajanja. Vrijeme razvoja ovih pukotina višestruko je kraće od prvog registriranja značajnih pukotina u eksploataciji.

➢ Procjena pouzdanosti ispitanih radnih kola

Pouzdanost elemenata turbine ovisi o tome kolika će biti duljina neke postojeće pukotine za određeno vrijeme rada elemenata turbine u zadanim uvjetima i da li će pukotina u tom vremenu biti u stabilnom području širenja ili će dostići svoju kritičnu duljinu. Na osnovi poznavanja sposobnosti materijala i provedenih izračuna primjenom mehanike loma, donosi se procjena pouzdanosti ispitanih elemenata turbina:

- Elementi turbina nisu pouzdani ukoliko su postignute sljedeće vrijednosti:
  - registrirane pukotine su veće od duljina kritičnih pukotina,
  - stijenke su stanjene više od 1/3 debljine istih,
  - registrirane pukotine su veće od duljina dopuštenih pukotina prema izračunima primjenom metoda mehanike loma.

U navedenim slučajevima, pouzdanost rada turbina je ugrožena i mora se pristupiti sanaciji oštećenih elemenata bez odlaganja.

- Elementi turbina i pored registriranih pukotina su pouzdani kada:
  - registrirane pukotine ne mogu dostići kritičnu duljinu pukotine,
  - registrirane pukotine su manje od dopuštenih prema izračunima primjenom metoda mehanike loma,
  - stanjenje stijenke ne prelazi 1/3 debljine iste

Ove pukotine potrebno je sanirati tijekom provođenja planiranih remonata ili će se donijeti nova procjena pouzdanosti na temelju provedenog ispitivanja u remontu.

6. LITERATURA

[1] H. Schumann: Metallographie, Leipzig 1962.

[2] H. Blumenauer: G Pusch, Bruchmechanik, VEB Leipzig 1985.

[3] M. Husnjak: Mehanika loma, Inženjerski priručnik, Školska knjiga, Zagreb 1996.

[4] Mazur, Poland: Izbor čelika na osnovi njihovih mehaničkih svojstava i žilavosti loma, Međunarodno savjetovanje: Introduction to fracture mechanics and fracture-safe design, Beograd 1980.

[5] M. Franz: Mehanička svojstva materijala, Sveučilište u Zagrebu, FSB Zagreb, 1998.

[6] K. K. Mehta: Über den zahlenmäßigen Zusammenhang zwischen der Bruchzähigkeit (K_{1C}) und der Kerbschlagzähigkeit, Thyssen Edelstahl Bericht 1970. Heft 3

[7] Merkblatt 488: Bruchmechanische bewerttung Stahl guss

[8] G. Fischer: Schweßreparaturen im Wasserturbinenbau, Sonderdruck aus Oerlikon Schweßmitteilungen 20 (1962), Nr 45

[9] M. Slijepac: Analiza nastajanja i širenja pukotina u radnim kolima i lopticama Francis turbina, Magistarski rad, FSB Zagreb 2004.

10. Savjetovanje o materijalima, tehnologijama, trenju i trošenju
10. Conference on Materials, Processes, Friction and Wear
MATRIB'05, Vela Luka, 23-25.06.2005.

THE EFFECT OF THERMAL TREATMENT ON THE STRUCTURE AND HARDNESS OF Co-Cr-Ti DENTAL ALLOY

Lj. Slokar, T. Matković, P. Matković
University of Zagreb, Faculty of Metallurgy, Sisak, Croatia

Abstract:

In this paper the effect of thermal treatment on the structure and hardness of dental Co-Cr-Ti alloy was investigated. Among twelve samples of Co-Cr-Ti alloys, wich were prepared by melting the pure elements in an arc-furnace under argon atmosphere $Co_{61}Cr_{35}Ti_4$ alloy was chosen as a representative because of the chemical composition close to the commercial Co-Cr base dental alloys.

Thermal treatment was performed at 400ºC, 600ºC, 800ºC and 1000ºC for 10 hours followed by quenching in water.

According to the results of quantitative metallography, the percentage of interdendritic region increases with the temperature of thermal treatment and also the hardness values. Data obtained by X-ray diffraction indicate that dendritic and interdendritic regions are Co-Cr-Ti solid solutions with hcp and fcc type of crystal structure at the 1000ºC and 800ºC, as well. However, at 600ºC and 400ºC there is no presence of fcc phase, but the σ-phase or intermetallic compound Co-Cr occurs. The corrosion measurement for $Co_{61}Cr_{35}Ti_4$ alloy shows high E_{pit} –value, indicating a very good corrosion properties.

From this study can be seen that the temperature of thermal treatment influences the crystal structure and properties of Co-Cr-Ti dental alloy.

Key words: Co-Cr-Ti dental alloys, thermal treatment, crystal structure, hardness

1. INTRODUCTION

Co-Cr base alloys have been used for many years in dentistry as implant materials due to its biocompatibility and excellent corrosion resistance to body fluids /**1,2**/. They have good properties for biomedical use, but the problem could be low ductility. In order to improve their relatively poor ductility and achieve better performances alloying with different elements has been intensively studied /**3**/.

Titanium and its alloys are widely used as dental and orthopeadic implants bacause of their outstanding properties, such as adequate strength, low modul of elasticity, high corrosion resistance and excellent biocompatibility /**4,5**/. Therefore, it may be expected improvement of some properties of base alloy by addition of titanium /**6**/.

The aim of this work was to present the results of an experimental study of the effect of thermal treatment at different temperatures on the structure and hardness of Co-Cr-Ti dental alloys.

2. MATERIALS AND METHODS

Samples of Co-Cr-Ti alloys were prepared by melting the pure elements in an arc-furnace under argon atmosphere. The buttons were remelted three times to achieve homogeneity. Casting of alloys was realised in the specially constructed copper anode cooled by water, which was used as casting mould.

Samples of representative alloy were thermally treated at 400ºC, 600ºC, 800ºC and 1000ºC for 10 hours and quenched in water. Their surfaces were grinded and polished for microscopy and etched with a freshly prepared solution of 50 ml HCl, 5 ml HNO_3 and 50 ml H_2O warmed on 80ºC.

The quantitative optical metallography of selected sample $Co_{61}Cr_{35}Ti_4$ was performed with corresponding programmes Olympus and Image Tool. Hardness was measured by Vickers method (30 N, 10 s) on the equipment of Otto-Wolpert-Werke.

Analysis by X-ray diffraction was carried out on polished discs surfaces from 10 to 100º of 2θ value using CuK_α radiation (Philips, PW 3710). Phase identification was accomplished by matching of each characteristic peak with the JCPDS file /**7**/.

Corrosion resistance of alloy was evaluated by electrochemical method of cyclic potentiodynamic anodic polarization at scanning rate of 2 mV/s between -600 and +1400 mV in aerated 0.9% NaCl solution at the room temperature. The counter electrode and reference electrode were platinum and saturated calomel electrode (S.C.E.) respectively.

3. RESULTS AND DISCUSSION

The effect of thermal treatment on the structure and hardness of Co-Cr-Ti alloys was investigated on selected sample $Co_{61}Cr_{35}Ti_4$.

It was chosen among twelve alloys with increasing Ti content (from 4 at.% to 12 at.%) as a representative because of the chemical composition close to the commercial Co-Cr base dental alloys /**8**/. The microstructural examination of the as-cast alloy by optical microscopy show typical two-phases eutectic dendritic microstructure, which consists of dendritic and interdendritic phase (**Figure 1**).

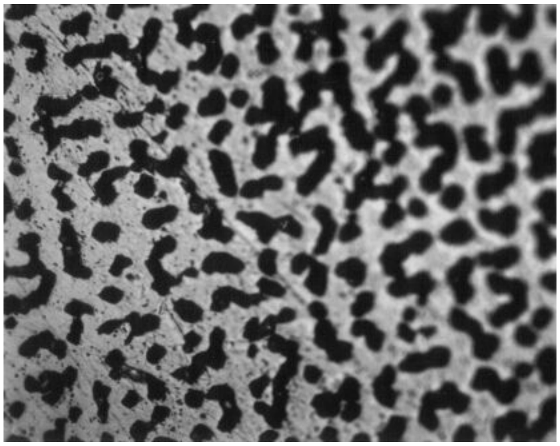

Figure 1. Microphotograph of as-cast $Co_{61}Cr_{35}Ti_4$ alloy (280x)

From the results of quantitative metallography (**Table 1**) can be seen that the percentage of interdendritic region increases with the temperature of thermal treatment, while the average area of grain decreases.

Table 1. The results of quantitative metallography for $Co_{61}Cr_{35}Ti_4$ alloy after different thermal treatments

Temp. of thermal treatment,°C	***Dendritic region, %***	***Interdendritic region, %***	***Average area of grains, μm²***	***Average perimeter of grains, μm***
400	50.11	49.89	112.88	79.61
600	35.37	64.63	74.45	52.04
800	29.68	70.32	54.37	46.72
1000	18.02	81.98	33.27	36.44

According to the data of hardness mesurements performed on $Co_{61}Cr_{35}Ti_4$ alloy (**Table 2**), hardness is not significantly influenced by thermal treatment and it is slightly increased with the temperature. In fact, hardness values depend on the content of interdendritic phase and increase with it.

Table 2. Hardness values for $Co_{61}Cr_{35}Ti_4$ alloy after different thermal treatments

Temp. of thermal treatment, °C	***Hardness (HV)***	$\overline{HV}$
400	326 322 327	325
600	367 364 374	368
800	419 408 419	415
1000	368 365 381	371

Data obtained by X-ray diffraction (**Table 3**) on $Co_{61}Cr_{35}Ti_4$ alloy thermally treated at the 1000ºC and 800ºC for 10 hours and quenched in water show the presence of the fcc and the hcp Co-rich solid solutions. At the 400ºC the hcp- phase and the intermetallic compound Co-Cr or σ- phase are present, so it could be concluded that a phase transformation has taken place. The appearance of σ- phase is expected, because it is known that in the carbon- free systems in addition to the Co-rich solid solution, σ- phase also occurs /**10**/.

Table 3. The results of X-ray diffraction for $Co_{61}Cr_{35}Ti_4$ alloy after different thermal treatments

at 1000ºC:

No.	***2θ, º***	***d_{obs}, nm***	***$d_{Co(hcp)}$, nm***	***$d_{Co(fcc)}$, nm***	***I_{rel}, %***
1.	42.26	0.214	0.217	-	8.6
2.	43.72	0.207	-	0.205	100.0
3.	45.83	0.198	0.202	-	10.6
4.	46.85	0.194	0.191	-	54.1
5.	50.79	0.180	-	0.177	43.5
6.	75.07	0.127	0.125	0.125	4.7
7.	91.08	0.108	0.107	0.107	26.3

at 800ºC:

No.	***2θ, º***	***d_{obs}, nm***	***$d_{Co(hcp)}$, nm***	***$d_{Co(fcc)}$, nm***	***I_{rel}, %***
1.	40.91	0.221	0.217	-	8.8
2.	43.76	0.207	0.202	0.205	100.0
3.	46.65	0.195	0.191	-	41.3
4.	50.73	0.180	-	0.177	8.1
5.	74.75	0.127	0.125	0.125	10.3
6.	83.07	0.116	0.115	-	6.5
7.	90.96	0.108	0.107	0.107	20.3
8.	96.69	0.103	0.102	-	3.2

at 600ºC:

No.	***2θ, º***	***d_{obs}, nm***	***$d_{Co(hcp)}$, nm***	***$d_{σ}$, nm***	***I_{rel}, %***
1.	41.06	0.220	0.217	-	2.0
2.	43.75	0.207	0.202	0.207	100.0
3.	46.89	0.194	0.191	0.193	14.8
4.	50.95	0.179	-	0.188	51.8
5.	75.09	0.127	0.125	-	5.3
6.	91.15	0.108	0.107	-	6.6

at 400ºC:

No.	*2θ,º*	*d_{obs}, nm*	*$d_{Co(hcp)}$, nm*	*$d_σ$, nm*	*I_{rel}, %*
1.	41.01	0.221	0.217	-	18.7
2.	43.84	0.207	0.202	0.207	46.9
3.	46.94	0.194	0.191	-	100.0
4.	50.99	0.179	-	0.188	67.8
5.	74.81	0.127	0.125	-	23.0
6.	83.62	0.116	0.115	-	7.7
7.	91.35	0.108	0.107	-	51.3
8.	61.97	0.150	-	0.148	10.6

The corrosion resistance of alloys can be evaluated on the basis of pitting potential E_{pit}, i.e. the potential of passive film breakdown. This is marked by a large and generally increasing polarizing current, due to the localized or pitting type corrosion as can be seen on **Figure 2**. E_{pit} values are criterion for corrosion resistance of alloys so that the greater E_{pit} value means the better corrosion properties.

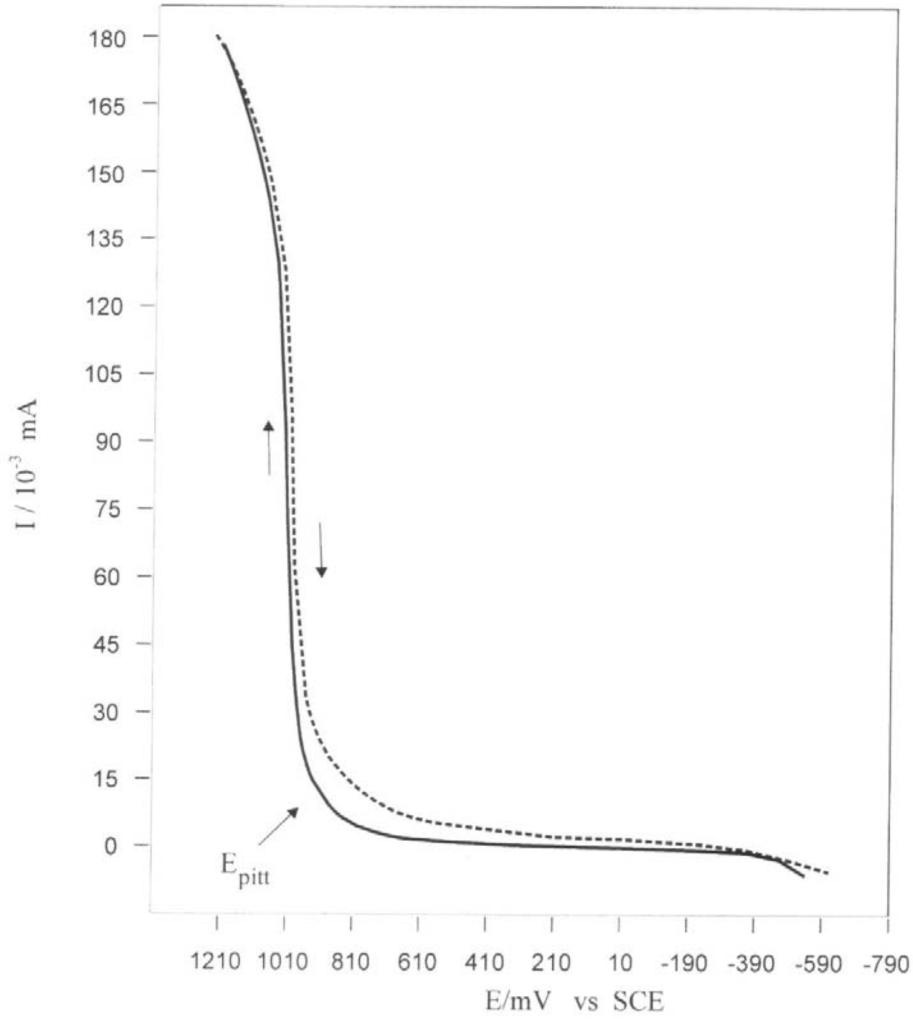

Figure 2. Anodic polarization curve of $Co_{61}Cr_{35}Ti_4$ alloy examined in 0.9% NaCl at 20ºC

In **Table 4** are given E_{pit} values for Co-Cr base dental alloys with addition of Mo, Ni /**9**/ and Ti. It can be seen that all three alloys have relatively high E_{pit}- values which means that they are chemically stable.

Table 4. Electrode potential E_{pit} (vs SCE) for Co-Cr-Ti, Co-Cr-Mo and Co-Cr-Ni alloys

Alloy composition, at.%	***E_{pit}, mV***
$Co_{61}Cr_{35}Ti_4$	1030
$Co_{60}Cr_{30}Mo_{10}$	1060
$Co_{60}Cr_{30}Ni_{10}$	1020

4. CONCLUSIONS

Study of the as-cast $Co_{61}Cr_{35}Ti_4$ alloy after different thermal treatments indicated the following results:

- according to the optical microscopy samples have two-phases dendritic structure which consists of dendritic and interdendritic region
- hardness values are dependent upon the percentage of the interdendritic phase
- the X-ray analysis reveals the fcc and hcp Co-rich solid solutions after thermal treatment at 1000ºC and 800ºC and the hcp and σ- phase at the 400ºC, which means that the allotropic transformation of metastable fcc to the hcp phase occurs
- a representative sample reveals a very good corrosion properties on the basis of E_{pit} value

5. REFERENCES

1. R. W. Cahn. P. Haasen, E. J. Kramer, *Materials Science and Technology,* Vol. 14: Medical and dental materials, D. F. Williams VCH Verlags, Weinheim, 1992.
2. K. Korber, K. Ludwig, *Zahnartzliche Werkstoffkunde und Technologie*, Georg Thieme Verlag, Stuttgart, 1993.
3. S. longquan, D. O. Northwood, C. Zhengwang, *Alloy design and microstructure of a biomedical Co-Cr alloy,* J. Mater. Sci., 28 (1993) 1312-1316
4. G. R. Parr, L. K. Gardner, R. W. Toth,*Titanium: The mystery metal of implant dentistry, Dental materials aspects,* J. Prosthet. Dent., 54 (1985) 410-413
5. M. Taira, J. B. Moser, E. H. Greener, *Studies of Ti alloys for dental castings*, Dent. Mater., 5 (1989) 45-50
6. Y. Igarashi, *Cobalt-chrome-titanium alloys dentitan, features and physical properties,* J. Dent. Tecnol., 13 (1985) 1195-1199
7. Powder Diffraction File Search Manual, JCPDS International Center for Diffraction data, Swarthmore, 1982.
8. Lj. Slokar, T. Matković, P. Matković, *Microstructure and hardness of Co-Cr-Ti alloys for dental castings,* Metalurgija, 43 (2004) 4, 273-277
9. P. Matković, T. Matković, J. Malina, *Usporedba svojstava biomedicinskih Co-Cr-Ni i Co-Cr-Mo slitina*, Strojarstvo 45 (2003) (1-3), 5-10
10. E. O. Hall, S. H. Algie, *The sigma phase*, Metallurg. Rev., 11(1966) 61-88

AN ANALYSIS OF STEEL MICROSTRUCTURE CHANGES DURING THE PLASMA AND GAS CUTTING PROCESSES

ANALIZA PROMJENA MIKROSTRUKTURE ČELIKA NAKON REZANJA PLAZMOM I PLINSKOG REZANJA

Božo Smoljan, Željko Gortan, Neven Tomašić
Faculty of Engineering Rijeka, Chair of Material Science and Engineering
Vukovarska 58, 51000 Rijeka

Abstract: The analysis will cover the change of a microstructure of microalloyed finegrained high quality steel during the plasma and gas cutting processes. The purpose of the analysis is to establish whether the surface changes during plasma or gas cutting processes require any subsequent finishing processes to be applied. The research is aimed at avoiding the necessity to apply additional manufacturing processes. The results of the research should enable the selection of adequate construction steel and cutting process meeting technological and economical requirements.

Key words: microstructure, construction steel, plasma cutting, gas cutting, steel manufacturing process

Sažetak: Analiza će uključivati promjenu mikrostrukture mikrolegiranog sitnozrnatog čelika tijekom rezanja plazmom i plinskog rezanja. Svrha analize je ustanoviti, da li su promjene površine nakon rezanja plazmom i plinskog rezanja takve da ne zahtijevaju primjenu naknadnih postupaka završne obrade. Cilj analize je izbjeći dodatne postupke u proizvodnom procesu. Rezultati istraživanja omogućit će odabir adekvatnog čelika i postupka rezanja u skladu s tehnološkim i ekonomskim zahtjevima.

Ključne riječi: mikrostruktura, konstrukcijski čelik, rezanje plazmom, plinsko rezanje, proizvodni postupci

1. Introduction

Gas cutting process, oxygen cutting or burning, is an economical method of cutting steel that provides good dimensional tolerances. It is much faster than any sawing or machining process, although the finished edges of finished parts are not as fine.

Plasma (arc) cutting (PAC) was developed in the 1950s for cutting of metals that could not be flame cut, such as stainless steel, aluminium and copper.

Plasmas are a practical alternative to gas cutting process and are used on many cutting machines. They are much faster than gas cutting process and work well on thin material but the equipment required is more sophisticated. Sometimes they prove more economical than oxygen cutting, even for mild steel, but much depends on the quantity and thickness of the materials to be cut.

The tendency in the processing of semi-finished products is to apply processes such as gas cutting, plasma cutting, welding, casting, forging etc., which do not require additional final processing. The difficulties arise due to changes of materials properties and surface roughness.

This paper is aimed at the analysis of microstructural changes during the manufacturing processes.

2. Overview of cutting processes

2.1. Gas cutting process

Gas cutting process lends itself well to small handheld cutting torches or large multi-torch automated machines. The process works on all steel products, but most large machines are particularly suited for cutting intricate shapes from sheet metal.

Steel is unique because the slag it creates melts at a slightly lower temperature than the parent metal. The slag is formed as a liquid in the heat of combustion and is easily blown away as a fine spray by the oxygen stream. This is a key factor, allowing for the uncut metal to remain intact, with a smooth, square cut face, while enabling at the same time the cut to continue and burn adjacent material.

The two main limitations on cutting speed are the quantity of pure oxygen available and the ability of the preheat flame to keep the top surface hot enough to continue the cut. The desired cutting quality must also be taken into consideration.

The combination of combustibility and a liquid slag makes steel one of the very few materials that can be cut by oxygen. Most other metals either do not burn in oxygen, or form a slag that does not flow away from the cut region.

Stainless steel will not burn because its high alloy content prevents oxidation and rusting. That is why the alloy is there - to prevent rust from forming, and rust is an oxide of iron, chemically similar to slag.

Many high alloy steels are more difficult to cut than mild steel because their ingredients also retard oxidation. Generally speaking, this results in a lower cutting speed. Cast iron does not burn easily because of its higher impurity content. A sweeping motion of the torch or a flux is required to cut it.

On the other hand, aluminium oxidizes readily, even in air at room temperature. But the aluminium oxide film that forms, while thin, is very hard and does not melt. It stays where it was created, obstructing the oxygen flow and so blocking any attempt on cutting.

Titanium is an exception. It reacts readily with oxygen and can be easily flame cut using conventional equipment. That reactivity explains why titanium cannot be welded without the use of a protective gas atmosphere. Cutting speeds will be 30 to 50% higher than on steel, with a wider cut slot. The cutting process will be accompanied by a huge amount of whitish smoke.

2.2. Plasma cutting process

Plasma (arc) cutting (PAC) was developed in the 1950s for cutting of metals that could not be flame cut, such as stainless steel, aluminium and copper. The PAC process uses electrically conductive gas to transfer energy from an electrical power source through a plasma cutting torch to the material being cut. Plasma arc cutting uses a high-speed electrically charged gas jet to cut the metal. This is often performed at extremely high temperatures. Commonly used plasma gases include argon, hydrogen, nitrogen and mixtures, plus air and oxygen.

The temperature of the plasma arc melts the metal and pierces the workpiece while the high velocity gas jet removes molten material from the bottom of the cut, also known as the kerf. In addition to high energy radiation (Ultraviolet and visible) generated by PAC, the intense heat of the arc creates substantial amounts of fumes and smoke by vaporizing metal in the kerf.

A variation, water-shielded plasma arc cutting, costs less to operate since water is cheaper than gas. Water shielding has a number of advantages. It reduces both top-edge material rounding and the amount of irritating smoke and fumes generated when cutting without the water.

There is an elevated level of interest in high-tolerance PAC, sometimes also known as high-definition or fine-plasma cutting. High-tolerance PAC can be used to cut metals from ~1mm to 10mm thick. High-tolerance PAC produces a cut quality rivalling laser cutting at a lower expense.

Plasmas present a practical alternative to gas cutting and are used on many cutting machines. They are much faster than gas cutting and work well on thin material, but for thicknesses of 200 mm for some materials current of 1000 A is needed and the equipment required is more sophisticated [1]. Sometimes they prove to be more economical than oxygen cutting, even for mild steel, but much depends on the quantity and thickness of materials to be cut.

3. The analysis of cut examples

For microstructure analysis testing examples from steel plate with 100 x 100 mm were cut. Microalloyed fine grained high quality steel (EN Norm: S690) was used as the test subject.

A power supply from Hypertherm Company was used for plasma arc cutting, model HyDefinition HD3070: Plasma Arc Cutting System with Automatic Gas Console. This unit houses a 100 A, 15kW chopper producing a constant current output variable from 15 to 100 A. It also contains a microprocessor control which regulates all plasma system functions: start sequence, machine interface functions, gas and cut parameters, and off sequence. The main power supply power on/off is controlled remotely by the CNC machine. The cutting current and pierce delay are also controlled by the CNC machine. The cooling system required to cool the torch is also housed by the main power supply. The main parameters for gas cutting process, with the same machine but with gas cutting process equipment are shown in Table 1.

Table 1. Main parameters for gas cutting process

Thickness (mm)	Preheat oxygen pressure during cutting (bar)	Preheat oxygen pressure (bar)	Cutting oxygen pressure (bar)	Piercing oxygen pressure (bar)	Cutting speed (mm/min)
20	0.7	2.5	7	1.5	480

The main parameters for plasma arc cutting process used for steel plate cutting examples are shown in Table 2.

Table 2. Main parameters for plasma arc cutting with

	Arc Voltage (V)	Preflow O_2 (%)	Preflow N_2 (%)	Shield O_2 (%)	Shield N_2 (%)	Plasma O_2 (%)	Cutting speed (mm/min)
Thickness 15 mm; 100 A	152	10	100	35	90	60	1450

The electrical energy consumption data for plasma arc cutting process is shown in table 3 and is calculated based on cutting speed of 1,45 m/min. Plasma cutting speed is three times higher than gas cutting speed.

Table 3. Electrical energy consumption for plasma cutting process .

Thickness (mm)	For 1 hour (kW)	For 1 meter of cut (kW)
15	15,2	0,17

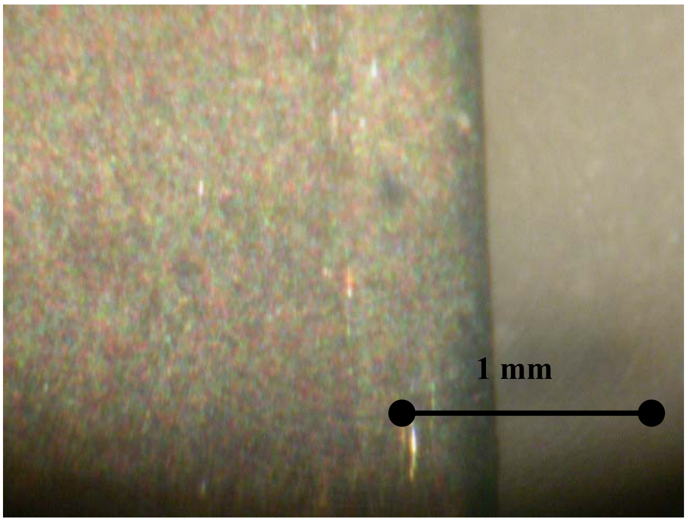

Fig.1. Plasma cutting edge

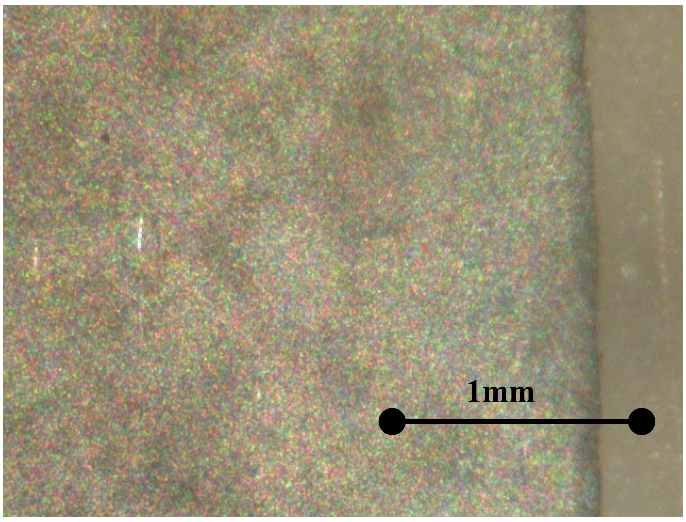

Fig.2. Gas cutting edge

Heat affected zone of plasma cutting is shown in figure 1. Heat affected zone of gas cutting is shown in figure 2. It can be seen that heat affected zone of gas cutting is much higher than heat affected zone of plasma cutting. Plasma cutting process is much more advantageous if surface without chemical and microstructural changes is needed due to surface hardening (induction quenching).

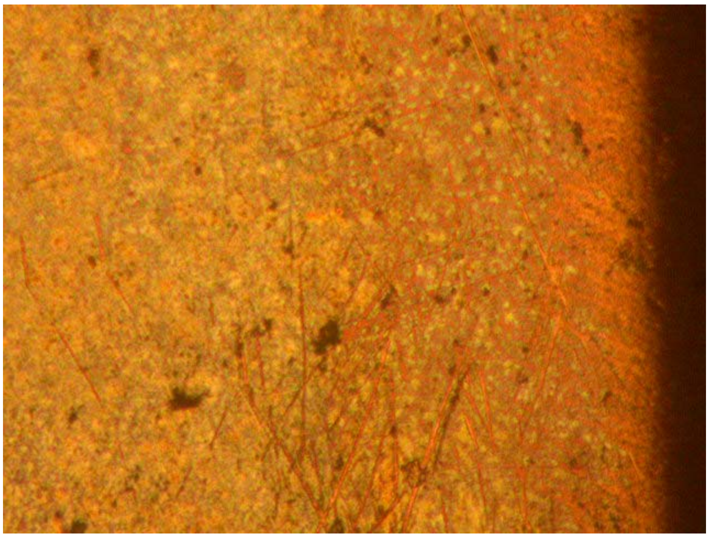

Fig. 3. Plasma cutting edge, decarbonised surface, Mag 100X

On figure 3 plasma cutting edge is shown. It can be seen that the surface is decarbonised. In microstructure beside the pearlite also ferrite can be found. Quantity of ferrite is decreasing by moving away from cutting edge. On distance of 500 µm from cutting edge microstructure of spheroidal pearlite is established.

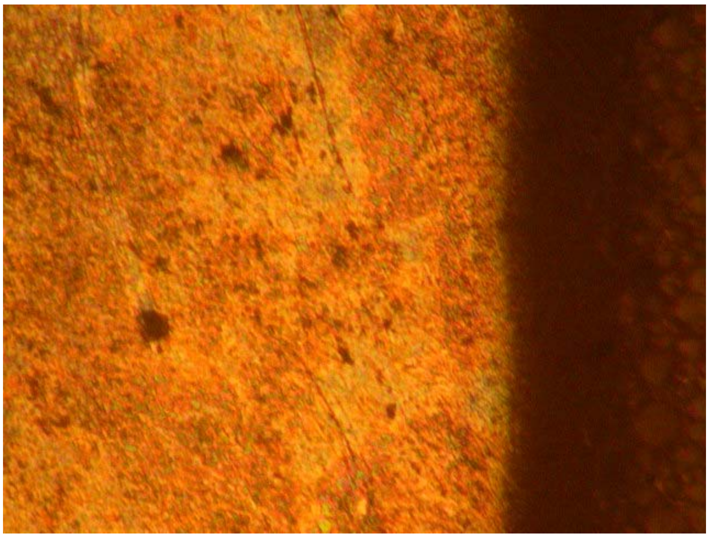

Fig. 4. Gas cutting edge, decarbonised surface, Mag 100X

On figure 4 gas cutting edge is shown. It can be seen that the surface is decarbonised in wider range than the surface of plasma cutting. In microstructure beside the pearlite also ferrite can be found.

The surface after gas cutting is rougher than after plasma cutting.

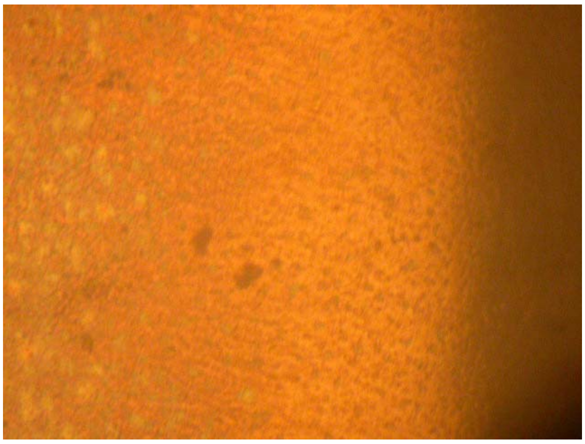

Fig. 5. Plasma cutting edge, Mag 200X

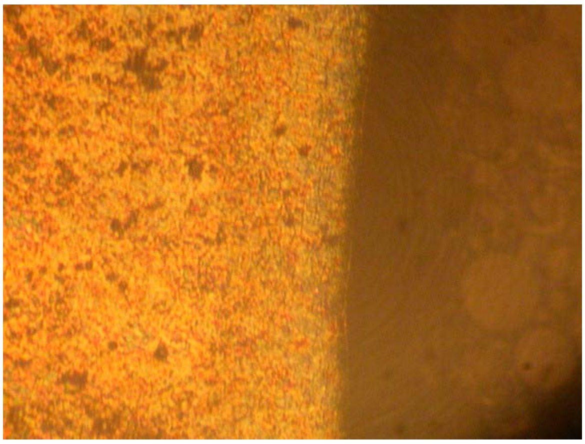

Fig. 6. Gas cutting edge, Mag 200X

Detailed plasma cutting edge is shown on figure 5 and detailed gas cutting edge is shown on figure 6. Magnification is 200. On both figures it can be seen decarbonising process and appearance of ferrite.

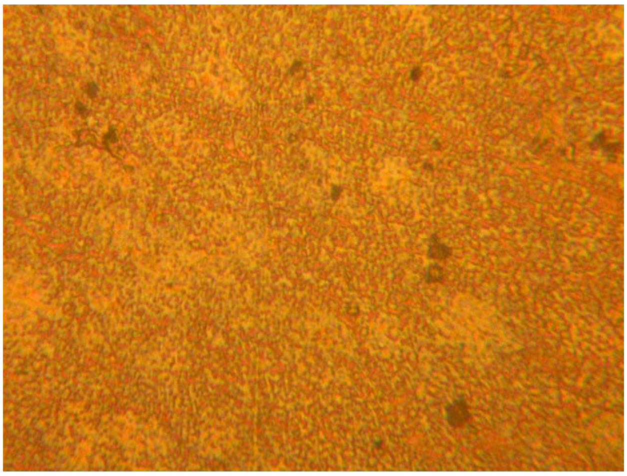

Fig. 7. Microstructure, Mag 500X

On figure 7 microstructure of investigated steel is shown. The microstructure of core is consisting of spheroidal pearlite

4. Conclusion

Gas cutting process is an economical method of cutting steel that provides good dimensional tolerances. Plasma (arc) cutting was developed for cutting of metals that could not be flame cut, such as stainless steel, aluminium and copper. Plasmas are a practical alternative to gas cutting process. They are much faster than gas cutting and work well on thin material, but for thicknesses of 200 mm current of 1000 A is needed and the equipment required is more sophisticated. Economical adequacy of usage of plasma cutting will be investigated in future work.

Heat affected zone of plasma cutting is smaller than heat affected zone of gas cutting. The cutting edge area after gas cutting is decarbonised in wider range than the surface area of plasma cutting. In microstructure beside the pearlite also ferrite can be found.

The surface after gas cutting is rougher than after plasma cutting. The resulting cut surface of plasma cutting has a very fine grain and is much more adequate as a final process unless additional demands are placed on precision.

5. Reference

1. Gojić Mirko, Tehnike spajanja i razdvajanja materijala, Sveučilište u Zagrebu, Zagreb, 2003.
2. Rose A et al, Atlas zur Wärmebehandlung der Stähle I, Verlag Stahleisen, Düsseldorf, 1958.
3. ASM Handbook, Vol.5 Surface Engineering, ASM International, Materials Park, Ohio, 1999.

10. Savjetovanje o materijalima, tehnologijama, trenju i trošenju
10. Conference on Materials, Processes, Friction and Wear
MATRIB'05, Vela Luka, 23-25.06.2005.

DETERMINATION OF WOOD-POLY(PROPYLENE) COMPOSITE REGENERATE MELT RHEOLOGY

Đurđica Španiček, Maja Rujnić-Sokele
Sveučilište u Zagrebu
Fakultet strojarstva i brodogradnje, I:Lučića 5, HR-10000Zagreb

Abstract: Due to their good properties polymer materials are present in almost all area of human life. The need for recycling of polymer materials has been recognized especially as a result of the growing awareness of environmental pollution by polymer waste. During processing and reprocessing at higher temperatures the polymer material is exposed to thermal, oxidative as well as shear induced degradation. Therefore, the physical and mechanical characteristic such as flow behaviour, tensile strength, and elongation or impact strength differ of those of initial material. The change in melt flow rate (MFR) can be used to study thermal degradation of polymer materials in processing. The paper deals with determination of MFR of wood-poly(propylene) composite regenerate of different cycle of reprocessing. Since the melt behaviour of the processed material is sensitive to the changes in molecular structure, knowledge of the MFR is useful for assessing the reprocessibility of polymer waste material.

Keywords: Wood-poly(propylene) composite, recycling, mechanical properties, melt flow rate (MFR)

Ključne riječi: drvo-poli(propilen) kompozit, recikliranje, mehanička svojstva, maseni protok taljevine (MFR)

Introduction

Because of very wide use of all types of polymer materials and therefore growing need for resources as well as growing awareness of environmental pollution, the need for their recycling has been well recognized. During polymer processing at higher temperatures the polymer material is exposed to thermal, oxidative as well as shear-induced degradation. Polymer materials are disperse systems, e.g. the macromolecules of which polymer are made of, and have identical chemical structure but different number of repeating units. Short-range macromolecules are subjected to the thermal degradation and they decompose into fragment of varying sizes. Therefore, the physical and mechanical characteristic such as the flow behaviour, tensile strength, and elongation or impact strength differ, generally inferior, to those of initial polymer.

Many environmental regulations force a production of environmental friendly materials. Therefore, tremendous efforts in last decade for production of polymer natural fiber composites are present. Wood and other natural fibres as reinforcements are environmental friendly and cost acceptable and therefore very suitable for productions. A lot of different natural fibers sources with great variety of properties are available. In table 1 the major potential world natural fibers sources are listed[1].

Table 1. Inventory of major potential world fiber sources (annual production)

Fiber source	**World** (Dry metric tons)
Wood	1.750. 000 000
Straw (wheat, rice, oat, barley, rye, flax, grass)	1.145.000 000
Stalks (corn, sorghum, cotton)	970.000 000
Sugar cane bagasse	75.000 000
Reeds	30.000 000
Bamboo	30.000 000
Cotton staple	15.000 000
Core (jute, kenaf, hemp)	8.000 000
Papyrus	5.000 000
Bast (jute, kenaf, hemp)	2.900 000
Cotton linters	1.000 000
Esparto grass	500 000
Leaf (sisal, abaca, henequen)	480 000
Sabai grass	200 000
TOTAL	**4.033.080 000**

Comparing with glass or carbon fiber-reinforced polymer composite natural fiber reinforced composite has some limitations.

First one is lower processing temperature. Limiting processing temperature for natural fibres are about 200^0 C. Higher temperatures is possible only in shorter time. Therefore, the choice of potential thermoplastics is limited to poly (propylene) (PP), poly (vinyl-chloride) (PVC), polyethylene (PE), polyamides (PA) and polystyrene (PS). Those thermoplastics constitute about 70% of total thermoplastics consumed by plastic industry.

Second limitation is higher moisture absorption of natural fibres. Water absorption can result in swelling of the fibres that leads to dimension instability. The fibers water absorption are minimized in the composite due to encapsulation by the polymer. It can be also reduced by using expensive surface barriers on the composite surface or by chemical modification of hydroxyl groups present in the fiber and most of all, by good fibre-matrix bonding, but those processes increase the costs of system.

The major reinforcement source in natural material reinforced thermoplastic is wood, because it is easily available. Wood-plastics composite are a new group of materials that extend the concept of wood composites from the traditional compressed materials to a new generation of high performace products. This new and rapidly developing generation of wood composites have good mechanical properties, high dimensional stability and can be use to produce complex shapes. There are two basic types of wood composite, depending on type of added wood: wood flour as a filler or wood fibers as reinforcement. Wood flour as filler increases the tensile and flexural moduli while has a little effect on the composite strength. Wood fibers have higher contribution to an increase in the moduli of composite and can also improve the strength of the composite when suitable additives are used to improve stress transfer between matrix and the fibers. The most common types of wood composite are produced by mixing wood flour and plastics to produce a material that can be processed just like plastic but have the best features of wood and plastic.

EXPERIMENTAL

Material

Tested basic composite was made by Isokon, Sl. Konjice, Slovenia, and has following content of components:

poly(propylene)	61 % by weight
wood flour (particles sizes 0,25-0,5 mm)	37 % by weight
compatibilizer (maleic anhydride grafted PP-MAPP)	2% by weight

Compatibilizer (or coupling agents) has to be used to improve the interaction and adhesion between non-polar matrix and polar wood particles. Entanglement between the poly(propylene) and MAPP molecules results in improved interphase properties and the strain to failure of the composite. It is important because cracs are usually initiated at places of high stress concentration or at the interface or interphase region where the adhesion between two phases is very poor. An extensive set of investigations[2] has shown that variations of as much as 50% in compressive strength and as much as two orders of magnitude in notched fatique life can be caused by altering just the interphase region, which may be as little as 1% of the total composite by weight.

Components were mixing in extruder and resulting composite blend was granulated and dried at 104^0 C for 4 hours to prevent swelling. Test specimens were made by injection moulding (Engel VC 330/60)[3]. Mixing the polar and hydrophilic fillers with non-polar and hydrophobic matrix, in spite of added compatibilizer, can result in difficulties in dispersing the fillers in matrix. The microscopic composite heterogenous structure is presented in figure 1.

Some of prepared specimens were selected for mechanical and thermal properties determination. All remaining specimens were granulated and injection molded again. This procedure was repeated of nine cycles, total 10 cycles of processing. Number of reprocessing cycles is marked as "generation of material". After every cycle some specimens (five for each mechanical properties determination) were randomly selected and tested for evaluation of reprocessing effect. First four generations were reprocessed in 48 hours after drying before first processing cycle. Other generations were reprocessed after 72 hours.

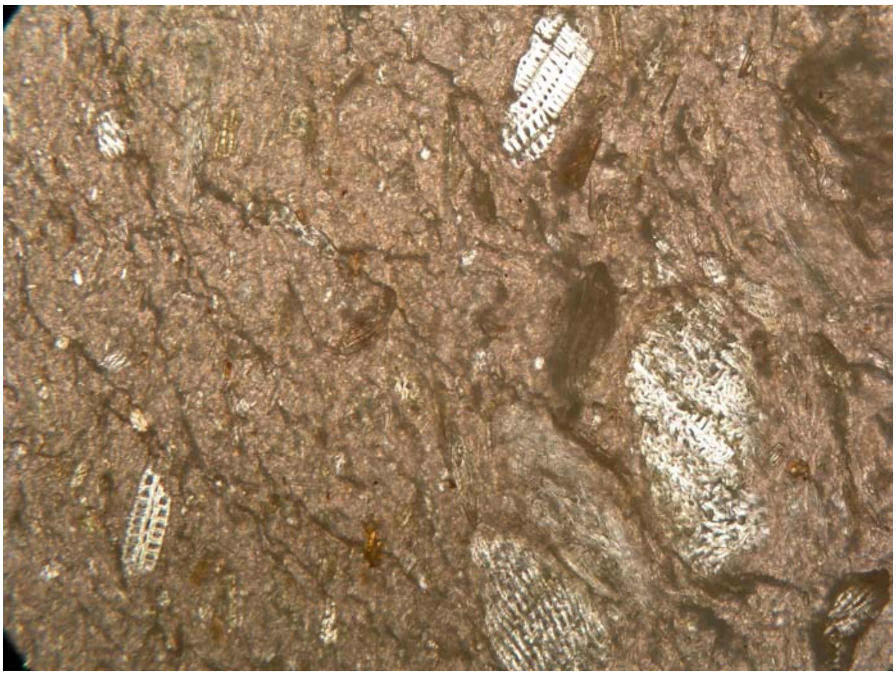

Figure 1. Heterogenous structure of wood-poly(propylene) composite
(Optical polarizing microscope, magnifications 400 x)

Results and discussion

Every generation of composite were subjected to following testing:

- Tensile modulus and strength (EN ISO 527-4)
- Flexural modulus and strength (EN ISO 14125)
- Impact strength (EN ISO 179-1)

Specimens for determination of impact strength were not made according standard, and therefore the obtained values are suitable only to compare tested composite generations.
Because of very small differences in properties of higher generation, generation 7, 8 and 9 were not tested. The obtained values for tested generations are given in table 2.

Table 2. Mechanical properties of tested generations

Generation of material	Tensile strength N/mm^2	Tensile modulus N/mm^2	Flexural strength N/mm^2	Flexural modulus N/mm^2	Impact strength mJ/mm^2
1	22,47	2570	40,19	1699	7,19
2	22,44	2737	39,79	1742	6,99
3	22,40	2749	41,47	1753	7,1
4	22,06	2704	41,77	1796	6,74
5	21,37	2506	40,49	1718	6,87
6	21,37	2477	40,57	1816	7,23
10	21,11	2490	38,22	1687	7,30

Note: All values are average value of 5 measurements

Because of the sensitivity of polymer materials melt rheology to small differences in molecular structure, knowledge of flow behavior is very important. The melt flow data are generally obtained by sophisticated methods requiring expensive instruments. The flow parameter easily available is the melt flow rate (MFR), which can be measured using a simple, inexpensive apparatus.

MFR is defined as the weight of polymer material in grams extruded in 10 minutes under application of specified load through melts flow apparatus (extrusion plastometer) at fixed temperature. The apparatus is basically an extrusion plastometer operating at a fixed temperature. The thermoplastic material, which is contained in a vertical cylinder, is extruded through a die by a loaded piston. MFR is a single point measurement and its utility is limited for process optimization. Nevertheless, the change in MFR can be used to study thermal degradation of polymer materials in processing, because is very good indicator of the processing history of material.

For generation 1, 2, 3, 6 and 10 melt flow rate was determined (EN ISO 133). The composite of different processing generation represent material with different melt flow rate. The results of tested generations are present in table 3.

Table 3: MFR for tested composite generations

Generation of material	**Melt flow rate (MFR) g/10 min**
1	2,61
2	2,625
3	2,835
6	2,895
10	3,043

The flow resistance measured by MFR represents the viscosity of tested material. Viscosity would be reduced with increasing free volume, decreasing entanglement density and weaker intermolecular forces or adhesion between components. The viscosity of the melt would therefore decrease with repeated processing, since the molecular weight of the polymer and bonding in composite are progressively reduced due to thermal and shear degradation in each processing cycle of tested generations. Therefore, the obtained MFR for every cycle of reprocessing is higher than previous one.

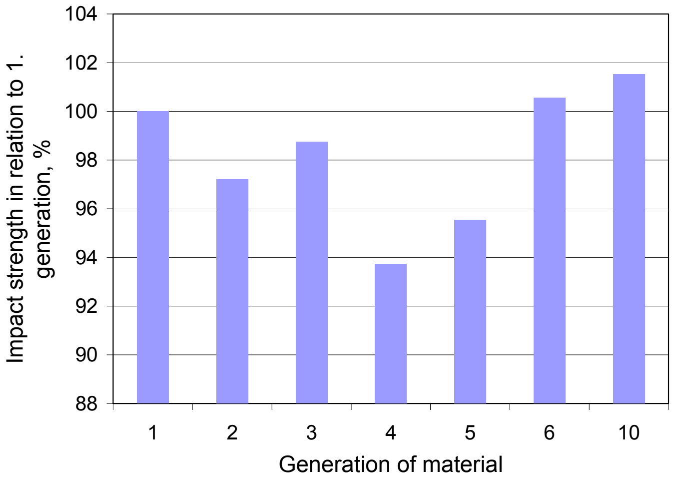

Due to degradation during reprocessing the estimated mechanical properties decrease with exception of impact strength (figure 3). After 4th cycle the impact strength is the lowest one and in further reprocessing the obtained value increases, in the 10th cycle is even greater than for generation 1. The explanation could be in the water absorption. After a few cycles of reprocessing, the wood particles are no longer completely encapsulated in polymer matrix and, because of wood hydrophility, it is difficult to entirely eliminate the absorbed moisture from composite. It is well known that in some polymer materials a low moisture content could provoke impact strength increase.

MFR determination is convenient method for indicating the value of the reprocessed material and whether it is viable for further reprocessing.

MFR of reprocessed composites are higher than basic one (generation 1), but without dramatic increase. That means, after 10 cycles of reprocessing composite properties are lower, (with exception of impact strength), but reprocessed material still has potential for use.

Literature:

1. R.M. Rowell, A.R. Sanadi and al., Utilization of natural fibers in plastic composites: Problems and opportunities, http://www.fpl.fs.fed.us/documents/PDF1997/ rowe197.d.pdf

2. K.L.Reifsnider, Modelling of the interphase in polymer-matrix composite material system, Composite, Vol.25. N^{o} 7, 1994, 461-469

3. M.Rujnić-Sokele, M.Šercer, B.Bujanić: Utjecaj recikliranja na mehanička svojstva drvno plastomernog kompozita, Polimeri 25,(2004), 1-2, 12-19

10. Savjetovanje o materijalima, tehnologijama, trenju i trošenju
10. Conference on Materials, Processes, Friction and Wear
MATRIB'05, Vela Luka, 23-25.06.2005.

ZERO STRESS CARBON (0SC) FILMS FOR MEMS APPLICATION

M. Šraml*, J. Flašker

University of Maribor, Faculty of Mechanical Engineering,
Smetanova 17, SI-2000 Maribor, Slovenia
*e-mail: sraml.matjaz@uni-mb.si

Abstract

Present paper is focused particularly on an application of the EU project in the frame of 6EU projects, "Nanotechnology" - within Specific Target Research Projects (STREP). This was first attempt and experience to taken the role in the nano-technology project for our research group as a "partner" of the project team "TRIBOMEMS". Our research contribution should be focused on the numerical calculations of new material tribo-parameters.

The primary objective of TRIBOMEMS is the development of Diamond Like Carbon (DLC) films with nearly zero stress that is "Zero Stress Carbon (0SC) Films" for Micro Electro Mechanical System (MEMS) devices. The present MEMS technology is based on Silicon (Si). If Si based MEMS are not touching or sliding against each other, tribology (friction and wear) is not a big issue. However, in some MEMS devices, such as micro-actuators, micro-gears and micro-motors, tribology becomes a dominant issue in their performance and reliability. It is well known that wear resistance of Si is not very good and the coefficient of friction between poly-Si and Si ranges from 0,25 to 0,35. These poor tribological properties of Si inspire us to
develop new innovative materials. In this respect, amorphous Carbon (a-C) or DLC films with nearly zero stress offer excellent mechanical and tribological properties to the rapidly expanding field of MEM.

Keywords: nano-technologies, Tribology in nano and micrometer scales, MEMS devices

1 INTRODUCTION

The investigation of nanostructures is a highly topical field of solid state physics and materials research. New, sophisticated characterization methods have been successfully developed during the last twenty years like the scanning tunnelling microscope (STM), for example, which has been established as standard instrument for scanning nanostructures on surfaces or the transmission electron microscope (TEM) combined with theoretical modelling for visualization of periodic structures. Even scattering methods (ions, electrons, X-rays, neutrons) have been improved to an extend which is hard to beat. Finally, spectroscopic information with high resolution has become available through the use of synchrotron radiation sources of the third generation [2].

What makes nanostructures different? They show significantly different properties compared to the bulk material. As is known from quantum mechanics the electronic states of nano-particles are considerably changed compared to the bulk. This is due to quantization effects caused by the spatial restriction. The electronic structure, on the other hand, is responsible for all those material properties like electronic conductivity, optical absorption, chemical reactivity or even the mechanical properties. Therefore, these nanostructures appear as particles with new material properties.

Here, one tendency is clearly recognizable: nanotechnology makes design the most important part of any development process. With nanotechnology the amount of design work increases enormously due to its complexity. To summarize, design will change radically under nanotechnology and for nano-engineers or nano-designers, respectively, a board knowledge will become even more important in the future.

2 PROJECT DESCRIPTION

A majority of Micro Electro Mechanical System (MEMS) devices have moving parts such as micro-actuators, micro-gears and micromotors, pistons, joints, etc. In these small devices, because of the large surface area to volume ratio, as the size scale decreases, the surface forces, such as adhesion and friction, start playing an important role and moreover they dominate over inertial and gravitational forces. Frictional forces between these moving parts as well as sticking may hinder the overall efficiency of the whole system. All tribology (friction, sticking and wear) happens on the micrometer and nanometer level, the real contacts between sliding surfaces involve asperities that are on the nanometer size scale. It is very important to have a control on this size scale in order to obtain materials with desired properties.

Therefore, materials of such surfaces must have a low coefficient of friction combined with other physical properties, such as high hardness, mechanical and thermal stability. If they are to be used in biological applications, then also biocompatibility is required. Furthermore, their process conditions must be compatible with the usual micro fabrication/production techniques. A family of carbon films, known with different names, such as Diamond Like Carbon (DLC) or amorphous Carbon (a-C) or hydrogenated amorphous Carbon (a:C-H) films, due to their excellent as well as tunable physical properties may satisfy requirements of MEMS. The carbon films are composed of 1 to 10 nanometer size turbo-stratic carbon crystallites. The overall physical and chemical properties of films are the function of properties of the nano-sized clusters. However, replacing existing technology, which is primarily based on Silicon (Si), with carbon films in MEMS productions, is a challenge. It is indeed a real challenge because of some intrinsic problems of carbon films, such as their high level of residual stress. It is well known that various properties of these films, such as hardness, adhesion, wear resistance, are influenced by the residual stress, which forms during the deposition.

Carbon films, in their various forms may become key materials for the manufacturing of MEMS even Nano Electro Mechanical System (NEMS) devices in the 21st century. Their well known forms are: Diamond, graphite, hydrogen free diamond like carbon (DLC), amorphous carbon (a-C), hydrogenated amorphous carbon (a-C:H), metal containing hydrogenated amorphous carbon (Me-a-C:H), disordered carbon or turbo-stratic carbon etc. Diamond films are deposited at very high temperatures (900 ºC and above), therefore, they are not yet compatible with the micro-fabrication techniques. On the other hand, DLC films in their different forms can be deposited at lower temperatures and may exhibit properties varying between those of diamond (sp^3 local bonding) and graphite (sp^2 local bonding) [1]. DLC is a form of a-C or a-C:H and is used in several applications due to its wide range of outstanding material properties which include high hardness, scratch and wear resistance, low coefficient of friction, biocompatibility, chemical inertness, hydrophobicity, high transparency (visible-IR), low electrical conductivity. These carbon films consist of only C and H atoms and the carbon atoms can form states with different types of hybridization sp^1, sp^2 and sp^3. This results in a wide range of optical, electrical and mechanical properties of carbon films [1].

These properties of the films are therefore closely related to the bonding structure which is governed by the deposition process. It is generally agreed that the sp^2 bonding is responsible for the electronic properties like band gaps, whereas the mechanical properties are governed by the sp^3 bonds [1]. It is clear from this information that DLC films with the best mechanical properties (high hardness, good adhesion, low coefficient of friction etc.) can be obtained when it is possible to deposit sp^3 rich or almost 100 % sp^3 amorphous DLC films. However, when the optimization of the sp^3 rich films is achieved the mechanical quality of DLC films, namely their stress and adhesion, becomes an issue which is related to the deposition process: the problem of residual stress which limits the thickness of the films as well as their adhesion to their substrates. The major advantage of the stress relief would be enabling the deposition of thick layers, such as 5-7 µm, without any loss of good adhesion properties to their substrates.

The residual stress may be invariably tensile or compressive in nature. Both tensile and compressive stress can take place in the films due to various reasons; deposition parameters, differences in the coefficients of thermal expansion of the film and substrate if the film material is deposited at elevated temperatures. Similarly large differences in the lattice parameters of the film and substrate material would also strain the deposited films.

The presence of a residual stress can be either useful or detrimental depending its value and potential applications. In general, brittle ceramic and DLC films have high compressive stress and this leads to their failure [1]. Large compressive stresses are present at sp^3 rich DLC films which are deposited even at low temperatures. This problem leads to poor adhesion between the coating and substrate, with large areas tending to spall off [1]. There are several methods of modifying and controlling the residual stresses developed in films during growth. Growing layers with alternatively tensile and compressive stresses that eventually offset each other can be a feasible approach to the problem. Periodically adding, alloying or reacting materials or mixing of materials can also lower stress in films. In proposed project, several methods both alone and in combinations should be utilized in order to obtain thick and well adherent 0SC films.

The main objective of this work is to remove obstacles related to tribology, mechanics, surface chemistry and materials science in the manufacturing and operation of some MEMS devices. We have understood very little about tribology and mechanical properties on micro to nanoscales carbon films in the construction of MEMS devices. The DLC films have been in use in the macro world for various applications for several years. However, the transfer of knowledge and experience from macro world to micro and nano-worlds is missing. It is the aim of this project to expose 0SC films to the attention of the MEMS community. MEMS is a rapidly expanding technology that offers new ways of combining sensing, signal processing and actuation on a miniature scale. MEMS are presently being considered for both micro-sensor and micro-actuator applications. Sensors detect physical and chemical signals. Actuators can drive micro-components, including optical mirrors, displays, photonic lattices, fluid controllers and turbines. Biological applications are now also under investigation. A vital reliability issue for MEMS structures whose parts are moving and rubbing against each other is the friction and wear which take place after sometime. Even non-rubbing parts, which are in contact, can experience adhesion or sticking, for example, at this size scale due to the ambient moisture on hydrophilic surfaces. In such cases, carbon coatings with their high hardness, lubricity and hydrophobicity can really prevent wear and adhesion in use. The majority of MEMS materials and processing techniques, for historical reasons in microelectronics, come from the Si wafer technology. Although Si is suitable for many applications, its low toughness, low creep strength, high wear rate and high friction coefficient limit its use in some MEMS devices.. Due to the high friction between the Si and SiO surfaces very high wear rates take place and limit the reliability of such MEMS devices. When one consider the MEMS scales, using of conventional lubricants may not be appropriate in these applications. But, all these problems can be overcome with new materials with better tribological properties which can provide both lubrication and hydrophobicity to prevent adhesion and high hardness combined with low coefficient of friction can offer extended life times by reducing high wear rates. The bottleneck is that the choice of materials is limited to a few materials when one has to really replace Si due to its poor tribological properties. The materials which have lifetime tribological advantages are: DLC, diamond, cubic boron nitride (c-BN), Silicon Carbide (SiC), carbon nitride (CN) and aluminium nitride (AlN).

This project proposes to measure the advantages of DLC films provided that their limiting problems are eliminated in contacting MEMS applications. Once the most limiting factor of DLC films, namely stress is lowered to minimal values, then 0SC based MEMS technology will be promising for other numerous optical and electrical applications. When metals are incorporated into the DLC films, their properties can be adjusted for more applications. For example, the Co containing DLC films have very good field emission property, which is promising in the field emission display applications [1]. Another example is Ti containing DLC films which have good conductivity therefore, they are promising in electrical applications [1]. DLC films are known to have poor electronic properties due to the excessive density of defect states in the band gap which act as trapping centres. High Energy (MeV) ion bombardment, implantation where the bombarding particles pass through the interfacial region has been known to increase film adhesion. The process can be thought as ballistic mixing or interface stitching. The ion bombardment and energy release may also anneal the films and reduce the residual stress. If the materials involved are miscible, the ion mixing results in interfacial reaction and diffusion, however if the materials are immiscible the interfacial region is not mixed but the adhesion may still be increased. The right doses of ions per square centimetres have to be found for the best results. It has been shown that the technique of ion implantation can be used to improve the adhesion and stress properties of DLC film, while maintaining the high hardness, low friction and wear.

3 APPLICATION OF THE PROJECT

The main objective of this work is to develop a process and create fundamental and technological knowledge in order to eliminate the limiting problems (high stress and limited thickness) of DLC films which prevent them from being a proper substitute for Si in MEMS devices. The details of scientific and technological objectives in a measurable and quantitative form can be summarized below:

- As briefly explained above, for historical reasons, the present MEMS technology is based on Si and Si micro-fabrication techniques. There are specific MEMS applications in which the poor tribological properties of Si hinder the lifetime and reliability of these MEMS devices. Therefore, a substitute for Si is a must! DLC films when they are made thick enough with nearly zero stress, then MEMS based on 0SC films will be available. We have to ensure that 0SC films, as a Si replacement, would meet performance specifications and life cycle cost reduction. Tribological data to obtain from this project, from ambient to extreme conditions will open the way for commercial availability of MEMS made from 0SC films.
- In order to obtain 0SC films we will have to first concentrate on growth conditions and parameters, which may contribute to the formation of residual stress. As for the growth methods both Physical Vapour Deposition (PVD) and Plasma Enhanced Chemical Vapour Deposition (PECVD) will be utilized. Various techniques, such as X-ray diffraction and Raman Scattering will be employed to determine the initial values of the obtained residual stress in our films. The thickness of the films will be measured with a Calotest method which grinds the films with a steel ball having diamond slurry on it.
- Influence of methane flow rates, substrate temperature, bias voltage, ion current density, growth rates on residual stress will be studied in detail and their optimized values will be determined for low stress in the films.
- Films having high stress levels will be annealed for stress relaxation. Together with stress relaxation we expect to see structural changes in the annealed films.
- Ion implantation experiments will be carried out to reduce stress and also improve adhesion of the films both before and after the deposition of the carbon films.
- Both carbide forming and non forming metals will be introduced to the films during growth. In addition to metal introducing, experiments of alloying with Si and doping with H & N will be done.
- Once we know that what causes what type of stress (compressive or tensile), then we will periodically grow layers with alternatively tensile and compressive stress that they will offset each other. We believe that the combination of these approaches which are briefly explained above will give us 0SC films with super properties such as hard, lubricious, hydrophobic, biocompatible, thermally and chemically stable etc.
- Mechanical, structural and tribological testing of the films will be done by various methods. All tribological testing will be done with recently developed instruments such as Nano-hardness tester, Nano-scratch tester and Nano-tribometer. The advantage of these instruments that they allow a much greater variation in contact conditions therefore they more suited to investigate the films at very low loads.
- Once we have a control of stress management, maximizing the film thickness experiments will be carried. Presently, these films can be grown up to 2-3 μm.

Growing films as thick as 5-7 μm will be extremely important and this may eventually lead to free standing membranes.

- The radically innovative materials processing aspect of this project are twofold: Developing the "0SC" films which would also lead to free standing membranes. The second equally innovative aspect will be the opening of carbon based MEMS application areas where the most conventional material Si would fail due to its insufficient tribological properties.
- For a complete understanding, experimental findings will be correlated theoretical calculations of minimizing stress and tribological properties of 0SC films.

4 CONCLUSIONS

To apply nanotechnology, researchers have to understand biology, chemistry, physics, engineering, computer science, and a lot of other special topics, such as protein engineering or surface physics. But the complexity of modern science forces scientists to specialize and the exchange of information between different disciplines is unfortunately not very common. So the breadth is one of the reasons why nanotechnology proves so difficult to develop.

The project *Zero stress carbon (0SC) films for MEMS application* therefore, was - for us - an attempt to participate in the new "TRIBOMEMS" design trends, with focusing on the numerical calculations of 0SC films and tribo-parameters.

As a conclusion, the following state can be made: design will change radically under nanotechnology and for nano-engineers, respectively, a broad knowledge will become even more important in the future.

ACKNOWLEDGMENT

The authors wish to thanks the co-ordinator of the project proposal Dr. Müzeyyen Ece Oral, from the *Teknoplazma Advanced Technology Materials, Industry and Trade*, for all private communication on this topic and all other participants in the project application as well.

REFERENCES

[1] TRIBOMEMS: Zero stress carbon (0SC) films for MEMS applications: Project applied for 6FW, edited by Müzeyyen Ece Oral, Turkey, 2004.
[2] Reith M. Nano-Engineering in Science and Technology: An introduction to the Word of Nano-Design. Word Scientific Publishing (first publishing 2003), reprinted 2004.

Authors' Address:

Dr. Matjaž ŠRAML, *Assistant Professor*
University of Maribor
Faculty of Mechanical Engineering
Smetanova 17
SI-2000 Maribor
Slovenia
Tel.: +386 2 220 7722
e-mail: sraml.matjaz@uni-mb.si

Dr. Jože FLAŠKER, *Full Professor,*
Head of Instutite of Structures and Design
University of Maribor
Faculty of Mechanical Engineering
Smetanova 17
SI-2000 Maribor
Slovenia
Tel.: +386 2 220 7700
e-mail: joze.flasker@uni-mb.si

ANALIZA POVRŠINSKIH GREŠAKA NA ODLJEVCIMA NODULARNOG LIJEVA KVALITETE HRN EN GJS 500-7

ANALISYS OF SURFACE DEFECTS ON NODULAR IRON CASTINGS QUALITY HRN EN GJS 500-7

K. Terzić*, F. Unkić*, Z. Glavaš*, T. Marjanović**

*K. Terzić, *Metalurški fakultet, Aleja narodnih heroja 3, Sisak*
*F. Unkić, *Metalurški fakultet, Aleja narodnih heroja 3, Sisak*
*Z. Glavaš, *Metalurški fakultet, Aleja narodnih heroja 3, Sisak*
**T. Marjanović, *Valjaonica cijevi ,Božidara Adžije 19, Sisak*

Sažetak:

U okviru rada provedena su ispitivanja površinskih grešaka (makro uključaka) na odljevcima nodularnog lijeva kvalitete HRN EN GJS 500-7. Na osnovi dobivenih rezultata metalografske analize te spektrometrijske emisije i difrakcije rendgenskih zraka utvrđeno je da su nastali kompleksni makro uključci, nastali na površini odljevka, uzrokovani reakcijom kalupne mješavine i taljevine. Provedene analize upućuju da su nastali uključci produkt reakcije magnezija s taljevinom i kalupnom mješavinom.

Ključne riječi: nodularni lijev, površinske greške, makro uključci

Abstract:

Research of surface defects (macro inclusions) on casting of nodular cast iron quality HRN EN GJS 500-7 have been performed in this paper. On the basis of obtained results of metallographic analysis, spectrum analysis and X-ray analysis, it has been ascertained that complex macro inclusions were formed on the casting's surface and that they are caused by reaction of green sand and melt. Performable analysis has shown that formed inclusions are product of reaction of magnesium with melt and green sand.

Key words: nodular cast iron, surface defects, macro inclusions

1.0 UVOD

Oblikovanje metala lijevanjem zasigurno je najstarija metoda kojom se brzo i ekonomično mogu ponovljivo izrađivati i najkompliciraniji konstrukcijski elementi. Zbog složenih uvjeta ljevarske proizvodnje i velikog broja faktora koji utječu na ostvarenu kvalitetu odljevaka, moguć je nastanak većeg broja ljevarskih pogrešaka, a samim tim i nastanak škartnih odljevaka. Unatoč suvremenim tehnologijama proizvodnje odljevaka, složeni postupak lijevanja nije moguće provesti bez pojave grešaka. Posebnu pažnju potrebno je posvetiti sprječavanju nastanka grešaka, odnosno nastale pogreške točno istražiti i utvrditi vezu između uzroka, mehanizma nastanka i mjera za sprječavanje nastanka pogrešaka [1-3]. U okviru ovog rada provedena je analiza makro uključaka na površini odljevka nodularnog lijeva kvalitete HRN EN GJS 500-7.

2.0 EKSPERIMENTALNI DIO

Ispitivanja su provedena na dva uzorka nodularnog lijeva kvalitete HRN EN GJS 500-7 s makro uključcima u udubljenjima na površini odljevaka. Temperatura lijevanja odljevka 1 iznosila je 1400˚C, a odljevka 2 1380˚C. Promjenom parametara lijevanja smanjen je nastanak grešaka, ali ne bitno. Da bi se uspješno spriječila pojava grešaka potrebno je utvrditi njihov uzrok. S tim ciljem u području grešaka izrezani su uzorci i provedena je metalografska analiza te analiza spektrometrijskom emisijom i difrakcijom rendgenskih zraka greške i mase za kalupovanje F 40 i P 40.

2.1 Metalografska analiza

Za analizu su pripremljeni presjeci uzoraka u području grešaka. Na mjestu greške u udubljenju na površini mjestimično je prisutan heterogeni sloj svjetlo i tamno sive boje, dubine do 1,1mm, odvojen od odljevka karakterističnim tankim slojem. U blizini grešaka došlo je do degeneracije nodula pri čemu se pojavljuje listićavi grafit. Ova pojava ukazuje na lokalno osiromašenje taljevine Mg, odnosno nastajanje oksidativnih uvjeta u tom dijelu odljevka. Na slikama 1a, 1b, 2a i 2b prikazana je mikrostruktura odljevaka u području grešaka.

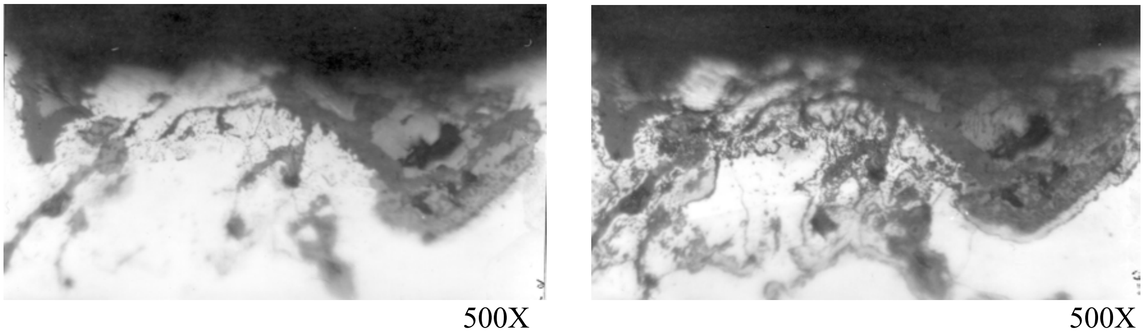

Slika 1. Heterogeni oksidni sloj u području grešaka na uzorku br. 1: a) nenagriženo stanje, povećanje 500x; b) nagriženo stanje (nital), povećanje 500x

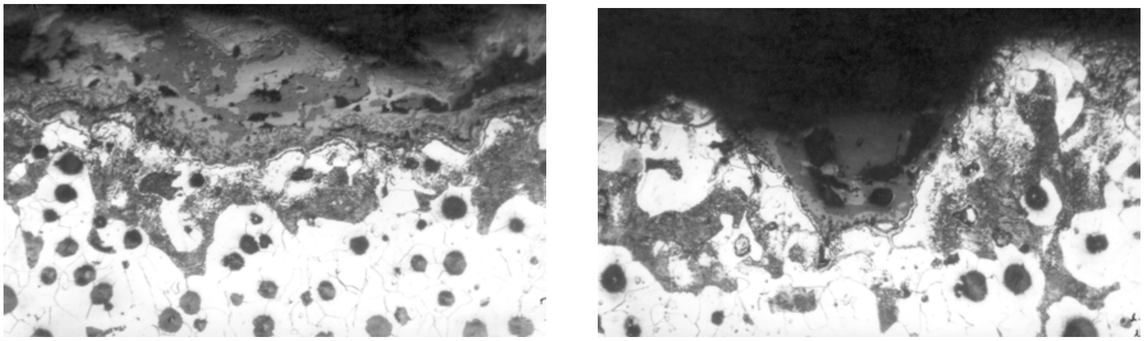

Slika 2. Heterogeni oksidni sloj u području grešaka na uzorku br. 2: a) nenagriženo stanje, povećanje 500x; b) nagriženo stanje (nital), povećanje 200x

2.2 Spektrometrijska emisija i difrakcija rendgenskih zraka

Za određivanje uzroka grešaka provedena su dopunska ispitivanja metodom spektrometrijske emisije i difrakcije rendgenskih zraka. Ispitani su:

-kalupna mješavina F 40 i P 40,
-uzorak 1 od odljevka lijevanog na višoj temperaturi,
-uzorak 2 od odljevka lijevanog na nižoj temperaturi,
-uzorak 3 koji predstavlja površinski sloj uzorka 2 dobiven brušenjem.

U tablici 1 prikazani su rezultati kvalitativne elementarne analize. Prema njima unutar osnove, koju čine Fe (uzorak 1 i 2) te Si (uzorak F 40 i P 40), u svim uzorcima identificirani su Mg, Al, Ca, Ti. U uzorku 1 i 2 identificirani su elemnti (P, Mn, Cu, Zn, As i Sb) koji se ne nalaze u uzorcima kalupne mješavine F 40 i P 40. U uzorku 1 identificirani su elementi (S, Cr, Ni, Sn) koji se ne nalaze u ostalim uzorcima.

Tablica 1. Rezultati kvalitativne elementarne analize

Element	Uzorak			
	1	2	F 40	P 40
Mg	-, +	+	+	+
Al	+	+	+	+
Si	+	+	+	+
P	-, +	+	-	-
S	+	-	-	-
K	+	-	+	+
Ca	+	+	+	+
Ti	+	+	+	+
Cr	+	-	-	-
Mn	+	+	-	-
Fe	+	+	+	+
Ni	+	-	-	-
Cu	+	+	-	-
Zn	+	+	-	-
As	+	+	-	-
Sn	+	-	-	-
Sb	+	+	-	-

Dobiveni rezultati ukazuju da dio elemenata identificiranih u uzorku 1 i 2 (Mg, Al, Si, K, Ca, Ti) potječe iz upotrijebljene kalupne mješavine i dijelom iz osnove uzorka 1 i 2, kao npr. Fe. Na ovakav zaključak upućuju i rezultati fazne analize, prikazane u tablici 2. Faze elemenata identificirane u uzorku 1 i 2 te uzorku 3 istovremeno su identificirane u uzorcima kalupne mješavine F 40 i P 40.

Tablica 2. Rezultati fazne analize

Identificirane faze	Uzorak				
	1	2	3	F 40	P 40
Fe_3O_4	+	+	+	-	-
αFe_2O_3	-	+	-	-	-
FeO	+	+	+	-	-
$2FeO\cdot SiO_2$	+	+	+	-	-
$2Cao\cdot SiO_2$	-	+	-	-	-
SiO_2 (kao kvarc)	+	+	+	+	+
SiO_2 (kao kristobalit)	-	-	-	+	+
$CaCO_3$	-	+	-	+	+
$CaMg(CO)_2$	-	+	+	+	+
$KAlSi_3O_8$	+	+	-	-	-
$Al_2SiO_5(OH)_4$	-	+	-	-	-
$FeTi_2O_5$	+	-	-	+	+
$Al_2SiO_5(OH)_4$	+	+	-	+	+
Al-Mg-Si-O-OH-Na	-	-	-	+	+
Faze netočno poznatog sastava Ti-O	-	-	-	+	+

U ovim uzorcima identificirane su i nove faze. $2FeO.SiO_2$, $FeTi_2O_5$ i $2CaO.SiO_2$ nastale kao produkt reakcije mase za kaluparenje i taljevine

3.0 ZAKLJUČAK

Na osnovu dobivenih rezultata metalografske analize te ispitivanja metodom spektrometrijske emisije i difrakcije rendgenskih zraka, može se zaključiti da su nastali makro uključci na površini odljevaka uzrokovani reakcijom kalupne mješavine i taljevine. U području grešaka detektiran je heterogeni sloj čija debljina je povezana s temperaturom lijevanja. Izgled grešaka upućuje na produkte reakcije magnezija s taljevinom i kalupnom mješavinom što potvrđuje i preliminarna fazna analiza. Oblik i lokacija grešaka kao i uvjeti lijevanja (temperatura lijevanja i sustav ulijevanja) ukazuju da uzrok nastale greške treba tražiti u načinu obrade taljevine i sustavu ulijevanja taljevine.

4.0 LITERATURA

[1] J. Campbell, Castings, Butterworth-Heinemann, Oxford, 2003.
[2] S. Hasse, Guß-und Gefügefehler, Giesserei-Verlag GmbH, Düsseldorf, 1998.
[3] Grupa autora, Ljevački priručnik, Savez ljevača Hrvatske, Zagreb, 1985

10. Savjetovanje o materijalima, tehnologijama, trenju i trošenju
10. Conference on Materials, Processes, Friction and Wear
MATRIB'05, Vela Luka, 23-25.06.2005.

COMPARISON OF NEURAL NETWORK DURABILITY MODELS FOR REINFORCED CONCRETE STRUCTURES

Neven Ukrainczyk, Tomislav Matusinović
University of Zagreb, Faculty of Chemical Engineering and Technology,
Marulićev trg 20, HR-10000 Zagreb, Croatia, e-mail: nukrainc@marie.fkit.hr

Velimir Ukrainczyk
Most projekt, Sveti Duh 36, HR-10000 Zagreb, Croatia, e-mail: mostprojekt@zg.htnet.hr

Abstract:
Data on relevant structural parameters gathered on eleven reinforced concrete structures in continental and three in Adriatic marine environment at various ages have been used for training artificial neural networks. Two separate models, for continental and marine environments have been developed. Data for modeling in continental environment were gathered at ten different ages of bridges and consists of 213 records. Data on marine environment were gathered at seven different ages of structures and consists of 124 records. The effects of the structure, properties of concrete and environmental conditions onto the degree of damage caused by steel corrosion have been investigated. The damages were classified into five categories based on the type of necessary remedial works. The artificial neural network for feature categorization was used as a tool for classification of damage and prediction of damage degree.
This paper demonstrates the use of artificial neural networks in modeling the durability of reinforced concrete structures in marine and continental environment. A comparison of the two models regarding the different environments is given. The models are able to recognize and evaluate the effect of individual parameters on the damages. The developed models could be useful for planning the maintenance of investigated structures and design of remedial works.

Keywords: reinforced concrete structure, durability, corrosion, damage categorization, artificial neural network, modeling, marine and continental environment.

1 Introduction

The safety of engineering concrete structures, whose expected service life is 120 years according to BS ISO15686-1, is often threatened in continental environment after only 20 to 30 years of exposure, and heavy repairs are necessary. In marine environment after only 15 years of exposure heavy repairs are needed. Besides the flaws in building standards, design and unsatisfactory construction, the direct causes are: a) accelerated carbonation, due to the higher carbon dioxide concentration on highways and in towns; b) de-icing chloride ions, which the fastest activate corrosion of steel; c) freezing and thawing cycles, which "find" the flaws in composition and curing of concrete. The products of corrosion occupy up to six times greater volume than the steel, and exert substantial stresses on the surrounding concrete, resulting in deterioration of concrete. The outward manifestations of the rusting include staining, cracking, and spalling of the concrete. Concurrently, the cross section of the steel is reduced. In time, structural distress may occur either by loss of bond between the steel and concrete due to cracking and spalling or as a result of the reduced steel cross-section area [1]. The principal factors influencing the rate of deterioration caused by reinforcement corrosion are known [1-6]. There are models [1,2,6] describing certain phases of the complex process of steel corrosion and destruction of concrete cover caused by rebar corrosion, namely: process of chloride penetration, carbonation, propagation of corrosion process, and destruction of reinforcement and concrete. However, overall analytical correlation between influential parameters and certain kinds of damages has not been established. Survey, diagnosis, and remedial works of the concrete structures have generated extensive experimental data over the years, but the analysis of such data using traditional tools has not produced reliable predictive models. Recently, there has been a growing interest in using artificial neural networks in engineering applications.

This research demonstrates the use of artificial neural networks (ANN) in modeling the durability of reinforced concrete structures in marine and continental environment. A comparison of the two models regarding the different environments is given. The model can be used for prediction of the extent of degree in the structure service life, for planning the maintenance, and can assist in designing and restoration of the investigated reinforced concrete structures.

2 ANN-based models

The architecture of ANNs mimics that of biological neurons and their operation essentially simulates the internal operation of the human brain[6]. In recent years, ANNs have shown exceptional performance as a regression tool, especially when used for pattern recognition and function estimation. They are highly nonlinear, and can capture complex interactions among input/output variables in the system without any prior knowledge about the nature of these interactions. A neural network is an empirical modeling tool, and it does operate by "curve-fitting". However, some notable differences exist between neural networks and typical, traditional empirical models[6]. In comparison to traditional methods, ANNs tolerate relatively *imprecise*, *noisy* or *incomplete* data, *approximate* results, are less vulnerable to outliers, have better *filtering capacity*, and are more *adaptive*. Moreover, ANNs are also *massively parallel*, that is, their numerous independent operations can be executed simultaneously. Some of the limitations of the neural networks are possible long training times, the need for large amount of reliable training data, and no guarantee of optimal results.

For the prediction of the most likely damage degree, for a given input pattern, classification network for characterization of distinct features was used. The classification networks[6] produce Boolean output responses, i.e., zero indicates that the input pattern is not within the specific class, and one indicates that it is. Actually, *fuzzy inferences* about the classifications are made.

3 Data gathering and damage categorization

Data on the effects of the structure and properties of concrete onto the degree of damage caused by steel corrosion have been gathered on eleven bridges located in continental environment [3,9]. The data were gathered at ten different ages of bridges: 1, 14, 22, 24, 28, 29, 31, 33, 55 and 91 years of exposure. The data consists of 213 records. The data on three concrete structures located in Adriatic marine environment [4,5] were gathered at seven different ages of concrete structures: 1, 20, 23, 27, 29, 31 and 73 years of exposure. The data consists of 60 records from the Vir bridge, 53 records from Krk bridge, and 11 records from former Torpedo factory. For the purpose of modeling data on damages caused by steel corrosion were interpreted as output. In addition, data on concrete properties and concrete compositions were considered as input parameters. Damages caused by steel corrosion were classified into five categories according to the criterion described in Table 1. The measurements of a half-cell potential, E (reference electrode $Cu/CuSO_4$), according to ASTM C 876-91 on the "undamaged" surfaces, indicate risks of corrosion occurrence.

Table 1: The categorization criteria for damages caused by steel corrosion.

DAMAGE CATEGORY	REINFORCED CONCRETE STRUCTURE STATE
0	No corrosion $E > -200$ mV (reference electrode $Cu/CuSO_4$)
1	Possible corrosion $E < -200$ mV
2	Cracks < 0.2 mm
3	Cracks > 0.2 mm, staining on the concrete surface
4	Large cracks, spalling, loss of bond between steel and concrete, reinforcement corroded on the surface
5	Spalling of concrete cover Significant loss of rebar cross section

Parameters that affect the steel corrosion in concrete (micro location conditions, structure, and properties of concrete) listed in Fig. 1 were used in this study for training the ANN models. Concrete cover depth, c was measured by profometer. Chloride ions concentrations at surface and rebar level, C_s and C_r represent water-soluble chloride content and are expressed in terms of the mass of concrete. They were determined on concrete powders obtained by drilling three holes in four layers, each two centimeters thick. The test methods for chloride extraction and titration recommended by the AFREM group were used. Chloride content values for C_s and C_r are averages of three samples tasted. Water-soluble chloride content is used as an appropriate parameter related to corrosion risk. The actual concrete strength, f_c was determined on one drilled core for each macro location. Representative location for drilling the core was chosen on the basis of broad testing of concrete homogeneity by Schmidt hammer. Carbonation depth, d (pH<9) was estimated on core by phenolphthalein test The porosity of concrete, p was measured on the 3 centimeters thick outer layer of the drilled core, as the general parameter of concrete quality. Moisture content in concrete, w was estimated as equilibrium value for average relative humidity of air measured throughout the year. The values for cement content (cc) and water-cement ratio (w/c) were taken from design documentation. The influence of the microclimate was considered through and with the parameters of: the orientation and exposure, OE (unexposed structural element is sheltered from the environment); the splashing zone, sz; the height above the sea level, h; and the horizontal distance from the sea, d. Average temperatures and relative environment humidity at the relatively close locations of the investigated structures are similar

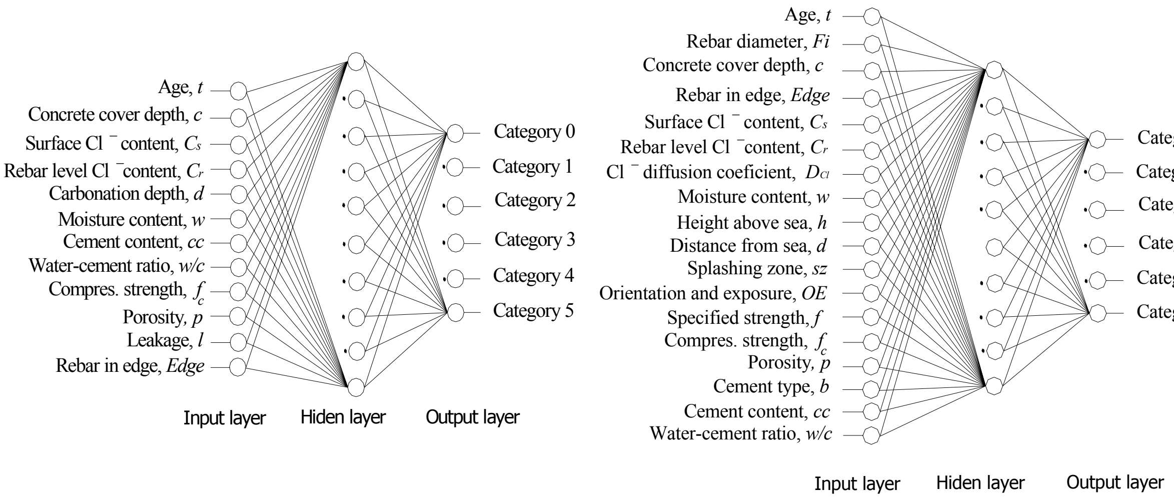

A) B)

Figure 1: Architecture of selected networks for A) continental and B) marine environment: one hidden layer with ten neurons (for clarity, not all neuron connections are shown).

for a given climate (continental or marine), so these influences were not considered as a possible parameter of a different impact to the rebar corrosion. As no data were available for influences of admixtures, type of blended cement, and freezing and thawing cycles these parameters were not considered. The data are arranged in a patterned format. Data used for network training, testing and validation contain sets of pairs, records. Each pair consists of an input vector of 12 (18-marine) influential parameters and an output vector of 6 attributes (damage categories), Fig. 1.

4 Training and validation of ANN models

For building and training the neural network several software packages were used [10-13]. To provide an ANN model with good generalization capability the data were divided into sets of 183 (94) training and 30 validation records. A feed-forward neural network using back-propagation algorithm was employed. The training procedure comprised iterative calculations of the weight coefficients by minimization of criteria function. After each epoch, the network predicted outputs using training (recall) and validation (generalization) records. To avoid over-fitting (over-training), and thus enable a good generalization capability, training was stopped when the misclassification rate of the validation records started to deviate from the misclassification rate of the training records. The chosen architecture is shown in Figure 1. The determination of the optimal number of hidden layers, the number of processing elements and the network parameters used was largely achieved by an educated trial and error process testing more than 100 networks. A sigmoid transfer function, *logsig*, was employed as an activation function with full connection adopted among units in different layers. Weights and biases were initialized randomly with an initial weight range = –0.3 to +0.3. The following values of network parameters were used: learning parameter = 0.5 and momentum = 0.5. A successfully trained network is characterized by its ability to predict damage category for the data it was trained on. The training process was completed with misclassification rate = 9.3%(7.4%). The validity of a successfully trained ANN model is determined by its ability to generalize its predictions beyond the training data and to perform well when it is presented with unfamiliar new data. The model was presented with a total of 30 records excluded from training. Validation of ANN model resulted with misclassification rate = 16.6%(13.3%). Misclassification rate is not high for this highly heterogeneous material.

Table 2: The number of correctly and falsely predicted categories by developed ANN models (continental/marine environment). The matrix diagonal represents correctly predicted categories.

continental/marine environment													
Training							Validation						
	Predicted							Predicted					
True	0	1	2	3	4	5	True	0	1	2	3	4	5
0	69/3	1/1	0/0	0/2	0/0	0/0	0	5/3	1/0	0/0	0/0	0/2	0/0
1	4/0	14/8	1/1	0/0	0/0	0/0	1	0/0	3/2	1/0	0/0	0/0	0/0
2	0/0	2/1	10/35	2/0	0/0	0/1	2	0/0	1/0	4/11	2/0	0/0	0/0
3	0/0	0/0	3/0	22/5	2/0	0/0	3	0/0	0/0	0/0	4/2	0/0	1/0
4	0/0	0/0	0/0	1/0	21/29	0/1	4	0/1	0/0	0/0	0/0	6/9	0/1
5	0/0	0/0	0/0	0/0	0/0	31/7	5	0/0	0/0	0/0	0/0	0/0	4/1

5 Comparison of ANN models for continental and marine environment

By adding absolute coefficient values of weights that connect one input signal to all the inner layer neurons, one gets a number for each input parameter named a contribution factor [3-5]. The contribution factor is a measure of the importance of respective parameter in predicting the network's output, relative to the other input parameters in the network [11]. However, neural networks are also capable of finding patterns among several parameters, none of which is highly correlated with the output but which together form a pattern that uniquely determines the output. Based on the final set of weights, given by the software [10-13], a contribution factor was calculated, fig. 2. In both environmental climates the Cover depth is the principal parameter. For the marine environment the top six influencing parameters in ascending order are the Rebar level chloride content, Splashing zone, Age, Rebar in an edge of the structural part, Orientation and exposure and Height above a sea. For the continental climate the top six are the Age, Carbonation depth, Rebar level chloride content, Compressive strength, Water-cement ratio and Water content.

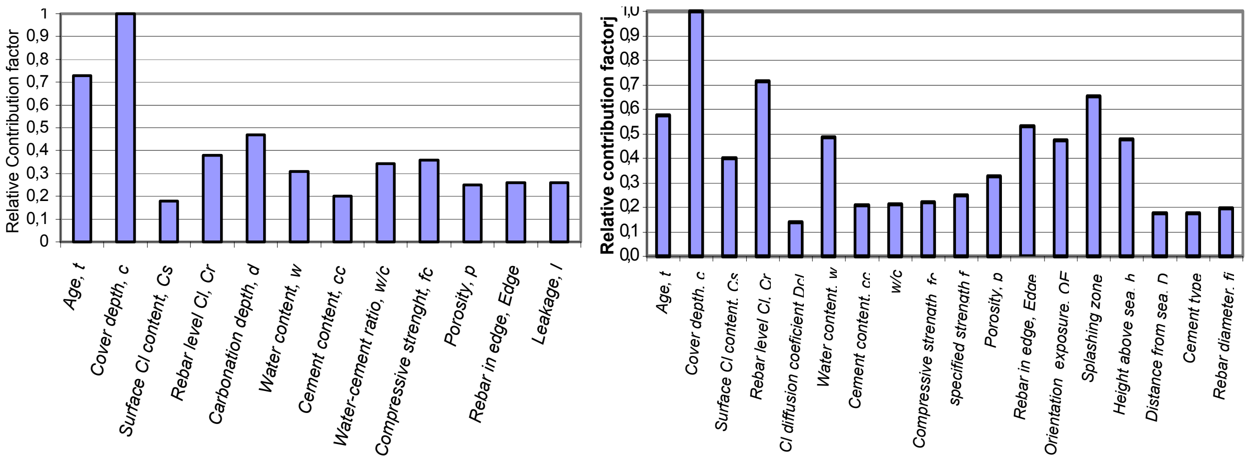

A) B)

Figure 2: Relative contribution factor for individual input parameters in predicting the damage category for the two models: A) continental and B) marine environment.

An example of the simulation results is illustrated in Figure 3 where *fuzzy inferences* about the classifications are made. A comparison shows how much the rate of the deterioration of structures in marine environment is faster than in the continental climate.

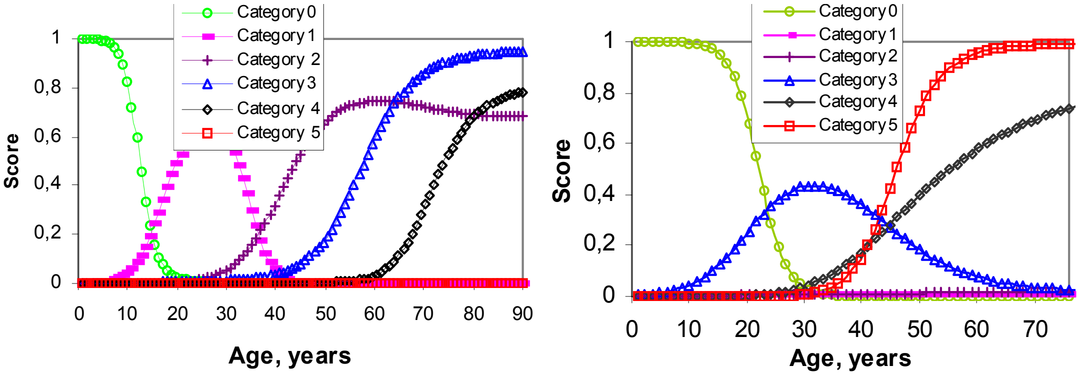

A) B)

Figure 3: Simulations with mean value parameters for A) continental and B) marine climate.

6 Conclusions

The models are able to recognize and evaluate the effect of individual parameters on the damages caused by steel corrosion. In both environmental climates the Cover depth is the principal parameter that determine the structural service life. The developed models could be useful for planning the maintenance of investigated structures and design of remedial works. Unfortunately, data on admixtures, type of blended cement, and freezing and thawing cycles were not available. Possibly, if included, ANN model would form a pattern that better determines its output.

7.0 References

1. ACI Committee 222R-89, *Corrosion of Metals in Concrete*, Detroit, 1990.
2. RILEM Report 14, ''Durability design of concrete structures,'' *Report of the Committee TC 130-CSL*, Edited by A. Sarja and E. Vesikari, E&FN Spon, 1996.
3. Ukrainczyk, N., Ukrainczyk, V., Use of Neural Network to Evaluate Rebar Corrosion in Continental Environment, 3th Int. Conf. *Construction Materials*, Vancouver, 2005.
4. Ukrainczyk, N., Banjad, P. I., and Bolf, N., Use of Neural Network to Evaluate Rebar Corrosion in Marine Environment, *ACI Materials Journal*, to be published.
5. Ukrainczyk, N., Banjad, P. I., and Ukrainczyk, V., Application of Neural Network in Predicting Damage of Concrete Structures Caused by Chlorides, International Symposium D*urability and Maintenance of Concrete Structures*, Dubrovnik, Croatia, 2004.
6. Siemes, A.; Vrouwenvelder, A., van den Beukel, A., ''Durability of buildings: reliability analysis,'' Heron, 30 (3), 1985.
7. Liu, Y. A., Baughman, D. R., *Neural Networks in Bioprocessing and Chemical Engineering*, Academic Press, Inc., San Diego, 1995.
8. Hammerstrom, D., '' Neural Networks at Work,'' *IEEE Spectrum*, July 1993, pp. 46-53.
9. Ukrainczyk, V., et all., Reports on State of *East Viaduct Sava-Odra*, *Bidj Highway S. Brod - V. Kopanica*, *Jasenovac*, *Mrežnica at Ostarije*, *Bednja at Tuhovec*, *Botovo-Drava, Kamenmost-Vrljika*, *Novi-Kupa*, *Jadranski-Sava, Ilova Highway Zagreb - Lipovac,* R.C. Bridge Structure and Design of Remedial Works'', (In Croatian), Mostprojekt, Zagreb.
10. Saha, A., Neural Network for Prediction and Classification – in Excel (www.geocities.com/adotsaha/NNinExcel.html)
11. Ward System group, *Neuroshell 2 release 1.5*, 1993.
12. Demuth, H., Beal, M., *Neural Network Tool Box for Use with MATLAB Release 13.*, The Math Works Inc., 2002.

HEAT TREATMENT OF BSt 500S STEEL REBAR

Dr.sc. Dražen Živković, doc., FESB – Split, Ruđera Boškovića bb.
Ante Alujević, dipl.ing., “ABP diesel”, d.o.o. – Split, Dugopolje

Abstract:

This paper deals with the analysis of mechanical properties of BSt500S steel rebar. First, the bars were quenched and self-tempered. Yield strength and ultimate tensile strength values have been investigated, as well as the distribution of hardness upon the bars cross-section. The chemical composition and microstructure of the processed samples have been controlled, too. The results of the mechanical properties and micro-structural tests were compared with the mechanical properties of ordinary steel (Č. 0551 – HR norm) rebar without heat treatment. The possible improvements (especially for continuous achieving of standard mechanical values) have been suggested in the conclusion.

Key words: Steel Rebar, BSt500S, Quenching

Sažetak:

Ovaj članak bavi se analizom mehaničkih svojstava rebrastih šipaka izrađenih iz čelika BSt500S. Šipke su najprije bile podvrgnute površinskoj toplinskoj obradi kaljenja, a zatim procesu samo-popuštanja. Provedena su ispitivanja vrijednosti granice razvlačenja i čvrstoće, kao i ispitivanja raspodjele tvrdoće po poprečnom presjeku. Također su kontrolirani kemijski sastav i mikro-struktura obrađenih uzoraka. Dobiveni rezultati uspoređeni su sa svojstvima čelične rebraste šipke iz čelika Č.0551, koja nije bila podvrgnuta toplinskoj obradi. U zaključku je dan prijedlog za moguća poboljšanja u smislu kontinuiranog ostvarivanja normiranih vrijednosti mehaničkih svojstava čelične rebraste šipke.

Ključne riječi: Čelična rebrasta šipka, BSt500S, površinsko kaljenje

1. INTRODUCTION

The parallel analysis of properties of two steel bars, made from similar steels, has been given in this paper. A group of specimens from BSt 500S were subjected to the surface heat treatment – quenching.

1.1. GENERAL WIEW ON PRODUCTION PROCESS OF STEEL REBAR IN "STEELWORKS SPLIT"

The production process of hot-rolled steel rebar in "Steelworks Split" consists of three basic processes. The first one takes place in the steel-plant, starting with melting of metal scrap in the direct electric arc furnace. The scarp has unknown chemical composition. After the chemical composition estimation, the corrections of chemical composition are made in crucible furnace. The corrected melt is now prepared for continuous casting. The molten metal is poured into a refractory-lined intermediate pouring vessel where impurities are skimmed off. The vessel holds as much as three tons of metal. The molten metal travels downward along a path supported by rollers *(pinch rolls)*. Before starting the casting process, a solid *starter* bar is inserted into the bottom of the mold. The molten metal is then poured and freezes onto the starter bar. The bar is withdrawn at the same rate the metal is poured. The cooling rate is such that the metal develops a solidified skin *(shell)* to support itself during its travel downward at speeds typically *25mm/s.* Additional cooling is provided by water sprays along the travel path of the solidifying metal. The dimensions of cast metal bar are *125x125x6000 mm.* The bars are air cooled at environment temperature.

Figure 1. " The direct electric arc furnace"

Figure 2. " The crucible furnace"

The next process starts in heat treatment furnace, where the bars are heated up to *1250 ^oC*. This high temperature is necessary for the hot-rolling. The bars are pushed out from the furnace to the rolling mill, for reshaping and reduction in thickness. During the rolling process the bar passes through the several rolling stands. All the rolling stands are placed in a line, and each consists of two rollers. The rolling bar passes through different rolling stands at the same time. The rolling speed is increasing from the first to the last rolling stand.

Figure 3. " The heat treatment furnace"

Figure 4. "The former rolling stand"

The third process is the heat treatment of the steel bar. This process consists in direct watering of the glowing hot steel rebar. The rebar, from the last rolling stand *(950 to 1000 ^oC)*, enters in cooling device, then passes through the water cooling head. The result is tempered surface layer. This process is called quenching. After quenching the rebar is cut off *(length 48 m)* and left on the cooling desk. The self-tempering process that occurs on the cooling desk is the last step in rebar production.

Figure 5. "The quenching device"

Figure 6. "The cooling desk"

2. THEORETICAL PRINCIPLES OF QUENCHING

The heat treatment of hot steel rolled rebar consists of direct water cooling and additional self-tempering. During this heat treatment the rebar is passing through three processes [2].

The first process is the fast water cooling that is applied on the hot rolled rebar after it leaves the last rolling stand. The cooling device efficiency in this first phase has to be adjusted as to fit the cooling ratio light higher than critical ratio for martensitic transformation. At the end of this phase the rebar has an austenitic core surrounded with a layer of austenite and martensite. The content of martensite is decreasing from the surface to the centre of the rebar. Duration of the first phase depends on the thickness of the surface martensite layer.

During the second process the rebar leaves the area of intensive water cooling and is additionally subjected to air cooling. The coefficient of heat transfer towards environment is low while the temperature gradient inside rebar is quite high. The hot rebar core heats again the rebar surface. As a result we have self-tempering previously formed martensite. This self-tempering assures better ductility with rather high yelled strength. This second phase finishes when the highest surface temperature is reached. This temperature is called the tempering temperature and is about *$600\ ^{o}C$.* Duration of the second phase depends on the bar diameter or on the cooling speed in the first phase. In the second phase untransformed austenite on the surface changes in to bainite, while in the core we still have austenite.

The third process starts on the cooling desk. It consists from quasi-isothermal process of austenitic transformation. As a final result of this transformation we have mixed phases of ferrite and pearlite or pearlite and bainite. The combination of those mixed phases depends on several factors as: chemical composition of steel, bar diameter, final rolling temperature and cooling device efficiency. The figure *7* shows the quenching process scheme and cooling curves.

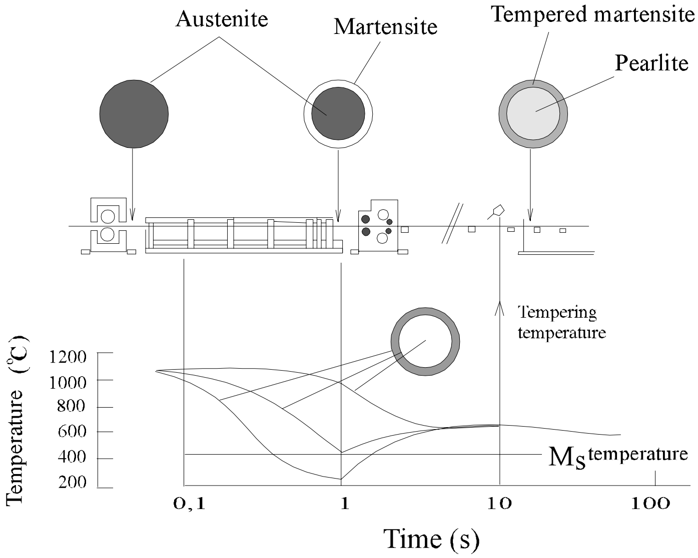

Figure 7. " Quenching process scheme and cooling curves" [3]

It may be considered that this quenching process consists of three physical phenomena:

1. heat transfer between rebar surface and environment,
2. heat conduction inside rebar,
3. allotropic modifications.

2.1. Heat transfer between rebar surface and environment

The heat transfer phenomena may be divided in three phases:

- quenching phase in which the rebar are intensively water cooled,
- air cooling phase (between the quenching device and the cooling desk),
- air cooling phase of parallel bars on the cooling desk.

Practically every phase may be defined by the *coefficient of heat transfer (α)* and *density of thermal flow (Φ):*

$$\Phi = \alpha\ (T_s - T_m)$$

- *T_s is the temperature of bar surface, T_m is the temperature of cooling media*

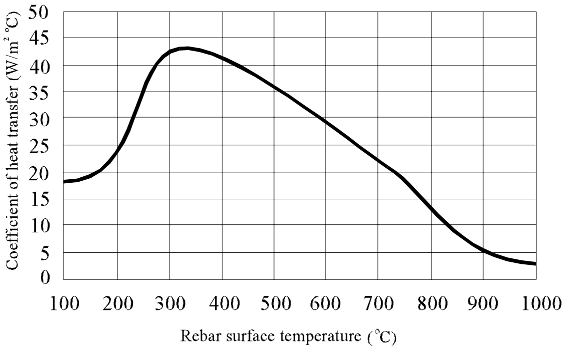

Figure 8. " Heat transfer coefficient inside the cooling device" [4]

During traveling from water cooling device to cooling desk the rebar is under coercion air cooling. This cooling process is combination of heat radiating and coercion air flow. The coefficient of heat transfer is a function of rebar surface temperature and relative rebar speed with reference to environmental air (Fig. 9).

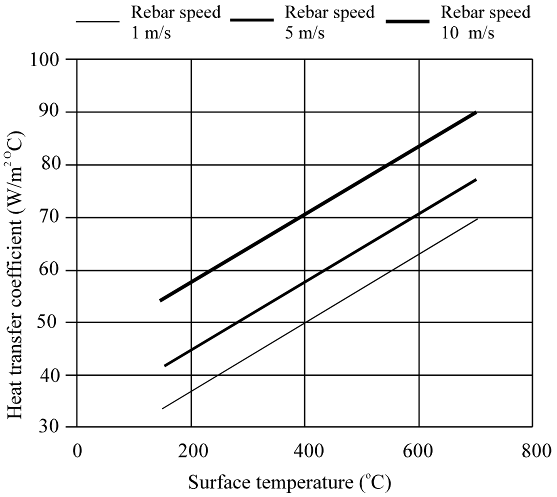

Figure 9. " Heat transfer coefficient during coercion air cooling" [4]

The heath transfer coefficient on the cooling desk is combination of heat radiating and convection air cooling. In other words the heath transfer coefficient depends on rebar temperature, rebar diameter and the free space between the rebar on cooling desk (Fig. 10).

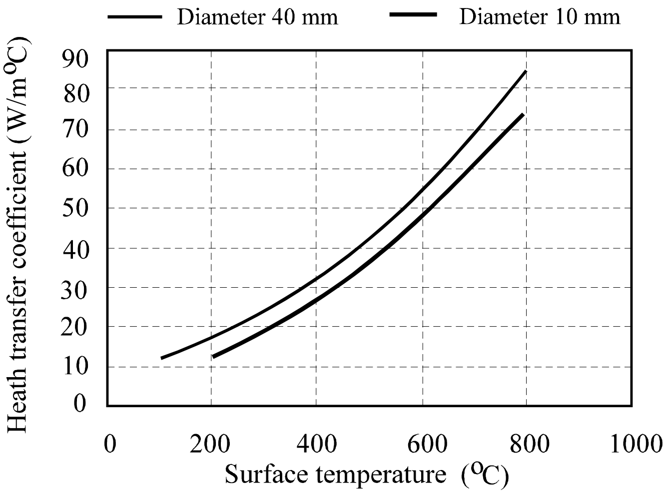

Figure 10. " The heat transfer coefficient on the cooling desk" [5]

2.2. Heat conduction inside rebar

Ultimate tensile strength of heat treated steel rebar depends on heat flow inside rebar in the moment of leaving the cooling device. Besides the heat transfer coefficient, it is necessary to estimate the heat properties of steel. From metallurgical point of view, knowing the heat field inside rebar gives the possibility to predict two essential parameters: voluminous martensite percentage and tempered temperature.

Voluminous martensite percentage

The martensite layer is formed as cylinder around the rebar axe. The martensite start temperature *(M_S)* is a function of chemical composition, and can be calculated from the following equation:

$$M_s = -361(\%C) - 39(\%Mn) + 500 \quad ({}^0C)$$

As the steel BSt 500S has an average chemical composition of *0,18 %C* and *0,8 %Mn*, its martensite transformation temperature is *400 °C.*

The voluminous martensite percentage can be calculated form the following equation:

$$p_M = 100 \cdot \left[1 - \left(\frac{2 \cdot r_M}{d} \right)^2 \right]$$

Tempering temperature

The temperature of tempering is defined as the maximum temperature achieved during self-tempering process. That is the maximum surface temperature during the cooling process on the cooling desk. It can be measured directly by the radiation pyrometer placed on the entry of the cooling desk. In this case tempering temperature is about *600 °C.*

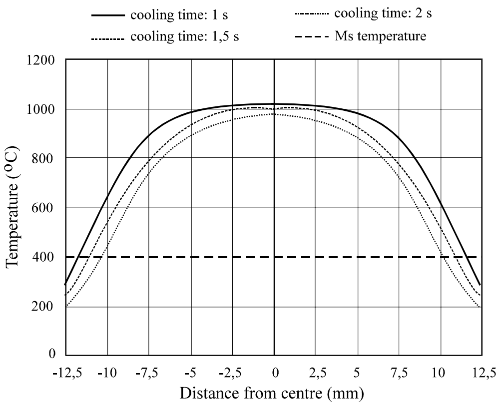

Figure 11. " The border radius of martensite layer as a function of treatment duration" [5]

3. EXPERIMENTAL WORK

The experimental work was based on the mechanical and chemical tests. In this part of the paper parallel analysis of the mechanical and chemical test results are given. The specimens were made from two similar steels *(Č.0551, BSt 500S – DIN 488)*. Those from *BSt500S* had been heat treated. Each group consisted of three bars with diameters: *12, 16* and *20 mm.*

3.1. Chemical composition

The bars with different diameters are continuously cast from different melt, so in *Table 1* the specimen chemical compositions are given.

Table 1. Chemical composition

Material	**Diameter (mm)**	**Chemical composition**							
Č.0551	*12*	**C**	**Si**	**Mn**	**P**	**S**	**Cu**	**Cr**	**Sn**
		0.2200	0.2910	0.8129	0.0025	0.0188	0.2679	0.1324	0.0149
		Al	**Mo**	**V**	**W**	**Ti**	**Ni**	**Nb**	**Fe**
		0.0055	0.0171	0.0003	0.0105	0.0023	0.0898	0.0030	98.10
BSt500S	*12*	**C**	**Si**	**Mn**	**P**	**S**	**Cu**	**Cr**	**Sn**
		0.1800	0.2115	0.6787	0.0101	0.0186	0.1771	0.0430	0.0121
		Al	**Mo**	**V**	**W**	**Ti**	**Ni**	**Nb**	**Fe**
		0.0045	0.0111	0.0004	0.0077	0.0021	0.0644	0.0029	98.50
Č.0551	*16*	**C**	**Si**	**Mn**	**P**	**S**	**Cu**	**Cr**	**Sn**
		0.1900	0.3030	0.8687	0.0123	0.0331	0.2462	0.1125	0.0164
		Al	**Mo**	**V**	**W**	**Ti**	**Ni**	**Nb**	**Fe**
		0.0063	0.0168	0.0005	0.0102	0.0028	0.0940	0.0025	98.02
BSt500S	*16*	**C**	**Si**	**Mn**	**P**	**S**	**Cu**	**Cr**	**Sn**
		0.1500	0.2170	0.8330	0.0178	0.0277	0.3088	0.1532	0.0161
		Al	**Mo**	**V**	**W**	**Ti**	**Ni**	**Nb**	**Fe**
		0.0066	0.0217	0.0023	0.0113	0.0024	0.1256	0.0035	98.07
Č.0551	*20*	**C**	**Si**	**Mn**	**P**	**S**	**Cu**	**Cr**	**Sn**
		0.2500	0.2652	0.8373	0.0091	0.0300	0.3021	0.0803	0.0160
		Al	**Mo**	**V**	**W**	**Ti**	**Ni**	**Nb**	**Fe**
		0.0008	0.0145	0.0002	0.0059	0.0026	0.0898	0.0021	98.07
BSt500S	*20*	**C**	**Si**	**Mn**	**P**	**S**	**Cu**	**Cr**	**Sn**
		0.1800	0.1925	0.6647	0.0406	0.0356	0.5956	0.1383	0.0215
		Al	**Mo**	**V**	**W**	**Ti**	**Ni**	**Nb**	**Fe**
		0.0010	0.0244	0.0002	0.0107	0.0020	0.1102	0.0015	97.99

The chemical composition control was achieved in the chemical laboratory of the *"Steelworks Split"*. The results presented in this table are average values.

3.2. Mechanical tests

The yield strength, ultimate tensile strength and hardness are tested mechanical properties.

Yield strength and ultimate tensile strength

Ultimate tensile strength and yield strength were tested by the tensile testing machine *(UHP 40 – MOHR-FEDERHAFF-LOSENHAUSEN)* on bare specimens in the laboratory for material testing of the *"Steelworks Split"*. The figure *12* shows the jaws of tensile testing machine with the bar specimen of *20 mm* in diameter.

Figure 12. " Testing of the bar Φ 20 mm – BSt500S"

The test results are given in *Table 2.*

Table 2. The test results of tensile properties

Material	**Bar dimensions (mm)**			**Yield strength** (MPa)	**Ultimate tensile strength** (MPa)	**Weight** (kg/m)
	Diameter	**Frame height**	**Frame width**			
Č.0551	12	1,4	2,7	489	601	0,980
BSt500S	11,8	1,5	2,4	528	627	0,940
Č.0551	15,5	2,0	2,7	517	617	1,650
BSt500S	15,6	1,8	3,1	673	752	1,620
Č.0551	19,4	1,8	3,5	588	695	2,490
BSt500S	19,6	1,6	3,6	687	767	2,470

Hardness test

Hardness test was conducted in *The Laboratory for Materials - FESB*[*] by the *Vickers testing microscope.* Hardness was tested on the cross-section from the surface to the centre of the specimen. The obtained results are shown in diagrams on figures *13, 14* and *15.*

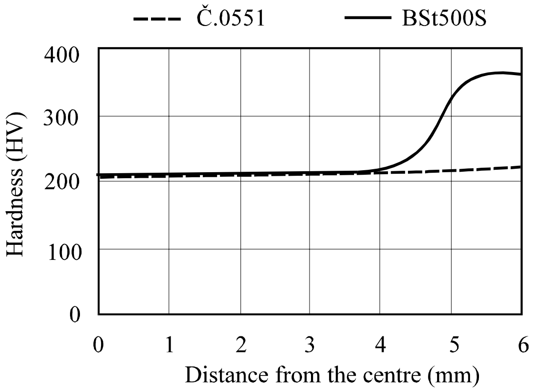

Figure 13. "Rebar Φ12"

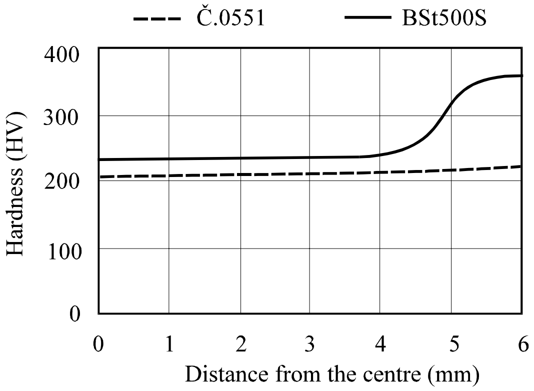

Figure 14. "Rebar Φ16"

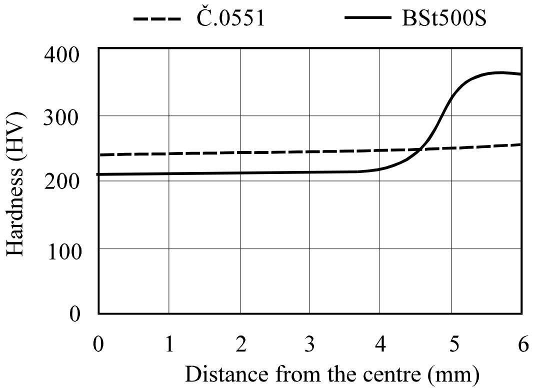

Figure 15. "Rebar Φ20"

---

[*] Faculty of Electrical Engineering, Mechanical Engineering and Naval Architecture, University of Split, Republic of CROATIA

3.3. Microstructure examination

The analysis of microstructure is the most common way for detecting changes caused by heat treatment. The microstructure examination has been done in the *Laboratory for materials – FESB,* with the *OPTON* microscope *AXIOSCOPE.* These examinations were applied on all specimens, but in this paper only three of them are presented.

On Fig.*16* the microstructure of the bar *Φ 12 mm* from Č.0551 steel is illustrated. The pearlite grains among the large ferrite grains are noticeable. The whole cross-section has the same microstructure.

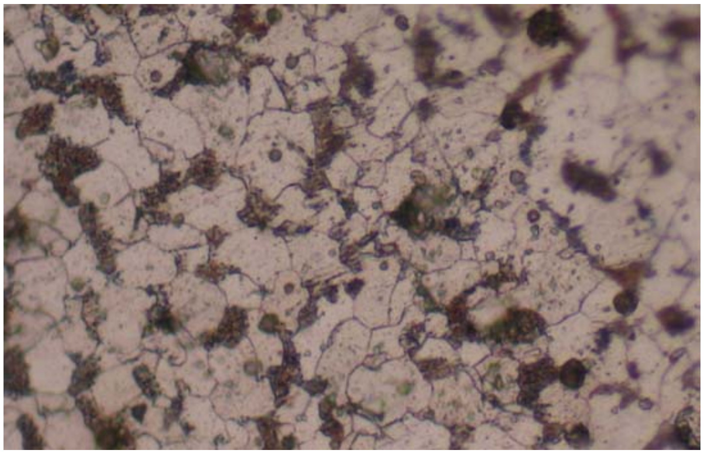

Figure 16. "Č.0551 steel rebar Φ12 - microstructure"

On Fig.*17* the microstructure of the core (bar *Φ 12 mm*) from BSt500S steel is illustrated. The pearlite grains among the large ferrite grains are noticeable.

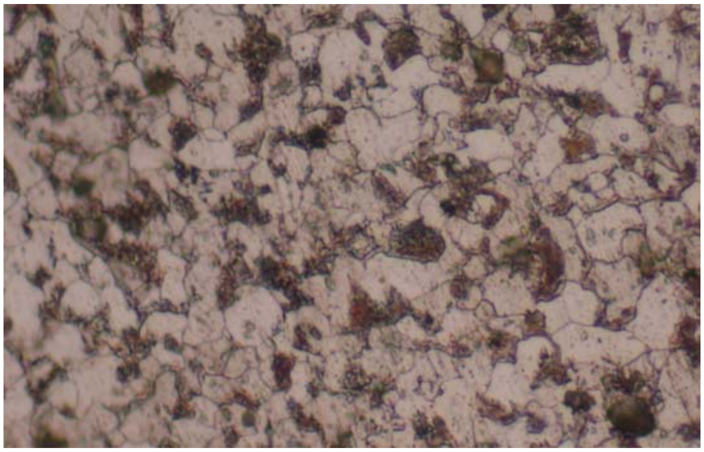

Figure 17. "BSt500S steel rebar core (Φ12) - microstructure"

On Fig.*18* the microstructure of the surface layer (rebar *Φ 12 mm*) from BSt500S steel is illustrated. The surface layer after the quenching consists of small martensite grains.

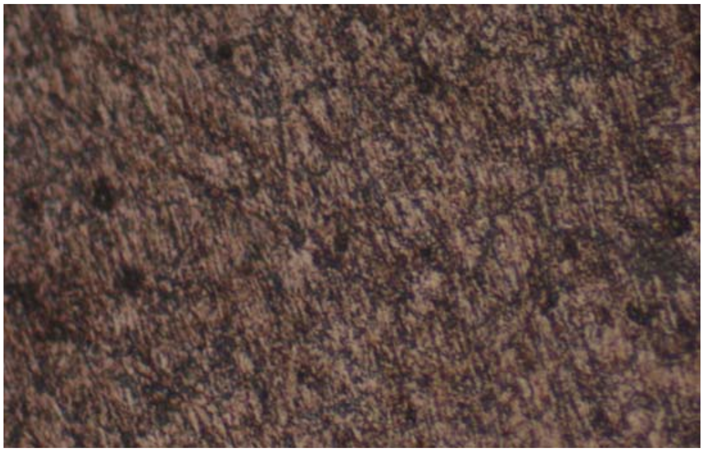

Figure 18. "BSt500S steel rebar surface (Φ12) - microstructure"

On Fig.*19* the microstructure of the transitive zone (surface layer – core - bar *Φ 12 mm*) from BSt500S steel is illustrated.

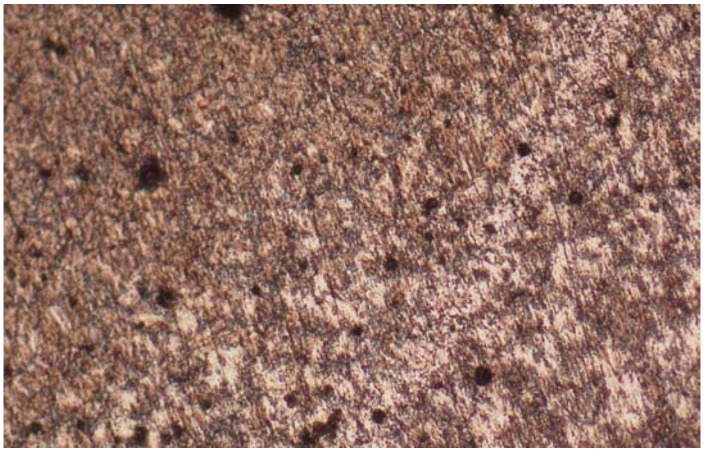

Figure 19. "BSt500S steel rebar transitive zone (Φ12) - microstructure"

4. **DISCUSION**

The analysis of the chemical composition shows significant difference in particular element content with the steels of similar designation. Thus, the carbon content of *Č.0551* differs from *0,19* to *0,25%*, while the silicon content is between *0,21* and *0,3%*. The manganese percentage is well-balanced. The specimens carbon percentage from BSt500S steel varies from *0,15* to *0,18%,* the silicon content is uniform, while there is a significant difference in manganese content *(from 0,66 to 0,83%).*

The mechanical properties test results show significant difference for yield strength as well as ultimate strength of material. Significant differences of mentioned properties are also noticeable between the specimens of the same dimensions from various steels. These differences are the result of various chemical compositions *(Č.0551)*, especially the carbon content. A part of differences are due to non uniform geometrical bar shape (rib dimensions).
The differences for the specimens of BSt 500S steel are more significant. They are mainly caused by non uniform surface heat treatment (quenching). Besides, if we compare obtained R_p and R_m value with the same properties of *DIN -488-84* norm *(R_p=500 MPa, R_m=550 MPa)* it is obvious that the obtained values for yield and ultimate strengths are higher. This fact points out that the applied heat treatment was inadequate according to the specified *DIN* norm [6]. Also according to the literature [ ] it may be concluded that tempering temperature was lower than needed temperature *(T_t =550 – 600^{o}C)*. That is the main reason for developing the phases of higher strength more deeply than needed.

The hardness test results of specimens from BSt 500S lead to the similar conclusion. Hardness of the surface layer *(1,5 – 2 mm beneath the surface)* was about *320 HV* while the core hardness was about *220 HV.*

The microstructure examination verified the existence of phases with higher strength in the specimen surface layers from BSt 500S steel. The phase uniformity across the whole section of specimen from *Č.0551* steel was also verified.

5. **CONCLUSION**

The analysis of the obtained results, without undoubtedly, show that surface heat treatment - quenching of steel rebar results in better mechanical properties. But if we want to have mechanical properties according to the *DIN norm* and also uniformity of mechanical properties for all diameters, it is necessary to have a permanent control of tempering temperature. This temperature control can be done by the radiation pyrometer on the entrance of the cooling desk.
It is therefore recommended to develop the computer program for controlling the water flow in the quenching machine. Basic parameters are: the chemical composition of steel and the rebar diameter. If it is possible to keep uniform chemical composition during the production process, the bar diameter will remain the only significant parameter for intensity of water flow.

6. **LITERATURE**

[1] R. Deželić: *Metals 2*, Faculty of electrical engineering, mechanical engineering and naval architecture, University of Split, Split 1989.

[2] A. Ćorluka: Graduation thesis, *Valjanje rebrastog čelika (Rolling technology of rebar steel),* Faculty of electrical engineering, mechanical engineering and naval architecture, University of Split, Split 2004.

[3] GETECO – Development Department: *Instruction book for Quenching device,* 2000.

[4] GETECO SRL*, Thermal treatment in - line for high yield strength steel,* Italy 2000.

[5] POMINI FARREL S.p.A., *Termex on - line bar treatment technology*, Italy 1999.

[6] *http://www.pittini.de/BSt500S.htm*

10. Savjetovanje o materijalima, tehnologijama, trenju i trošenju
10. Conference on Materials, Processes, Friction and Wear
MATRIB'05, Vela Luka, 23-25.06.2005.

UTJECAJ OTIRANJA OTISAKA NA SUVREMENIM MATERIJALIMA NA KVALITETU OFSETNOG TISKA

THE RUBBING INFLUENCE OF PRINTS ON CONTEMPORARY MATERIALS ON THE QUALITY OF OFFSET PRINTING

I. Zjakić, S. Bolanča, N. Mrvac, M. Milković

Sažetak:
Razvoj grafičke tehnologije omogućio je da se proizvod izrađuje po ujednačenim normama kvalitete tiska u skoro cijelom svijetu. Međutim, kako ne bi došlo do razilaženja u shvaćanju kvalitete otiska, razvoj materijala povlači za sobom i problem standardizacije parametara koji omogućuju izradu kvalitetnog proizvoda, a koji se odnose na materijale koji su po svojim karakteristikama vrlo problematični za otiskivanje tehnikom ofsetnog tiska. Zbog toga je vrlo važno praćenje razvoja materijala i znanstveno dokazivanje standarda koji slijede takav razvoj. Eksperimantalni rezulatati u ovom radu pokazuju vrijednosti prirasta rastertonskih vrijednosti otisaka nastalih na metaliziranim tiskovnim podlogama i to prije i nakon mehaničkih utjecaja na površinu materijala.

Ključne riječi: tisak, prirast rastertonskih vrijednosti, otiranje, kvaliteta

Abstract:
Development of the printing technology enabled the product to be made according to standards of printing quality in almost all the world. However, in order not to disagree in the conception of print quality, the development of materials includes the problem of parameter standardization which enables the production of the qualitative product, which refers to the materials that are very problematic for printing in the offset printing technique. Because of that the monitoring of the material development and the scientific proof of standards which follow such development is very important. Experimental results in this work show the values of the dot gain of prints made on tinted printing surfaces before and after mechanical influence on the material surface.

Key Words: Printing, Dot Gain, Rubbing, Quality

1. UVOD

Proizvođači grafičkih materijala ulažu ogromna sredstva u razvoj materijala koji bi omogućili povećanje kvalitete tiska i time utjecali na povećanje konkurentnosti na tržištu. Jedan od glavnih ograničenja povećanja kvalitete tiska je nemogućnost da se iznad kritične točke debljine sloja bojila bojilo kvalitetno prihvati za tiskovnu podlogu. Jedan od glavnih uzroka povećanja kvalitete tiska danas, razvoj je novih metaliziranih tiskovnih podloga koje imaju povećanu sposobnost prihvaćanja veće količine bojila. Međutim, značajno povećanje kvalitete tiska onemogućeno je povećanjem prirasta rastertonskih vrijednosti u tisku. Cilj svake grafičke reprodukcije je osim da što točnije prikaže original je i da taj prikaz čim dulje ostane nepromijenjen, odnosno da se što manje mijenja s obzirom na različite utjecaje. U tom smislu su u ovom radu i istraživane promjene otiska na različitim metaliziranim tiskovnim podlogama nakon izlaganja otiranju kako bi se u što većoj mjeri definirala i ta dimenzija kvalitete otiska.

2. PRIRAST RASTERTONSKIH VRIJEDNOSTI

U tiskarskom postupku veliki broj čimbenika može utjecati na povećanje rastertonske vrijednosti. Na prirast rastertonske vrijednosti između ostaloga utječe vrsta tiskarskog bojila, temperatura, vrsta rastera i njegove karakteristike, rastertonska vrijednost, vrsta gumene navlake, pritisak na tiskovnu podlogu, vrsta tiskarskog stroja, vlaženje, vrsta tiskovne podloge, itd. Ukupni prirast rastertonskih vrijednosti, za jednobojne reprodukcije, moguće je izračunati Yule -Nielsenovom jednadžbom:

$$R(a) = (a\, R_S^{1/n} + (1\text{-}a)\, R_0^{1/n})^n$$

gdje je $1 \leq n \leq 2$, za refleksiju tiskovnih R_S i netiskovnih R_0 elemenata.

Uslijed prolaska svjetlosti kroz tiskovnu podlogu, dio svjetlosti vraća se reflektirana od unutarnjih slojeva tiskovne podloge. Rezultat takve refleksije svjetlosti je doživljaj proširenja rasterskog elementa koji se naziva optički prirast rastertonskih vrijednosti.

Slika 1. Prikaz optičkog prirasta rastertonskih vrijednosti

Refleksija svjetlosti R(x, y) uslijed upadnog intenziteta svjetlosti I(x, y) tvori kovolucijsku funkciju:

$$R(x,y) = [(I(x,y)\ T(x,y)) \times P(x,y)]\ T(x,y)$$

gdje je T(x, y) transparentnost sloja bojila, a P(x, y) integralna funkcija refleksije površine tiskovne podloge. Navedena jednadžba odnosi se na jednobojne reprodukcije. Kod višebojnog tiska potrebno je uzeti i parametre distribucije svjetlosti, pa se optički prirast rastertonskih vrije-dnosti može prikazati kao:

$$R(x,y,l) = [(I(x,y,\ l),\ T(x,y,\ l)) \times P(x,y,\ l)]\ T(x,y,\ l)$$

gdje je λ valna dužina svjetlosti.
Uslijed niza interakcija u realnoj grafičkoj proizvodnji, rasterski element nije oštar i nanos bojila nije jednoličan po svim dijelovima rasterskog elementa kako je prikazano na slici 2:

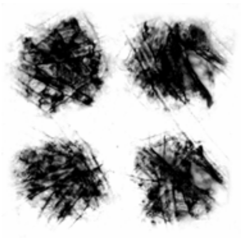

Slika 2. Prikaz realnog rasterskog elementa

Kad bi reprodukcija rasterskih elemenata bila takva da je pokrivenost po cijelom elementu jednolika, a element potpuno geometrijski jednoličan, onda bi se slika mogla prikazati binarno H(x, y), gdje vrijednost 0 predstavlja površinu bez pokrivenosti bojilom, a vrijednost 1 površinu u potpunosti pokrivenu bojilom.
Rezultat reprodukcije uslijed realnog prirasta rastertonskih vrijednosti može se prikazati kao:

$$(x,y) = 10^{-Ds(H(x,y)Q(x,y))}$$

gdje je D_S, integralna gustoća obojenja pune površine, a Q(x, y) funkcija rasipanja svjetlosti s površine. Kada je reprodukcija višebojna, navedena jednadžba može se prikazati za svaku boju odvojeno:

$$T_C(x,y,l) = 10^{-D_C(l)(H_C(x,y)Q(x,y))}$$
$$T_M(x,y,l) = 10^{-D_M(l)(H_M(x,y)Q(x,y))}$$
$$T_Y(x,y,l) = 10^{-D_Y(l)(H_Y(x,y)Q(x,y))}$$
$$T_K(x,y,l) = 10^{-D_K(l)(H_K(x,y)Q(x,y))}$$

Rezultat tiska sve četiri boje ukupnog prirasta rastertonskih vrijednosti prikazuje se kao produkt:

$$T(x,y,l) = T_C(x,y,l), T_M(x,y,l), T_Y(x,y,l), T_K(x,y,l)$$

3. EKSPRIMENTALNI DIO

Ispitivani otisci u ovome radu napravljeni su na četiri vrste metaliziranih tiskovnih podloga (Sappi) koje su različite po svojstvima hrapavosti. Karakteristike navedenih materijala dane su u slijedećoj tablici:

Tablica 1. Površinske karakteristike ispitivanih materijala

Vrsta papira	hrapavost po Bendsenu [ml min^{-1}]	gramatura [gm^{-2}]
uzorak 1	21	135
uzorak 2	22	135
uzorak 3	46	135
uzorak 4	72	135

Otiskivanje je provedeno provedeno u realnim uvjetima na ofsetnom stroju KBA Rapida. Otopina za vlaženje bila je demineralizirana voda umjetno otvrdnuta s vrijednostima vodljivosti od 700-1100 mS, 5-8 ^{0}dH (njem.), te 5,3-5,5 pH. Otiskivanje je obavljeno u standardiziranim uvjetima unutar dopuštenih granica tolerancije[9]. Korištene tiskovne forme u otiskivanju bile su napravljene termalnim sistemom CtPlate na uređaju Topsetter pf 102. Kompresibilne gumene navlake na ofsetnom cilindru bile su od proizvođača Vulcan, s tvrdoćom 80 SH^{0}. Izračun prirasta rastertonskih vrijednosti i konstrukcija krivulje reprodukcije napravljena je programom Heidelberg PrintOpen, dok je izračun gamuta napravljen programom Monaco GW. Otiranje otisaka rađeno je uređajem Pira Wallace.

4. REZULTATI ISTRAŽIVANJA I DISKUSIJA

Nakon otiskivanja s gustoćama obojenja preporučenih normi ISO 12647-2:1996. otisci su podvrgnuti otiranju i nakon mjerenja elemenata kontrolnog stripa, ustanovljen je odnos rastrirane površine otisaka prije i nakon otiranja za različite rastertonske vrijednosti:

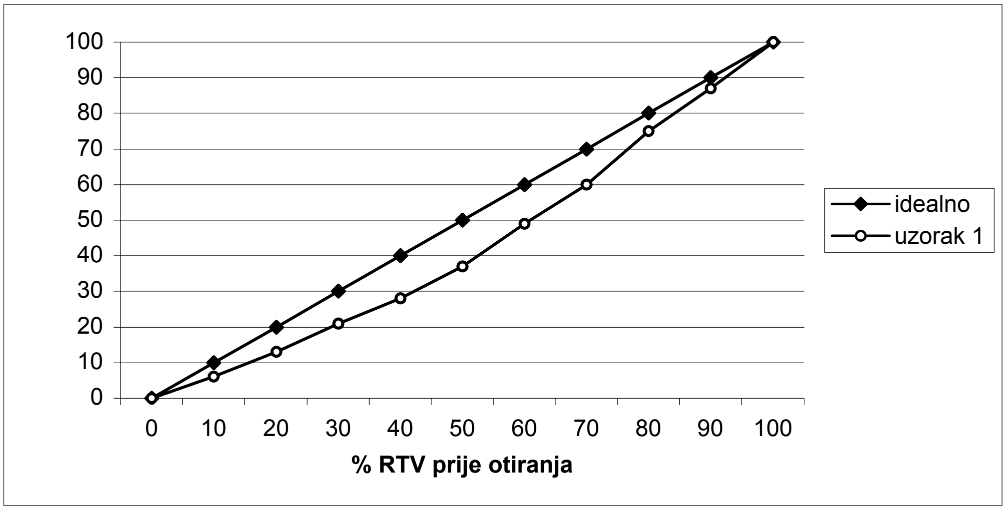

Slika 3. Odnos reprodukcije uzorka 1

Kako je prirast rastertonskih vrijednosti ovisan o rasterskim elementima i gustoći obojenja punog tona, iz navedene krivulje vidi se da je deformacija rastertonskih elemenata uzorka 1 (s najmanjom hrapavosti) nakon otiranja veća na dijelovima reprodukcije s punim tonovima, odnosno otisak nakon otiranja ima veći prirast rastertonskih vrijednosti. Također je izračunat odnos rastrirane površine otisaka prije i nakon otiranja uzorka 2:

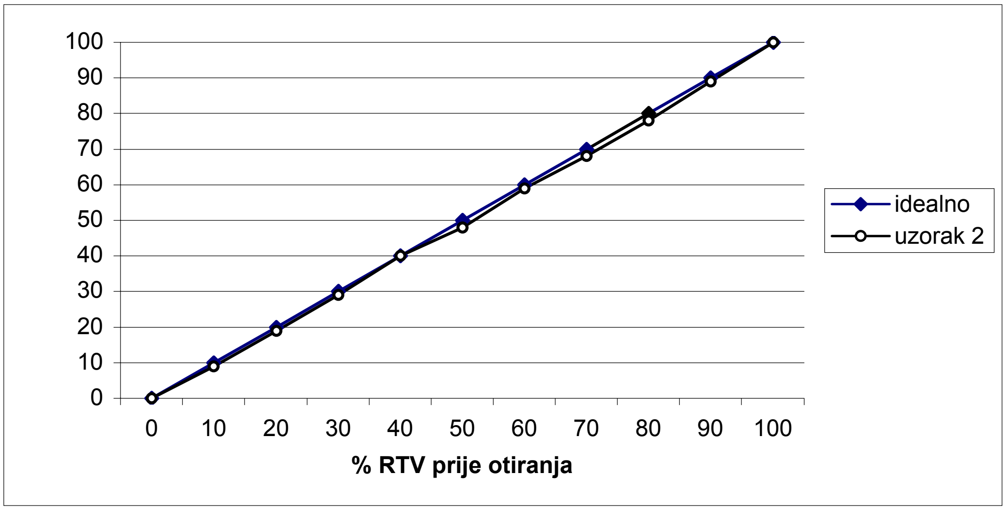

Slika 4. Odnos reprodukcije uzorka 2

Ovim dijagrmom vidljivo je da je deformacija hrapavije tiskovne podloge ujednačenija kod rasterskih elemenata i punog tona. Izračunat je i odnos rastrirane površine otisaka prije i nakon otiranja uzorka 3:

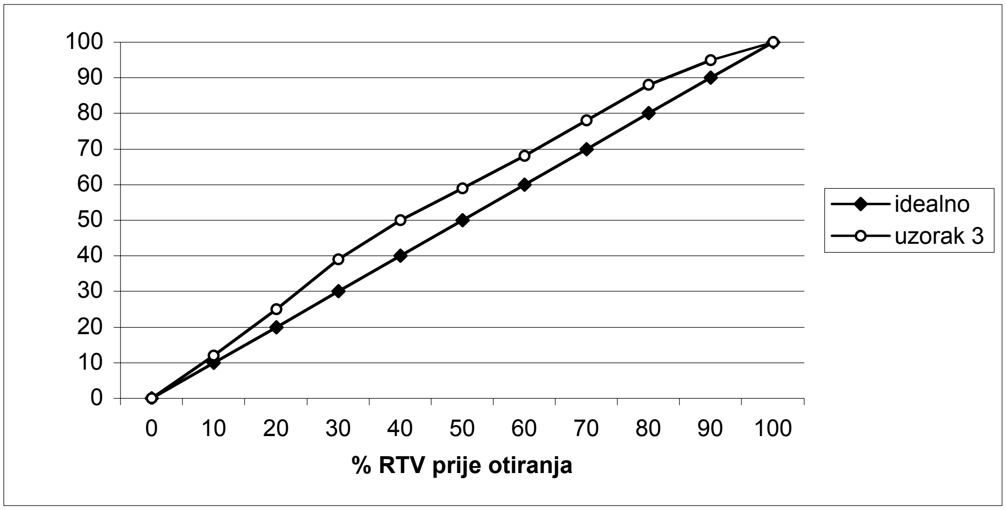

Slika 5. Odnos reprodukcije uzorka 3

Ovim dijagrmom vidljivo je da je deformacija hrapavije tiskovne podloge manja nakon otiranja na dijelovima reprodukcije s punim tonovima, odnosno otisak nakon otiranja ima manji prirast rastertonskih vrijednosti. Također je izračunat i odnos rastrirane površine otisaka prije i nakon otiranja uzorka 4:

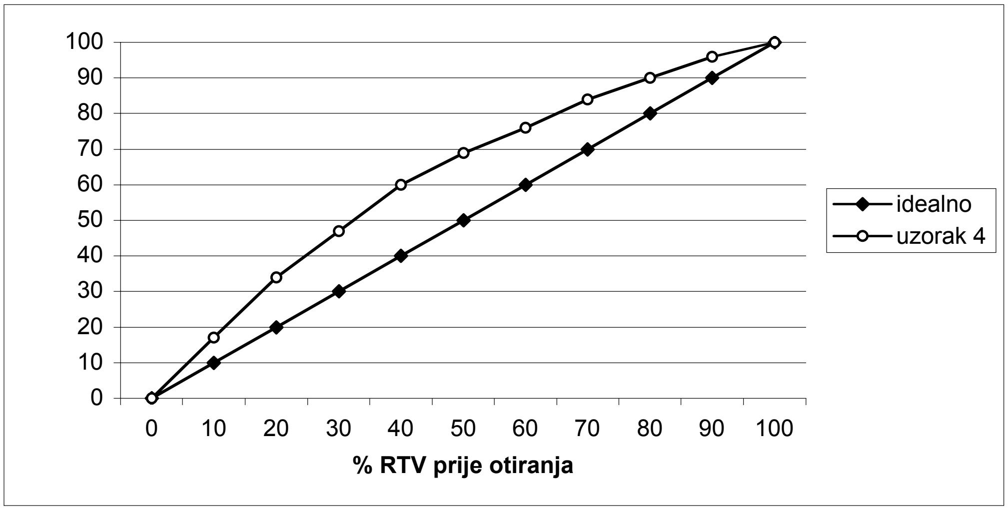

Slika 6. Odnos reprodukcije uzorka 4

Iz ovog dijagrama je vodljivo da je najmanji prirast rastertonskih vrijednosti nakon otiranja ustanovljen kod najhrapavije tiskovne podloge, što dovodi do zaključka da je otiranje djelovalo podjednako na rasterske elemente kao i na puni ton.

5. ZAKLJUČAK

Radom je dokazano da su prirasti rastertonskih vrijednosti različiti s obzirom na hrapavost tiskovne podloge. Na ispitivanim otiscima načinjenim na metaliziranim tiskovnim podlogama nakon izlaganja otiranju došlo je do pada kvalitete otiska.

Rezultati također ukazuju da izlaganje otiska načinjenog na metaliziranoj tiskovnoj podlozi otiranju dovodi do nejednolikog gubitka otisnute grafičke informacije s obzirom različite rastertonske vrijednosti.

Provedenim istraživanjima utvrđeno je da je krivulja reprodukcije nakon otiranja najmanje promijenjena kod tiskovnih materijala hrapavosti površine 21 do 46 [ml min^{-1}] po Bendstenu. U tom smislu u svrhu povećanja kvalitete dobivenih otisaka u realnim uvjetima grafičke proizvodnje pri gramaturi papira od 135 gm^{-2} preporučuje se korištenje metaliziranih tiskovnih površina hrapavosti površine 21 do 46 [ml min^{-1}] po Bendstenu.

6. LITERATURA:

D. Ricards, P. James: "New age solutions", Digital Demand (2001) 38, 66-69.

J. MacPheem: "Fundamentals of lithographic printing", GATFPress, Sewickley (PA) 1998.

J. R. Franck: "GATF Encyclopedia of Graphic Communications", GATFPress, Pittsburgh 1998.

M. Wedin, B. Cruse: "Mechanical and Optical Dot Gain in Halftone Colour Prints", IS&T 11th International Congress on Advances in Non-Impact Printing Technology, Conference Proceedings, New York, 1995.

N. Mrvac, S. Bolanča, I. Zjakić: "Influence of Register Error of Particular Colour on the Visual Evaluation of the Print Quality", GATFPress, Pittsburgh 2001.